Društvo za tehniku zavarivanja Slavonski Brod
Welding Society in Slavonski Brod

ISNN: 2806-755X

13. MEĐUNARODNO ZNANSTVENO-STRUČNO SAVJETOVANJE SBZ 2025

„STROJARSKE TEHNOLOGIJE U IZRADI ZAVARENIH KONSTRUKCIJA I PROIZVODA, SBZ 2025.“

13. INTERNATIONAL SCIENTIFIC-PROFESSIONAL CONFERENCE SBW 2025

„ENGINEERING TECHNOLOGIES IN MANUFACTURING OF WELDED CONSTRUCTIONS AND PRODUCTS, SBW 2025.“

Urednik/Editor: Ivan Samardžić, Josip Pavić, Dejan Marić

SLAVONSKI BROD 08. i 09. 05 2025.

13. Međunarodno znanstveno-stručno savjetovanje SBZ 2025
„STROJARSKE TEHNOLOGIJE U IZRADI ZAVARENIH KONSTRUKCIJA I PROIZVODA, SBZ 2025.“
Slavonski Brod (08. i 09. 05. 2025.)

13. International scientific-professional conference SBW 2025
„ENGINEERING TECHNOLOGIES IN MANUFACTURING OF WELDED CONSTRUCTIONS AND PRODUCTS, SBW 2025“
Slavonski Brod (08. i 09. 05. 2025.)

ZBORNIK RADOVA
CONFERENCE PROCEEDINGS

Urednici/Editors
Ivan Samardžić
Josip Pavić
Dejan Marić

Slavonski Brod, 2025

Naslov/Title
ZBORNIK RADOVA - „STROJARSKE TEHNOLOGIJE U IZRADI ZAVARENIH KONSTRUKCIJA I PROIZVODA, SBZ “/CONFERENCE PROCEEDINGS - „ENGINEERING TECHNOLOGIES IN MANUFACTURING OF WELDED CONSTRUCTIONS AND PRODUCTS, SBW“

Urednici/Editors:
Ivan Samardžić, Josip Pavić, Dejan Marić

Tehnički urednik/Technical editor:
Tomislav Šolić

Organizacija/Organized by:
Sveučilište u Slavonskom Brodu, Strojarski fakultet u Slavonskom Brodu/University of Slavonski Brod,Mechanical Engineering Faculty in Slavonski Brod,
Faculty of Mechanical Engineering, University of Maribor
Faculty of Materials Science and Technology in Trnava
Društvo za tehniku zavarivanja (DTZ), Slavonski Brod/Welding Society Slavonski Brod
Đuro Đaković Grupa d.d. Slavonski Brod/Đuro Đaković Group - Slavonski Brod

Pokrovitelj/Patrons:
Sveučilište u Slavonskom Brodu/University of Slavonski Brod

Nakladnik/Publisher:
Sveučilište u Slavonskom Brodu/University of Slavonski Brod
E-mail: dtzsb@unisb.hr
URL: https://dtzsb.unisb.hr/

ISNN: 2806-755X

PROGRAMSKI ODBOR
SCIENTIFIC COMMITTEE

Aračić Stjepan, Croatia
Avdić Sead, Bosnia & Herzegovina
Bajić Darko, Montenegro
Barta Jozef, Slovakia
Bártová Katarína, Slovakia
Bauer Branko, Croatia
Bošnjaković Mladen, Croatia
Buranský Ivan, Slovakia
Burzić Meri, Serbia
Burzić Zijah, Serbia
Cumin Josip, Croatia
Čambál Miloš, Slovakia
Despotović Božo, Croatia
Dunđer Marko, Croatia
Ergić Todor, Croatia
Garašić Ivica, Croatia
Gojić Mirko, Croatia
Grabulov Vencislav, Serbia
Grizelj Branko, Croatia
Gubeljak Nenad, Slovenia
Ivandić Željko, Croatia
Javor Franjo, Croatia
Juraga Ivan, Croatia
Karakašić Mirko, Croatia
Kladarić Ivica, Croatia
Klobčar Damjan, Slovenia
Kolumbić Zvonimir, Croatia
Kondić Živko, Croatia
Konjatić Pejo, Croatia
Köveš Arpad, Slovenia
Kozak Dražan, Croatia
Kožuh Zoran, Croatia
Lujić Roberto, Croatia
Maglić Leon, Croatia
Manjgo Mersida, Bosnia & Herzegovina
Marić Dejan, Croatia
Marônek Milan, Slovakia
Marušić Vlatko, Croatia
Milčić Dragan, Serbia
Milović Ljubica, Serbia
Mišina Nedjeljko, Croatia
Novoselović Daniel, Croatia
Pašić Omer, Bosnia & Herzegovina
Samardžić Ivan, Croatia
Stoić Antun, Croatia
Stojšić Josip, Croatia
Šimeková Beáta, Slovakia
Vuherer Tomaž, Slovenia

ORGANIZACIJSKI ODBOR
ORGANISING COMMITTEE

Deanović Iva
Despotović Božo, zamjenik predsjednika
Jagnjić Mario
Lukačević Tomislav
Lulić Damir
Marić Dejan, tajnik
Marsenić Tihomir
Mazurek Miroslav
Pavić Josip predsjednik
Samardžić Ivan
Samardžić Mijat
Senić Mirjana
Sigurnjak Ivan
Šolić Tomislav
Zovko Marko

POČASNI PROGRAMSKI ODBOR

Dr. Duspara Mirko, Mayor of the city Slavonski Brod, Croatia

Dr.sc. Danijel Marušić, dr.med.vet., Perfect of Brodsko-posavska county, Croatia

red. prof. dr. Matej Vesenjak, Dean of the Faculty of mechanical engineering, University of Maribor, Slovenia

prof. Ing. Miloš Čambál, CSc. Dean of Faculty of Materials Science and Technology in Trnava, Slovakia

Prof.dr.sc. Ivan Samardžić, Rector of the University of Slavonski Brod, Croatia

Prof.dr.sc. Goran Šimunović, Dean of the Mechanical engineering faculty in Slavonski Brod, University of Slavonski Brod, Croatia

Jadranka Eržišnik, Croatian Welding Society, Zagreb, Croatia

Mato Sigurnjak, dipl.ing.str., Director of company Sigmat, Slavonski Brod, Croatia

Marko Čosić, President of management bord of company Đuro Đaković Group Plc., Slavonski Brod, Croatia

Pavel Maroushek, Member of management bord of company Đuro Đaković Group Plc., Slavonski Brod, Croatia

Vjekoslav Galić, dipl.ing.str., Executive manager of company Industroremont, Slavonski Brod, Croatia

Anto Pivac, Executive manager of company Đuro Đaković Montaža, Slavonski Brod, Croatia

Prskalo Zdenko, Executive manager of company Magma, Požega, Croatia

Danijela Brajdić Cirković, dipl.ecc., Manager of company Đuro Đaković Kompenzatori, Slavonski Brod, Croatia

DRUŠTVO ZA TEHNIKU ZAVARIVANJA SLAVONSKI BROD - DANAS I SUTRA

Društvo za tehniku zavarivanja Slavonski Brod osnovano je 1955. godine pri industriji i za potrebu industrije „Đuro Đaković“. Može se reći da je industrija „Đuro Đaković“ trebala Društvo za tehniku zavarivanja Slavonski Brod, ali isto tako slobodno možemo reći da Društvo za tehniku zavarivanje Slavonski Brod ne bi opstalo ovoliki niz godina bez industrije „Đuro Đaković“. Jedan od temeljnih ciljeva Društvo za tehniku zavarivanja Slavonski Brod je povezivanje kolega u metaloprerađivačkoj industriji, te razmjena iskustava sa svima koji se susreću sa tehnikom zavarivanja.

Rad i aktivnosti Društva za tehniku zavarivanja Slavonski Brod usko su povezani sa Sveučilištem u Slavonskom Brodu i Strojarskim fakultetom. Obrazovanje i znanost ključni su čimbenici razvoja i pri tome važan razvojni potencijal predstavljaju Sveučilište u Slavonskom Brodu i Strojarski fakultet, pogotovo njihovi obrazovni programi usmjereni na suradnju s gospodarskim sektorom. Važnu ulogu u obrazovanju i stručnom osposobljavanju članova društva imaju i Hrvatsko društvo za tehniku zavarivanja Zagreb, te Certifikacijske kuće prisutne u tvrtkama kroz nadzor, kvalifikacije postupaka zavarivanja i zavarivača te certificiranju sustava.

SVEUČILIŠTE U SLAVONSKOM BRODU
UNIVERSITY OF SLAVONSKI BROD

Strojarski fakultet
Mechanical Engineering Faculty

Društvo za tehniku zavarivanja Slavonski Brod djeluje u Brodsko-posavskoj županiji koja je tradicionalno središte industrije i poduzetništva u snažnom zamahu prema zelenom, inovativnom, digitalnom gospodarstvu i zadovoljnom društvu. Središte županije je grad Slavonski Brod u kojem živi više od trećine svih stanovnika županije i u kojem je koncentrirana većina društvenog i gospodarskog života. Drugi grad po veličini u Brodsko-posavskoj županiji je Nova Gradiška koja je središnje mjesto zapadnog dijela županije. Glavna konkurentska prednost Brodsko-posavske županije jest njezin izvanredni geostrateški položaj s obzirom na to da je smještena na križanju dvaju europskih prometnih koridora. Županijom prolaze željeznički, cestovni i vodeni putevi, telekomunikacijska mreža i naftovod. Četiri glavna grada (Zagreb, Budimpešta, Beograd i Sarajevo) nalaze se u radijusu od 350 km od Slavonskog Broda, sjedišta županije. Najvažnija gospodarska djelatnost jest prerađivačka industrija u kojoj prevladavaju poduzetnici iz metaloprerađivačke djelatnosti, prerade drva i proizvodnje namještaja, proizvodnje kemijskih te prehrambenih proizvoda. Prerađivačka industrija ima i najveći udio u prihodima od izvoza. Poduzetnici Brodsko-posavske županije najviše izvoze u Njemačku, Italiju, Austriju, Bosnu i Hercegovinu te Belgiju.

Društvo za tehniku zavarivanja Slavonski Brod, od ove godine, član je Hrvatske gospodarske komore i Strukovne grupe metaloprerađivačke industrije HGK – Županijske komore Slavonski Brod i HGK – Županijske komore Požega, koja ima regionalni karakter i osnovana je 21. rujna 2023. godine u HGK – Županijskoj komori Slavonski Brod.

Članice Strukovne grupe metaloprerađivačke industrije udružile su se radi promicanja, zaštite i usklađivanja zajedničkih interesa, boljega tržišnog pozicioniranja, unapređivanja rada i stručnih znanja te razvoja djelatnosti. Udruženje metaloprerađivačke industrije djeluje u Odjelu prerađivačke industrije Sektora za industriju i održivi razvoj Hrvatske gospodarske komore.

Snažna gospodarska aktivnost i metaloprerađivačka industrija privukla je i proizvođače opreme za zavarivanje, dodatnih materijala za zavarivanje i opreme za obradu metala. Direktno i/ili putem svojih zastupnika oprema svih vodećih svjetskih proizvođača zastupljena je u pogonima tvrtki metaloprerađivačke industrije Brodsko-posavske županije. Stručna suradnja Društva za tehniku zavarivanja Slavonski Brod sa proizvođačima opreme i njihovim zastupnicima ostvarena je putem organizacije jednodnevnih stručnih seminara i prezentacijom dijela tehnologije, opreme i procesa, te organizacijom edukativnih posjeta tvrtkama proizvođačima opreme.

Društvo za tehniku zavarivanja Slavonski Brod, svake dvije godine, od 2001.g. organizira međunarodna znanstveno-stručna savjetovanja. Kroz međunarodna savjetovanja stručna suradnja je ostvarena i sa kolegama iz industrije, znanstvenim institucijama i društvima za tehniku zavarivanja iz regije i šire (Austrija, Bosna i Hercegovina, Crna Gora, Italija, Makedonija, Njemačka, Slovačka, Slovenija, Srbija). Pored prezentacije znanstveno-stručnih radova, u programu savjetovanja nezaobilazna je izložba opreme za zavarivanje, pokazna zavarivanja, posjete tvrtkama, te zajedničko druženje sudionika u gradu Slavonskom Brodu i okolici. Želja organizatora je postići ugodno druženje u opuštenom okruženju sa ciljem razmjene iskustava sa kolegama, stjecanje novih kontakata, jačanje povjerenja, umrežavanje, poticanje i proširenje poslovne suradnje.

Danas, kao rezultat rada proteklih godina, Društvo za tehniku zavarivanja Slavonski Brod ima svoje prepoznatljivo mjesto i ulogu u povezivanju vodećih strojarskih kadrova iz metaloprerađivačke industrije, znanstvene zajednice lokalno i u međunarodnim okvirima. Pri tome ne možemo zanemariti utjecaj i ulogu tvrtki metaloprerađivačke industrije iz koje dolaze naši članovi, te utjecaj i ulogu Sveučilišta u Slavonskom Brodu i Strojarskog fakulteta. Zahtjev industrije za obrazovanim, stručnim kadrovima, prilagodljivim, inovativnim i spremnim za cjeloživotno obrazovanje je permanentan. Povezivanje i suradnja nameće se sama od sebe.

U naredno periodu, program rada i ciljevi Društva za tehniku zavarivanja Slavonski Brod ostaju isti, ali će se mijenjati pristup. Danas sve što nije objavljeno na društvenim mrežama nije se dogodilo. Komunikacija, povezivanje, suradnja i razmjena iskustava on line putem web stranice društva zadatak je za sve zainteresirane na suradnju sa Društvom za tehniku zavarivanja Slavonski Brod.

Želja nam je da web stranica društva bude mjesto za:

- suradnju i zajednički rad,
- razmjenu iskustava,
- uvid u najnovije tehnologije,
- inovacije i zanimljivosti u metaloprerađivačkoj industriji,
- predstavljanje i promociju tvrtki,
- predstavljanje i promociju proizvoda,
- predstavljanje i promociju opreme.

Više o Društvu za tehniku zavarivanja Slavonski Brod možete pronaći na: https://dtzsb.unisb.hr/.

Predsjednik DTZ SB
Josip Pavić, dipl.ing.

Glavni sponzor

SIGMAT d.o.o. za proizvodnju, inženjering i trgovinu

Dr.Franje Tuđmana 35, naselje Gromačnik, 35252 Sibinj, Croatia

E-mail: sigmat@sigmat.hr

voestalpine Böhler Welding CEE GmbH

Böhler-Welding-Straße 1

8605 Kapfenberg, Austria

E-mail: goran.nadrcic@voestalpine.com

Sponzori

JUŽNI PROLAZ	**Južni prolaz d.o.o.** 10000 Zagreb, Majstorska 3, Croatia E-mail: ivo.belan@juzniprolaz.hr
Eurotehnika	**Eurotehnika d.o.o.** 10000 Zagreb, Susedsko polje 2B, Croatia E-mail: info@eurotehnika.hr
KOŽUL	**Kožul d.o.o.** Vinogradska cesta 2G 35 000 Slavonski BrodCroatia E-mail: kozul@kozul.hr
TÜVNORD	**TÜV NORD Adriatic d.o.o.** Bani 110, Zagreb, HR - 10 010 Buzin E-mail: perkusic@tuv-nord.com
INDUSTROREMONT d.o.o. SLAVONSKI BROD - HRVATSKA	**Industroremont d.o.o.** 35000 Slavonski Brod, Ulica 108. brigade ZNG 88, Croatia E-mail: info@industroremont.hr
summa-chem	**SUMMA-CHEM, d.o.o.** Prilaz Gjure Deželića 42, Zagreb E-mail: gordan.habekovic@summachem.hr
LINCOLN ELECTRIC	**Lincoln Electric Italia S.r.l.** Località Casalmenini, 3, 37010 Rivoli Veronese, Italy
TREA TRADE d.o.o.	**TREA TRADE d. o. o.** Marinići, Blažići 2A, Viškovo, E-mail: info@treatrade.hr
CHI-TECH HIGH INTELLIGENCE cutting TECHNOLOGY	**CHI-TECH d.o.o.** Videkovići 46, 10431 Sveta Nedelja, Croatia, E-mail: info@chitech.com.hr
Industrijska defektoskopija	**Idef d.o.o.** 10000 Zagreb, Kranjčevićeva 30, Croatia E-mail: idef@idef.hr
CROMATEC	**Cromatec d.o.o.** Hrvatske bratske zajednice 2, 10430 Samobor, Croatia, E-mail: info@cromatec.hr
YASKAWA	**Yaskawa Slovenija d.o.o.** Lepovče 23, 1310 Ribnica, Slovenija, E-mail: Denis.Medved@yaskawa.eu
RAOS 3M Authorised Distributor Industrial Products	**RAOS, d.o.o.** Savica I 111 (CMP Savica Šanci), 10000 Zagreb, E-mail: info@raos.hr
metalvar	**Metalvar d.o.o.** HR-10000 Zagreb, Črnkovečka 2D E-mail: metalvar@metalvar.hr

Partneri

	**Đuro Đaković Specijalna vozila d.d.** 35000 Slavonski Brod, Ulica 108. brigade ZNG 40, Croatia E-mail: marketing@ddsv.hr
 ANDRITZ TEP d.o.o.	**ANDRITZ TEP d.o.o.** Croatia, Ulica 108. brigade ZNG 84 35000 Slavonski Brod E-mail: info-tep@andritz.com
	**Magma d.o.o.** Industrijska 27, 34000 Požega, Croatia E-mail: magma@magma-pz.hr
	**Đuro Đaković Kompenzatori d.o.o.** 35000 Slavonski Brod, Ulica 108. brigade ZNG 62, Croatia E-mail: ddk@kompenzatori.com
	**ĐURO ĐAKOVIĆ-Centar za istraživanje i razvoj d.o.o.** Ul. 108. brigade ZNG 26, 35000, Slavonski Brod, Croatia E-mail: ddcir@ddcir.hr
	**Đuro Đaković Montaža d.o.o.** Ulica 108. brigade ZNG 94 35000 Slavonski Brod, Hrvatska E-mail: info@ddmontaza.hr

Sadržaj

Društvo za tehniku zavarivanja Slavonski Brod

13. Međunarodno znanstveno-stručno savjetovanje SBZ 2023

„STROJARSKE TEHNOLOGIJE U IZRADI ZAVARENIH KONSTRUKCIJA I PROIZVODA, SBZ 2025."
Slavonski Brod, 08. i 09. 05. 2025.

Fracture mechanics properties of welding joints made by duplex stainless steel 1.4462

T. Vuherer[1,*], D. Bajić[2], M. Manjgo[1], M. Manjgo[3], G. Lojen[1]

[1] Univerza v Mariboru, Fakulteta za strojništvo, Slovenia
[2] Faculty of Mechanical Engineering, University of Montenegro, Montenegro
[3] Faculty of Mechanical Engineering in Mostar, University "Džemal Bijedić", Bosnia and Herzegovina

[*] Corresponding Author. E-mail: tomaz.vuherer@um.si

Abstract

Duplex stainless steel 1.4462 combines the good properties of austenite and ferrite and has good resistance to pitting corrosion, surface and intergranular corrosion and has higher resistance to stress corrosion. The material also has good mechanical properties with a strength up to 2 times higher than AISI304 stainless steel and the steel is well weldable. Due to these excellent properties and corrosion resistance, this material is often used in many areas of the marine industry for different structures which are usually made by welding. Therefore, good mechanical properties, good impact toughness and, above all, adequate fracture toughness are expected from the individual parts of the weld (weld metal - WM, fusion line - FL, heat affected zone - HAZ). Welding with inappropriate heat input in certain zones of the weld such as WM and HAZ often results in very low impact and fracture toughness. This is precisely what this paper is concerned with, identifying the different mechanical properties such as impact toughness and fracture toughness in the individual parts of the welds and comparing them with the properties of the base material.

Keywords: Weld joint, mechanical properties, impact toughness, fracture toughness

1. Uvod

Primjena dupleks čelika je u ekspanziji u praktično svim značajnim grana industrije. Dominantna primjena je u termoenergetici, procesnoj industriji, prehrambenoj industriji itd. Ograničena zavarljivost ovih čelika zahtijeva studiozan pristup pri definisanju adekvatne tehnologije zavaribvanja.
Specifičnost dupleks nerđajućih čelika je njihova mikrostukturna građa koju čine jednaki udjeli austenitne i feritne faze (50 – 50%). Zbog ograničene korozione postojanosti i otežane zavarljivosti

[1, 2] primjena ovih čelika do 80-ih godina XX vijeka bila je izuzetno mala. Treba spomenuti da su ovi čelici dobijeni 30-ih godina XX vijeka.
Dupleks čelici posjesuju najbolje karakteristike austenitne i feritne strukture. Unapređenje u svojstvima ovih materijala je postignuto zahvaljujući pojednim legirajućim elementima u svojstvu faznih stabilizatora: azot, nikl, molibden, volfram, bakar, silicijum. Austenitna faza obezbjeđuje izrazitu duktilnost na niskim temperaturama i visoku otpornost prema opštoj koroziji. Feritna faza povećava čvrstoću i otpornost pojavi toplih prslina i prslina usled naponske korozije [3].
Budući da dupleks čelike karakteriše njihova lamelarna građa, neophodna posebna pažnja pri njihovoj proizvodnji i samom oblikovanju. Zavarljivost ovih čelika je uspješna ukoliko se tehnologijom obezbjeđuje zadržavanje početnog odnosa austenitne i feritne faze (50 – 50%) u metalu šava. Važnu ulogu u ovom procesu ima prisustvo azota. U nedostatku azota javlja se feritizacija strukture metala šava, čime se pogoršava njihova zavarljivost, a time i njegove mehaničke karakteristike. Ključ uspjeha za dobijanje kvalitetnog zavarenog spoja je održavanje ograničenog sadržaju azota, kontrolisanom unosu toplote i termičkoj obradi zavareni spoja kod elemenata veće debljine [2, 4]. Azot i nikl su glavni gamageni, a hrom i molibden alfageni legirajući elementi.
Zavareni spoj dupleks čelika očvršćava kao 100% ferit, dok se austenit formira i raste u čvrstom stanju [5].

2. Osnovni i dodatni materijal

Osnovni materijal je koroziono postojani dupleks čelik 1.4462 (DIN X2CrNiMoN 22-5-3). Hemijski sastav čelika 1.4462 dat je u tabeli 1, a u tabeli 2 njegova mehanička svojstva.

Tabela 1. Hemijski sastav osnovnog materijala 1.4462

Maseni udio (wt. %)											
C	Si	Mn	P	S	Cr	Ni	Mo	Nb	Cu	Co	N
0.017	0.31	1.34	0.028	0.001	22.29	5.66	3.16	0.004	0.23	0.13	0.168

Tabela 2. Mehnička svojstva materijala 1.4462

Yield strength, $R_{p0,2}$, MPa	Tensile strength, R_m, MPa	Elongation, A_5, %	Hardness, HB	Impact thougness, K_v, J/cm^2
647	832	34	264	238

Čelik 1.4462 ima veliku upotrebu za izradu elemenata koji funkcionišu u agresivnim sredinama. Ovaj čelik ima dobru zavarljivost i nije potrebna preventivna (predgrijavanje) ili naknadna termička obrada. Zahvaljujući niskoj vrijednosti koeficijenta toplotnog širenja, kod zavarenog spoja ovog čelika se javlja minimalna vrijednost zaostalih napona.

Koroziono postojani dupleks čelik 1.4462 je magnetičan. Prema preporuci [6], za čelik 1.4462 maksimalna temperatura međuprolaza je 150 – 250 °C, a energija električnog luka 0.5 – 3.5 kJ/mm.

Za SMAW zavarivanje korišćena je dodatni materijal puna žičana elektroda G 22 9 3 NL (ISO 14343-A) Ø1 mm. Hemijski sastav pune žičane elektrode dat je u tabeli 3, a u tabeli 4 njena mehanička svojstva.

Tabela 3. Hemijski sastav pune žičane elektrode G 22 9 3 NL

Maseni udio (wt. %)															
C	Si	Mn	P	S	Cr	Mo	Ni	Nb	Cu	Ti	Al	Co	N	B	V
0.01	0.52	1.44	0.018	0.0005	23.2	3.44	8.2	0.01	0.07	0.01	0.006	0.02	0.13	0.002	0.05

Tabela 4. Mehnička svojstva pune žičane elektrode G 22 9 3 NL

Yield strength, $R_{p0,2}$, MPa	Tensile strength, R_m, MPa	Elongation, A_5, %
450	550	20

3. Zavarivanje uzoraka

Zavarivani su uzorci dimenzija 360x240x4 mm. Dužina zavarenog spoja je 360 mm. Za zavarivanje uzoraka postupcima SMAW izvršena je priprema stranica spoja u obliku V žljeba (Slika 1).

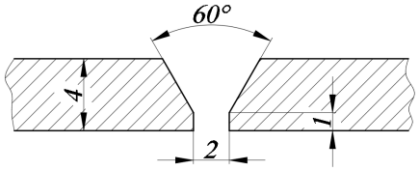

Slika 1. Priprema V žljeba

Za SMAW (135) zavarivanje korišćen je uređaj VARSTROJ – VARMIG 600 D44 Synergy TIG 220 DC HF FV. Zavarivanje je izvršeno u dva prolaza. Koriščeni zaštitni gas je EN ISO 14175: M13 (Ar 98%, O_2 2%), a za korijensku stranu gas M21 (Ar 82%, O_2 18%). Temperatura međuprolaza je 150 °C. Parametri zavarivanja dati su u tabeli 5.

Tabela 5. Parametri SMAW zavarivanja

	Napon U, V	Struja I, A	Brzina zavarivanja v, cm/min	Protok zaštitnog gasa, l/min
Prvi prolaz	23	135	35	17
Drugi prolaz	24.8	167.4	35	17

Izgled zavarenog spoja prikazan je na slici 2.

Slika 2. Izgled zavarenog spoja (lice i korijen)

4. Rezultati ispitivanja zatezanjem

Ispitivanje zatezanjem je izvršeno u skladu sa standardnom EN ISO 6892-1 [7]. Epruvete za određivanje mehaničkih svojstava zavarenog spoja su pravougaonog poprečnog presjeka (slika 3).

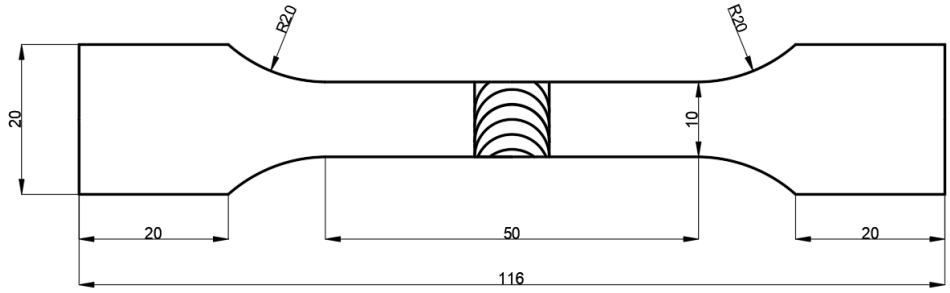

Slika 3. Geometrija epruvete za ispitivanje zatezanjem

U tabeli 6 su date srednje vrijednosti parametara ispitivanog osnovnog materijala (5 epruveta)

Tabela 6. Srednje vrijednosti parametara [1]

E_t, GPa	σ_{x1}, Mpa	σ_{x2}, MPa	σ_{x3}, MPa	σ_{x4}, MPa	σ_M, MPa	ε_M, %	σ_B, MPa	ε_B, %	Z, %	h, mm	b, mm	A_0, mm^2
169.8	694.2	731.2	755.8	773.6	802.2	8.4	359.8	13.3	81.78	4	10.1	39.36

Na slici 4 je prikazan snimak epruvete OM3 nakon razaranja. Ova epruveta zbog nehomogenosti materijala odstupa od ostale četiri i kontrakcija je manja za 4.33% od srednje vrijednosti, tabela 6.

Slika 4. Epruveta OM3 nakon ispitivanja sa izraženom kontrakcijom

U tabeli 7 su date srednje vrijednosti parametara ispitivanih SMAW zavarenih spojeva duplex čelika (5 epruveta).

Tabela 7. Srednje vrijednosti parametara zavarenih spojeva [1]

E_t, GPa	σ_{x1}, MPa	σ_{x2}, MPa	σ_{x3}, MPa	σ_{x4}, MPa	σ_M, MPa	ε_M, %	σ_B, MPa	ε_B, %	Z, %	h, mm	b, mm	A_0, mm^2
165	724.8	768.8	796.2	813.4	834.4	7.12	429.8	10.58	77.6	3.91	10.13	39.61

Na slici 5 je prikazan snimak epruvete 3M nakon razaranja. Površina preloma na ovoj epruveti je izrazito svijetle boje i površina iznosi 8.6 mm^2 dok je kontrakcija 78.16% i od prosjeka je veća za 0.56%.

Slika 5. Epruveta 3M nakon ispitivanja sa izraženom kontrakcijom

5. Rezultati ispitivanja Charpy udaren žilavosti

Određivanje Charpy udarne žilavosti izvršeno je prema standardu EN ISO148-1 [8] koristeći "V" zarez. Materijal odnosno zavareni spoj ima izraženu duktilnost. Dobijene vrijednosti energije loma ispitivanih uzoraka su prikazani u tabeli 8.

Tabela 8. Srednje vrijednosti Charpy udarne žilavosti zavarenih spojeva

	OM	ZUT	LS	MŠ
E_u, J	100.7	86.7	67.1	44.8

6. Rezultati ispitivanja mehanike loma

Eksperimentalno ispitivanje parametara mehanike loma (J integral i K_{IC}) izvedeno je prema standardu ASTM E1820 [9]. Prema tom standardu korištene su SENB ispitivani uzorci dimenzija: debljina materijala B = 4 mm, visina uzorka W=10 mm, rastojanje između oslonih valjaka S = 48 mm, debljina potpore za postavljanje senzora Z = 0.5 mm.
Određeni su dijagrami ispitivanja F – *CMOD* za osnovni materijal (slika 6) i metal šava (slika 7). Eksperiment se zaustavljao na vrijednosti *CMOD* od 0.8 mm. Korištena je normalizacijska metoda prema navedenom standardu za dobijanje rezultata i krivih otpornosti.

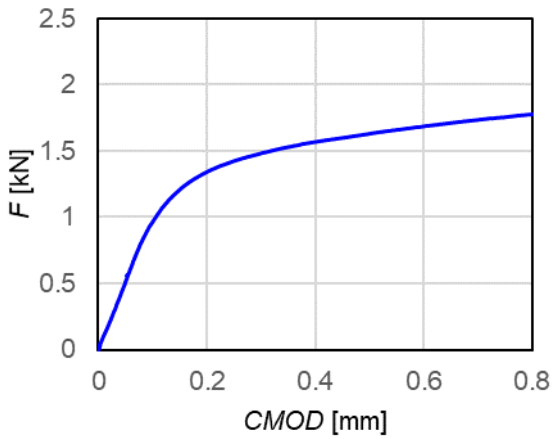

Slika 6. *F-CMOD* za osnovni materijal (OM)

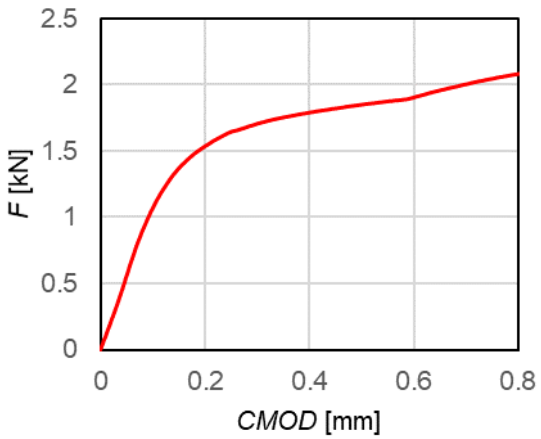

Slika 7. *F-CMOD* za metal šava (MŠ)

Zbog malih dimenzija ispitivanih uzoraka (debljina 4 mm) teško je postići RDS i zbog toga je mali kapacitet ispitivanog uzorka. Plastična zona materija koja je formirana je praktično došla do ruba uzorka. Nijesu zadovoljeni uslovi standarda ASTM E1820: debljina B>25 J_Q/σ_y i inicijalni ligament b_0>25 J_Q/σ_y.
Za MŠ dobijena je kriva otpornosti J-Δa (slika 8), dok za OM nije bilo moguće nacrtati jer nije bilo dovoljnog rasta pukotine (vidno iz slika prelomnih površina), tako da je eksperiment zaustavljen u zoni zatupljenja vrha pukotine (bluntingu).

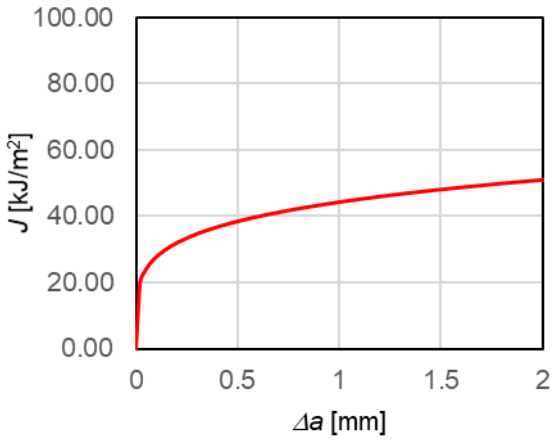

Slika 8. Kriva otpornosti *J-Δa* za metal šava (MŠ)

U tabeli 9 prikazani su rezultati – parametri mehanike loma. Za osnovni materijal K_Q je usvojena vrijednost žilavosti materijala, što je 2.5 – 3 puta manja vrijednost zbog nedovoljnog rasta pukotine. Prema podacima iz literature [10], vrijednost K_{IC} za OM je 180 – 200 MPam^{0,5}. Kod ispitivanog uzorka MŠ, napredovanje pukotine je bilo dovoljno, te su dobijeni rezultati validni.

Tabela 9. Parametri mehanike loma

	K_Q [MPam^{0,5}]	J_{IC} [kJ/m^2]	J [kJ/m^2] kod *CMOD* 0,8 mm
OM	67 (180-200[1])	-	139.1
	K_{IC} [MPam^{0,5}]	J_{IC} [kJ/m^2]	J [kJ/m^2] kod *CMOD* 0,8 mm
MŠ	87.9	32.8	175.3

[1] Blunting područje K_{IC} = 200 MPam^{0,5}

Na slici 9 prikazane su prelomne površine oba ispitivana uzorka, gdje se jasno vidi da kod OM nije bilo dovoljnog napredovanja rasta pukotine (za OM Δa = 0.049 mm), dok je kod MŠ Δa = 0.299 mm.

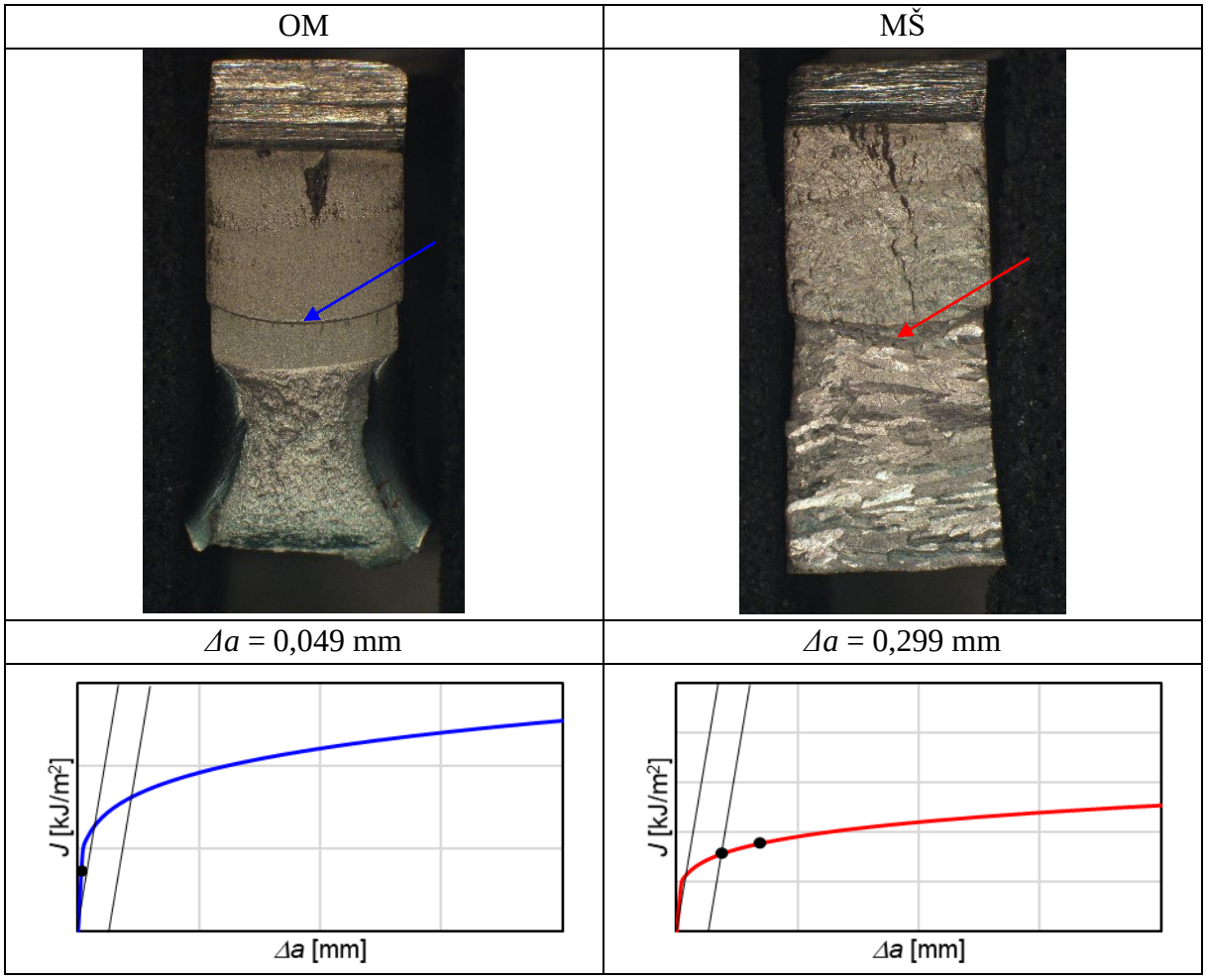

Slika 9. Prelomne površine ispitivanih uzorak as a adekvatnim krivim otpornosti *J-Δa*

7. Zaključci

Iz shematskog prikaza se vidi da za osnovni materijal nismo dostigli dovoljan rast pukotine, te da je posljednja tačka eksperimenta ostala u blunting području. Dobijena žilavost za osnovni materijal bi trebala biti 2,5 – 3 puta veća kada bi napredovanje pukotine bilo minimalno 0,2 mm. Za metal šava, kriva otpornosti i parametri mehanike loma su potpuno validni. Tačke na shematskoj slici prikazuju vrijednost J_{IC} (gdje konstrukcijska linija pri Δa = 0,2 mm presijeca krivu otpornosti), te posljednju tačku eksperimenta pri Δa = 0,299 mm.

Parametri mehanike loma za duktilne materijale male debljine, kao što je slučaj sa dupleks čelik 1.4462 debljine 4 mm, teško je dobiti jer nijesu stvoreni preduslovi RDS.

Rezulati duktilnosti materijala koji je definisan Charpy ispitivanjem potvrđuju da je osnovni materil izuzetno velike duktilnosti u odnosu na metal šava (>2 puta).

8. Literatura

[1] Delić, Dejan. (2022). Ocjena kvaliteta zavarenih spojeva dupleks čelika 1.4462 ostvarenih REL i MAG postupcima, Master rad, Mašinski fakultet, Univerzitet Crne Gore, Podgorica.

[2] Russel, Steven W.; Lundin, Carl D. (2005). The Development of Qualification Standards for Cast Duplex Stainless Steel. Final report, Vol. 2. The University of Tennessee, Knixville, Submitted to U.S. Departnemt of Energy, Award Number - DE-FC07-00 ID13975.

[3] https://www.stainless-structurals.com/blog/ferritic-stainless-steel/ / pristupano 07.02.2022.

[4] Delić. D., Bajić D., Manjgo Mirza, Manjgo Mersida, Vuherer T. (2023). Comparative analysis of the quality of welded joints of duplex steel 1.4462 made by electric arc methods, 12. Međunarodno znanstveno-stručno savjetovanje SBZ 2023, „STROJARSKE TEHNOLOGIJE U IZRADI ZAVARENIH KONSTRUKCIJA I PROIZVODA, SBZ 2023.", Slavonski Brod, 26. i 27. 04. 2023. i Požega 28. 04. 2023., pp.45-54

[5] Kotecki, Damian J. (2011) Some Pitfalls in Welding Duplex Stainless Steels. *Welding & Welded Structures*, 56, 63-69. (Translation: Milica Antić).

[6] Leif. K. (2018). Welding duplex stainless steels: A review of current recommendations. *Welding & Welded Structures*. 63. 29-35. https://doi.org/10.5937/zzk1801029K.

[7] EN ISO 6892-1:2019, Metallic materials - Tensile testing - Part 1: Method of test at room temperature.

[8] EN ISO148-1:2009, Metallic materials – Charpy pendulum impact test – Part 1: Test method.

[9] ASTM E1820-18, Standard Test Method for Measurement of Fracture Toughness

[10] Sieurin H., Westin E. M., Liljas M., Sandström R. (2009) Fracture Toughness of Welded of Commercial Duplex Stainless Stainless. *Welding & Welded Structures*, 1/2009, 21-32. (Translation: Milica Antić).

Lifetime assessment for newly developed friction stir welding tool

J. Bárta[1,*], F. Jurina[1], I. Buranský[1], R. Kukuča[1], B. Pätoprstý[1]

[1]Faculty of Materials Science and Technology, Slovak University of Technology in Bratislava, Slovakia

[*] Corresponding Author. E-mail: jozef.barta@stuba.sk

Abstract

Friction Stir Welding (FSW) is a revolutionary solid-state joining process that has transformed the way metals, particularly aluminium alloys, are welded. FSW tools are nowadays a big topic due to differences in industrial applications and materials used. Many producers are creating different geometries to acquire a good quality weld joint while obtaining a good lifetime of their tools. Paper deals with the lifetime assessment of a new tool for welding aluminium alloy AW7075-T651. Two different materials were used for a probe production in order to compare the lifetime of the tool and identify the wear on tool edges. It was found that extreme hardness of the probe can lead to the reduction of tool lifetime. The shortest achieved tool life was 960 hours. The probe made of tungsten carbide showed the small wear on leading edges.

Keywords: Friction Stir Welding (FSW), Lifetime, AW7075-T651

1. Introduction

Unlike conventional fusion welding techniques, FSW does not rely on melting the base material, which significantly reduces defects such as porosity, cracking, and distortion. Instead, a rotating tool generates heat through friction, softening the material and allowing it to be mechanically stirred into a seamless joint. This process results in superior mechanical properties, making it an ideal choice for industries requiring high-strength, defect-free welds [1]. Since its inception in 1991, it has gained widespread adoption across various industries, including aerospace (Figure 1), automotive, marine, and railway manufacturing. The ability to produce high-quality welds without the need for filler materials or shielding gases has made FSW an attractive alternative to traditional welding methods [2]. The FSW process involves a specially designed non-consumable tool that consists of a rotating shoulder and a pin. As the tool is plunged into the workpiece, frictional heat is generated, causing the material to soften without reaching its melting point. The rotating pin stirs the softened material,

creating a solid-state bond. The shoulder of the tool helps contain the material flow, ensuring a smooth surface finish [3].

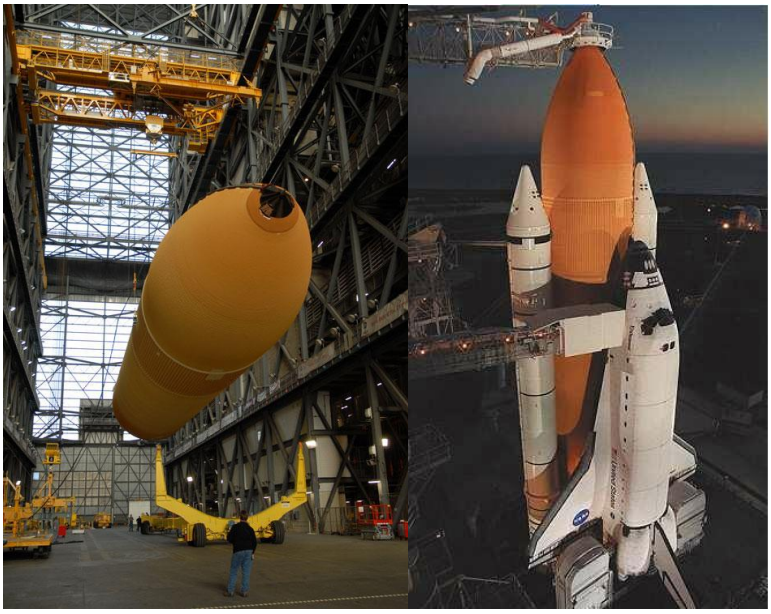

Figure 1. The retractable pin tool developed at Marshall Space Flight Center fully enables friction stir welding (FSW) for circumferential and tapered thickness welds, like those needed to assemble the space shuttle's external tank. [4]

Key parameters influencing the quality of FSW joints include rotational frequency, traverse speed, tool geometry and axial force. FSW offers several advantages compared to traditional fusion welding techniques, like improved mechanical properties, minimum distortion, environmental benefits, energy efficiency, or ability to join dissimilar materials [1].

Recent studies have focused on optimizing FSW parameters to enhance weld quality. Researchers have explored hybrid FSW techniques that incorporate additional heat sources, such as laser or induction heating, to improve weld penetration and reduce tool wear. Additionally, advancements in tool materials and designs have led to increased durability and efficiency in welding high-strength alloys. Due to the issues of weldability of aluminum alloys by fusion welding methods, FSW provides a great alternative.

Aluminum 7075 is a high-strength alloy widely used in aerospace, automotive, and military applications due to its excellent mechanical properties. However, it is traditionally considered difficult to weld using conventional fusion welding methods due to its susceptibility to hot cracking and loss of mechanical strength in the heat-affected zone (HAZ). FSW has emerged as a promising solution for welding 7075 aluminum, as it eliminates the need for melting and significantly reduces the formation of defects. Studies have shown that FSW produces a fine-grained microstructure in the

weld nugget, leading to improved mechanical properties. The process also minimizes residual stress, which is common in fusion-welded joints [5].
The latest research in FSW of AW7075 showed benefits like microstructural improvements where fully recrystallized fine-grain weld nugget enhanced strength and ductility, as well as findings that heat-affected zone experience localized softening due to coarsened precipitates, which can affect tensile strength [5]. Research in hybrid FSW techniques suggests that incorporating additional heat sources, such as laser-assisted FSW, can further improve weld penetration and reduce tool wear [6]. FSW of 7075 aluminum is increasingly being adopted in aerospace and automotive industries, where high-strength joints are essential. Ongoing research focuses on optimizing welding parameters and developing advanced tool materials to enhance weld quality and tool durability [7].
The aim of the paper is to evaluate the lifetime of the newly developed tool for friction stir welding for welding the AW 7075T651 aluminum alloy. The goal of the lifetime test was set to 1000 meters of weld trajectory.

2. Methodology

Material used within the experiment was aluminum alloy AW7075-T651 with the thickness of 80 mm. This plate was used for evaluation of FSW tool lifetime using multiple passes, summing total length of weld seams until tool destruction or systematic weld defect appears.
Tool geometry was developed in cooperation with MASAM Ltd., and the tool consists of 2 parts. Shoulder, made of tool steel had 3 spiral grooves, whereas the probe, made of tungsten carbide, was truncated quadrilateral pyramid with a thread on the circumference as shown in Figure 2. As two different materials for probes were used the tools were marked as 06 and 08. The characteristics of both materials are provided in Table 1.

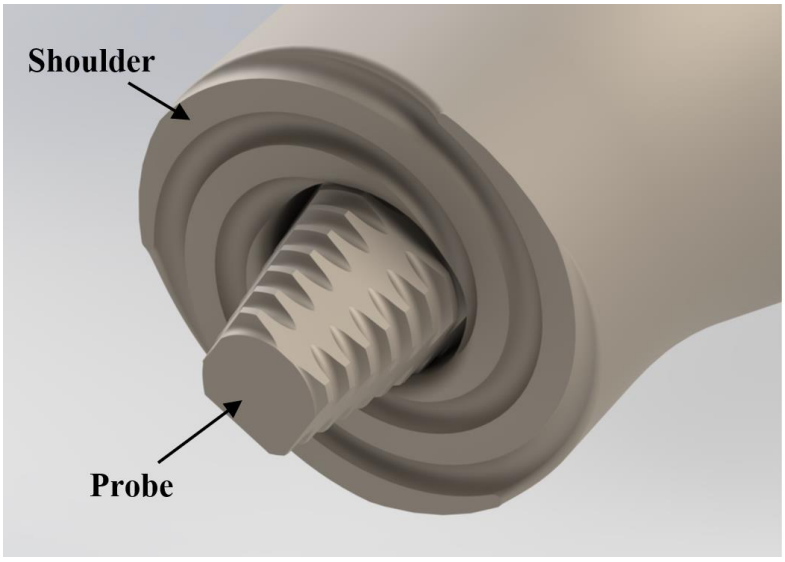

Figure 2. Geometry of the tool used in experiment

Table 1. Probe material characteristics

Sample designation	06	08
ISO Group	K05-K10	K01-K05
Structure	Ultra fine	Ultra fine
Grain size [µm]	≤ 0.6	≤ 0.6
Co content ± 0.5 [%]	6	8
Hardness HV30	1840	2010
TRS [N.mm^{-2}]	3 500	3 700
Fracture toughness K_{IC} [MPa.m$^{-0.5}$]	8.0	8.6

The tool life investigation in FSW will be carried out at constant welding parameters. The tool rotation frequency used will be 1000 min^{-1} and the welding speed will be 500 mm.min^{-1}. The shoulder immersion will be 0.1 to 0.2 mm. These parameters were chosen based on previous experiments made on the same material, using the same tool geometry.

The welds will be arranged in a row pattern to effectively use the entire surface of the plate. The path is created so that the gap between the welds is at least 7 mm. Each individual layer of weld will be made 10 meters long. To maintain the quality of the process and eliminate the effect of end holes that occur at the end of individual welds, the end point of a new layer of welds will never be identical to the end point of the previous layer of welds. For this reason, a straight part at the edge of the plate is included in the path, where end holes will occur next to each other. The plate will be attached to the working surface of the device using four screws. The representation of the melt path, dimensions and location is shown in Figure 3.

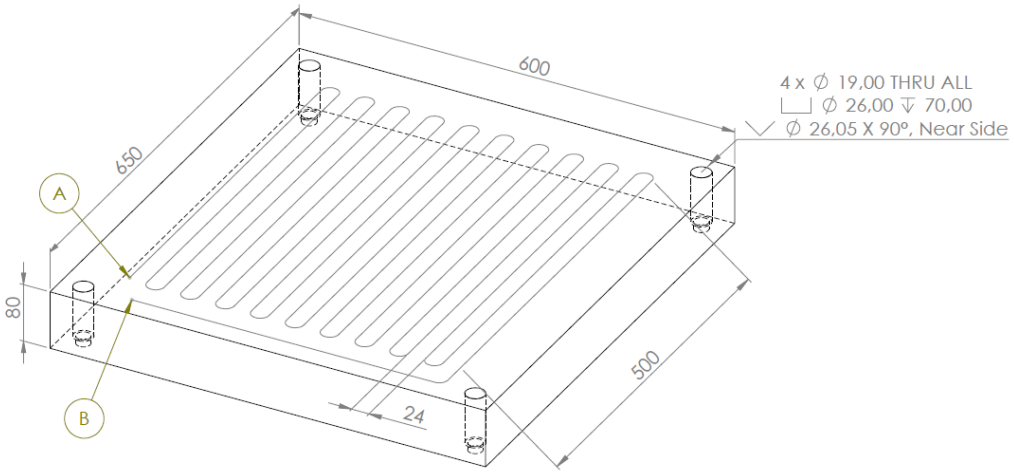

Figure 3. Scheme of aluminum plate with tool path

After each welded layer, the plate will be cooled to a temperature of less than 30 °C. This cooling will minimize deformation and preserve mechanical properties of the material. Subsequently, a 0.5 mm thick layer is milled from the plate surface, ensuring a uniform surface for the subsequent layer. A face milling cutter with a diameter of 64 mm will be used to mill the surface, which will ensure precise and effective material removal. Cooling will be used during the milling process to avoid heat generated during machining. Also, to maintain the same conditions, the surface will be cleaned and degreased after each cooling to prevent changes in friction and the generated temperature due to the presence of lubricants in the cooling liquid. After cleaning, the next layer of weld is then applied, and the whole process is repeated.

A control weld was performed every 20 meters, which corresponds to every second weld pass. A control weld over the entire thickness of the material will be performed on a separate plate with a thickness of 5 mm (full penetration weld), where the length of the control weld will be 150 mm. The control weld was realized to reveal possible internal defects, whereas the surface condition of the control welds will be evaluated by visual inspection according to the ISO EN 25239 standard. The uniformity of the weld width, the uniformity of the weld bead pattern, the presence of surface defects and the depth of the arm immersion were evaluated specifically. If a surface defect is detected by visual inspection, the given control melt will be checked by X-ray - CT analysis. When internal defects are detected, previous control melts are also subjected to X-ray - CT analysis to verify the presence of defects and to identify a systematic defect and subsequently determine the tool life. Alicona InfiniteFocusSL microscope was used to analyze the geometry of the tools.

Lifetime will be determined as a tool path until the systematic defect will occur. Occurrence of the systematic defect will mean that the wear of the tool is significant and can't be used any longer. Different materials with different mechanical properties of the probe will give us an idea of the hardness influence on tool wear (and lifetime).

3. Experiment

The experiment was realized according to the methodology (Figure 4). The FSW tool marked as 08 was used as first. The tool trajectory was programmed into the milling machine and repeated multiple times. As the test was carried out and the thickness of the material was getting thinner, there were adjustments in the Z-axis to ensure constant tool immersion.

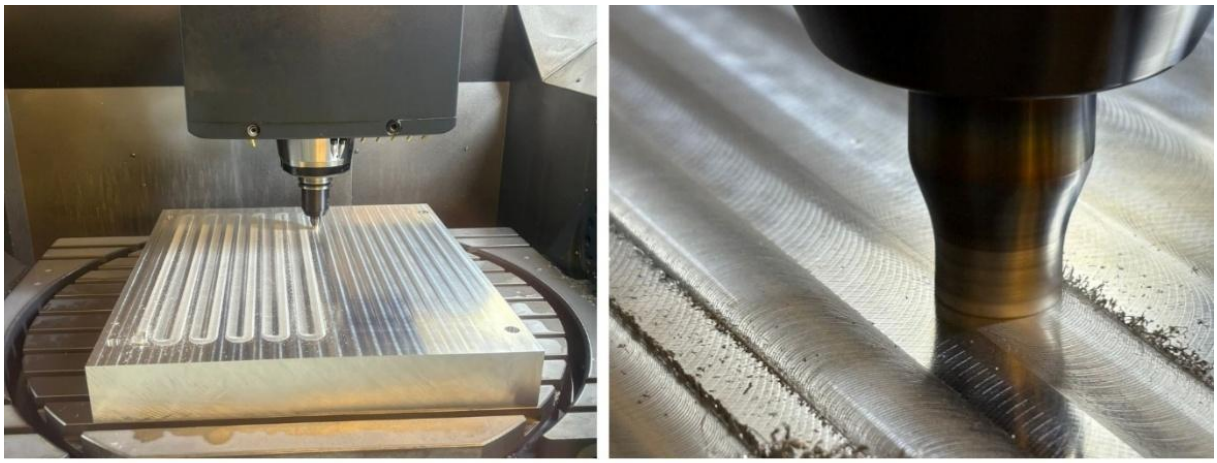

Figure 4. Lifetime test setup
a) welding trajectory, b) detail on FSW tool 08 while welding

After every pass, the material was present on the tool (Figure 5). This material does not represent any complication as it is removed in the next pass of plasticized and pushed into the material again. This material can be cleaned using NaOH solution with water however the cleaning was not applied to avoid any chemical disruption (corrosion) of the tool. The temperature of the material after the welding pass was about 60 °C. The temperature of the tool was about 240 °C and temperature of the Weldon tool clamp was approximately 80 °C.

Figure 5. FSW tool 08 appearance after welding

The welding tool was broken after 980 meters of welding during control weld. For this reason, the control melts were evaluated by computer tomography to detect possible internal defects. Specifically, control melts 980, 960 and 940 m were analyzed. Voids were observed in the control melt 960 m, but no defects were found in the control melt 940 m. Figure 6 shows the X-Ray CT analysis of the last control weld after 980 meters where destruction of the FSW occurred. The white color represents the high-density material, which is tungsten carbide in our case. The control weld was realized from right to left in this case and tool destruction happened approximately 20 mm after the too immersion point (starting point). The scan is breaking out due to the high amount of high-density material, therefore it was clear that the probe stayed in the material. Small white particles were observed near the surface. This was caused by the material originated from the probe fracture and the shoulder that was still running the last pass was pushing these leftovers from tool destruction into the material surface.

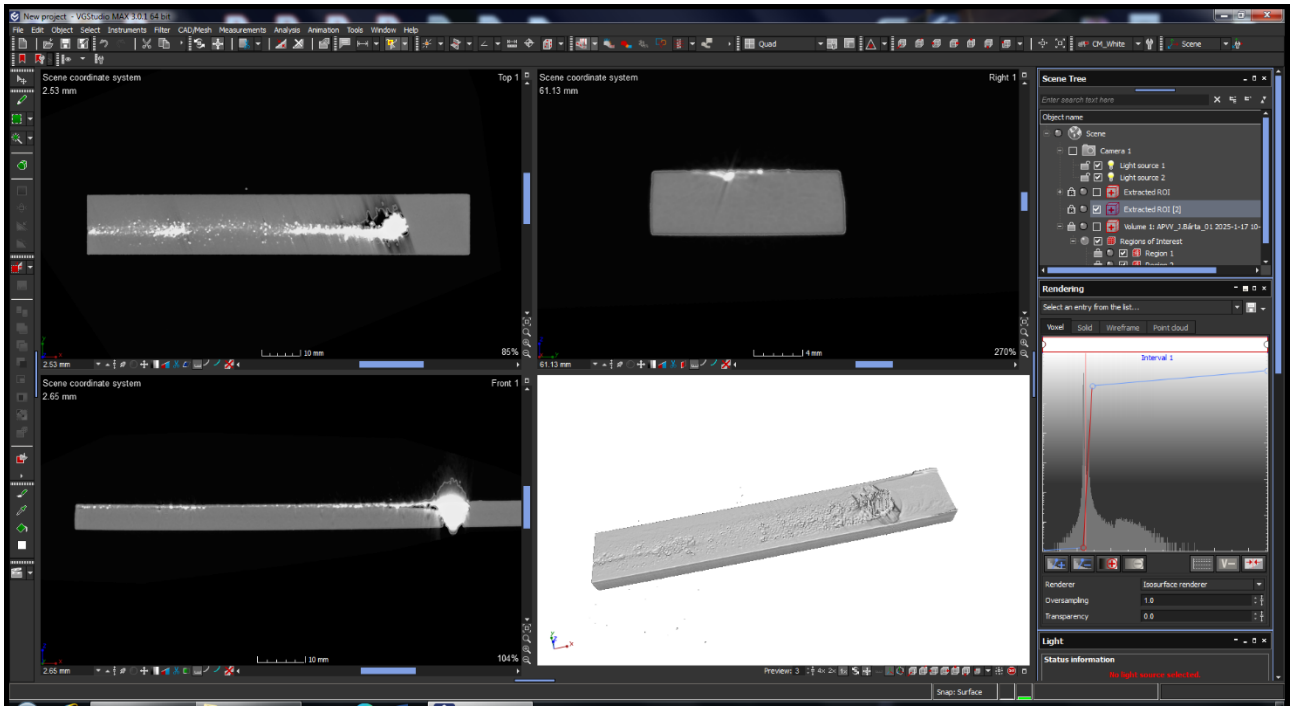

Figure 6. X-Ray CT scan of control weld after 980 meters

The more detailed scan was realized to observe the tool probe itself. Aluminum was filtered from the scan using the difference in density. Figure 7 confirms that the probe was present in material and some residuals from fracture stayed near the surface. We were not able to observe a clear image of the probe from X-Ray CT scan.

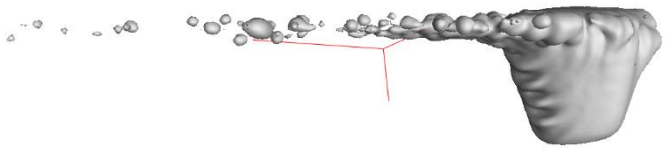

Figure 7. X-Ray CT scan of tool probe present in aluminum after fracture

According to the methodology we made the X-Ray CT analysis for previous control welds as well. Figure 8 documents the control weld after 960 m, which appears to contain the voids. In cross-section images of Xray CT scan can be seen the formation of a tunnel defect in the bottom part of the control weld however it was observed in approximately 20 millimeters of control weld which represents 13.3 % of total weld length. In this same length the imperfections in uniformity of the weld bead surface was observed. These imperfections can be seen in the bottom right 3D picture of the scan. Despite the fact that this defect was short and observed at the beginning of the welding process, the lifetime of the tool was determined to be 940 meters since the scan of control weld after 940 m was clear from defects.

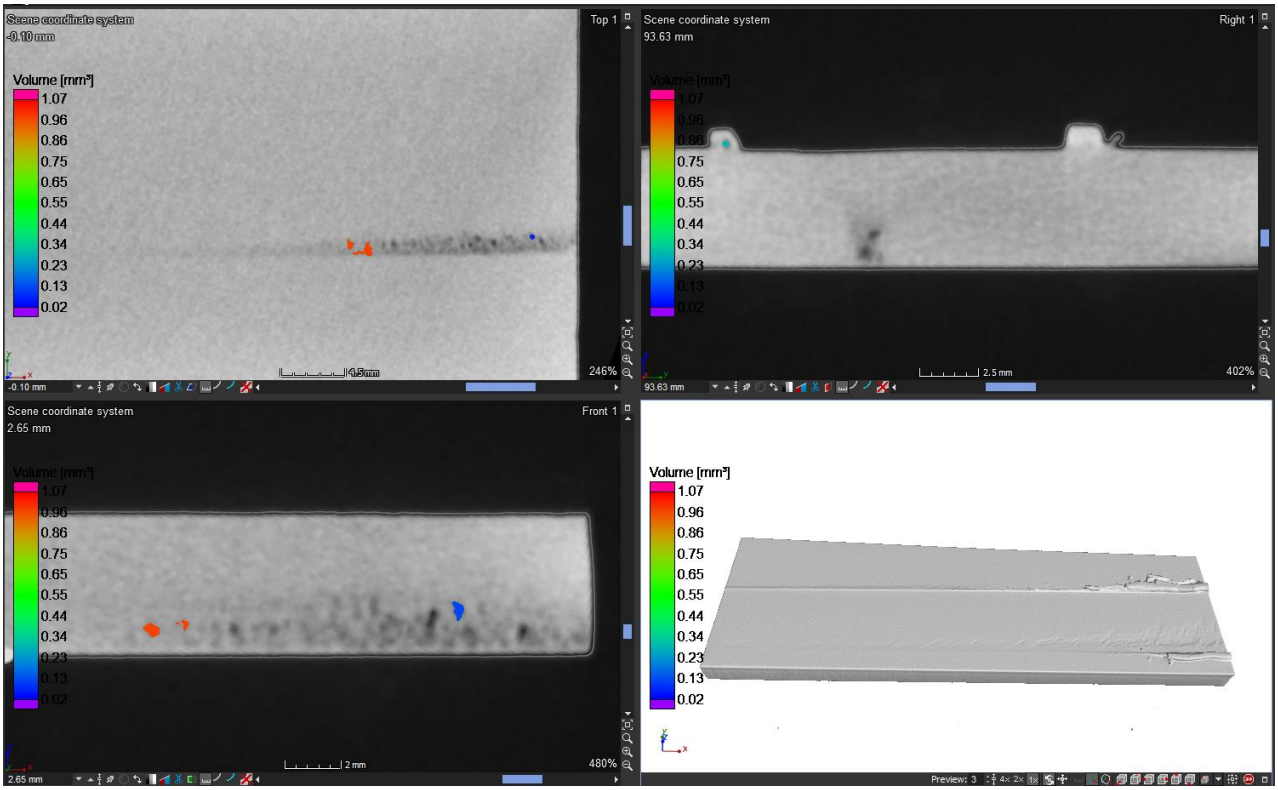

Figure 8. X-ray CT analysis of control weld after 960 m

After this test, the next tool marked as number 06 was used and the whole process was repeated. In contrast to the previous FSW tool, this one lasted 1060 m without any damage to the tool. As our

target welding trajectory was 1000 m, we decided to end the test and rather check the changes in geometry of the tool. The reason for the probe lasted longer was probably due to lower hardness and higher fracture toughness. Alicona FocusX microscope was used to evaluate the wear of the shoulder and the probe of the tool was realized using the Zeiss Inspect software. This tool, marked as 06, after welding 1060 m, was compared to a new tool, produced at the same time with the same geometry. Figure 9 shows a 3D scan of the analyzed used tool. Simultaneously a color deviation map is shown, which quantifies the geometric differences between this scan and a reference 3D model of a new tool through a best-fit alignment method.

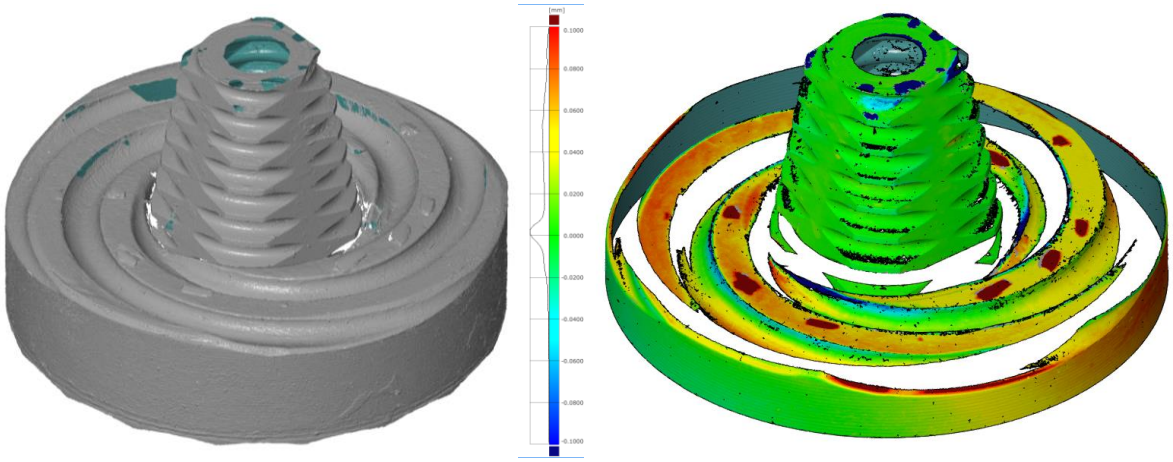

Figure 8. Color deviation map of used and new tool

Color deviation map showed that the leading edge of the tool was rounded, and a radius of 0.3 mm was observed. The wear of the tool was caused by the hardened aluminum, but it is not significant.

4. Conclusions

Friction stir welding is probably the most innovative technology for joining similar and dissimilar materials nowadays.

The lifetime of the newly developed FSW tool was realized with proposed methodology. Two types of probe materials were tested within the experiment. The results showed that softer tungsten carbide perform better probably due to the better fracture resistance. The harder tool probe marked as 08 was damaged by a brittle fracture and the small particles from the fracture were pressed and stirred into the soft aluminum surface. Tests on probe 08 were stopped after reaching 1060 meters of weld trajectory as the goal was met. From the deviation map we can say that the tool is not at its lifetime regarding the geometry, however attention must be paid to the structural properties of the probe since the fracture is brittle and there is no warning before the failure. The used tool 06 will be further examined for structural changes.

5. Acknowledgement

This work was supported by the Slovak Research and Development Agency under the contract No. APVV-21-0111.

6. References

[1] Kolli, Murahari; Sunnapu, Chendrasekhar; Medikondu, Nageswara Rao. (2025). Multi-response optimization of friction stir welding process parameter of AA 5083 with Taguchi-VIKOR approach. *J. Eng. Appl. Sci.* 72, 2. https://doi.org/10.1186/s44147-024-00572-xhttps://link.springer.com/article/10.1007/s40194-024-01847-w **(journal article)**

[2] Mohan, Dhanesh G; Wu, ChuanSong. (2021). A Review on Friction Stir Welding of Steels. *Chin. J. Mech. Eng.* 34, 137. https://doi.org/10.1186/s10033-021-00655-3 **(journal article)**

[3] NasaSpinoff; Innovative Tools Advance Revolutionary Weld Technique, 2009, Accessed 14.4.2025: https://spinoff.nasa.gov/Spinoff2009/ip_5.html (Website)

[4] Mahoney MW; Rhodes CG; Flintoff JG; Bingel WH; Spurling RA; Properties of friction-stir-welded 7075 T651 aluminum. (1998). *Metall Mater Trans A.* 29(7):1955–64. https://link.springer.com/article/10.1007/s11661-998-0021-5 **(journal article)**

[5] https://link.springer.com/article/10.1007/s12008-024-01922-y

[6] https://www.academia.edu/81382509/Friction_Stir_Welding_of_Aluminum_7075_Alloys

Iskustava u procesu remonta unutrašnjosti reaktora za proizvodnju amonijaka

Experiences in proccess of refurbishment of the inside of ammonia converter

D. Bičanić[1,*], M. Rajić[1], M. Teskera[1], I. Kolundžić[1]

[1]Industroremont d.o.o, 108. brigade ZNG 88, 35000 Slavonski Brod, Croatia

[*] Corresponding Author. E-mail: d.bicanic@industroremont.hr

Sažetak

Remonti, sanacije te bilo kakvi oblici radova na već postojećim objektima predstavljaju svojevrsne izazove. Ovaj rad opisuje neke od problema koji su se pojavili pri remontu reaktora za proizvodnju amonijaka, izrađenog od austenitnog nehrđajućeg čelika. Ova iskustva uključuju zavarivanje novih elemenata na već postojeće – vrlo stare elemente, rad u vrlo uskim, skučenim i visokim prostorima, a dotiče se i zaštite na radu pri unosu topline u kemijski reaktivnu okolinu. Nečistoće i prljavština, koje imaju negativan utjecaj na ljudstvo, također i posebice otežavaju zavarivanje austenitnih nehrđajućih čelika te legura nikla i kroma budući da navedeni čelici zahtijevaju posebnu čistoću površine.

Abstract

Refurbishments, repairs or any kinds of works on already existing facilities present unique challenges. This paper describes some of the problems that appeared during the refurbishments of an ammonia production reactor made of austenitic stainless steel. These experiences include welding new elements to existing – very old elements, working in very narrow, confined and high spaces, and also includes occupational safety when heat is brought into chemically reactive environment. Impurities and dirt, which have a negative impact on personnel, also make welding austenitic stainless steels and nickel-chromium alloys particularly difficult, since the aforementioned steels require special surface cleanliness.

Ključne riječi: austenitni nehrđajući čelici, nikl-krom legure, zaštita na radu, skučeni prostori

Keywords: austenitic stainless steels, nickel-chromium alloys, health and safety, confined spaces

1. Uvod

Austenitni nehrđajući čelici te legure nikla vrlo se često koriste u postrojenjima izloženima kemijskim djelovanjima i visokim temperaturama radi svoje otpornosti na navedeno. Također se smatraju i vrlo delikatnim materijalima za koje je potrebna posebna pažnja pri zavarivanju, najviše radi čistoće površine. Prilikom remonta, ovaj uvjet je ponekada vrlo teško postići, a čak i uz dovoljno pažnje, mogu se i dalje pojaviti neočekivani problemi vezani uz zavarivanje ovih materijala te uz zaštitu na radu - pogotovo ako se radi o zatvorenim prostorima.

2. Osnovni podaci o remontu

Izvođenje radova provodilo se na području Europe, a prema prethodno napisanom Tehničkom elaboratu te vrlo detaljnim uputama kupca i nadzora pod kojim se provodio remont. Zbog stavki navedenih u Ugovoru između Izvođača radova i Kupca, nije moguće imenovati navedene strane uključene u izvođenje radova.

Remont se izvodio prema osnovnim standardima/pravilnicima PED 2014/68/EU, ASME VIII Div.1, te europskim standardima za zavarivanje EN ISO 3834-2, EN ISO 15614-1.

3. Predmet remonta – reaktor za proizvodnju amonijaka

Osnovni podaci o reaktoru koji su bili definirani su sljedeći:

- tip posude: vertikalni
- unutarnji promjer posude: 3200 mm
- ukupna visina: približno 26,4 m

Reaktor je prikazan na slici 1.

Slika 1. Reaktor

Materijali koji se nalaze u reaktoru su:

- austenitni nehrđajući čelik - AISI 321 (X6CrNiTI18-10): grupa 8.1 prema ISO/TR 15608
- austenitni nehrđajući čelik AISI 310S (X8CrNi25-21): grupa 8.2 prema ISO/TR 15608
- legura nikla i kroma INCONEL 600 (UNS N06600): grupa 43 prema ISO/TR 15608

Reaktor se sastoji od tri dijela koja dijele podnice ovalnog oblika pod blagim nagibom, a remont se većinu vremena radio u isto vrijeme na sve tri podnice – kada god je to bilo moguće. Dispozicija reaktora prikazana je na slici 1 – zelenom bojom označeni su dijelovi koje je bilo potrebno zamijeniti, a crvenom oni koji su ostali stari.

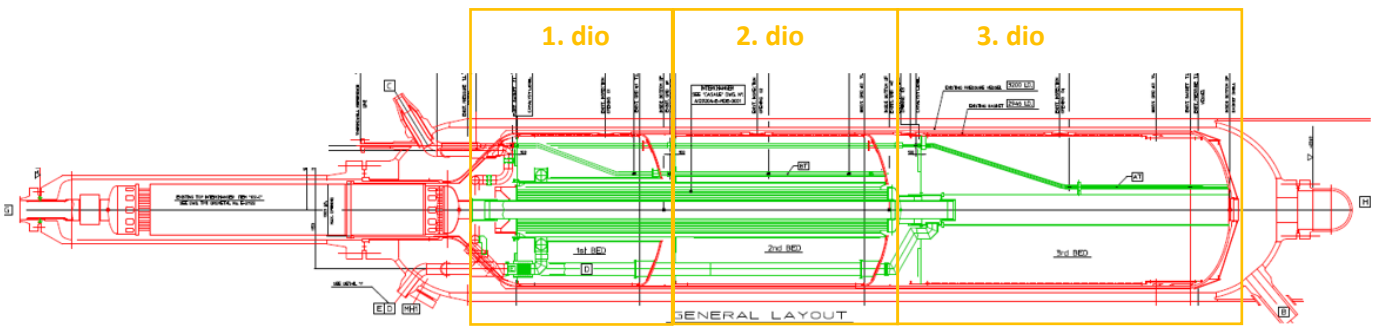

Slika 1. Dispozicija reaktora (okrenuta horizontalno)

4. Izvođenje radova zavarivanja

4.1 Tehnika zavarivanja

Zavarivanje se izvodilo postupcima TIG, REL i TIG+REL, uz prijedloge uputa dostavljenih od trećih strana. Međutim, zbog praktičnih ograničenja, neke od uputa morale su biti prilagođene specifičnim uvjetima na terenu. U Tablici 1 su dani popisi materijala, postupaka i korištenog dodatnog materijala.

Tablica 1. Postupci zavarivanja

POSTUPAK	OSNOVNI MATERIJALI	ŽICA/ELEKTRODA	TRGOVAČKI NAZIV - ŽICA/ELEKTRODA
TIG	321/321	ER 347	Thermanit H-347
REL	321/321	E 347-16	SAS2-A
TIG	310S/310S	ER 310 / E 310-16	FFB-IG / FFB-A
TIG+REL	321/310S	ER 347 / E 347-16	Thermanit H-347 / SAS2-A
TIG	321/310S	ER 347	Thermanit H-347
TIG	INC.600/INC.600	ER NiCr-3	UTP A 068 HH
TIG	321/INC.600	ER NiCr-3	UTP A 068 HH

4.2 Čistoća površine

Reaktor na kojemu su izvođeni radovi star je preko 35 godina te je toliko i u funkciji. Unutrašnjost reaktora popunjena je katalizatorom koji je sačinjen od vrlo sitnih čestica, za izvođača radova tada nepoznatog kemijskog sastava. Nakon neutralizacije i vađenja starog katalizatora (koja je rađena od strane treće tvrtke), unutrašnjost samog reaktora ostala je vrlo prljava te obložena slojevima nečistoća nepoznatih debljina, preko kojih je zavarivanje, naravno, bilo nemoguće. Prema informacijama kupca i nadzora, unutarnji dijelovi reaktora, izloženi djelovanju temperature i kemije katalizatora, bili su podložni stvaranju nitriranog sloja.

Nitriranje je toplinsko-kemijska obrada čelika kojom se postiže otvrdnjavanje površine. Ovaj proces se odvija kada čelik dolazi u kontakt sa amonijakom ili drugim spojevima sa dušikom, pri povišenim temperaturama. Razgradnjom amonijaka nastaje atomski dušik, koji difuzijom ulazi u metal i stvara slojeve nitrida.

Upravo zbog ove pojave se u reaktoru pojavljuju i legure nikla i kroma, koje pokazuju najveću otpornost prema nitriranju. No, za nehrđajuće austenitne čelike, koji su najzastupljeniji u reaktoru, postoji veća opasnost od pojave nitriranog sloja – koji je bilo potrebno u potpunosti skinuti prije zavarivanja na postojeće, stare dijelove reaktora. Ovaj nitrirani sloj bio je nepoznate debljine, a ukljanjao se prema uputama kupca i nadzora - brušenjem te zagrijavanjem na temperaturu od 500°C (tzv. 'pečenje'). Nakon ohlađivanja, bilo je potrebno provjeriti je li uklonjen nitrirani sloj pomoću

5%-tne dušične kiseline. Nanošenjem kiseline na brušeni dio, kiselina bi promjenila boju u plavičastu – ukoliko nitridni sloj nije u potpunosti bio uklonjen. Tada bi se ponovno pristupalo uklanjanju na isti način, dok površina ne bi bila čista i spremna za zavarivanje. Također, pri samom brušenju moglo se djelomično ustanoviti je li sloj uklonjen – ako je prisutan nitridni sloj, iskrenja nije bilo ili ga je bilo minimalno, dok kada bi se sloj uklonio, pojavilo bi se intenzivnije iskrenje pri brušenju.

Međutim, nijedna od ovih metoda nije u potpunosti davala točne rezutate uklonjenog nitridnog sloja jer su se i dalje pojavljivale greške pri zavarivanju. Austenitni nehrđajući čelici te niklove legure zahtjevaju čistu površinu, nerijetko odmašćenu i očišćenu od bilo kakve prljavštine, bojila i naslaga, a koji su obavezno prisutni prilikom remonta starih dijelova – kako bi se omogućilo zavarivanje bez pojave grešaka. Prilikom zavarivanja preko navedenih slojeva prljavštine te nitriranih slojeva, dolazilo je do pojave tzv. 'pjenjenja' zavara, koje je posljedično uzrokovalo pojavu pora i naljepljivanja. Upravo radi ovoga, bilo je potrebno provesti ispitivanje penetrantima na 100% zavara. Neke od grešaka koje su se javljale su prikazane na slici 3.

Slika 3. Greške naljepljivanja uslijed lose očišćene površine

4.3 Zavarivanje s podloškom postupkom TIG / TIG+REL

Unutarnji kolektor reaktora zavarivan je uz pripremu sa podloškom, prema slici 4.

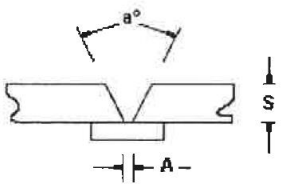

Slika 4. Priprema zavara uz pripremu sa podloškom

Lim podloške bio je debljine 3 mm, dok je lim materijala cilindra bio 8 mm. Predviđena zračnost u korijenu žlijeba je 2-3 mm (oznaka 'A' na Slici 4). Budući da se radi o relativno maloj debljini, svi zavarivači morali su proći probu zavarivanja sa podloškom, TIG+REL postupkom, sa dodanim materijalom dostavljenim od treće strane. Dostavljeni dodatni materijal bila je žica promjera Φ2,0 te elektroda najmanjeg promjera Φ3,25 mm. Već na probama je ustanovljeno da je, uz ovakvu pripremu,

gotovo nemoguće zavariti zavar uz dovoljno protaljivanje podloške, a bez da je se propali. Slika 5 prikazuje jednu od proba.

Slika 5. Proba zavarivanja - neprotaljena podloška

Nakon uspješno položenih proba sa većom zračnosti u korijenu žlijeba zavara, dobivene su prihvatljive probe. No, nedostatak odgovarajuće elektrode nastavio je stvarati probleme unutar reaktora - zbog vrlo uskih tolerancija na već pripremljenim komadima velikih dimenzija, spremnim za ugradnju. Zbog ovoga je, uz dogovor svih strana, prihvaćena nova uputa za zavarivanje gdje su se ovakvi zavari odradili samo TIG postupkom.

4.4 Zavarivanje mrežice katalizatora

Unutrašnjost reaktora po cijelom obodu je obložena mrežicom koja služi kako bi zadržala katalizator gdje bi trebao biti. Ova mrežica je izrađena od nikl-krom legure INCONEL 600 (UNS N06600), debljine svega 0,9 mm. Mrežica je prikazana na slici 6 (a, b).

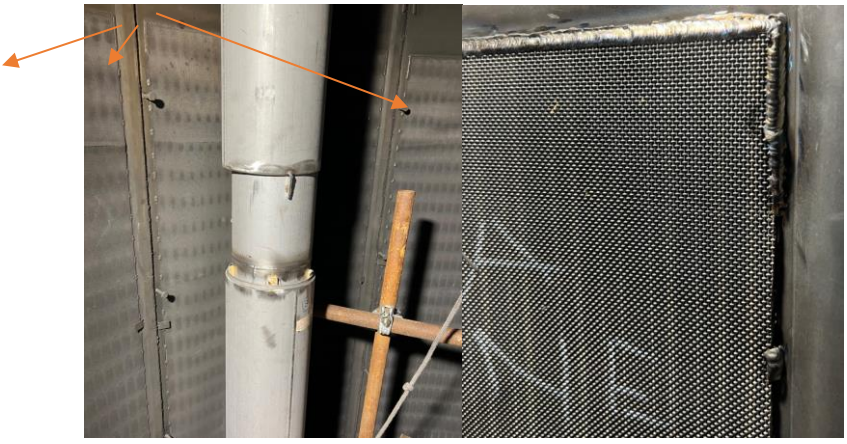

a) **b)**

Slika 6. Mrežica katalizatora po unutrašnjem obodu plašta reaktora (a); prikaz zavara mrežice na plašt reaktora (b)

Na mrežicama su odrađeni zavari prema dvije upute za zavarivanje:

- zavarivanje između stare mrežice i plašta (grupa 8.2 sa grupom 43) – sastojalo se od uklanjanja starog zavara, uklanjanja nitriranog sloja te ponovnog zavarivanja već postojeće mrežice – prikazano na slici 7.

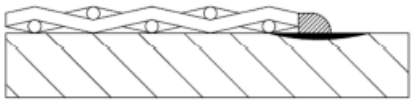

Slika 7. Zavarivanje između stare mrežice i plašta

- zavari između mrežica (grupa 43 sa grupom 43) – sastoji se od zavarivanja (pripajanjem, odnosno, tzv. 'heftovima') nove mrežice preko stare mrežice, prikazano na slici 8

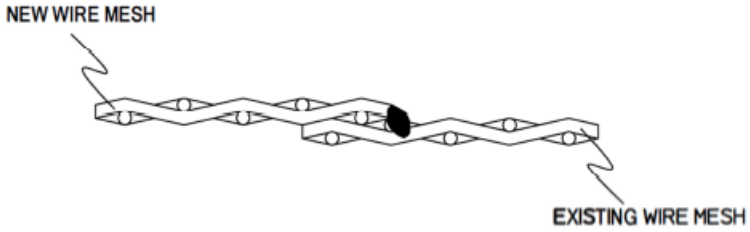

Slika 8. Zavari između stare mrežice i nove mrežice

Popravci su rađeni tako da su se dijelovi mrežice zavarivali preko već postojeće, oštećene mrežice. Na pojedinim dijelovima, gdje su se radi drugih razloga (procesne greške u reaktoru) stare mrežice morale u potpunosti ukolniti, postavljane su potpuno nove na plašt reaktora. Zavare na mrežicama izvodili su isključivo zavarivači koji su prethodno prošli obuku upravo za zavarivanje mrežica te ostalim zavarivačima nije bilo dozvoljeno odrađivati ove zavare. Unatoč uputama kupca i nadzora, debljina mrežice bila je vrlo kritičan parametar pri zavarivanju mrežice na mrežicu te se vrlo teško moglo zavariti bez da se mrežica ne propali. Nakon mnogo pokušaja i uz suradnju zavarivača, inženjera i nadozora, došlo se do nove upute za zavarivanje koja je uključivala pulsno zavarivanje TIG postupkom, prema parametrima prikazanima na slici 7.

Slika 7. Parametri pulsnog TIG zavarivanja mrežice katalizatora

5. Problemi zaštite na radu unutar reaktora

Jedan od najvećih izazova ovoga projekta bila je zaštita na radu u vrlo skučenom prostoru. Otežan rad na više visinskih kota u isto vrijeme te potrebno vrlo dobro dodatno osvjetljenje stvaralo je dodatne probleme, a ventilacija prostora u nekim slučajevima nije bila dovoljna da se održe sigurni uvjeti za rad. Slika 8 samo djelomično prikazuje unutrašnjost reaktora u kojima su izvođeni radovi.

Slika 8. Unutrašnjost reaktora

Najveći izazov tijekom čišćenja za pripremu zavara bilo je zagrijavanje površina na 500°C u kombinaciji s primjenom 5%-tne dušične kiseline. Naime, uslijed već postojećih nečistoća unutar

starog reaktora te velikog unosa topline, uz prisustvo vrlo reaktivnih kemijskih otopina, neočekivano su se počeli pojavljivati problemi pojave ugljikovog monoksida unutar skučenog prostora reaktora. Ugljikov monoksid (CO) je bezbojni plin, bez mirisa i okusa, koji ne iritira sluznice te ga je vrlo teško uočiti, a vrlo je opasan za ljude jer istiskuje kisik iz organizma te izaziva gušenje.
Budući da su u zatvorenim prostorima radnici obavezni nositi detektore plinova, ovaj problem je, na sreću, na vrijeme otkriven. Slijedom reakcije prisutnog inženjera, nakon oglašavanja uređaja za detekciju plinova, svi radnici su na vrijeme izašli iz područja kontaminiranog ugljikovim monoksidom. Svi daljnji radovi su zaustavljeni do detaljnog pregleda odgovorne osobe za zaštitu na radu nadležnog postrojenja. Uzrok pojave ugljikovog monoksida tada nije bio poznat, pa su odgovorne osobe iz postrojenja provele dodatne provjere kako bi spriječile moguće katastrofe – uvedene su i potpisivane dozvole za rad svakih sat vremena.
Naknadno je zaključeno da se monoksid pojavljuje svaki puta odmah po paljenju plamenika za zagrijavanje površina (i vrlo često na površinama koje su prethodno bile premazivane dušičnom kiselinom. Uz suradnju nadležnog postrojenja, koje je organiziralo zagrijavanje svih površina unutar reaktora, pod zaštitnim maskama i uz boce kisika, problem pojave monoksida je uspješno riješen te su se daljnji radovi mogli nesmetano nastaviti – uz dodatne sigurnosne mjere.

6. Zaključak

Remont reaktora za proizvodnju amonijaka, koji je obuhvatio složene zadatke zavarivanja austenitnih nehrđajućih čelika i legura nikla, pokazao je značajne izazove, od tehničkih poteškoća u zavarivačkim postupcima do problema zaštite na radu. Ključni problemi bili su vezani uz čistoću površina, što je zahtijevalo preciznu kontrolu kvalitete.
S obzirom na specifične uvjete rada u zatvorenom prostoru, zaštita na radu postala je najvažniji izazov. Uz dodatne mjere sigurnosti i kontinuiranu kontrolu radnih uvjeta, problemi su uspješno riješeni, no bitno je naglastiti važnost stalnog opreza u radnom okruženju s potencijalno opasnim kemijskim i fizičkim uvjetima.
Ovaj projekt pokazuje važnost preciznosti u izvođenju radova na kompleksnim industrijskim postrojenjima, kao i potrebu za stalnim usavršavanjem tehnoloških postupaka i osiguravanjem sigurnosti svih radnika.

7. Literatura

[1] Tehničke specifikacije projekta
[2] Standard ISO/TR 15608
[3] Industroremont upute za zavarivanje
[4] Khoshnaw Fuad, Gubner Rolf. (2020) Corrosion Atlas Case Studies, Part II: Corrosion Topics, *Elsevier Science (liii).* https://doi.org/10.1016/B978-0-12-818760-9.02003-1 **(članak u časopisu)**

Društvo za tehniku
zavarivanja Slavonski Brod

13. Međunarodno znanstveno-stručno savjetovanje SBZ 2025

„STROJARSKE TEHNOLOGIJE U IZRADI ZAVARENIH KONSTRUKCIJA I PROIZVODA, SBZ 2025."
Slavonski Brod, 08. i 09. 05. 2025.

The effect of arc current in plasma transferred arc (PTA) weld deposition on the hardness of Stellite 12 hardfacing on S235 structural steel

D. Milčić[1,*], V. Krstić[2] , M. Milčić[1] , D. Klobčar[3], A. Đurić[4]

[1]Faculty of Mechanical Engineering, University of Niš, Aleksandra Medvedeva 14, 18000 Niš, Serbia
[2]Pedagogical faculty in Vranje, University of Niš, Partizanska 14, 17500 Vranje, Serbia
[3]Faculty of Mechanical Engineering, University of Ljubljana, Aškerčeva cesta 12, 1000, Ljubljana, Slovenija
[4]Faculty of Mechanical Engineering, University of East Sarajevo, Vuka Karadžića 30, 71123 East Sarajevo, Bosnia and Herzegovina

[*] Corresponding Author. E-mail: dragan.milcic@masfak.ni.ac.rs

Abstract

Hardfacing is the oldest method of surface engineering for obtaining diverse characteristics and extending the life of materials. Hardfacing is typically done to worn rebuilt gear, but it can also be applied to new equipment to make it more wear-resistant. Hardfacing parts from older equipment can save you anywhere from 25 to 75 percent on replacement costs. Hardfacing can help extend the life of parts on latest equipment by up to 300 percent. The substrate material can be a material with advantageous mechanical and plastic properties, and the coating can provide corrosion or abrasion (wear) resistance. Among coating application techniques, plasma transfer arc (PTA) weld deposition can be used. The PTA process is easily automated, providing a high degree of reproducibility of the weld overlays. In addition, because of the highly concentrated heat source, this process benefits from high powder utilization and can achieve a very low level of iron dilution in the overlay. Because the hardfacing materials are in powder form, it is possible to produce overlays from many different materials and combinations of materials with a wide range of hardness and other properties. The paper analyzes the effect of arc current in plasma transferred arc (PTA) weld deposition on the hardness of Stellite 12 hardfacing on S235 structural steel.

Keywords: Hardfacing Alloy, Stellite12, Plasma Transfer Arc (PTA), Hardness

1. Introduction

Hardfacing is a technique used to enhance surface properties of metallic components under harsh conditions of aerospace, gas turbines, petrochemical, mining industries and power plants [1, 2]. Multicomponent Co, Ni and Fe-based alloys are homogeneously deposited on the surface of a soft material (carbon and low alloy steels) by welding or cladding, with the purpose of increasing hardness, wear and corrosion resistance without significant loss in ductility and toughness of the substrate. Several arc welding techniques such as gas metal arc welding (GMAW), shielded metal arc welding (SMAW), submerged arc welding (SAW), gas tungsten arc welding (GTAW) and plasma transferred arc (PTA) welding and laser cladding can be used for hardfacing [1]. Plasma transferred arc (PTA) weld deposition represents a very good alternative to other surface welding processes. It has advantages over conventional welding techniques in terms of its high deposition rate, lower heat input, excellent arc stability and most importantly the wide range of choices of materials. It also have advantages over laser cladding because of its lower capital and maintenance costs, higher thickness capability, higher deposition efficiency and rate, and ease of integration into certain production settings due to its small size [2-4]. Stellite hardfacing alloys derived from the Co–Cr–W–C type can be found in several modifications and commercial grades such as Stellite1, 12 and 6. [3]. The hardness and tribological properties of Stellite alloys at room temperature depends on strengthening and crystallographic nature of cobalt-rich solid solution, type and amount of carbides and intermetallic compounds formed during solidification [4]. In these alloys, carbides are considered as the primary strengthening agent while solid solution hardener including chromium and tungsten are considered as the secondary strengthening agent [5].

Stellite can be welded on elements subject to impact loads, such as tools used in plastic working [6,7]. Stellites' hardness is up to 670 HV. The morphology and the carbide content affect the hardness of the stellite. Despite the fact that stellites are plastically deformable materials [8], thanks to the plastic deformation-induced structural transformation in the cobalt austenite network, they have the ability to accumulate impact loads, which significantly extends the scope of their applications. They are used for the production of components used in a demanding work environment, such as components of internal combustion engines (high-temperature corrosion, mechanical loads, abrasive wear and fatigue processes).

The variation in arc current during the PTA weld deposition of Stellite 12 alloy on S235 structural steel significantly affects the properties of the deposited layer. An increase in current leads to higher energy input into the material, resulting in deeper penetration and greater dilution of the base material. This can negatively impact the wear resistance and hardness of the deposited layer, as higher dilution may reduce the concentration of hard phases characteristic of the Stellite 12 alloy. On the other hand, lower currents can produce shallower deposits with less dilution but may affect the bonding of the layer to the base material. Therefore, optimizing the arc current is crucial to achieving the desired combination of hardness, wear resistance, and the quality of the bond between the deposited layer and the base material.

The present investigation aims to study the effect of arc current on the hardness of Stellite12 hardfacing on S235 structural steel using PTA weld deposition.

2. Experimental Procedures

The plasma transferred arc (PTA) weld deposition was carried out with surfacing machine with a maximal current of about 330A (Figure 1). The cladding process was performed using the following gas flow rates: plasma gas (Ar) = 1.5 l/min, carrier gas (Ar) = 3,5 l/min and shielding gas (Ar) = 11 l/min.

Figure 1. View of the PTA process

Stellite 12 coating powder with particle size of 50 to 145 μm were deposited on quenched and tempered S235 JRG1 steel by PTA welding machine. The nominal composition of the Stellite12 alloy powder is listed in Table 1. The surface layer was deposited using the plasma transferred arc (PTA) process on specimens having dimensions of 250 mm × 150 mm × 20 mm, made of S235 JRG1 structural steel (Table 2).

Table 1. Nominal chemical composition of Stellite 12 powder in wt%

Co	C	Si	Mn	Cr	Ni	W	Fe
Balance	1,65	1,52	0,98	29,54	2,21	8,5	2,43

Table 2. Nominal chemical composition of S235 JRG1 (1.0036) in wt%

Fe	C	Mn	P	S
Balance	□0,21	□1,5	□0,005	□0,005

The PTA deposition process was implemented under constant parameters which were a current of 89, 118, 125, 142 and 160 A, a voltage of 18 to 19 V and a travel speed of 130 mm/min. Deposition procedures were carried out in a single layer with a thickness of 2 mm. An schematic of PTA process used for deposition hardfacing layer are depicted in Fig. 2. In the PTA process the powder is continuously transported from the hopper through flexible tubes to the torch by an inert carrier gas and introduced into the plasma arc and heated and accelerated to the substrate surface. Transferred arc produces the energy density needed to melt both the base metal and the feedstock materials. A molten pool formed on the surface of substrate is protected against oxidative atmosphere by a curtain of inert gas as shielding gas.

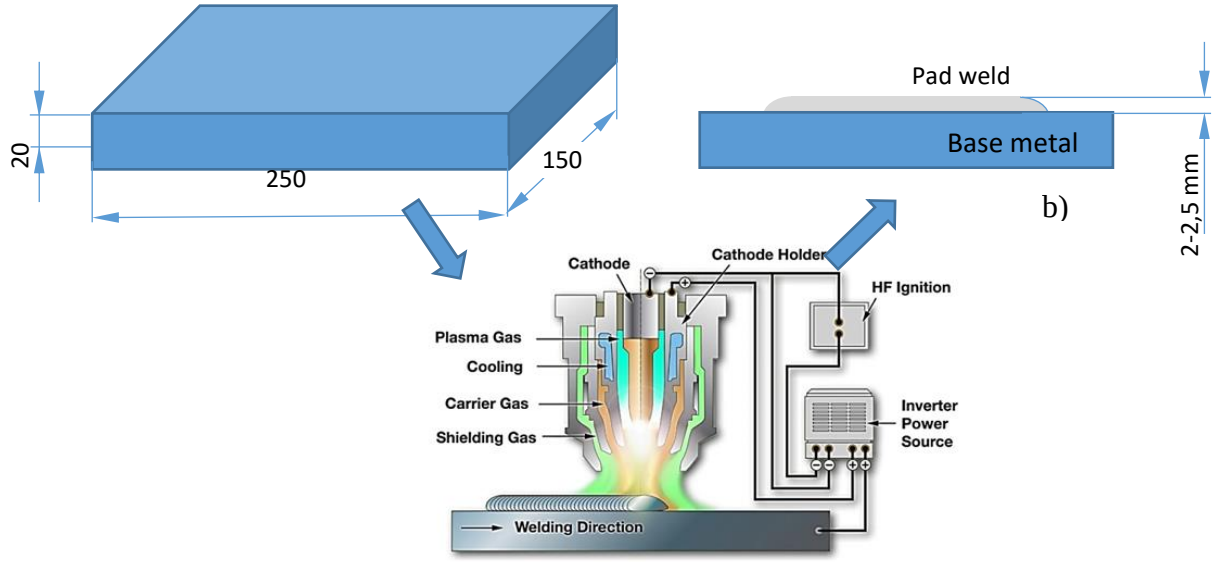

Figure 2. An schematic of the PTA process used for deposition hardfacing layer (a) Image of the prepared structural steel plate sample used for the study, including its dimensions (b) Schematic image of the cross-section of the final product after surface coating

The input parameters are considered for process PTA weld deposition is shown in table 3.

Table 3. Deposition parameters for PTA weld deposition

		Sample 1	Sample 2	Sample 3	Sample 4	Sample 5
Welding current	A	89	118	125	142	160
Arc voltage	V	18-19	18-19	18-19	18-19	18-19
Coating thickness	mm	2				
Welding speed	mm/min	160				
Gas type		Argon				
Plasma gas flow rate	l/min	1,5				
Shield gas flow rate	l/min	11				
Carrier gas flow rate	l/min	3,5				
Oscillation	mm	62				
Preheat temperature	°C	300				

Figure 3 shows the wiew of the plate with pad weld and the macrostructure of Stellite 12.

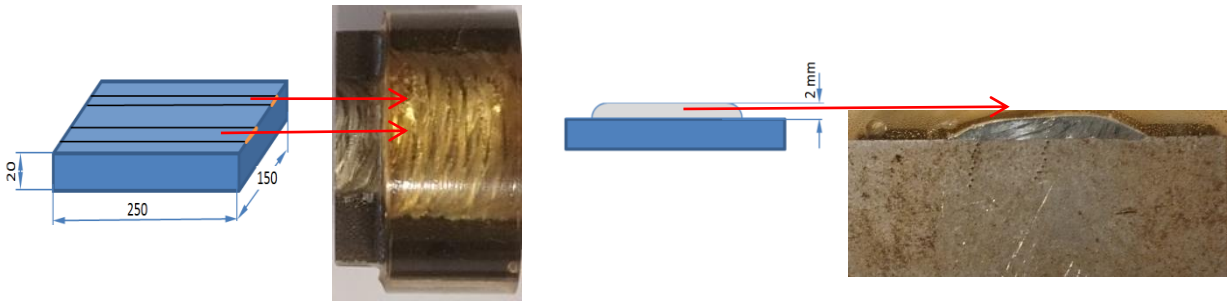

Figure 3. View of the plate with pad welds

The samples for microstructural analysis were polished and etched following conventional procedures. Etching was performed using Marble's etchant: 50 ml HCl, 10 ml HNO_3, 10 g $FeCl_3$, 100 ml H_2O, with an etching time of 30 seconds.

Hardness was measured by the Vickers method according to SRPS EN ISO 6507-1:2023 on the HV10 scale. The Wilson VH1150 hardness tester was used for hardness measurements. The measurement was performed on the cross-section of the padding welds along a defined path, with indentations spaced approximately 1 mm apart, extending from the surface of the padding weld to the steel substrate, as shown in Figure 4. Each measurement included 11 to 16 indentations.

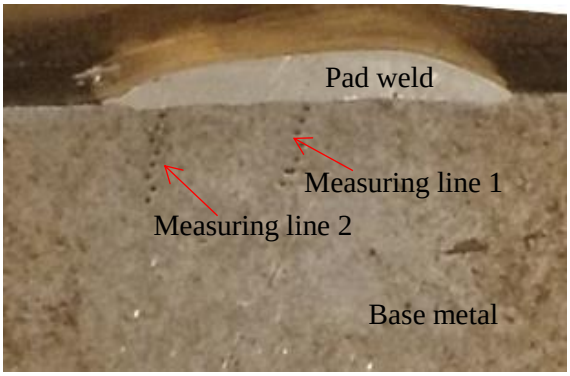

Figure 4. Scheme of hardness HV10 testing on samples' cross-section

3. Results and Discussion

Figure 5(a) shows the fusion line between substrate and coating. The dilution zone of the coating is shown as red rectangles in Figure 5(b). The microstructure of the welded layers has a dendritic structure (Figure 6). The dendritic region consists of a cobalt-based austenite matrix strengthened by elements such as chromium, tungsten, and impurities of iron, manganese, and silicon. Dendrites grow from the melting line towards the axis of the welded layer. The interdendritic eutectic regions, which contain carbides, are rich in tungsten and chromium. The carbides have an increased concentration of chromium and have been identified as phases Cr_7C_3 and $Cr_{23}C_6$, with cobalt and tungsten occupying the position of chromium [9, 11].

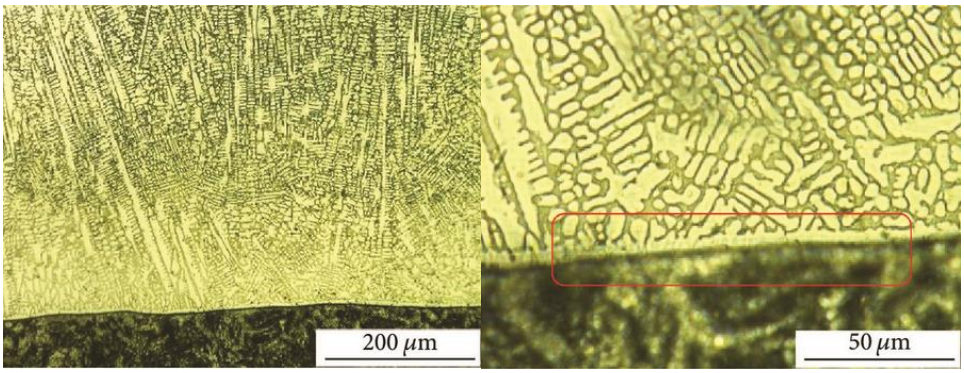

a) b)

Figure 5. Microstructure of hardfacing layer (a) fusion line, (b) dilution zone

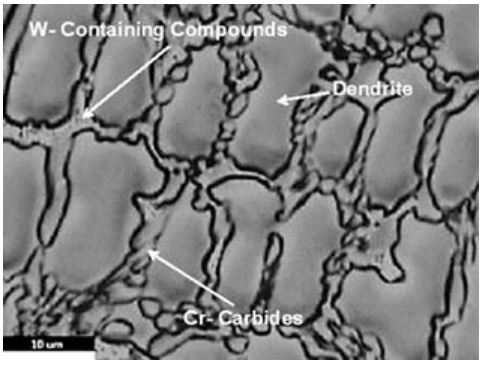

Figure 6. SEM micrograph of cross-section of PTA deposited Stellite 12

The welding current in the PTA process significantly influences the hardness of the Stellite 12 alloy and the occurrence of defects, such as pores, in the welded layer. With the increase in current intensity, the amount of energy input increases, leading to the dilution of the base material.
The hardness of the weld pad and base metal was measured in two directions: at the center of the weld pad and at the edge of the weld pad. Hardness HV10 distribution of pad weld and substrate in cross-section is shown in Table 4. From this table, it can be observed that the Vickers hardness of the base material was significantly lower than that of the coatings. The hardness of the base material was approximately 145 HV in all cases. The welding current used in the PTA deposition process varied, with values of 89, 118, 125, 142, and 160 A. For sample 1.1 (Table 4a and b), welding was performed with a current of 89 A, and the average hardness of the weld pad was 404 HV. The hardness of the weld pad closest to the surface was the lowest, measuring 385 HV. The hardness of the weld pad near the edge (measurement line 2) closest to the surface was around 300 HV. As the current increased to 118 A, 125 A, and 142 A, the average hardness of the weld pad decreased. For the highest current of 160 A (Table 4j and k), the hardness of the weld pad was the highest, around 500 HV, but defects, such as pores, appeared in the weld pad.

Table 4. Hardness HV10 distribution of pad weld and substrate in cross-section

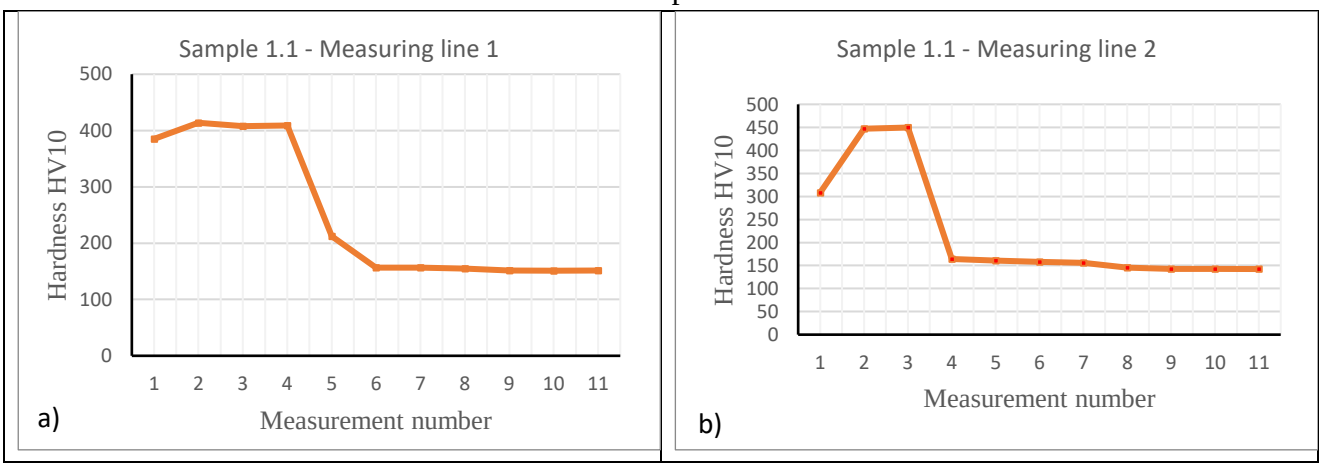

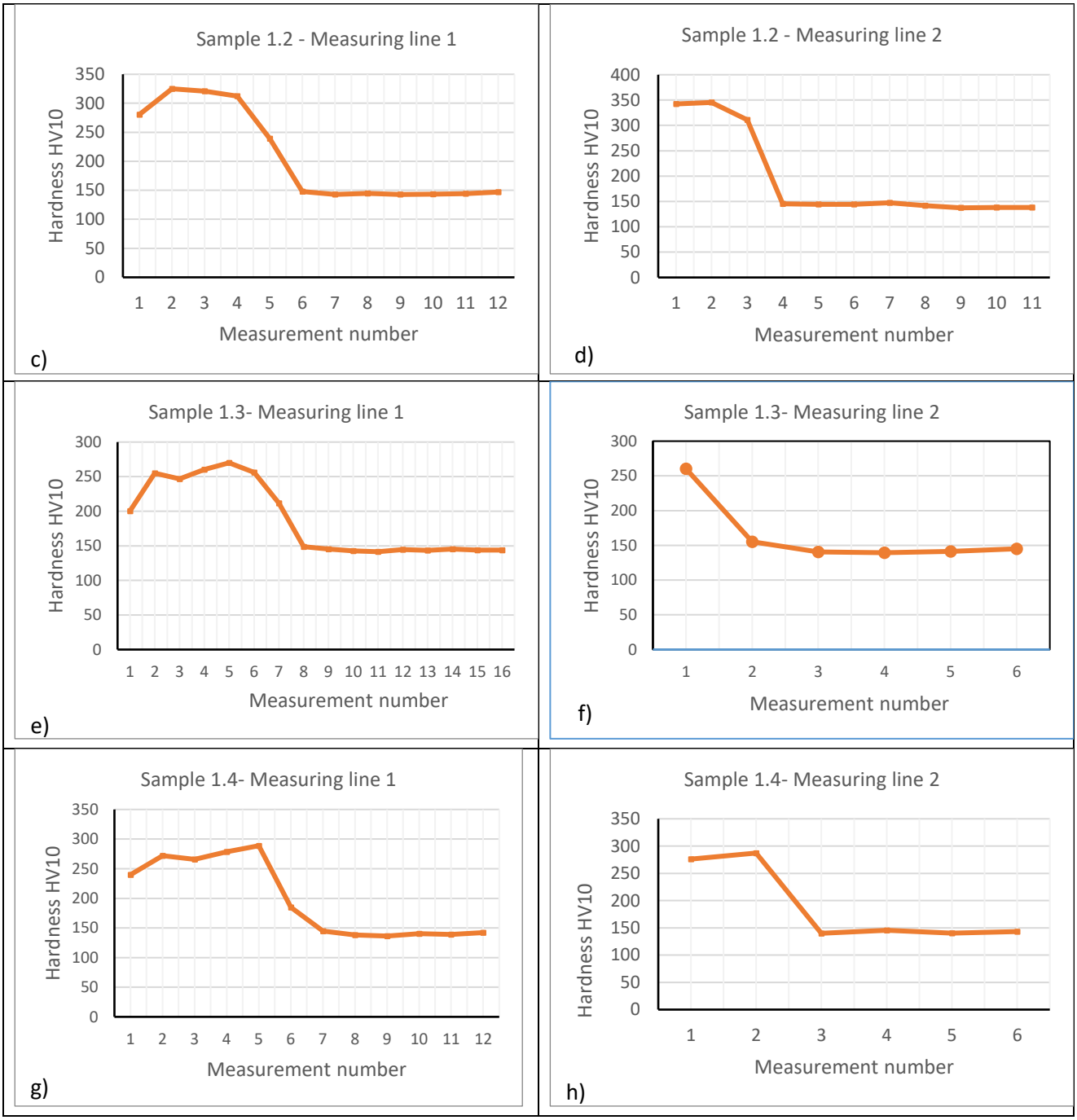
Sample 1.2 - Measuring line 1
Hardness HV10
Measurement number
c)
Sample 1.2 - Measuring line 2
Hardness HV10
Measurement number
d)
Sample 1.3- Measuring line 1
Hardness HV10
Measurement number
e)
Sample 1.3- Measuring line 2
Hardness HV10
Measurement number
f)
Sample 1.4- Measuring line 1
Hardness HV10
Measurement number
g)
Sample 1.4- Measuring line 2
Hardness HV10
Measurement number
h)

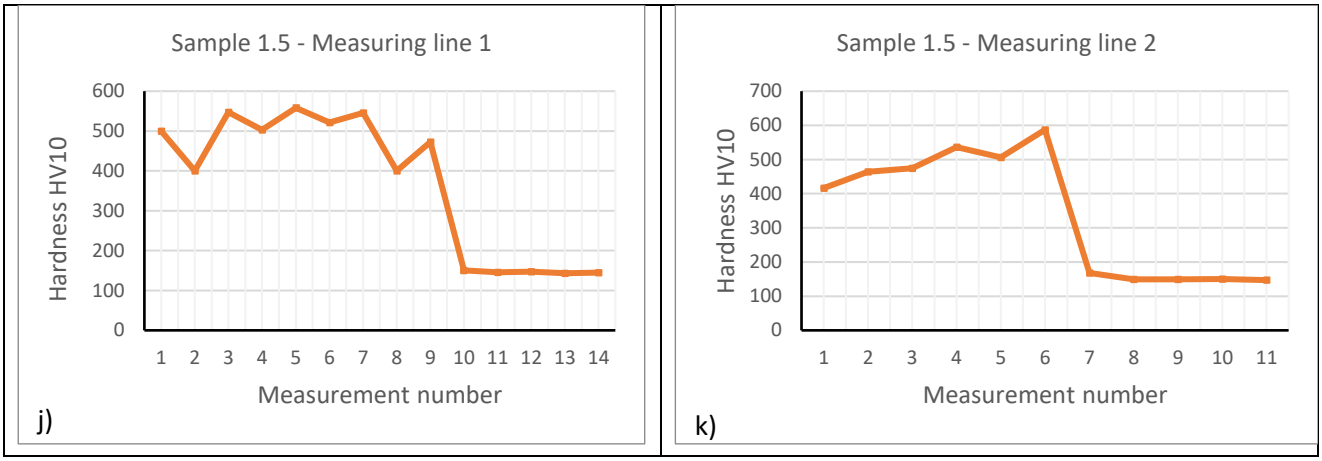

Maximum hardness of 404 HV was observed in the pad weld of sample 1.1 and decreases with increasing arc current for the other samples [11]. As the current increases, both the melting temperature and the amount of energy input into the material rise. This leads to deeper penetration of the welded layer and increased dilution of the base material. As a result, the hardness of the welded layer decreases due to a lower concentration of hard phases, such as carbides, which are the primary contributors to high hardness.

4. Conclusions

Structural steel S235 was hardfaced with Stellite 12 alloy using the PTA deposition process. The hardfacing process was characterized by a hardening mechanism and the formation of a dendritic microstructure. The microstructure of Stellite 12 consisted of dendrites and interdendritic eutectic carbides, with dendrites arranged in a planar, cellular, and columnar manner, forming towards the surface of the coating. The PTA process enabled a high coating deposition rate with reduced iron dilution from the base material.

Based on the obtained results, it can be concluded that the arc current in the PTA deposition process significantly affects the hardness of the pad weld layer, as well as the presence of defects in the material. The PTA deposition process was implemented under constant parameters: a current of 89 to 160 A, a voltage of 28.5 V, and a travel speed of 130 mm/min.

At the lowest current of 89 A, the average hardness of the pad weld layer was 404 HV, while the hardness closest to the surface was 385 HV. With an increase in current to 118 A, 125 A, and 142 A, the average hardness of the pad weld layer decreased, indicating increased dilution of the base material and a reduction in the concentration of hard phases in the layer.

At the highest current of 160 A, an increase in the hardness of the pad weld layer (around 500 HV) was observed, but with the occurrence of porosity, indicating excessive melting and increased gas release during the process.

It was observed that the hardness at the edge of the pad weld layer was lower compared to the central part, which may indicate microstructural inhomogeneity due to different cooling rates and solidification.

5. References

[1] M. F. Buchely, J. C. Gutierrez, L. M. León, and A. Toro. (2005). The effect of microstructure on abrasive wear of hardfacing alloys. *Wear, 259,* 52-61. https://doi.org/10.1016/j.wear.2005.03.002

[2] D. Chen, D. Liu, Y. Liu, H. Wang, and Z. Huang. (2014). Microstructure and fretting wear resistance of γ/TiC composite coating in situ fabricated by plasma transferred arc cladding. *Surface and Coatings Technology, 239,* 28-33. https://doi.org/10.1016/j.surfcoat.2013.11.012

[3] M. X. Yao, J. B. C. Wu, and Y. Xie. (2005). Wear, corrosion and cracking resistance of some W- or Mo-containing Stellite hardfacing alloys. *Materials Science and Engineering: A, 407,* 234-244. https://doi.org/10.1016/j.msea.2005.06.062

[4] W. C. Lin and C. Chen. (2006). Characteristics of thin surface layers of cobalt-based alloys deposited by laser cladding. *Surface and Coatings Technology, 200,* 4557-4563. https://doi.org/10.1016/j.surfcoat.2005.03.033

[5] A. Khoddamzadeh, R. Liu, M. Liang, and Q. Yang. (2012). Novel wear-resistant materials–Carbon fiber reinforced low-carbon Stellite alloy composites. *Composites Part A: Applied Science and Manufacturing, 43,* 344-352. https://doi.org/10.1016/j.compositesa.2011.11.023

[6] Foster J., Cullen C., Fitzpatrick S., Payne G., Hall L., Marashi J. (2019). Remanufacture of hot forging tools and dies using laser metal deposition with powder and a hard-facing alloy Stellite 21®. *Journal of Remanufacturing, 9,* 189-203. DOI: 10.1007/s13243-018-0063-9.

[7] G.P. Rajeev, M. K., Bakshi S.R. (2017) Hardfacing of AISI H13 tool steel with Stellite 21 alloy using cold metal transfer welding process. *Surface and Coatings Technology, 326,* 63–71. https://doi.org/10.1016/j.surfcoat.2017.07.050

[8] L.E. Falqueto, D.J. Butkus, J.D.B. De Mello, A.C. Bozzi, C. Scandian. (2017). Sliding wear of cobalt-based alloys used in rolling seamless tubes. *Wear, 376–377,* 1739–1746. https://doi.org/10.1016/j.wear.2017.01.009

[9] A. Motallebzadeh, E. Atar, H. Cimenoglu. (2015). Microstructure and Tribological Properties of PTA Deposited Stellite 12 Coating on Steel Substrate. *Manufacturing Science and Technology, 3(5),* 224 - 228. DOI: 10.13189/mst.2015.030505.

[10] W. Henzler, M. Sawa, P. Trębicki, M. Szala, G. Winiarski. (2021) Influence of austenitic interlayer on the properties of stellite padding welds after impact-hardening. *Welding Technology Review 93(2),* 13-20. https://doi.org/10.26628/wtr.v93i2.1134.

[11] D. Deng, J. Lu, X. Li. (2013) The Effect of Arc Current on the Microstructure and Wear Characteristics of Stellite12 Coatings Deposited by PTA on Duplex Stainless Steel. *Materials Transactions, 54(9),* 1851-1856. doi:10.2320/matertrans.M2013103.

Društvo za tehniku
zavarivanja Slavonski Brod

13. Međunarodno znanstveno-stručno savjetovanje SBZ 2025

„STROJARSKE TEHNOLOGIJE U IZRADI ZAVARENIH KONSTRUKCIJA I PROIZVODA, SBZ 2025."
Slavonski Brod, 08. i 09. 05. 2025.

Machines with guaranteed travel

B. Grizelj[1,*], M. Duspara[1], B. Kovačević[1], M. Stoić [1], V. Starčević[1]

[1]Mechanical Engineering Faculty in Slavonski Brod, University of Slavonski Brod, Croatia

[*] Corresponding Author. E-mail: Branko Grizelj@unisb.hr

Abstract

Machines with a guaranteed travel are part of the metal forming machines, which depend on the operation of the main drive. Machines with a guaranteed travel play a major role in the economy, because they are used to economically produce parts in metal forming. They are later used for heavily loaded parts of various machines, as well as the majority of metal parts and consumer elements of various masses. The data required in practice are given.

Keywords: metal forming, machines, guaranteed travel

1. Introduction

In metal forming, the workpiece is most often deformed in one or more steps, where the tool used most often consists of two parts. Metal forming machines have the task of providing the necessary forces, moments or deformation work and guiding the tools.
The division of metal forming machines cannot be made according to the type of metal forming, because different processes can be performed on one machine (bending, deep drawing, cutting, punching, etc.). Therefore, it is carried out not according to the type of forming, but according to the type of machine. These include: rolling machines, machines with guaranteed energy (pistons and spindle presses), machines with guaranteed force, machines with guaranteed travel and machines for metal forming by means of an active medium and active energy.

2. Characteristic sizes

The close relationship that exists within the manufacturing process between metal forming machines and metal forming by deformation seems necessary, because the deformation is carried out by means of a machine. The requirements of the forming process on a forming machine and its properties can be described by means of characteristic quantities [1-5]. In addition to knowledge of the various characteristic quantities, it is necessary to know the numerical values of the characteristic quantities in order to specify the machines.

According to Lange [3], three groups of machines are distinguished according to their characteristic quantities:

1. force and energy
2. time
3. accuracy in unloaded and loaded machines.

3. Machines with guaranteed travel

In machines with guaranteed stroke, the stroke of the machine ram is determined by the kinematics of the main drive. The ram force F_{St} depends on the ram position Figure 1. It can theoretically be infinite. Since in these machines the drive and the press body can withstand the corresponding forces, the nominal force F_N must not be exceeded in these machines.

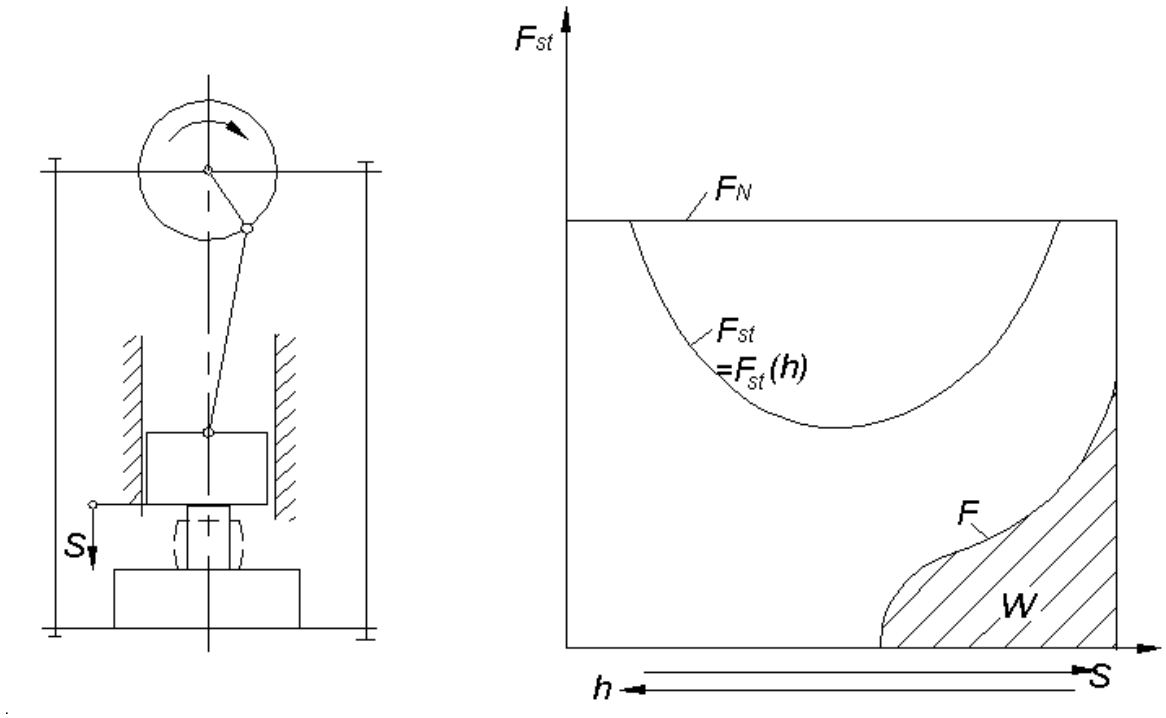

Figure 1 Machines with guaranteed stroke. Crank press (schematic and force limitation) [1]

The most important characteristic quantities are the hammer force $F_{St} = F_{St}(h)$ and the nominal force F_N. Machines with a guaranteed stroke operate with an energy reservoir (flywheel). During the working stroke, energy (nominal energy E_N) is available, which is obtained by the design of the reservoir. The working power is therefore a further characteristic value of machines with a guaranteed

stroke. Representatives of these machines are presses with a crank mechanism drive (eccentric presses, crank presses, lever presses and curve presses).

4. Force and Moment (with guaranteed travel)

If a torque M_K acts on the knee (connecting rod), the tangential force F_t will act in the connecting rod in the direction of movement, the radial force F_r will act perpendicular to the movement, and the force in the direction of the motor lever F_s will act, Figure 2 and Figure 3.

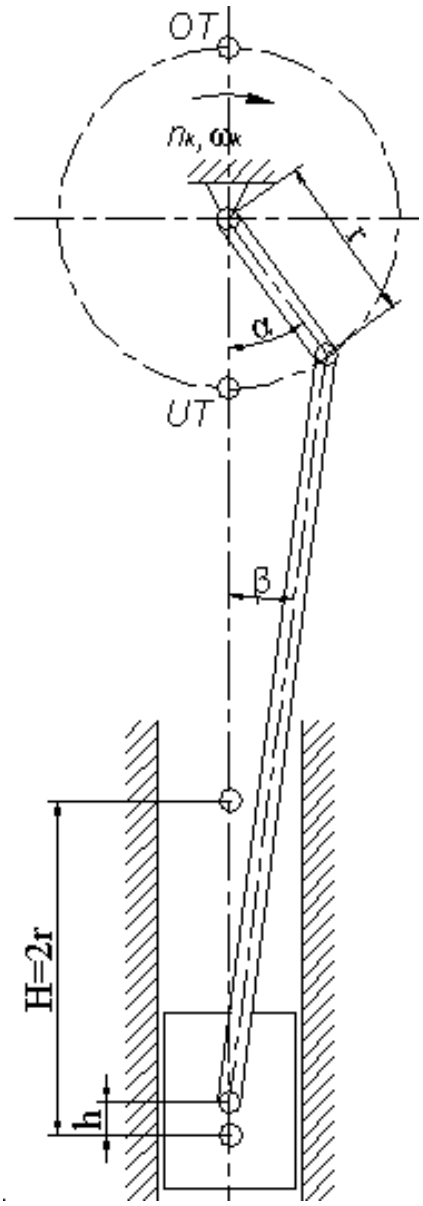

Figure 2. Markings on the crank press

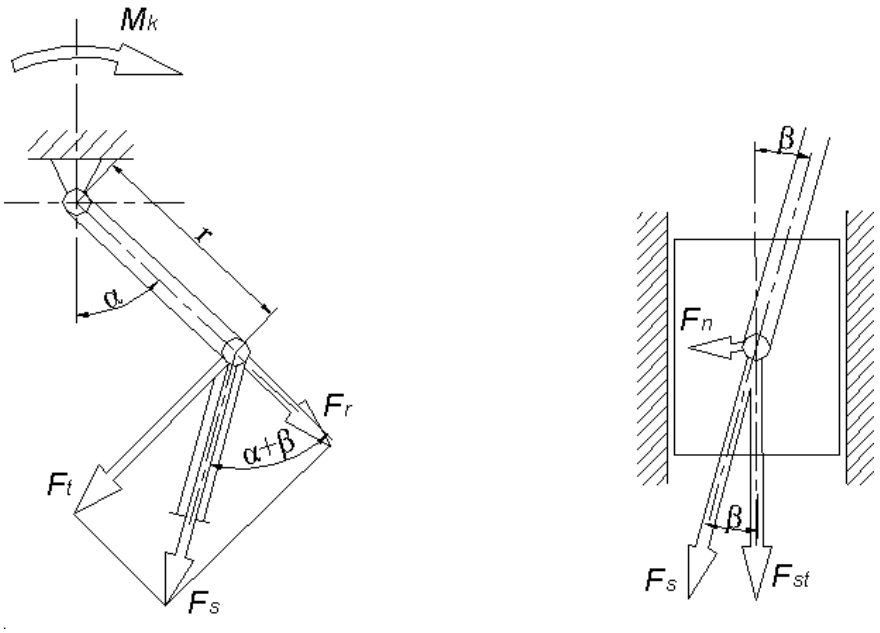

a b

Figure 3. Forces on a crank press: a – connecting rod sleeve; b – motor lever sleeve

By neglecting friction, forces can be calculated.
Tangential force

$$F_t = \frac{M_K}{r}$$

force in the direction of the motor lever

$$F_s = \frac{F_t}{\sin(\alpha+\beta)} = \frac{M_K}{r}\frac{1}{\sin(\alpha+\beta)}$$

Radial force

$$F_r = F_s \cos(\alpha+\beta) = \frac{M_K}{r}\frac{1}{\tan(\alpha+\beta)}$$

On the push rod sleeve, the force F_s induces a force in the direction of the hammer stroke F_{st} and perpendicular to the direction of the hammer stroke F_n (Figure 10 b). The following applies to these forces:

force of the hammer

$$F_{st} = F_s \cos\beta = \frac{M_K}{r} \frac{\cos\beta}{\sin(\alpha+\beta)}$$

normal force

$$F_n = F_s \sin\beta = \frac{M_K}{r} \frac{\sin\beta}{\sin(\alpha+\beta)}$$

$$F_n = \frac{F_{st} \sin\beta}{\cos\beta} = F_{st} \tan\beta$$

If the connecting rod lever is denoted by r and the length of the motor lever by l, then $r/l=\lambda$ called the ratio of the radius of the connecting rod to the length of the engine lever. Size λ is 1/4 to 1/15. In practice, it is most often λ is 1/10. For this value the angle is β very small. For λ=0,1 for example follows:

$$\sin\beta = \lambda \cdot \sin\alpha \Rightarrow \beta_{max} = 6^o$$

For cosβ≅1 and sin($\alpha + \beta$)~ sin α follows

$$F_{st} = \frac{M_K}{r} \frac{1}{\sin\alpha} \qquad (1)$$

For a press, the nominal force F_N and the nominal angle are important α_N, because the press is calculated and dimensioned for the nominal force and nominal angle. If the angle of the connecting rod α_N put into expression (6) it follows from it:

$$M_K = F_N \cdot r \cdot \sin\alpha_N \qquad (2)$$

$$F_{st} = F_N \cdot \frac{\sin\alpha_N}{\sin\alpha} \qquad (3)$$

α_N nominal connecting rod angle corresponding to the nominal force of the press
F_N nominal press force.

From expression (2and3) for the nominal connecting rod angle $\alpha_N = 30^o$the connecting rod torque is:

$$M_K = F_N \cdot r \cdot \sin 30^o = F_N \cdot \frac{r}{2} \tag{4}$$

$$F_{st} = F_N \cdot \frac{\sin 30^o}{\sin \alpha} = \frac{F_N}{2} \frac{1}{\sin \alpha}. \tag{5}$$

Figure 4 shows the relative dependence of the hammer force Fst/F_N on the connecting rod angle α according to expression (5).

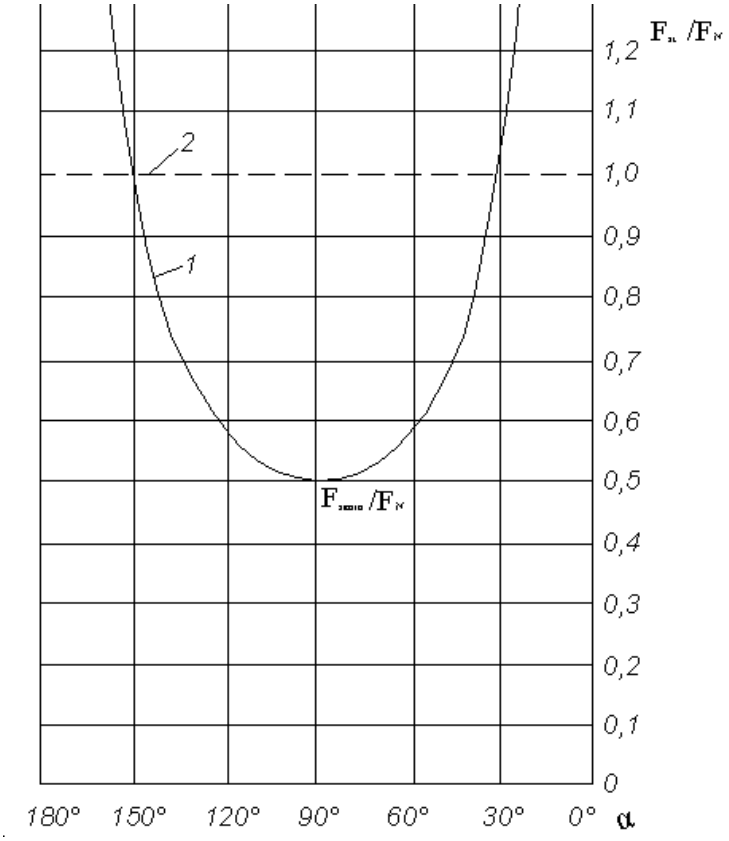

Figure 4. Limiting forces of the hammer Fst/F_N depending on the connecting rod angle α. 1- limiting force given over the permissible load, for rotating drive parts, 2- limiting force given over the permissible load for non-rotating drive parts (nominal force of the press)

The flow of hammer force in the area should be observed. $0^o \leq \alpha \leq 90^o$ corresponding to the total stroke.

1. For $\alpha > 30^o$ the available force decreases with increasing angle.
For the hammer force *F*st=0.5 F_N. The connecting rod is subjected to a torque that is greater than necessary and there is a risk of overloading the rotating drive parts. For $30^o \le \alpha \le 90^o$ the permissible force is less than the maximum force available.

2. For $\alpha < 30^o$ the force increases suddenly and theoretically for $\alpha = 0^o$ it amounts to infinity. The press parts can only withstand the nominal force (the press is dimensioned accordingly) and this should be taken into account (the nominal force F_N in this case is for the nominal angle α_N= 30°).

In presses with guaranteed stroke, only the dependence of the permissible hammer force on the angle α but on the hammer stroke *h* is important.

From Figure 9 it follows:

$$h = r\left[(1-\cos\alpha)+\frac{1}{2}\cdot\lambda\cdot\sin^2\alpha\right] \tag{6}$$

Figure 5 shows the dependence of the connecting rod angle on the hammer path for $\lambda = 0{,}1$.

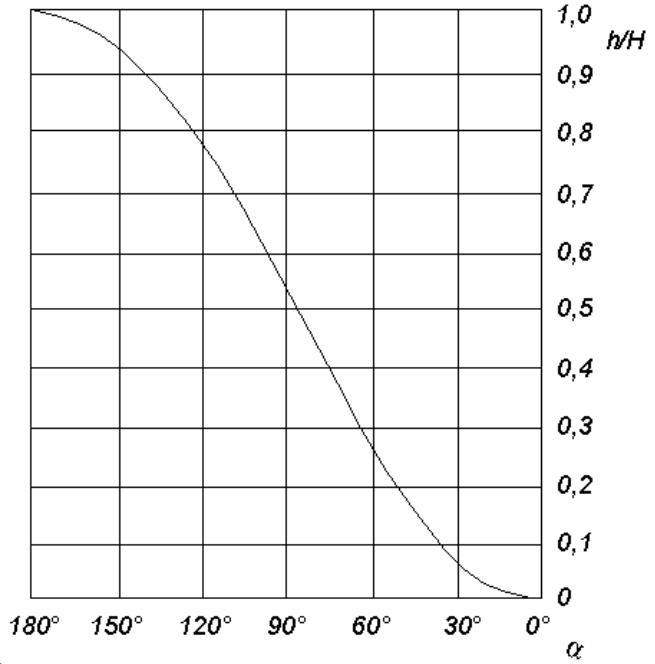

Figure 5. Dependence of the sledgehammer path on the angle of the connecting rod

Figure 6 shows the flow of permissible hammer force depending on the hammer path.

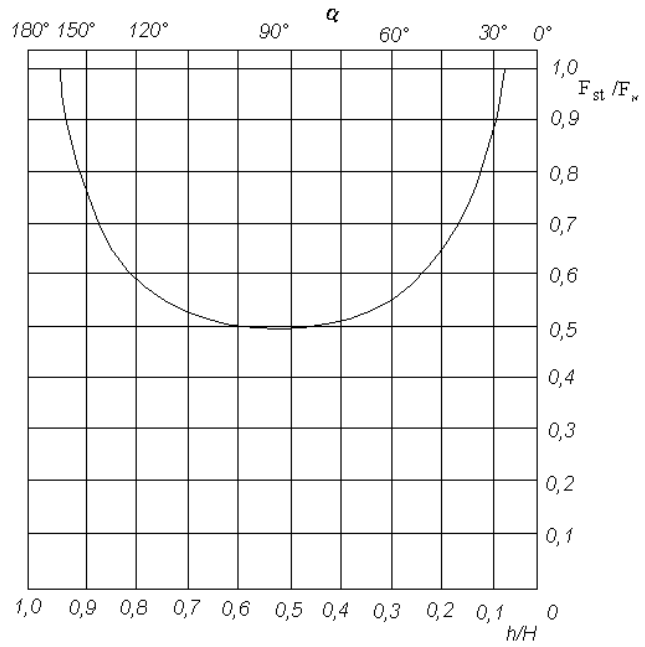

Figure 6. Dependence of the permissible force on the hammer path for $\lambda = 0{,}1$

Table 1 shows the most important data of toggle presses.

Table 1. The most important data of elbow presses

Nominal angle α_N	h_N/H	F_{stmin}/F_N	M_K/M_{K30}	Using
10°	0,008	0,17	0,35	forging in a forge
20°	0,033	0,34	0,68	stamping
30°	0,073	0,50	1,00	universal
45°	0,158	0,71	1,41	extrusion
60°	0,269	0,87	1,73	deep pull
75°	0,398	0,97	1,93	deep pull

Ratio h_N/H	α_N	F_{stmin} / F_N
0,008	10°	0,17
0,02	16°	0,28
0,04	22°	0,37
0,08	31°	0,52
0,16	45°	0,71
0,24	56°	0,83
0,32	66°	0,91

Figure 7 shows the dependence of Fst/F_N on h/H for different α_N.

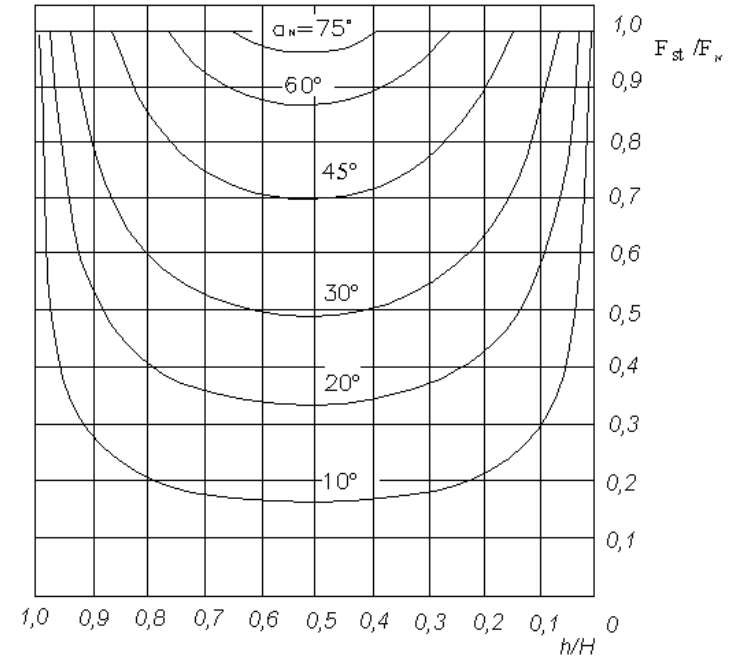

Figure 7. Dependence of Fst/F_N on h/H for different

Figure 8 shows the dependence of Fst/F_N on h/H for different h_N/H.

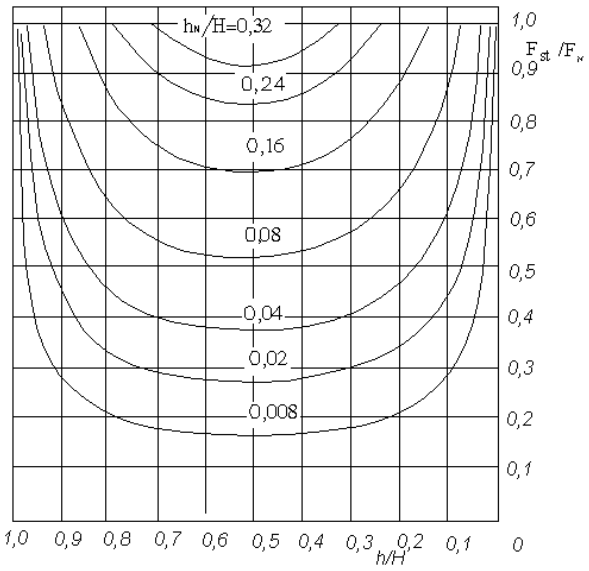

Figure 8. Dependence of Fst/F_N on h/H for different h_N /H

5. Conclusions

Machines with a guaranteed path are part of the metal forming machines, which depend on the operation of the main drive.

When buying machines, it is important to consider what the machine is being purchased for. It does not matter whether the machine is being purchased for forging in forges or deep drawing. For example, the nominal force F_N or the nominal angle α_N.

If the nominal force of the machine for forging in the forge is 10 MN, it is many times cheaper than the same nominal force (10 MN) in deep drawing. That is why in production it is not good to forge pieces on a deep drawing machine. The price of such parts is many times more expensive.

6. References

[1] Grizelj, Branko. (2007). Strojevi za oblikovanje metala deformiranjem. Slavonski Brod : Strojarski fakultet u Slavonskom Brodu. (ISBN 978-953-6048-42-7) **(book)**

[2] Grizelj, Branko. (2018). Oblikovanje metala deformiranjem Umformtechnik Metal forming. Slavonski Brod : Strojarski fakultet u Slavonskom Brodu. (ISBN 978-953-6048-88-5) **(book)**

[3] Lange, Kurt. (1988-1993). Lehrebuch der Umformtechnik. Berlin/Heidelberg/New York. Spring Verlag **(books)**

[4] Lange, Kurt. (1985). Handbook of metal forming. McGraw-Hill **(book)**

[5] Grizelj, Branko. (1995). Doprinos analizi aksijalno simetričnog savijanje lima. Zagreb FSB **(doktorska disertacija mentor prof.dr.sc. Povrzanović Aleksandar)**

Društvo za tehniku
zavarivanja Slavonski Brod

13. Međunarodno znanstveno-stručno savjetovanje SBZ 2025

„STROJARSKE TEHNOLOGIJE U IZRADI ZAVARENIH KONSTRUKCIJA I PROIZVODA, SBZ 2025."
Slavonski Brod, 08. i 09. 05. 2025.

Finite element analysis of the thermal field in a butt-welded joint with three weld passes

I. Dunđer[1,*], P. Konjatić[1], I. Gelo[1], M. Katinić[1]

[1]Mechanical Engineering Faculty in Slavonski Brod, University of Slavonski Brod, Croatia

[*] Corresponding Author. E-mail: idunder@unisb.hr

Abstract

The finite element analysis of the thermal field during butt welding of structural steel is carried out using ANSYS software. The analysis includes a discretized finite element model of steel plates with a V-shaped weld preparation used for the simulation of thermal welding with three welding passes. Key features of the simulation include moving heat source, material deposition and temperature-dependent material properties. To accurately model the gradual addition of filler metal, the element birth and death technique was used. The propagation and magnitude of the thermal field was analyzed using transient thermal analysis which allowed tracking the temperature values during across all three weld passes. A good correlation between numerically obtained results and experimental results has been established and presented in the paper to serve as a verification of the numerical analysis.

Keywords: welding, thermal field, transient-thermal finite element method, butt-welded joint, birth and death technique.

1. Introduction

Welding is a widely used fabrication technique across various industries, including automotive, construction, shipbuilding, pressure vessels, and steel bridges. During the welding process, materials are exposed to intense heat input, resulting in the formation of residual stresses. These stresses can have a significant impact on the structural integrity and overall performance of the welded joint. Therefore, it is essential to estimate welding deformations and analyze the effects of different welding conditions. With advancements in computing, the finite element method has become an effective tool for predicting and assessing welding deformations, which vary based on production factors such as welding materials, dimensions, and process parameters. Finite element simulations have been widely utilized to predict the thermal, material, and mechanical effects of welding, offering both efficiency and flexibility in modeling the complex welding process. [1]-[3]

The thermal cycle during welding influences not only the heat distribution within the welded parts, but also the phase transformations that occur when the molten metal solidifies. Monitoring the thermal field during welding is crucial to ensure compliance with welding procedures and key parameters such as the preheating temperature (ϑ_p) the cooling time ($t_{8/5}$) between 800 °C and 500 °C, and the cooling rate (c_r). [4]

The cooling time $t_{8/5}$ represents the time required for the weld bead and its heat-affected zone to cool down from 800 °C to 500 °C. The preheat temperature refers to the minimum temperature that the base material must reach before welding begins. An incorrect selection of welding parameters can lead to undesirable structural changes that ultimately affect the mechanical properties of the welded joints.

Understanding thermal history is crucial for accurately estimating the stresses and deformations in welded components. Numerous scientific studies have introduced finite element models capable of simulating complex welding processes. However, due to the simultaneous occurrence of thermal and mechanical phenomena, developing numerical models for welded structures presents significant challenges. To address these complexities, various strategies can be applied to improve the accuracy and reliability of simulations [5]. Florea [6] explored the use of infrared thermography for monitoring the thermal field during fusion welding. The method was validated by comparing infrared measurements with those obtained from contact thermocouples. The resulting temperature profiles enabled calculation of the $t_{8/5}$ parameter, which influences phase transformations during cooling.

Numerous researchers have employed the finite element method (FEM) to analyze heat transfer characteristics in welding. The modelling of a moving heat source, as a typical transient process, is a critical concern in the welding simulation. Some studies have also focused on estimating heat source model parameters for various fusion welding processes. The technique of element birth and death had been implemented by various researchers, due to its ability in representing the filler deposition during the welding process. Armentani et al. [7,8] has adopted a parametric model and the element birth and death technique are used in single-pass butt welded joint to simulate weld filler variation with time. Hashemzadeh et al. [9] investigated thermal field and residual stresses in a multi-pass butt welded joints using an FE model, based also on the element birth and death technique, validated by comparing numerical and experimental results.

The present work builds on previous studies that have investigated the thermal field during welding and the application of the finite element method (FEM) to evaluate the influence of welding parameters. Transient thermal FEA was performed to evaluate the temperature distribution in a three-pass butt-welded joint. The aim of the study was to thoroughly analyze the thermal cycles occurring during welding, to investigate the influence of different preheating conditions on the evolution of the thermal field and to validate the developed numerical model by comparing it with experimental data obtained with contact thermocouples and infrared thermography.

2. Problem description

2.1 Heat input and welding process parameters

The heat input Q generated by the moving heat source on the entire elements of the welded joint is expressed by the following relation:

$$Q = \frac{\eta \cdot I \cdot U}{v}$$

where:

- Q - heat input (J/mm),
- I - welding current (A),
- U - voltage (V),
- v – travel speed (mm/s)
- η - coefficient thermal efficiency, defined according to relevant standards (EN ISO 1011-1:2009).

In order to achieve a high-quality welded joint, the welding process was carried out in three passes, as shown in Figure 1. This approach ensures gradual heat input into the material, thereby reducing residual stresses and distortions while improving the weld microstructure. According to reference [6], for the numerical simulation of the welding process of the S890QL material, the parameters for the MAG welding process were used. The parameters used in the welding simulation are given in Table 1.

Table 1. The welding parameters used in the simulation

I, A	U, V	v, mm/s	η
260	26	10	0,8

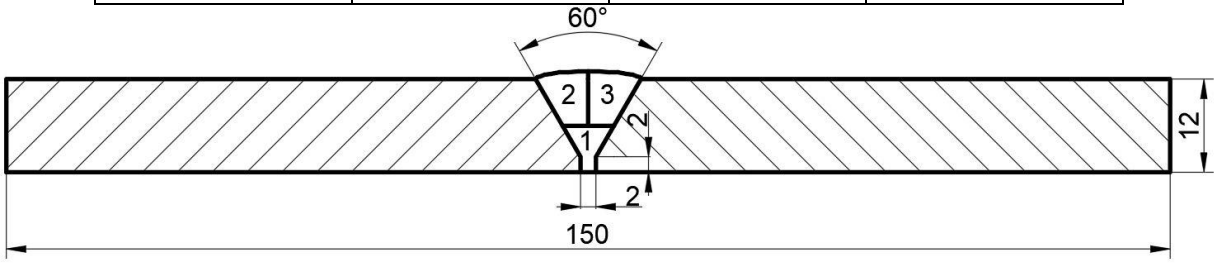

Figure 1. Sketch of the welded joint cross-section

The initial conditions and boundary conditions were applied accordingly. Prior to welding, the effect of preheating the base material was also considered. Preheating was modeled by applying a thermal input with value adjusted to achieve the desired initial material temperatures prior to welding.

In accordance with the recommendations for welding high-strength steel S890QL [6], two different preheating conditions were considered in the simulations: ϑ_{p1}=100°C and ϑ_{p2}=150°C. During welding and cooling, heat loss is considered through convection, and the radiation heat loss was ignored. The boundary condition was applied to free surfaces of the plate exposed to the ambient temperature set at 22°C.

2.2. Material properties

In the present study, the steel S890QL was analyzed using two plates with the dimensions 300 x 74 x 12 mm. The temperature-dependent material properties of the steel were used to achieve more realistic simulation of the transient heat transfer during the welding process. The specific values of these temperature-dependent properties can be found in Table 2. It can be seen that the modulus of elasticity (E) of the steel decreases significantly with increasing temperature. The other parameters, including the specific heat capacity (C), the coefficient of thermal expansion (α) and the thermal conductivity (K), were considered as constant values throughout the simulation.

Table 2. Temperature-dependent material properties of the steel S890QL [9,11]

T, °C	E, GPa	C, J/kg·K	α, µm/m·K	K, W/m·K
20	210	460	9,1	41
100	195			
210	195			
330	185			
420	168			
540	118			
660	52			
780	12			
985	11,8			
1320	10,4			
1420	10,2			
1500	10			

The general mechanical properties and chemical composition of the low-alloy high-strength steel S890QL are listed in Tables 3 and 4 respectively[6].

Table 3. Chemical composition of the steel S890QL

Material	C	Si	Mn	Cr	Ni	Mo	V	N	Nb	Ti	Cu	Zr	S	P
S890QL	0,2	0,8	1,7	1,5	2	0,7	0,12	0,015	0,06	0,05	0,5	0,15	0,01	0,02

Table 4. Mechanical properties of the steel S890QL

Material	Tensile strength R_m, MPa	Yield strength R_e, MPa	Elongation A, %
S890QL	940-1100	≥ 890	11

3. Numerical procedure

3.1. Finite element method

In this study, a transient thermal analysis was performed using the finite element method (FEM) to simulate the welding process. The analysis was carried out taking into account suitable finite elements, material properties, boundary conditions and a defined heat input model representative of the welding process. The result of this phase is the temperature distribution at each node and at every consecutive second of welding and cooling process, which serves as the initial condition for the subsequent thermal load.

The finite element analysis was performed using the commercial software ANSYS (2023) [10]. The element Solid 279, a thermal hexahedral element with 20 nodes, was used for the thermal analysis. The model consisted of 8,356 elements and 43,864 nodes. The mesh density was determined by a mesh sensitivity analysis to ensure an optimal balance between computational efficiency and result accuracy. The element size in the heat-affected zone (HAZ) and weld area was set to 3 mm, while a coarser element size of 10 mm was used in the base material. Geometry model discretized with finite element mesh is shown in Figure 2.

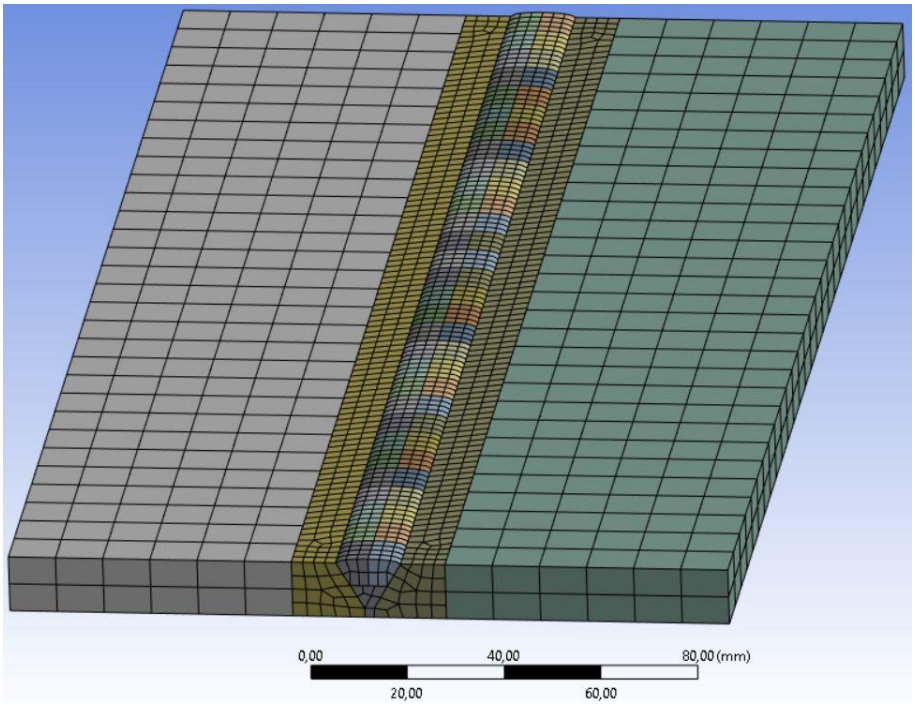

Figure 2. Geometry model discretized with finite element mesh

3.2 Element birth and death technique application

The finite element (FE) model was constructed using the birth-and-death element technique. All elements, including those representing weld joint to be activated in the subsequent phases, were defined at the beginning of the analysis. However, the elements along the weld path were initially treated as 'inactive' or 'dead', reflecting their non-existence in the actual structure prior to welding. As the weld progresses during the simulation, these elements are progressively 'activated' and treated as 'alive' to simulate material deposition.
The deactivation of elements (the death of elements) does not involve their physical removal from the model. Instead, the relevant material properties, such as stiffness, thermal conductivity or other analogue properties are drastically reduced by applying a significant reduction factor. Conversely, reactivation (the birth of an element) occurs sequentially depending on the movement of the welding torch. This is done by resetting the material properties of the affected elements, such as stiffness and mass, to their original values. This approach allows an accurate representation of the transient nature of material addition during the welding process.

4. Results

The results of the thermal analysis, which refer to specific observation points located at 150 mm from the top of the plate where each weld pass starts for all three passes using birth and death element, are shown in Figure 3. Each thermal cycle is followed by a cooling phase of 30 seconds, indicating a relatively rapid temperature drop after the passage of the welding arc. As the legend on the Figure 3. shows, there are unrealistic negative temperature values obtained during the welding process. These values occur only at the several isolated nodes at the furthest edges of the plates and do not represent the realistic values, nor do they affect the remaining results, and thus can be neglected.

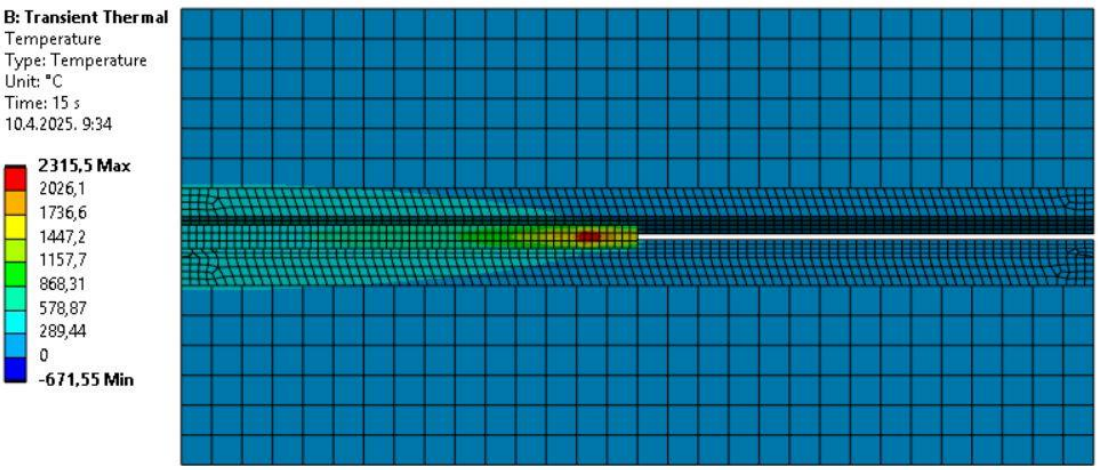

a)

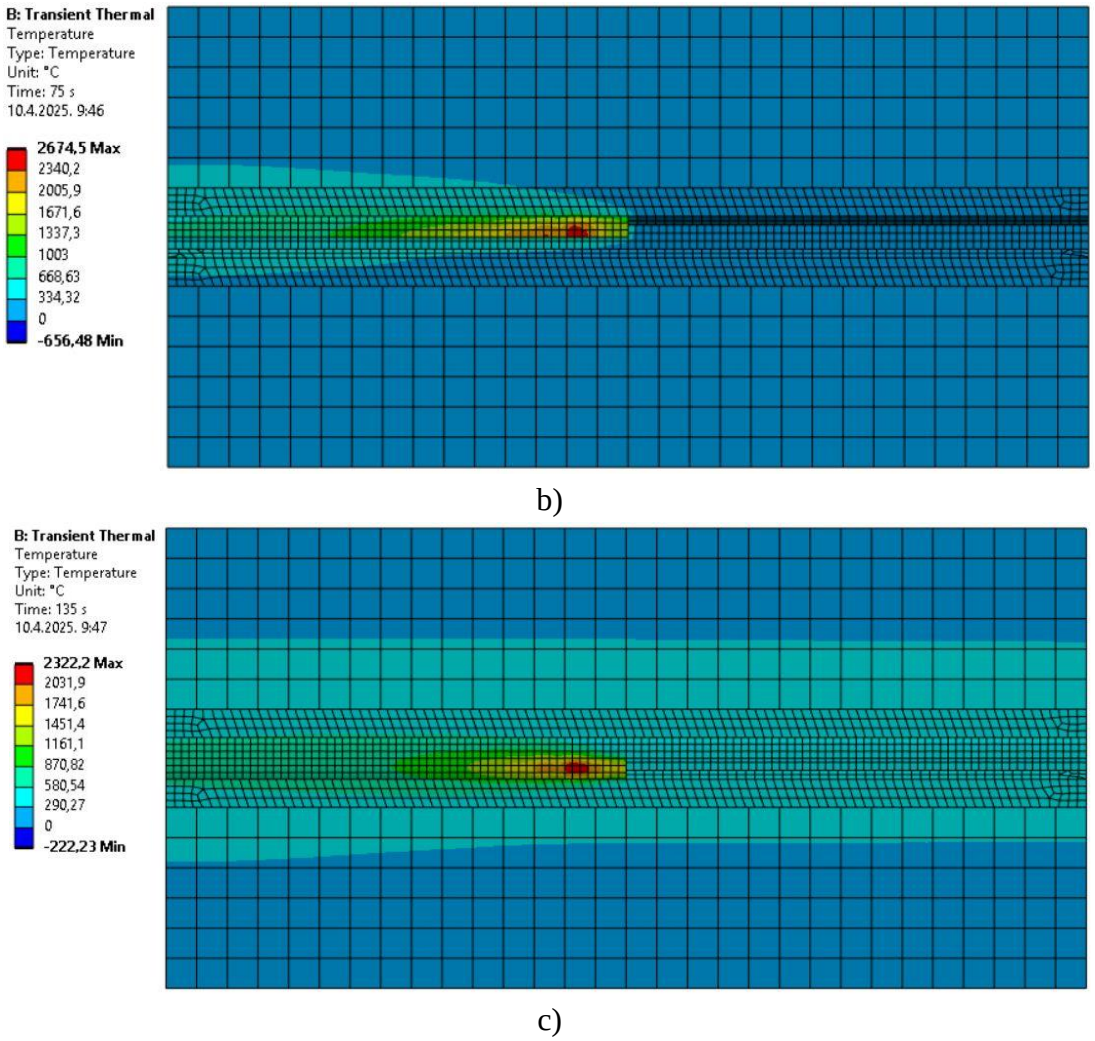

Figure 3. Birth and death technique in multi-pass welding: a) first pass, b) second pass, c) third pass

Figure 4 illustrates the maximum temperatures reached in the welded joint under preheating conditions. Although two different preheating temperatures are applied, the maximum temperatures reached during the welding process are approximately the same. The highest temperature values are observed during the second welding pass. This increased thermal effect is further enhanced by the fact that the second pass takes place over the area that was affected by the first pass, and which has not yet cooled down completely. Consequently, the residual heat from the previous pass leads to an accumulation of thermal energy, resulting in higher peak temperatures.

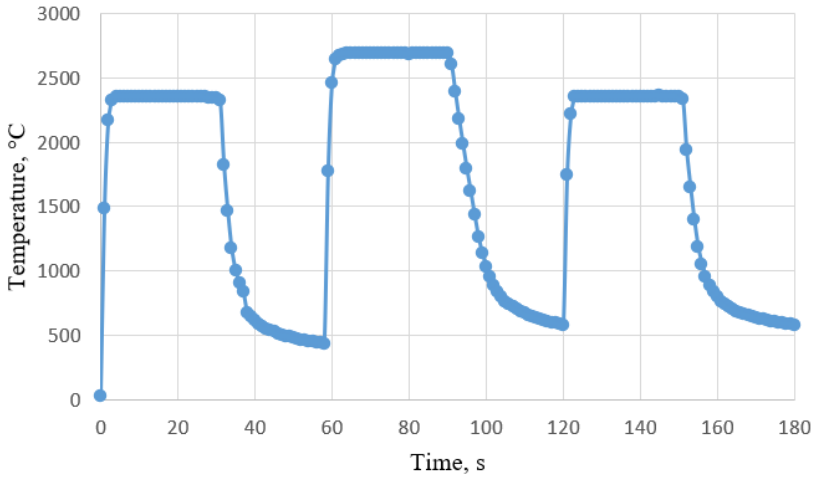

Figure 4. Maximum temperatures in the welded joint

The experimental welding procedure for the S890QL steel with a thickness of 12 mm was adopted from a previously conducted study [6]. In order to analyze the thermal cycles during welding, temperature measurements were carried out using two methods: Contact thermocouples and an infrared thermographic camera. Based on the recorded data, plots of the temperature–time change were created for each measurement method. The results of the thermocouple measurements and the infrared thermography were then compared with the results of the numerical simulation, which are shown in Figure 5 and Figure 6. This comparison enables the validation of the numerical model and provides a more comprehensive understanding of the thermal behavior during welding of S890QL steel. Figure 5 and 6 shows a good agreement between numerical and experimental results.

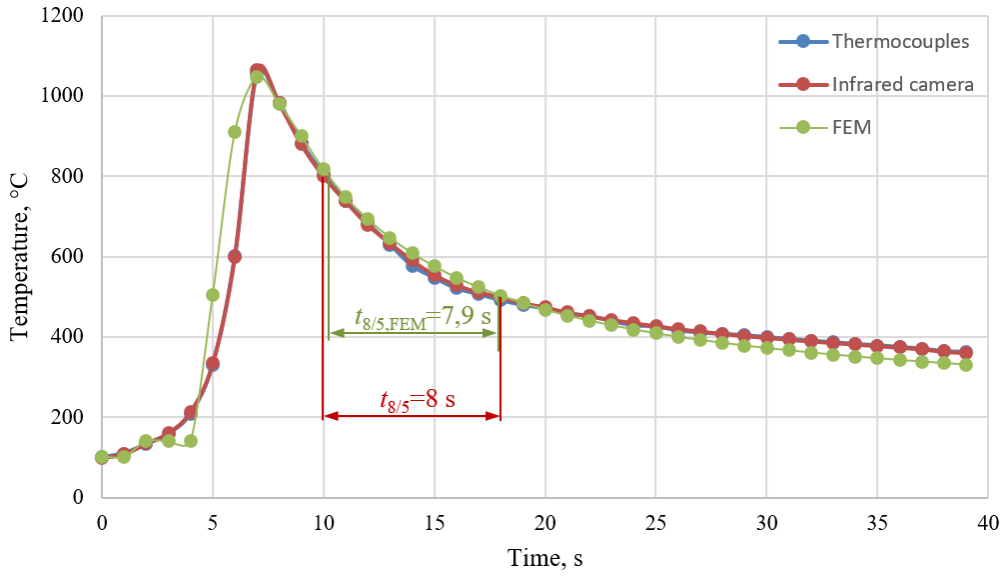

Figure 5 Variation of thermal cycle temperatures with preheat temperature ϑ_{p1} = 100°C

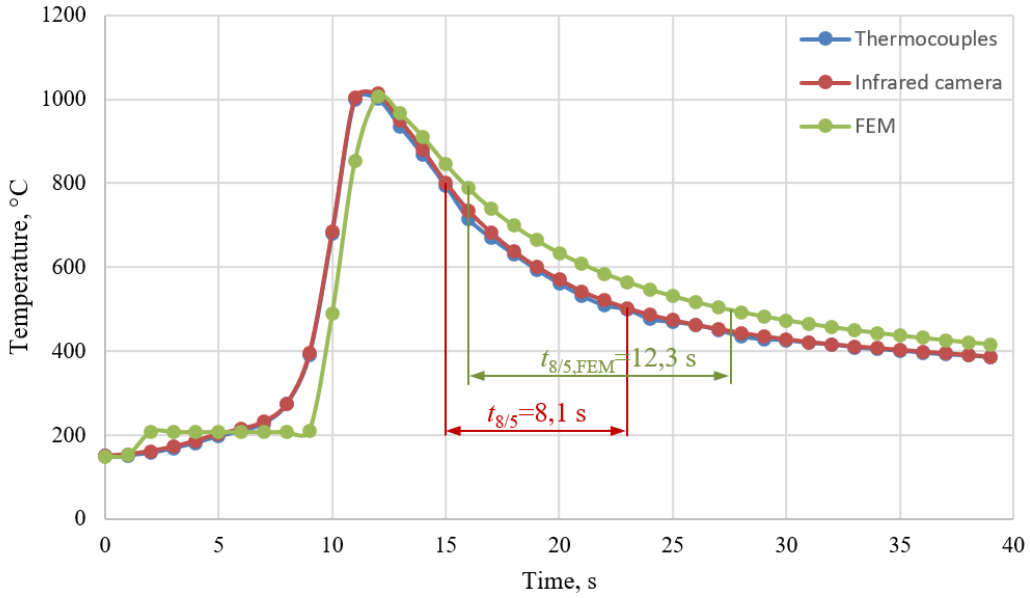

Figure 6 Variation of thermal cycle temperatures with preheat temperature ϑ_{p2} = 150°C

5. Conclusions

This study presents a numerical simulation of the welding of a butt-welded joint made of steel S890QL. The application of the "birth and death" technique is successfully used to simulate a three-pass welding process and allowed a realistic modelling of the gradual material deposition. This method proved to be effective in tracking the thermal fields and temperature distribution in the weld zone.

The experimental results showed a good correlation with the numerical results, thus validating the methodology used for numerical simulation.

The finite element analysis showed that preheating significantly influences the cooling time $t_{8/5}$. Higher preheating temperatures lead to increased heat input into the elements, which requires longer cooling times. These findings are crucial for controlling microstructural changes and preventing the formation of cracks in the welded joint.

The results contribute significantly to the understanding of thermal processes in the welding of high-strength steel, to the optimization of welding parameters. The reliability of the FEM as a tool for analyzing thermal effects and deformations in welded joints was confirmed.

Future research is recommended to further analyze residual stresses in welded joints and evaluate their effects on structural durability. Further work could include the experimental validation of residual stress simulation and the investigation of the effects of different heat treatment processes on the reduction of stress concentrations.

6. References

[1] Li Li, Khurram Asifa, Hong Li, Shehzad Khurram. (2012). FE Simulation Methods to Predict Welding Residual Stresses. *Key Engineering Materials, 525,* 281-284. https://doi.org/10.4028/www.scientific.net/KEM.525-526.281 (**journal article**)

[2] Locatelli, Fábio Renck; Casas, Walter J. P.; Filho, Ricardo F. L. (2014). Assessment of the Influence of Welding Parameters on Distortion. *Applied Mechanics and Materials*, *597*, 208-212. https://doi.org/10.4028/www.scientific.net/AMM.597.208 (**journal article**)

[3] Stamenković, Dragi; Vasović, Ivana. (2009). Finite Element Analysis of Residual Stress in Butt Welding Two Similar Plates. *Scientific Technical Review, 59,* 57-60. http://doi.org/ntp/rad2009/1-09/drag/219.673 (**journal article**)

[4] R. Celin, J. Berneti, D. Anica, S. Balanti; (2014) Welding of the steel grade S890QL. *Materials and technology*, *48*, 931–935.

[5] Sepe, R.; De Luca, A.; Greco, A.; Armentani, E. (2020) Numerical evaluation of temperature fields and residual stresses in butt weld joints and comparsion with experimental measurments. *Fatigue and Freacture of Engineering Materials and Structures*, *44-1*, 182-198. https://doi.org/10.1111/ffe.13351 (**journal article**)

[6] Florea,A., Petriceanu, S.C., Rontescu, C., Bogatu, A. M., CICIC, D. T. (2023) Thermal field measurement during welding using infrared thermography. Scientific bulletin, 48, 167-178

[7] Armentani, E.; Esposito, R.; Sepe, R;(2007.) The effect of thermal proper-ties and weld efficiency on residual stresses in welding. *Journal of Achiev. in Materials and Manuf. Engineering*, *20*, 319-322 https://hdl.handle.net/11588/203634 (**journal article**)

[8] Armentani E.; Esposito, R; Sepe, R; (2006) Finite element analysis ofresidual stresses on butt welded joints.*Fatigue and Fracture, Heat Transfer, Internal Combustion Engines, Manufacturing, and Technology and Society*, *4*, https://doi.org/10.1115/ESDA2006-95125 (**journal article**)

[9] Hashemzadeh, M.; Chen, B. Q.; Guedes Soares, C. (2018). Evaluation of multi-pass welding-induced residual stress using numerical and experimental approaches.*Ships and Offshore Structures*,*13*(8), 847–856 https://doi.org/10.1080/17445302.2018.1470453 (**journal article**)

[10] ANSYS (2023)

[11] Celin,R., Berneti,J., Skobir Balanti, D. A. (2014) Welding of the steel grade S890QL. *Materials and Technology*, *48-6*, 931-935. http://mit.imt.si/izvodi/mit146/celin.pdf (**journal article**)

Društvo za tehniku zavarivanja Slavonski Brod

13. Međunarodno znanstveno-stručno savjetovanje SBZ 2025

„STROJARSKE TEHNOLOGIJE U IZRADI ZAVARENIH KONSTRUKCIJA I PROIZVODA, SBZ 2025."
Slavonski Brod, 08. i 09. 05. 2025.

Comparison of the robotic WiseThin MAG and conventional MAG welding process

M. Frajzman[1*],Z. Kožuh[1], I. Garašić[1], M. Šutalo[2], J. Eržišnik[1]

[1]Faculty of Mechanical Engineering and Naval Architecture, University of Zagreb, Croatia
[2]Cromatec d.o.o., Croatia

[*] Corresponding Author. E-mail: marko.frajzman@fsb.hr

Sažetak

Suvremeni zahtjevi tržišta te neprestani razvoj industrije doveli su do nastanka različitih inačica konvencionalnih postupaka zavarivanja. Razvoj novih materijala i potreba za povećanom produktivnošću potaknuli su inovacije u tehnologiji zavarivanja te time omogućili iskorak u produktivnosti, kontroli procesa i kvaliteti zavara. Jedan od produkata tih inovacija je razvoj WiseThin MIG/MAG postupka zavarivanja. Ovaj modificirani proces namijenjen je za zavarivanje tankostjenih radnih komada, pri čemu se kontroliranim prijenosom metala postiže stabilniji luk, manji unos topline i omogućuje precizna kontrola procesa zavarivanja u usporedbi s konvencionalnim postupkom. U eksperimentalnom radu provedeno je jednostrano kutno zavarivanje šest uzoraka od čelika S235JR robotiziranim MAG-D i WiseThin MAG postupkom. Iz tehnoloških razloga, odabrane su tri različite debljine radnih komada te su parametri zavarivanja prilagođeni u svrhu dobivanja jednake visine kutnog zavara za istu debljinu radnog komada. Cilj eksperimentalnog rada bio je usporediti značajke konvencionalnog MAG-D i WiseThin MAG postupka. Analizom rezultata ispitivanja dane su preporuke za zavarivanje tankostjenih radnih komada WiseThin MAG postupom.

Ključne riječi: MAG, WiseThin MAG, geometrija zavara

Abstract

Modern market demands and the continuous development of industry have led to the emergence of various versions of conventional welding processes. The development of new materials and the need for increased productivity have encouraged innovations in welding technology, thereby enabling a breakthrough in productivity, process control, and weld quality. One of the outcomes of these innovations is the development of the WiseThin MIG/MAG welding process. This modified process is intended for welding thin-walled workpieces, where controlled metal transfer achieves a more stable arc, and lower heat input and enables precise control of the welding process compared to the

conventional process. In the experimental work, single-sided fillet welding of six samples of S235JR steel was carried out using the robotic MAG-D and WiseThin MAG processes. For technological reasons, three different workpiece thicknesses were selected and the welding parameters were adjusted to obtain the same fillet weld height for the same workpiece thickness. The experimental work aimed to compare the characteristics of the conventional MAG-D and WiseThin MAG processes. Based on the analysis of the test results, recommendations were provided for welding thin-walled workpieces using the WiseThin MAG process.

Keywords: MAG, WiseThin MAG, weld geometry

1. Uvod

U tehnologiji spajanja metala zavarivanjem, MIG/MAG (engl. Metal Inert Gas/Metal Active Gas) postupak je najrelevantniji zbog svoje svestranosti u zavarivanju širokog spektra metala i njihovih legura koji se koriste u različitim granama industrijske proizvodnje [1]. Ovaj postupak zavarivanja se može primijeniti za zavarivanje ugljičnog, visokolegiranog i niskolegiranog čelika te za ostale vrste metala kao što su aluminij, bakar, titan i legure nikla [1]. Samim time, ovaj postupak se odlikuje i visokom produktivnošću, pouzdanošću, relativno jednostavnom edukacijom zavarivača te visokom mogućnošću automatizacije i robotizacije [2]. Automatizacija i robotizacija MIG/MAG postupka značajno povećava kontrolu i preciznost što rezultira poboljšanjem kvalitete zavara uz rast produktivnosti [3]. Zbog svoje svestranosti, razvijene su i različite modifikacije ovog postupaka u cilju povećanja produktivnosti, kvalitete zavara i smanjenja unosa topline tijekom procesa zavarivanja [2]. Jedna od najpoznatijih modifikacija ovog postupka je primjena pulsnog načina prijenosa metala čime se značajno doprinosi fleksibilnosti i stabilnosti uz manji unos topline u usporedbi s prirodnim prijenosom metala (Kratki spojevi, prijelazni luk i štrcajući luk) [2]. Jedna od najranijih modifikacija MIG/MAG postupka je primjena tandem zavarivanja ili dvostruke žice čime je značajno povećana produktivnost, međutim time dolazi i do velikog unosa topline u metal čime dolazi do povećanja zaostalih naprezanja i nastanka deformacije radnog komada [4]. Ovakvim povećanjem produktivnosti, dolazi do rasta proizvodnih troškova zbog potrebe za obradom radnog komada nakon zavarivanja u pogledu toplinske obrade i različitih mehaničkih zahvata [4]. Samim time, glavni cilj u razvoju modificiranih inačica MIG/MAG postupka bio je postizanje zavarenih spojeva zahtijevane kvalitete uz visoku produktivnost i mali unos topline [5]. Time su nastali modificirani postupci kao što su CMT (engl. Cold Metal Transfer), AC-MIG/MAG (engl. Alternating Current MIG/MAG), SA-MIG/MAG (engl. Spin-Arc MIG/MAG), NG-MIG/MAG (engl. Narrow Gap MIG/MAG), laser-MIG hibridno zavarivanje, te mnoge druge inačice različitih proizvođača izvora struje za zavarivanje [5]. Unatoč visokoj produktivnosti, postizanje zavarenih spojeva zahtijevane kvalitete modificiranim MIG/MAG postupcima ograničeno je manjkom istraživanja pojedinačnih inačica i prilagodbom samih parametra zavarivanja za konkretnu primjenu u industriji [5]. Također, razvojem umjetne inteligencije otvara se prostor za njenu implementaciju u sklopu

tehnologije zavarivanja čime bi se omogućila bolja kontrola procesa te prilagodba parametra zavarivanja u realnom vremenu [6].
U sklopu ovog rada analiziran je i testiran modificirani MIG/MAG postupak proizvođač opreme za zavarivanje Kemppi, pod nazivom WiseThin MAG. Ova inačica je razvijena u cilju jednostavnijeg zavarivanja tankostjenih radnih komada.

2. WiseThin MIG/MAG postupak zavarivanja

WiseThin modificirani MIG/MAG postupak zavarivanja karakterističan je po tome što koristi preciznu kontrolu parametara zavaravanja kao što su napona luka, brzina dodavanja žice i količina protok zaštitnog plina. Time se omogućuje primjena ovog postupka u industrijama koje zahtijevaju zavarivanje tankostjenih radnih komada kao što su automobilska, zrakoplovna i elektronička. WiseThin postupak temelji se na preciznom mjerenju i kontroli napona električnog luka u realnom vremenu pomoću povratnog kabela koji se spaja na radni komad koji se zavaruje kako je prikazano na **Pogreška! Izvor reference nije pronađen.**. Time se pomoću povratnog kabela omogućuje da modul izvora struje za zavarivanje prepozna kratki spoj kroz pad napona pri čemu struja zavarivanja raste i tali vrh žice stvarajući kapljicu „pinch" efektom. Kada izmjereni napon postigne odgovarajuću vrijednost, struja se smanjuje prije nego što se kapljica dodatnog metala odvoji i padne u talinu čime bi se završio kratki spoj (**Pogreška! Izvor reference nije pronađen.**). Samim time, kratki spoj završava u trenutku niže vrijednosti struje (**Pogreška! Izvor reference nije pronađen.**) u usporedbi s konvencionalnim prijenosom metala kratkim spojevima što rezultira prijenosom dodatnog materijala uz smanjenje rasprskavanja. Nakon prekida kratkog spoja, stvara se impuls struje koji zagrijava talinu, ali ne uzrokuje prijenos dodatnog materijala (**Pogreška! Izvor reference nije pronađen.**). [7]

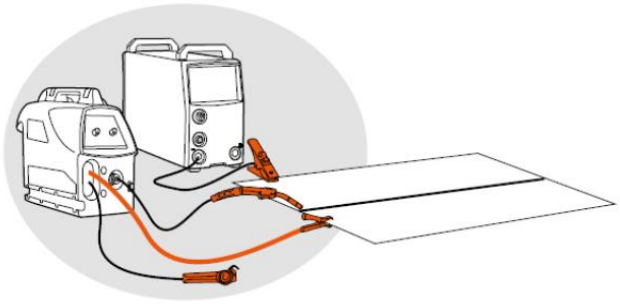

Slika 1 Shematski prikaz opreme za WiseThin MIG/MAG postupak [7]

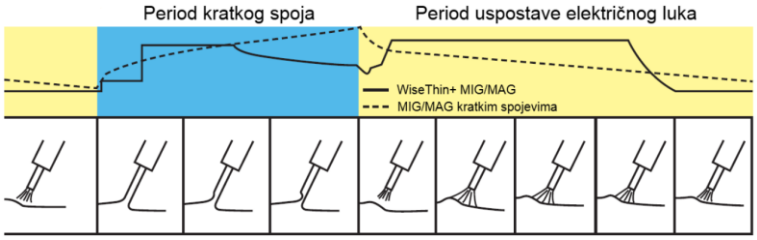

Slika 2 Usporedba WiseThin s konvencionalnim MAG prijenosom metala kratkim spojevima [7]

Glavne prednosti WiseThin MIG/MAG postupka su značajno smanjenje rasprskavanja te smanjenje unosa topline, a time i zaostalih naprezanja i deformacija. Također, ovim modificiranim postupkom se omogućuju veće brzine zavarivanja i kraće vrijeme proizvodnog ciklusa uslijed smanjenja obrade radnih komada nakon zavarivanja. [7]

3. Eksperimentalni dio

U sklopu ovog ispitivanja izrađeno je šest uzoraka od konstrukcijskog čelika oznake S235JR (Tablica 1) prema normi HRN EN 10027-1:2016. Uzorci su laserski rezani u obliku pravokutnih ploča dimenzije 300x150 mm pri čemu su se debljine odabranog osnovnog materijala varirale te su bile 1,5 mm, 2 mm i 3 mm. Jednostrano kutno zavarivanje ploča ispitnih uzoraka provedeno je u PA položaju robotiziranim MAG-D i WiseThin postupkom u cilju dobivanja jednake visine kutnog zavara. Iz tehnoloških razloga za debljinu osnovnog metala od 1,5 mm odabrana je visina kutnog zavara 2 mm, za debljinu od 2 mm odabrana je visina kutnog zavara 2,5 mm te za debljinu od 3 mm odabrana je visina kutnog zavara od 3 mm. Tijekom zavarivanja je korištena dvokomponentna mješavina zaštitnog plina u volumnom omjeru 82 % Ar i 18 % CO_2, oznake M21 ArC 18 prema normi HRN EN ISO 14175:2008. Uzorci su time podijeljeni u 3 skupine ovisno o debljini osnovnog metala te je za svaku debljinu izrađen jedan uzorak MAG-D i WiseThin postupkom prema parametrima prikazanim u Tablica 2. Vrijednosti struje i napon tijekom procesa zavarivanja su bile konstantne, stoga je električni luk bio stabilan. Kod WiseThin postupka, za istu jakost struje i napona zavarivanja kao kod MAG postupka, brzina dobave žice je veća u odnosu na MAG postupak zavarivanja. Samim time, bila je nužna prilagodba brzine zavarivanja kako bi se postigla što ujednačenija geometrija zavara ali uz manji unos topline (Tablica 2).

Tablica 1 Kemijski sastav čelika S235JR prema normi HRN EN 10025-2:2019

Maseni udio legirnih elementa, %					
C	Mn	P	S	N	Cu
≤ 0,17	≤ 1,4	≤ 0,035	≤ 0,035	≤ 0,12	≤ 0,55

Tablica 2 Parametri zavarivanja uzoraka

Uzorak	1	2	3	4	5	6
Debljina osnovnog materijala, mm	1,5	1,5	2,0	2,0	3,0	3,0
Postupak zavarivanja	MAG-D	WiseThin	MAG-D	WiseThin	MAG-D	WiseThin
Protok plina, l/min	15					
Vrsta zaštitnog plina	M21 ArC 18					
Duljina slobodnog kraja žice, mm	10					
Položaj zavarivanja	PA					
Struja zavarivanja, A	131	145	125	125	161	161
Napon zavarivanja, V	17,4	17,2	17,2	17,2	18,5	18,0
Brzina dobave žice, m/min	5,0	6,3	4,5	5,3	6,0	6,6
Brzina zavarivanja, cm/min	55	70	37,5	41	34	40
Unos topline, kJ/cm	2,065	1,710	2,752	2,517	4,204	3,478

Zavarivanje uzoraka provedeno je na robotskoj stanici (Slika 3a) koja se sastoji od robota za zavarivanje FANUC ArcMate 100iD, upravljačke jedinice, izvora struje za zavarivanje Kemppi A7 MIG s pripadajućim hladnjakom, stanice za održavanje i čišćenje pištolja za zavarivanje te dvoosnog pozicionera A05B-1220-J201. Kao dodatni materijal koristila se puna žica promjera 1,0 mm za zavarivanje ugljičnih i niskolegiranih čelika oznake G 42 4 M21 G 3Si1 (HRN EN ISO 14341:2017). Prije samog zavarivanja, izrezane ploče radnog komada su temeljito očišćene i odmašćene 96 % denaturiranim etanolom te je u steznoj napravi izvršeno njihovo međusobno pripajanje po duljini u T-spoj (Slika 3b) kako bi se osigurala krutost spoja i time spriječilo njihovo eventualno pomicanje tijekom procesa zavarivanja. Nakon pripajanja, uzorci su stegnuti na pozicioner robota čime je omogućeno jednostrano kutno zavarivanje u PA položaju kako je prikazano na Slika 3c. Korištena je lijeva tehnika rada s kutom nagiba pištolja za zavarivanje od 10 °.

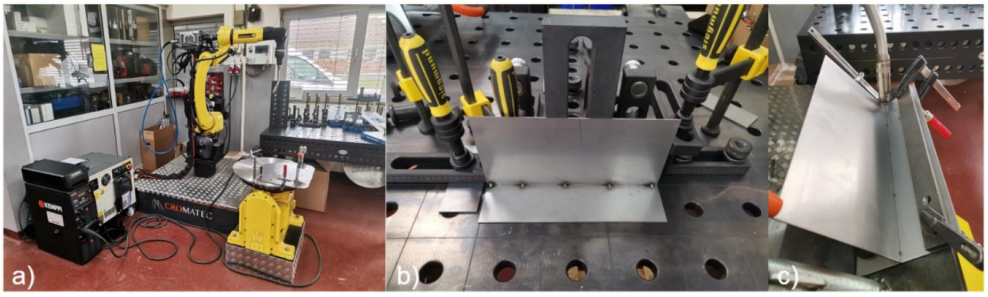

Slika 3 Priprema uzoraka za zavarivanje

Nakon zavarivanja uzorci su ostavljeni da se ohlade na zraku te ponovno očišćeni četkom, te su odmašćeni 96 % denaturiranim etanolom kako bi se dobio čim bolji uvid u izgled lica zavara ovisno o tome dali su uzorci zavareni MAG-D ili WiseThin postupkom. Pregledom lica zavara svih šest ispitnih uzoraka uočeno je manje rasprskavanje kod uzoraka 2, 4 i 6 (Slika 4) koji su zavareni WiseThin postupkom. Također, tragovi rasprskavanja su manji kod uzoraka 2, 4 i 6 (Slika 4).

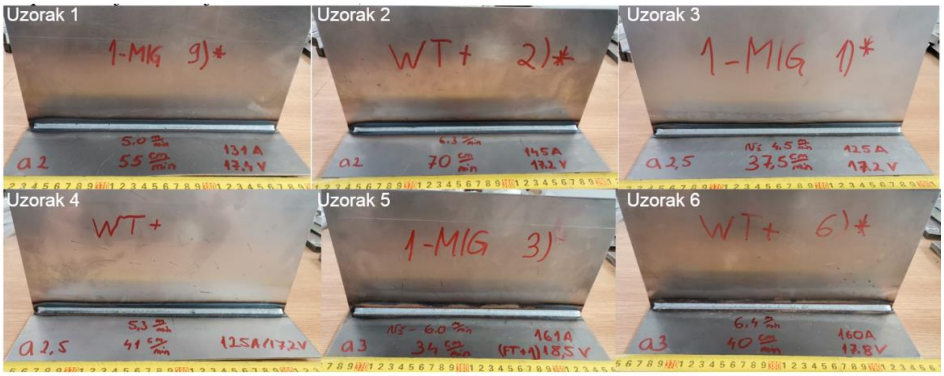

Slika 4 Uzorci nakon provedenog zavarivanja

Pregleda površine uzoraka, kutni spojevi režu se tračnom pilom na označenim presjecima na dimenzije 25x50x35 mm. Provedenim izrezivanjem uzoraka, provodi se grubo brušenje na uređaju Mecatech 250 s različitim granulacijama brusnog papira: P240, P320 i završno P400. Poliranje uzoraka provedeno je na uređaju Mecatech 250 sa sljedećim granulacijama brusnog papira: P600, P1000, P2400 i završno superpoliranje P4000. Provedenim poliranjem, uzorci su kemijski nagrizani u 3 % otopini dušične kiseline i alkohola te isprani vodom kako bi se prekinula kemijska reakcija te su nakon toga osušeni na zraku. Nakon sušenja, na uzorcima se jasno može razlikovati metal zavara i osnovni metal, a zona utjecaj topline nije vidljiva kao što se može vidjeti na Slika 5.

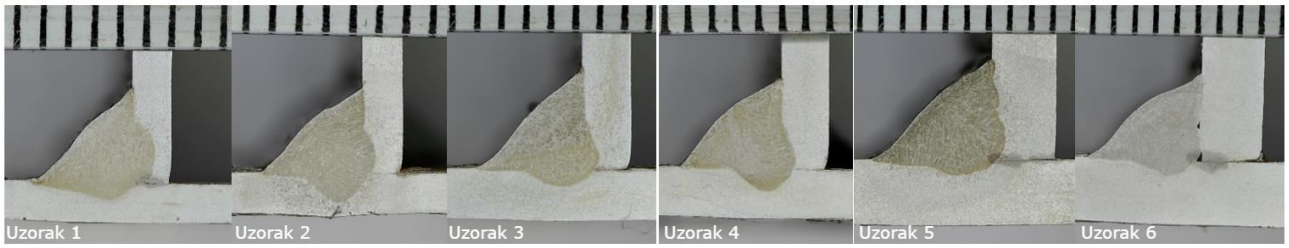

Slika 5 Makroizbrusci ispitnih uzoraka

4. Analiza rezultata

4.1 Kvantitativna analize makrostrukture

Uzorci se nakon nagrizanja fotografiraju te se s pomoću dobivenih fotografija analizira makrostruktura. U programu ImageJ provedeno je mjerenje geometrijskih karakteristika kao što su

katete kutnog zavara (z1, z2), visina kutnog zavara (a), širina (b), nadvišenje (h) i penetracija korijena (p) metala zavara kao što je prikazano na Slika 6. Također, mjerena i površina metala zavara (P), a rezultati mjerenja svih navedenih veličina prikazani su u Tablica 3.

Tablica 3 Rezultati mjerenja geometrijskih karakteristika zavara

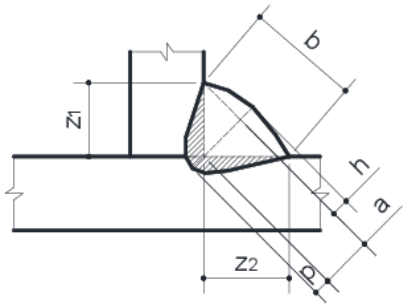

Slika 6 Oznake mjernih veličina

Oznaka uzorka	z1 [mm]	z2 [mm]	a [mm]	h [mm]	b [mm]	p [mm]	P [mm^2]
Uzorak 1	3,557	4,091	2,519	0,185	5,418	0,277	10,717
Uzorak 2	3,148	3,725	2,226	0,544	4,877	0,221	9,518
Uzorak 3	4,090	4,284	2,883	0,206	5,940	0,429	11,834
Uzorak 4	3,738	4,315	2,635	0,680	5,683	0,561	12,513
Uzorak 5	4,688	5,661	3,315	0,612	7,331	0,187	17,892
Uzorak 6	3,941	5,431	2,787	1,020	6,706	-	14,265

Uspoređujući rezultate mjerenja prikazanih u Tablica 3 i Slika 7 može se vidjeti da su vrijednosti visine kutnog zavara (a) kod svih šest ispitnih uzoraka veće kod uzoraka 1, 3 i 5 koji su zavareni MAG-D postupkom (Slika 7). Za debljine radnog komada od 1,5 i 2 mm kod sva četiri ispitna uzoraka je postignuta željena visina kutnog zavara (Slika 7). Međutim, za debljinu radnog komada od 3 mm, kod uzorka 6 zavarenog WiseThin postupkom, visina kutnog zavara iznosi 2,787 mm te time nije postignuta željena visina kutnog zavara od 3 mm (Slika 7), a kod uzorka 5 zavarenog MAG-D postupkom je postignuta te iznosi 3,315 mm. Lice metala zavara je kod svih šest uzoraka konveksnog oblika, pri čemu je veće nadvišenje (h) postignuto kod uzoraka 2, 4 i 6 koji su zavareni WiseThin postupkom. Uspoređujući vrijednosti širine metala zavara (b), jasno je vidljivo (Slika 7) da je kod uzoraka 2, 4 i 6 koji su zavareni WiseThin kod sve tri debljine radnog komada postignuta manja širina zavara u odnosu na uzorka 1, 3 i 5 koji su zavareni MAD-D postupkom (Slika 7). Vrijednosti penetracije korijena (p) značajno se razlikuju ovisno o debljini radnog komada koji se zavaruje (Slika 7). Za debljine radnog komada od 1,5 postignuta je manja penetracija kod uzorka 2 (p=0,221 mm) koji je zavaren WiseThin postupkom u odnosu na uzorak 1 (p=0,277 mm) koji je zavaren MAG-D postupkom . Međutim, za debljinu radnog komada od 2 mm, kod uzorka 4 koji je zavaren WiseThin postupkom postignuta je veća penetracija korijena (p=0,561 mm) u odnosu na uzorak 3 (p=0,429

mm) zavaren MAG-D postupkom. Kod debljine radnog komada od 3 mm, kod uzorka 5 je postignuta penetracija korijena od 0,187 mm čime je i to najmanja vrijednost od svih uzoraka zavarenih MAG-D postupkom (Slika 7). Također, kod uzorka 6 koji je zavaren WiseThin nije postignuta penetracija korijena te je i sam metal zavara djelomično nalijepljen (Slika 5). Površine metala zavara (P) također se značajno razlikuju ovisno o debljini radnog komada. Kod debljine radnog komada od 1,5 mm veća površina je postignuta kod uzorka 1 koji je zavaren MAG-D postupkom te je razlika 1,2 mm^2 u površini metala zavara. Za debljinu radnog komada od 2 mm, veća površina metala zavara postignuta je kod uzorka 4 koji je zavaren WiseThin postupkom, a razlika u površini metala zavara iznosi 0,68 mm^2. Međutim, kod debljine radnog komada od 3 mm, veća površine metala zavara postignuta je kod uzorka 5 zavarenog MAG-D postupkom te je razlika u površinama značajno veća i iznosi 3,327 mm^2 što je i najveća razlika za sve debljine radnog komada.

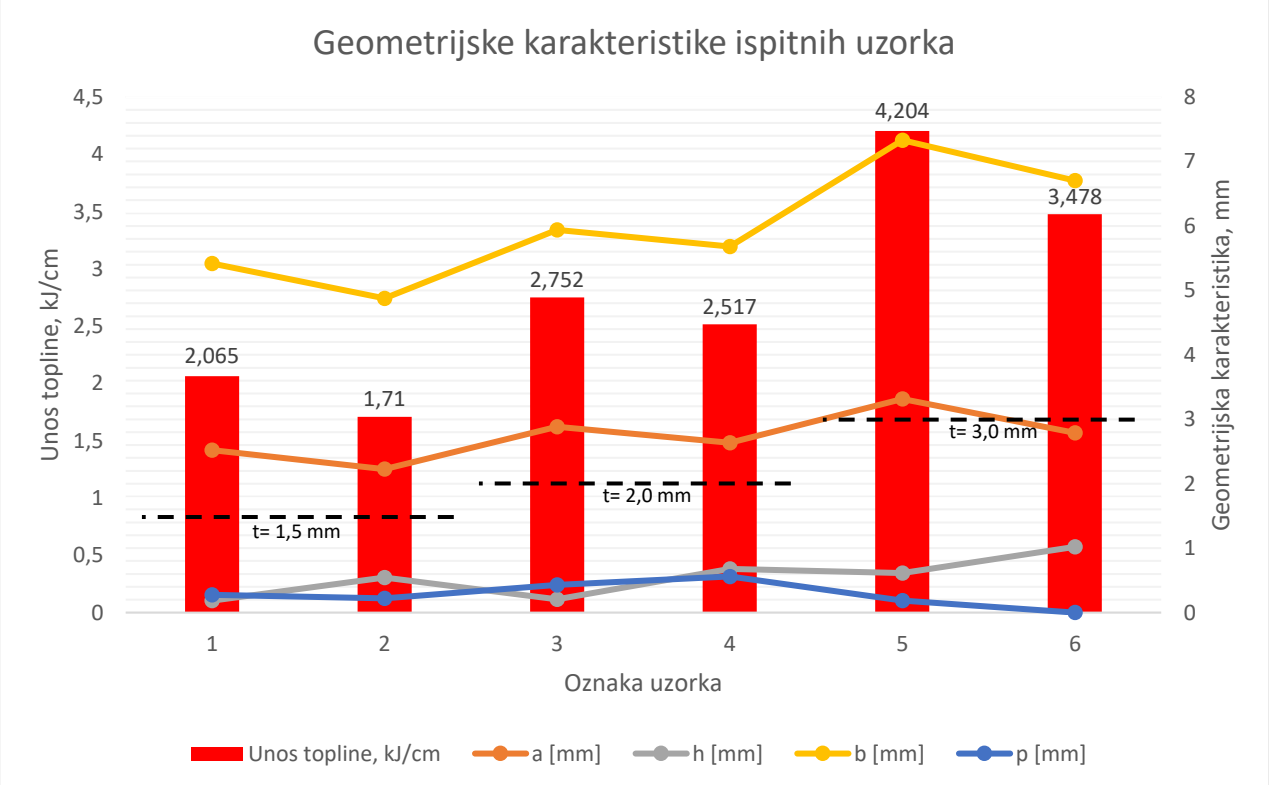

Slika 7 Graf odnosa unosa topline i geometrijskih karakteristika ispitnih uzoraka

5. Zaključak

Na temelju kvantitativne analize makrostrukture ispitnih uzoraka, doneseni su sljedeći zaključci o prikladnosti WiseThin MIG/MAG postupka za zavarivanje tankostjenih radnih komada:

- WiseThin postupkom se postiže veće nadvišenje zavara i manje rasprskavanja u odnosu na konvencionalni MAG-D postupak,

- uz manji unos topline, WiseThin postupkom se postiže željena visina kutnog zavara kod debljina radnog komada od 1,5 i 2 mm,
- za debljinu radnog komada od 3 mm, WiseThin postupkom se ne postiže željena visina kutnog zavara od 3 mm, te su uočene nepravilnosti naljepljivanja i nedovoljnog provara u korijenu,
- širina kutnog zavara, je za sve tri debljine ranog komada manja kod WiseThin postupka.

Samim time, preporučuje se primjena WiseThin MIG/MAG postupka kod zavarivanja tankostjenih radnih komada do 2 mm debljine. Time se postižu tražene geometrijske karakteristike metala zavara uz manji unos topline i povećanu produktivnost u usporedbi s konvencionalnim MAG-D postupkom. Za zavarivanje većih debljina radnog komada od 2 mm, potrebna je dodatna prilagodba parametara zavarivanja povećanjem struje a time i brzine dobave žice za istu brzinu zavarivanja. Također, moguća je modifikacija parametara primjenom neutralne ili desne tehnike rada.

6. Literatura

[1] A. Trindade, 'Innovation in Welding in Terms of Processes, Weldability or Design Connections', 2024. doi: 10.5772/intechopen.1005436.

[2] J. C. Dutra, R. H. Gonçalves e Silva, K. C. Riffel, and C. Marques, 'High-performance GMAW process for deep penetration applications', Welding in the World, vol. 64, no. 6, pp. 999–1009, Jun. 2020, doi: 10.1007/s40194-020-00889-0.

[3] G. Tukahirwa, C. Wandera, G. Tukahirwa, and C. Wandera, 'Influence of Process Parameters in Gas-Metal Arc Welding (GMAW) of Carbon Steels', in Welding - Materials, Fabrication Processes, and Industry 5.0, IntechOpen, 2023. doi: 10.5772/intechopen.1002730.

[4] E. Spaniol et al., 'Development of a highly productive GMAW hot wire process using a two-dimensional arc deflection', Welding in the World, vol. 64, no. 5, pp. 873–883, May 2020, doi: 10.1007/s40194-020-00880-9.

[5] G. M. S. Silveira et al., 'Microstructural characterization and mechanical properties of high-strength steel weld metals obtained by GMAW process with rotating electrode (GMAW-RE)', Journal of the Brazilian Society of Mechanical Sciences and Engineering, vol. 43, no. 4, p. 221, Mar. 2021, doi: 10.1007/s40430-021-02932-7.

[6] R. Thompson Martínez, G. Alvarez Bestard, A. Martins Almeida Silva, and S. C. Absi Alfaro, 'Analysis of GMAW process with deep learning and machine learning techniques', Journal of Manufacturing Processes, vol. 62, pp. 695–703, Feb. 2021, doi: 10.1016/j.jmapro.2020.12.052.

[7] Kemppi Oy: WiseThin+, Internal Document, Kemppi Oy, Lahti, Finska, 2022.

Properties of the heat affected zone of high-strength steels

M. Horvat[1,*], Z. Botak[1], K. Pisačić[1], Z. Busija[1], K. Nová[2]

[1]Sveučilište Sjever, Varaždin, Hrvatska
[1]Sveučilište u Slavonskom Brodu, Strojarski fakultet u Slavonskom Brodu, Hrvatska

[*]Corresponding Author E-mail: marko.horvat@unin.hr

Sažetak

Zona utjecaja topline (ZUT) je dio osnovnog materijala, koji se nalazi uz rastaljenu zonu zavarenog spoja, a gdje dolazi do promjene mikrostrukture i mehaničkih svojstava zbog topline unesene procesom zavarivanja. Ova zona vrlo često predstavlja najveće izazove u projektiranju tehnologije zavarivanja. S obzirom na primjenu kombinacije različitih mehanizama očvrsnuća s ciljem dobivanja specifičnih mehaničkih svojstava visokočvrstog čelika, zona utjecaja topline ove grupe čelika razlikuje se od zone utjecaja topline konvencionalnih nelegirani čelika. U radu su prezentiranme mikrostrukturne promjene i specifičnosti zone utjecaja topline visokočvrstih QT čelika.

Ključne riječi: visokočvrsti čelici, zona utjecaja topline

Abstract

Heat affected zone (HAZ) is the part of the base material that is located next to the molten zone of the welded joint, where changes in microstructure and mechanical properties occur due to the heat input during the welding process. This zone often presents the greatest challenges in the design of welding technology. Given the application of a combination of different strengthening mechanisms aimed at achieving specific mechanical properties in high strength steels, the heat affected zone of this group of steels differs from the heat affected zone of conventional unalloyed steels. The paper presents microstructural changes and specific characteristics of the heat affected zone of high strength QT steels.

Keywords: heat affected zone, high strength steels

1. Uvod

Zona utjecaja topline (ZUT) igra ključnu ulogu u svojstvima zavarenih spojeva, osobito kod visokočvrstih čelika. Za razliku od konvencionalnih ugljičnih čelika, visokočvrsti čelici, posebno oni

isporučeni u poboljšanom stanju (kaljeni i popušteni – QT), pokazuju specifična svojstva u ZUT-u koja su posljedica primjene različitih mehanizama očvrsnuća. U ovom radu opisane su mikrostrukturne promjene i mehanička svojstva koja se javljaju u ZUT-u QT čelika u procesu zavarivanja. [1-6]

2. Zona utjecaja topline kod visokočvrstih QT čelika

Zona utjecaja topline (ZUT) kod visokočvrstih QT čelika pokazuje specifične mikrostrukturne promjene uslijed toplinskih ciklusa tijekom zavarivanja. Zbog njihove početne mikrostrukture, koja je rezultat termomehaničkih obrada, ovi čelici posebno su osjetljivi na promjene u ZUT-u, koje mogu narušiti njihova izvorna mehanička svojstva. ZUT kod visokočvrstih QT čelika sastoji se od četiri karakteristične zone.

- zona pogrubljenja zrna (CGHAZ – Coarse-Grained Heat-Affected Zone)
- zona normalizacije/zona sitnog zrna (FGHAZ – Fine-Grained Heat-Affected Zone)
- zona djelomične rekristalizacije (ICHAZ – Intercritical Heat-Affected Zone)
- zona popuštanja (temperatura ispod 700 °C) [1-6]

2.1. Zona pogrubljenja zrna (CGHAZ – Coarse-Grained Heat-Affected Zone)

Zona pogrubljenja zrna (CGHAZ) smještena je uz liniju staljivanja, granicu sa zonom taljenja i metalom zavara, gdje temperature tijekom zavarivanja dosežu od približno 1100 °C do 1500 °C. U ovom temperaturnom rasponu dolazi do značajnog povećanja veličine zrna, koja ostaju povećana nakon hlađenja na sobnu temperaturu. Najveća zrna nalaze se u dijelu koji je najbliži zavaru, gdje su temperature bile najviše. Zrna u CGHAZ-u obično su 5-15 puta veća od zrna u osnovnom metalu na sobnoj temperaturi, a njihov rast ovisi o kemijskom sastavu čelika. Manji unos topline tijekom zavarivanja rezultira užim područjem krupnih zrna, uz prisutnost manjih zrncima u ostatku zone.

Ciklus temperature u CGHAZ-u, koji traje kratko, čini ovu zonu uskom u odnosu na druge dijelove ZUT-a. Mikrostruktura pri vršnim temperaturama uglavnom je austenitna, a nakon hlađenja transformira se u martenzit, bainit ili njihovu kombinaciju, ovisno o brzini hlađenja i kemijskom sastavu čelika. Povećanje veličine zrna obično smanjuje žilavost, što čini CGHAZ najniže žilavom zonom u cijelom ZUT-u. [1-6]

2.2. Zona normalizacije/zona sitnog zrna (FGHAZ – Fine-Grained Heat-Affected Zone)

Zona normalizacije, odnosno zona sitnog zrna (FGHAZ), obuhvaća područje koje tijekom zavarivanja dostiže temperature u rasponu od približno 900 °C do 1100 °C. U tom temperaturnom području dolazi do potpune austenitizacije i rekristalizacije, pri čemu se formiraju sitna zrna. Fina mikrostruktura u ovoj zoni doprinosi povećanoj žilavosti i stabilnosti mehaničkih svojstava.

Tijekom hlađenja, austenit se transformira u martenzit, bainit ili njihovu kombinaciju, ovisno o kemijskom sastavu čelika i brzini hlađenja. Fina veličina zrna u ovoj zoni pozitivno utječe na otpornost prema krhkom lomu i umanjuje negativne učinke koji se javljaju u zonama s krupnijom mikrostrukturom, poput CGHAZ-a. [1-6]

2.3. Zona djelomične rekristalizacije (ICHAZ – Intercritical Heat-Affected Zone)

Zona djelomične rekristalizacije (ICHAZ) nalazi se između FGHAZ-a i zone popuštanja, a tijekom zavarivanja doseže temperature u rasponu od približno 700 °C do 900 °C. Budući da se radi o interkritičnom području, dolazi do djelomične austenitizacije – pri čemu dio mikrostrukture prelazi u austenit, dok ostatak ostaje u izvornom stanju.

Nakon hlađenja, nova faza (najčešće martenzit) formira se unutar matrice prethodno popuštenog martenzita ili bainita, što dovodi do heterogene mikrostrukture. Ova mikrostrukturna nehomogenost često uzrokuje smanjenje čvrstoće i žilavosti u odnosu na zone s homogenijom strukturom. Zrna u ICHAZ-u ostaju relativno mala, ali su veća nego u FGHAZ-u, a lokalna kemijska segregacija može dodatno negativno utjecati na mehanička svojstva. [1-6]

2.4. Zona popuštanja

Zona popuštanja je dio zone utjecaja topline (ZUT) u kojem vršne temperature tijekom zavarivanja ostaju ispod približno 700 °C. U ovom temperaturnom rasponu ne dolazi do austenitizacije (strukturnih promjena) niti do značajnog rasta zrna. Unatoč tome, mogu se pojaviti mikrostrukturne promjene u obliku precipitacije karbida i intermetalnih spojeva, kao i promjene u distribuciji sekundarnih čestica koje su prethodno pridonosile očvršćivanju materijala. To može rezultirati smanjenjem tvrdoće i čvrstoće u ovoj zoni.

Nakon hlađenja na sobnu temperaturu, mikrostruktura obično uključuje popušteni martenzit, bainit ili njihovu kombinaciju. Iako je ova zona strukturno stabilna, lokalno smanjenje mehaničkih svojstava može nepovoljno utjecati na cjelokupnu pouzdanost zavarenog spoja. [1-6]

3. Usporedba s konvencionalnim ugljičnim čelicima

Zona utjecaja topline (ZUT) u visokočvrstim QT čelicima značajno se razlikuje od one u konvencionalnim ugljičnim čelicima zbog njihove početne mikrostrukture i prisutnosti više mehanizama očvrsnuća, čiji se efekt može izgubiti tijekom zavarivanja. Visokočvrsti QT čelici u poboljšanom stanju podvrgnuti su procesu kaljenja i popuštanja, čime se dobiva mikrostruktura s

izraženim mehaničkim svojstvima. Zavarivanjem se ti efekti mogu narušiti, osobito u pojedinim zonama ZUT-a.

Za razliku od visokočvrstih čelika, kod konvencionalnih ugljičnih čelika ZUT obuhvaća sljedeće zone: djelomično rastaljena zona, zona pregrijanja, zona normalizacije, zona djelomične prekristalizacije, rekristalizacijska zona, zona starenja i zona plavog loma. Ove zone obično pokazuju predvidljivije mikrostrukturne promjene pri zavarivanju i manju osjetljivost na gubitak mehaničkih svojstava.

Visokočvrsti QT čelici zbog većeg udjela legirajućih elemenata i prisutnih mehanizama očvrsnuća dodatno su osjetljivi na toplinske cikluse, a mikrostrukturne transformacije u njihovom ZUT-u uključuju fazne promjene koje mogu nepovoljno utjecati na žilavost i čvrstoću. Nadalje, zbog izraženije toplinske vodljivosti i manjeg dopuštenja za rast zrna, ZUT u ovim čelicima zahtijeva pažljivu kontrolu parametara zavarivanja kako bi se spriječile degradacije svojstava. [1-6]

5. Zaključak

Razumijevanje mikrostrukturnih promjena u ZUT-u visokočvrstih QT čelika ključno je za optimizaciju procesa zavarivanja i osiguranje željenih mehaničkih svojstava zavarenog spoja. Svaka od karakterističnih zona ZUT-a – zona pogrubljenja zrna, zona normalizacije/sitnog zrna, zona djelomične rekristalizacije i zona popuštanja – ima specifičan temperaturni raspon i mikrostrukturne transformacije koje utječu na čvrstoću, žilavost i krhkost zavarenog spoja.

Osim toga, nekoliko drugih faktora igra ključnu ulogu u oblikovanju svojstava ZUT-a. Na primjer, pogrešno odabrane vrijednosti parametra vremena $t_{8/5}$ mogu značajno negativno utjecati na vrijednosti prijelazne temperature, stvaranje poligonalnog ferita te smanjenje žilavosti i čvrstoće. također, isti parametar može utjecati i na stvaranje nepovoljnog martenzita i povećati rizik od hladnih pukotina. Također, minimizacija "jarka tvrdoće" u dijelu ZUT-a između temperature popuštanja i A1, kao i kontrola ulaska atomarnog vodika u zavareni spoj, smanjuju mogućnost pojave hladnih pukotina.

Važan utjecaj na ZUT imaju i mikrolegirni elementi koji oblikuju razvoj precipitata i intermetalnih spojeva, te niže vrijednosti primarnog unosa topline, poput temperature predgrijavanja, koje mogu pozitivno utjecati na mikrostrukturalne transformacije. Nemogućnost primjene naknadnih toplinskih obrada i pojava zaostalih naprezanja također predstavljaju izazove koji mogu negativno utjecati na svojstva zavarenog spoja.

U konačnici, precizna kontrola svih ovih faktora tijekom zavarivanja i pravilno upravljanje parametrima procesa ključni su za smanjenje negativnih učinaka ZUT-a i postizanje željenih

svojstava zavarenih spojeva, čime se doprinosi poboljšanju dugoročne pouzdanosti i funkcionalnosti konstrukcija.

6. Reference

1. Lüder, K., & Löffler, J. F. (2012). Heat-affected zone and weldability of high-strength steels. Materials Science and Engineering: A, 536, 1-9.
2. Yuan, H., Liu, Z., & Guo, X. (2016). Microstructure and mechanical properties of the heat-affected zone in high strength low alloy steels. Science and Technology of Welding & Joining, 21(6), 453-460.
3. Tóth, L., & Balázs, T. (2010). Effect of heat input on the microstructure and mechanical properties of the heat-affected zone in welded joints of high-strength steels. Journal of Materials Processing Technology, 210(10), 1413-1419.
4. Marrs, D., & Houldcroft, P. (2014). Welding of high-strength steels: Effect of welding parameters on microstructure and properties. Journal of Constructional Steel Research, 98, 104-112.
5. Rajasekaran, S., & Suresh, S. (2018). Effect of welding on microstructure and mechanical properties of high-strength steels. Materials Characterization, 137, 165-178.
6. SSAB., SSAB Welding Handbook, A Guide to Better welding of Hardox and Weldox

Cold cracks in welded joints of high strength steels

M. Horvat[1,*], Z. Botak[1], K. Pisačić[1], Z. Busija[1], I. Samardžić[2]

[1]Sveučilište Sjever, Varaždin, Hrvatska
[2]Sveučilište u Slavonskom Brodu, Strojarski fakultet u Slavonskom Brodu, Hrvatska

[*]Corresponding Author E-mail: marko.horvat@unin.hr

Sažetak

S obzirom na mehanička i kemijska svojstva čelika te stanje mikrostrukture, čelici pokazuju veću ili manju sklonost prema određenim pogreškama uslijed primjene procesa zavarivanja. Daleko najopasnije pogreške u zavarenim spojevima predstavljaju pukotine. Unutar grupe visokočvrstih čelika poseban problem predstavljaju hladne pukotine. U radu su prikazani osnovni uzročnici nastajanja hladnih pukotina te osnovne mjere za sprečavanje istih.

Ključne riječi: hladne pukotine, visokočvrsti čelici

Abstract

Given the mechanical and chemical properties of steel and the state of the microstructure, steels show a greater or lesser tendency towards certain defects due to the application of the welding process. The most dangerous defects in welded joints are cracks. Within the group of high strength steels, cold cracks present a particular problem. The paper presents the main causes of cold cracks and the basic measures for their prevention.

Keywords: cold cracks, high strength steels

1. Uvod

Visokočvrsti čelici pokazuju specifične karakteristike u pogledu otpornosti na različite vrste pogrešaka u zavarenim spojevima, među kojima se posebno izdvaja problem hladnih pukotina. Hladne pukotine, poznate i kao vodikove pukotine, nastaju uslijed prisutnosti vodika u spoju i mogu se formirati u ZUT-u (zoni utjecaja topline) i ZT-u (zoni taljenja). Zbog izraženih mehaničkih svojstava i specifičnog mikrostrukturnog stanja, visokočvrsti čelici imaju povećan rizik od nastanka ovog tipa pogrešaka. Pravilnim projektiranjem tehnologije zavarivanja, uključujući kontrolu unosa

topline (primarnu i sekundarnu), uvjeta ohlađivanja i primjenu odgovarajućih dodatnih materijala, moguće je značajno smanjiti rizik od nastanka hladnih pukotina. [1]

2. Uzroci nastanka hladnih pukotina

Hladne pukotine nastaju tijekom hlađenja zavarenog spoja nakon završetka zavarivanja, obično kada temperatura u spoju padne ispod 200 °C. Ove pukotine mogu se inicirati i razviti nekoliko sati nakon završetka zavarivanja, a detekcija potencijalnih pukotina najčešće se provodi unutar 16 do 48 sati). Formiranje (nastanak) hladnih pukotina uvjetovano je interakcijom tri osnovna faktora:

a) udjelu legirnih elemenata u osnovnom i/ili dodatnom materijalu:

- legirajući elementi poput ugljika, mangana, silicija i drugih često prisutnih elemenata mogu povećati sklonost nastanku hladnih pukotina
- legirni elementi mogu utjecati na raspodjelu naprezanja i smanjiti duktilnost materijala, čime osiguravaju povoljne uvjete za nastanak pukotina
- visoki sadržaj ugljika povećava krhkost čelika, što povećava rizik od razvoja hladnih pukotina.

b) visoka koncentracija vodika u spoju

- vodik, koji može doći iz okoliša, zavarivačkih plinova, potrošnog materijala ili neadekvatnih uvjeta zavarivanja, igra ključnu ulogu u formiranju hladnih pukotina
- obzirom na to da vodik smanjuje duktilnost materijala, povećava sklonost čelika ka krhkosti, osobito pri nižim temperaturama
- sadržaj vodika u spoju mora biti dovoljan da bi došlo do inicijacije pukotine, a visoki udio vodika može značajno smanjiti sposobnost materijala da podnese naprezanja, čak i u slučajevima niskih naprezanja.

c) prisutnost naprezanja u spoju

- naprezanja koja nastaju tijekom procesa zavarivanja, osobito zbog nejednolikiih brzina hlađenja ili stazanja materijala, mogu stvoriti uvjete pogodne za nastanak hladnih pukotina
- naprezanja mogu biti izazvana i velikim temperaturnim gradijentima, što dovodi do stvaranja napetosti u spoju, čime se povećava vjerojatnost nastanka pukotina, osobito kada su u kombinaciji s visokim koncentracijama vodika.

Interakcija ovih čimbenika omogućuje da čak i pri nižim vrijednostima naprezanjima, uz povećanu koncentraciju vodika u spoju, može doći do razvoja pukotina. Iako postoje brojni modeli koji nastoje opisati međusobnu povezanost ovih faktora, mehanizam inicijacije hladnih pukotina nije potpuno razjašnjen. Razumijevanje ovih interakcija ključno je za smanjenje rizika i implementaciju

učinkovitih preventivnih mjera. Kada dođe do nastanka hladne pukotine, ona se obično širi okomito na smjer glavnih naprezanja u spoju.

U kontekstu visokočvrstih čelika, preporučuju se različiti modeli koji pomažu u procjeni otpornosti prema hladnim pukotinama, temeljenih na ekvivalentu ugljika (CE). Ovaj parametar izračunava se na temelju kemijskog sastava čelika, uzimajući u obzir udio ključnih legirajućih elemenata, čime se omogućuje predviđanje sklonosti materijala prema nastanku hladnih pukotina. Preporučuje se način izračuna ekvivalenta ugljika sukladno preporukama proizvođača osnovnog materijala. [1-9]

3. Ključni čimbenici za pojavu i sprječavanje hladnih pukotina u visokočvrstim čelicima

A. Utjecaj legirnih elemenata u osnovnom materijalu
Sadržaj legirnih elemenata u visokočvrstim čelicima obično je nizak, no specifični legirni elementi imaju ključnu ulogu u postizanju željenih mehaničkih svojstava (sudjeluju u ostarivanju specifičnih mehanizama očvrsnuća). Ipak, i vrlo niski udjeli nekih od legirnih elemenata mogu povećati osjetljivost na vodikove pukotine, osobito u zoni utjecaja topline (ZUT). Temeljem navedenog, kao vrlo važan alat u spečavanju pojave hladnih pukotina može se upotrijebiti izračun vrijednosti ekvivalenta ugljika pomoću CET ili CEV modela. Ovaj parametar omogućuje procjenu sklonosti materijala prema pojavi hladnih pukotina uz dodatno razmatranje primjene procesa predgrijavanja. Ipak, obzirom na primjenjene mehanizme očvrsnuća u visokočvrstom čeliku, preporuke za predgrijavanje temelje se na detaljnim analizama, uključujući primjenu standardnih laboratorijskih metoda za procjenu sklonosti prema hladnim pukotinama. [1-9]

B. Utjecaj legirnih elemenata u nelegiranim i niskolegiranim dodatnim materijalima
Izbor dodatnih materijala za zavarivanje visokočvrstih čelika može značajno utjecati na rizik od nastanka hladnih pukotina. U tom slučaju važno je poznavati i vrijednost ekvivalenta ugljika dodatnog materijala (izračunava se isključivo prema CET metodi). CET vrijednost dodatnog materijala trebala bi odgovarati ili premašiti onu osnovnog materijala kako bi se smanjio rizik od pukotina u zavarenom spoju (ove zahtjeve važno je poštovati prilikom upotrebe dodatnih materijala čija vrijednost granice razvlačenja prela 700MPa uz napomenu prilagodne i temperature predgrijavanja ukoliko se taj postupak primjenjuje). [1-9]

C. Sadržaj vodika u spoju
Vodik, a kao atom najmanjeg promjera, vrlo lako ulazi u metal zavara tijekom izvođenja procesa zavarivanja, a njegova prisutnost jedan je od osnovnih uvjeta pojave hladnih pukotina. Izvor vodika može uključivati osnovni materijal (stanje površine, tvornički primeri i sl.), dodatni i potrošni materijal, okolišne uvjete i dr. Rizik od hladnih pukotina prvenstveno je povezan s tzv. difuzijskim vodikom koji migrira iz ZTu ZUT ili osnovni materijal. Održavanje niskih koncentracija vodika ključno je za sprječavanje nastanka pukotina. [1-9]

D. Predgrijavanje/temperatura predgrijavanja
Predgrijavanje pomaže u ubrzavanju difuzije vodika iz zavarivnog metala, čime se smanjuje rizik od hladnih pukotina. Ovo je osobito važno za deblje pozicije ili kada se zavarivanje izvodi pod uvjetima s visokim toplinskim opterećenjem. Preporuke za predgrijavanje temelje se na debljini pozicija osnovnog materijala, konfiguraciji spoja i uvjetima u radnom okolišu. Kod predgrijavanja visokočvrstih čelika vrlo je važno pratitit upute proizvođača osnovnog materijala kako nebi došlo do narušavanja mikrostrukture i gubitna mehaničkih svojstava. [1-9]

E. Zaostala naprezanja
Proces zavarivanja izaziva nastanak zaostalih naprezanja zbog temperaturnih gradijenata koji nastaju tijekom procesa hlađenja. Ova naprezanja mogu značajno povećati rizik od hladnih pukotina pukotina. Preporučuje se poduzimanje mjera za smanjenje zaostalih naprezanja, kao što je pravilan odabir i geometrija privremenih spojeva (pripoja), točaka početka i završetka zavarivanja, geometrija korijenskih zazora, primjena prednaprezanja, stezanja i sl.. [1-9]

F. Primjena dodatnog materijala austenitnog tipa
Primjena dodatnog materijala austenitne mikrostrukture (npr. AISI 307 ili 309) nude izuzetnu otpornost na hladne pukotine zbog svoje mikrostrukture. Austenitna mikrostruktura ima sposobnost otapanja većih količina vodika, čime se smanjuje rizik od pukotina u ZT-u i ZUT-u. Pri tome valja obratiti pozornost na vrijednosti čvrstoća u spoju koje ponekada mogu biti nedovoljne obzirom na tip osnovnog materijala (visokočvrstog čelika). [1-9]

G. Odabir metode predgrijavanja
Pravilnim odabirom metode predgrijavanja omogućuje se ravnomjernija raspodjela primarno unešenog toplinskog inputa što je ključno za sprječavanje neravnomjernog hlađenja koje može uzrokovati pukotine. Ovdje je važno napomenuti i važnost primjene kontrole temperature predgrijavanja (odabir pravilne metode) kao i temperature međuprolaza kod višeprolaznog zavarivanja. [1-9]

H. Toplinske obrade nakon zavarivanja
Toplinske obrade nakon zavarivanja mogu se provoditi kako bi se dodatno smanjio rizik prema pojavi hladnih pukotina pukotine. Ako je takva toplinska obrada nužna, potrebno ju je specificirati već unutar procesa projektiranja tehnologije zavarivanja, imajući pri tome na umu tip i vrstu visokočvrstih čelika (visokočvrsti čelici čija se mehanička svojstva temelje na mehanizmima očvrsnuća dobivenim putem toplinskih obrada nakon zavarivanja se toplinski više ne obrađuju!) [1-9]

4. Zaključak

Pojava hladnih pukotina u zavarenim spojevima visokočvrstih čelika predstavlja jedan od najsloženijih izazova u zavarivanju, s obzirom na kombinirani utjecaj vodika, mikrostrukture ZUT-a i razine zaostalih naprezanja. Kako bi se umanjio rizik od hladnih pukotina, nužno je provesti niz mjera u postupku projektiranja tehnologije zavarivanja. Ključno je održavati nizak sadržaj difuzijskog vodika u spoju, što se postiže uporabom potrošnih materijala s niskim udjelom vodika (do 5 ml H_2/100 g zavarenog metala), osiguravanjem čistoće spoja, pravilnim skladištenjem dodatnih materijala i primjenom odgovarajuće temperature predgrijavanja (ukoliko se primjenjuje). Dodatno, važno je primjeniti sve dostupne mjere koje će eliminirati ili zadržati zaostala naprezanja u niskim vrijednostima. Kod primjene višeprolaznog zavarivanja preporučuje se upotreba dodatnih materijala različite čvrstoće – prvi prolazi zavaruju se dodatnim materijalima niže čvrstoće, dok se završni prolazi izvode potrošnim materijalima visoke čvrstoće, čime se dodatno smanjuje rizik od nastanka hladnih pukotina.

Temeljem navedenog, može se zaključiti da je za smanjivanje rizika od nastanka i uspješno sprječavanje hladnih pukotina potreban sveobuhvatan pristup koji uključuje pravilan odabir osnovnih i dodatnih materijala, tehnologije zavarivanja i poznavanje interakcije mikrostrukturnih i mehaničkih čimbenika u zoni utjecaja topline. Sustavno provođenje ovih mjera temelj je za osiguranje pouzdanosti zavarenih spojeva kod visokočvrstih čelika.

5. Literatura

1. SSAB., SSAB Welding Handbook, A Guide to Better welding of Hardox and Weldox
2. Pokhodnya, I.K., & Shvachko, V.I. (1996). Cold cracks in welded joints of structural steels. *Materials Science*, 32(1), 45–55.
3. Kim, H.J., & Kang, B.Y. (2003). Effect of microstructural variation on weld metal cold cracking of HSLA-100 steel. *ISIJ International*, 43(5), 706–713.
4. Mikami, Y., Kawabe, N., Ishikawa, N., & Mochizuki, M. (2016). Evaluation of cold cracking in high-strength steel weld metal based on local critical conditions incorporating stress and diffusible hydrogen distributions. *Quarterly Journal of the Japan Welding Society*, 34(2), 67–80.
5. Schwedler, O., Holtschke, N., & Jüttner, S. (2016). Hydrogen-assisted cold cracking in welded joints of press-hardened 22MnB5. *Welding in the World*, 60, 1063–1070.
6. Kasatkin, G.O. (1994). Hydrogen embrittlement mechanisms in high-strength steels on welding. *Avtomat. Svarka*, 1, 3–7.
7. Ahn, D.C., Sofronis, P., & Dodds, R.H. (2007). On hydrogen-induced plastic flow localization during void growth and coalescence. *International Journal of Hydrogen Energy*, 32(16), 3734–3742.
8. Moore, P.L., Howse, D.S., & Wallach, E.R. (2004). Microstructures and properties of laser/arc hybrid welds and autogenous laser welds in pipeline steels. *Science and Technology of Welding and Joining*, 9(4), 314–322.

9. Chen, Y.-S., Huang, C., Liu, P.-Y., Yen, H.-W., Niu, R., Burr, P., Moore, K.L., Martínez-Pañeda, E., Atrens, A., & Cairney, J.M. (2024). Hydrogen trapping and embrittlement in metals

Optimisation of a simple rod structure - case study

K. Pisačić[1,*], M. Horvat[1], Z. Botak[1], Z. Busija[1]

[1]Sveučilište Sjever, Varaždin, Hrvatska

[*]Corresponding Author E-mail: katarina.pisacic@unin.hr

Abstract

Engineers need to make decisions about product design, technology, maintenance, and management at different levels. The main goal to either use fewer resources or achieve better results is achieved by optimisation procedures. We can describe the resources or results using mathematical functions called objective functions or criteria. This article describes theoretical text book examples optimised in Matlab and alternatively in Ansys 2019 R1. The procedure is thoroughly explained and can be used as a template for optimising different kinds of structures.

Keywords: optimisation, rod structure, case study

1. Uvod

Optimiranje je vječita tema istraživača i njegova popularnost kontiunirano raste što se vidi na kratkom primjeru broja rezultata prepraživanja objavljenih radova, koristeći slovensku bazu UM:NIK, koja pristupa Scopusu, WOS-u i drugim relevantnim citatnim i cjelovitim bazama radova. Slika 1 pokazuje broj radova koji u sažetku sadrže ključne riječi "structural" i "optimization". Unošenjem dodatnih uvjeta za prepraživanje, broj rezultata vezanih na temu optimizacije bi se vjerojatno i povećao
Mnogi alati za simboličko programiranje, kao što su Mathcad, Matlab, Mathematica, sadrže ugrađene algoritme za optimiranje, a slične algoritme često sadrže i alati za numeričke analize, kao primjerice Ansys. U radu u nastavku će se prikazati usporedno postupci optimiranjam, a koji su razvijeni uz literaturu [1-9]

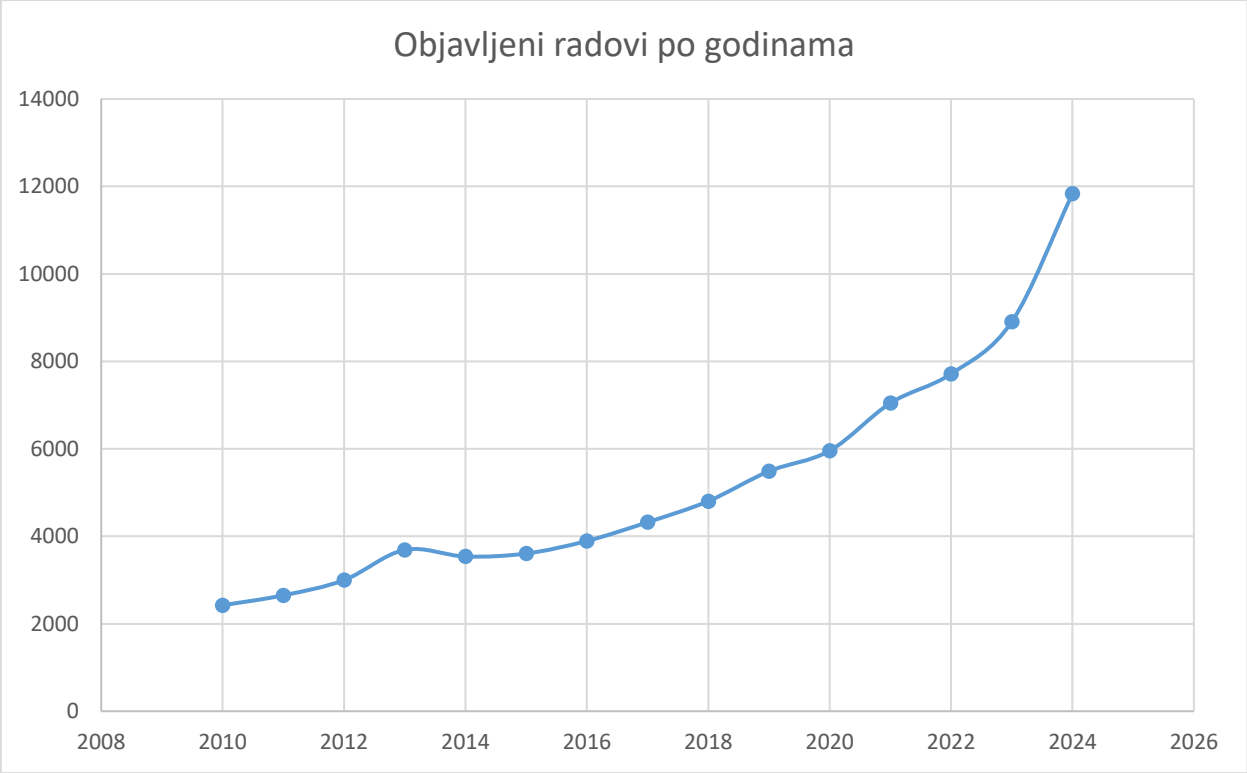

Slika 1. Broj objavljenih radova na temu structural optimization zadnjih godina

2. Definiranje problemskog zadatka

Sustav prema slici 2 je simetričan obzirom na os y. Bezdimenzijski omjeri $x_1 = \frac{x}{h}$ i $x_2 = \frac{A}{A_{ref}}$ tretirani su kao dizajnerske varijable. Koordinate čvora 3 smatraju se konstantnima. Potrebno je minimizirati:

a) težinu konstrukcije f_1 i

b) ukupni pomak čvora 3 pod opterećenjem f_2 bez prelaženja dopuštenog opterećenja σ_0 te

c) minimalne vrijednosti varijabli za funkciju cilja ($f_1 + f_2$).

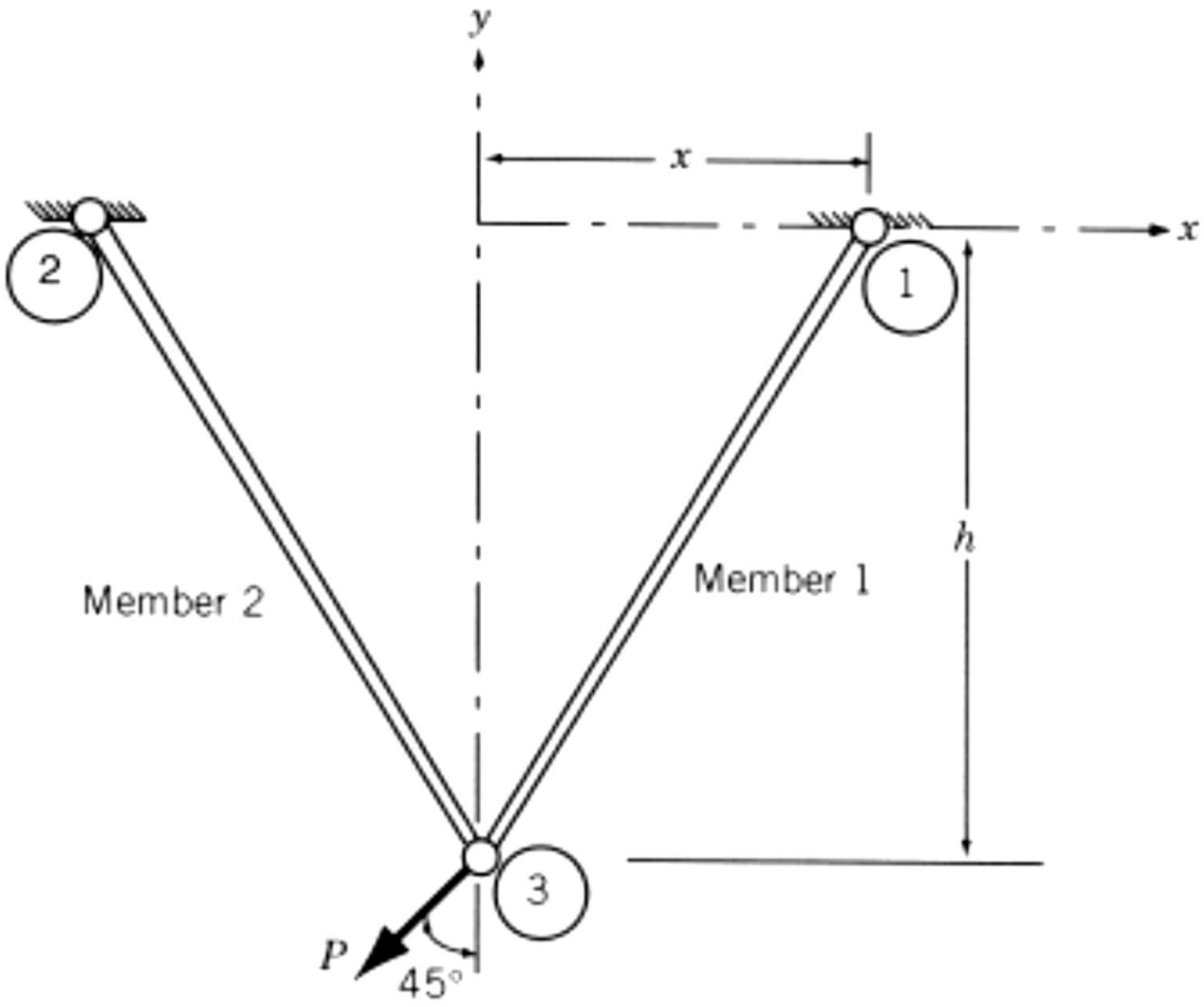

Slika 2. Sustav štapova [1]

Težina konstrukcije i pomak čvora 3 mogu se prikazati izrazima

$$f_1(x) = 2\rho h x_2 \sqrt{1 + x_1^2}\, A_{ref} \qquad (6.1)$$

$$f_2(x) = \frac{Ph(1 + x_1^2)^{1.5}\sqrt{1 + x_1^4}}{2\sqrt{2}Ex_1^2 x_2 A_{ref}} \qquad (6.2)$$

Gdje je ρ težinska gustoćo, P je sila opterećenja, a E Youngov modul elastičnosti. Naprezanje u štapovima 1 i 2 (σ_1 i σ_2) dani su izrazima:

$$\sigma_1(x) = \frac{P(1+x_1)\sqrt{(1+x_1^2)}}{2\sqrt{2}x_1x_2A_{ref}} \qquad (6.3)$$

$$\sigma_2(x) = \frac{P(x_1-1)\sqrt{(1+x_1^2)}}{2\sqrt{2}x_1x_2A_{ref}} \qquad (6.4)$$

Pri čemu su gornja i donja granica konstrukcijskih varijabli $x_i^{\min} \le x_i \le x_i^{\max}$; $i = 1,2$, a zadane su vrijednosti:

$E = 30 \cdot 10^6$ psi
$\rho = 0.283$ lb/in^3
$P = 10000$ lb
$\sigma_0 = 20000$ psi
$h = 100$ in
$A_{ref} = 1$ in^2
$x_1^{\min} = 0.1$
$x_2^{\min} = 0.1$
$x_1^{\max} = 2.0$
$x_2^{\max} = 2.5$

2. MATLAB rješenja

Zadatak je podijeljen u tri dijela te se u sljedeća tri odlomka prikazuju sva tri rješenja dobivena pomoću MATLABA.

2.1. Optimiranje težine

Glavna programska datoteka naziva primjer_stapa_a.m sadrži naredbe:

```
x0 = [1;1];
A=[ ];
```

```
b=[ ];
Aeq=[ ];
beq=[ ];
LB = [0.1;0.1];
UB = [2;2.5];
[xopt, fopt] = fmincon('fun_a', x0, A, b, Aeq, beq, LB, UB, 'nonlcon')
```

Datoteka funkcije cilja fun_a.m sadrži sljedeći niz naredbi:

```
function f = fun_a(x)
E=30*10^6;
ro=0.283;
P=10000;
sigma=20000;
h=100;
Aref=1;
f = 2*ro*h*x(2)*sqrt(1+x(1)^2)*Aref;
```

Datoteka s nelinearnim ograničenjima ima naziv nonlcon.m i sadrži:

```
function [C,Ceq] = nonlcon(x)
E=30*10^6;
ro=0.283;
P=10000;
sigma=20000;
h=100;
Aref=1;
C(1)=(P*((1+x(1))*sqrt(1+x(1)^2)))/(2*sqrt(2)*x(1)*x(2)*Aref)-sigma;
C(2)=(P*((x(1)-1)*sqrt(1+x(1)^2)))/(2*sqrt(2)*x(1)*x(2)*Aref)-sigma;
Ceq = [ ];
```

Nakon izvođenja glavne programske datoteke dobivena su rješenja:

```
xopt =
   0.6573
   0.5334
fopt =
  36.1273
```

Što je u skladu s rješenjem u knjizi [1] $X^* = \{0.65,\ 0.53521\}$

2.2. Ukupni pomak čvora

Glavna programska datoteka naziva primjer_stapa_b.m sadrži naredbe:

```
x0 = [1;1];
A=[ ];
b=[ ];
Aeq=[ ];
beq=[ ];
LB = [0.1;0.1];
UB = [2;2.5];
[xopt, fopt] = fmincon('fun_b', x0, A, b, Aeq, beq, LB, UB, 'nonlcon')
```

Datoteka funkcije cilja fun_b.m sadrži sljedeći niz naredbi:

```
function f = fun_b(x)
E=30*10^6;
ro=0.283;
P=10000;
sigma=20000;
h=100;
Aref=1;
f =(P*h*(1+x(1)^2)^1.5*sqrt(1+x(1)^4))/(2*sqrt(2)*E*x(1)^2*x(2)*Aref);
```

Datoteka s nelinearnim ograničenjima ima naziv nonlcon.m i sadrži:

```
function [C,Ceq] = nonlcon(x)
E=30*10^6;
ro=0.283;
P=10000;
sigma=20000;
h=100;
Aref=1;
C(1)=(P*((1+x(1))*sqrt(1+x(1)^2)))/(2*sqrt(2)*x(1)*x(2)*Aref)-sigma;
C(2)=(P*((x(1)-1)*sqrt(1+x(1)^2)))/(2*sqrt(2)*x(1)*x(2)*Aref)-sigma;
Ceq = [ ];
```

Nakon izvođenja glavne programske datoteke dobivena su rješenja:

xopt =

0.8645
2.4999

Što je u skladu s rješenjem u knjizi [1] $X^* = \{0.9,\ 2.5\}$

2.3 Optimiranje glavne funkcije

Glavna programska datoteka naziva primjer_stapa_b.m sadrži naredbe:

```
x0 = [1;1];
A=[ ];
b=[ ];
Aeq=[ ];
beq=[ ];
LB = [0.1;0.1];
UB = [2;2.5];
[xopt, fopt] = fmincon('fun_c', x0, A, b, Aeq, beq, LB, UB, 'nonlcon')
```

Datoteka funkcije cilja fun_c.m sadrži sljedeći niz naredbi:

```
function f = fun_c(x)
E=30*10^6;
ro=0.283;
P=10000;
sigma=20000;
h=100;
Aref=1;
f1 = 2*ro*h*x(2)*sqrt(1+x(1)^2)*Aref;
f2 =(P*h*(1+x(1)^2)^1.5*sqrt(1+x(1)^4))/(2*sqrt(2)*E*x(1)^2*x(2)*Aref);
f=f1+f2;
```

Datoteka s nelinearnim ograničenjima ima naziv nonlcon.m i sadrži:

```
function [C,Ceq] = nonlcon(x)
E=30*10^6;
```

```
ro=0.283;
P=10000;
sigma=20000;
h=100;
Aref=1;
C(1)=(P*((1+x(1))*sqrt(1+x(1)^2)))/(2*sqrt(2)*x(1)*x(2)*Aref)-sigma;
C(2)=(P*((x(1)-1)*sqrt(1+x(1)^2)))/(2*sqrt(2)*x(1)*x(2)*Aref)-sigma;
Ceq = [ ];
```

Nakon izvođenja glavne programske datoteke dobivena su rješenja:

```
xopt =
   0.6581
   0.5332
```

Što je u skladu s rješenjem u knjizi [1] $X^* = \{0.65,\ 0.5352\}$

3. Optimiranje mase konstrukcije u ANSYS-u

U ovom poglavlju opisuju se glavne značajke sučelja za rad s parametrima konstrukcije, detaljan opis mogućnosti optimiranja u ANSYS Workbenchu te će biti prikazano rješenje istog primjera za usporedbu s analitičkim rezultatima dobivenim korištenjem Matlaba. Postupak optimiranja pomoću Ansys-a koristi se u brojnim radovima, također su vrlo korisni i brojni edukacijski video materijal [1,2].

3.1 Optimizacijski alat u Ansys-u

Kako bismo mogli provoditi optimiranje u Ansys-u, potrebno je proučiti mogućnosti i ulogu Desing Explorer sučelja korištenje alata za optimiranje u Ansys-u. DesignXplorer (DX) se koristi za sažeti pregled parametara konstrukcije te njihovo bolje razumijevanje i konačno optimiranje. Prilikom dizajniranja novog ili redizajniranja postojećeg proizvoda ili konstrukcije važna su sljedeća pitanja:

- Koji su ključni parametri konstrukcije?
- Kako utječu parametri jednog dijela na druge dijelove konstrukcije u fazi izrade i eksploatacije
- Pri kojim uvjetima će konstrukcija dati najbolje rezultate?
- Koliko je konstrukcija robustna?

Slika 3. Upotreba parametara u dizajnu [9]

Što ako analiza se automatski provodi za specificirane točke dizajna. Na taj način može se provesti korelacijska analiza tj. odrediti utjecajne i manje utjecajne parametre. Također može se odrediti koliko je funkcijska veza konstrukcijakih konstrukcije linearna ili kvadratna.
Kod planiranja pokusa definira se vrsta plana pokusa, raspon svake parametarske varijable i tip (kontinuirana, diskretna, proizvodna). Točke dizajna su odabrane automatski kako bi se učinkovito provela analiza parametarskog prostora. Alat za odzivne površine generira surogat model, može se koristiti za određivanje minimuma i maksimuma, izradu 2D i 3D dijagrama, provjeru lokalne osjetljivosti i procjenu kvalitete odzivne površine.Za provođenje postupka optimiranja nužno je definirati ciljeve, ograničenja i ulazne parametre. Ako se optimiranje temelji na odzivnoj površini može se provesti analiza tisuća konfiguracija u kratkom vremenu, a ako se temelji na izravnom postupku, konvergencija rješenju je definirana odabranim algoritmom. Ciljevi Six sigma analize su razumjeti kako će tolerancije dizajna utjecati na izvedbu, na koliko će se dijelova pojaviti kvarovi i koje ulazne parametre je potrebno najstrože kontrolirati.

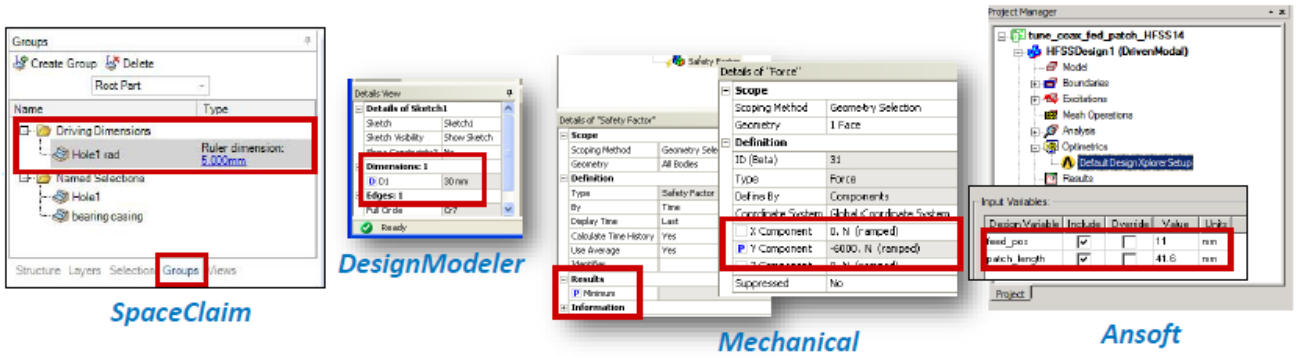

Slika 4. Postupak parametriziranja u raznim sučeljima unutar Ansysa [9]

Optimiranje u Ansysu

Koristeći alat DesignXplorer moguća su dva radna toka [10]:

- Optimiranje odzivnom površinom - Temelji se na planiranju pokusa i odzivnim i simulacijsko vrijeme se troši za vrijeme koraka planiranja pokusa mijenjanje kriterija i ponavljanje postupka optimiranja je gotovo bez utroška vremena. Optimalne rezultate bi trebalo provjeriti
- Direktno optimiranje - Izravno je i temelji se na "stvarnim" rješenjima. Promjena parametara optimiranja i ponovno izvođenje postupka je vremenski iscrpno. Optimalni rezultati temelje se na pravim rješenjima

Koraci u provođenju optimiranja u Ansys-u:

1. definiranje područja optimiranja
2. definiranje relacija ulaznih parametara
3. odabir metode optimiranja
4. konvergencija rješenja i naknadna obrada rezultata

Područje, domena optimiranja obuhvaća granice i tipove parametara. Kod optimiranja odzivne površine parametri su definirani prilikom planiranja pokusa, ali granice se mogu reducirati prilikom optimiranja. Moguće je usmjeriti postupak optimiranja na određeno područje interesa.

Relacije ulaznih parametara mogu biti definirane kao nejednakosti i eliminiraju beskorisne kombinacije ulaznih vrijednosti.

Može se definirati jedna ili nekoliko funkcija cilja, pri čemu treba obratiti pozornost na to da neki algoritmi ne podržavaju višekriterijsko optimiranje. Svakoj funkciji cilja može se pridružiti težinski parametar i može se definirati jedna ili više funkcija ograničenja. Tipovi funkcija cilja: minimum, maksimum, traženje mete. Tipovi ograničenja: vrijednost <= granica, vrijednost >= granica, donja granica <= vrijednost <= gornja granica.

U Design Explorer-u na raspolaganju je 6 metoda optimiranja:

Screening (pomaknuti Hammersley)

MOGA (Multi Objective Genetic Algorithm)

NLPQL (Non-linear Programming by Quadratic Lagrangian)

MISQP (Mixed-Integer Sequential Quadratic Programming Method)

Adaptive Single-Objective(samo za direktno optimiranje)
Adaptive Multiple-Objective
Optimiranje odzivne površine treba se temeljiti na preciznoj odzivnoj površini, u kratkom vremenu analizira brojne konfiguracije i omogućava korištenje nekolicine različitih algoritama kako bi se odabrao kandidat. Ukoliko je definirana jedna funkcija cilja, preporuča se Screening metoda te nakon nje NLPQL ili MISQP, za više definiranih funkcija cilja koristi se MOGA.
Direktno optimiranje je robusno i izravno, omogućava korištenje nekoliko algoritama za pronalaženje optimalnog kandidata. Dobar je početni pristup ukoliko je definirana jedna funkcija cilja te ako su ulazni parametri kontinuirani, nemaju zavisnosti i broj ulaznih parametara <10 koristiti Adaptive Single-Objective, inače koristiti MISQP. Ako je definirano više funkcija cilja i ako su neki parametri diskretni preporuča se koristiti MOGA, inače se preporuča Adaptive Multiple-Objective.

3.2 Rješavanje problemskog zadatka

Kako bi se problem mogao optimirati u Ansys-u, uvedeno je pojednostavljenje te je za udaljenost uzeto optimalno rješenje iz odlomka 6.2.1 $x_1 = 0.6573$, prema čemu je izračunat razmak između oslonaca $x_1 = 65.73$ in . Područje raspona polumjera je suženo u odnosu na zadatak iz odlomka 6.2.1 zbog ograničenja geometrije. Kako bi se složio sklop potrebno je kreirati dva štapa i tri osovine kao zasebne komponente. Kako bi geometrijski model zadržao integritet dimenzije polumjera je potrebno prilagoditi dijelu štapa na kojem se nalaze rukavci osovine te su ograničene vrijednosti polumjera, definirano je područje polumjera $0.35 \text{ in} < r < 0.7 \text{ in}$.
Kako bi se provelo optimiranje potrebno je kreirati novi projekt u Ansys Workbench-u, definirati geometriju i fizikalni model te sve ulazne i izlazne parametre koji će se povezati s optimizacijskim alatom te nakon toga provesti optimiranje.

3.3 Definiranje geometrije

Prethodno odabrati Static Structural alat i povući ga na radnu površinu.

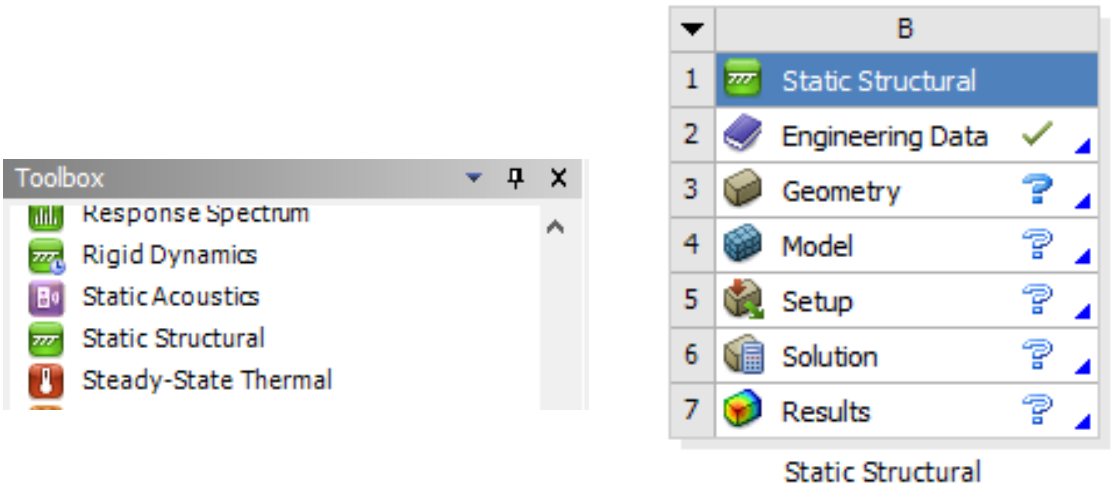

a) b)

Slika 5. Static Structural alat u Ansys Workbench-u

Najprije je potrebno zadati koji će se materijali koristiti u simulaciji, klikom na polje Engineering Data (slika 5 b)) otvara se popis, te su na slici 6 prikazana dva materijala koja će se koristiti u simulaciji.

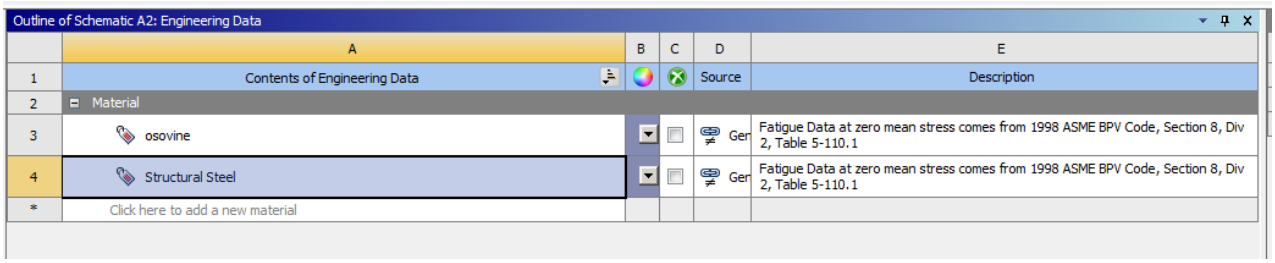

Slika 6. Engineering dana

Zatim je potrebno definirati geometriju, desnim klikom iznad polja Geometry (slika 5 b)) otvara se izbornik te je potrebno odabrati New SpaceClaim Geometry. Koristeći Ansys SpaceClaim alat za modeliranje kreiran je model sustava štapova na slici 7.

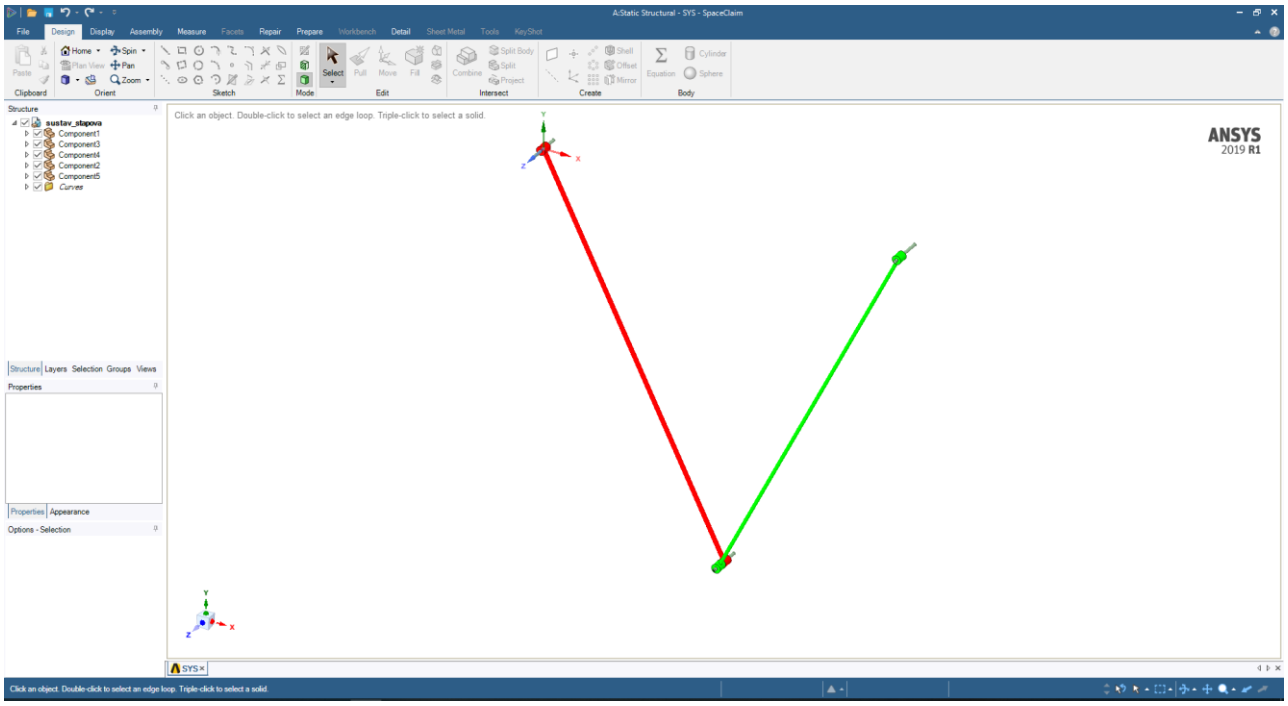

Slika 7. Model sustava štapova

SpaceClaim alati za modeliranje nalaze se na alatnoj traci Design (slika 8). Sketch skupina naredbi služi za crtanje sketch-a, dvodimenzionalne skice, dok su alati za kreiranje trodimenzionalnih tijela grupirani u skupinama naredbi Edit i Intersect. Neke od važnijih naredbi su Pull koja kreira tijelo iz dvodimenzionalne skice, ali služi i za editiranje i Move koja omogućava pomicanje segmenata, zatim Combine koja između ostalog omogućava spajanje nekoliko geometrijskih tijela u jedno.

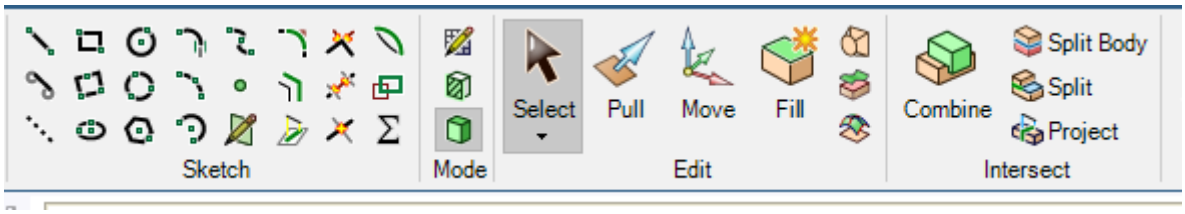

Slika 8. Alati za modeliranje

Spaceclaim je alat za direktno modeliranje te ne postoji stablo značajki već prikazuje strukturu datoteke koja se može sastojati od komponenti (kada se slaže sklop) koje sadrže tijela (Solid) kao što se vidi na slici 7.8.

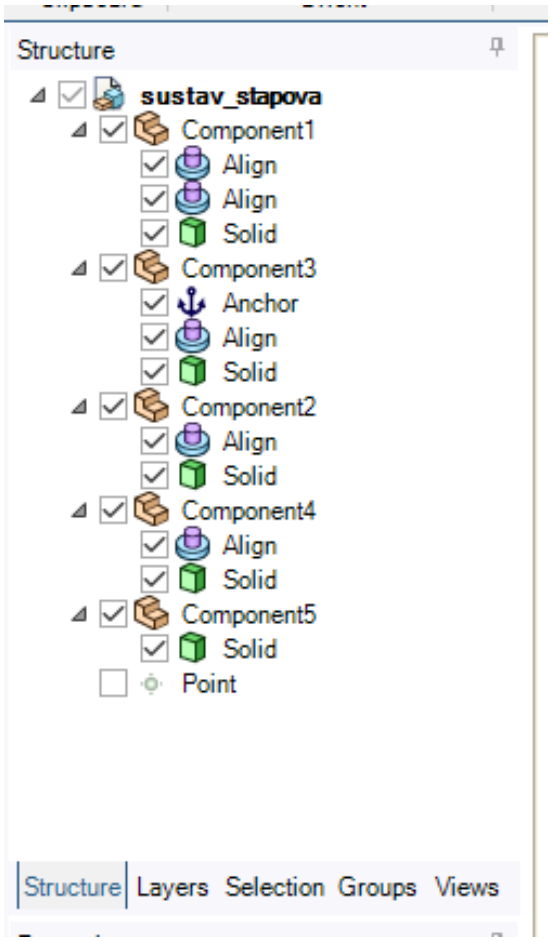

Slika 9. Struktura modela u Spaceclaim-u

Komponentama u sklopu (Assembly) mogu se dodavati poravnanja (Align), slika 7.9.

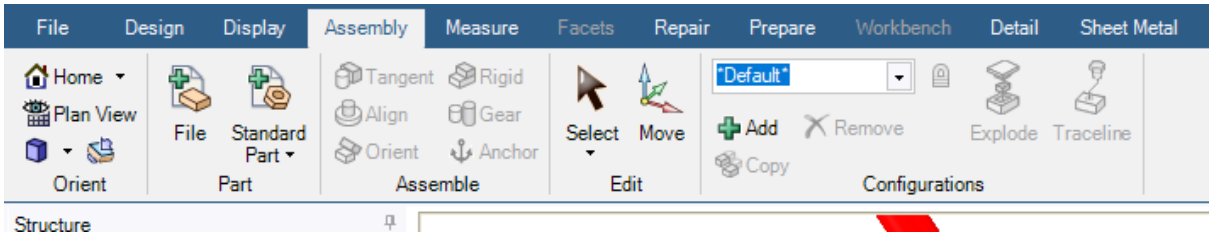

Slika 10. Vrpca Assembly

Koristeći naredbe iz skupina Sketch, Edit i Assemble kreiran je model kao na slici 11.

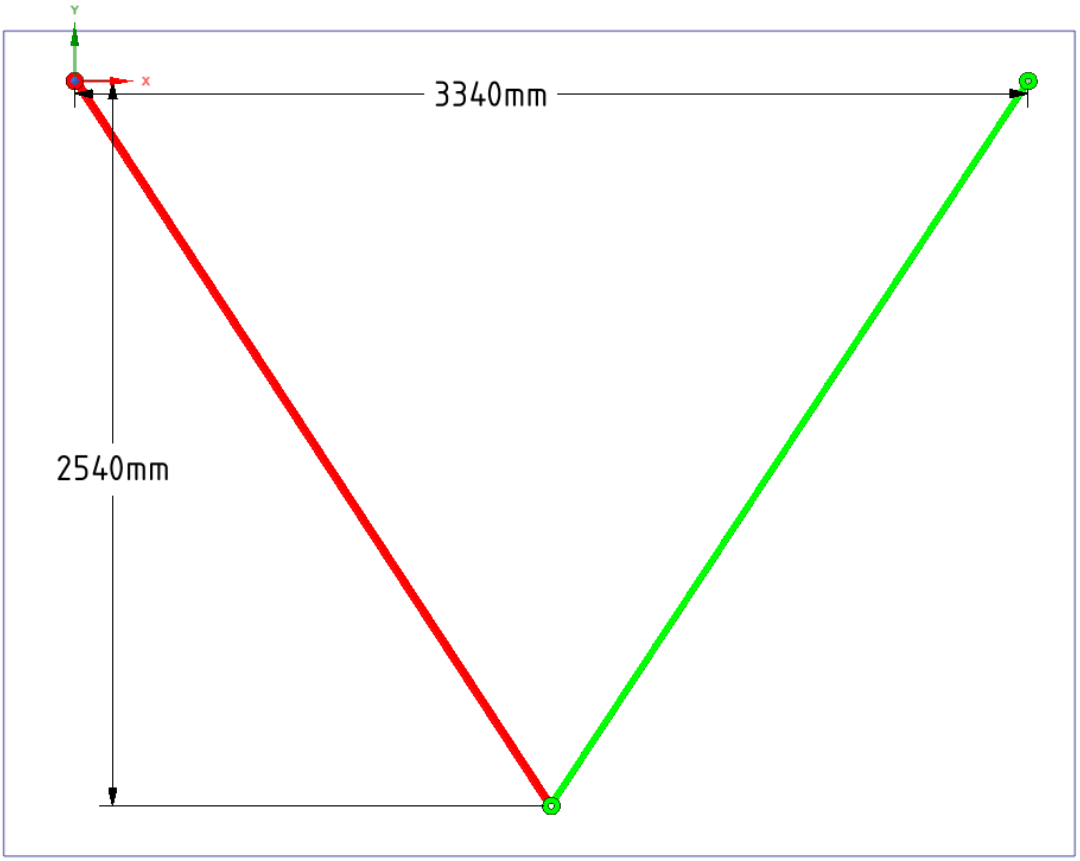

Slika 11. Dimenzije modela u Spaceclaim-u

Pojednostavljeni model je parametriziran tako što se koristila naredba Pull te uz mjesto za upis dimenzije javlja se oznaka P na koju je potrebno kliknuti te je parametre moguće pregledati na kartici Groups (slika 12)

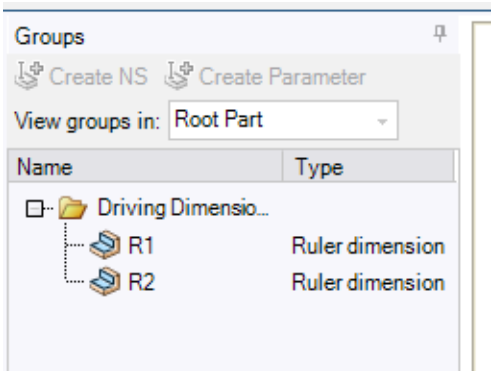

Slika 12. Parametri

Prilikom definiranja modela uočeno je nekoliko nedostataka SpaceClaim-a u odnosu na primjerice SolidWorks. Postavljanje poravnanja kod kreiranja sklopa je vrlo jednostavno, ali nažalost i mogućnosti su mu ograničene u odnosu na SolidWorks koji dozvoljava poravnanje obzirom na neku globalnu ishodišnu ravninu ili ishodišnu ravninu nekog lokalnog koordinatnog sustava, kao i zadavanje nekih uvjeta brojčano definiranih. Ukoliko su takve opcije i moguće, procedura je složena i stoga ovaj dio alata SpaceClaim nije dovoljno prilagođen korisniku.
Još jedan nedostatak u odnosu na SolidWorks je što nije moguće izravno parametre povezivati međusobno formulama već je potrebno koristiti Excel komponentu i svaki puta nakon promjene jednog parametra učitavati datoteku, što bi moguće stvorilo komplikacije prilikom Optimiranja.

3.4 Definiranje fizikalnog modela

Nakon pripreme geometrije može se pristupiti postavljanju simulacije, kako izgleda projekt u Ansys Wokrbench-u prikazano je na slici 13.

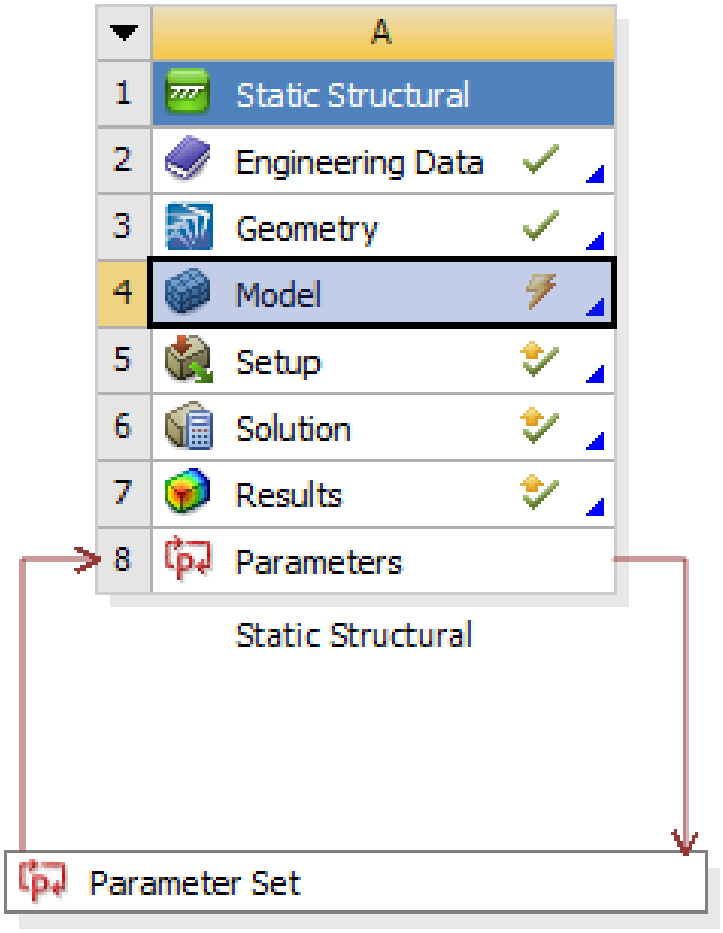

Slika 13. Shema projekta u Ansys Workbench-u

Kada se u Ansys Workbench-u klikne na Model, u ovom slučaju, otvara se prozor Static Structural – Mechanical, gdje se postavljaju uvjeti za simulaciju. Definirana je mreža konačnih elemenata, postavljeni oslonci u osovinama koje drže štapove i zadana sila koja djeluje vertikalno prema dolje slika 14.

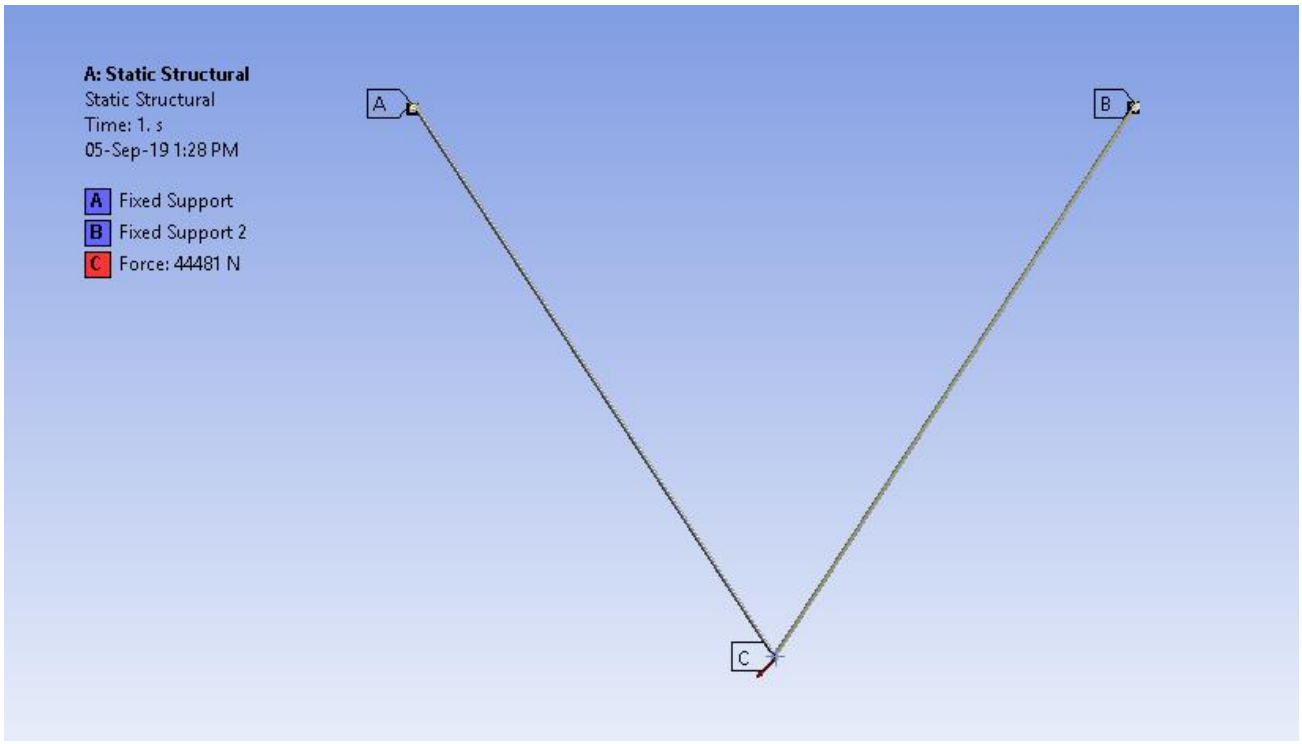

Slika 14. Postavljena ograničenja modela

Obzirom da je jedan kriterij optimiranja masa, potrebno je odabrati masu kao parametar što se vrši klikom na prazni kvadratić pokraj oznake Mass i tada se pojavi plavo slovo P što znači da je masa odabrana kao izlazni parametar (slika 15)

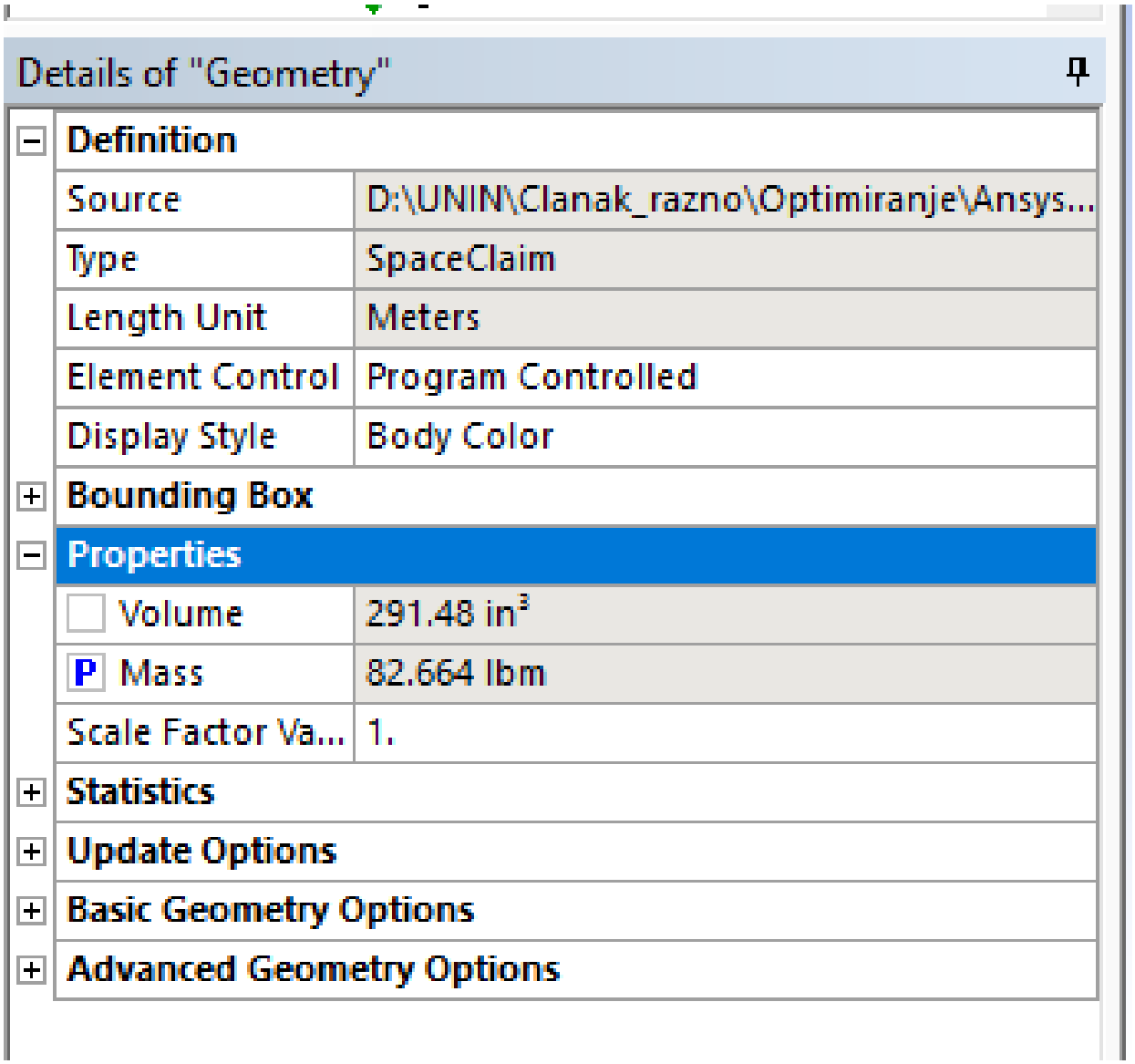

Slika 15. Izbor mase kao izlaznog parametra

Osim mase, sustav je potrebno optimirati tako da se postigne minimalni pomak za zadano naprezanje pa su pomak i normalno naprezanje označeni kao izlazni parametri (slika 16).

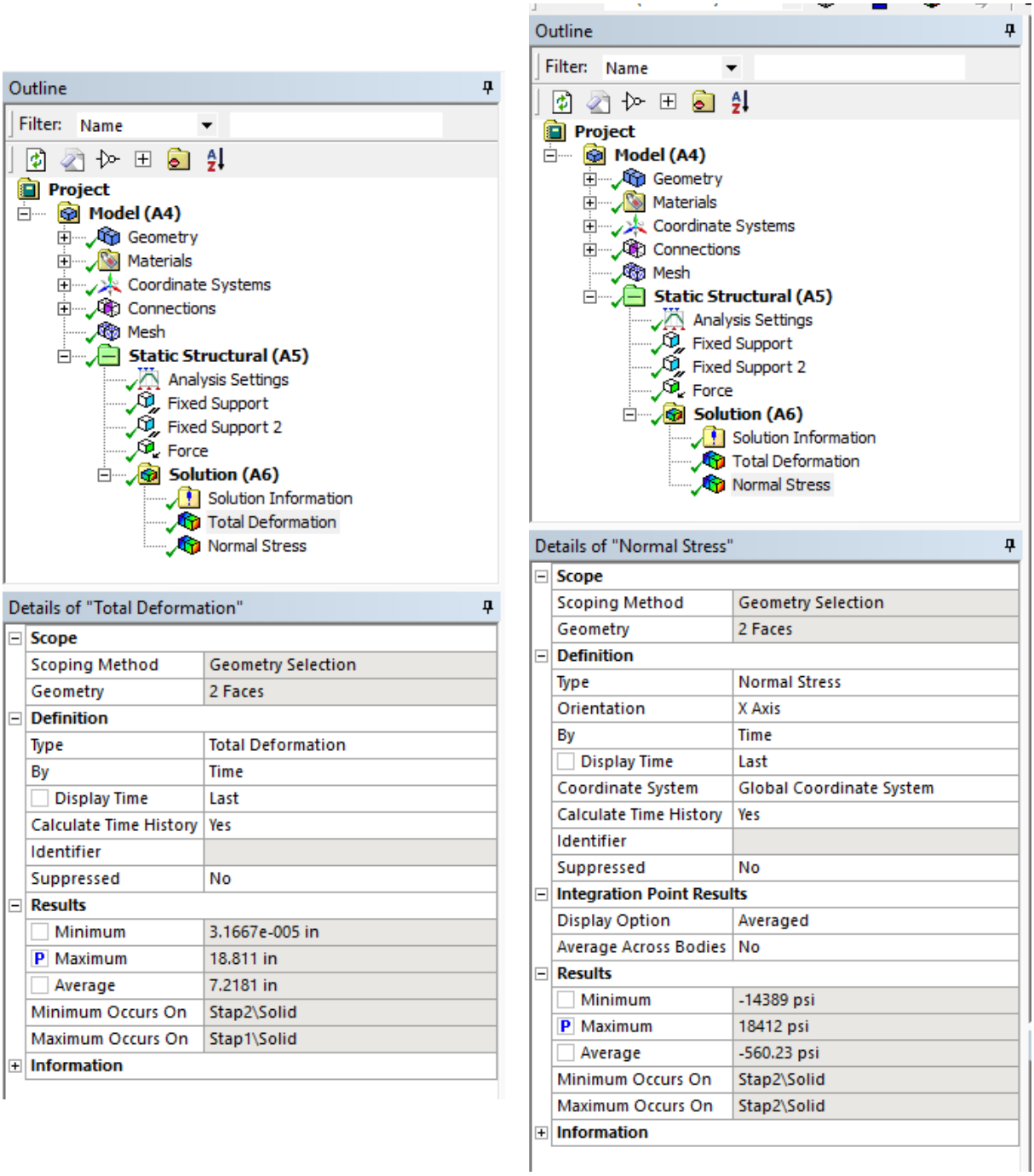

a) pomak b) normalno naprezanje

Slika 16. Izlazni parametri deformacija i naprezanje

Klikom na Parameter Set u shemi projekta (slika 17) otvara se prozor Parameters u kojem je moguće pregledati sve parametre, parametri u ovom zadatku su prikazani na slici 7.16.

Outline of All Parameters

	A	B	C	D
1	ID	Parameter Name	Value	Unit
2	Input Parameters			
3	Static Structural (A1)			
4	P7	R1	0.75	in
5	P8	R2	0.75	in
*	New input parameter			
7	Output Parameters			
8	Static Structural (A1)			
9	P4	Normal Stress Maximum	18412	psi
10	P5	Geometry Mass	82.664	lb
11	P6	Total Deformation Maximum	18.811	in
*	New output parameter			
13	Charts			

Slika 17. Pregled parametara

Potrebno je napomenuti da iako je definirano da će se za projekt koristiti anglo-saksonski sustav mjernih jedinica, ipak u pojedinom sučelju treba ponovno odabrati sustav jedinica.

3.5 Analiza korelacije parametara

Prije provođenja optimiranja korisno je najprije analizirati korelaciju tj. međusobnu zavisnost parametara. Alat za analizu korelacije u Ansys Workbenchu se nalazi u skupini alata Design Exploration (slika 18)

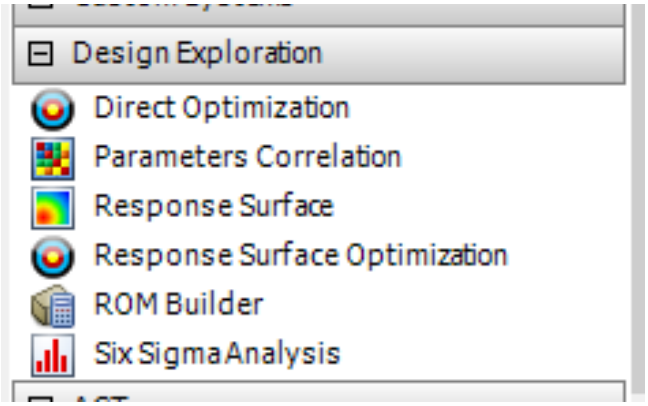

Slika 18. Alati za analizu parametara

Lijevim klikom se „povuče“ Parameters Correlation alat na shematski prikaz projekta i u stablu se veže na postojeću Static Structural analizu (slika 19).

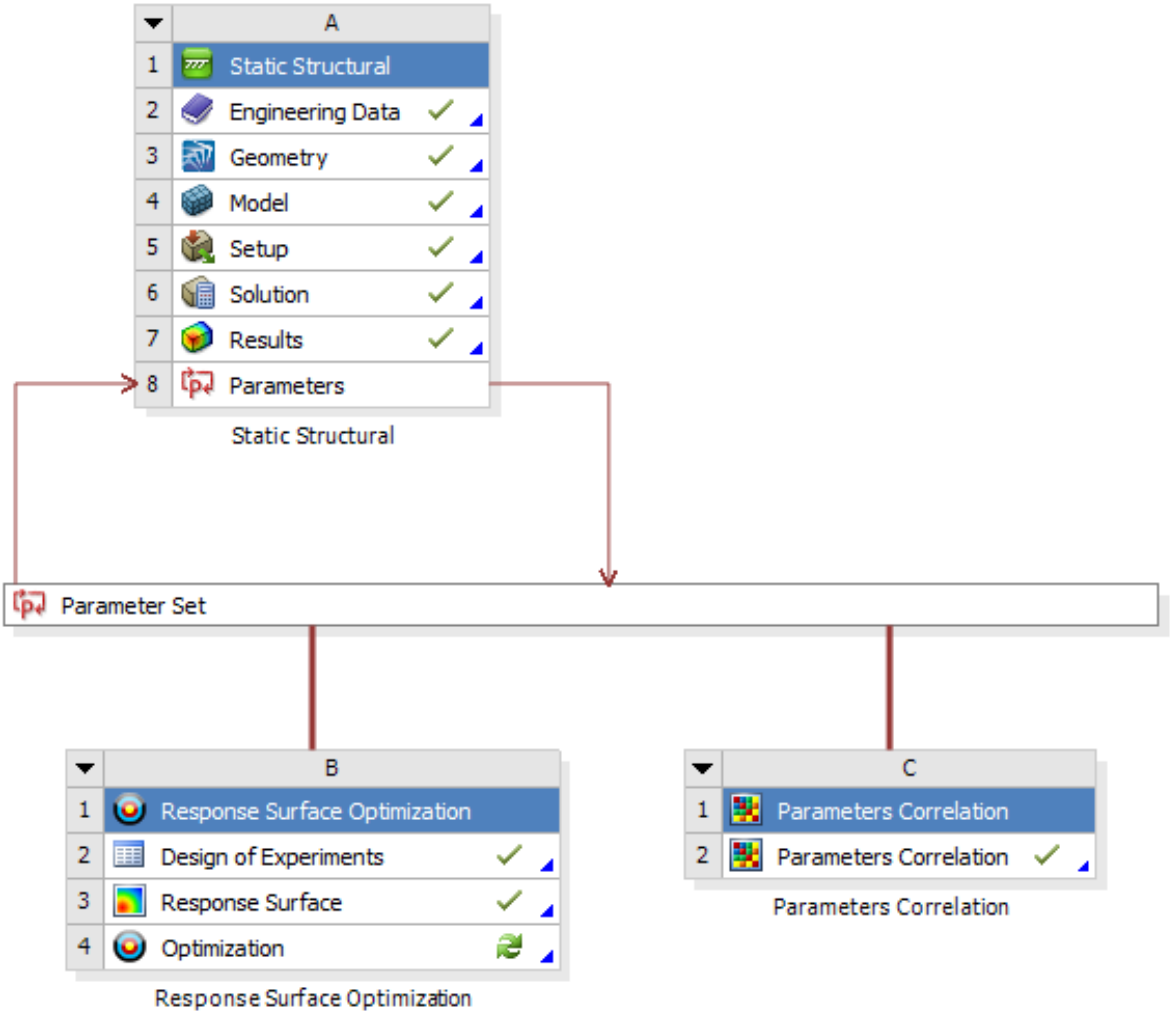

Slika 19. Shematski prikaz projekta

Potrebno je kliknuti na parametre i definirati gornje i donje granične vrijednosti, slika 20.

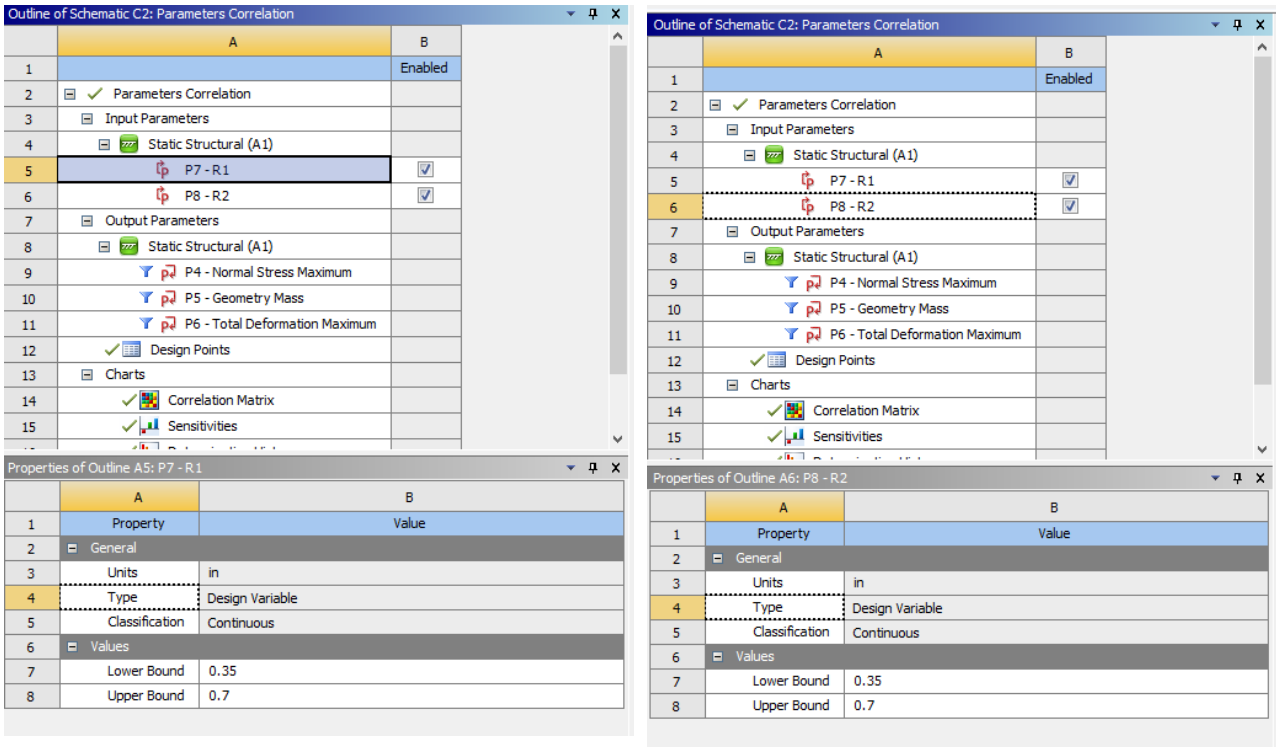

Slika 20. Granične vrijednosti ulaznih parametara

Osim graničnih vrijednosti potrebno je definirati i broj točaka koje će se generirati, predefinirana vrijednost je 100 što je prilično mnogo te je u ovom primjeru odabran nešto manji broj točaka kako bi se uštedilo na vremenu (slika 21).

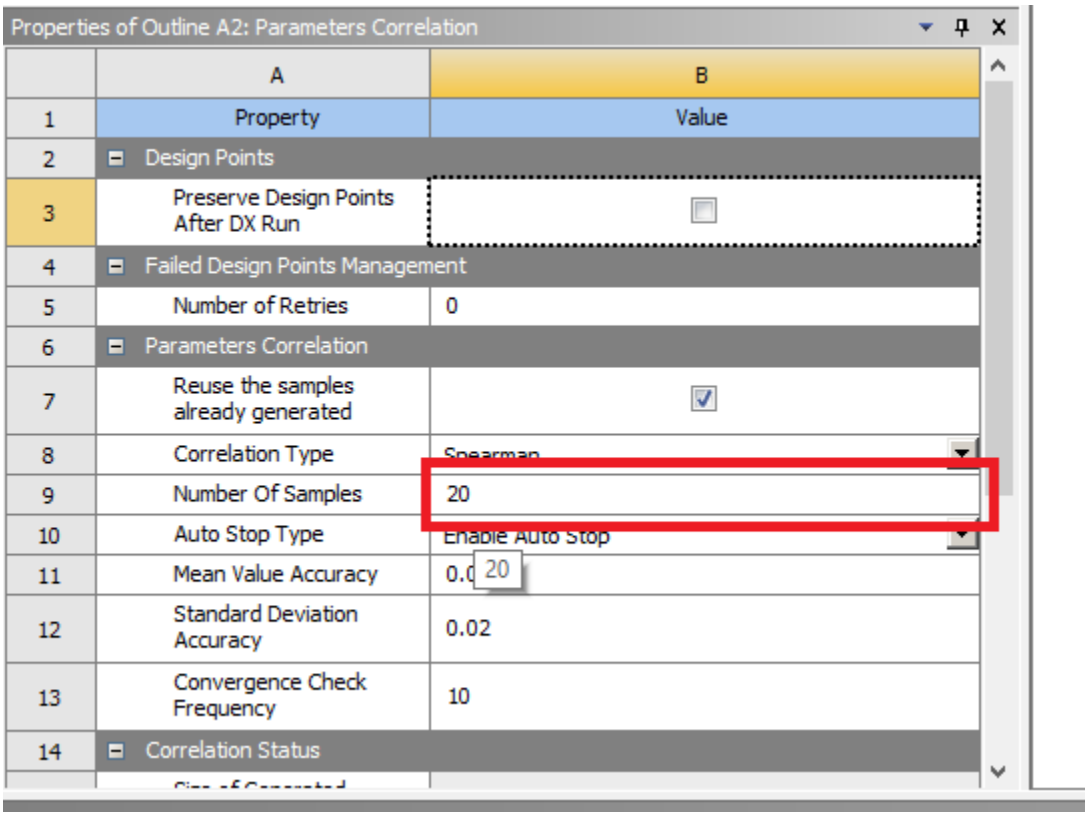

Slika 21. Postavljanje parametara analize korelacije

Nakon izvršene analize korelacije parametara moguće je prikazati matricu korelacija (slika 21) iz koje se očitava koliko neki parametar korelira s nekim drugim parametrom. Vidljivo je da ulazni parametri međusobno ne koreliraju, što je vrlo važno provjeriti. Vidljiva je i snažna veza između izlaznih faktora naprezanje i pomaka, također dimenzije štapova utječu na naprezanje i donekle na deformaciju, niske razine korelacije su posljedica toga da je kao izlazni parametar odabrano samo maksimalno normalno naprezanje i maksimalna ukupni pomak, ali je očito da veza između ulaznih i izlaznih parametara postoji.

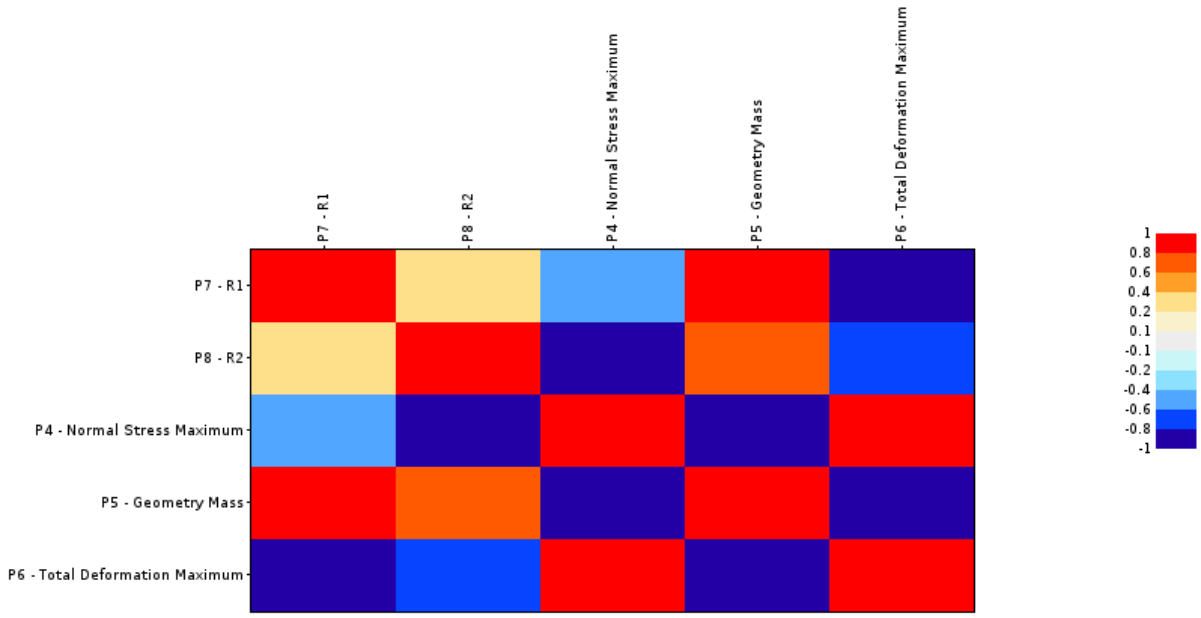

Slika 22. Matrica korelacija

3.6 Optimiranje planom pokusa

Alat za optimiranje odzivne površine također se nalazi u grupi Design Exploration (slika 17), a kada se povuče u shematski prikaz projekta i spoji sa parametrima statičke analize dobiva se stablo kao na slici 19. Kako bi se provelo optimiranje potrebno je izvršiti tri koraka (slika 23):

- Kreiranje plana pokusa (Design of Experiments)
- Analiza odzivne površine (Response Surface)
- Optimiranje (Optimisation)

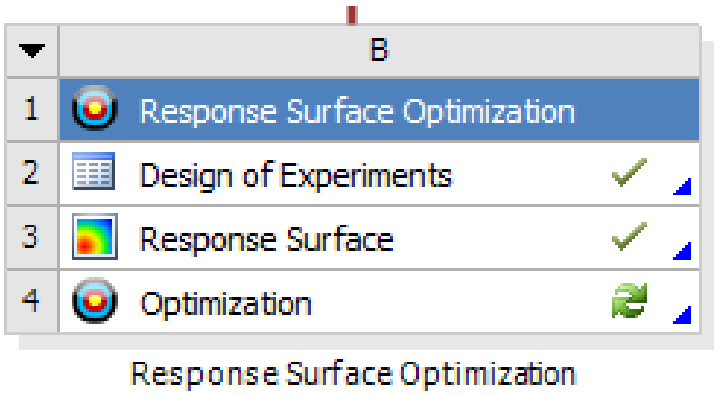

Slika 23. Optimiranje odzivne površine

Kod kreiranja plana pokusa potrebno je podesiti neke parametre. Najprije potrebno je definirati granične vrijednosti ulaznih parametara. Kako je objašnjeno na početku poglavlja, zbog ograničenja dizajna ciljano područje je suženo pa su granične vrijednosti parametara prikazane na slici 24.

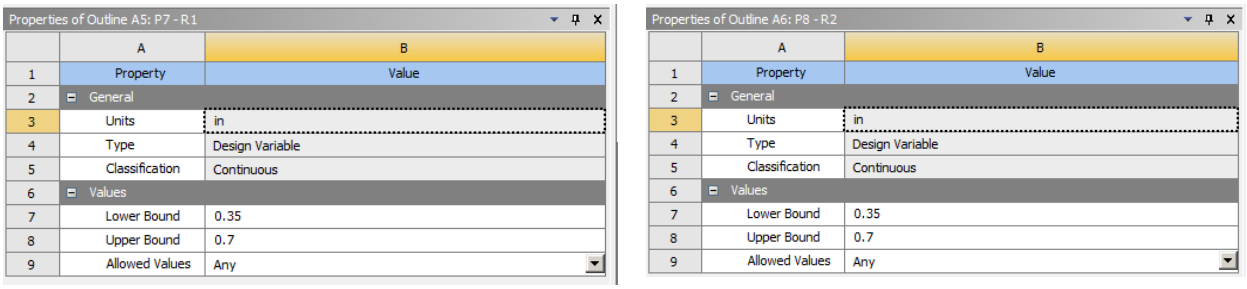

Slika 24. Granične vrijednosti ulaznih parametara

Nakon definiranja granica i odabira vrste plana pokusa (ovdje je korišten predefinirani centralno kompozitni plan pokusa), može se kreirati plan klikom na Update naredbu, slika 25.

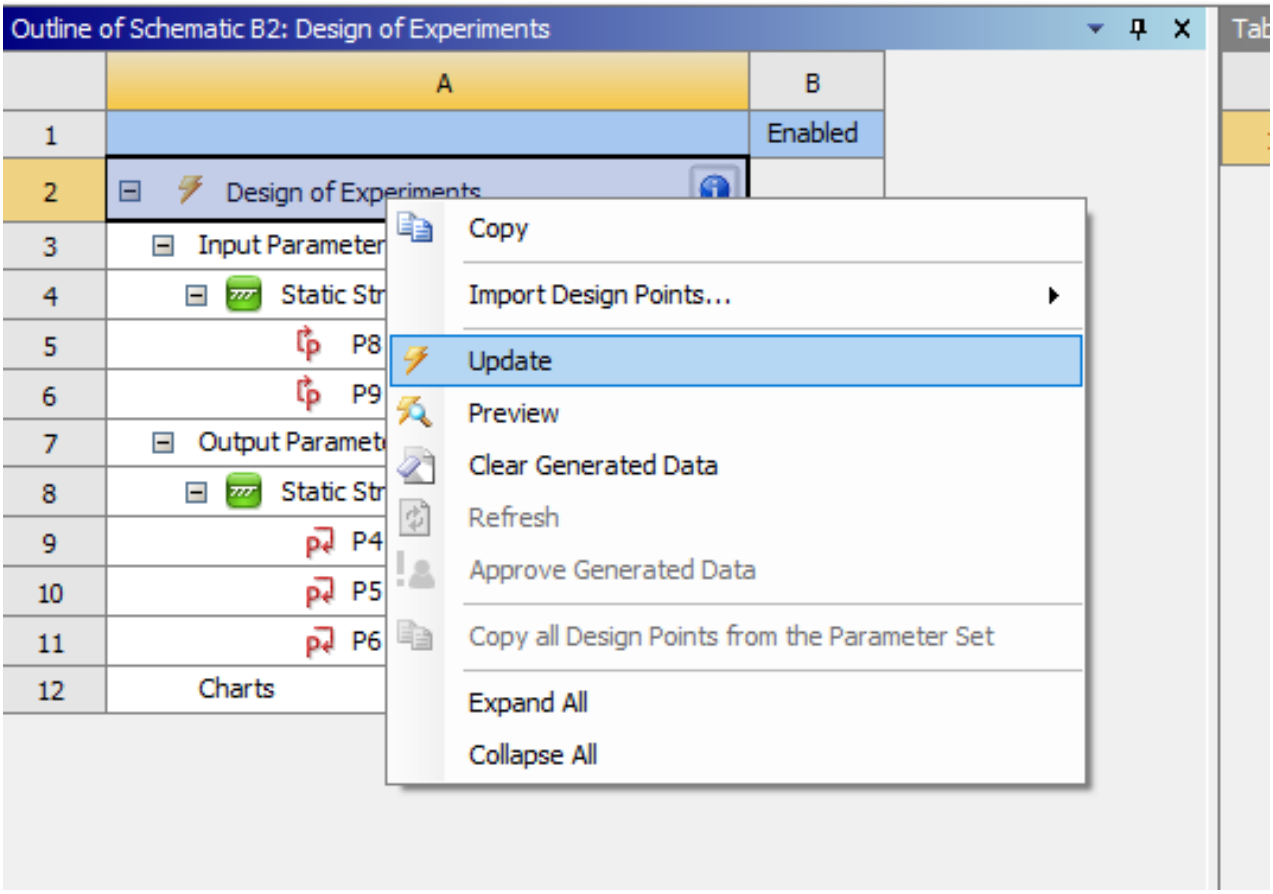

Slika 25. Pokretanje plana pokusa

Nakon odabira naredbe Update pokreće se izrada plana pokusa tj. Ansys pokreće glavnu komponentu na koju je vezan plan pokusa, u ovom slučaju je to strukturna analiza i korak po korak mijenja vrijednosti ulaznih parametara. Za svaki set ulaznih parametara izračunava izlazne parametre te daje tablični prikaz svih parametara (slika 26).

Table of Schematic B2: Design of Experiments (Central Composite Design : Auto Defined)

	A	B	C	D	E	F
1	Name	P7 - R1 (in)	P8 - R2 (in)	P4 - Normal Stress Maximum (psi)	P5 - Geometry Mass (lb)	P6 - Total Deformation Maximum (in)
2	1	0.525	0.525	31669	68.448	29.008
3	2	0.35	0.525	30664	52.275	38.987
4	3	0.7	0.525	25086	91.141	14.41
5	4	0.525	0.35	76060	52.275	47.831
6	5	0.525	0.7	17663	91.141	19.052
7	6	0.35	0.35	75915	36.103	86.829
8	7	0.7	0.35	44622	74.968	16.404
9	8	0.35	0.7	21384	74.968	23.398
10	9	0.7	0.7	13879	113.83	11.684

Chart: No data

Slika 26. Ulazni parametri i izlazne vrijednosti

Nakon postavljanja plana pokusa analizira se odzivna površina. Za svaku odzivnu točku moguće je dobiti dijagram paukove mreže kao na slici 27. Ova slika prikazuje odzivnu površinu za ulazne parametre $r_1 = 0.525$ in i $r_2 = 0.525$ in .

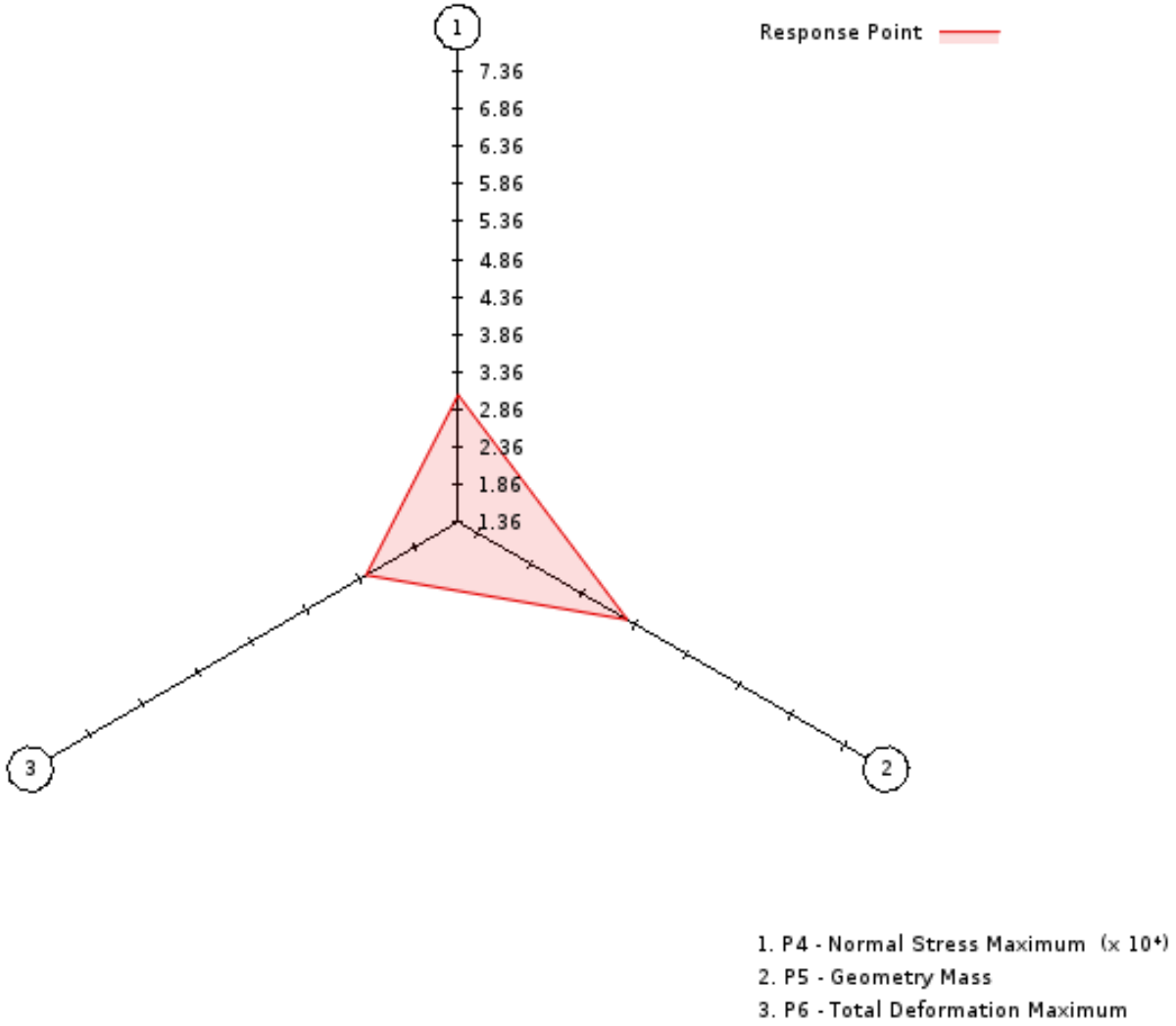

Slika 27. Dijagram paukove mreže

Osim ovog dijagrama omogućeni su i drugi grafički prikazi kao dijagram odziva i osjetljivosti pojedine izlazne varijable o ulaznoj za sve točke odziva, čiji je ukupni broj definiran na početku postupka analize odzivne površine. Kako je u ovoj analizi za odzivnu funkciju odabran oblik polinoma drugog reda, moguće je napraviti i provjeru koliko je dobra regresija odzivne funkcije (slika 28) tj. koliko se predviđene vrijednosti iz funkcije odzivne površine poklapaju sa promatranim vrijednostima dobivenim analizom za ulazne parametre.

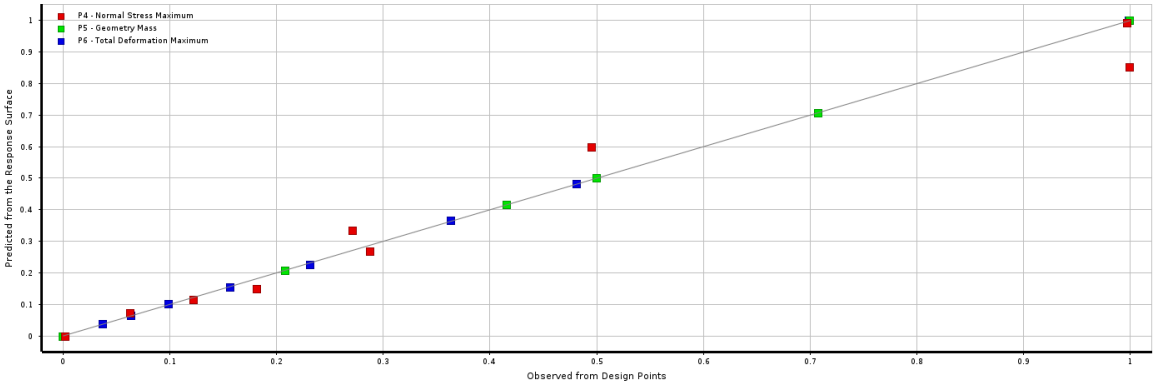

Slika 28. Analiza regresijske funkcije

Nakon analize odzivne površine slijedi optimiranje odzivne površine. Potrebno je zadati koji izlazni parametri se optimiraju, tj. predstavljaju funkciju cilja, a koji predstavljaju funkcije ograničenja. Za prvi dio zadatka funkcija cilja je pronaći minimalnu masu, a ograničenje dopušteno naprezanje.

Outline of Schematic B4: Optimization

	A	B	C
1		Enabled	Monitoring
2	Optimization		
3	Objectives and Constraints		
4	Minimize P5		
5	P9 <= 20000 psi		
6	Domain		
7	Static Structural (A1)		
8	P7 - R1	☑	
9	P8 - R2	☑	
10	Parameter Relationships		
11	P7 >= P8	☑	
12	Convergence Criteria		
13	Results		
14	Candidate Points		
15	Tradeoff		
16	Samples		
17	Sensitivities		

Slika 28. Postupak optimiranja

Postavljena je ovisnost između parametara, P7>=P8, tj. definirano je da $r_1 >= r_2$ kako bi se algoritam prisilio da odabere rješenje u kojem su $r_1 \approx r_2$.

Table of Schematic B4: Optimization

	A	B	C	D
1	Input Parameters			
2	Name	Lower Bound	Upper Bound	
3	P7 - R1 (in)	0.35	0.7	
4	P8 - R2 (in)	0.35	0.7	
5	Parameter Relationships			
6	Name	Left Expression	Operator	Right Expression
7	P7 >= P8	P7	>=	P8
*	New Parameter Relationship	New Expression	<=	New Expression

Slika 29. Ovisnost parametara

Table of Schematic B4: Optimization , Candidate Points

	A	B	C	D	E	F	G	H	I
1	Reference	Name	P7 - R1 (in)	P8 - R2 (in)	P5 - Geometry Mass (lb)		P6 - Total Deformation Maximum (in)	P9 - Normal Stress Maximum (psi)	
2					Parameter Value	Variation from Reference		Parameter Value	Variation from Reference
3	○	Candidate Point 1	0.32413	0.31652	31.833	-0.97%	0.6916	19804	0.97%
4	○	Candidate Point 2	0.32341	0.31822	31.897	-0.77%	0.68745	19487	-0.64%
5	◉	Candidate Point 3	0.32767	0.31753	32.144	0.00%	0.68676	19613	0.00%
*		New Custom Candidate Point	0.4	0.4					

Slika 30. Optimalna rješenja

Osim tablice optimalnih rješenja (slika 30.) moguće je prikazati brojne dijagrame, kao što su dijagrami promjene izlaznih parametara ovisno o koraku optimiranja, slike 31. i 32.. Ovi dijagrami pokazuju kako su se izlazne vrijednosti mijenjale sa svakim korakom optimiranja.

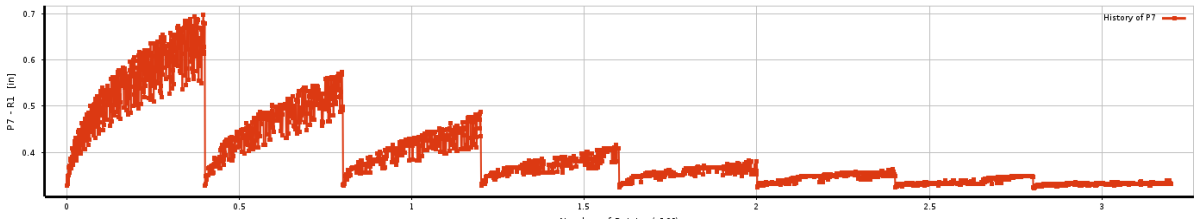

Slika 31. Dijagram povijesti optimiranja mase

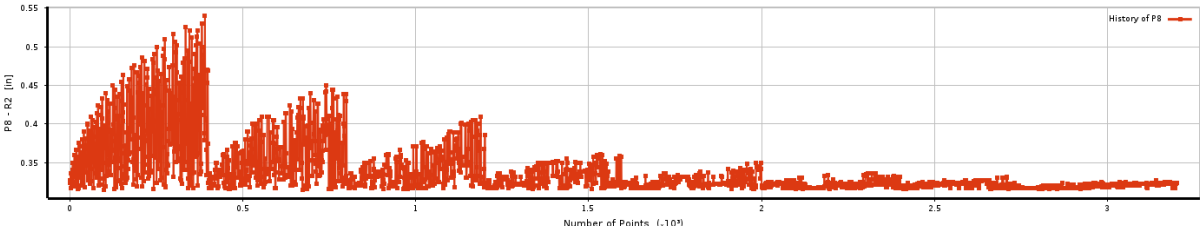

Slika 32. Dijagram povijesti normalnog naprezanja

Moguće je promatrati konvergenciju, osjetljivost i druge rezultate. Također moguć je i ručni odabir optimizacijskog algoritma i podešavanje parametara optimiranja. Rješenje ovog algoritma daje vrijednost koja je vrlo blizu rješenjima dobivenim u Matlab-u.
Rješenja dobivena u Matlab-u

$$x_2 = 0.5443 \quad (7.1)$$

Parametar x_2 predstavlja omjer površina

$$x_2 = \frac{A}{A_{ref}} \quad (7.2)$$

Za štap okruglog presjeka površina se računa:

$$A = r^2\pi \quad (7.3)$$

Iz površine presjeka slijedi polumjer

$$r = \sqrt{\frac{x_2 \cdot A}{\pi}} = 0.3 \text{ in} \quad (7.4)$$

Rješenja dobivena u Ansys-u za problem optimiranja radijusa iznose, slika 7.27:

$$r_1 = 0.32767 \text{ in} \quad (7.5)$$

$$r_2 = 0.31753 \text{ in} \quad (7.6)$$

Rezultati pokazuju da su rješenja dobivena optimiranjem funkcije cilja u Matlab-u i planom pokusa u Ansys-u vrlo bliska.

4. Zaključak

Ukoliko je poznato analitičko rješenje ili je relativno jednostavno postaviti zadatak kako bi se došlo do izraza funkcija cilja korištenjem alata za simboličko programiranje moguće je optimirati funkciju cilja uz zadana ograničenja. Matlab ali i većina drugih programskih paketa kao primjerice Mathcad

ili Mathematica nude gotove optimizacijske algoritme, kojima je moguće optimirati funkciju, pri tome je moguće birati odgovarajući postupak optimiranja kao i parametre optimiranja.
Ukoliko je analitičko rješenje složeno, softverski paketi kao primjerice Ansys koji vrše analizu metodom konačnih elemenata ili konačnih volumena, ovisno o vrsti problema, nude često i mogućnost optimiranja. U ovom radu je prikazana usporedba postupka optimiranja u Matlabu i Ansys-u. U Ansys-u je korišten algoritam za optimiranje plana pokusa, a moguće je i direktno optimiranje.
Iako je korištenje Ansys-a za inženjerske simulacije vrlo uvriježeno među stručnjacima i znanstvenicima, zahtjeva prilično mnogo vremena kako bi se istražile brojne mogućnosti, softver je složen i sadrži brojna ograničenja koja je moguće obići, ali to iziskuje dodatne napore. Novi alati i mogućnosti koje se pojavljuju u novijim verzijama softvera često olakšavaju rad, ali redovita nadogradnja je prilično skupa. S druge strane na internetu su brojne grupe i online društva koja pružaju pomoć u radu, a i stručnjaci iz kompanija koje prodaju i održavaju softver voljni su pomoći kada korisnik naiđe na poteškoće prilikom rješavanja problema.

5. Literatura

[1] Rao, Singiresu S.: Engineering Optimization, Theory and Practice, Wiley & Sons, Inc., 2009. (book/chapter in book)
[2] Konjicija, Samim: Optimizacija resursa, Uvodno predavanje, Sarajevo, 2016. (course materials)
[3] Bertoša, Branimir: Optimizacija, Predavanje 5, Matematičke metode u kemiji 2, https://www.pmf.unizg.hr/chem/predmet/mmuk2, dostupno 12.7.2019. (course materials)
[4] Bui, Lam Thu, Alam, Sameer: Multi-Objective Optimization in Computational Intelligence: Theory and Practice, Information science reference, Hershey, 2008. (book/chapter in book)
[5] Miettinen, Kaisa: Nonlinear multiobjective optimization, Kluwer Academic Publishers, 1999.
[6] Messac, Achille: Optimization in practice with Matlab® for engineering students and professionals, Cambridge university press, 2015. (book/chapter in book)
[7] https://www.youtube.com/watch?v=yKQax0PTUnc (web video)
[8] https://support.ansys.com/staticassets/ANSYS/Conference/Confidence/Houston/Downloads/optimization-in-ansys-workbench.pdf (web site)
[9] Module 01: Introduction - Introduction to ANSYS DesignXplorer (course materials)
[10] Module 05: Optimization - Introduction to ANSYS DesignXplorer (course materials)

Handheld laser welding of different materials - shielding gases and applications

Michael Wolters[1,*], Tomislav Klobucarevic[2,*]

[1]Messer SE & Co. KGaA, Department of Development, Krefeld, Germany
[2]Messer Croatia Plin d.o.o., Zapresic, Croatia

[*] Corresponding Author. E-mail:
Michael.wolters@messergroup.com
tomislav.klobucarevic@messergroup.com

Abstract

Manual laser welding has been increasingly used in industry and small and medium-sized companies for a few years now. In the future, this welding process could replace a significant part of TIG, MIG and MAG welding tasks.
Manual laser welding cannot yet keep up with the established welding processes. Special technological properties of the welded joints are required.
Obtaining a welding procedure qualification is still difficult and is limited to low sheet thicknesses. This welding process is currently still in the development phase.
The presentation shows the influencing welding parameters and their different effects on the welding process. These parameters include, for example, the scan frequency, scan width, focus position, wire feed speed, welding speed, welding torch position and welding power. These influence the welding depth and the formation of the weld pool. They can lead to different heat input into the component and contribute to different mechanical pore formation and degassing.
In connection with metallurgical aspects, the effects of different shielding gases and shielding gas mixtures are investigated. Most manufacturers recommend the use of argon or nitrogen, but there is usually no specification or justification for one of the gases.
Argon is an inert gas that has no influence on melting metallurgy. Nitrogen, on the other hand, is absorbed by the liquid melt and later stored in the metal structure. The formation of nitrides with the different metals and alloying elements cannot be ruled out. Nitrogen is known to be harmful to structural steel. Even small amounts can later lead to embrittlement. As is already known from the now banned Thomas steel. When hand-laser welding austenitic steels, nitrogen has been proven to increase strength and hardness.
An important aspect when examining shielding gases is also their influence on pore formation.

Keywords: handheld laser welding, stainless steel, mild steel, aluminum, shielding gases

1. Introduction

Laser welding is now an established welding process. It is used in large and medium-sized companies. The laser beam source is no longer the cost driver for this process. Software and automation of the welding process account for a large proportion of the costs.
Laser beam sources are now produced inexpensively in the Far East. This has led to the development of a new welding process. Manual laser welding has been entering the Euro-pean market for a few years now. It is also already widespread in the USA.
In this process, a laser beam is guided via a fiber optic cable to a manual welding torch. This laser creates a molten pool that must be protected by a shielding gas. An external supply of a wire-shaped welding consumable is optional. It is required for filling fillet welds.
The use of manual laser welding requires various protective measures. These must be met before the process is introduced, especially in America and Europe. Adequate protection of the welders and all personnel and equipment in the vicinity must be ensured. In addition, the handheld laser welding device must comply with the applicable local regulations. Certified devices have been available in Europe since the end of 2022. These devices have been available in China and the USA for some time.
Handheld laser welding allows common metals and metal alloys to be easily welded. It is therefore seen as a competitor to traditional arc welding. Above all, the price of laser beam generation has become so affordable that these devices have become a real alternative to arc welding. Laser sources for handheld laser welding are available for under €10,000. These are non-certified machines without approval. However, the devices can still be purchased from China. Certified machines are available starting at €20,000.

2. Process Description

For handheld laser welding, both thermal conduction welding and deep penetration weld-ing or keyhole welding can be used.
In thermal conduction welding, the material to be welded is melted at the surface by the laser beam. A molten pool forms through heat conduction.
Deep penetration welding occurs at very high energy density. The material is vaporized by the laser beam. The vapor serves to transfer the heat to the remaining material. The laser beam essentially drills into the material and forms a vapor capillary. This then transfers the heat to the surrounding material.

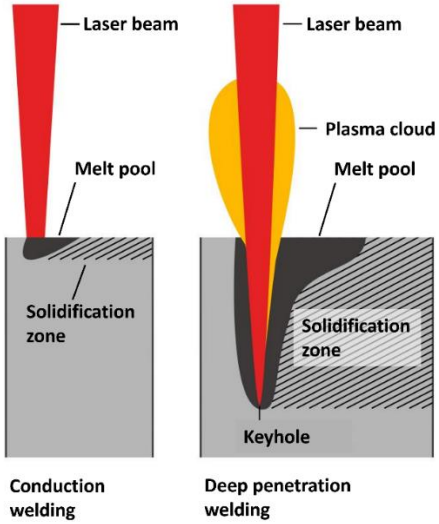

With thermal conduction welding, penetration depths of tenths of a millimeter can be achieved.
The most commonly used handheld laser welding process, however, is deep penetration welding. This currently achieves penetration depths of approximately 10 mm. However, this penetration depth is not yet usable in production.
A special feature of handheld laser welding is the wobble function.

3. Influencing Factors

As with conventional welding processes, this process also has a multitude of influencing factors. The conventional influencing factors include those known from established arc welding processes.

Conventional influences:

- Material
- Material thickness
- Power
- Welding speed
- Wire feed

However, with handheld laser welding we encounter influencing factors that are unknown in conventional arc welding processes.

Special influences (especially for handheld laser welding):

- Beam characteristics, heat distribution
- Focus position
- Wobble (wobble frequency, wobble width)

- Torch position
- Shielding gas

In the following, the influencing factors and their influences that differ from the usual influencing factors are discussed in more detail.
The torch position likely has a different influence on the welding result than with arc welding processes. Since welding is performed with a very narrow vapor capillary, degassing of the molten pool is difficult. This is strongly influenced by the torch position.
Since all tests were conducted manually, the influence of the torch position could not be investigated.

3.1. Beam characteristics, heat distribution

Two different laser beam sources were used for the welding tests. This was done to investigate the influence of the laser beam sources and their beam characteristics.

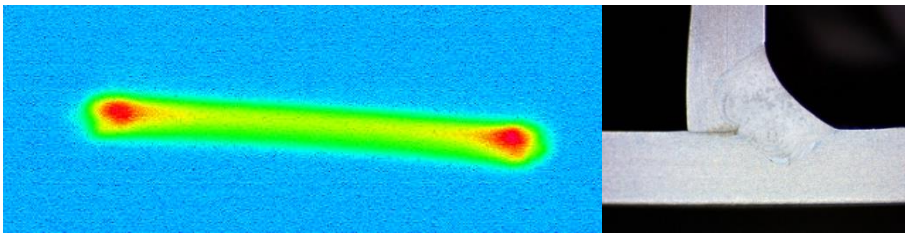

The first welding system had a maximum power of 1.5 kW. It was equipped with a simple wobble function. This meant that the laser beam was continuously bounced back and forth by a mirror. The image above shows a visual representation of the heat distribution without any welding movement. It can be seen that there is increased heat input at the ends of the wobble section. This naturally also affects the penetration. There is increased penetration at the weld flanks. The unfavorable heat distribution makes it difficult to detect the root.

The second system exhibits an irregular wobble motion. The wobble speed decreases to-ward the center of the wobble section. This results in increased heat input in the center of the wobble section.

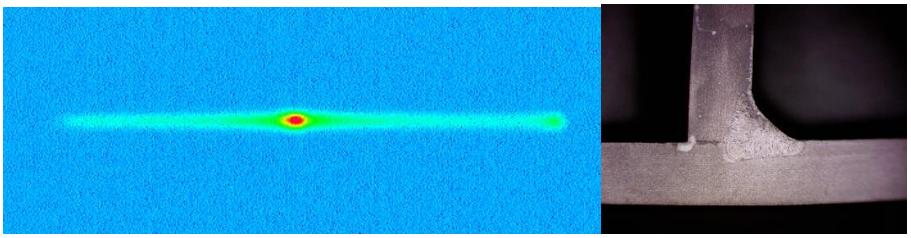

This has a corresponding effect on the penetration profile. There is no increased penetration at the weld flanks. The concentrated heat input in the center significantly facilitates penetration of the root.

3.2. Focus position

Another important influencing factor is the focal position. The focal position can be neutral, positive, or negative. With a neutral focal position, the focal point is directed toward the sheet surface. A positive focal position means the focal point is above the sheet sur-face. If the focal position is negative, the focal point is below the sheet surface.

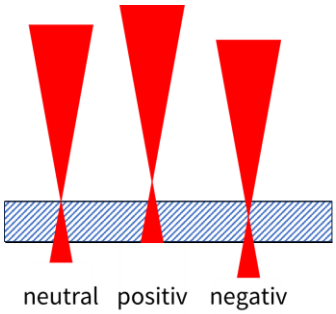

Since the surface power of the laser beam is highest at the focal point, the position of the focal point is of great importance.
With a neutral position of the focal point, the highest possible surface power is directed onto the surface. This enables good laser coupling.
With negative defocusing, the energy density on the surface is lower. The bottom of the vapor capillary is then charged with a high energy density, and the vapor capillary extends further into the depth. More pores are formed.
Positive defocusing also reduces the energy density at the surface. As the vapor capillary continues, the energy density decreases further, and the evaporation of the material de-creases. This results in a shallower penetration depth and fewer pores.

3.3. Wobbling

Wobbling is the back-and-forth movement of the laser using a mirror in the welding torch. The amplitude can be adjusted in mm and the frequency in Hz. The wobbling occurs perpendicular to the welding direction.

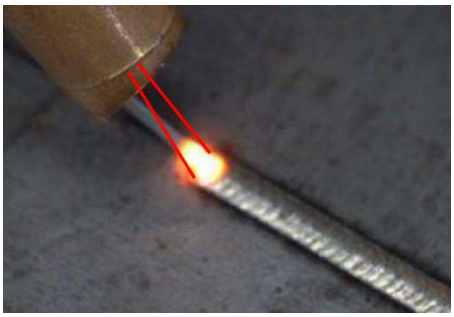

Wobbling is necessary because the laser beam is focused to a diameter of approximately 20 µm to approximately 150 µm at the material surface. Focusing the laser beam achieves the desired energy density.
With such a small "weld spot" no welder would be able to reach a welding gap and complete a weld.

3.4. Shielding gases

Unlike conventional arc welding processes, shielding gases and their components play a different role in the handheld laser welding process. In arc welding, shielding gases and their mixtures influence the physics of the arc. The arc can expand or contract. The heat distribution within the arc is also affected. In handheld laser welding, gas properties such as thermal conductivity can be utilized. Components with metallurgical properties, such as oxygen, can also positively influence the welding process. Many manufacturers recommend nitrogen as a universal shielding gas. However, compatibility with different materials and their alloying elements must be considered. While argon and helium are inert gases, nitrogen, oxygen, CO2, and hydrogen are reactive gases.

- Argon and helium are inert gases; they cannot be dissolved in liquid metals and do not participate in any chemical reactions.
- Nitrogen dissolves in the liquid melt and can later be interstitially incorporated into the atomic lattice or form nitrides with alloying elements.
- Oxygen reacts with metals to form oxides.
- Hydrogen diffuses into the liquid melt pool and can remain interstitially dissolved there during solidification or form pores.

In the individual applications, it must now be taken into account which gas components can react with a material or alloying element and which reaction products can be formed.

4. Preliminary tests on stainless steel

Our initial welding tests were conducted using the manufacturer's recommended parameters. In addition to the recommended shielding gas nitrogen, we also used other gases and gas mixtures.

The external appearance of the welded T-joints was positive. The top surfaces of the welds were bright, and there was hardly any tarnish visible on the back (root side).
We then took samples for microsections. The results were less satisfactory under the microscope. In addition to the noticeable pore formation with argon and argon mixed gases, an unusual penetration profile was observed. The rectangular penetration profile resulted in intensive penetration of the weld flanks. The root, however, was not sufficiently penetrated. The following images show the effect of the individual gases and gas mixtures on the penetration behavior.

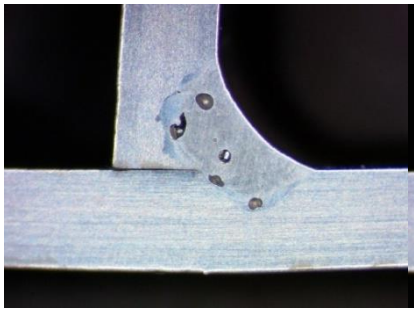

Argon

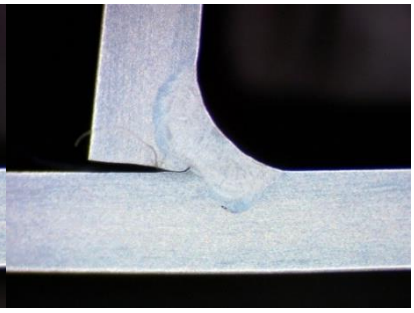

Nitrogen

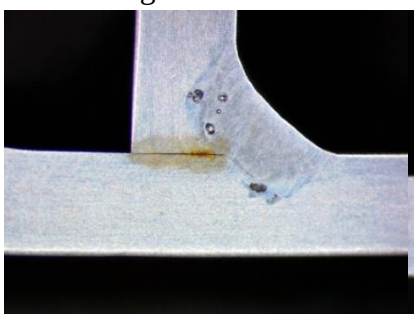

Argon, 30% Helium

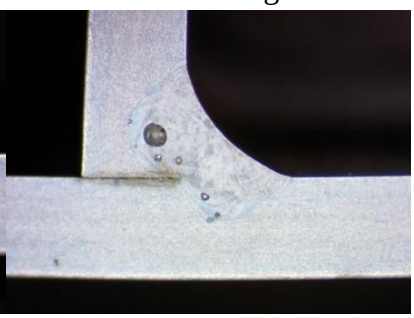

Argon/Nitrogen/Hydrogen

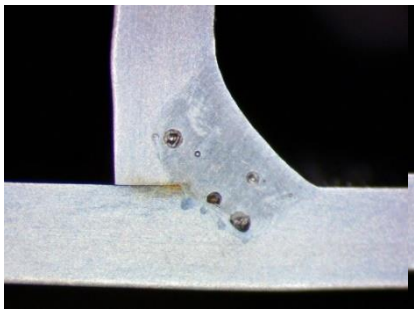

Argon/Hydrogen

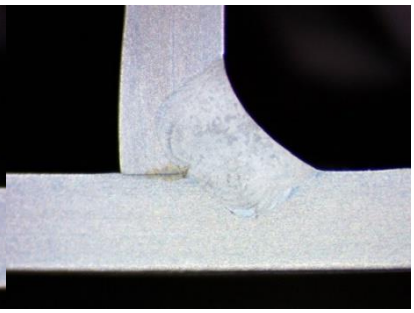

Nitrogen/Hydrogen

5. Influence of nitrogen

Nitrogen is not an inert gas. It is known from metallurgy that nitrogen is interstitial in the microstructure and, depending on the material, can lead to strain and hardening of the microstructure

or form intermetallic compounds. We wanted to demonstrate nitrogen uptake using the stainless-steel specimens we welded.
To this end, we compared the hardness of the base material and the weld metal of specimens welded using argon or nitrogen.

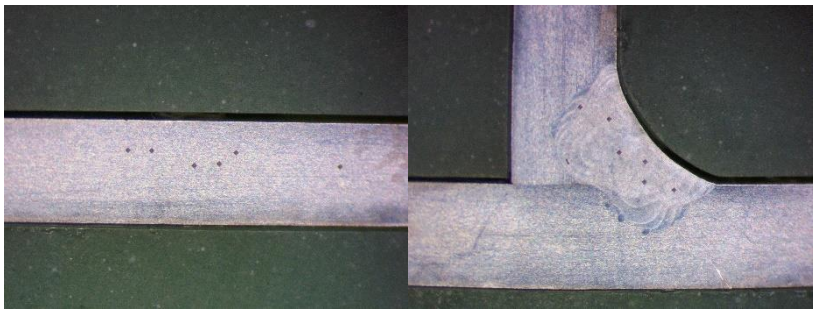

Hardness test, base material Hardness test, weld metal

Vickers Hardness Test of base material and weld metal

Gas	Vickers hardness [HV1], single values										hardness average		
	BM1	BM2	BM3	WM1	WM2	WM3	BM4	BM5	BM6		BM 1-3	Weld metal	BM 4-6
Argon	190	184	186	183	196	188	195	193	191		186,7	189,0	193,0
nitrogen	176	179	180	204	220	210	187	184	193		178,3	211,3	188,0
Ar/N2, H2	191	183	180	203	198	216	195	200	186		184,7	205,7	193,7
N2/H2	195	193	193	210	209	210	191	183	190		193,7	209,7	188,0
average values		186			209*			191					

*) only nitrogen-containing welds included

An average hardening of approximately 10% was observed. This provided evidence that nitrogen was absorbed by the weld metal. In the case of stainless steel 1.4301, this fact is not dramatic, as the toughness of the mate-rial is only slightly reduced. There is a risk of nitride formation with metals or alloying elements such as molybdenum (Mo), vanadium (V), titanium (Ti), manganese (Mn), magnesium (Mg), or aluminum (Al). Depending on the shape of these intermetallic compounds, embrittlement of the material can occur, as is known from ferritic alloys such as structural steels. Therefore, material compatibility must be checked in advance.

6. Welding tests

The following welding tests specifically demonstrate the influences of wobble frequency, focus position, and individual gases and gas mixtures. In addition, the results of two laser beam sources

with different beam characteristics are presented. Depending on the material, the different beam characteristics of the laser beam sources had different effects. Macro sections are shown, with the corresponding X-ray images on the upper side.

7. Welding tests on structural steel

7.1. Preliminary tests

For the preliminary tests, the welding parameters recommended by the manufacturer were used.

Laser 01 (Multi Mode)

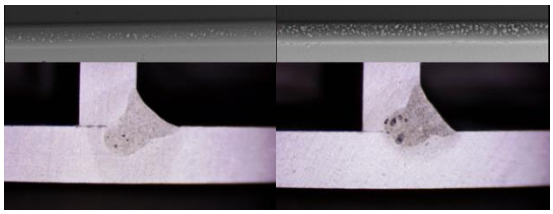

Nitrogen Argon

Laser 02 (Single Mode)

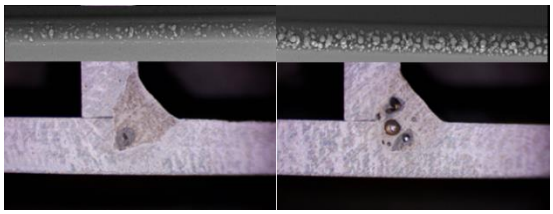

Nitrogen Argon

A significant difference in pore formation was observed with similar penetration.
Since ferritic steels have a strong tendency to form nitrides, the focus for the subsequent optimization of the welding parameters was on argon and argon-based gas mixtures.

7.2 Influence of the wobble frequency for different laser sources

Laser 01 (Multi Mode)

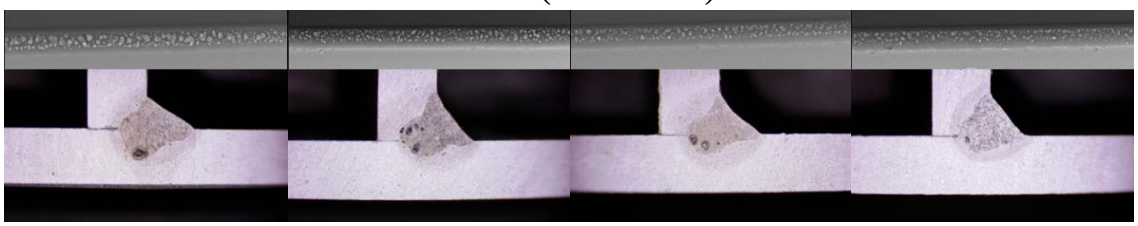

WF 30 Hz WF 60 Hz WF 120 Hz WF 250 Hz

Laser 02 (Single Mode)

WF 60 Hz WF 75 Hz WF 90 Hz

With the multi-mode laser, increasing the wobble frequency only results in a slight reduction in pore formation and penetration. With the single-mode laser, welding was performed with lower energy. Here, a reduction in penetration can be seen due to the increased wobble frequency. The reduction in pore formation can be attributed to both the increased wobble frequency and the reduced penetration caused by the lower welding energy.

7.3. Influence of the focus position

Laser 01 (Multi Mode)

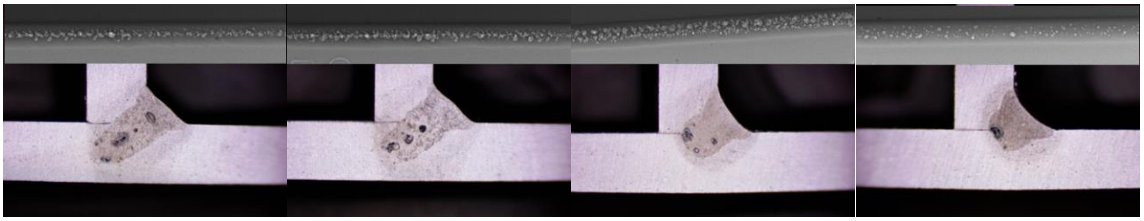

FP -5 mm FP 0 mm FP +5 mm FP +10 mm

Laser 02 (Single Mode)

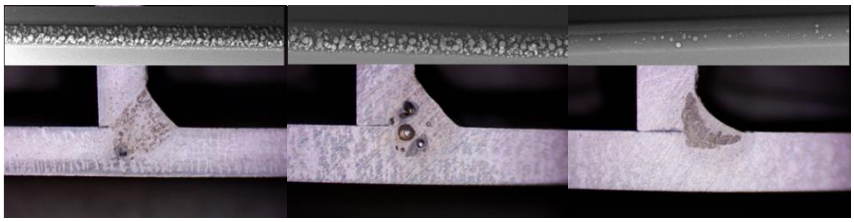

FP -5 mm FP 0 mm FP +5 mm

For both laser beam sources, a significant reduction in penetration and pore formation can be observed due to the positive defocusing.

7.4. Best results with different shielding gases

The following images show the best results that could be achieved with different shielding gases.

Laser 01 (Multi Mode)

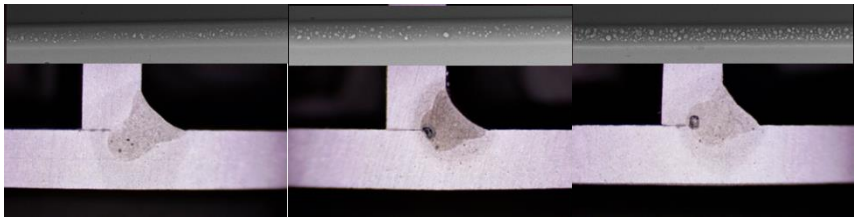

Nitrogen Argon Argon/Oxygen

Laser 02 (Single Mode)

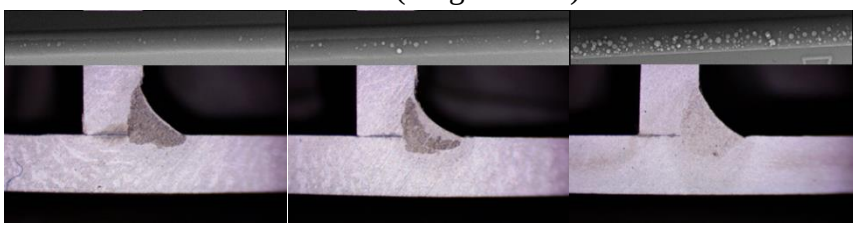

Nitrogen Argon Argon/Oxygen

Both laser beam sources were able to produce low-porosity welds using nitrogen.
When using argon, more pores were observed. The single-mode laser showed slightly less pore formation. Oxygen increased penetration with both laser beam sources. However, pore formation also increased.

8. Welding tests on stainless steel

8.1. Preliminary tests

For the preliminary tests, the welding parameters recommended by the manufacturer were used.

Laser 01 (Multi Mode)

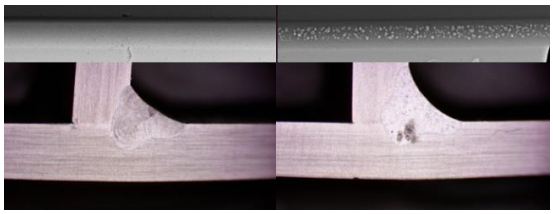

Nitrogen Argon

Laser 02 (Single Mode)

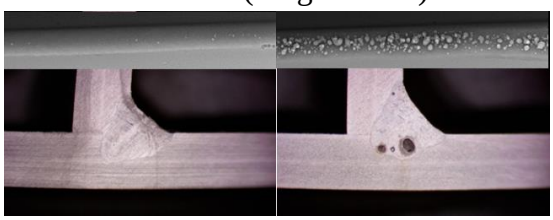

Nitrogen Argon

A significant difference in pore formation was observed with similar penetration. To optimize the welding parameters, argon and nitrogen gas mixtures with hydrogen and oxygen were considered.

8.2. Influence of the wobble frequency on single-mode lasers

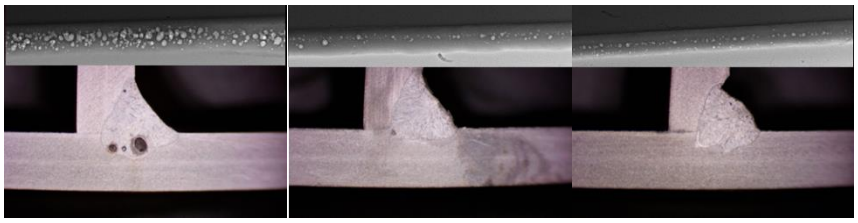

WF 60 Hz WF 120 Hz WF 220 Hz

The single-mode laser shows a significant reduction in pore formation with a slight reduction in penetration when the wobble frequency is increased. However, an excessively high wobble frequency leads to penetration problems. The penetration becomes irregular, and undercuts may occur.

8.3. Influence of the focus position on single-mode lasers

Argon

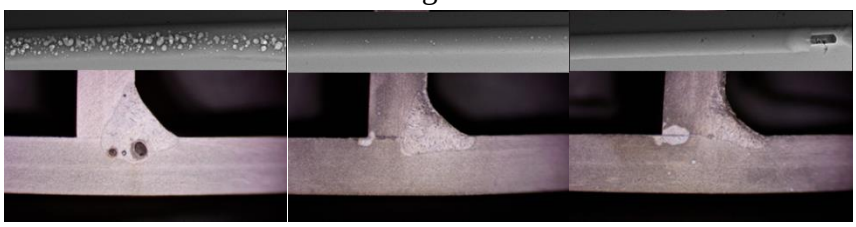

FP 0 mm FP +5 mm FP +10 mm

Nitrogen

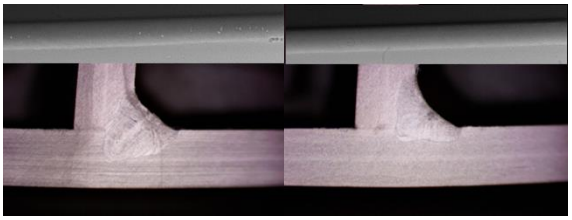

FP 0 mm FP +5 mm

Positive focusing leads to a reduction in penetration in single-mode lasers. A significant reduction in pore formation can be achieved, especially when using argon.

8.4. Best results with different shielding gases

For metallurgical reasons, stainless steels allow the use of many gas components. Argon, nitrogen, hydrogen, and oxygen were used for the gas mixtures. The following images show the best results achieved with different shielding gases.

Laser 01 (Multi Mode)

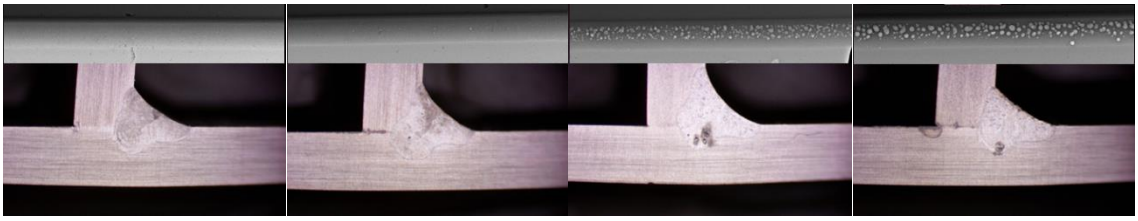

Nitrogen Nitrogen/Hydrogen Argon Argon/Hydrogen

Laser 02 (Single Mode)

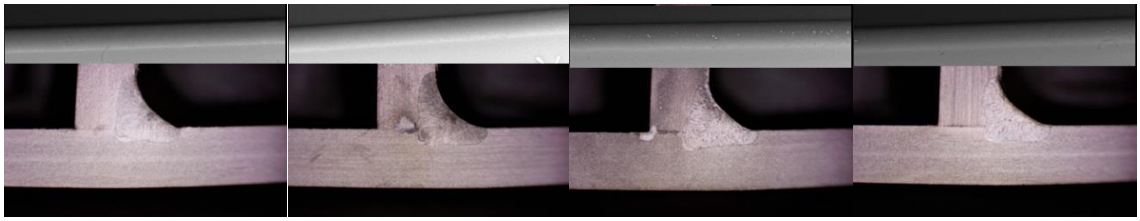

Nitrogen Nitrogen/Hydrogen Argon Argon/Hydrogen

Oxygen led to severe pore formation in both laser beam sources and was therefore not included in the evaluation. Nitrogen and nitrogen/hydrogen mixtures produced very good welding results with the multi-mode laser. Argon and argon/hydrogen mixtures still led to severe pore formation. With the single-mode laser, nitrogen, nitrogen-hydrogen mixtures, argon, and argon/hydrogen mixtures showed very good welding results.

9. Welding tests on aluminum

9.1. Preliminary tests

For the preliminary tests, the welding parameters recommended by the manufacturer were used.

Laser 01 (Multi Mode)

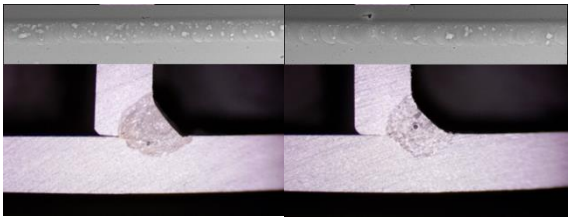

Nitrogen Argon

Laser 02 (Single Mode)

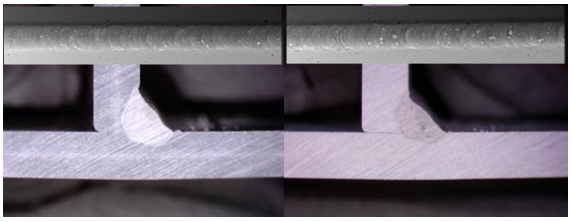

Nitrogen Argon

Aluminum shows a different behavior during handheld laser welding than mild steel and stainless steel. While nitrogen resulted in significantly less pore formation in these steels, this effect was not observed when welding aluminum. Due to the nitride formation of aluminum, magnesium, and titanium, the focus was again on argon in subsequent welding tests. The welding tests with the single-mode laser all showed a strong tendency toward pore formation. Therefore, the results with the single-mode laser were not included in the evaluation.

9.2. Influence of the wobble frequency on multi-mode lasers

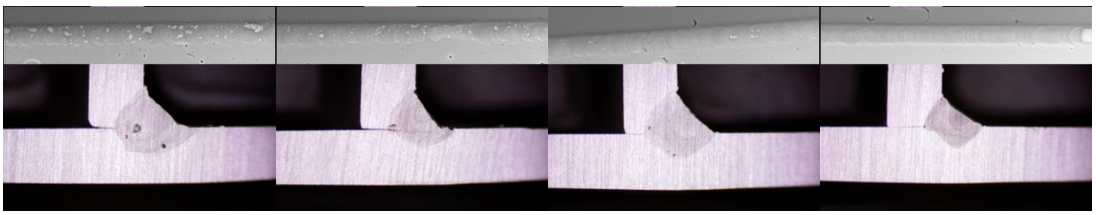

WF 30 Hz WF 60 Hz WF 120 Hz WF 250 Hz

Increasing the wobble frequency has only a minor effect on penetration. A lower frequency leads to a more rounded penetration. Increasing the frequency results in a significant re-duction in pore formation.

9.3. Influence of the focus position on multi-mode lasers

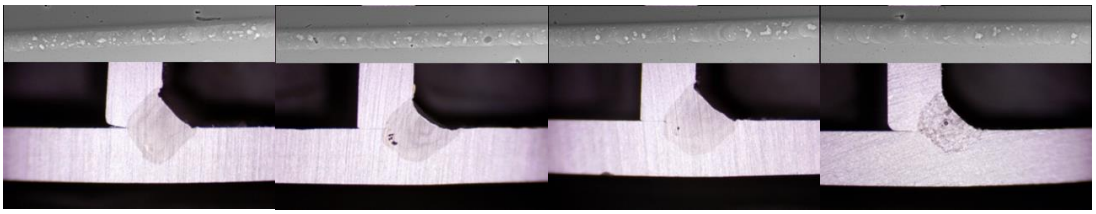

FP -2 mm FP 0 mm FP +2,5 mm FP +5 mm

Positive defocusing also leads to a reduction in pore formation in aluminum.

9.4. Best results with different shielding gases

The following images show the best results that could be achieved with different shielding gases.

Laser 01 (Multi Mode)

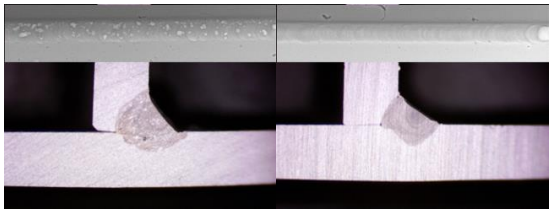

Nitrogen Argon

The multi-mode laser has shown good results in welding aluminum. In contrast to steel, better welding results were achieved with argon than with nitrogen.

10. Conclusion

The handheld laser welding process is influenced by many factors. The factors examined here can be summarized as follows:

- Wobble Frequency
  Increasing the wobble frequency leads to more uniform heat input. The consequences are less penetration and fewer pores.
- Focus Position
  At a neutral focus position, the energy density on the sheet surface is highest. This provides good coupling to the laser beam. The energy input is very high and leads to increased pore formation via intensive vaporization of the material. Negative focusing reduces the energy density but introduces a lot of energy into the vapor capillary. This also leads to intensive vaporization of the material with increased pore formation. The best results were achieved with positive focusing.
- Laser Beam Source
  The beam source has a significant influence on the welding result due to the type of wobble function and the energy distribution in the wobble motion. As the welding tests on steel showed, the single-mode laser produced a completely different penetration behavior than the multi-mode laser. Pore formation was also significantly reduced. When welding aluminum, the welding results of the revised beam source with the single-mode and intermittent wobble motion were less satisfactory.

11. Literature

[1] International Journal of Heat and Mass Transfer: Elucidation of keyhole induced bubble formation mechanism in fiber laser welding of low carbon steel, Dongsheng Wu, Xueming Hua ⇑, Lijin Huang, Fang Li, Yan Cai

[2] SUPPLEMENT TO THE WELDING JOURNAL, OCTOBER 2015: The Effect of Ar and N2 Shielding Gas on Laser Weld Porosity in Steel, Stainless Steels, and Nickel, BY J. W. ELMER, J. VAJA, H. D. CARLTON, AND R. PONG

[3] The International Journal of Advanced Manufacturing Technology (2023) 127:1887–1894: The influence of shielding gases on keyhole-induced porosity and nitrogen absorption in SS 304 stainless steel fiber laser welds, Hafez Khalid M.

[4] BIAS – Bremer Institut für angewandte Strahltechnik, Band 63: Dynamik und Stabil-ität der Dampfkapillare beim Laserstrahltiefschweißen, Jörg Volpp

[5] Acta Materialia Transylvanica 7/1. (2024) 44–47: The Effects of Laser Power and Travel Speed on Weld Geometry in the case of Manual Laser Welding, Virág SIMON, Balázs VARBAI, Károly ABAFFY, László GYURA

[6] The International Journal of Advanced Manufacturing Technology (2024) 134:1947–1964: Gap bridging in laser welding of EN AW 5083 with different joint configura-tions via beam oscillation and filler wire (Received: 20 April 2024 / Accepted: 30 July 2024 / Published online: 12 August 2024), Kenan Kaan Yetil, Daniele Colombo, Yusuf Ayan, Ali Gökhan Demir

[7] Effect of Oscillation Parameters on Weld Surface Morphology during Laser Beam Oscillation Welding of Stainless Steel, Binxin Donga, Zhiyong Lia, Bo Chena, Xiuli He

ANALIZA ZAVARENOG SPOJA NA CIJEVIMA OD TITANA

ANALYSIS OF WELDED JOINT ON TITANIUM PIPES

R. Hamzić[1,*], N. Džibrić[1], S. Avdić[1]

[1]Institut za zavarivanje d.o.o. Tuzla, Bosne Srebrene broj 6, Tuzla, Bosna i Hercegovina

e-mail: resul.hamzic@izz-bh.ba

Rezime

U ovom istraživanju provedena je analiza mehaničkih svojstava i mikrostrukture zavarenog spoja na cijevi od titana Gr.2. Zavareni spojevi pripremljeni su primjenom odgovarajuće tehnologije zavarivanja, nakon čega su provedena mehanička ispitivanja s ciljem određivanja čvrstoće i tvrdoće. Rezultati su potvrdili zadovoljavajuće mehaničke karakteristike.
Metalografska analiza obuhvatila je ispitivanje makrostrukture i mikrostrukture zavarenog spoja, omogućavajući uvid u faktore koji imaju uticaja na njegova svojstva. Na temelju provedenih mehaničkih ispitivanja i metalografske analize donesen je zaključak da zavareni spoj ispunjava zahtjeve standarda i predviđene primjene.
Provedeno istraživanje omogućava jasniji uvid u svojstva zavarenih spojeva od titana Gr.2 te pruža smjernice za unapređenje zavarivačkih postupaka i poboljšanje njihovih karakteristika u industrijskoj primjeni.

Ključne riječi: Zavareni spoj, Titan Gr.2, Mehanička ispitivanja, Mikrostruktura, Svojstva

Abstract

This study analyzes the mechanical properties and microstructure of a Grade 2 titanium welded pipe joint. The welded joint were created via an appropriate welding technology, after which the welded joint were mechanically tested for hardness and strength. The results confirmed acceptable mechanical properties.
Metallographic investigation comprised examination of the macrostructure and microstructure of the welded joint and a survey of the effect on properties of influencing factors. The conclusion with

respect to requirements of standards and intended application after conducted mechanical testing and metallographic examination is that the welded joint meets these.
The conducted research provides a greater understanding of Grade 2 welded titanium joints and offers recommendations regarding the optimization of welding processes as well as establishing their characteristics under industrial conditions.

Keywords: Welded joint, Titanium Gr.2, Mechanical properties, Microstructure, Properties

1. Uvod

Zavarivanje titana i njegovih legura igra ključnu ulogu u raznim industrijama, od vazduhoplovstva i automobilske industrije do hemijske obrade i medicinske opreme. Svojstva i kvalitet zavarenih spojeva od iznimne su važnosti kako bi se osigurao integritet i pouzdanost komponenti ili konstrukcija.
Ovo istraživanje fokusirano je na analizu mehaničkih svojstava, makro i mikrostrukture zavarenog spoja na cijevima od titana Gr.2. Osnovni cilj je proučiti makro i mikrostrukturu, zatim mehaničke osobine zavarenog spoja kako bi dobili informacije o njegovoj prikladnosti za određene industijske primjene.
Analiza uključuje pripremu zavarenih spojeva na cijevima od titana Gr.2, primjenom odgovarajuće tehnike zavarivanja. Nakon toga će se provesti niz mehaničkih ispitivanja kako bi se procijenile ključne mehaničke karakteristike, uključujući čvrstoću, žilavost i tvrdoću. Provest će se metalografska analiza kako bi se proučila makro i mikrostruktura zavarenog spoja, uključujući strukturu zrna, faze i moguće nedostatke.
Ocjena zavarenog spoja temeljit će se na rezultatima dobivenim iz mehaničkih ispitivanja i metalografske analize.

2. Priprema i zavarivanje uzorka

Uzorak koji je korišten u istraživanju je cijev dimenzija D60,3 t5,54 [mm] od titanijuma Gr.2. Titan Gr.2 je legura titanijuma koja se sastoji od 99,2 [%] čistog titanijuma sa malim udjelom ugljika od 0,1 [%]. Ova legura se često koristi u raznim industrijskim aplikacijama zbog svojih izuzetnih mehaničkih svojstava, visoke otpornosti na koroziju i dobre zavarljivosti.
Dimenzije uzorka su odabrane u skladu sa zahtjevima standarda EN ISO 15614-5:2024 (slika 2.1) koji propisuje specifikacije za ispitivanje zavarenih spojeva na titanu i njegovim legurama.

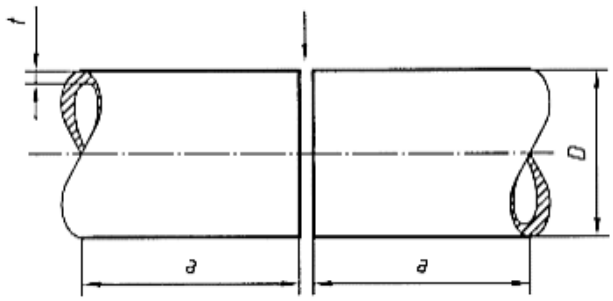

a - minimalna dužina 150 [mm];
D - vanjski prečnik cijevi,
t - debljina stijenke cijevi

Slika 2.1 - Dimenzije uzorka cijevi za sučeono zavarivanje

Priprema cijevi za zavarivanje uključuje niz koraka kako bi se osigurala čista i prikladna površina za postizanje što boljeg kvaliteta zavarenog spoja.
Nakon mašinske pripreme žlijeba (slika 2.2), provedeno je temeljito čišćenje površine cijevi kako bi se uklonile nečistoće, masnoće i oksidi koji mogu negativno utjecati na zavareni spoj. Čišćenje se vrši otopinom za dekapiranje koja sadrži fluorovodičnu kiselinu (48% koncentracija) i azotnu kiselinu (70% koncentracija). Preporučen omjer kiselina je između 1:5 i 1:9 (5%HF i 35%HNO_3 pokazalo se kao učinkovito rješenje). Čišćenje se provodi na sobnoj temperaturi, 1-5 minuta.
Zavarivanje uzorka vršeno je TIG (Tungsten Inert Gas) postupkom u zaštiti inertnog plina. Kao zaštitni plin korišten je argon (Ar), koji se koristio također za zaštitu korijenog prolaza. Ovakvim načinom pripreme površine i izborom postupka zavarivanja teži se osiguranju visoke kvalitete zavarenog spoj.

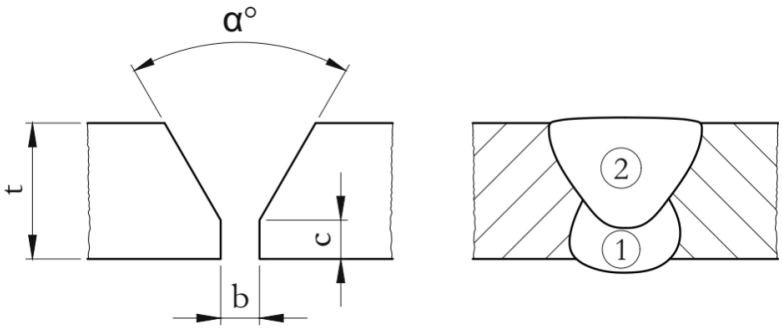

Slika 2.2 - Priprema spoja i redoslijed zavarivanja

Kako bi se osigurala optimalna kvaliteta spoja korišten je dodatni materijal S Ti 0120 (Ti99,6). U tabeli 2.1 su prikazane karakteristike dodatnog materijala uključujući sastav, mehaničke osobine i preporučene parametre zavarivanja.

Tabela 2.1 - Karakteristike dodatnog materijala

Hemijski sastav dodatnog materijala					
C	**Ti**	**Fe**	**N**	**O**	**H**
0,01	REST	0,05	0,005	0,12	0,002
Mehaničke osobine dodatnog materijala					
Rp 0,2	**Rm**		**A**	**Z**	**T**
≥ 250 MPa	≥ 345 MPa		≥ 20%	-	20°C
- Struja zavarivanja: 70-100 [A] - Napon: 9-10 [V] - Zaštitni plin: I1 (100%Ar)					

U toku procesa zavarivanja, važno je kontrolisati parametre zavarivanja. To uključuje pravilno podešavanje struje zavarivanja koja je u ovom slučaju 90 [A], brzine kretanja i dodavanja dodatnog materijala, te protok zaštitnog gasa. Zavarivanje cijevi izvedeno je u položaju H-L045 (ISO 6947:2019), odnosno pod nagibom od 45° u odnosu na vodoravnu osu, a zavar je izvođen u smjeru od donje prema gornjoj strani cijevi.

3. Ispitivanja bez razaranja i priprema uzorka za mehanička i metalografska ispitivanja

Prije pripreme uzoraka za ispitivanja sa razaranjem, izvršena je vizuelna, penetrantska i radiografska kontrola. Navedena ispitivanja nisu otkrila prisutnost nedostataka na uzorku prije njihove pripreme za daljnja ispitivanja.
U tabeli 3.1 dati su parametri radiografskog ispitivanja, koji uključuju napon i struju, fokusnu udaljenost i ekspozicijsko vrijeme.

Tabela 3.1 - Parametri radiografskog ispitivanja cijevi D60,3 t5,54 od titanijuma Gr.2

Parametar	**Vrijednost**
Napon [kV]	150
Struja [mA]	6
Fokusna udaljenost [mm]	550
Ekspozicijsko vrijeme [sec.]	15

Uzorci za mehanička i metalografska ispitivanja pripremljeni su u skladu sa zahtjevima standarda EN ISO 15614-5:2004 (Slika 3.1).

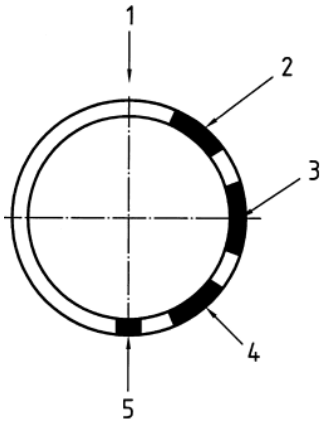

1 - Vrh cijevi.

2 - Uzorci za ispitivanje zatezne čvrstoće i savijanja.

3 - Uzorci za ispitivanje udarne žilavosti.

4 - Uzorci za ispitivanje zatezne čvrstoće i savijanja.

5 - Uzorci za makro analizu i ispitivanje tvrdoće.

Slika 3.1 - Lokacija ispitnih uzoraka na sučeono zavarenoj cijevi

3.1. Ispitivanje zatezne čvrstoće prema EN ISO 4136:2022

Priprema epruvete za ispitivanje zatezne čvrstoće prema standardu EN ISO 4136:2022 uključuje izrezivanje uzoraka prema specificiranim dimenzijama i obliku.
Nakon pripreme epruveta za ispitivanje zatezne čvrstoće, pristupilo se njihovom kidanju na kidalici. Dobiveni rezultati kidanja prikazani su dijagramom koji je prikazan na slici 3.2.

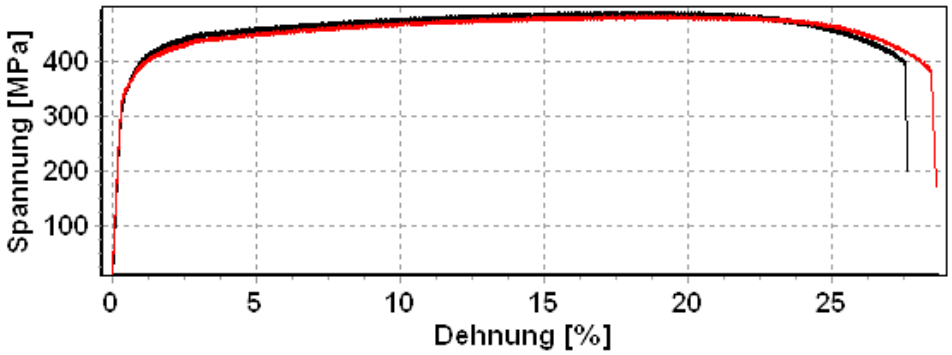

Slika 3.2 - Dijagram napon-deformacija za slučaj ispitivanja titana Gr.2

Vrijednost napona tečenja za ispitni uzorak iznosi 355 [MPa], a zatezna čvrstoća zavarenog spoja koja predstavlja maksimalni napon koji zavareni spoj može podnijeti pri zatezanju prije nego dođe do loma ima vrijednost od 491 [MPa], odnosno u drugom slučaju 484 [MPa]. Vrijednost zatezne čvrstoće i žilavi lom u osnovnom materijalu, ukazuju da je se radi o jakom i otpornom zavarenom spoju, te da ne postoje prisutni nedostaci unutar istog.

3.2. Metalografska analiza zavarenog spoja od titana Gr.2

Priprema uzoraka za metalografsku analizu, odnosno za makro i mikro analizu uključuje nekoliko koraka. Nakon izrezivanja prema specificiranim dimenzijama i obliku uzorci su mehanički obrađeni kako bi se dobila ravna površina za daljnju analizu. Nakon mehaničke obrade, uzorci su podvrgnuti brušenju kako bi se uklonile neravnine i nepravilnosti. Brušenje se izvodi koristeći postupno finije brusne papire i vodeno hlađenje. Nakon brušenja, uzorci se poliraju kako bi se postigla još finija površina. Poliranje se obavlja pomoću finih abrazivnih materijala i polirnih pasti.
Nakon poliranja, uzorci su podvrgnuti nagrizanju, koje ima za cilj otkriti makro i mikrostrukturu uzorka. Kao reagens za nagrizanje spoja od titana Gr.2 korišten je Kellerov reagens (HNO_3 + HF + HCl).
Makroizbrusak slika 3.3, je posmatran pod makroskopom na uvećanju od x3.6, u cijelosti. Nisu uočene nepravilnosti u metalu šava, niti u zoni uticaja toplote (ZUT). Zavareni spoj ima dovoljnu penetraciju.

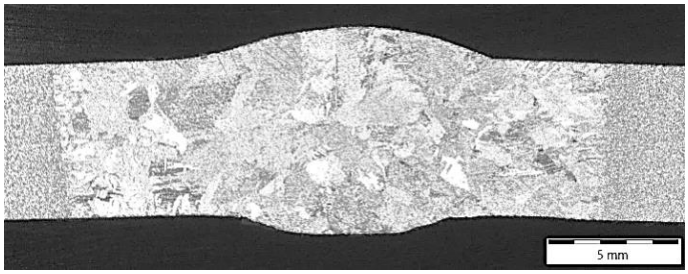

Slika 3.3 - Makroizbrusak na uvećanju x3,6

Uzorak je posmatran pod mikroskopom kako bi se detaljnije proučila mikrostruktura zavarenog spoja. Na slici 3.4 prikazana je mikrostruktura osnovnog materijala na uvećanju od x200.

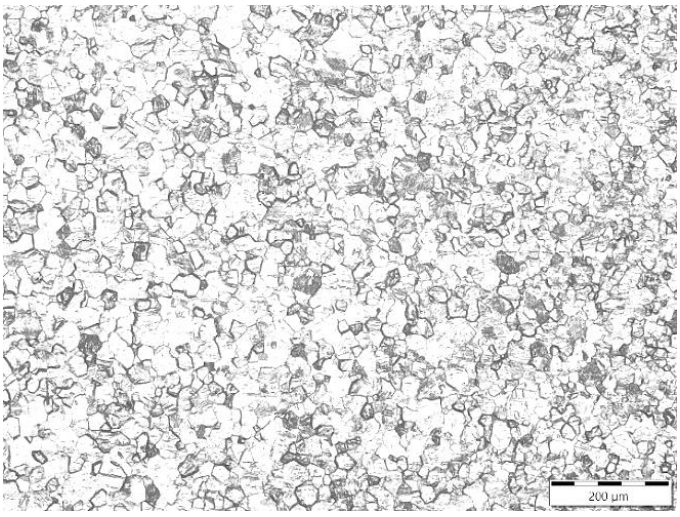

Slika 3.4 - Mikrostruktura osnovnog materijala titana Gr.2 na uvećanju x200

Uočljivo je da se radi o alfa fazi titana, koja je osnovna i dominantna faza u nezavarenom materijalu. Prisutnost alfa faze u mikrostrukturi titana važna je za postizanje željenih mehaničkih osobina.
Na slici 3.5 prikazana je mikrostruktura osnovnog materijala, zone uticaja toplote i zavara na uvećanju od x200.
Proces zavarivanja, odnosno sporo hlađenje nakon zavarivanja uzrokovalo je stvaranje alfa faze kao Widmanstätten ploča, odnosno specifičnog oblika organizacije nazubljene alfa faze u metalu.
Widmanstätten ploče su posebno vidljive zbog prisutnosti alfa i beta faza u mikrostrukturi. Prisutnost Widmanstätten ploča dovelo je do povećanja tvrdoće u metalu šava. Opservacijom i analizom nije uočeno prisustvo uključaka u mikrostrukturi.

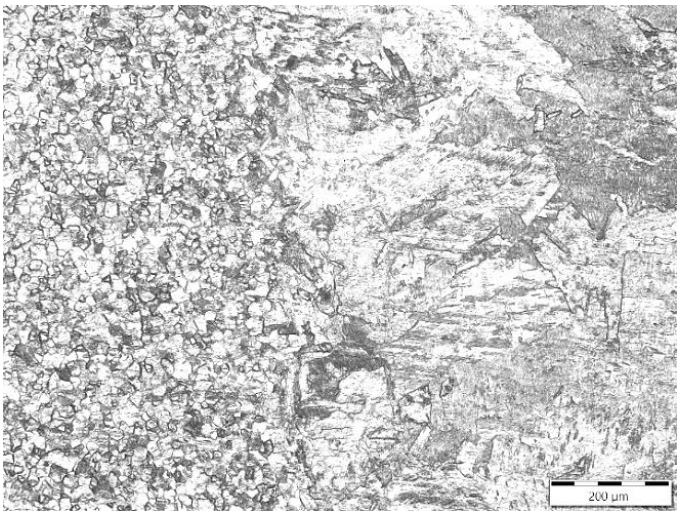

Slika 3.5 - Mikrostruktura osnovnog materijala, zone uticaja toplote i zavara titana Gr.2 na uvećanju x200

3.3. Ispitivanje tvrdoće po Vikersu

Tvrdoća uzorka je ispitana metodom Vickers, koristeći silu utiskivača od HV10. Važno je da tvrdoća u zavaru prema specifičnom zahtjevu ne smije premašiti 50 HV10 u odnosu na tvrdoću osnovnog materijala.
Na slici 3.5 dat je uvid u vrijednosti izmjerene tvrdoće makroizbruska.

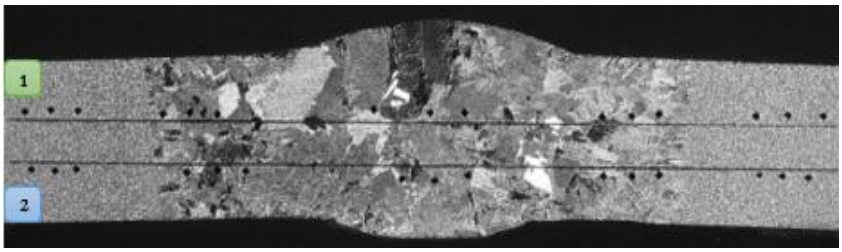

Red mjerenja	OM			ZUT			MŠ			ZUT			OM		
1 – 15	171	173	178	183	188	191	175	169	162	188	183	180	176	171	170
16 – 30	170	175	179	181	185	186	172	175	173	185	180	179	174	172	169

Slika 3.5 - Tvrdoća zavarenog ispitnog uzorka

4. Završni komentar

Na temelju provedenog ispitivanja na cijevi D60,3 t5,54 [mm] od titana Gr.2 mogu se izvesti zaključci:

- Makrostruktura zavarenog spoja i zona uticaja toplote (ZUT) su bez vidljivih nepravilnosti, zavareni spoj ima dovoljnu penetraciju.
- Mikrostruktura osnovnog materijala, zone uticaja toplote i zavar pokazuju prisustvo Widmanstätten ploča, posebne strukture koja se javlja zbog sporog hlađenja beta faze.
- Analizom mikrostrukture nije uočeno prisustvo uključaka, što ukazuje na visoku čvrstoću materijala i kvalitetno izvedeno zavarivanje.
- Ispitivanje tvrdoće pokazalo je da tvrdoća zavarenog spoja ne prelazi 50 HV10 u odnosu na tvrdoću osnovnog materijala, što je u skladu sa specifičnim zahtjevima.

Na temelju navedenih rezultata, možemo zaključiti da zavareni uzorak, odnosno tehnologija zavarivnaja koja je primijenjena za zavarivanje cijevi od titana Gr.2 zadovoljava kriterije. Tvrdoća i struktura su prikladne za širok raspon industrijskih primjena.

Društvo za tehniku
zavarivanja Slavonski Brod

13. Međunarodno znanstveno-stručno savjetovanje SBZ 2025

„STROJARSKE TEHNOLOGIJE U IZRADI ZAVARENIH KONSTRUKCIJA I PROIZVODA, SBZ 2025."
Slavonski Brod, 08. i 09. 05. 2025.

Pojednostavljena ručna muzilica za koze

I. Lacković[1,*], S. Jularić[1], P. Nakić[1], S. Šimunić[1]

[1] Technical department of University of Slavonski Brod, Trg Ivane Brlić Mažuranić 2, Slavonski Brod 35000, Republic of Croatia, ilackovic@unisb.hr

[*] Corresponding Author. E-mail: ilackovic@unisb.hr

Abstract

The goal of this paper is to describe how to use man's associated energy to facilitate hard physical work easier and faster, as well as to enable work faster and cheaper in regions where there is no electricity.
Making a manual milking machine improves the finished product's quality and hygiene. The milker's operation is based on the imitation of udder sucking. Rubber membranes are utilised in this process, which are put on the udder and generate a vacuum. When the device is turned on, pressure is created, which causes the milk to flow into the tanks. The use of a milking machine promotes faster milk production in goats while maintaining good hygiene standards.
A major issue occurs while milking goats in areas where there is no access to electricity using existing milking devices. Milking by hand is a time-consuming and physically demanding task; the sanitary conditions are also poor, and the milk is of lesser quality and filthy. Lactation lasts less than when milking using milkers, resulting in a substantially lesser profit.
The paper describes the project, calculated the main structural elements and created a 3D model of the device.

Keywords: goats, milking equipment, 3D model, construction calculation

1. UVOD

Koze su jedne od najstarijih domaćih životinja koje je čovjek među prvima pripitomio. Postoje znanstvene studije koje dokazuju da je čovjek koristio kozje mlijeko prije 7000 godina. Razlog pripitomljavanju koza je njihova vrlo visoka iskoristivost. Nisu zahtjevne životinje, vrlo su snalažljive i same si mogu pronaći hranu, te potrebna briga za njih, u odnosu na ostale domaće životinje, vrlo je minimalna. [1]
U prošlosti, koze su bile jedne od glavnih domaćih životinja, međutim, dolaskom industrijalizacije, u Europi, a i u svijetu, veliki i masovni uzgoji koza znatno su pali na ljestvici, iz razloga što je njihova

laktacija u odnosu na krave značajno manja, kao i doprinos mesa i dlake. Međutim, u siromašnijim zemljama Azije i Afrike, koze su i dalje glavna domaća životinja, upravo zbog jednostavnog i jeftinog održavanja i dobivanja visokokvalitetnog proizvoda.
U današnje vrijeme, koze se uzgajaju većinom na manjim privatnim gospodarstvima, koja su u većini slučajeva smještena u brdima i obroncima planina, gdje je smanjena dostupnost električne energije i pitke vode, ali i na velikim gospodarstvima čiji je glavni cilj proizvodnja kozjeg sira. [2]
Najveća dobrobit koza je njihovo mlijeko. Zbog njihove raznolike prehrane, kozje mlijeko se smatra visokokvalitetnim proizvodom s ljekovitim svojstvima. Ono sadrži mnoštvo vitamina, među kojima su vitamini B1, B2, B6 i B12, vrlo značajni za jačanje živčanog sustava, te različiti minerali koji doprinose čvrstoći kostiju i jačanju imuniteta. Također se koristi i za liječenje različitih dišnih i srčanih bolesti te u smanjenju alergija, a zbog svoje visoke probavljivosti ne djeluje opterećujuće na organizam čovjeka.
Laktacija koze traje u prosjeku od 200-300 dana u godini, te za to vrijeme koza proizvede 10 do 20 puta više mlijeka od svoje tjelesne mase, stoga se koze smatraju mliječnim životinjama.
Tokom godine, njihova laktacija se mijenja, te se može reći da najveća laktacija koze počinje u ožujku, kada je obično razdoblje jarenja, te se prema kraju godine smanjuje i potpuno prestaje 3 mjeseca prije jarenja. To razdoblje se naziva suhostaj. [1]

1.1 Vrste mužnje

Mužnju koza možemo podijeliti prema načinu izvođenja, i to na:
- Ručna mužnja
- Automatska mužnja.

1.1.1 Ručna mužnja

Ručna mužnja koza se u pravilu koristi kod mužnje manjih stada koza (do 5 grla), gdje nabava opreme za mužnju ne bi bila isplativa, ili kod gospodarstava koja nisu u mogućnosti financirati opremu za strojnu mužnju ili je iz nekog drugog razloga strojna mužnja onemogućena.
Čovjek pomoću šake imitira sisanje vimena te koza ispušta mlijeko u posudu (slika 1.1). Može se izvoditi i metodom prstohvata, gdje se prstima također imitira sisanje vimena. [1]

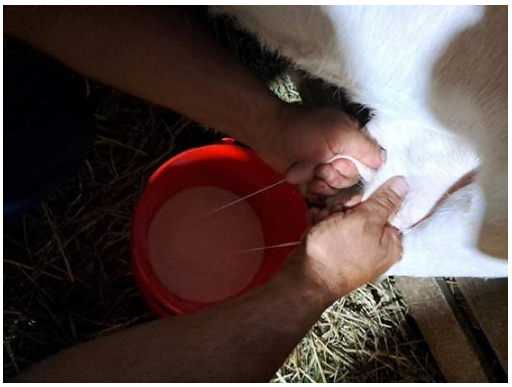

Slika 1.1 Ručna mužnja koza (OPG Zdjelarević)

Ukoliko je stado veće od 5 grla, ručna mužnja postaje jako fizički naporan i težak posao. Budući da se mlijeko ispušta u otvorenu posudu, koja nije zaštićena, u nju upadaju i ostale nečistoće i prljavština (dlake, prašina i sl.).

1.1.2 Automatska mužnja

Automatska mužnja ili mužnja uz pomoć različitih strojeva se može okarakterizirati kao mužnja uz pomoć ručnih muzilica i potpuno automatska mužnja. Kod mužnje uz pomoć ručnih muzilica (slika 1.2), čovjek ručnom silom uzastopno stišće ručicu te proizvodi imitaciju sisanja vimena te na taj način ispušta mlijeko u zaštićeni spremnik. Također je moguće upotrijebiti elektromotor, da bi se olakšalo pokretanje muzilice (slika 1.3).

Slika 1.2 Mužnja pomoću ručne muzilice [3]

Slika Pogreška! U dokumentu nema teksta navedenog stila**..3** Mužnja pomoću ručne muzilice
pokretane elektromotorom (OPG Zdjelarević)

Ovakve muzilice se koriste kod manjih stada (<10 grla) te kod stada gdje je iz određenog razloga onemogućena automatska mužnja. Negativna strana ručnih muzilica je što je ručna mužnja i dalje

fizički zahtjevan posao, a na mjestima gdje nema dostupnosti električne energije, nije primjenjiva muzilica s elektromotorom. Opcija korištenja umjetnih izvora struje (npr. agregat), nije prihvatljiva, iz razloga što su koze vrlo plahe životinje te visokom uznemirenosti dolazi do smanjenja laktacije.
Kod automatske mužnje, muzilica se spaja na vime te se, uz pomoć elektromotora i imitacije sisanja vimena ispušta mlijeko, bez kontakta sa zrakom, u zatvorenu posudu ili rashladni uređaj (laktofriz). Muzilice mogu biti stacionarne i pokretne. Slika 1.6 prikazuje opremu uza automatsku mužnju, koja se značajno razlikuje od ručne mužnje.
Stacionarne muzilice se nalaze na jednom mjestu i ne mogu se pomicati (Slika 1.4 i 1.5). Najčešće se koriste kod velikog i masovnog uzgoja koza. Kod takvih postrojenja, motor za pokretanje obično se nalazi u drugoj prostoriji, pokraj mjesta mužnje, da bi se smanjila buka i spriječila uznemirenost životinje, te samim time i povećala laktacija. Moguće je istovremeno vršiti mužnju i do 50 grla.

Slika 1.4 Jednoredno izmuzište [4]

Slika 1.5 Suvremeno dvoredno izmuzište [5]

Pokretne muzilice su značajno manje od stacionarnih i mogu se prenositi. Rade na vrlo sličnom principu kao i stacionarne, ali su puno tiše, te ih nije potrebno odvajati u posebnu prostoriju. Posuda za prikupljanja mlijeka obično je kapaciteta 18-20 l, te je moguće vršiti istovremeno mužnju do 2 grla. Vrlo su praktične, zadovoljavaju visoke higijenske uvjete, ali im je nedostatak dugotrajno čišćenje nakon svake mužnje, što na mjestima gdje nije dostupna voda predstavlja veliki problem.

2. POJEDNOSTAVLJENA RUČNA MUZILICA

2.1 Nedostupnost električne energije

Kod već postojećih muzilica, veliki problem nastaje prilikom obavljanja mužnje na mjestima gdje nema dostupnosti električne energije. Veliki broj gospodarstava u Republici Hrvatskoj na kojima se uzgajaju koze ne koriste automatske muzilice jer nemaju pristupa električnoj energiji ili zbog previsoke cijene nabave i održavanja automatske muzilice.
Mužnja rukama je jako dugotrajan i fizički težak posao, niskih higijenskih uvjeta i mlijeko je niže kvalitete.

2.2 Opis muzilice

Cilj ove muzilice je pokretanje pomoću čovjekove snage, omogućiti lakše i brže obavljanje teškog fizičkog posla i na mjestima gdje električna energija nije dostupna, podizanje kvalitete i higijene gotovog proizvoda, te niskim ulaganjem, povećati profit.
Princip rada se zasniva na imitaciji sisanja vimena. Pri tome se koriste mliječne čašice na kojima se nalaze sisne gume, koje se postavljaju na vime, te stvaraju vakuum prilikom upotrebe. Uređaj se pokreće okretanjem ručice koja je spojena na ručno kolo na kojem se nalaze konusni nastavci. Konusni nastavci pritišću ručicu koja podiže silikonsku membranu, stvara se podtlak, te mlijeko protječe, kroz silikonska crijeva, u kolektor. Pod utjecajem gravitacije, mlijeko se slijeva u sito, koje se nalazi na vrhu zatvorene posude, te se zaostale nečistoće zadržavaju u njemu.

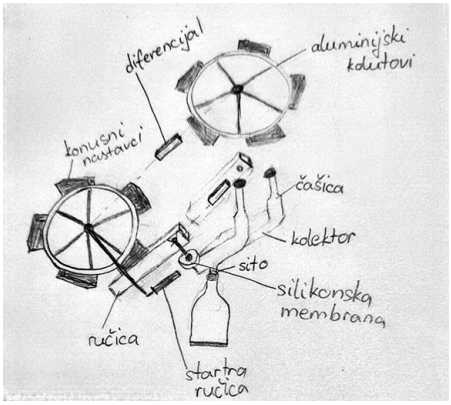

Slika 2.1 Skica ručne muzilice

Muzilica ima dva ručna kola, međusobno spojena osovinom. Na svakom ručnom kolu je zavareno 3 konusna nastavaka. Postavljeni su prema skici. Također, u središtu vrtnje postavljena je startna ručica, koja se okreće pod djelovanjem vanjske sile (čovjekova snaga ruku). Startna ručica pokreće ručna kola, te konusni nastavci pritišću ručice postavljene u neposrednoj blizini. Ručice odižu silikonske membrane koje povlače zrak i stvaraju podtlak koji djelovanjem na vime izvlači mlijeko. Pomoću udaljenosti između konusnih nastavaka, dobivamo otpuštanje ručice, samim time i otpuštanje silikonske membrane. Okretanje ručice, odnosno ručnih kola omogućava ritmičko podizanje i otpuštanje silikonske membrane, povlačenje i otpuštanje vimena, što predstavlja imitaciju sisanja vimena.

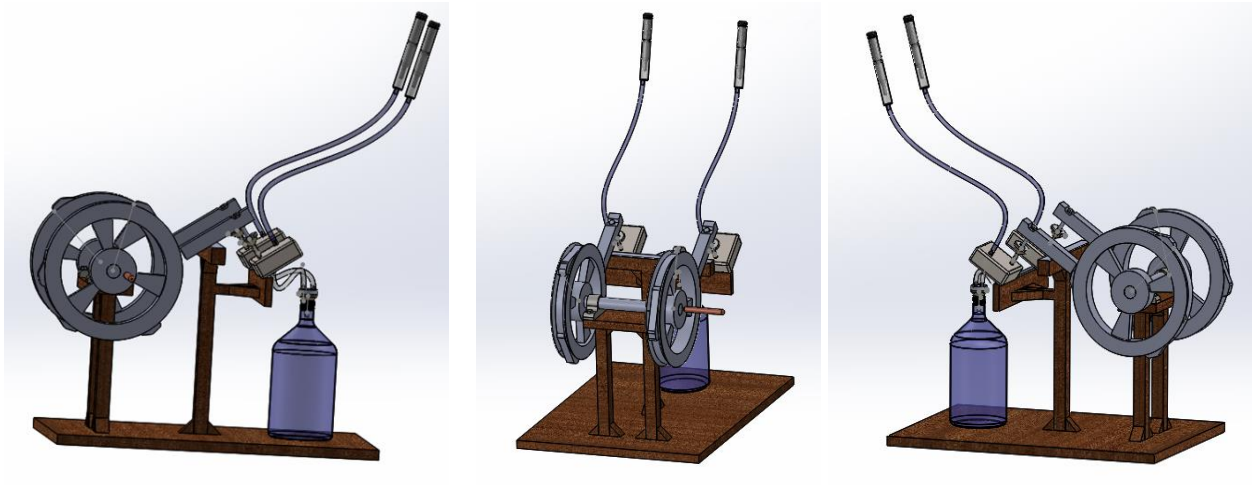

Slika 2.2 Model ručne muzilice

3. POJEDNOSTAVLJENA RUČNA MUZILICA – Opis dijelova

3.1 Startna ručica

Startna ručica je izrađena od polivinil-klorida, kojim je presvučen opći konstrukcijski čelik. PVC omogućuje bolje ležanje u ruci, te samim time lakše rukovanje. Pričvršćena za jedno od dva ručna kola. Osoba koja izvršava mužnju ju okreće snagom ruku. Značajna je jer s njom počinje proces mužnje.

3.2 Ručno kolo

Ručna kola su načinjena od općeg konstrukcijskog čelika, te je na svakom od njih zavareno po 3 konusna nastavaka. U središtu vrtnje nalazi se ručica koja se pokreće vanjskom silom, odnosno čovjekovom snagom. Konusni nastavci pritišću ručicu koja odiže silikonsku membranu. Konusni nastavci su postavljeni tako da konusni nastavak drugog ručnog kola je pomaknut za dužinu konusnog nastavka prvog ručnog kola, zbog toga da prilikom vrtnje ne stisnu obadva konusna nastavka obadvije ručice u isto vrijeme, zbog prevelikog opterećenja vimena. Zahtjev muzilice je imitirati sisanje vimena, a budući da je moguće obaviti mužnju obadva vimena u isto vrijeme (radi skraćenja vremena rada), potrebno je jedno vime otpustiti da bi iz drugog vimena poteklo mlijeko.

3.3 Osovina

Između kola se nalazi osovina koja spaja međusobno dva ručna kola, drži ih na određenoj udaljenosti i prenosi rotacijsko gibanje. Osiguranje od ispadanja i sigurnost za prijenos gibanja, osiguravaju kuglični ležajevi pričvršćeni za postolje muzilice vijcima.

3.4 Ručica

Ručica je izrađena od čelika. Njezina je uloga da u trenutku kada je opterećena konusnim nastavkom, odigne silikonsku membranu, te stvori podtlak. Na vrhu se nalazi zatik koji je pričvršćen na silikonsku membranu i pritiskanjem ručice on se povlači, te podiže membranu.

3.5 Silikonska membrana

Silikonska membrana se nalazi na ulazu u kolektor. Izrađena je od silikonske gume. Najvažniji je prijenosnik pulzacije. Dopuštena brzina pulzacije je 60-70 pulseva/min.

3.6 Kolektor

U kolektoru se, pomicanjem silikonske membrane stvara podtlak. Najveći dopušteni podtlak koji se smije stvoriti je 40-50 kPa. Također služi kao privremeni sakupljač mlijeka iz vimena.

3.7 Sito

Sito služi za pročišćavanje gotovog proizvoda (mlijeka) od zaostalih nečistoća, koje nisu očišćene prije mužnje, Služi kao završna kontrola gotovog proizvoda prije ulaska u spremište. Dimenzijom odgovara ulazu u spremište (grlu boce).

3.8 Mliječne čaše

Mliječne čaše se postavljaju na vime koze. Na vrhu imaju sisnu gumu, koja stavljanjem vimena u mliječnu čašu, stvara vakuum te mliječnu čašu zadržava na vimenu. Mliječne čaše imaju zapremninu 50-60 ml, a sisna guma je dimenzije Ø8-Ø20 x 159 mm.

3.9 Silikonska crijeva

Silikonska crijeva služe za odvođenje gotovog proizvoda u kolektor iz mliječnih čaša, ili odvođenje iz kolektora do spremnika za mlijeko. Maksimalni dopušteni promjer silikonskih crijeva je $D \leq 20$ mm.

3.10 Spremnik gotovog proizvoda

Spremnik je zatvorena posuda (boca) koja služi za zaprimanje gotovog proizvoda (mlijeka). Spojeno je silikonskim crijevima na kolektor. Na samom ulazu se nalazi sito. Zapremnina spremišta je 5 l.

3.11 Postolje

Postolje muzilice izrađeno je od drvene konstrukcije. Na mjestima kritičnih presjeka postavljena su drvena ojačanja (trokutaste tzv. „kajle"). Na mjestima gdje je potrebno povećati otpornost na trošenje, pričvršćen je tanki sloj lima od nehrđajućeg čelika. Ležajevi su za postolje pričvršćeni vijcima s metričkim navojem, te je u taj dio postolja upresana unutarnja matica (Unit matica).

4. PRORAČUN

4.1 Proračun brzine vrtnje startne ručice

Ukoliko se jedan okret startne ručice promatra kao jedan period, odnosno frekvencija, brinu vrtnje možemo izračunati prema sljedećem proračunu:

$$\omega_r = \frac{n_{rk}*\pi}{30} \rightarrow n_{rk} = \frac{30*\omega_r}{\pi} = 11{,}14\ min^{-1} \qquad (4.1)$$

Što predstavlja:
ω_r - maksimalan dopušten broj pulzacija [min-1]
n_{rk} – brzina vrtnje ručnog kola [min-1]

4.2 Proračun maksimalne slike koja smije opteretiti zavar startne ručice i ručnog kola

Maksimalnu sliku koja smije opteretiti zavar moguće je izračunati pomoću smičnog naprezanja. [6]

$$\tau_z = \frac{F}{\Sigma(a*l)} \rightarrow F = \tau * a * l = 90 * 0{,}003 * 0{,}150 = 0{,}04\ kN \qquad (4.2.)$$

Što predstavlja:
τ_z - maksimalno dopušteno smično naprezanje u zavaru [MPa]
Za opći konstrukcijski čelik τ_{dop} = 90 Mpa
F – sila koja djeluje u površini zavara [kN]
a – dubina zavara, za ravne kutne zavare, a_{min} = 3 mm
l – duljina zavara, odgovara duljini konusnog nastavka [mm], iz modela očitano, l = 150 mm

4.3 Proračun vlačne čvrstoće i granice elastičnosti vijka

Izabrani vijci za spoj ležaja s drvenim postoljem su prema DIN 933 vijci metričkog navoja M6x30, 8,8 Zn te pripadajuće unit matice.
Vlačnu čvrstoću odrediti će se prema:

$$R_m = 8 * 100 = 800\ MPa \qquad (4.3)$$

Gdje je:
R_m - vlačna čvrstoća vijka [MPa]

Granicu elastičnosti odrediti će se prema:

$$R_e = 800 * 0{,}8 = 640\ MPa \tag{4.4}$$

R_e – granica elastičnosti vijka [MPa]

4.4 Proračun provjere samokočnosti vijka

Osovina je izrađena od čelika s faktorom trenja μ=0,1. Samokočnost navoja će se provjeriti prema:

$$\rho' > \alpha \tag{4.5}$$

Gdje je:
ρ' – korigirani kut trenja [º]
α – kut uspona zavojnice [º]

$$\tan\rho' = \mu' = \frac{\mu}{\cos 30°} = \frac{0{,}1}{\cos 30°} \rightarrow \rho' = 6°35'37'' \tag{4.6}$$

Kut uspona zavojnice:

$$\tan\alpha = \frac{n*P}{\pi*d_2} \tag{4.7}$$

Gdje je:
n – vojnost navoja, kod metričkog navoja n=1
P – korak navoja [mm]
d_2 – promjer bokova navoja [mm]
$d_2 = 5{,}35$ mm (prema DIN 13 (JUS M.B0.009 do 045)

$$\tan\alpha = \frac{1*1}{\pi * 5{,}35} \rightarrow \alpha = 3°24'72''$$

Budući da je rezultat korigirani kut trenja veći od kuta uspona zavojnice, vijak je samokočan.
Proračun vijeka trajanja ležaja

4.5 Proračun vijeka trajanja ležaja

Vijek trajanja ležaja izračunati će se prema:

$$L = 10^6 (\frac{C}{F})^X \quad (4.8)$$

Gdje je:
L – nominalni vijek trajanja [okr.]
C – dinamička nosivost normalnog ležaja [kN], očitano iz *K.H. Decker, Elementi strojeva, tab. 81, str. 233*, za d=20 mm, C=5,1 kN [7]
x – eksponent vijeka trajanja, prema *K.H.Decker, Elementi strojeva,* za sve kuglične ležajeve x=3
F – dinamičko ekvivalentno opterećenje, u ovom slučaju F = F_r = 0,04 kN
Stoga prema gore navedenom, vijek trajanja ležaja iznosi:

$$L = 10^6 (\frac{5,1}{0,04})^3 = 2,1 * 10^{12}\ okr.$$

4.6 Proračun naprezanja zatika na savijanje i smik

Naprezanje zatika na savijanje i smik, izračunati će se prema sljedećem proračunu;
Naprezanje na savijanje:

$$\sigma_f = \frac{0,5F*0,5a}{0,1d^3} \quad (4.9)$$

Što predstavlja:
σ_f – naprezanje zatika na savijanje [MPa]
F – pogonska sila koja opterećuje zatik na savijanje [kN]
a – duljina površine najvećeg opterećenja sa savijanje [mm]
d – promjer zatika [mm] – iz modela očitano d=8 mm

Pogonska sila opterećuje ručicu u koju je pričvršćen zatik, duljina površine najvećeg opterećenja će biti širina ručice na dijelu gdje je pričvršćen zatik. Iz modela je očitano a= 26 mm.

$$\sigma_f = \frac{0,5 * 0,04 * 0,5 * 26}{0,1 * 8^3} = 5,08 * 10^{-3}\ MPa$$

Naprezanje na smik:

$$\tau = \frac{F}{2A} \quad (4.10)$$

Što predstavlja:
τ – naprezanje na smik [MPa]
F – pogonska sila koja opterećuje zatik na smik [kN]
A – površina presjeka zatika na djelu spoja s ručicom [mm^2]

$$A = d * a = 8 * 26 = 208\ mm^2 \qquad (4.11)$$
$$\tau = \frac{0{,}04}{2*208} = 9{,}62 * 10^{-5} MPa$$

4.7 Proračun volumenskog protoka

Kod većine automatskih muzilica, prosječna vrijednost volumenskog protoka iznosi oko 200 l/h. Za potrebe ovog proračun ta vrijednost uzeti će se kao relevantna.
Q = 200 l/h ≈ 0,06 l/s
Sakupljanje mlijeka iz vimena, kroz silikonska crijeva u kolektor i istjecanje iz njega predstavlja nestlačivo strujanje fluida, te protok mlijeka kojim ulazi se u kolektor mora biti jednak protoku izlaza. Kod nejednolikog strujanja izračunava se srednja brzina istjecanja. [8]

$$Q = v_{sr} * A \qquad (4.12)$$

Gdje je:
Q – volumenski protok [l/min, s, h]
v_{sr} – srednja brzina istjecanja [m/s]
A – površina poprelnog presjeka (u ovom slučaju, uzima se površina poprečnog presjeka silikonskog crijeva, jer se promatra istjecanje tekućine u spremnik. [m]
D_{max} = 20 mm – maksimalni dopušten promjer silikonskog crijeva

$$v_{sr} = \frac{Q}{A} = \frac{Q}{r^2 * \pi} = \frac{0{,}06}{0{,}01^2 * \pi} = 190{,}96\ m/s$$

5. ZAKLJUČAK

Upotrebom uređaja za mužnju koza moguće je značajno povećati brzinu rada, fizički olakšati posao, dobiti visoke higijenske uvjete i povećati količinu i kvalitetu gotovog proizvoda.
Izradom ovog projekta, omogućili bismo mužnju ručnim muzilicama i na mjestima gdje nema električne energije, te lakše obavljanje posla, a da se pri tome postignu visoki higijenski uvjeti. Cijena ove muzilice bi bila znatno niža u odnosu na automatske muzilice, te bi samim time bila puno konkurentnija na tržištu.
Muzilicu je moguće i dodatno razvijati, npr. postavljanjem točkića na postolje, te bi samim time dobila još jednostavnije korištenje.

6. LITERATURA

[1] Felhafer S., Banožić S., Antunac N., Uzgoj i hranidba koza, Hrvatska mljekartska udruga, Zagreb, 1994.
[2] Šakić V, Velija K, Ferizbegović J., Uzgoj koza, Sarajevo, 2011.
[3] https://garden.desigusxpro.com/hr/kozy/kak-doit.html
[4] https://www.agroportal.hr/wp-content/uploads/muznja-koza.jpg
[5] https://gumexplus.hr/oprema-za-muznju/
[6] Katedra za elemente strojeva, Elementi strojeva (osovine, vratila, rukavci i veze s glavinom), Fakultet strojarstva i brodogradnje, Zagreb
[7] Decker K.H., Elementi strojeva, 2.popravljeno izdanje, Zagreb
[8] Virag Z., Mehanika fluida (odabrana poglavlja, primjeri i zadaci), Sveučilište u Zagrebu, Fakultet strojarstva i brodogradnje, Zagreb, 2002

Društvo za tehniku
zavarivanja Slavonski Brod

13. Međunarodno znanstveno-stručno savjetovanje SBZ 2025

„STROJARSKE TEHNOLOGIJE U IZRADI ZAVARENIH KONSTRUKCIJA I PROIZVODA, SBZ 2025."
Slavonski Brod, 08. i 09. 05. 2025.

Svojstva i primjena kobaltovih superlegura

Properties and applications of cobalt superalloys

S. Kladarić [1,*], I. Kladarić [2], D. Ćorić [3]

[1] Sveučilište u Slavonskom Brodu, Tehnički odjel, Hrvatska
[2] Sveučilište u Slavonskom Brodu, Strojarski fakultet u Slavonskom Brodu, Hrvatska
[3] Sveučilište u Zagrebu, Fakultet strojarstva i brodogradnje, Hrvatska

[*] Autor za korespodenciju. E-mail: skladaric@unisb.hr

Sažetak

Superlegure su legure na osnovi nikla, željeza i nikla te kobalta koje sadrže velike količine legirnih elemenata, a namijenjene su za proizvodnju dijelova od kojih se zahtijeva visoka čvrstoća i otpornost na puzanje na povišenim i visokim temperaturama do 1000 °C te otpornost na koroziju.
Visoka čvrstoća i otpornost puzanju ovih legura posljedica je FCC kristalne strukture u području povišenih i visokih temperatura, visokog tališta i očvrsnute mikrostrukture.
Superlegure se koriste za izradu različitih dijelova u zrakoplovnoj, naftnoj, petrokemijskoj i drugim industrijama, u energetici, medicini itd.
U usporedbi s drugim superlegurama, kobaltove superlegure imaju višu temperaturu tališta, bolju otpornost na koroziju pri visokim temperaturama i trajnost te bolju zavarljivost. Očvršćuju kombiniranim djelovanjem kristala mješanaca i karbida.
U radu je prikazana podjela kobaltovih superlegura, opisan je utjecaj legirnih elemenata i mehanizmi njihovog očvrsnuća te su navedena mehanička, tehnološka i ostala svojstva, kao i primjeri primjene.

Ključne riječi: superlegure na osnovi kobalta, mehanizmi očvrsnuća, struktura, svojstva, primjena

Abstract

Superalloys are alloys based on nickel, iron and nickel and cobalt that contain large amounts of alloying elements and are intended for the production of parts that require high strength and creep resistance at elevated and high temperatures up to 1000 °C as well as corrosion resistance.
The high strength and creep resistance of these alloys results from the FCC crystal structure at elevated and high temperatures, the high melting point and the hardened microstructure.

Superalloys are used for the production of various parts in the aerospace, oil, petrochemical and other industries, the energy sector, medicine, etc.
Compared to other superalloys, cobalt superalloys have a higher melting point, better corrosion resistance at high temperatures and a longer service life, as well as better weldability. They harden through the combined effect of solid solutions and carbides.
The article presents the classification of cobalt superalloys, describes the influence of alloying elements and their hardening mechanisms and lists mechanical, technological and other properties as well as application examples.

Keywords: Cobalt-based superalloys, hardening mechanisms, structure, properties, application

1. Općenito o superlegurama

Superlegure su višekomponentni sustavi na osnovi nikla, željeza i nikla te kobalta koje sadrže visoke udjele kroma i manje udjele visokotaljivih elemenata molibdena i volframa te titana i aluminija.
Razvoj superlegura započeo je krajem tridesetih godina prošlog stoljeća zbog povećane potražnje za metalnim materijalima koji mogu izdržati povišene i visoke radne temperature u zrakoplovnoj i energetskoj industriji.
Superlegure su korozijski postojani materijali koji zadržavaju vlačnu čvrstoću, otpornost na umor i otpornost na puzanje do temperatura $0{,}7 \cdot T_t$ (T_t – talište, K), a pojedine od njih su kratkotrajno primjenjive i na višim temperaturama.
Visoka čvrstoća i otpornost puzanju ovih legura posljedica je FCC kristalne strukture u području povišenih i visokih temperatura, visokog tališta i očvrsnute mikrostrukture.
Plošno centriranu kubičnu (FCC) rešetku karakterizira oko 100 puta manji koeficijent difuzije nego prostorno centriranu kubičnu (BCC) rešetku. Značajno manja pokretljivost atoma bitno otežava gibanje dislokacija i tako sprečava puzanje materijala.
Superlegure očvršćuju otapanjem legirnih elemenata u kristalima mješancima matrice i precipitacijom intermetalnih spojeva i/ili karbida u austenitnoj matrici. [1, 2, 3]

2. Svojstva i primjena kobalta

Kobalt (lat. *cobaltum*) je kemijski element atomskog (rednog) broja 27 i relativne atomske mase 58,933. U periodnom sustavu elemenata kobalt, kemijskog simbola Co, pripada skupini prijelaznih metala. Otkrio ga je 1735. godine švedski kemičar Georg Brandt te naknadno opisao njegova svojstva i otkrio magnetičnost.
Gustoća kobalta iznosi 8900 kg/m^3. Temperatura tališta je 1495 °C, a vrelišta 2927 °C.
Elementarni kobalt na prijelomu je srebrnastobijele boje (slika 1.), vrlo tvrd, žilav i otrovan. Feromagnetičan je sve do 1127 °C (po nekim izvorima do 1150 °C). Usporedbe radi, željezo je feromagnetično do 769 °C, a nikal, ovisno o stupnju čistoće, do temperature 358…362 °C.

Slika 1. Elementarni kobalt [4]

Tvrdoća lijevanog kobalta iznosi 124 HB, a elektrolitičkog 300 HB. Vlačna čvrstoća lijevanog kobalta iznosi 237,4 N/mm^2, vučenog 689,4 N/mm^2, dok je savojna čvrstoća lijevanog kobalta 827,7 N/mm^2.
U Zemljinoj kori ima ga samo 0,0037 % vezanog u spojevima te je u malim količinama široko rasprostranjen u prirodi. U elementarnom stanju može se pronaći isključivo u meteoritima. Prisutan je uz nikal, bakar i druge metale u pojedinim mineralima iz kojih se složenim pirometalurškim i hidrometalurškim postupcima dobiva kao sporedni proizvod. Najvažniji su minerali kobaltit (CoAsS) i skuterudit ($CoAs_3$).
Kobalt se javlja u dvije alotropske modifikacije (slika 2.). Heksagonska α-modifikacija (HCP – gusto slagana heksagonska rešetka) prelazi pri ugrijavanju na temperaturi od 417 °C u kubičnu β-modifikaciju (FCC – plošno centrirana kubična rešetka) postojanu sve do tališta koje iznosi 1495 °C.

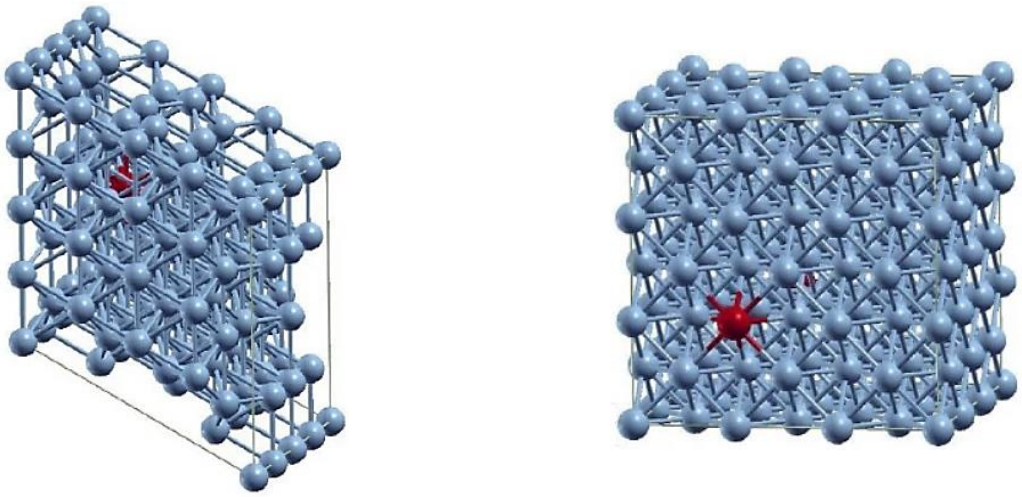

Slika 2. Raspored atoma kobalta (plave boje) u HCP (lijevo) i FCC (desno) kristalnoj rešetci (crvene boje je supstitucijski rastvoren atom tantala) [5]

Zbog svoje kristalne strukture, kobalt je dobro toplo oblikovljiv, ali ograničeno hladno oblikovljiv, kao i ostali metali s gusto slaganom heksagonskom rešetkom (Ti, Mg, Zn) kod kojih se deformacija ostvaruje samo klizanjem baznim ravninama HCP jedinične ćelije.

Površina mu je stabilna na zraku sve do 300 °C. S lužinama gotovo ne reagira, ali reagira s jakim kiselinama, na povišenoj temperaturi i s vodenom parom, kisikom i s većinom nemetala (osim s vodikom i dušikom).
U praškastom je stanju samozapaljiv, a u spojevima je najčešće dvovalentan i trovalentan.
Postoji samo jedan prirodni izotop kobalta, ^{59}Co i veliki broj umjetno proizvedenih. Najpoznatiji je radioaktivni izotop ^{60}Co koji kao jaki γ-emiter služi u industriji za ispitivanje bez razaranja odljevaka i zavara te u medicini za radioterapiju.
Čisti kobalt se rijetko upotrebljava kao tehnički materijal. Vrlo je važan kao legirni element za proizvodnju permanentnih i praškastih magneta (elektroindustrija i elektronika), korozijski i temperaturno postojanih superlegura (energetska postrojenja, aeronautika…), materijala za navarivanje otpornih na trošenje, brzoreznih čelika, sinteriranih tvrdih metala, zubarskih legura i legura za implantate u kirurgiji.
Kao legirni element u čelicima, kobalt pripada skupini gamagenih legirnih elemenata koji proširuju austenitno područje. Supstitucijski rastvoren u rešetki željeza usporava rast zrna pri povišenim temperaturama što doprinosi postojanosti mikrostrukture i otpornosti na popuštanje alatnih čelika za topli rad i brzoreznih alatnih čelika.
Kobaltovi spojevi, posebice oksidi, koriste se u proizvodnji stakla, emajla, keramike, pigmenta za modru glazuru, slikarskih boja, katalizatora za organsku sintezu, sušila za boje (kobaltove organske soli), nevidljive tinte (kobaltov(II) klorid) i dodataka stočnoj hrani i umjetnim gnojivima.
Kobalt je esencijalan mikroelement za čovjeka jer njegov spoj cijanokobalamin, poznat kao vitamin B12, sudjeluje u izgradnji eritrocita, a njegov nedostatak može uzrokovati anemiju. [1, 6, 7]

3. Kobaltove superlegure

3.1. Podjela i kemijski sastav

Kobaltove superlegure potiču od legura „Stellite" koje je početkom 1890-tih patentirao Elwood Haynes. Kasnije, od 1922. do 1950. godine, Haynes je u svojoj tvrtki Haynes International registrirao veliki asortiman superlegura otpornih na koroziju. [3]
Superlegure se općenito koriste u lijevanom i gnječenom stanju (valjane, ekstrudirane, kovane) te oblikovane postupcima metalurgije praha.
Legure za gnječenje su općenito homogenije i sitnozrnate mikrostrukture zbog čega posjeduju izvrsna vlačna svojstva i visoku dinamičku izdržljivost. Superlegure kobalta proizvedene kovanjem imaju različitu mikrostrukturu od onih proizvedenih lijevanjem. Kristalna zrna su manja i sfernog oblika. Raspršeni karbidi i mala veličina zrna čine ove legure mehanički vrlo otpornima.
Legure za lijevanje su segregirane i grubozrnate mikrostrukture koju karakterizira veća statička izdržljivost, odnosno bolja otpornost puzanju. Karbidi izlučeni po granicama zrna predstavljaju glavni mehanizam očvrsnuća kobaltovih superlegura koje se proizvode lijevanjem.
U tablici 1. naveden je kemijski sastav kobaltovih superlegura za gnječenje, a u tablici 2. naveden je kemijski sastav kobaltovih superlegura za lijevanje.

Tablica 1. Kemijski sastav kobaltovih superlegura za gnječenje [3]

Oznaka	Kemijski sastav, mas. %										
	Cr	Ni	Co	Mo	W	Nb	Ti	Al	Fe	C	Ostali
Superlegure na bazi kobalta											
Haynes 25	20,0	10,0	50,0	...	15,0	...	...	...	3,0	0,10	1,5 Mn
Haynes 188	22,0	22,0	37,0	...	14,5	...	...	...	3,0 maks.	0,10	0,90 La
S-816	20,0	20,0	42,0	4,0	4,0	4,0	...	...	4,0	0,38	...
MP35-N	20,0	35,0	35,0	10,0	...	...	...	...	...	...	...
MP	19,0	25,0	36,0	7,0	...	0,6	3,0	0,2	9,0	...	...
Ste	30,0	1,0	61,5	...	4,5	...	...	...	1,0	1,0	...
UMCo	28,0	...	49,0	...	...	...	...	...	21,0	0,12	...

Tablica 2. Kemijski sastav kobaltovih superlegura za lijevanje [3]

Oznaka	Kemijski sastav, mas. %												
	C	Ni	Cr	Co	Mo	Fe	Al	B	Ti	Ta	W	Zr	Ostali
Superlegure na bazi kobalta													
AirResist 13	0,45	...	21	62	...	...	3,4	...	...	2	11	...	0,1 Y
AirResist 213	0,20	0,5	20	64	...	0,5	3,5	...	...	6,5	4,5	0,1	0,1 Y
AirResist 215	0,35	0,5	19	63	...	0,5	4,3	...	...	7,5	4,5	0,1	0,1 Y
FSX-414	0,25	10	29	52,5	...	1	...	0,01	...	...	7,5	...	...
Haynes 21	0,25	3	27	64	...	1	...	...	...	...	...	...	5 Mo
Haynes 25; L-605	0,10	10	20	54,0	...	1	...	...	...	...	15,0	...	...
J-1650	0,20	27	19	36	...	...	...	0,02	3,8	2	12	...	...
MAR-M 302	0,85	...	21,5	58	...	0,5	...	0,005	...	9	10	0,2	...
MAR-M 322	1,0	...	21,5	60,5	...	0,5	...	...	0,75	4,5	9	2	...
MAR-M 509	0,6	10	23,5	54,5	...	...	...	...	0,2	3,5	7	0,5	...
MAR-M 918	0,05	20	20	52	...	...	...	...	...	7,5	...	0,5	...
NASA Co-W-Re	0,40	...	3	67,5	...	...	...	...	1	...	25	1	2 Re
S-816	0,4	20	20	42	...	4	...	...	...	...	4	...	4 Mo, 4 Nb, 1,2 Mn, 0,4 Si
V-36	0,27	20	25	42	...	3	...	...	...	...	2	...	4 Mo, 2 Nb, 1 Mn, 0,4 Si
Wi-52	0,45	...	21	63,5	...	2	...	...	...	...	11	...	2 Nb+Ta
X-40 (Stellite 31)	0,50	10	22	57,0	...	1,5	...	...	...	...	7,5	...	0,5 Mn; 0,5 Si

Kobaltove superlegure se, prema primjeni, mogu podijeliti na; legure otporne na visoke temperature, legure otporne na trošenje i legure otporne na koroziju.

Legirni elementi volfram, molibden, tantal i niobij bitno poboljšavaju otpornost na oksidativne i sulfatizirajuće sredine pri vrlo visokim temperaturama (700 °C do 1200 °C).

U matičnoj kobaltno-kromovoj leguri ovi dodaci pospješuju stvaranje stabilnih karbida u mikrostrukturi koji daju čvrstoću, vatrootpornost i kemijsku postojanost pri visokim temperaturama. Upotrebljavaju se za izradu dijelova turbina koje su izložene visokim temperaturama.

Tipični predstavnici ove skupine vatrootpornih legura su L-605 i Haynes 188. Ove legure imaju sposobnost dugotrajnog podnošenja niskih naprezanja na visokim temperaturama.

Superlegure Stellite serije 6, 21 i 31 su poznate kao legure s dobrom otpornošću na trošenje. Stellite 6 je legura s najboljom duktilnošću i čvrstoćom iz navedene serije, a svoju otpornost na trošenje

zadržava i na temperaturama do 1050 °C. Zbog visokog sadržaja kroma otporna je i na oksidaciju, a primjenu nalazi u plinskim i parnim turbinama. Visoka otpornost prema vrućim korozijski agresivnim plinovima ima za posljedicu dulji životni vijek ovih postrojenja te lakše održavanje.
Sve legure na bazi kobalta se mogu proizvoditi kovanjem i lijevanjem. Neke legure s korozijskom postojanošću se također mogu proizvoditi i metalurgijom praha. [3]

3.1. Utjecaj legirnih elemenata

Kobaltove superlegure su po sastavu mnogo jednostavnije od niklovih superlegura.
Kobaltove superlegure sadrže 30…65 %Co, 15…30 %Cr, 0…32 %Ni, 0…20 %Fe i 0,1…1,1 %C.
Visok sadržaj kroma osigurava antikorozivnost i očvršćuje leguru otapanjem u kristalima mješancima i stvaranjem kromovih karbida. Udio kroma može se smanjiti u legurama kod kojih nije izrazito bitna korozijska otpornost na visokim temperaturama te u slučajevima kada se površina može oplemeniti dodatnim difuzijskim slojevima.
Dodatak nikla u ovim legurama ima dvostruko djelovanje; očvršćuje kristale mješance i stabilizira kubičnu plošno centriranu strukturu pri nižim temperaturama.
Ostali legirni elementi; W, Mo, V, Ti, Nb, Ta, Zr i B dodaju se isključivo zbog stvaranja karbida. Ovisno o sastavu, izlučuju se karbidi oblika TiC, NbC, TaC, WC, ZrC, BC ili neki od karbida kao što su Cr_7C_3, $Cr_{23}C_6$ te rjeđe $W_{23}C_6$ i $Mo_{23}C_6$.
Porastom udjela ugljika dolazi do povećanog izlučivanja karbida što rezultira povišenjem statičke izdržljivosti uz istovremeno sniženje žilavosti i dinamičke izdržljivosti.
Karbidi u superlegurama općenito imaju tri funkcije;

- karbidi po granicama zrna očvršćuju granice sprečavajući ili usporavajući klizanja uzduž zrna
- karbidi unutar zrna povećavaju njegovu čvrstoću, što je osobito važno kod kobaltovih superlegura koje nisu očvrstljive izlučivanjem intermetalnih spojeva
- karbidi mogu spriječiti određene elemente da formiraju nestabilne faze tijekom eksploatacije. [1, 2, 3]

3.2. Mehanizmi očvrsnuća

Kobaltove superlegure očvršćuju kombiniranim djelovanjem kristala mješanaca i karbida. Nisu precipitacijski očvrstljive jer kod njih nije moguća precipitacija intermetalnih faza kao kod nikal i željezo-nikal superlegura, što djelomično ograničava njihovu primjenu.

3.3. Toplinska obrada

Kobaltove superlegure se toplinski obrađuju žarenjem i precipitacijskim očvršćivanjem.
Žarenje se provodi radi rekristalizacije, mekšanja materijala kod hladnog ili toplog oblikovanja, smanjenja zaostalih naprezanja nakon zavarivanja te homogenizacije lijevanih ingota.

Žarenje za redukciju zaostalih naprezanja kovanih obradaka ograničeno je na legure koje se ne obrađuju precipitacijom. Parametri žarenja ovise o metalurškim karakteristikama legure te o vrsti i veličini zaostalih naprezanja. Parametri žarenja za redukciju zaostalih naprezanja lijevanih obradaka ovise o geometriji obradaka i prethodnim obradama. [8]
Žariti se mogu i gotovi dijelovi radi postizanja sitnozrnate mikrostrukture u primjenama koje zahtijevaju čvrstoću i dinamičku izdržljivost.
Precipitacijsko očvršćivanje provodi se rastvornim žarenjem na temperaturama do 1240 °C, gašenjem i naknadnim zagrijavanjem na temperaturama 650…850 °C.
Na slici 3. prikazana je metalografska slika mikrostrukture kobaltove superlegure Haynes 25 koja je toplinski obrađena rastvornim žarenjem na temperaturi 1205 °C i dozrijevanjem na temperaturi 870 °C u trajanju od 340 h. U strukturi su vidljivi precipitirani karbidi tipa M_6C i intermetalni spoj Co_2W rastvoreni u FCC matrici.

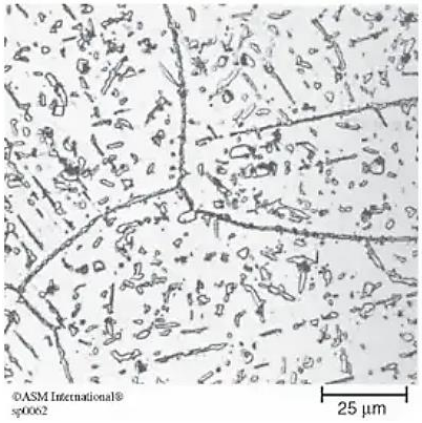

Slika 3. Precipitacijski očvrsnuta superlegura Haynes 25 (uvećanje 500×) [8]

Na slici 4. prikazan je dijagram postupka toplinske obrade kobaltove superlegure CoCr20Ni20W. Rastvornim žarenjem pri 1175 °C otapaju se intermetalni spojevi i karbidi te prelaze u čvrstu otopinu. Nakon gašenja u vodi i dodatnog zagrijavanja na 760 °C izlučuju se sitni karbidi koji usporavaju gibanje dislokacija i otežavaju klizanje granica zrna.

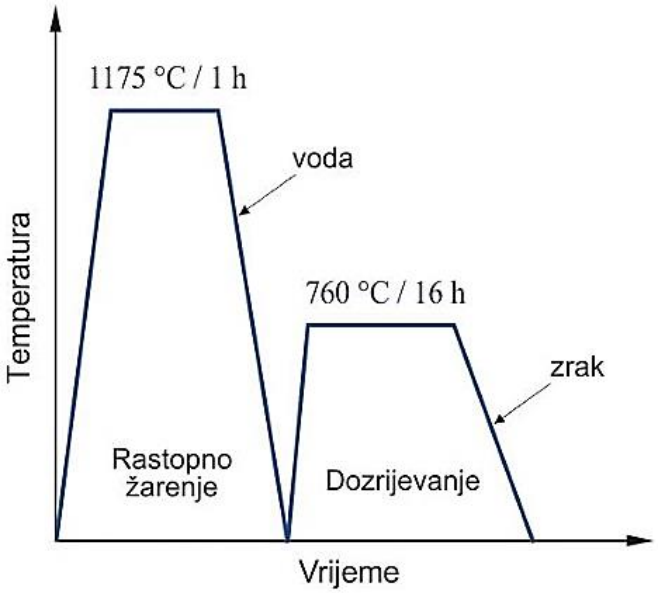

Slika 4. Postupak precipitacijskog očvrsnuća kobaltove superlegure CoCr20Ni20W [2, 3]

U tablici 3. navedene su vrijednosti mehaničkih svojstava rastvorno žarenih i dozrijevanih legura CoCr20Ni20W i CoCr20W15Ni.

Tablica 3. Parametri toplinske obrade i mehanička svojstva superlegura Haynes 25 i Vaccutherm 8–13 H [2, 3]

Oznaka legure	Sastav ostalo %	Precipitacija		R_m min. MPa	A min. %	KU DVM min. J	Maksimalna temperatura primjene
		Rastopno žarenje	Dozrijevanje				
CoCr20W15Ni Zapp *Haynes 25* Böhler *Turbotherm* 20Co50 *Hastelloy*	10 Ni maks. 3 Fe	1230 °C / voda	-	930	60	35	950 °C
CoCr20Ni20W Zapp *Vaccutherm* 8–13 H	4 Mo 4 W maks. 5 Fe 4 Nb	1175 °C / voda	760 °C / 16 h	1000	25	20	900 °C

3.4. Svojstva i primjena

Kobaltove superlegure karakterizira dobra livljivost i zavarljivost te visoka toplinska otpornost i otpornosti na koroziju.
Postojane su do 1000 °C i koriste se za slične namjene kao i toplinski otporne niklove superlegure.

Kobaltove superlegure nisu prikladne za mehanički izrazito opterećene dijelove jer im je čvrstoća pri visokim temperaturama niža u odnosu na niklove superlegure. Stoga se koriste za statički opterećene (nerotirajuće) dijelove dugotrajno izložene manjim naprezanjima.
Kobaltove superlegure, jednako kao i one niklove, ne preporučuje se upotrebljavati iznad gornje granične temperature zbog otapanja intermetalnih faza i karbida u čvrstoj otopini odnosno njihove koagulacije čime padaju vrijednosti čvrstoće. [1, 2, 3]
Kobaltove superlegure često se koriste za dijelove većih dimenzija zbog dobre otpornosti prema toplinskom umoru, budući da imaju nešto veći koeficijent toplinske provodnosti i niži koeficijent toplinske dilatacije u odnosu na niklove superlegure. [3]
Superlegure na bazi kobalta koriste se za izradu dijelova u plinskim turbinama, svemirskim letjelicama, raketnim motorima, nuklearnim reaktorima, elektranama i kemijskoj opremi (slika 5).

Slika 5. Neka područja primjene kobaltovih superlegura [9]

Dobra otpornost na toplinski umor koji nastaje uslijed učestale promjene temperature omogućuje primjenu kobaltovih superlegura za dijelove avionskih motora koji su izloženi učestalom gašenju i paljenju.
Kobalove superlegure imaju visoku otpornost na koroziju koja se javlja pri izgaranju vrućih plinova što također omogućuje primjenu za komponente avionskih motora.
U postrojenjima za eksploataciju nafte i plina kobaltove superlegure se koriste za izradu alata za bušenje, ventila i druge opreme koja mora raditi u visoko korozivnim uvjetima te pri visokim temperaturama i mehaničkim naprezanjima.
Kobaltove superlegure su najčešće korišteni materijali za kirurške implantate zbog svoje čvrstoće, otpornosti na trošenje, otpornosti na koroziju i biokompatibilnosti.
Za izradu umjetnih kukova i koljena u primjeni su lijevane Co-Cr-Mo (F-75) i vruće kovane Co-Ni-Cr-Mo (F-799) superlegure. [3]
Preostali dio primjene uključuje: industrijske plinske turbine, medicinske implantate i stomatološke proteze, raketne motore, opremu za toplinsku obradu, rezne alate za visokotemperaturnu obradu, industriju celuloze i papira, kemijsku i petrokemijsku industriju itd. [3, 9, 10]

4. Zaključak

Kobaltove superlegure su suvremeni metalni materijali koji se koriste u vrlo zahtjevnim uvjetima eksploatacije. Karakterizira ih dobra mehanička otpornost na povišenim i visokim radnim temperaturama, visoka korozijska postojanost, otpornost na trošenje i dugotrajnost.
U usporedbi s željezo-nikal i niklovim superlegurama, kobaltove superlegure imaju višu temperaturu tališta, bolju otpornost na koroziju pri visokim temperaturama i trajnost te bolju zavarljivost.
Kobaltove superlegure su vrlo složenog kemijskog sastava, a očvršćuju kombiniranim djelovanjem kristala mješanaca i karbida.
Dijelovi izrađeni od kobaltovih superlegura proizvode se postupcima tehnologije lijevanja, oblikovanja deformiranjem i metalurgije praha. Toplinski se obrađuju žarenjem i precipitacijskim očvršćivanjem.
Visoka cijena proizvoda izrađenih od superlegura posljedica je visoke cijene legirnih dodataka i složenog procesa proizvodnje. Međutim, ista je opravdana zbog specifičnih zahtjeva u eksploataciji koje ovi materijali mogu ispuniti.

5. Literatura

[1] Filetin, Tomislav; Kovačiček, Franjo; Indof, Janez. (2002). Svojstva i primjena materijala. Zagreb: Sveučilište u Zagrebu, Fakultet strojarstva i brodogradnje. (ISBN 953-6313-77-4)
[2] Ćorić, Danko. (2017). Posebni metalni materijali – III. dio. Zagreb: Sveučilište u Zagrebu, Fakultet strojarstva i brodogradnje. (ISBN 978-953-7738-58-7)
[3] Sunulahpašić, Raza; Oruč, Mirsada. (2020). Superlegure. Zenica: Univerzitet u Zenici, Metalurško-tehnološki fakultet. (978-9958-785-44-3)
[4] https://www.britannica.com/science/cobalt-chemical-element
[5] Sewak, R., Dey, C.C. & Toprek, D. Temperature induced phase transformation in Co. Sci Rep 12, 10054 (2022). https://www.nature.com/articles/s41598-022-14302-x
[6] https://enciklopedija.hr/clanak/kobalt
[7] https://tehnika.lzmk.hr/tehnickaenciklopedija/kobalt.pdf
[8] Matthew J. Donachie; Stephen J. Donachie. (2002). Superalloys: A Technical Guide. (Second Edition). ASM International. ISBN electronic: 978-1-62708-267-9
[9] https://www.cobaltinstitute.org/essential-cobalt-2/cobalt-innovations/superalloys/
[10] Cobalt based alloys – Benefits, Chemical Composition and more https://bortec-group.com/glossary/cobalt-based-alloys/

Društvo za tehniku zavarivanja Slavonski Brod

13. Međunarodno znanstveno-stručno savjetovanje SBZ 2025

„STROJARSKE TEHNOLOGIJE U IZRADI ZAVARENIH KONSTRUKCIJA I PROIZVODA, SBZ 2025."
Slavonski Brod, 08. i 09. 05. 2025.

Preliminary Investigation of Additive Manufacturing of Duplex Stainless Steel Parts with Vibrational Assistance

U. Patrick[1,*], Š. Klarić[1], S. Havrlišan[2]

[1]Faculty of Science and Technology, Charles Darwin University, Australia
[2]Mechanical Engineering Faculty in Slavonski Brod, University of Slavonski Brod, Croatia

[*]Corresponding Author. E-mail: uhamir.patrick@students.cdu.edu.au

Abstract

Duplex stainless steel (DSS) parts fabricated by Gas Metal Arc Welding - Additive Manufacturing (GMAW-AM) process are mostly characterised by challenges such as highly austenitic microstructure and sigma phase formation due to retention at elevated temperature for extended periods of time. For their designed purpose to be achieved, it is quite important for the fabricated DSS components to have a suitable ferrite-austenite phase ratio. This phase ratio is influenced by chemical composition of filler and base materials, shielding gas or combination of shielding gases, interlayer temperature maintained, deposition energy input, and secondary mechanisms assisting the process. In this paper, research literature featuring secondary mechanism-assisted GMAW-AM of DSS parts has been reviewed and analysed. Furthermore, preliminary findings from ultrasonic vibration-assisted deposition of DSS beads using the GMAW-AM process are presented.

Keywords: GMAW, AM, DSS, in-situ ultrasonic vibration, weld appearance

1. Introduction

It is now beyond doubt that Additive Manufacturing (AM) is the answer to the quest for efficient, effective, economic, and sustainable manufacturing [1, 2]. Since its inception, it has motivated global scientific community to aim at developing competencies and capabilities for additively manufactured parts with properties comparable to counterparts manufactured by conventional processes [3]. Diverse materials have been successfully employed for AM ranging from basic materials such as plastics, ceramics and concrete to advanced and complex metals, alloys and functionally graded materials [4]. Due to this versatility, AM processes have become relevant to wide range of industries including biomedical, marine, chemical, petroleum and gas, automotive and aerospace [5]. AM processes employ various techniques and methods for three-dimensional (3D) printing of metals. Some processes employ feed metal in the form of powder whereas some in the form of wire.

Similarly, feed material could be deposited on a substrate (base material) via sources such as laser, spray, electron beam, and welding arc [6]. Depending on the nature of the method and material employed, AM processes are classified into different types such as Powder Bed Fusion, Binder Jetting and Directed Energy Deposition (DED) [7].

Wire and arc additive manufacturing (WAAM) is a DED process employing metal fed by filler wire to a welding robot. The torch of the robot sticks out wire which is ignited by a welding arc and turned into molten droplets which are then deposited on the substrate while the torch travels along its path, as presented in Figure 1. The deposition path is assigned to the welding robot by certain computer aided designing / computer aided manufacturing (CAD/CAM) model. WAAM is further classified into Tungsten Arc Welding, Plasma Arc Welding and Gas Metal Arc Welding (GMAW) AM [8].

Of these processes, GMAW-AM is attractively characterised by higher material deposition rates and suitable economy [9]. Added to that is the feasibility of the process, as it does not require isolated working environment, and therefore, can be executed in open space. Also, the filler wire is fed by the welding torch in GMAW-AM, compared to other WAAM processes in which filler wire is externally fed [10]. Available literature on GMAW-AM indicates that the process has been employed for a range of metals and alloys including Aluminium, Copper, Titanium, Inconel and Stainless Steels [11]. Among these materials, the merit of research on GMAW-AM with Duplex Stainless Steels (DSSs) is quite high because there is only moderate amount of literature currently available in this area.

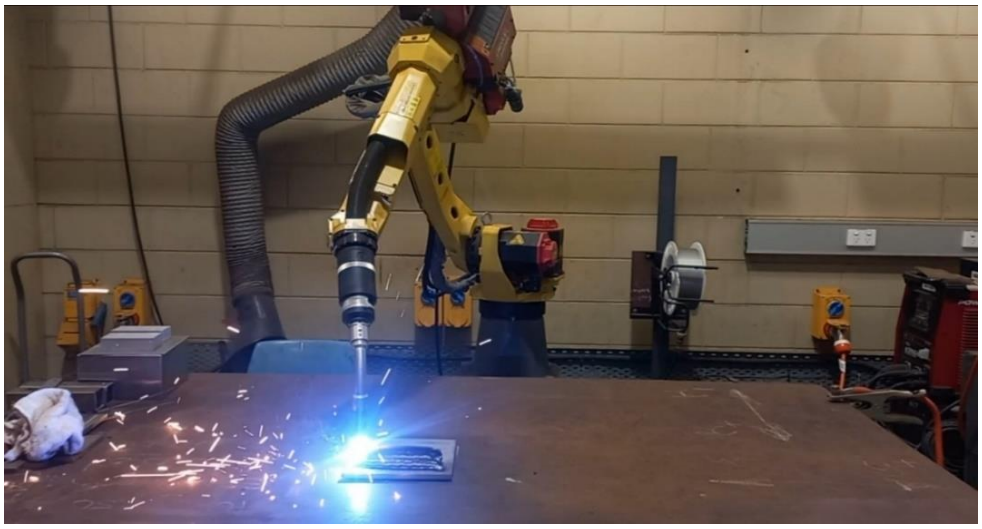

Figure 1. GMAW-AM equipment at Charles Darwin University (Casuarina), Australia

Therefore, this paper is a contribution to existing and available research works on fabrication of DSS parts using GMAW-AM process. Most importantly, the paper is aimed at presenting preliminary findings from ultrasonic vibration assisted deposition of DSS beads by GMAW process. Comparative analysis has been undertaken between two types of beads, ones obtained with high deposition (arc/heat) energy input and others with low heat input, with and without the assistance of ultrasonic

vibrations. Along with macroscopic features such as bead width, height, reinforcement area, depth and area of penetration, microscopic analysis using optical microscopy was carried out. The fabrication process and microscopic analysis were carried out using in-house facilities available at Charles Darwin University (CDU), Australia (Figure 1).

2. Literature Review

To begin with, DSS fabrication by GMAW-AM is an infant research area, still in its formative stages [12-14]. Analysis of research methods, as reported in these articles, brings out that among the available 56 articles, 46 articles are based on process optimization whereas only a meagre 4 and 6 articles involve combination of shielding gases and secondary mechanism assisted fabrication, respectively. This means that over 82% per cent of the existing and available research database is on parametric optimization of GMAW-AM process for development of satisfactory DSS parts, as shown in Figure 2. Finally, literature specifically on in-operando mechanisms assisted GMAW-AM based fabrication of DSS parts was reviewed and quantified, as shown in Figure 3.

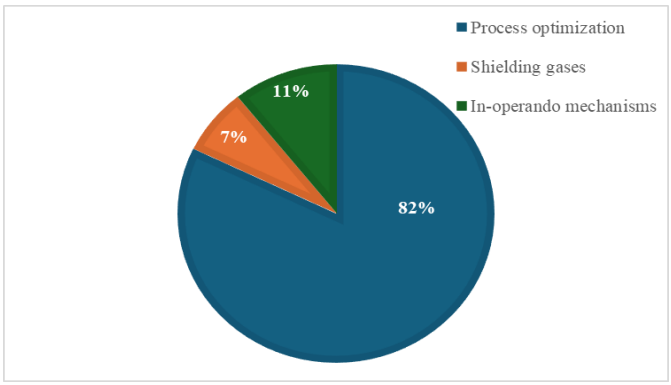

Figure 2. Literature segregation on DSS fabrication by GMAW-AM according to methods

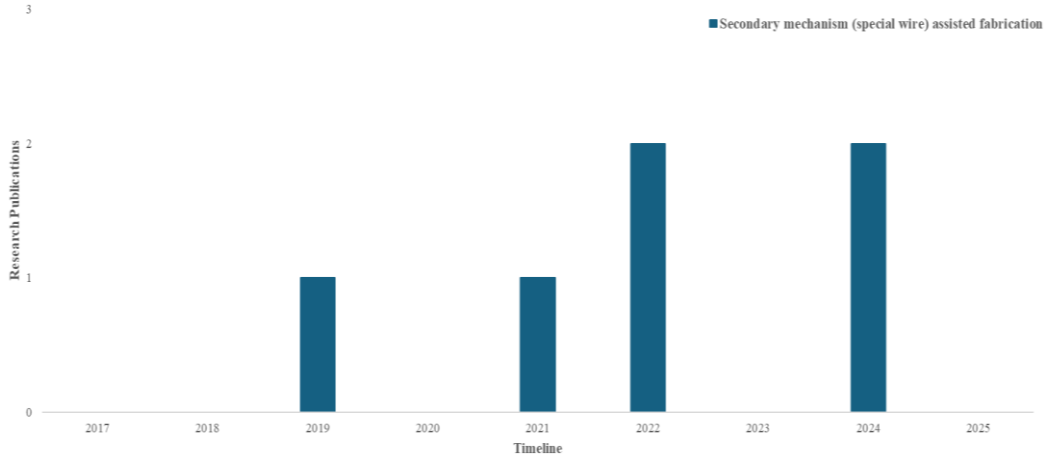

Figure 3. Timeline of research works on secondary mechanism assisted GMAW-AM of DSS

On the basis of literature review and analysis presented above, it is established that there is ample opportunity for investing research efforts in developing DSS parts with suitable internal (microstructural) characteristics and external (mechanical) properties by aiding GMAW-AM process with secondary (in-situ/in-operando/in-process) mechanisms.

Following paragraphs briefly present research works involving secondary mechanism (and specific wire type) assisted fabrication of DSS components by GMAW-AM process:

By employing an additional lean DSS2205 cold wire with DSS2209 wire during cold metal transfer (CMT) GMAW-AM process, ferrite percentage in the deposited structure was successfully increased to 72% from 39% in case with only DSS2209 feed wire [15]. This was made possible by maintaining the filler wire to cold wire ratio of 3.3:1. Due to adjustment in the feed ratio, nickel equivalent (Ni_{eq}) and chromium equivalent (Cr_{eq}) adjusted in such a manner that suitable percentages of ferrite and austenite phases were measured in the deposit.

Flux-cored (FC) DSS wires for GMAW-AM process successfully adjusted ferrite-austenite phase ratio in the deposited structure to satisfactory and suitable levels [16]. The structure deposited using commercial DSS2209 wire registered 74% austenite content. The two FC wires developed, that is, FCWA-AM-DSS-#1 and FCWA-AM-DSS-#2 successfully reduced the austenite contents to 37% and 45%, respectively.

Rotation-extrusion assisted CMT GMAW-AM process with DSS2209 filler wire was successfully performed to fabricate wall structure [17]. Phase quantification by Electron Back Scattered Diffraction (EBSD) analysis showed that austenite phase increased from 52.5% in as-deposited (non-assisted) structure to 87.7% by in-situ rotation-extrusion treatment of deposited layers. The increase in the austenite content was associated with the frictional heat induced in the layers generated by in-situ mechanism. The additional heat and eventual slow cooling rate favoured an increased austenite recrystallization.

FC super DSS (SDSS) wire specially designed for GMAW-AM process was successfully employed to fabricate a three-dimensional (3D) printed wall [13]. This FCWA-AM SDSS wire had a Cr_{eq}/Ni_{eq} ratio of 2.23 which reduced the austenite content from 74% to approximately 45% in the deposit and improved their corrosion resistance and tensile properties.

FC SDSS wire was successfully employed with in-situ addition of Titanium (Ti) during GMAW-AM process [14]. The results indicated that the Ti addition of 1% in the overall chemical composition of deposited structure completely transformed the grain structure of ferrite from epitaxial columnar (39 μm size) to fine equiaxed (12-19 μm size). The research also suggested that in-situ Ti could help to reduce anisotropy of mechanical properties by producing fine equiaxed ferrite grains in the microstructure.

In light of mentioned literature, it is understood that the material characterization of DSS components fabricated by GMAW-AM process is currently an area of research focus. Efforts toward understanding the influence of complex thermal cycles of the fabrication process on microstructure remain a high priority for the research community. The studies already undertaken premise on two significant aspects, chemical composition and thermal history of printed parts. This understanding is

being developed by both experimental and simulation techniques and methods. Comprehension of these aspects will be beneficial to map material characteristics with mechanical ones, suggesting improvements to the process and enabling the production of parts with satisfactory and reliable attributes.
In this regard, this research work is an effort to understand the effect of in-situ ultrasonic vibrations on the microstructure of DSS2209 beads produced by GMAW process.

3. Research Method

3.1 Process and equipment

The GMAW process was carried out at CDU's in-house facility, as illustrated in Figure 1. The system used is a LINCOLN ELECTRIC AUTODRIVE® integrated with a FANUC® ARC Mate 100iC robotic arm. This welding robot is operated via a FANUC® R-30iB Plus controller and powered by a LINCOLN ELECTRIC Power Wave® S500CE welding source. The complete setup, including all associated equipment and accessories, is shown in Figure 4.

(a) (b) (c)

Figure 4. (a) LINCOLN ELECTRIC AUTODRIVE® SA FANUC® Robot ARC Mate 100iC (b) FANUC® Controller R-30iB Plus (c) LINCOLN ELECTRIC Power Wave® S500CE

For the purpose of inducing ultrasonic vibrations of 20 kHz frequency in the deposited layers, Derui V1.3 Ultrasonic Generator TU series, which is connected with DS-2020 Ultrasonic Transducer Plate (Figure 5). Two sets of deposition parameters were employed, one for high heat input and another one for low heat input. Both sets of parameters were applied to deposit beads with and without the assistance of ultrasonic vibrations. The GMAW-AM process parameters are provided in Table 2. Therefore, four beads were deposited, two with each set of parameters with and without ultrasonic vibrations, respectively. A constant interpass temperature of 50 °C was maintained.

Figure 5. Ultrasonic vibration generator (left) with ultrasonic vibrating plate (right)

Table 2. GMAW process parameters employed for beads deposition

Process Parameters	**Low heat input ~0.189 kJ/mm**	**High heat input ~0.368 kJ/mm**
Torch Speed	40 cm/min	30 cm/min
Wire Feed Speed	400 cm/min	600 cm/min
Voltage	18.9 V	20.8 V
Current	~66.7 A	~88.6 A
Shielding gas (Argon) flow rate	20 l/min	
Nozzle tip-to-contact distance	15 mm	
Filler wire stick out	10 mm	
Wire tip to base plate distance	5 mm	
Vibration frequency	20 kHz	

3.2 Filler, base and shielding materials

DSS2209 was used as filler wire with a diameter of 1.2 mm. DSS2205 plate with a length, width and thickness of 200 mm, 100 mm and 10 mm, respectively, was used. Argon gas was used for shielding. Each of the deposited bead had a length of 150 mm. The distance between two consecutive beads was kept at 25 mm.

3.3 Experimental tests and method

Considering the preliminary nature of this research work, bead geometry measurements and optical microscopic analysis were carried out. A total of 6 specimens from centre of each bead were sectioned using bandsaw with coolant and metallographic specimens were prepared. For grinding and polishing, Struers TegraPol-15 equipment was employed. Beraha's in combination with modified Kalling's etchants were used for etching purposes. For geometric measurements of beads, OLYMPUS

microscope was used. Nikon ECLIPSE MA100 was used to capture the micrographs, and the images were analysed using ImageJ software.
Picture of beads and samples after sectioning and metallographic preparation are shown in Figure 7.

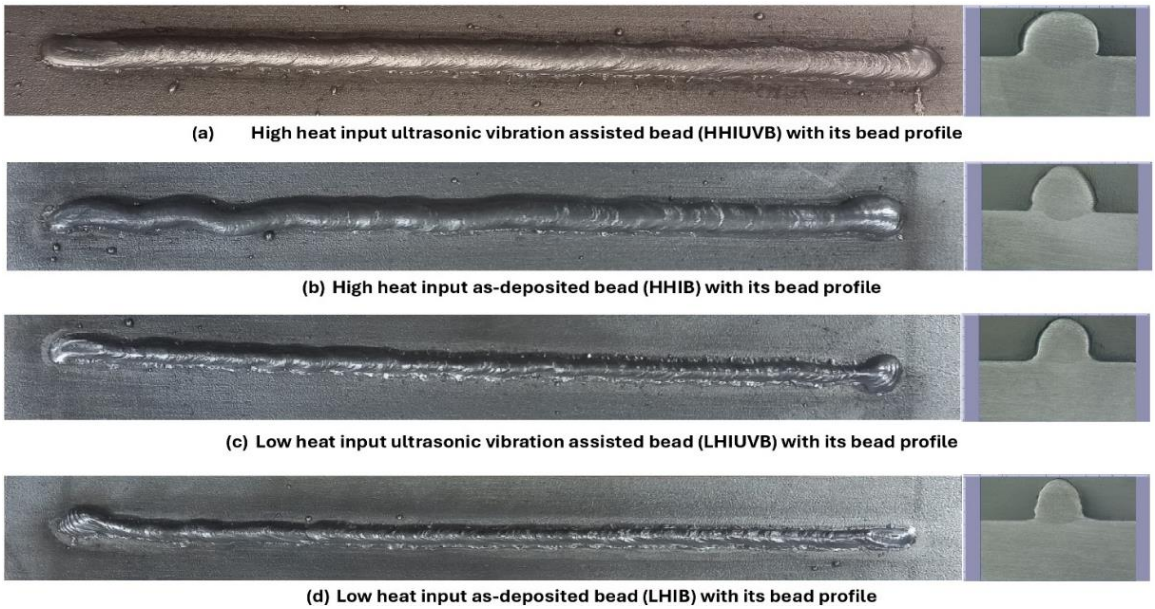

Figure 7. Beads with their corresponding sectioned metallographic samples

4. Results and Discussion

4.1 Bead geometric measurements

Based on image analysis and data acquisition results obtained from the micrographs using ImageJ software, it was found that ultrasonic vibrations influenced the overall bead geometry, including its width, height and reinforcement area. Vibration-assisted beads, in the case of both high and low heat inputs, had higher widths compared to as-deposited beads under the same conditions. This contrast in geometrical appearance of beads is presented in Table 3.

Table 3. Bead geometric measurements

	Average Width / mm	**Average Height / mm**	**Average Area / mm²**
High Heat Input Ultrasonic Vibration Assisted Bead	2.987	2.176	5.394
High Heat Input As-Deposited Bead	2.922	2.052	5.455
Low Heat Input As-Deposited Bead	2.023	1.557	2.382
Low Heat Input Ultrasonic Vibration Assisted Bead	2.079	1.562	2.528

4.2 Metallographic analysis

Micrographs using 10× magnification lens of optical microscope were obtained from all three sections of the samples, that is, weld metal (WM), heat affected zone (HAZ) and base metal (BM). The micrographs showed that ultrasonic vibrations in case of both, high and low, heat input conditions influenced not just the bead profiles, but also their dendrite formation patterns, respectively. This is shown in Figures 8 and 9. This is a potential indication of the possible grain refinement in 3D printed DSS walls using GMAW-AM process assisted with ultrasonic vibrations.

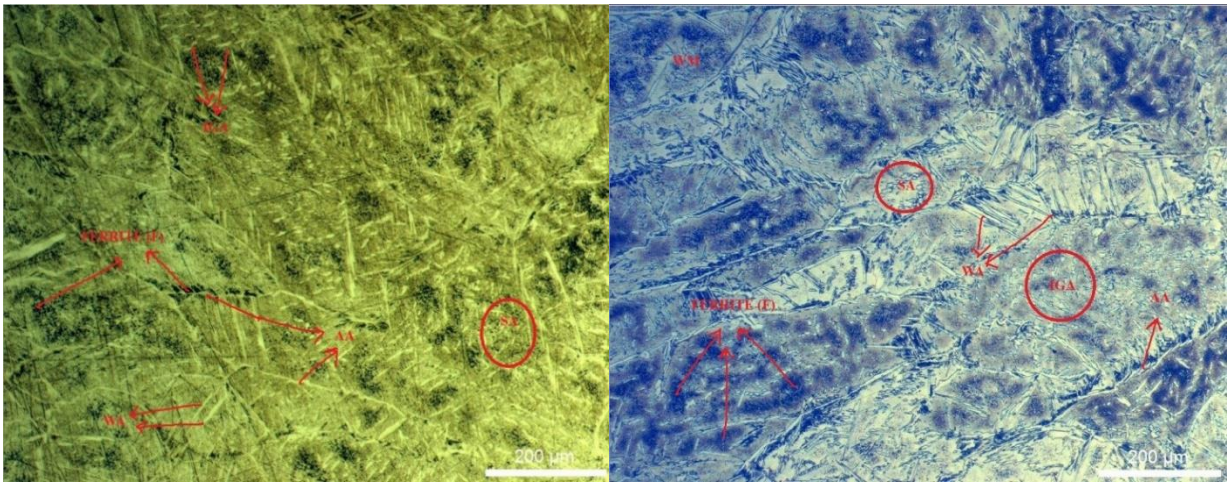

Figure 8. High heat input as-deposited (left) and ultrasonic-vibration-assisted (right) beads (weld metal) microstructures

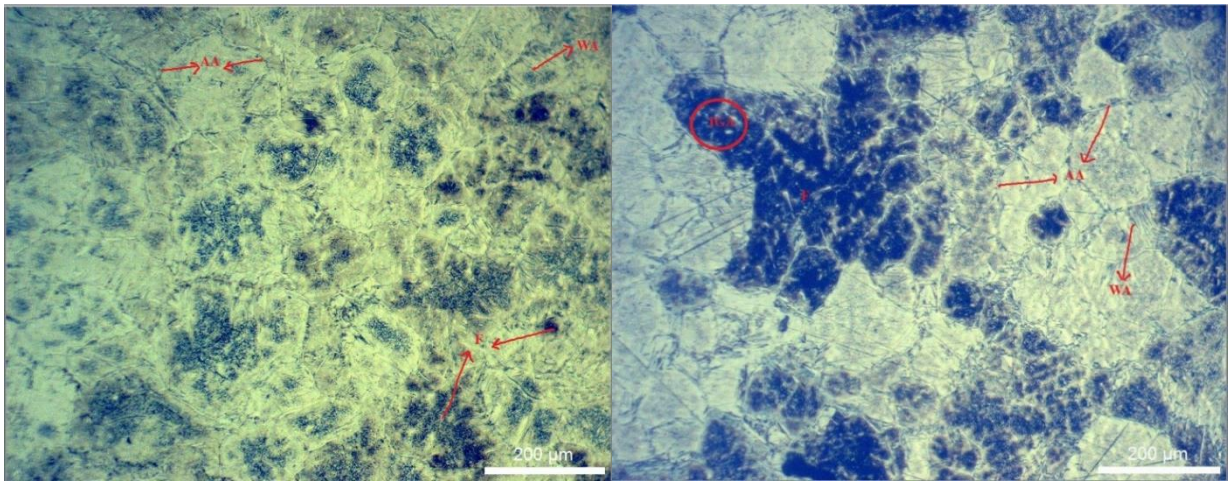

Figure 9. Low heat input as-deposited (left) and ultrasonic-vibration-assisted (right) beads microstructures

It was observed that various types of austenite formation took place, including Widmanstätten Austenite (WA), Intragranular Austenite (IGA), Allotriomorphic Austenite (AA), and Secondary

Austenite (SA), while ferrite matrix is more prominently observed in ultrasonic vibration assisted samples.

In Figure 8, it can be seen that the as-deposited bead lacks ferrite formation. Also, the austenite formation is more led by AAs and SAs, while WAs were not found in as much concentration as in the case of ultrasonic vibration assisted bead deposited with same heat input.

Both, in Figures 8 and 9, there is some evidence suggesting pro-ferrite growth in ultrasonic vibration assisted beads possibly due to quick cooling of the weld pool and enhanced pool fluidity due to vibrations. It would be interesting to see if the same is the case with multilayered structures due to ultrasonic vibration and its effect on the grain structure and chemical composition of deposited walls.

5. Conclusion

From the present preliminary study carried out with DSS 2209 filler wire beads deposited by GMAW process on DSS 2205 base plate under high and low heat input conditions with and without the assistance of ultrasonic vibrations, it is concluded that:

- Geometric measurements show that the bead morphology is influenced by ultrasonic vibrations. Based on this outcome, a potential relationship between vibration assisted deposition and microstructure can thus be hypothesised and considered as a future research direction.
- Macroscopic properties such as bead height, width and area of reinforcement remained uniform in the case of ultrasonic vibration assisted beads, which indicates the possibility of fabricating multilayered structures with uniform and stable geometry.
- The ultrasonic vibration might be favourable for more ferrite formation in the deposited beads, possibly due to higher solidification rate due to higher weld pool fluidity. Whether this holds true in case of multilayered walls will be investigated.
- Various austenite morphologies were observed in higher heat input samples, compared to lower heat input ones.

Future research should focus on analysis of isotropy, or otherwise anisotropy, of hardness, toughness and tensile properties of 3D printed DSS structures with the assistance of ultrasonic vibrations during GMAW-AM process.

6. References

[1] Pérez, Mercedes; Carou, Diego; Rubio, Eva María; Teti, Roberto. (2020). Current advances in additive manufacturing. *Procedia CIRP, 88,* 439-444. https://doi.org/10.1016/j.procir.2020.05.076

[2] Rodríguez-Martín, Manuel; Domingo, Rafael; Ribeiro, Joao. (2024). Mapping and prospective of additive manufacturing in the context of Industry 4.0 and 5.0. *Rapid Prototyping Journal, 30*(7), 1393-1410. https://doi.org/10.1108/RPJ-11-2023-0410

[3] Martínez-García, Asunción; Monzón, Mario; Paz, Rubén. (2021). Standards for additive manufacturing technologies: Structure and impact. Additive Manufacturing. Elsevier.

[4] Asami, Karim; Crego-Lozares, José María; Ullah, Abid; Bossen, Bastian; Clague, Leighton; Emmelmann, Claus. (2024). Material extrusion of metals: Enabling multi-material alloys in additive manufacturing. *Materials Today Communications*, *38*, 107889.

[5] https://doi.org/10.1016/j.mtcomm.2023.107889

[6] Jin, Wanwan; Zhang, Chaoqun; Jin, Shuoya; Tian, Yingtao; Wellmann, Daniel; Liu, Wen. (2020). Wire arc additive manufacturing of stainless steels: A review. *Applied Sciences*, *10*(5), 1563. https://doi.org/10.3390/app10051563

[7] Rodrigues, Tiago A.; Duarte, Vítor; Miranda, R. M.; Santos, Telmo G.; Oliveira, J. Pedro. (2019). Current status and perspectives on wire and arc additive manufacturing (WAAM). *Materials*, *12*(7), 1121. https://doi.org/10.3390/ma12071121

[8] Koltsaki, Maria; Mavri, Maria. (2024). A comprehensive overview of additive manufacturing processes through a time-based classification model. 3D Printing and Additive Manufacturing, 11(1), 363–382. https://doi.org/10.1089/3dp.2022.0167

[9] Wang, Huifeng; Klarić, Stefanija; Havrlišan, Sara. (2024). Preliminary study of bead-on-plate welding bead geometry for 316L stainless steel using GMAW. *FME Transactions*, *52*(4), 563-572. https://doi.org/10.5937/fme2404563w

[10] Laghi, Vittoria; Palermo, Michele; Tonelli, Lavinia; Gasparini, Giada; Ceschini, Lorella; Trombetti, Tomaso. (2020). Tensile properties and microstructural features of 304L austenitic stainless steel produced by wire-and-arc additive manufacturing. *The International Journal of Advanced Manufacturing Technology*, *106*, 3693-3705. https://doi.org/10.1007/s00170-019-04868-8

[11] Pattanayak, Suvranshu; Sahoo, Susanta Kumar. (2021). Gas metal arc welding based additive manufacturing - a review. *CIRP Journal of Manufacturing Science and Technology*, *33*, 398-442. https://doi.org/10.1016/j.cirpj.2021.04.010

[12] Rathinasuriyan, C.; Elumalai, P. V.; … Shahapurkar, Kiran. (2023). Welding-based additive manufacturing processes for fabrication of metallic parts. *Composites and Advanced Materials*, *32*, 26349833231210572. https://doi.org/10.1177/26349833231210572

[13] Zhang, Di; Liu, Aobo; Yin, Bangzhao; Wen, Peng. (2022). Additive manufacturing of duplex stainless steels - a critical review. *Journal of Manufacturing Processes*, *73*, 496-517. https://doi.org/10.1016/j.jmapro.2021.11.036

[14] Zhang, Yiqi; Wu, Shaojie; Cheng, Fangjie. (2022). A specially-designed super duplex stainless steel with balanced ferrite:austenite ratio fabricated via flux-cored wire arc additive manufacturing: Microstructure evolution, mechanical properties and corrosion resistance. *Materials Science and Engineering: A*, *854*, 143809. https://doi.org/10.1016/j.msea.2022.143809

[15] Wu, Shaojie; Zhang, Yiqi; Xue, Manye; Cheng, Fangjie. (2024). Grain refinement of flux-cored wire arc additively manufactured duplex stainless steel through in-situ alloying of Ti. *Materials Characterization*, *209*, 113749. https://doi.org/10.1016/j.matchar.2024.113749

[16] Stützer, Juliane; Totzauer, Tom; Wittig, Benjamin; Zinke, Manuela; Jüttner, Sven. (2019). GMAW cold wire technology for adjusting the ferrite–austenite ratio of wire and arc additive manufactured duplex stainless steel components. *Metals*, *9*(5), 564. https://doi.org/10.3390/met9050564

[17] Zhang, Yiqi; Cheng, Fangjie; Wu, Shaojie. (2021). The microstructure and mechanical properties of duplex stainless steel components fabricated via flux-cored wire arc-additive manufacturing. *Journal of Manufacturing Processes*, *69*, 204-214. https://doi.org/10.1016/j.jmapro.2021.07.045

[18] Yu, Chen; Zhao, Yunqiang; … Miao, Shu. (2022). Trailing rotating-extrusion-assisted wire arc additive manufacturing of duplex stainless steel. *Science and Technology of Welding and Joining*, *27*(8), 629-637. https://doi.org/10.1080/13621718.2022.2105993

Društvo za tehniku
zavarivanja Slavonski Brod

13. Međunarodno znanstveno-stručno savjetovanje SBZ 2025

„STROJARSKE TEHNOLOGIJE U IZRADI ZAVARENIH KONSTRUKCIJA I PROIZVODA, SBZ 2025."
Slavonski Brod, 08. i 09. 05. 2025.

Dwelling Time Analysis in GMAW Additive Manufacturing of 316L Stainless Steel

H. Wang[1,*], Š. Klarić[1], S. Havrlišan[2]

[1]Faculty of Science and Technology, Charles Darwin University, Australia
[2]Mechanical Engineering Faculty in Slavonski Brod, University of Slavonski Brod, Croatia

* Corresponding Author. E-mail: huifeng.wang@students.cdu.edu.au

Abstract

As an important parameter of Wire Arc Additive Manufacturing process (WAAM), interlayer temperature (IT) has a significant impact on the microstructure, mechanical properties, and surface quality of Additive Manufacturing (AM) products. To keep IT within an acceptable range (around 150 °C), a dwell time (DT) is introduced. From the perspective of effective products, a constant DT is not suitable for a multi-layer AM process, because only a short DT is required at the beginning of welding, while as the number of layers increases heat accumulates and a longer DT is required. In this paper, the relationship between DT and IT was obtained through numerical simulation method. It revealed that the efficiency of DT in IT control reduced with the layers number increasing. Under a constant DT strategy, 5160s is required, but using variable DT, the total time can be reduced by 40%. The experiment results verified that the DT strategy was an effective way to improve the manufacturing speed and the quality of the WAAM process.

Keywords: Wire Arc Additive Manufacturing process (WAAM), Interlayer Temperature (IT), Dwell Time (DT), Numerical Simulation, 316L stainless steel

1. Introduction

Additive manufacturing (AM), which is a layer-by-layer deposition process, has rapidly developed in the last three decades [1, 2]. GMAW additive manufacturing is Wire Arc Additive Manufacturing (WAAM) process where the accumulation of melted/joined metallic materials is utilized to manufacture products [3]. Besides other advantages of the AM process, GMAW AM can also manufacture large-scale metal products, with a higher deposition rate and lower cost compared to other AM methods [4, 5].

The interlayer temperature (IT) is an important parameter in the WAAM processes, besides parameters such as the wire feed speed (WFS), the travel speed (TS), and welding voltage. The

review of IT influence on the quality of AM product will be focus of this review [6, 7]. IT can influence the AM structure significantly, from microstructures and mechanical properties to surface qualities. For example, Chen Shen et al. [8] indicated that inter-pass temperature was critical for preventing stress-induced cracking. Xiong J. et al. [9] revealed that when the interlayer temperature increased, the macro-cracks gradually disappeared, the layer width increased, and the layer height decreased.

As shown in the related reference [10-12] that the IT between 100 and 500 °C is suitable for steel materials, AM process. Many methods exist to control the IT to a suitable range before the next deposition, such as a water-cooling system [13, 14], a gas-cooling system [15, 16], and dwelling/idle time. Among them, while extra cooling system can reduce the IT quickly, it will also increase the complexity of the system, so researchers are still focused on using DT to control IT. The influence of the idle time on the inter-pass temperature was researched by F.W.C. Farias et al. for AWS ER90S-B3 wire and the results showed that with an idle time of 150 s, the temperature of the top layer can be reduced to 300 °C, while idle time of the 90 s can lead to 450 °C [17]. B. Prasanna Nagasai et al. [18] applied low carbon steel (ER70S-6) with a wire diameter of 1.2 mm as the fill metal to study the effect of interlayer delay on welding bead. The results showed that the wall width was decreased, and the height of the wall was increased with an increase in the interlayer dwell time from 40 to 120 s. The hardness of the deposited parts was increased with an increase in interlayer delay due to fine grain microstructure. Study by Batuhan Turgut et al. [19], also showed that for low carbon low alloy steel, 120 s dwelling time can meet the requirements of the IT (the highest temperature of the top layer is about 150 °C), while the 60 s DT lead to 250 °C and no DT lead to the temperature of more than 500 °C. Considering the current research of IT and the relationship between IT and DT, to meet the requirements of AM process, in this paper, IT under 300 °C, and DT under 210 s will be chosen FEM (Finite Element Analysis) is a useful method to predict the thermal cycle during the AM process, which is also a method to help determine the relationship of IT and DT. For example, Dong, B. L. et al. [20] carried out a numerical model to simulate the thermal process during WAAM in a high alloyed quaternary Al-Zn-Mg-Cu alloy. The calculated thermal cycles of the fabricated components were compared with the measured results to validate the reliability of the numerical model.

In Ref [17] the FEM simulation estimated the effect of the idle time on the IT, and with the layers increasement, the efficiency of the heat transfer mechanism via conduction to the substrate was reduced; longer idle time could be considered to decrease the overall temperature of the built part. Hackenhaar W. et al. [21] showed that when using AWS ER70S-6 as filler materials for AM processing, an FE simulation can accurately predict the overall trend of the substrate temperature.

As mentioned above, IT can impact the AM parts significantly, from the mechanical properties of 3D parts to the microstructure and geometry. To get a lower IT, introducing a DT during layers deposition is one of the options. However, considering the heat accumulation layer by layer, a DT strategy should be developed, in which the DT is not a constant value, but its value increases with the layer buildup. In this paper FEM simulation will be carried out for consideration of the optimal DT strategy.

2. Materials and methods

2.1 The properties of the materials

In previous research, the optimal welding parameters were obtained when considering the geometry of welding beads, which were the voltage of 19 V, wire feed speed (WFS) of 500 cm/min, and travel speed (TS) of 15 cm/min [22]. As per [22], in this study carbon steel was applied as the substrate and the wire material is 316L stainless steel. The thermal properties of carbon steel and 316L stainless steel were shown in Figure 1, obtained from ANSYS materials data and engineering data sources. So the mechanical properties of the 316lL at room temperature were the following: The melting temperature is 1370 °C.

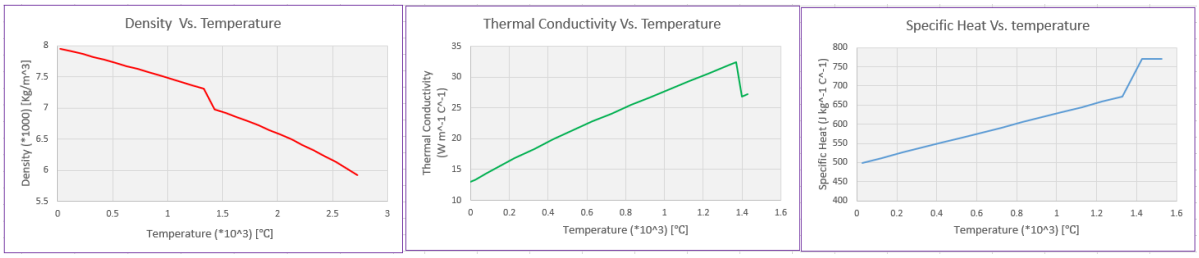

Figure 1. The thermal properties of 316L stainless steel. [Ansys]

2.2 Simulation model and procedure

2.2.1 3D model and Elements

A single pass 20-layer wall of 316L stainless steel was deposited on a carbon steel substrate of 120 × 40 × 10 mm. The geometry 3D model and its dimensions were shown in Figure 2 to utilize birth and death elements for the metal deposition process. There were 15 birth and death elements defined in each layer and the size of each element was 8 × 4 × 8 mm. All the information would be considered in the analysis setting process with the welding parameters mentioned above.

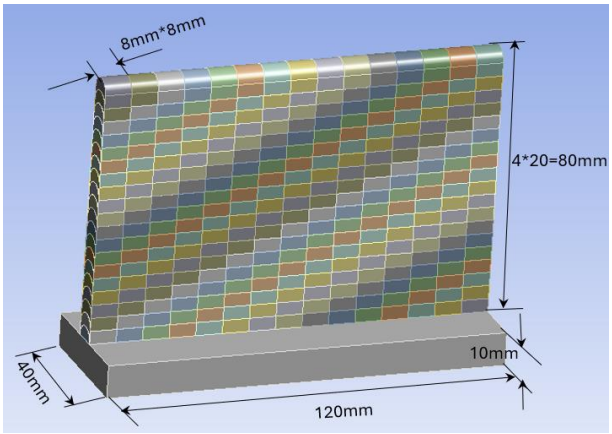

Figure 2. 3D model and dimensions for the simulation process

To be similar to the actual welding bead appearance, two types of shapes were applied which were semi-cylinder and a special shape shown in Figure 3(a). The former type was applied only on the first layer and the next 19 layers used the second type. After the mesh process, 20,196 Hexahedral elements are applied for this simulation, among them 216 elements for the substrate part, and there were 113,298 Nodes, as shown in Figure 3(b).

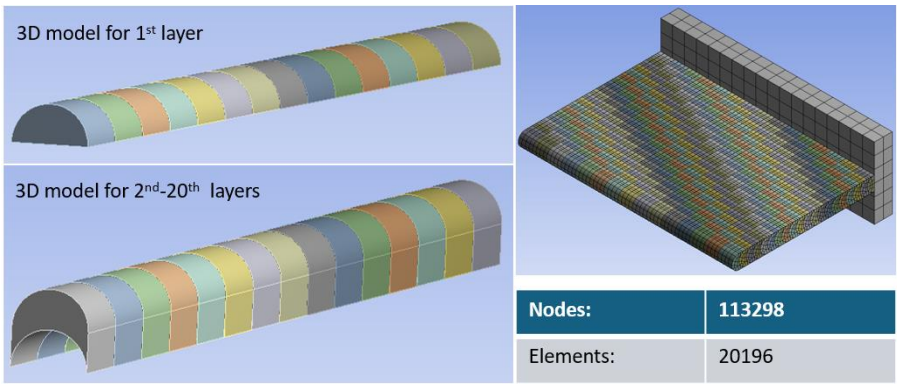

Figure 3. Different layer shapes (a) and model after meshing (b)

2.2.2 Heat distribution

Among all the heat source modeling methods, the Gaussian heat source distribution is the most popular one for welding and similar processes . The Schematic diagram of Gaussian heat source distribution was shown in Figure 4. The heat flux density distribution of Gaussian heat source was described by introducing the Gaussian mathematical model, as shown in Equation 1 [23].

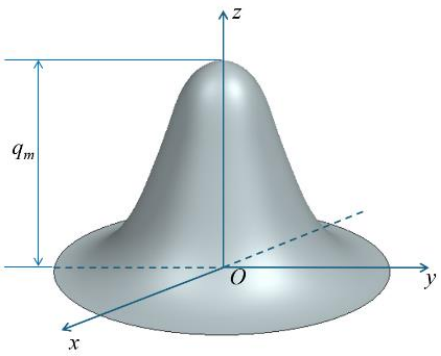

Figure 4. Schematic diagram of Gaussian heat source distribution [23]

$$q(r) = \frac{Q}{2\pi\sigma_q^2}\exp\left(-\frac{r^2}{2\sigma_q^2}\right) \quad (1)$$

Where, $q(r)$ is heat flux and the unit was J/ (m^2·s); r is the distance from the centre of the spot (m); Q was the effective power (J); σ_q is the Gaussian distribution parameters.

During the heat source application process, the reciprocating addition path was also considered to reduce the nonuniform material deposition in welding start and welding end sections, as shown in Figure 5.

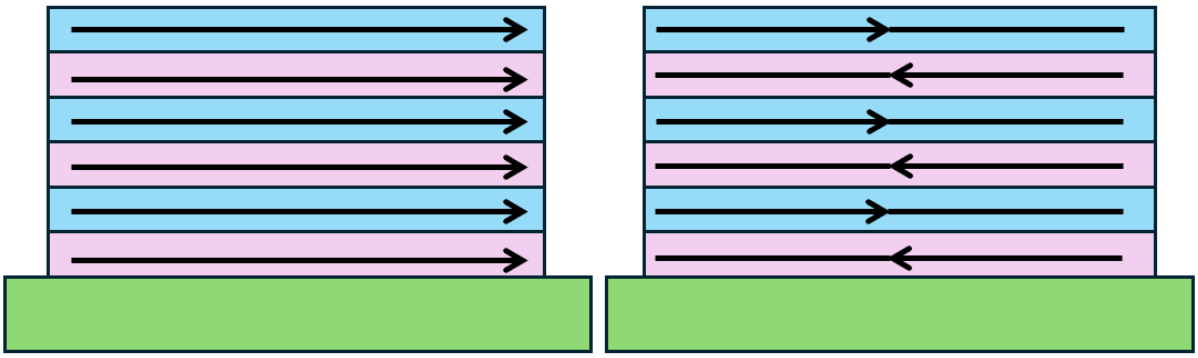

(a) Unidirectional addition (b) Reciprocating addition

Figure 5. Heat source application(welding) path

2.2.3 DT Design

Using DT is a way to let the temperature drop during the process, in theory, longer DT could lead to lower interlayer temperature. However, from an efficiency view, shorter DTs should also be considered. So, the following dwelling strategy was introduced in this section.

Five DT schedules would be applied according to the literature review [17-19] and experience from the experiments. The DTs were shown in Table 1. In the strategy of DT = 0 the next layer of welding started without any cooling time. The total times were from 960 s to 5160 s for each DT strategy, and the constant DT was applied during the first four strategies, while variable DT was utilized in the 5th strategy.

Table 1. DT strategy for simulation process.

Run	Strategy	Total Time
1	Constant DT: DT = 0 s	960
2	Constant DT: DT = 90 s	2760
3	Constant DT: DT = 150 s	3960
4	Constant DT: DT = 210 s	5160
5	Layer 1-10: DT = 90 s; Layer 11-16: DT = 150 s, Layer 17-20: DT = 210 s	3720

2.3 Welding experiment

Fanuc Robot was used as the main experiment equipment to verify the validation of the simulation. The welding robot arm, including the welding nozzle, is shown in Figure 6.

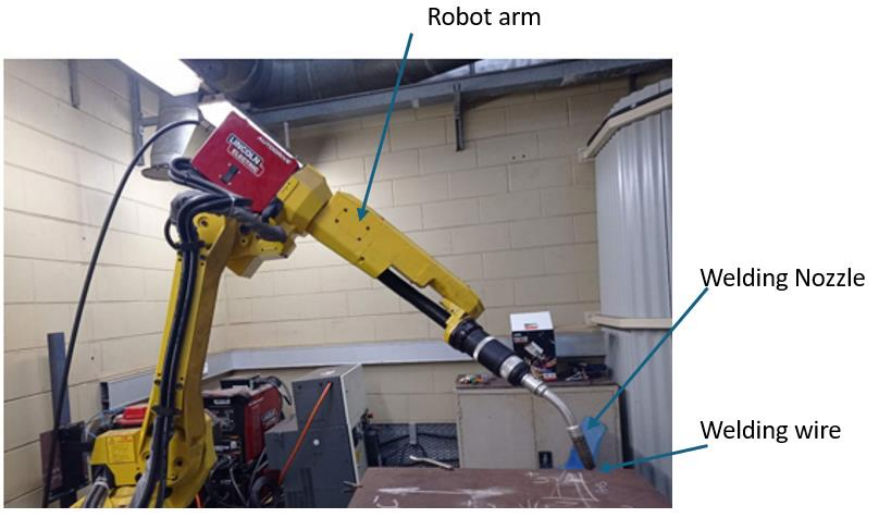

Figure 6. Welding robot used in the experimental part

3. Results and Discussion

The simulation temperature cloud was obtained from the ANSYS 2019 R2 as shown in Figure 7. The temperature close to the substrate was lower than the other part of the 3D structural wall, and the temperature gradually increases from bottom to top.

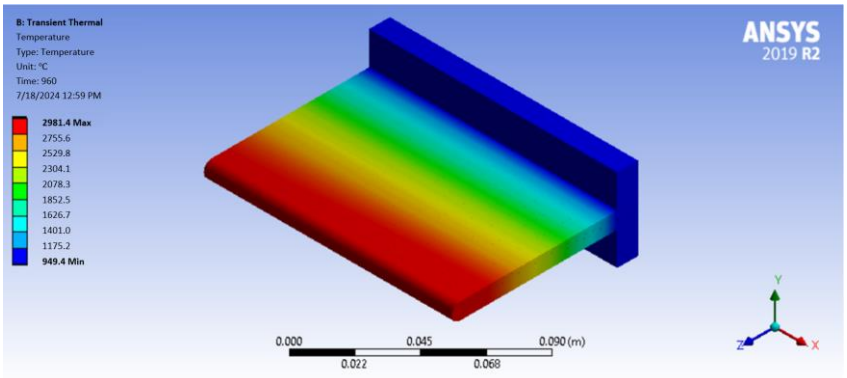

Figure 7. The simulation temperature cloud in solution of DT = 0

A thermal cycle could be used to track the temperature changes during GMAW additive manufacturing. Numerical simulation could easily obtain the temperature changes during the entire welding process.

Figure 8 shows examples of simulations for DT = 0 and DT = 90 s and revealed that when DT = 0, due to the continuous accumulation of heat, the interlayer temperature exceeds 1200 °C in all the 20th layer. This temperature is too high to maintain the normal additive manufacturing process. When DT = 90 s, the highest interlayer temperature reaches 700 °C, and the temperature is better controlled compared to DT = 0.

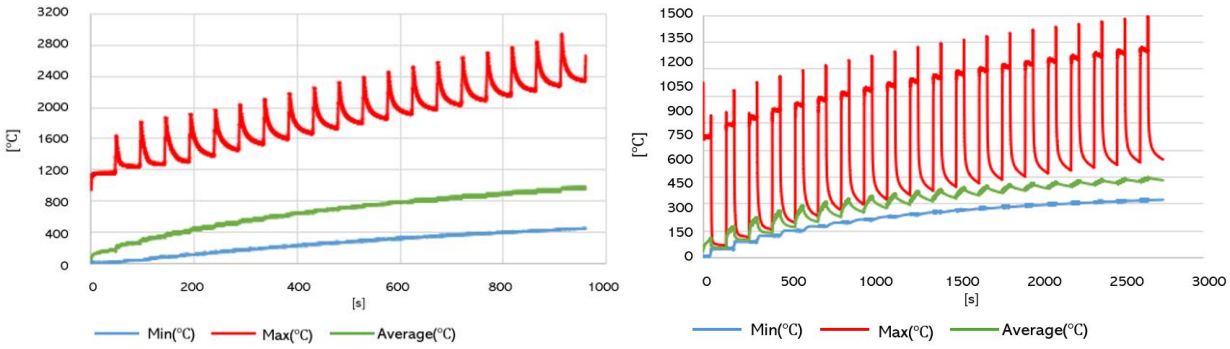

(a) DT = 0 s (b) DT = 90 s

Figure 8. Thermal cycle in AM process of DT = 0 and DT = 90

Based on the simulation results, the lowest interlayer temperature under different DTs is shown in Figure 9. The analysis showed that when DT was set to 210 s, the interlayer temperature (IT) could be controlled within 200 °C. However, under this setting, the entire additive manufacturing process took 5160 s to complete. After further optimizing DT and adopting a different DT solution, IT could still be effectively controlled within 200 °C, but the total manufacturing time was shortened to 3720 s. Therefore, a different DT could effectively reduce the manufacturing time, while ensuring that the temperature was controlled within a reasonable range and optimizing the efficiency of additive manufacturing.

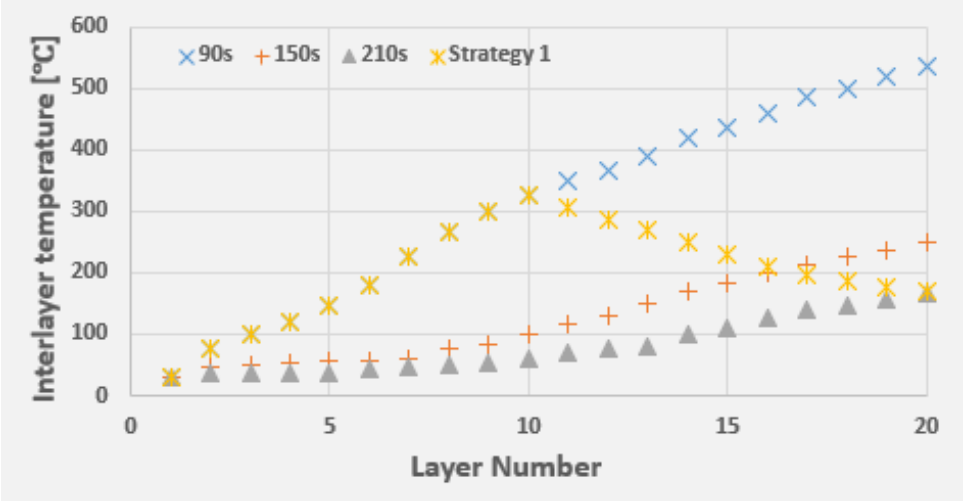

Figure 9. The interlayer temperature with different DT

4. Validation using Experiment

To verify the simulation results, a welding process was conducted using the wire feed speed of 500 cm/min, voltage of 19 V and the tavel speed of 15 cm/min. As discussed in Section 3, when there was no DT applied, the interlayer temperature would increase rapidly and reach above 1000 ℃ after the 8th layer. It was hard for the metal wall to solidify, and the additive manufacturing process could not continue. Figure 10(b) showed that with the appropriate DT strategy the more even AM wall appearance can be obtained.

(a) DT=0s (b) With variable DT strategy

Figure 10. Additive manufacturing process with DT=0 and varible DT strategy

5. Conclusion

This study uses a variable DT (DT) design to obtain an acceptable interlayer temperature and analyzes the effect of heat accumulation on cooling time during welding through numerical simulation. The study showed that as welding heat continues to accumulate, the required cooling time gradually increases. If a fixed DT was used, the overall efficiency of additive manufacturing would be reduced. The strategy of using a smaller DT in the early stage and a longer DT in the later stage could effectively control the interlayer temperature within 200 °C and improve manufacturing efficiency. Actual additive manufacturing experiments have also verified the feasibility and effectiveness of this method.

6. Reference

[1] Int, Anthony. (2013). Standard terminology for additive manufacturing technologies.

[2] Zhang, Dong; Wei, Zhiyuan; Xu, Jian; Wu, Zhiqiang; Yu, Lichao. (2022). Additive manufacturing of duplex stainless steels-A critical review. *Journal of Manufacturing Processes*, 73, 496-517. https://doi.org/10.1016/j.jmapro.2022.01.016

[3] Haden, Christopher V.; Peters, Gavin; Kumar, Ravi. (2017). Wire and arc additive manufactured steel: Tensile and wear properties. *Additive Manufacturing*, 16, 115-123. https://doi.org/10.1016/j.addma.2017.01.009

[4] Yuan, Yu-Heng; Zhang, Hongbo; Xu, Wei; Wang, Dong. (2022). Experimental and Numerical Investigation of CMT Wire and Arc Additive Manufacturing of 2205 Duplex Stainless Steel. *Coatings*, 12(12). https://doi.org/10.3390/coatings12121806

[5] Langelandsvik, Geir; Ferraz, Luís M. G.; Gaspar, António. (2020). Comparative study of eutectic Al-Si alloys manufactured by WAAM and casting. *International Journal of Advanced Manufacturing Technology*, 110(3-4), 935-947. https://doi.org/10.1007/s00170-020-05856-1

[6] Wang, Zhi-Yu; Zhang, Jian; Wei, Cheng; Liu, Hongyu. (2021). Prediction of bead geometry with consideration of interlayer temperature effect for CMT-based wire-arc additive manufacturing. *Welding in the World*, 65(12), 2255-2266. https://doi.org/10.1007/s40034-021-00297-6

[7] Vázquez, Luis; Peña, Manuel; González, Ricardo. (2020). Influence of interpass cooling conditions on microstructure and tensile properties of Ti-6Al-4V parts manufactured by WAAM. *Welding in the World*, 64(8), 1377-1388. https://doi.org/10.1007/s40034-020-00297-x

[8] Shen, Chao; Yang, Jian; Zheng, Xiaodong. (2017). Influences of deposition current and interpass temperature to the Fe Al-based iron aluminide fabricated using wire-arc additive manufacturing process. *International Journal of Advanced Manufacturing Technology*, 88(5-8), 2009-2018. https://doi.org/10.1007/s00170-017-0372-9

[9] Xiong, Jian; Liu, Guang-Chao; Zhang, Guo-Jiang. (2023). Influence of interlayer temperature on microstructure and mechanical properties of TiAl alloys in wire and arc additive manufacturing. *Journal of Manufacturing Processes*, 94, 278-288. https://doi.org/10.1016/j.jmapro.2023.02.029

[10] Ali, Yasser; Khalid, Imran; Zafar, Muhammad; Mirza, Muhammad. (2019). Wire arc additive manufacturing of hot work tool steel with CMT process. *Journal of Materials Processing Technology*, 269, 109-116. https://doi.org/10.1016/j.jmatprotec.2019.03.022

[11] Knezovic, Nikola; Garasic, Ivan; Juric, Ivan. (2020). Influence of the Interlayer Temperature on Structure and Properties of Wire and Arc Additive Manufactured Duplex Stainless Steel Product. *Materials*, 13(24). https://doi.org/10.3390/ma13245855

[12] Xiong, Yu-Bin; Zhang, Wei; Liu, Hui; Zhao, Ping. (2022). Effect of interlayer temperature on microstructure evolution and mechanical performance of wire arc additive manufactured 300M steel. *Materials Science and Engineering A-Structural Materials Properties Microstructure and Processing*, 831. https://doi.org/10.1016/j.msea.2022.142000

[13] da Silva, Luis J.; Santos, José; Moreira, João. (2020). Concept and validation of an active cooling technique to mitigate heat accumulation in WAAM. *International Journal of Advanced Manufacturing Technology*, 107(5-6), 2513-2523. https://doi.org/10.1007/s00170-020-05909-9

[14] Scotti, Fabio M.; Moreira, João; Ferraro, Giuseppe. (2020). Thermal management in WAAM through the CMT Advanced process and an active cooling technique. *Journal of Manufacturing Processes*, 57, 23-35. https://doi.org/10.1016/j.jmapro.2020.02.029

[15] Ma, Chao; Liu, Shuang; Zhao, Yifan. (2021). Investigation of the in-situ gas cooling of carbon steel during wire and arc additive manufacturing. *Journal of Manufacturing Processes*, 67, 461-477. https://doi.org/10.1016/j.jmapro.2021.03.039

[16] Wu, Bao-Tao; Zhang, Long; Wang, Jinyang. (2018). The effects of forced interpass cooling on the material properties of wire arc additively manufactured Ti6Al4V alloy. *Journal of Materials Processing Technology*, 258, 97-105. https://doi.org/10.1016/j.jmatprotec.2018.03.029

[17] Farias, Filipe W.C.; Payao, João D.; Oliveira, Vitor H. P. M. E. (2021). Prediction of the interpass temperature of a wire arc additive manufactured wall: FEM simulations and artificial neural network. *Additive Manufacturing*, 48. https://doi.org/10.1016/j.addma.2021.102389

[18] Nagasai, Bhuvana P.; Malarvizhi, Shanmugan; Balasubramanian, Venkatesh. (2023). Effect of interlayer delay on microstructure and bead geometry of wire arc additive manufactured low carbon steel components. *International Journal of Interactive Design and Manufacturing - IJIDEM*, 17(2), 939-946. https://doi.org/10.1007/s12055-023-00741-0

[19] Turgut, Burak; Gürol, Umut; Onler, Ramazan. (2023). Effect of interlayer dwell time on output quality in wire arc additive manufacturing of low carbon low alloy steel components. International Journal of Advanced Manufacturing Technology, 126(11-12), 5277-5288. https://doi.org/10.1007/s00170-023-09749-0

[20] Dong, Bao-Lin; Xie, Cheng; Ma, Junfeng. (2021). Effects of interlayer temperature on the microstructures of wire arc additive manufactured Al-Zn-Mg-Cu alloy: Insights into texture responses and dynamic precipitation behaviors. *Additive Manufacturing*, 48. https://doi.org/10.1016/j.addma.2021.102316

[21] Hackenhaar, Wilhelm; Kubelka, Milan; Fechter, Maximilian. (2020). An experimental-numerical study of active cooling in wire arc additive manufacturing. *Journal of Manufacturing Processes*, 52, 58-65. https://doi.org/10.1016/j.jmapro.2020.02.019

[22] Wang, Huifeng; Klarić, Štefanija; Havrlišan, Sara. (2024). Preliminary Study of Bead-On-Plate Welding Bead Geometry for 316L Stainless Steel Using GMAW. *FME Transactions*, 52(4), 563-572. https://doi.org/10.5937/fme2104563w (journal article).

[23] Nascimento, Edson J. G.; Magalhães, Edson D.; Paes, Luiz E. D. (2023). A literature review in heat source thermal modeling applied to welding and similar processes. International Journal of Advanced Manufacturing Technology, 126(7-8), 2917-2957. https://doi.org/10.1007/s00170-023-09751-6

Personell certification in non-destructive magnetic particle testing

T. Brlić[1,*], M. Franjković[2], G. Filipan[1], S. Rešković[1]

[1]University of Zagreb Faculty of Metallurgy, Sisak, Croatia
[2]STSI Ltd., Lovinčićeva 4, Zagreb, Croatia

[*] Corresponding Author. E-mail: tbrlic@simet.unizg.hr

Abstract

This paper presents the STSI Ltd. staff preparation for the certification process procedure during non-destructive (NDT) magnetic particle testing. The preparation of NDT staff for the certification process procedure was carried out by testing metallic materials using the magnetic particle testing method. The importance of staff certification for non-destructive magnetic particle testing in accordance with the requirements of HRN EN ISO 9712:2022 was determined by testing of metal parts with and without welds.

Keywords: certification, non-destructive testing (NDT), NDT personell, magnetic particle testing

1. Introduction

It is known that certification is an assessment procedure carried out by an independent certification body to confirm whether a product, service or process meets certain requirements, and for the purpose of ensuring a satisfactory level of quality or safety [1].

Employees in the field of non-destructive testing are NDT personnel. They conduct tests using non-destructive methods with the aim of characterizing the condition of the tested material and timely detection of errors that can prevent damage and accidents, such as various explosions, dangerous chemicals in the environment, bursting of reservoirs, etc. Detection of defects in metallic materials, as well as their interpretation, is a complex process and requires trained personnel. Therefore there are qualification and certification bodies that are carried out certification procedure according to international standards.

The non-destructive (NDT) personell certification procedure is of great importance, since additional training and knowledge testing is confirmed by the ability of candidates to perform responsible jobs [2,3].
The international standard HRN EN ISO 9712:2022 specifies the requirements for the qualification of personnel for non-destructive testing in industry. Non-destructive testing is performed on various materials such as forgings, castings, welded and brazed products, pipes, rolled products, composites, and is used in manufacturing, railway maintenance, aviation, etc. [4-6].

NDT personnel are divided into three levels according to qualifications and each level has certain expertise and responsibilities that are verified and confirmed in accordance with the HRN EN ISO 9712:2022 standard. Level 1 certificate confirms NDT personell ability to conduct material testing using the appropriate non-destructive method according to written instructions and under the supervision of level 2 or 3 personnel. Certified level 2 have proven NDT personell ability to perform and conduct testing using non-destructive methods in accordance with international standards. Level 3 personnel have proven their ability to implement and supervise non-destructive testing procedures for the method for which they are certified and that they have sufficient practical knowledge of the materials being tested, the production process, non-destructive testing techniques for these materials, as well as the ability to evaluate and analyze test results [7,8].

The aim of this paper is to present the certification procedure of NDT personnel preparation in the company STSI d.o.o on testing metallic materials with and without welds using the non-destructive method of magnetic particles.

2. Experimental work

The test equipment used to train and prepare NDT personnel for the certification process of non-destructive magnetic particle testing is listed below. The workplace illumination test was carried out with a Tiede lux meter shown in Figure 1.

Figure 1. Lux meter

The test specimens used in the non-destructive magnetic particle testing are a metal plate with a weld, Figure 2, and a metal shaft without a weld, Figure 3. The cleaning of the test specimens was carried out mechanically using the MR 79 cleaner.

Figure 2. Test specimen - metal plate with weld

Figure 3. Test specimen - metal shaft without weld

A electromagnetic yoke Tiede GmbH + Co, W. Germany D-73457 was used to establish a magnetic field on the tested metallic materials, Figure 4.

Figure 4. Electromagnetic yoke Tiede GmbH + Co, W. Germany D-73457

Magnetic field strength measurements were performed using the Tiede FSM 2, Figure 5. Magnetic particles MR 76 S and contrast agent MR 72 were used for magnetic particle testing and were applied to the test specimens.

Figure 5. Magnetic field strength meter

3. Results and discussion

The preparation of the STSI Ltd. NDT personell for the certification process was carried out using the non-destructive magnetic particle test.

It was important to determine adequate illumination in the workplace for testing metallic materials using the magnetic particle testing. Therefore, the NDT personnel carried out a illumination check using a lux meter. The measured value was 617 lux, which complies with the requirements of the ISO 17637:2016 standard in which states that the minimum recommended illumination is 500 lux, Figure 6.

Figure 6. Measurement of workplace illumination with a lux meter

Surface preparation and cleaning of the test specimens was carried out by removing various impurities, such as oil and rust, mechanically and with the MR 79 cleaner, Figure 7.

Figure 7. Cleaning the surface of a metal plate with a weld

The magnetic field strength was then tested by lifting a test specimen of a metal plate weighing more than 4.5 kg. It was found that the magnetic yoke was able to lift and hold the metal plate in the air, proving that the required magnetic field strength was achieved, Figure 8.

Figure 8. Magnetic field strength testing

The exact value of the magnetic field strength was 42.0 A/cm, confirming that a satisfactory magnetic field required for the magnetic particle testing has been achieved, Figure 9.

Figure 9. Measurement of magnetic field strength

The MR 72 contrast agent and MR 76 S magnetic particles were applied to the test specimens immediately before the testing procedure, Figure 10.

a) b)

Figure 10. Contrast agent and magnetic particles on test specimens: a) metal plate with weld and b) metal shaft without weld

The testing procedure was initiated by establishing a magnetic field between the poles of the magnetic yoke, Figure 11.

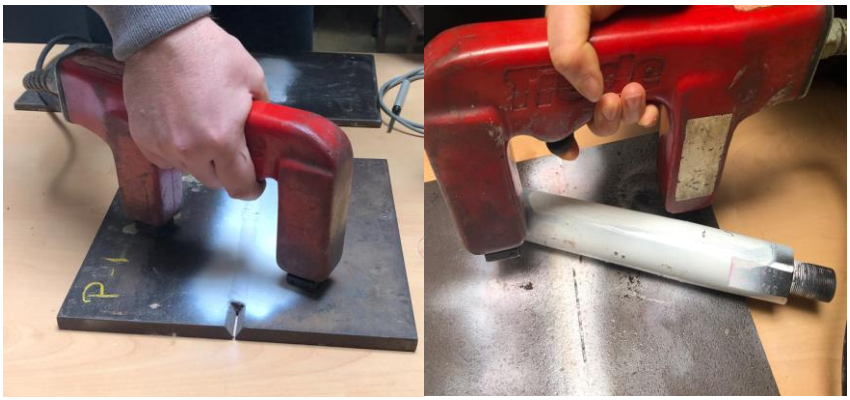

Figure 11. Specimen testing procedure with electromagnetic yoke

NDT personnel then proceeded to find areas of clustering of magnetic particles that indicate the occurrence of a defect or indication. A minor defect was found on the test specimen of the metal plate with a weld, Figure 12 a, while on the metal shaft without weld, the defect was clearly determined along the entire length of the test specimen, Figure 12 b.

a) b)

Figure 12. Surface analysis of test specimens after the test: a) metal plate with weld and b) metal shaft without weld

NDT personell was made a report of the performed inspection on the appropriate form after surface analysis of specimens. The exact defect location on the tested specimens was determined and measured, which is listed in the inspection report, Figure 13.

Figure 13. Determination of the position and dimensions of the metal shaft defect

The magnetic particles then were cleaned by rinsing and wiping. NDT personnel then began the demagnetization process. The demagnetization process was carried out by moving the electromagnetic yoke away from the metal shaft surface, Figure 14. The magnetic field strength was measured before the demagnetization process and it was 4.2 A/cm, Figure 15 a. After the demagnetization process, the magnetic field strength was 1.4 A/cm, Figure 15 b.

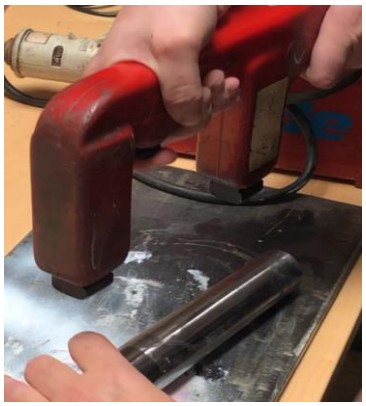

Figure 14. Demagnetization procedure

a) b)

Figure 15. Measurement of the magnetic field strength: a) before demagnetization and b) after demagnetization

4. Conclusions

The paper presents the importance of NDT personnel preparation for the certification process in non-destructive magnetic particle testing. The preparation of NDT personnel has proven to be an indispensable and significant step for the quality analysis of the magnetic particle tests. The most important steps identified during the testing are the preparation of test specimens, the testing procedure, the preparation of a report inspection of the tested metallic materials, the determination of the defects presence in the tested material and the demagnetization procedure. Defects were identified on the tested metal specimens, which were marked and listed by the NDT personnel in the inspection report in accordance with the requirements of the certification process and standards, which represents one of the key steps in the personnel certification process in magnetic particle testing.

5. References

[1] Rešković, Stoja; Brlić, Tin. (2019). Upravljanje kvalitetom. Sisak: Sveučilište u Zagrebu Metalurški fakultet.
[2] HDKBR d.o.o. (2022). Priručnik sustava upravljanja certifikacijskim tijelom, Zagreb.

[3] https://www.nde-ed.org/NDEEngineering/POD/index.xhtml, preuzeto 14.04.2023.
[4] ISO 9712:2021. (2021). Non-destructive testing - Qualification and certification of NDT personnel, Geneva, Switzerland.
[5] Rešković, Stoja. (2009). Ispitivanje materijala. Sisak: Sveučilište u Zagrebu, Metalurški fakultet.
[6] Brlić, Tin. (2009). Ultrazvučna kontrola izmjenjivača topline. Sisak: Sveučilište u Zagrebu, Metalurški fakultet.
[7] HDKBR d.o.o. (2022). Opći uvjeti kvalifikacije i certifikacije osoba za područje nerazornih ispitivanja. Zagreb.
[8] STSI d.o.o. (2022). Radna uputa: Inspekcija zavarenih spojeva magnetskim česticama.

Društvo za tehniku zavarivanja Slavonski Brod

13. Međunarodno znanstveno-stručno savjetovanje SBZ 2025

„STROJARSKE TEHNOLOGIJE U IZRADI ZAVARENIH KONSTRUKCIJA I PROIZVODA, SBZ 2025."
Slavonski Brod, 08. i 09. 05. 2025.

Application of control charts in the determination of dimensional deviations of hot-rolled welded pipes

T. Brlić[1,*], S. Rešković[1], I. Samardžić[2], B. Grizelj[2]

[1]University of Zagreb Faculty of Metallurgy, Sisak, Croatia
[2]University of Slavonski Brod, Mechanical Engineering Faculty in Slavonski Brod, Croatia

[*] Corresponding Author. E-mail: tbrlic@simet.unizg.hr

Abstract

The paper presents the results of pipe wall thickness and diameter deviations during several months of monitoring. The obtained results are determined using the control charts. It was determined that there were no significant deviations in the tested dimensions of hot-rolled welded pipes during production.

Keywords: quality management system, control charts, hot-rolled welded pipes, pipe diameter, pipe wall thickness

1. Introduction

The technology of hot-rolled, longitudinally welded pipes is very complex. The hot-rolled strip is cut to a specific width, welded into a pipe and heated first to the normalizing temperature and then to the hot-rolling temperature. Pipes with different diameters and wall thicknesses are then rolled from a pipe dimension, that is always the same, using stretch reduction technology [1-3]. The process for producing hot-rolled longitudinally welded pipes is a continuous process and consists of welding the cut strip into a continuous strip, forming the strip into a pipe, high-frequency welding the pipe and heating the pipe to the normalization temperature, to arrange the microstructure in the weld and the heat-affected zone, reheating to the hot rolling temperature, hot rolling the pipe by reducing or stretch-reducing to the final dimension, cooling, finishing, testing and packaging the pipe [3,4].

The stretch-reducing unit consists of several stretch-reducing stands arranged in a row, which are positioned at an angle of 120° to the preceding ones. The caliber of the stretch-reducing stand is closed by two, three or four rollers. The most favorable design of the caliber is with three rollers. The diameter reduction is carried out in calibers. All calibers, except the last one, have an oval shape. The last caliber has a round shape and determines the diameter of the pipe [5,6].

The reduction of the pipe wall is achieved by stretching the caliber. It is determined by the coefficient of plastic elongation *Z* and depends on the velocity of the pipe before entering and after leaving the caliber. The pipe wall thickness can be influenced by changes in the strip thickness. It is known that hot rolled strip has a lower thickness at the beginning of leaving the last rolls than at the end. The reason for this is that there is a certain temperature drop during rolling, which influences the reduction of the strip and therefore its thickness.

The standards specify pipe dimensions that must be taken into account. In addition to the nominal dimension, dimensional tolerances are always prescribed depending on the standard, i.e. maximum and minimum diameter and maximum and minimum wall thickness of the pipe. They are checked regularly during the production process. Control charts are a very reliable tool for checking dimensions and eliminating unacceptable deviations [1].

Control charts are one of the oldest and basic tools used for the statistical control of products or production processes [7]. They are forms for the graphical representation of data obtained through continuous measurements and for comparison with control limits. They are used to detect deviations from the planned flow of the process and to adjust the influential parameters so that the measured values are within the specified limits. Control charts contain three basic control limits: upper control limit (UCL), control line (CL) and lower control limit (LCL) [7,8].

Measurements outside the control limits indicate that a significant cause for the measurement deviation has occurred in the process. When measurement data is outside the control limits, the term "process is unstable" is used. This is a statistical term that indicates that the process only fluctuates under the influence of random, process-specific influences [7,9].

In addition to the precise creation of control charts, their correct interpretation is also of great importance. The analysis of the individual control charts should be carried out very seriously and carefully. Based on the results of the control chart, it is possible to improve the production process, eliminate undesirable causes and deviations, reduce production costs and thus increase profits.

There are a number of terms used in the interpretation of control charts to describe a particular state in a control chart that shows that a process is "under control". Run (flow or tendency) – occurs when seven points in a row are above or below the control line, but within the control limits. This visualization of the control chart indicates that there are irregularities in the process that need to be corrected. Trend (slope) – if there is a series of points on the control chart whose values are continuously decreasing or increasing, this indicates that the process is out of control and the machine normally needs to be calibrated. Periodicity – indicates when cyclical changes within the process occur at the same intervals. Hugging – an irregularity that occurs when the measured values are very close to the control line or control limits [7,8,10].

This paper presents the results of continuous monitoring of pipe dimensions using control charts. A problem that could have led to considerable deviations in the pipe diameter was identified and eliminated. If pipes with dimensional deviations were reach the customer, they could be the cause of complaints with financial problems.

2. Experimental work

Measurements were taken while rolling 60,3 x 3,65 mm pipes. The pipes were rolled in accordance with standrad BS1387. The tolerances for the pipe diameter were + 0,5 and – 0,32 mm, while the tolerances for the pipe wall thickness were + 0,35 and – 0,37 mm. After every four hours of continuous operation, three pipes were removed and the diameter and wall thickness measured. The mean values of the measurements are listed in Table 1. The prescribed tolerances in the plus range were used for the upper control limits and the prescribed tolerances in the minus range were used for the lower control limits.

Table 1. Measured pipe dimensions

Number of the measurement	Pipe diameter, mm	Pipe wall thickness, mm	Number of the measurement	Pipe diameter, mm	Pipe wall thickness, mm
1	60,00	3,64	21	60,35	3,70
2	60,00	3,58	22	60,43	3,72
3	60,10	3,63	23	60,48	3,65
4	60,00	3,65	24	60,56	3,75
5	60,10	3,65	25	60,62	3,68
6	60,10	3,60	26	60,58	3,65
7	60,17	3,65	27	60,62	3,64
8	60,10	3,45	28	60,64	3,62
9	60,12	3,59	29	60,68	3,60
10	60,15	3,68	30	60,69	3,54
11	60,10	3,60	31	60,70	3,55
12	60,20	3,48	32	60,71	3,60
13	60,18	3,50	33	60,75	3,88
14	60,20	3,68	34	60,72	3,65

15	60,24	3,65	35	60,76	3,65
16	60,21	3,65	36	60,76	3,62
17	60,23	3,67	37	60,77	3,60
18	60,28	3,70	38	60,76	3,68
19	60,30	3,65	39	60,77	3,70
20	60,24	3,75	40	60,78	3,70

3. Results and discussion

Control charts for the pipe diameter and wall thickness were created from the measured data in accordance with Table 1. The control charts are shown in Figures 1 and 2.

Table 2. Control limits of the measured data

	Pipe diameter, mm	Pipe wall thickness, mm
Lower control limit, mm	59,98	3,28
Nominal dimension, mm	60,4	3,64
Upper control limit, mm	60,80	4,0

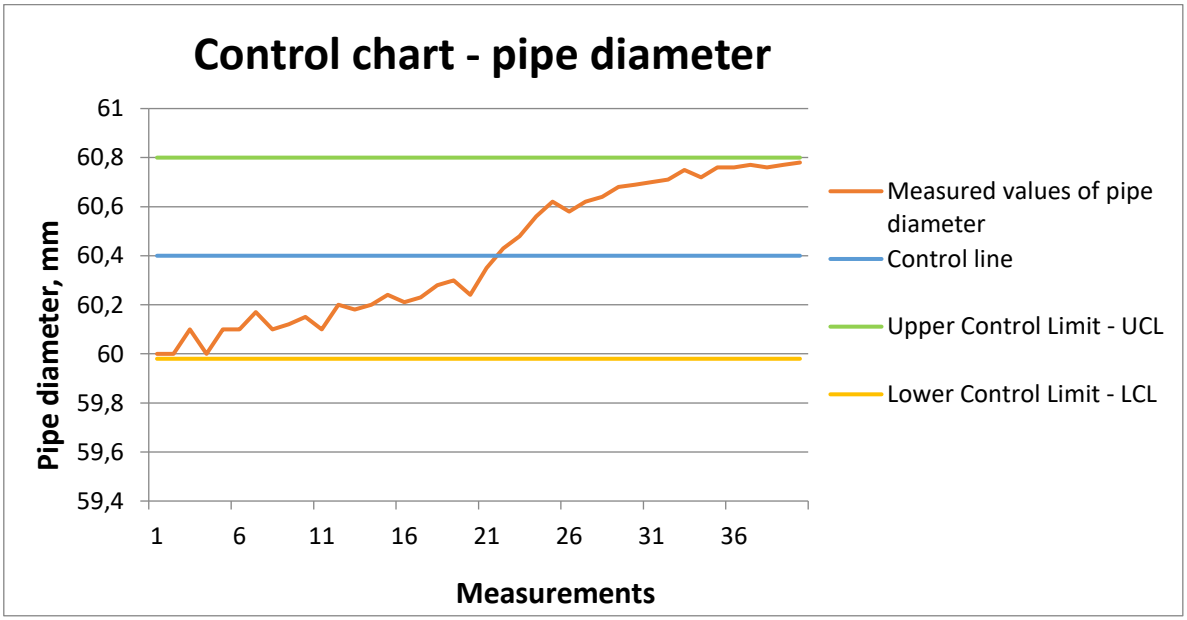

Figure 1. Control chart for the pipe diameter

Figure 1 shows that the pipe diameter is within the upper and lower control limits for all measurements, i.e. within the prescribed maximum deviations. However, a trend of increasing pipe

diameter can be observed during the measurement. As already mentioned, the pipe diameter defines the caliber opening, i.e. the diameter of the working part of the rollers at the stretch-reducing unit. As there were no other deviations in the process during the measurement, it was concluded that the rollers were worn during operation. The rollers were replaced and during further operation the pipes showed minor deviations in diameter. When the rollers were replaced, their working part was measured and it was confirmed that in the last caliber, the diameters of the working part of the rollers were close to the minimum value.

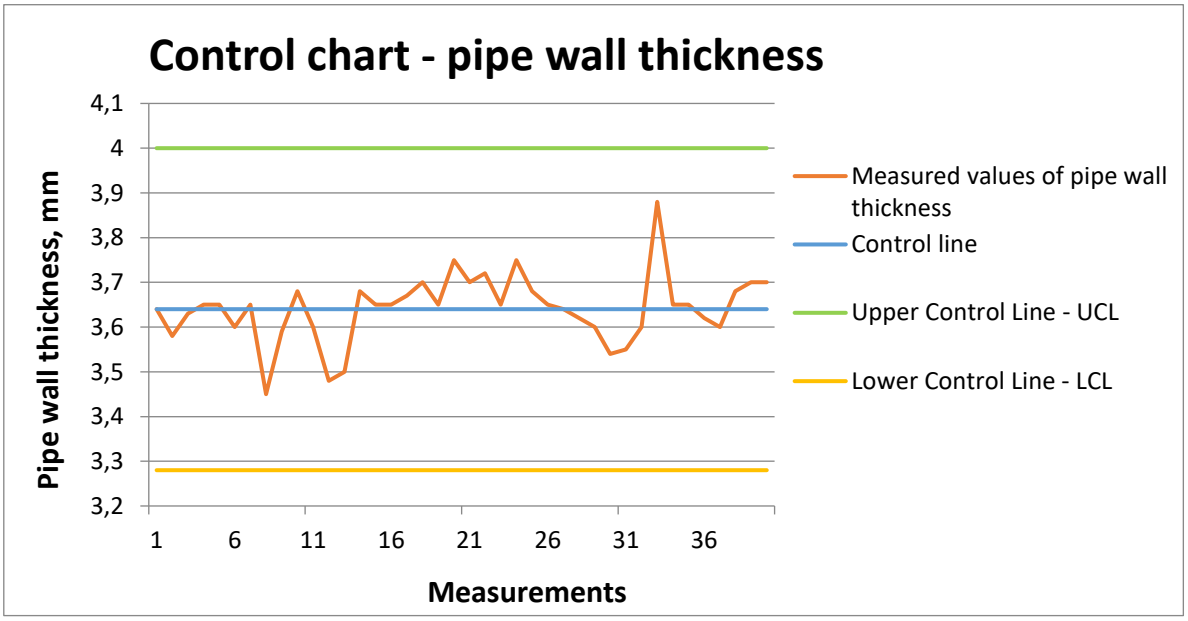

Figure 2. Control chart for the pipe wall thickness

The control chart in Figure 2 shows that the pipe wall thickness is within the upper and lower control limits for all measurements, and it can be concluded that this is a stable process. All pipes had wall thicknesses within the prescribed tolerances, i.e. within the prescribed maximum deviations, Figure 2. Certain minor deviations are mainly due to changes in strip thickness.

4. Conclusions

Measurements of the pipe dimensions using control charts showed that all pipes had dimensions within the tolerances prescribed by the standard. However, a continuous increase in pipe diameter dimensions was observed over time, which was a result of roller wear, i.e. an increase in the cross-section of the caliber that occurred after long-term operation. The timely replacement of the rolls at the stretch reducing mill prevented major non-conformity and thus possible customer complaints due to deviations in the pipe diameters.

5. References

[1] Rešković, Stoja; Jandrlić, Ivan. (2022). Tehnologije oblikovanja deformiranjem. Sisak: Metalurški fakultet Sveučilišta u Zagrebu.

[2] Stefański, Krzysztof; Kubiński, Wiktor. (2010). Diminishment of internal polygonization of tubes in hot stretch-reducing mill. *Metallurgy and Foundry Engineering*, *36*, 21-29.

[3] Rešković, Stoja; Vodopivec, Franc. (2008). An investigation of the stretch reducingof welded tubes. *Materiali in tehnologije*, *42*, 257-262.

[4] Samardžić, Ivan; Rešković, Stoja; Grizelj, Branko; Brlić, Tin; Marić, Dejan. (2023). The influence of hot deformation on the quality of welding of niobium microalloyed seam pipes intended for plumbing installations // *PLIN 2023 - ZBORNIK RADOVA 14. MEĐUNARODNOG SKUPA O PRIRODNOM PLINU, TOPLINI I VODI.* Slavonski Brod: Sveučilište u Slavonskom Brodu, 2023. str. 250-260.

[5] Rešković, Stoja; Križanić, Rade; Vodopivec, Franc. (2010). Numerical design of hot-stretch-reducing process for welded tubes. *Materiali in Tehnologije*, *44*, 243-250.

[6] Pavlić, D. (1990). Studija toplog valjanja uzdužno zavarenih šavnih cijevi na valjačkom reducirnom stanu. Fakultet strojarstva i brodogradnje. Zagreb.

[7] Rešković, Stoja; Brlić, Tin. (2019). Upravljanje kvalitetom. Sisak: Metalurški fakultet Sveučilišta u Zagrebu.

[8] Mudronja, Vedran; Baršić, Gorana; Katić, Marko; Šimunović, Vedran. (2014). Indeks sposobnosti procesa i statističke polerancije. *14. Hrvatska konferencija o kvaliteti i 5. Znanstveni skup Hrvatskog društva za kvalitetu*. Baška, otok Krk, 231-240.

[9] Kovačić, Goran; Kondić, Živko. (2012). Statistička analiza sposobnosti procesa proizvodnje stretch folije. *Tehnički glasnik*, *6*, 191-198.

[10] Svijet kvalitete - Portal o kvaliteti http://www.hgk.hr/category/sektor-centar/centar-kvaliteta,.com/index.php, preuzeto: 20.1.2018.

Društvo za tehniku zavarivanja Slavonski Brod

13. Međunarodno znanstveno-stručno savjetovanje SBZ 2025

„STROJARSKE TEHNOLOGIJE U IZRADI ZAVARENIH KONSTRUKCIJA I PROIZVODA, SBZ 2025."
Slavonski Brod, 08. i 09. 05. 2025.

Influence of impeder position on weld quality in high-frequency pipe welding

S. Rešković[1], I. Samardžić[2], T. Brlić[1,*], D. Marić[2]

[1]University of Zagreb Faculty of Metallurgy, Sisak, Croatia
[2]University of Slavonski Brod, Mechanical Engineering Faculty in Slavonski Brod, Croatia

[*] Corresponding Author. E-mail: tbrlic@simet.unizg.hr

Abstract

The paper presents the results of the influence of impeder position and welding parameters on the weld quality of welded pipes during high-frequency welding. It was determined that incorrect impeder position results in poor weld quality and higher electricity consumption.

Keywords: impeders, welded pipes, welding

1. Introduction

In the rolling mill for hot-rolled longitudinally welded pipes, a reconstruction was carried out on the high-frequency pipe welding machine. After a short period of continuous operation, problems were detected which resulted in a failure of the installed equipment and poor quality of the pipe welds. A detailed analysis revealed that the impeder was burning out.

The process of welding pipes with high-frequency current is based on the skin effect, according to which a high-frequency current flows along the surface of the conductor (the strip formed into the pipe) along the line of least resistance or impedance. The induced current is concentrated on the edges of the strip and thus heats the slot A-O-B, Figure 1. At point O, the metal melts and the edges of the strip are connected and welded by pressure rollers with relatively little force [1-5].

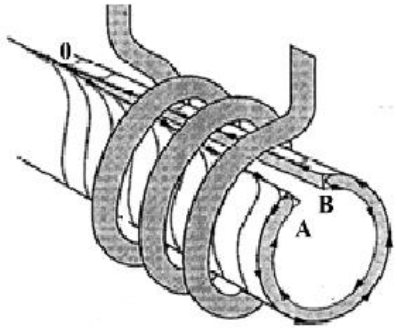

Figure 1. Schematic representation of high-frequency pipe welding [4].

Ferrite cores (impeders) are used to reduce the losses inside the pipe, Figure 2. Ferrite rods (magnetic cores) are placed in a specific position inside of the impeder. The magnetic core is completely filled with ferrite rods in a pipe with diameter of 30 mm. The ferrite core is placed closer to the weld for pipes with a larger diameter [1,4,5].

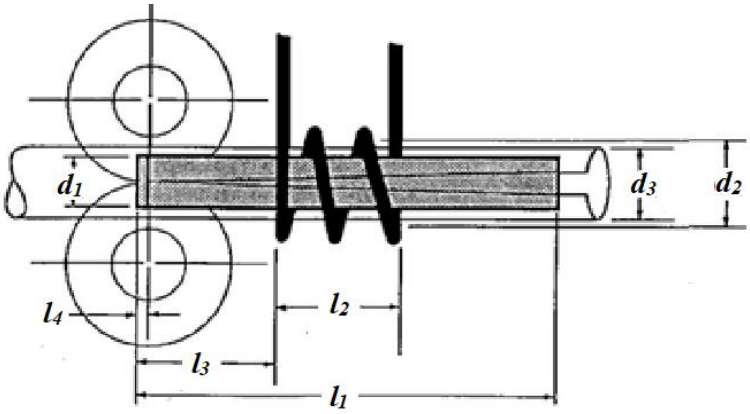

Figure 2. Impeder position

Symbols in Figure 2: d_1 – diameter of the impeder, d_2 – diameter of the inductor, d_3 – inner diameter of the pipe, l_1 – length of the impeder, l_2 – length of the inductor, l_3 – length defining the position of the impeder in relation to the axis of the welding rollers and the inductor, l_4 – length defining the position of the impeder in relation to the axis of the welding rollers.

Ferrite rods can be solid, tubular and fan-shaped. Solid and fan-shaped rods offer better performance, but since it is difficult to achieve adequate cooling, their application usually does not lead to the desired goal. Impeders are manufactured using open and closed cooling methods. Open impeder systems have a free drainage of the cooling water, while closed impeder systems have systems for recirculating the cooling water. Open cooling methods are preferred as the design is simpler and cheaper. However, impeder systems with closed cooling are always used for continuous lines.

Impeders are used for welding pipes with a diameter of 8 – 529 mm and a wall thickness of 0,3 to 10 mm. The current used for welding pipes is high frequency (400 – 500 kH). The main advantages of welding machines with impeders are the possibility of significantly increasing the speed of welding pipes (> 150 m/min) and at the same time improving the quality of the weld, the possibility of welding pipes made of low and high alloy steels, non-ferrous metals and rare alloys, as well as a significant reduction in specific power consumption per ton of finished pipes.

This paper examines the optimum position of the impeder to ensure uninterrupted operation of the system and good quality of the pipe weld seams.

2. Experimental work

The paper involved testing the quality of the pipes and the operation of the device at three impeder positions: A) 7 mm behind the axis of the welding rollers (existing condition), B) in the axis of the welding rollers and C) 15 mm in front of the axis of the welding rollers. Samples were taken and the quality of the weld seams on the pipes was tested by radiography, flattening of the pipes and macrostructures on the weld seam.

3. Results and discussion

In order to determine the optimum position of the impeder, it is necessary to explain the role of the impeder in high-frequency pipe welding in detail. The role of the impeder and its position in relation to the inductor in high-frequency pipe welding is of great importance. When current flows through the inductor, a magnetic field appears. The magnetic field is intersected by the shaped pipe passing through the inductor (Figure 2). In this way, an electric current is induced. A current with a frequency of up to 500 kH is applied, which is accepted as the standard frequency of industrial plants. The induced current flows in different paths, but for the purpose of consideration it can be simplified to assume that the current flows in two paths: along the edges of the "V" slot of the pipe (A-O-B) and along the circumference of the pipe, Figure 1. The electrical resistance of the heated edges of the "V" slot of the pipe (A-O-B) is the working resistance, and the resistance of the circuit around the circumference of the pipe is a useless resistance. These resistances can be considered to be connected in series as the induced current flows first around the circumference of the pipe and then along the edges of the "V" of the slot to the weld point O, Figure 1. In addition to the observed resistances which are resistively connected, there is an inductive resistance when the high frequency current flows through. The lowest possible operating resistance is required for the highest possible utilization of the induced current.

In order to make optimum use of the magnetic flux induced by the welding current, ferrite cores or impeders are fitted inside the pipe. The role of the impeder is to reduce the loss of the induced current

flowing on the inside, i.e. to conduct almost all of the induced current to the edges of the "V" slot lamella, Figure 1. In this way, the efficiency of high-frequency welding is increased. For maximum utilization of the welding current, the inductor and impeder must have the correct dimensions and be in the correct position in relation to each other and to the pipe to be welded.

The impeder is positioned so that it covers the length of the inductor and the welding point in the transverse direction. Three impeder positions have been defined in relation to the welding spot. There are different, contradictory opinions about the most optimal impeder position, i.e. the optimum distance between the front end of the ferrite cores and the welding spot, which is determined by the axis of the welding (pressure) rollers. This distance can be calculated empirically and depends on several factors. As a rule, it is "0" or 5 mm in front of or 30 mm behind the axis of the welding rollers, Figure 2, which is related to the welding speed.

The manufacturer placed the impeder 7 mm behind the axis of the welding rollers during installing the device. This resulted in high power consumption. At the V-groove, Figure 1, the edges of the formed pipe were heated over a larger area, and at point O the temperature was 1400°. This resulted in an excessive amount of internal weld, metal leakage, buildup on the impeder and burnout [6, 7].

Important properties to consider when selecting a material are the permeability and the Curie point and their relationship. Ferrite rods are heated to a temperature of 150 - 160 °C, and above this temperature they begin to lose their magnetic properties. If the temperature is below the Curie point for steel and during normal rolling mill operation, the impeders do not heat up above this temperature. However, if molten metal escapes from the internal weld through the impeder, the ferrite cores will certainly overheat and lose their magnetic properties.

The results obtained for different impeder positions are shown in Figures 3 and 4 and in Table 1. The X-ray images of the pipe welds taken for all three impeder positions are shown in Figure 3.

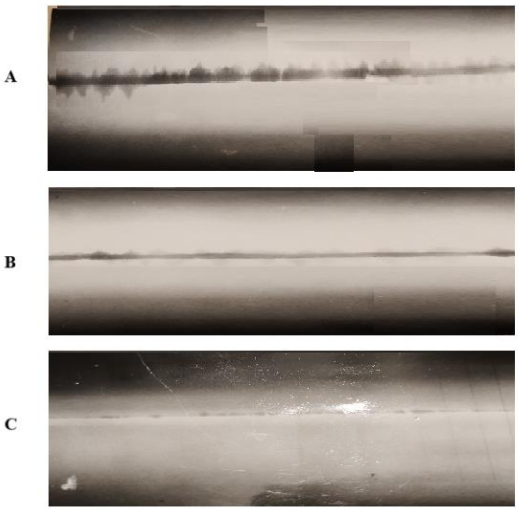

Figure 3. X-ray images of the pipe at different impeder positions

The X-ray images show a significant influence of the position of the impeder on the size of the inner weld seam excess of the pipe. In position A the internal weld excess is large and scattered, while in position B the internal weld excess is constant and of optimum size. In position C, the internal weld excess is very small and intermittent.

The recorded macrostructures of the pipe weld (at 100x magnification) are shown in Figure 4.

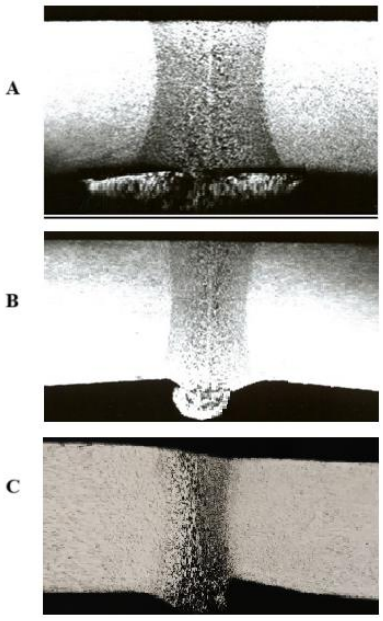

Figure 4. Macrostructure of pipe welds at different impeder positions

Figure 4 clearly shows the influence of the impeder position on the quality of the weld seam. If the impeder is in position A, the excess in the weld is significant, and the heat-affected zone is quite wide. If the impeder is in the axis of the welding rollers, i.e. in position B, the weld excess is optimal and the heat-affected zone is uniform. In position C, the internal weld excess is small and the heat-affected zone is uniform.

All pipes were also tested for hydrostatic pressure at 90 bar, with group A pipes passing 92%, group C 38% and group B 100%.

Six pipes were taken from each group for flattening tests. The pipes were flattened to 2/3 of their diameter. The tests were carried out in such a way that three samples were flattened by applying force along the weld and three perpendicular to the pipe weld. The results are shown in Table 1.

Table 1. Results of pipe flattening tests after welding

Flattening force	Test sample	Position of the impeder in relation to the axis of the welding rollers		
		A	B	C
Along the weld 	1	+	+	+
	2	+	+	-
	3	+	+	+
Perpendicular to the weld 	1	+	+	-
	2	-	+	-
	3	+	+	-
+ no cracks found, - crack at the weld				

The Table 1 shows that when testing group A pipes, a crack was observed in the heat-affected zone during flattening perpendicular to the weld. For group B pipes, all pipes met the requirements and no cracks were observed on the pipes. Cracks occurred on four group C pipes, all perpendicular to the weld and one per weld. No cracks were observed on two pipes during flattening along the weld. In addition, cracks occurred when the pipes were drawn, which occurred during rolling.

4. Conclusions

The tests have shown that the position of the impeder in relation to the axis of the welding rollers is very important both for the uninterrupted continuous operation of the rolling mill and for the quality of the welded pipe and power consumption. Placing the impeder behind the axis of the welding rolls, as the supplier did when assembling the device, is unacceptable both for the quality of the weld seam

and for the power consumption and frequent downtimes in the continuous production process of hot-rolled longitudinally welded pipes. The placement of the impeder in front of the axis of the welding rollers is also unacceptable as the quality of the pipe weld is not satisfactory. The obtained results clearly show that the optimum position of the impeder is in the axis of the pressure rollers, i.e. in position B. It should be noted that lower power consumption was achieved with the B position of the impeder.

5. References

[1] Rešković, Stoja; Jandrlić, Ivan. (2022). Tehnologije oblikovanja deformiranjem. Sisak: Metalurški fakultet Sveučilišta u Zagrebu.
[2] https://ahssinsights.org/joining/solid-state-welding/high-frequency-tube-pipe-welding/, preuzeto: 4.3.2025.
[3] Rogale, Dubravko; Firšt Rogale, Snježana; Knezić, Željko; Fajt, Siniša; Časar Veličan, Daniel; Jukl, Nikolina. (2024). Process Parameters of High Frequency Welding. *Materials, 17*, 517.
[4] Rešković, Stoja. (1998). Optimalizacija potrošnje električne energije pri visokofrekfentnom zavarivanju cijevi. PC Šavne cijevi. Željezara Sisak, Sisak.
[5] Rešković, Stoja; Križanić, Rade; Vodopivec, Franc. (2010). Numerical design of hot-stretch-reducing process for welded tubes. *Materiali in Tehnologije*, *44*, 243-250.
[6] Rešković, Stoja. (1998). Optimalizacija parametara visokofrekfentnog zavarivanja preciznih šavnih cijevi, *Zavarivanje*, *31*, 15-23.
[7] Rešković, Stoja. (1988). Određivanje temperature vara kod visokofrekfentnog zavarivanja cijevi, *Zavarivanje*, *31*, 231-239.

Društvo za tehniku
zavarivanja Slavonski Brod

13. Međunarodno znanstveno-stručno savjetovanje SBZ 2025

„STROJARSKE TEHNOLOGIJE U IZRADI ZAVARENIH KONSTRUKCIJA I PROIZVODA, SBZ 2025."
Slavonski Brod, 08. i 09. 05. 2025.

Glavni troškovi kod elektrolučnog zavarivanja

Main costs at arc welding process

L. Sigurnjak[1,*], J. Eržišnik[2], I. Samardžić[3], M. Dunđer[3]

[1]University of Slavonski Brod, Department of Social Science and Humanities, Croatia, Croatia
[2]Faculty of Mechanical Engineering and Naval Architecture, University of Zagreb, Croatia, Croatia
[3]Mechanical Engineering Faculty in Slavonski Brod, University of Slavonski Brod, Croatia

[*] Corresponding Author. E-mail: lsigurnjak@unisb.hr

Sažetak

U radu se obrazlažu glavni troškovi kod elektrolučnog zavarivanja taljenjem. Daju se osnovne formule za izračun pojedinih troškova i ukupnih troškova za primjer ručnog elektrolučnog zavarivanja, a kroz praktični primjer daje se usporedba troškova zavarivanja kod primjene različitih postupaka elektrolučnog zavarivanja.

Ključne riječi: elektrolučno zavarivanje, troškovi, koeficijent taljenja, depozit

Key words: arc welding, costs, fusion coefficient, deposit

1. Uvod

Proračun glavnih troškova kod elektrolučnog zavarivanja vrlo su važni kod analize tehnologičnosti u proizvodni zavarenih konstrukcija. Glavni troškovi kod elektrolučnog zavarivanja su: trošak rada zavarivača/operatera, trošak dodatnog materijala, trošak opreme za zavarivanje i trošak utrošene električne energije. Ti se troškovi mogu svesti na jedinične troškove po metru duljine zavara ili što je češći slučaj jedinične troškove po kilogramu rastaljenog (deponiranog) materijala. U nastavku se daju analitički izrazi za izračunavanje glavnih troškova kod elektrolučnog zavarivanja iskazani po kilogramu depozita.

2. Glavni troškovi kod elektrolučnog zavarivanja taljenjem

Troškovi kod zavarivanja razmatraju parcijalno i na kraju svih analiza i izračuna sumiraju se, pa se temeljem toga donose izabire ono rješenje koje je najprihvatljivije za proizvodnu tvrtku. Vrlo važna parcijalna analiza tehnologičnosti je analiza glavnih troškova kod elektrolučnog zavarivanja taljenjem. Nakon što je odabran postupak zavarivanja i oblik žlijeba za zavarivanje, izračunava se potrebna masa dodatnog materijala (depozita) koji će popuniti žlijebove za zavarivanje na način da će se ostvariti kvalitetni nerastavljivi spojevi. Masa utrošenog (deponiranog) materijala dobije se kao umnožak površine poprečnog presjeka zavara (A), duljine zavara (l) i specifične mase dodatnog materijala (ρ).

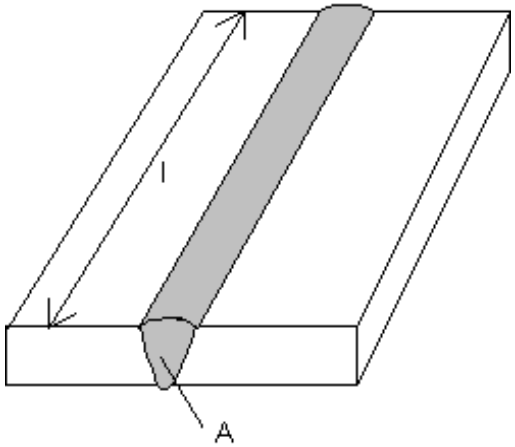

Masa depozita *(količina istaljenog DM):*

$G_{dep} = A \cdot l \cdot \rho$, kg

ρ … specifična masa, kg/m^3

A ....površina presjeka deponiranog dodatnog materijala (žlijeba), m^2

l ... duljina zavara, m

Slika 1. Inicijalne dimenzije sučeonog zavara kao polazište za izračunavanje glavnih troškova zavarivanja

Glavni troškovi ručnog elektrolučnog zavarivanja taljivom obloženom elektrodom (REL) su:

troškovi elektroda, $T_{elektroda}$
troškovi električne energije, $T_{el.energije}$
troškovi osobnog dohotka – plaće radnika, T_{ODI}
troškovi izvora struje (stroja) za zavarivanje, T_{stroja} .

1. Troškovi elektroda

$$T_{elektroda} = C_{1\ elektroda}\left[\frac{€}{kg\ elektroda}\right] \cdot k_t'\left[\frac{kg\ elektroda}{kg\ depozita}\right] \quad , \quad \frac{€}{kg\ depozita}$$

Gdje je:
$C_{1elektroda}$ ... jedinična cijena elektroda €/kg elektroda
k'_t ... koeficijent taljenja elektrode koji iskazuje iznos mase elektroda zajedno sa oblogom koja je potrebna da se rastali (deponira) 1 kg depozita.

2. Troškovi električne energije

$$T_{el.energije} = \left[\frac{U \cdot I}{1000 \cdot \quad_{s}} + N_o(1 - \ )\right] \cdot \frac{1}{k_t.} \cdot C^1_{el.en.}, \frac{€}{kg\ depozita}$$

Gdje je:

N_o … snaga praznog hoda izvora struje za zavarivanje

U – napon električnog luka; orijentacijski za REL 20 – 25 V

I – struja zavarivanja; približno 40 · promjer elektrode, A

η_s – stupanj korisnog djelovanja stroja: - rotacijski agregat …….. 0,55 – 0,65

- transformator……. 0,80 – 0,95

- ispravljač …….. 0,75 – 0,85

ε – intermitencija, vrijeme uključivanja električnog luka

$$\varepsilon = \frac{vrijeme\ gorenja\ luka}{ukupno\ radno\ vrijeme\ (8\ h\ napr.)}$$

Vrijednost □ za REL zavarivanje je obično oko 0,3, a samo u dobro organiziranoj proizvodnji može iznositi do 0,5. Za automatska zavarivanja mogu se postići više vrijednosti.

N_o – Snaga koju stroj za zavarivanje koristi u praznom hodu, kada luk ne gori. Snaga se tada troši za rad ventilatora, trenje, rasipanje magnetskog polja i zagrijavanje vodiča u stroju. N_o iznosi približno za: - agregate ……..… 1,0 kW

- ispravljače …….. 0,7 kW

- transformatore …… 0,5 kW

k_t – koeficijent taljenja elektrode, $\frac{g}{A \cdot h}$ ili $\frac{kg\ depozita}{h}$ i iskazuje efikasnost taljenja elektroda i različit je za pojedine vrste i promjere elektroda.

Orijentacijska vrijednost iznosi oko 10 $\frac{g}{A \cdot h}$. Ako zavarujemo sa elektrodom □ 4 mm i strujom 160 A, tada se k_t može izraziti i u kg dep/h:

$k_t = 160\ A \cdot 10 \frac{g}{A \cdot h} = 1{,}6 \frac{kg\ dep.}{h}$

Koeficijent taljenja ovisi o vrsti elektrode, količini Fe praška u elektrodi, u materijalu obloge elektrode i jakosti struje zavarivanja.

$C^1_{el.en.}$ – jedinična cijena električne energije €/kWh.

3. Troškovi osobnog dohotka izrade

$$T_{ODI} = \frac{ODI\left[\frac{€}{h}\right]}{k_t\left[\frac{kg\ dep}{h}\right] \cdot \varepsilon}, \frac{€}{kg\ depozita}$$

Gdje je:

ODI - bruto iznos osobnog dohotka, koji se dobije, ako se neto osobnog dohotka dodaje u obavezna davanja društvenoj zajednici (mirovinsko i zdravstveno osiguranje i ostala izdvajanja)

4. Troškovi stroja

$$T_{stroja} = T_s^1\left[\frac{€}{h}\right] \cdot \frac{1}{k_t \cdot \varepsilon}\left[\frac{h}{kg\ depozita}\right]$$

$$= \frac{C_N(amort. + osig. + održavanja + kamate + PF)}{broj\ sati\ rada\ godišnje}, \frac{1}{k_t \cdot \varepsilon}, \frac{€}{kg\ depozita}$$

Gdje je:

T_s^1 … Troškovi stroja računato po satu rada za 1 godinu.

$$T_s^1 = \frac{C_N(amort. + osiguranje + održavanje + kamate + PF)}{broj\ sati\ rada\ godišnje}, \frac{€}{h}$$

Broj sati godišnje rada stroja u jednoj ili više smjena ovisi o stvarnom korištenju stroja.

C_N - nabavna cijena stroja, €
amort - godišnja stopa amortizacije, npr. 0,1 (10% od C_N godišnje) otpis stroja za 10 god.
osiguranje - premija osiguranja godišnje npr. 0,01; 1% od C_N
održavanje - godišnji iznos za održavanje npr. 0,04 ; 4% od C_N

Ukupno glavni troškovi izračunavaju se prema izrazu:

$$T_s^1 = \frac{C_N(amort. + osiguranje + održavanje + kamate + PF)}{broj\ sati\ rada\ godišnje}, \frac{€}{h}$$

Glavni troškovi MAG/MIG i TIG zavarivanja

Izračunavanje troškova zavarivanja kod MIG/MAG zavarivanja je analogno izračunavanju troškova kod REL zavarivanja, uz dodatak troška plina za zavarivanje, dok se umjesto elektrode koristi žica. Parametri zavarivanja se također razlikuju u odnosu na REL postupak.

Glavni troškovi EPP zavarivanja

Kod EPP zavarivanja kao i kod MAG/MIG zavarivanja ulogu žica ima ulogu elektrode, a umjesto zaštitnog plina upotrebljava se prašak. Parametri zavarivanja se također razlikuju u odnosu na REL postupak.

3. Primjer izračuna glavnih troškova zavarivanja

Za izračunavanje glavnih troškova kod elektrolučnog zavarivanja može se koristiti ms office Excel aplikacija. U nastavku, na slici 2 se daje prikaz sučelja Excel datoteke u koju su uneseni ulazni podaci za izračunavanje glavnih troškova kod REL (ručnog elektrolučnog zavarivanja taljivom elektrodom), te iznos pojedinih komponenti koje sve zajedno čine ukupne glavne troškove zavarivanja. Na slici 3 su prikazani glavni troškovi REL zavarivanja, dok su na slikama 4 i 5 prikazani glavni troškovi kod MAG zavarivanja (elektrolučno zavarivanje taljivom elektrodom u zaštiti aktivnog plina), te EPP zavarivanje (elektrolučno zavarivanje taljivom elektrodom pod zaštitnim praškom).

	A	B	C	D	E	F	G	H	I	J	K
1	**Unos podataka za izračunavanje troškova zavarivanja kod REL zavarivanja**										
2											
3	a) TROŠKOVI ELEKTRODE										
4										Dijagram	
5	Jedinična cijena elektrode (€/kg):						C1elektrode =	3,00			
6	Koeficijent taljenja elektrode (kg elektroda/ kg depozita):						kte =	1,70		Povratak na početak	
7	**Troškovi elektrode** (€ / kg depozita):						T elektroda =	5,10			
8											
9	b) TROŠKOVI ELEKTRIČNE ENERGIJE										
10											
11	Napon zavarivanja (V):						U =	22,00			
12	Jakost struje zavarivanja (A):						I =	160,00			
13	Stupanj iskorištenja energije stroja za zavarivanje										
14	(za ispravljač iznosi 0.75 - 0.85):						η =	0,80			
15	Intermitencija pogona (za dobro organiziran pogon 0.3, za odlično										
16	organiziran pogon 0.5):						ε =	0,50			
17	Snaga praznog hoda stroja (kW):						No =	40,00			
18	Specifični koeficijent taljenja (kg depozita/h):						kts =	1,60			
19	Jedinična cijena koštanja električne energije										
20	(industrijska struja - 0.183 €/kWh):						C1struja =	0,18			
21	**Troškovi električne energije (€/ kg depozita):**						T struja =	5,078			
22											
23	c) TROŠKOVI OSOBNOG DOHOTKA IZRADE										
24											
25	Osobni dohodak izrade (€/h):						ODIN =	15,00			
26	Izdvajanja iz osobnog dohotka izrade										
27	za potrebe mirovinskog, zdravstva, ... (%):						IODI =	1,40			
28	**Troškovi osobnog dohotka izrade (€/ kg depozita):**						TODI =	26,25			
29											
30	d) TROŠKOVI STROJA ZA ZAVARIVANJE										
31											
32	Nabavna cijena stroja (€):						Nc =	15000,00			
33	Broj sati rada godišnje (h):						BSR =	4368,00			
34	Obavezna izdvajanja na osnovi nabavne cijene stroja										
35	(npr. 10% amortizacija stroja, 1% osiguranje stroja,										
36	4% godišnje održavanje stroja, ...):						OI =	0,15			
37	**Troškovi stroja za zavarivanje (€/ kg depozita):**						T stroja =	0,644			
38											
39	**UKUPNI GLAVNI TROŠKOVI (€/ kg depozita):**						T =	37,072			

Slika 2. Excel sučelje za unos ulaznih podataka za izračunavanje pojedinih komponenata glavnih troškova kod REL zavarivanja, te rezultati izračuna kao i ukupni glavni troškovi kod REL zavarivanja.

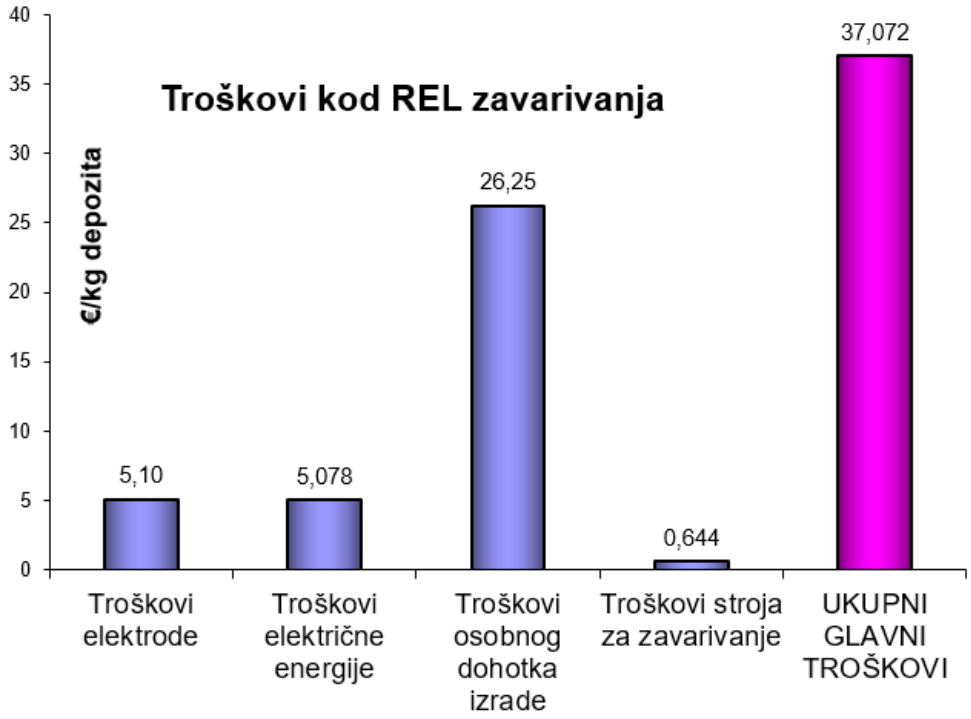

Slika 3. Pojedinačni troškovi zavarivanja i ukupni glavni troškovi zavarivanja kod REL postupka zavarivanja opće konstrukcijskog čelika.

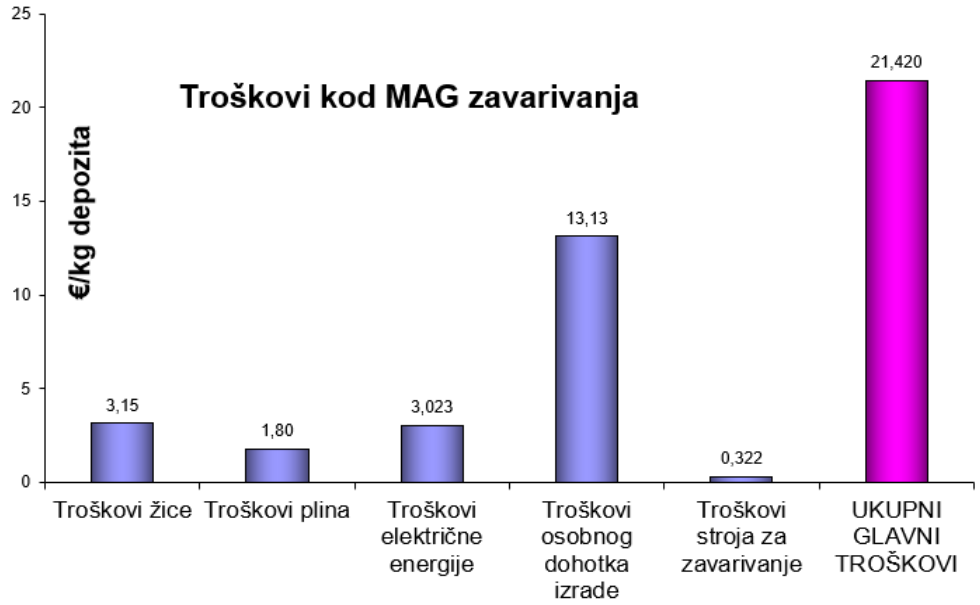

Slika 4. Pojedinačni troškovi zavarivanja i ukupni glavni troškovi zavarivanja kod MAG postupka zavarivanja opće konstrukcijskog čelika.

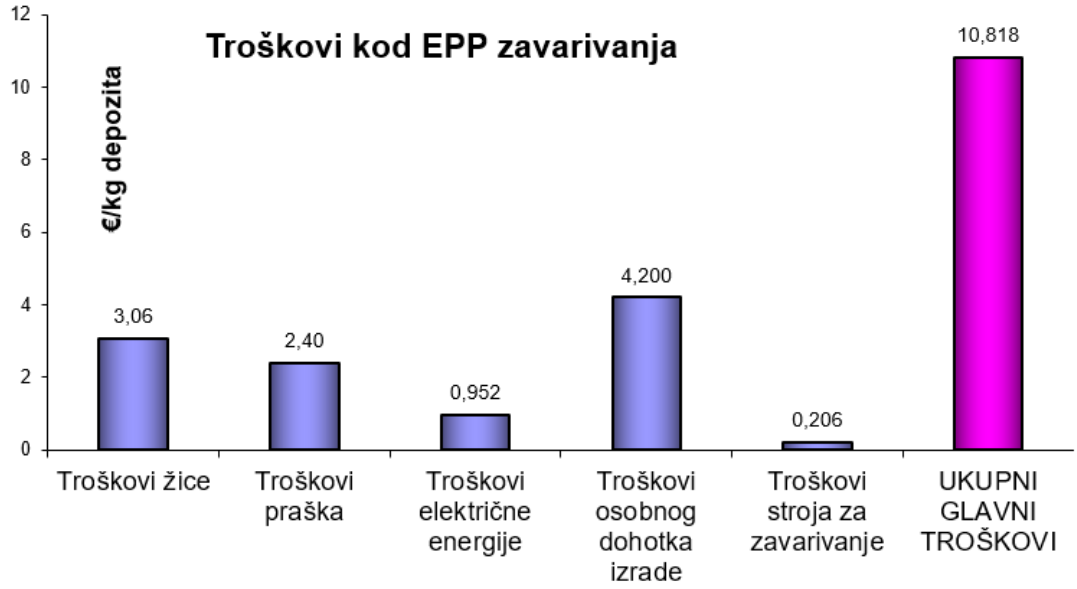

Slika 5. Pojedinačni troškovi zavarivanja i ukupni glavni troškovi zavarivanja kod EPP postupka zavarivanja opće konstrukcijskog čelika.

Usporedbom ukupnih troškova sa slika 3,4 i 5 vidljivo je da su ukupni jedinični troškovi zavarivanja kod REL postupka najviši, odnosno kod EPP postupka su najniži. To svakako ide u prilog činjenici da je ekonomski isplativa primjena poluautomatskog i automatskog zavarivanja u proizvodnim procesima u kojima je zastupljenost tehnologije zavarivanje velika. Kako su ulazni podaci za izračun troškova zavarivanja podložni promjenama na tržištu, kao i ovisni od dobavljača do dobavljača, te veličine narudžbe za pojedine elemente (napr. cijena dodatnog materijala, cijena zaštitnog plina i zaštitnog praška …), jasno je da potrebno pratiti kako promjene na tržištu, tako i glavne troškove elektrolučnog zavarivanja kako bi se ostvarili maksimalni benefiti proizvodnje.

4. Zaključak

Glavni troškovi zavarivanja (troškovi rada zavarivača/operatera, troškovi dodatnog materijala, troškovi opreme za zavarivanje i troškovi električne energije) u značajnoj mjeri određuju ekonomsku isplativost proizvodnog pogona (što je vrlo značajan element koji determinira tehnologičnost proizvoda i proizvodnje, odnosno cost efficiency). U radu se daju izrazi za izračunavanje pojedinih komponenata glavnih troškova kod elektrolučnog zavarivanja, kao i primjer izračuna troškova kod zavarivanja opće konstrukcijskog čelika REL, poluautomatskim MAG i automatskim EPP postupkom zavarivanja. Kod prikazanog primjera pokazalo se da su jedinični troškovi zavarivanja najpovoljniji kod EPP zavarivanja opće konstrukcijskog čelika, a najviši kod REL zavarivanja. U proizvodnim pogonima gdje se zahtjeva veća količina depozita kod zavarivanja opće konstrukcijskih čelika, primjena automatskog EPP postupka zavarivanja je opravdana i ekonomski isplativa.

5. Literatura

1. Lukačević, Zvonimir. Zavarivanje. Strojarski fakultet u Slavonskom Brodu, 1998.
2. https://www.hep.hr/ods/korisnici/poduzetnistvo/tarifne-stavke-cijene-161/161
3. Samardžić, Ivan i dr. Analiza tehnologičnosti zavarenih konstrukcija. Digitalni udžbenik, 2000. https://sfsb.unisb.hr/portal-merlin/diplomski-studij/d851-zavarivanje/zavarivanje-digitalni-udzbenik/

Primjena METALOCK postupka hladnog spajanja

D. Marić[1,*], I. Deanović[1], M. Krneta[2], I. Samardžić[1], T. Šolić[1]

[1]Mechanical Engineering Faculty in Slavonski Brod, University of Slavonski Brod, Croatia
[2]STSI - Integrirani tehnički servisi d.o.o., Lovinčićeva 4, 10000 Zagreb, Croatia

[*] Corresponding Author. E-mail: dmaric@unisb.hr

Sažetak

U radu se obrazlaže METALOCK postupak hladnog spajanja koji se najčešće koristi kod reparature oštećenih pozicija od sivog lijeva (blokovi različitih motora s unutrašnjim izgaranjem, kućišta lijevanih reduktora, kućišta alatnih strojeva od sivog lijeva, kućišta preša od sivog lijeva itd.). Kroz praktični primjer prikazani su koraci kod primjene ovog postupka spajanja koji je u praksi prisutan oko 100 godina i koji i danas ima značajnu primjenu kod specifičnih vrsta oštećenja strojarskih proizvoda.

Ključne riječi: METALOCK, reparatura, hladno spajanje, sivi lijev

1. Uvod

METALOCK je inženjerski postupak hladnog popravka napuknutih, polomljenih ili s greškom lijevanih dijelova strojeva izrađenih najčešće od lijevanog materijala. Postupak je moguće primijeniti na različite materijale (napr. Al legure, Mg legure, sve vrste lijevova na bazi željeza i dr.). Različitim tehničkim rješenjima, metalok može riješiti i najkompliciranije slučajeve lomova strojnih dijelova. Po potrebi, metalok garantira svoje popravke na nepropusnost, protiv daljnjeg produženja napuknuća. METALOCK postupak se javlja se 20. stoljeća u SAD-u, a 1937. goddine patentirao ga je L.B. Scott. Nakon isteka prava na patent osnovana je međunarodna METALOCK udruga u pedesetim godinama prošlog stoljeća.

2. METALOCK postupak

2.1. Kratak opis METALOCK postupka

Za hladni popravak ili popravak po metalock postupku upotrebljavaju se tri elementa (slika 1):

- METALACE vijci ili cilindrični zatici
- METALOCK ključevi

- MASTERALOCK ploče

METALACE (vijci) • Izrađuju se od niskougljičnog čelika oznake 3.6 • U praksi se koriste vijci oznake 8.8 koji su prethodno otpušteni • Stavljaju se po pukotini	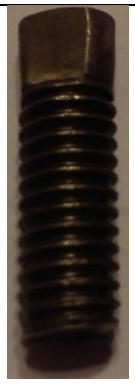
METALOCK ključ • Materijal: Č 4130 (EN 34 Cr 4) • Čvrstoća: 40-50 HRC • Izrađuju se lijevanjem • Kupuju se u šipkama duljine 500 mm	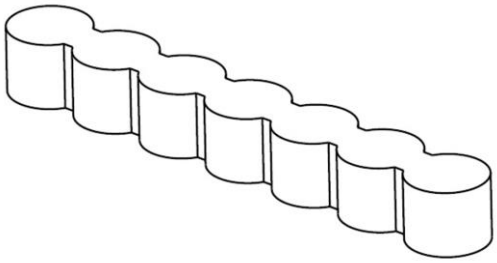
MASTERLOCK ploča	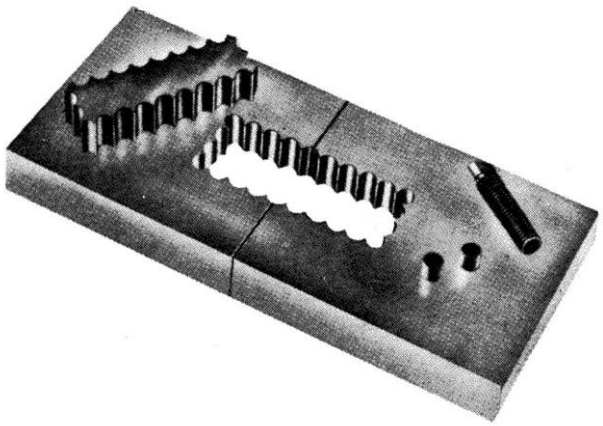

Slika 1. METALCK spajanje – 3 glavna elementa postupka spajanja. [1]

2.2. Primjena METALOCK postupka

- Ovaj postupak se provodi najčešće na strojnim dijelovima izrađenih od sivog lijeva.
- Glavni cilj ovog postupka je zaustaviti pukotinu da se ne širi dalje.
- Spada u skupinu hladnog spajanja, što znači da se materijalu ne mijenja struktura.
- Postupak se izvodi na licu mjesta, radi čega proizvodni pogoni ne trpe gubitke.

2.3. Primjena Metalock postupka spajanja

METALOCK postupak spajanja nailazi na široku primjenu u praksi, najčešće kod reparaturnih postupaka spajanja u sljedećim područjima:

- offshore industrija
- kemijska i procesna industrija
- vojna industrija
- željeznice
- energetska postrojenja
- industrija celuloze i papira
- naftna postrojenja
- brodogradnja
- strojarstvo
- ostale grane proizvodnje i industrije s većim postrojenima (lijevanim pozicijama)

2.4. Shematski prikaz spajanja METALOCK elemenata

Na slici 2 daje se shematski prikaza spajanja METALOCK elementima:

METALOCK ključ	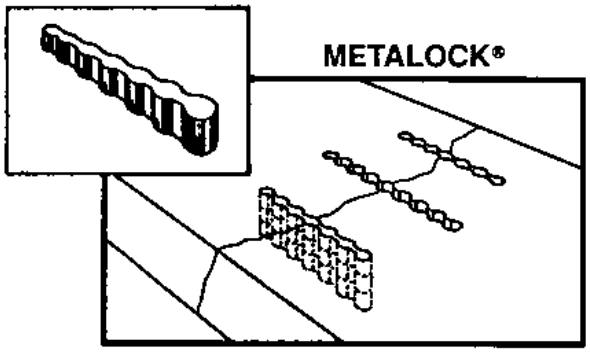
METALACE vijci	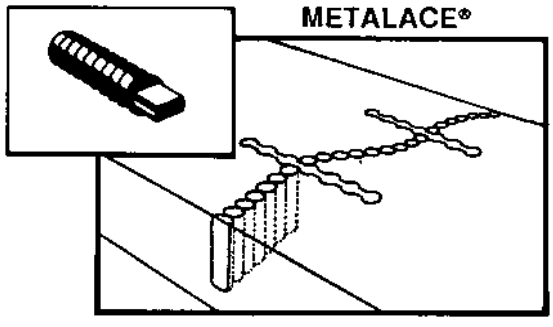

MASTERLOCK ploča	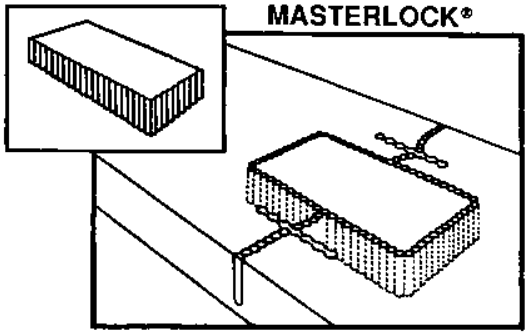

Slika 2. Shematski prikaza spajanja METALOCK elementima. [1]

3. Primjer praktične primjene METALOCK postupka spajanja

Tijekom izrade diplomskog rada oštećeni odljevak (poziciju) prikazanu na slici 3 trebalo je sanirati METALOCK postupkom.

Slika 3. Polomljenja pozicija prije sanacije METALOCK postupkom. [2]

Slika 4. Bušenje rupa za METALOCK ključeve [2]

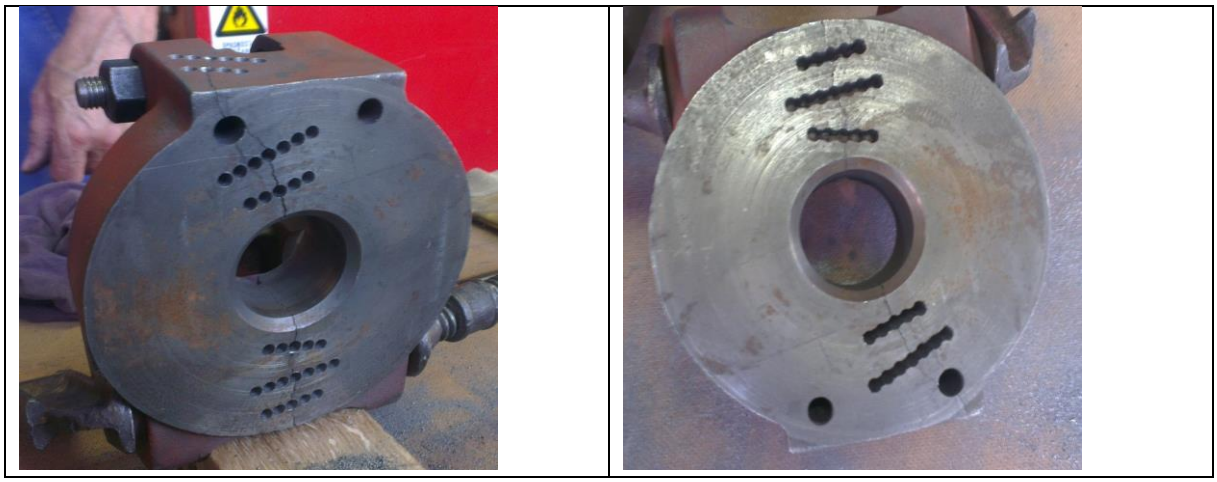

Slika 5. Rupa nakon bušenja i spajanje rupa u oblik pogodan za postavljanje METALOCK ključa. [2]

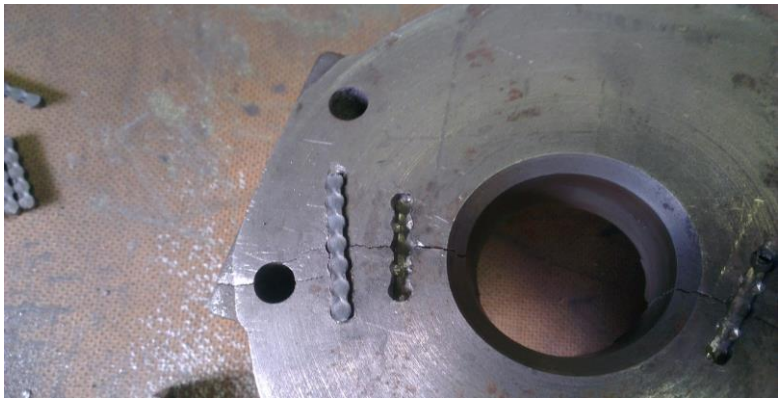

Slika 6. Postavljanje METALOCK ključeva. [2]

Slika 7. Bušenje rupa za METALACE vijek i postavljanje METALACE vijaka. [2]

Slika 8. Raskivanje METALACE vijaka i METALOCK ključeva. [2]

Slika 9. Obilježavanje i odvajanje materijala kao priprema za postavljanje METALOK pločice. [2]

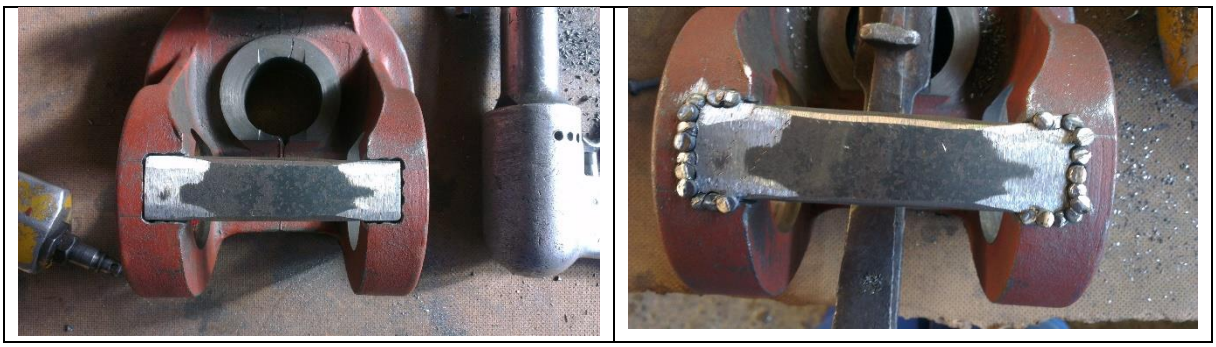

Slika 10. Postavljanje METALOCK pločice i postavljanje METALACE vijaka nakon bušenja rupa. [2]

Slika 11. Raskivanje METALACE vijaka i brušenje površine. [2]

Nakon provedenog postupka sanacije METALOCK postupkom uz primjenu MASTERLOCK ploče, METALOCK ključeva i METALACE vijaka obnovljena pozicija je poprimila izgled kako je prikazano na slici 12.

Slika 12. Izgled obnovljene pozicije nakon primjene sanacije METALOCK postupkom

Nakon aktivnosti kontrole kvalitete, pozicija ja spremna za površinsku zaštitu i eksploataciju. [2]

4. Zaključak

U radu je opisan METALOCK postupak reparature oštećenih dijelova, najčešće od odljevaka. Ovaj postupak je daleko od idealnog spajanja materijala, no ponekad predstavlja nužnost iz razloga što u relativno kratkom vremenskom roku nije moguće nabaviti određenu poziciju ili ju uopće nije moguće nabaviti (ukoliko se radi o starijim strojevima). Pored toga, kod popravljanja blokova motora gdje je uslijed izloženosti motornom ulju došlo do površinskog upijanja ulja, nije moguće primijeniti tehnologiju zavarivanja, a da se prije toga ne odstrani ulje iz površinskog sloja na mjestu zavarivanja. [3] Također ponekad zavarivanje nije moguće ukoliko je u blizini strojno obrađena površina čije se dimenzije mogu promijeniti zbog utjecaja topine pri elektrolučnom zavarivanju. Ukoliko ovaj postupak provodi osoba koja je pravilno obučena i certificirana od strane METALOCK udruge, onda

se za određene slučajeve može dobiti i garancija za obavljeni posao, kao i garancija na nepropusnost (napr. Blokovi brodskih diesel motora i sl.).
Uz različita tehnička rješenja, ovim postupkom uspješno se repariraju lomovi, pukotine i druge greške nastale u samom tehnološkom procesu izrade proizvoda ili greške nastale tijekom eksploatacije.

5. Literatura

1. Krneta M(2017) Application procedure Metalock connections material, Graduate work at Mechanical Engineering Faculty of University in Slavonski Brod, 2017. URN:https://urn.nsk.hr/urn:nbn:hr:153:020916
2. Krneta M, Samardžić I, Ivandić Ž, Marić D (2018) Joining materials by metlock repair method, Metalurgija, Vol 57, No.1-2
3. Marić, Dejan i drugi. Metalock crack sanation. The international Journal of Advanced Manufacturing Technology, 2018. https://link.springer.com/article/10.1007/s00170-018-2155-y

Tehnologična izrada zavarenih proizvoda

J. Eržišnik[1], S. Šimunović[2], M. Samardžić[2,*], I. Samardžić[2]

[1]Faculty of Mechanical Engineering and Naval Architecture, University of Zagreb, Croatia, Croatia
[2]Mechanical Engineering Faculty in Slavonski Brod, University of Slavonski Brod, Croatia

[*] Corresponding Author. E-mail: samardzic.mijat@gmail.com

Sažetak

U radu se obrazlaže pojam tehnologičnosti proizvoda koji je važan sa stajališta projektiranja i konstruiranja proizvoda, ali se benefiti ovog pristupa očituju kroz praktičnu primjenu i eksploataciju zavarenih proizvoda u praksi. Tehnologičnost obuhvaća troškove, kvalitetu, pouzdanost, uštedu materijala i energije, te estetski izgled proizvoda, pa je izuzetno važno naglašavati značaj tehnologičnog pristupa proizvodu kako kod obrazovanja, tako i kod cjeloživotnog obrazovanja i usavršavanja stručnjaka koji rade na poslovima od projektiranja i konstruiranja, pa sve do izrade i na koncu zbrinjavanja zavarenog proizvoda nakon završenog životnog vijeka.

Ključne riječi: tehnologičnost, zavarivanje, pouzdanost, kvaliteta

1. Uvod

Termin tehnologičnost je prihvaćen iz ruskog jezika.[1] U drugim jezicima nema odgovarajuća riječ. Tako npr. u engleskom jeziku je odgovarajući termin "cost effective design" (ekonomično oblikovanje). Tehnologično rješenje je ono, koje osigurava ispravno funkcioniranje proizvoda s traženom razinom pouzdanosti, u predviđenom vijeku eksploatacije, a uz najmanje troškove, najmanji utrošak materijala, najmanji utrošak energije i uz najmanje zagađivanje biološke okoline. Inženjeri koji se bave tehnologijom zavarivanja provode analize tehnologičnosti tijekom projektiranja tehnologije izrade zavarene konstrukcije ili zavarenog proizvoda, ali isto tako i tijekom trajanja proizvodnog procesa ukoliko se procjeni da je došlo do bitnih promjena koje mogu rezultirati reduciranje, odnosno smanjenje troškova proizvodnje, poboljšanje pouzdanosti, kvalitete ili

2. Općenito o tehnologičnosti

Od više mogućih rješenja u izradi proizvoda bit će tehnologično ono rješenje koje ispunjava sljedeće kriterije:

- Najniži troškovi
- Najmanje zagađenje okoline
- Najmanji utrošak energije
- Minimalni utrošak materijala
- Zadovoljavajuća kvaliteta i pouzdanost
- (Ponekad i zadovoljavajući estetski izgled proizvoda).

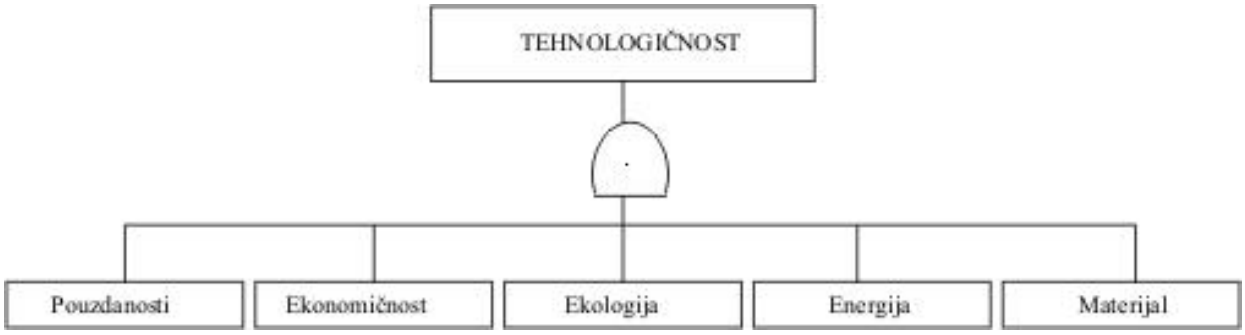

Slika 1. Tumačenje pojma tehnologičnosti proizvoda.[1]

Bez obzira što su kod razmatranja tehnologičnosti zavarenog proizvoda važni svi navedeni elementi, većina inženjera se u prvom osvrtu posveti analizi troškova izrade zavarenog proizvoda, gdje su glavni troškovi zavarivanja (troškak rada zavarivača ili operatera, trošak dodatnog materijala, trošak amortizacije opreme za zavarivanje i trošak električne energije) samo dio troškova izrade zavarenog proizvoda.

Smanjenje troškova izrade zavarene proizvoda ostvarivo je kroz:

- smanjenje mase (težine) zavarene konstrukcije (primjena visokočvrstih čelika, primjena lakih legura (Al-legure, Ti-legure, visokočvrsti čelici, …)
- ispravno konstrukcijsko oblikovanje (design) i proračun detalja zavrenog proizvoda
- smanjenje trajanja zavarivanja (naprave za dovođenje radnog komada u povoljniji položaj zavarivanja, automatizacija, robotizacija, visokoučinski postupci zavarivanja i prateće tehnologije, …)

Pri analizama tehnologičnosti proizvoda treba imati na umu da je tehnologičnost veličina ovisna o vremenu, tj. da se mijenja ovisno o proizvodnim mogućnostima, kapacitetima i infrastrukturi proizvodnog pogona, te ovisno o raspoloživim kadrovima koji sudjeluju u proizvodnom procesu izrade i kontrole zavarenog proizvoda.

Parcijalnim analizama tehnologičnosti proizvoda fokusira se na pojedine faze životnog vijeka proizvoda, pa se u nastavku navode neke od značajnijih.

1. Ugovor. *Definiraju se izbor propisa, opseg i metode kontrole, kriteriji prihvatljivosti, toplinska obrada, zahtijevana dokumentacija, rokovi, uvjeti garancije …*

2. Projektiranje i konstruiranje. *Proračunske formule, koeficijenti, dopuštena naprezanja, pretjerana zaokruženja na više vrijednosti. Povezivanje opsega kontrole i koeficijenta slabljenja zavara.*

Klasifikacija proizvoda i zavarenih spojeva unutar proizvoda. Oblikovanje detalja. U fazi projektiranja i konstruiranja treba koristiti standardizaciju, tipizaciju i principe grupne tehnologije.
3. Izbor materijala. *U fazama konstruiranja i projektiranja, ugovaranja i izbora materijala definira se oko 70-90% zahvata u izradi. Zbog toga je neophodo da u fazi projektiranja zajednički rade projektant (konstruktor) i tehnolog zavarivanja (nužno je poznavanje proizvodnih mogućnosti proizvođača).*
4. Izrada i montaža. *Izabiru se postupci obrade i zavarivanja, režimi, oblici žljebova i dodatni materijali, strojevi, radne površine, kadrovi, rokovi. Moguće je predvidjeti nekoliko rješenja, ali uvijek uz uvjet da se ostvari zahtijevana kvaliteta i uz što niže troškove.*
5. Osiguranje i kontrola kvalitete u izradi, montaži i eksploataciji proizvoda. *Različite aktivnosti osiguranja kvalitete: atestiranja zavarivača, postupaka zavarivanja i opreme za zavarivanje, sušenje dodatnog materijala za zavarivanje, baždarenja mjernih instrumenata i dr..*
Oprema, metode kontrole i osoblje se moraju provjeravati (atestirati).
6. Zbrinjavanje proizvoda. *Životni vijek proizvoda završen je tek nakon recikliranja i/ili ekološkog zbrinjavanja proizvoda, što je također vrlo važan segment koji se reflektira na sve elemente koji determiniraju tehnologičnost proizvoda.*

3. Analize tehnologičnosti sa stajališta izbora postupka zavarivanja

Koji postupak zavarivanja primijeniti za izradu zavarenog proizvoda/konstrukcije jedno je od prvih pitanja koja si postavljaju direktori proizvodnje i tehnolozi zavarivanja. Na izgled jednostavan zadatak, ali u praksi to i nije baš jednostavno jer može imati dalekosežne negativne posljedice u slučaju pogrešno izabranog postupka zavarivanja.

Mogući su različiti kriteriji za izbor postupka zavarivanja. Neki od kriterija su:

- debljina osnovnog materijala koji se zavaruje,
- oblik žlijeba za zavarivanje,
- položaj zavarivanja,
- potrebna količina depozita,
- vrsta/vrste osnovnog materijala,
- zahtjevi za kvalitetu zavarenih spojeva
- raspoloživa oprema i kadrovi za izvođenje zavarivačkih radova, te ranija iskustva iz primjene određenih visokoučinskih postupaka zavarivanja i dr.

U tablici 1 je prikazana orijentacijska količina depozita (čistog metala zavara) koja se može realizirati kod primjene uobičajenih postupaka zavarivanja taljenjem kod primjene dodatnog materijala odgovarajućeg promjera. Pored toga se navodi i vrijednost dilucije (miješanja osnovnog i dodatnog materijala), što je izuzetno važno kod tehnologije navarivanja (napr. navarivanje korozijsko

postojanog materijala na općekonstrukcijski čelik ili navarivanje tvrdog materijala na mekšu podlogu u cilju povećanja otpornosti na trošenje).

Tablica 1. Orijentacijska količina rastaljenog depozita – "deposition rate" (kg/h), te uobičajeno miješanje osnovnog i dodatnog materijala (%) za pojedine elektrolučne postupke zavarivanja i određene promjere dodatnog materijala. [2]

Postupak zavarivanja	**Promjer dodatnog materijala, mm**	**Količina depozita, kg/h**	**Uobičajeno miješanje, %**
MMA	3.25	1.5	30
MMA	5.00	3	35
MIG (spray arc)	1.20	2 – 5	30
MIG (spray arc)	1.60	3 – 7	30
TIG	2.40	1 – 2	20
SAW (wire)	3.20	4 – 8	35
SAW (strip)	0.5 x 60	15 – 17	15
Elektroslag (strip)	0.5 x 60	20 – 22	10
FCAW	1.20	3 – 6	25

Izvor: Avesta Welding AB, Sweden

Gdje je:

- **MMA** (Manual Metal Arc or Shielded Metal Arc Welding) – ručno elektrolučno zavarivanje taljivom obloženom elektrodom (REL zavarivanje)
- **MIG** (metal Inert Gas welding) – elektrolučno zavarivanje taljivom elektrodom pod zaštitom inertnog plina; postupak je izvorno poluautomatski, no može biti automatski i robotiziran
- **TIG** (Tungsten Inert Gas welding) – elektrolučno zavarivanje netaljivom elektrodom pod zaštitom inernog plina (argon, helij ili njihova mješavina); postupak je izvorno ručni, ali može biti poluautomatski, automatski i robotiziran
- **SAW** (Submerged Arc Welding) – elektrolučno zavarivanje taljivom elektrodom pod zaštitnim praškom (EPP zavarivanje); postupak je automatski
- **FCAW** (Flux Cored Arc Welding) – elektrolučno zavarivanje praškom punjenom žicom (taljiva praškom punjena žica s ili bez dodatnom plinskom zaštitom električnog luka); varijanta MAG zavarivanja
- **ES welding** (ElectroSlag welding) – elektrootporno zavarivanje pod troskom

Na slici 2 je prikazana ovisnost količine depozita i brzine zavarivanja kod različitih visokoučinskih postupaka zavarivanja. U nekim slučajevima se zahtjeva veća brzina zavarivanja pa je onda tehnologičan postupak zavarivanja LaserHybrid postupak (napr. u automobilskoj industriji), dok je u

nekom drugom slučaju kada se traži velika količina rastaljenog dodatnog materijala (depozita) tehnologičan postupak zavarivanja varijanta TimeTwin Digital postupak zavarivanja.

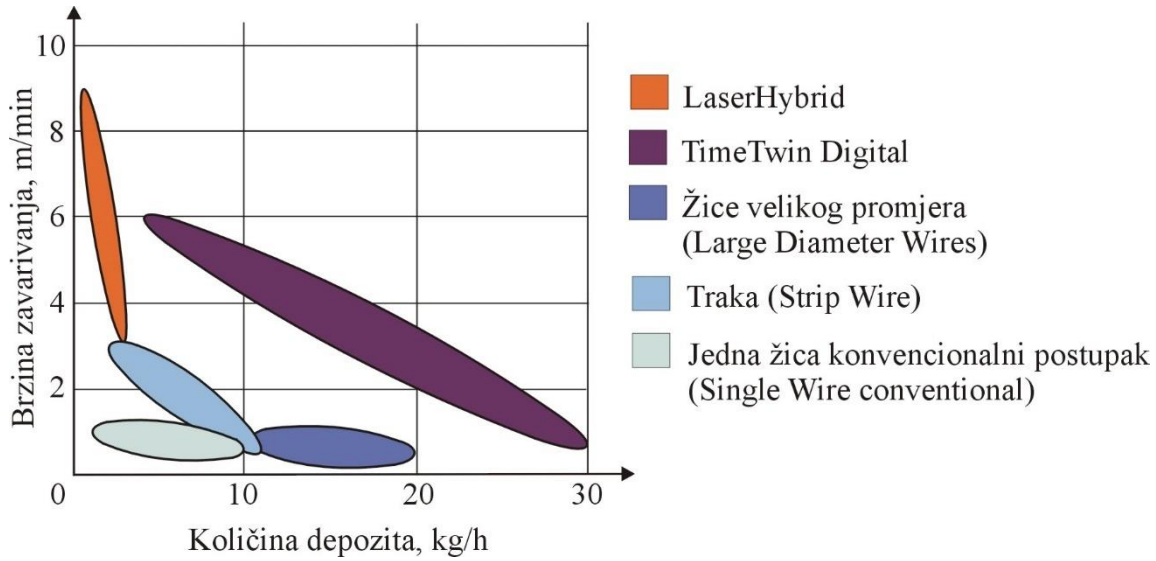

Izvor: Fronius International Gmbh

Slika 2. Brzina zavarivanja i količina depozita za visokoučinske postupke zavarivanja.[2]

Veća količina depozita od stvarno potrebne količine ne predstavlja samo trošak dodatnog materijala, već može imati čitav niz negativnih posljedica kao što su:

- veće deformacije i zaostale napetosti zbog većeg nepotrebnog unošenja topline u materijal,
- dulje trajanje proizvodnje zbog nepotrebno više vremena za zavarivanje (taljenje dodatnog materijala),
- više potrebne energije i veća potrošnja energije (el. energija za elektrolučno zavarivanje), te
- više i nepotrebne troškova stroja (amortizacija, održavanje, osiguranje, kamata na osnovna sredstva); oprema bi se mogla koristiti za druge aktivnosti zavarivanja na istom ili drugim proizvodima.

4. Izbor žlijeba za zavarivanje

Nakon što je izabran postupak zavarivanja, logičan je slijed izbora oblika žlijeba za zavarivanje ukoliko se radi o elektrolučnom zavarivanju sučeonih spojeva. Logika kojom se vodi je prvenstveno da se postigne minimalno zahtjevana kvaliteta zavarenog spoja, uz minimalan utrošak dodatnog materijala i minimalno trajanje zavarivanja. Pri tome svakako treba voditi računa i o položaju zavarivanja koji je često uvjetovan veličinom zavarenog proizvoda i postupkom zavarivanja (napr. EPP postupak zavarivanja moguć je u horizontalnom položaju i u nekim slučajevima u zidnom položaju). Na slici 3 je prikazana teorijska površina žlijeba za elektrolučno zavarivanje za različite oblike žlijebova, dimenzije osnovnog materijala i tehnike pripreme žlijeba.

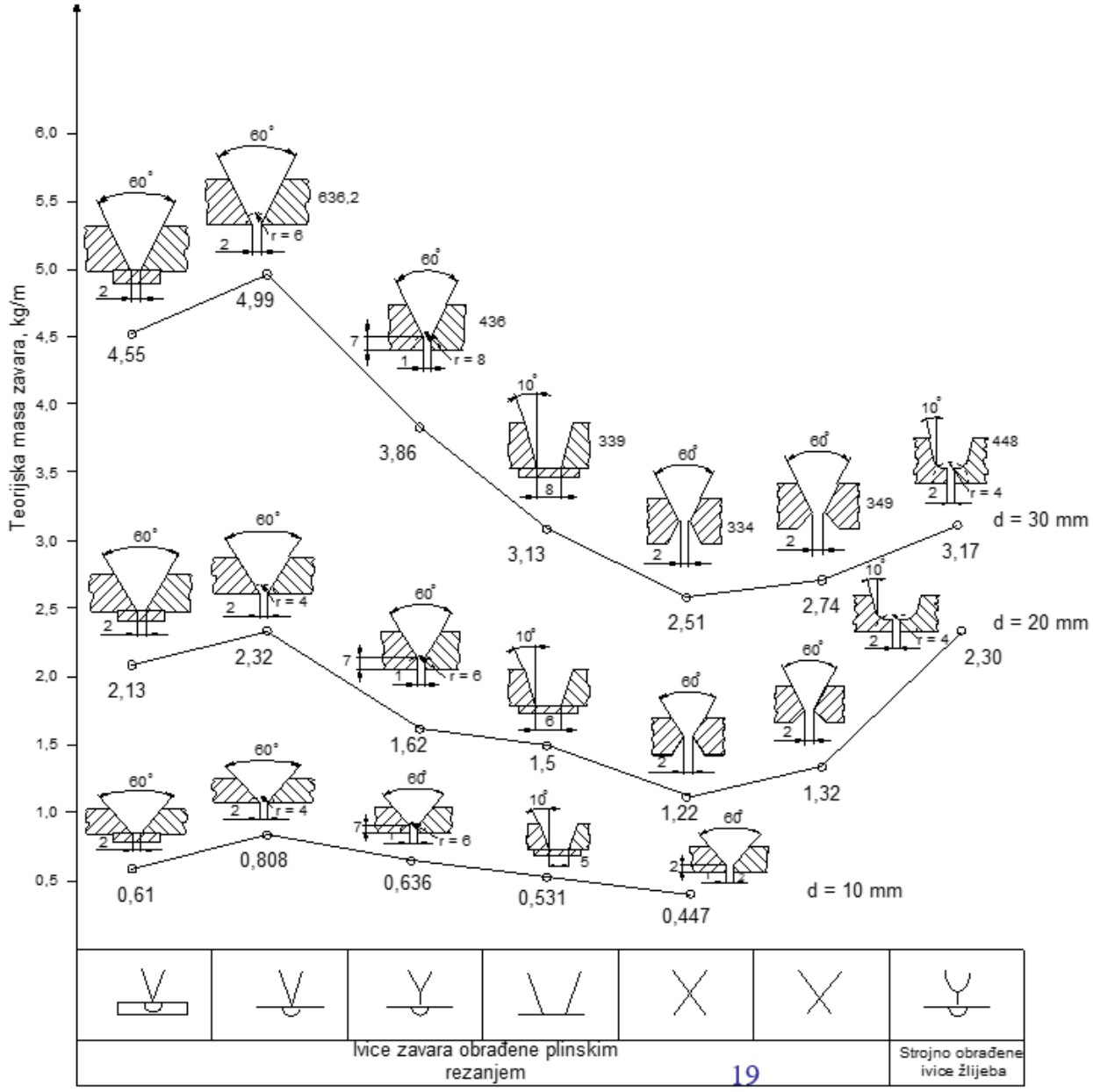

Slika 3. Teorijska površina žlijeba (bez nadvišenja zavara) za zavarivanje za različite oblike žlijebova, dimenzije osnovnog materijala i tehnike pripreme žlijeba.[3]

U Svakom slučaju, poželjno je radni komad dovesti u najpovoljniji položaj zavarivanja, a to je horizontalni položaj jer se na taj način skraćuje trajanje zavarivanja i troškovi zavarivanja (slika 4), jer je to najpovoljniji položaj za zavarivanje (najmanja vjerojatnost grešaka, lakši i humaniji rad, više vrijednosti parametara zavarivanja, manji troškovi zavarivanja, …). Nepovoljne položaje zavarivanja potrebno je izbjegavati već u fazi projektiranja konstrukcije, a kako bi se radni komad doveo u najpovoljniji položaj za zavarivanje koristiti se različite naprave za zavarivanje (pozicioneri,

okretaljke, okretno-nagibne stolove, …) što povećava troškove zavarivanja, ali u konačnici analize tehnologičnosti pokazat će isplativost kod većeg broja zavarenih proizvoda.

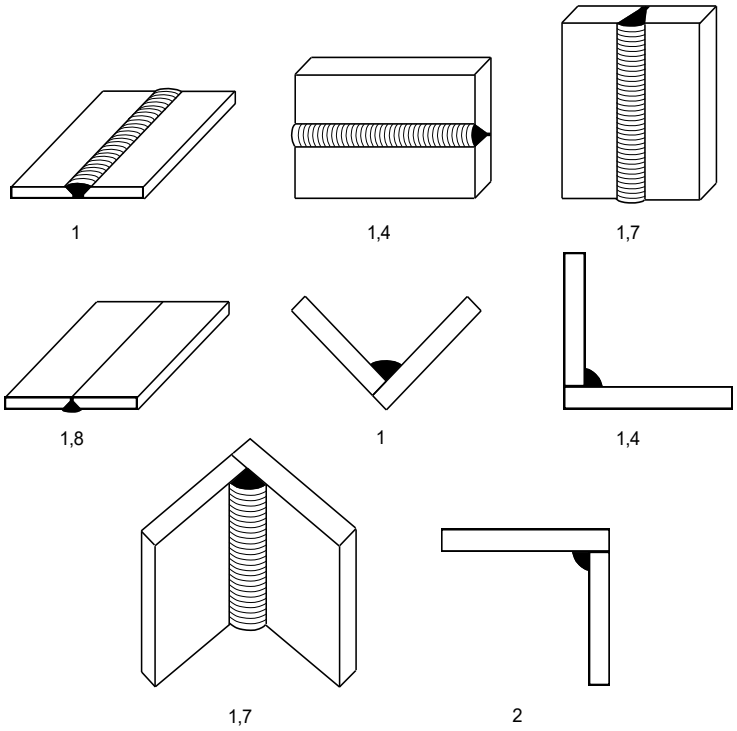

Slika 4. Relativni troškovi elektrolučnog zavarivanja sučeonih i kutnih zavarenih spojeva ovisno o položaju zavarivanja.

Na slici 5 kvalitativno su prikazani jedinični troškovi zavarivanja I nosača različitim postupcima elektrolučnog zavarivanja u najpovoljnijem tj. horizontalnom položaju zavarivanja. Veći stupanj automatizacije smanjuje jedinične troškove zavarivanja što se kod većeg broja proizvoda pokazuje kao isplativo rješenje.

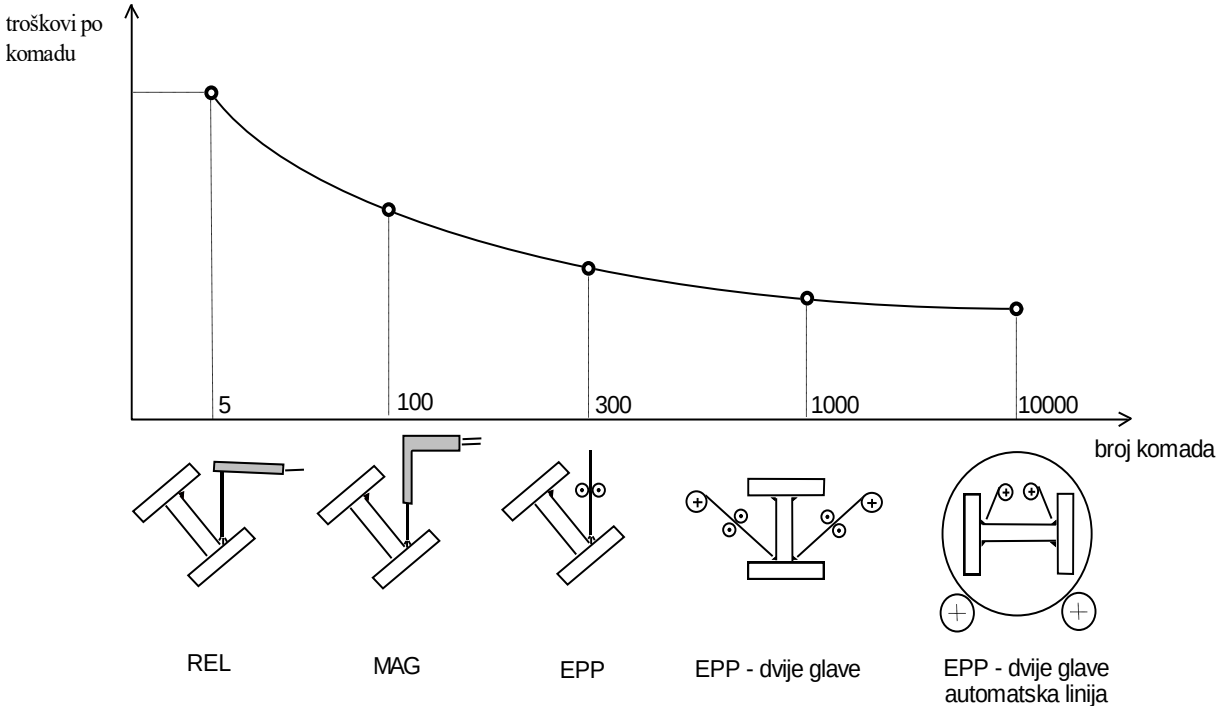

Slika 5. Jedinični troškovi zavarivanja I nosača različitim postupcima elektrolučnog zavarivanja [3]

5. Primjeri tehnologičnih rješenja sa stajališta smanjenja troškova na zavarenim proizvodima

U nastavku se navode tri jednostavna primjera, često uočljiva u proizvodnim pogonima, koja se odražavaju na troškove zavarivanja, a o kojima je potrebno voditi računa kako ne bi nastajali nepotrebni troškovi.

a) Preveliko nadvišenje zavara, konveksan zavar i „nalijeganje" zavara

Nepotrebnim povećanjem debljine kutnog zavara (slika 5e) nepotrebno se povećava količina depozita s kvadratom povećanja debljine zavara. „Nalijeganje" zavara (slika 5c) također predstavlja odstupanje od teorijskog idealnog položaja (slika 5a), što je nepotrebni gubitak dodatnog materijala i svih ostalih troškova i negativnih posljedica povezano s tim. Poželjno je da je kutni zavar konkavan (slika 5d), dok konveksan oblik lica zavara (slika 5b) pored povećanja mase zavara predstavlja i veću koncentraciju naprezanja u odnosu na konkavni izgle lica zavara (slika 5d).

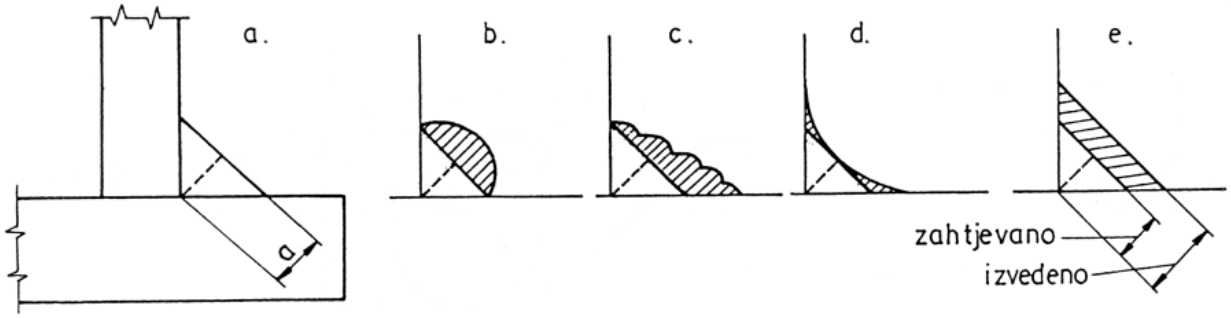

Slika 6. Odstupanja od teorijske dimenzije debljine kutnog zavara.[1]

b) Povećana penetracija kod postupaka zavarivanja s povećanom penetracijom (MAG/MIG, EPP, plazma).

Ako bi kod REL postupka zavarivanja trebao izvesti kutni zavar debljine a=7 mm, a kod EPP postupka kutni zavar debljine a=5 mm (zbog dodatne povećane penetracije koja postoji kod ovog postupka zavarivanja i koja je za primjer autora ovoga rada eksperimentalno utvrđena i iznosi e_{min} = 4 mm). Usporede li se dobivene vrijednosti površine kutnog zavara za vrijednost a= 7 mm i a=5 mm dobije se:

$A_{REL} / A_{EPP} = a_{REL}/a_{EPP} = 49/25 = 1,96$, odnosno može se uočiti da je potrošnja deponiranog materijala povećana za 96 % u slučaju kada se koristi REL postupak zavarivanja.

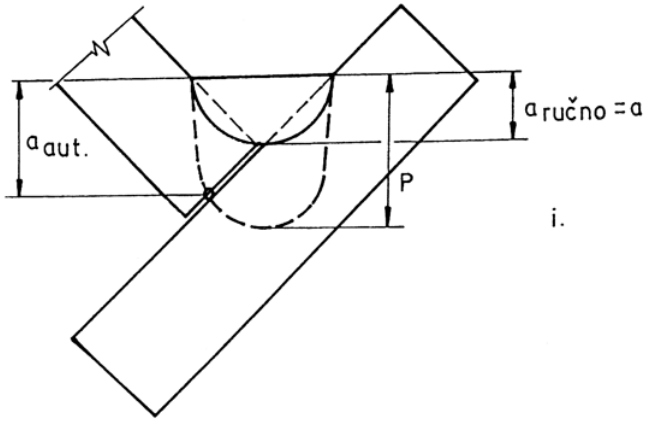

Slika 7. Povećanje penetracije kod postupaka zavarivanja s povećanom penetracijom u odnosu na REL zavarivanje.[1]

c) Otvor sučeonog V žlijeba kod REL i MAG zavarivanja

Kod REL zavarivanja sučeonih zavarenih spojeva potrebno je ostaviti otvor žlijeba dovoljno velik kako bi elektroda odgovarajućeg promjera (napr. fi2,5 mm ili fi 3,25 mm) mogla rastaliti žlijeb u korijenu spoja. U tom slučaju je potreban kut žlijeba 60°). Ako bi se zavarivanje izvodilo MAG postupkom zavarivanja gdje se koristi dodatni materijal žica puno manjeg promjera (bapr. fi 1mm ili

fi 1,2 mm), tada bi otvor žlijeba za zavarivanje mogao biti 45 °. Na ta način moguće je ostvariti uštede u utrošku dodatnog materijala i s tim povezane druge benefite.

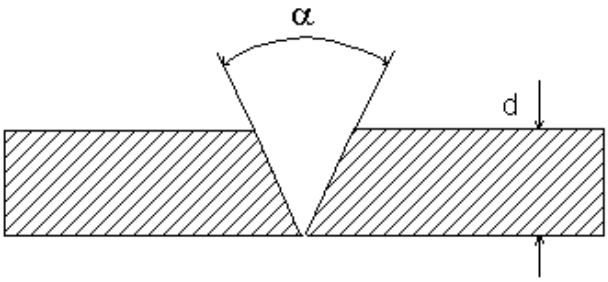

- za otvor žlijeba α = 60° masa depozita G = 0,865 kg dep. / m šava
- za otvor žlijeba α = 45° masa depozita G = 0,573 kg dep. / m šava.

6. Zaključak

Inženjerski pristup uvijek je orijentirati se tehnologičnim rješenjima, bez obzira o kojoj se proizvodnji radilo. Smanjenje troškova, smanjenje zagađenja okoliša, ušteda energije, što humaniji rad, što viša kvaliteta i pouzdanost proizvoda i estetski prihvatljiv izgled proizvoda, to su najvažniji elementi koji determiniraju tehnologičnost proizvoda. Ovaj pristup je posebno važan kod zavarenih proizvoda jer se često radi o izuzetno odgovornim proizvodima (posude pod tlakom, tračnička vozila, brodovi, zrakoplovi, …) kod proizvodnje kojih je velika konkurencija na svjetskom tržištu i svaki pozitivni pomak ima značajan utjecaj na tehnologičnost. U radu se nastojalo približiti tehnologičnost kroz neke primjere koji su češće zastupljeni u našim proizvodnim pogonima kako bi se potaknulo inženjere da i sami osmisle nove načine unaprjeđenja tehnologičnosti. Tehnologičnost je komparativno svojstvo. Što znači da uvijek ima novih načina kako se nešto može osmisliti i izraditi, a inženjer uvijek traži nove i bolje načine.

7. Literatura

1. Lukačević, Zvonimir. Zavarivanje. Strojarski fakultet u Slavonskom Brodu, 1998.
2. Avesta Welding AB, Sweden.
3. Samardžić, Ivan i dr. Analiza tehnologičnosti zavarenih konstrukcija. Digitalni udžbenik, 2000. https://sfsb.unisb.hr/portal-merlin/diplomski-studij/d851-zavarivanje/zavarivanje-digitalni-udzbenik/
4. https://www.hep.hr/ods/korisnici/poduzetnistvo/tarifne-stavke-cijene-161/161

Društvo za tehniku
zavarivanja Slavonski Brod

13. Međunarodno znanstveno-stručno savjetovanje SBZ 2025

„STROJARSKE TEHNOLOGIJE U IZRADI ZAVARENIH KONSTRUKCIJA I PROIZVODA, SBZ 2025."
Slavonski Brod, 08. i 09. 05. 2025.

Metode kontrole kvalitete zavarenih spojeva

Z. Markešić[1], I. Deanović[2,*], M. Samardžić[2], I. Samardžić[3]

[1]Faculty of Mechanical Engineering and Naval Architecture, University of Zagreb, Croatia, Croatia
[2]Mechanical Engineering Faculty in Slavonski Brod, University of Slavonski Brod, Croatia

[*] Corresponding Author. E-mail: ivaa.samardzic@gmail.com

Sažetak

U radu se obrazlaže uloga kontrole kvalitete u svim fazama životnog vijeka zavarene konstrukcije ili zavarenog proizvoda. Navode se metode kontrole kvalitete s i bez razaranja koje se koriste u praksi. Pored toga se navode i neke od prednosti i ograničenja pojedinih metoda kontrole kvalitete zavarenih spojeva.

Ključne riječi: NDT, DT, zavareni spoj, kvaliteta

1. Uvod

S obzirom na zahtjeve u izradi i eksploataciji koji se postavljaju prema zavarenim konstrukcijama i proizvodima (sigurnost za ljude i čovjekov okoliš, te potencijalni gubitak imovine), osiguranje i kontrola kvalitete zavarenih spojeva izuzetno je važan inženjerski izazov kojem se sve više pridaje značaj u praksi. Rizici od otkaza na posudama pod tlakom, komponentama energetskih postrojenja i drugim zavarenim proizvodima i konstrukcijama mogu imati nesagledive posljedice. Sa stajališta otkaza posuda pod tlakom posebno je bila nepovoljna 1984. godina kada je došlo do nekoliko otkaza s katastrofalnim posljedicama:

- Eksplozija i razaranje spremnika za skladištenje LPG u Mexico City koja je prouzročila smrt oko 500 i ranjavanje oko 7 000 ljudi.
- Tragedija propuštanja spremnika u kemiskoj tvornici u gradu Bhopal, India. Oko 2000 tisuće ljudi je poginulo i još je oko 200 000 ljudi pretrpjelo trajna oštećenja zdravlja.
- U Chicago Oil Co. eksplodirala je vertikalna PPT (amin-absorber) pri čemu je poginulo 17 ljudi.

Nakon 1984. godine bilo je još katastrofalnih otkaza vagonskih cisterni s ukapljenim naftnim plinom, kao i velikih požara u rafinerijama (vidljivi video zapisi na internetu). Iako ovakvi otkazi ne moraju biti nužno povezani s greškama u zavarenim spojevima, logično je da bi eventualne nedozvoljene

greške u zavarenim spojevima mogle dovesti do sličnih ili još gorih katastrofa. Rizici od otkaza upućuju na bezrezervno inzistiranje na kvaliteti zavarenih spojeva na zavarenim konstrukcijama i proizvodima, počevši od faze projektiranja i konstruiranja, kroz fazu proizvodnje i izrade, te tijekom eksploatacije zavarenih konstrukcija i proizvoda. Kontrola i osiguranje kvalitete zavarenih spojeva usko je povezano s tehnologijom izrade zavarene konstrukcije jer samo kvalitetna zavarena konstrukcija može stvoriti novu vrijednost krajnjem korisniku i proizvodnoj tvrtki.

2. Greške u zavarenim spojevima

Postoje različite klasifikacije grešaka u zavarenim spojevima, a jedna od njih je prema (HRN EN 26520) HRN EN ISO 6520-1:

- greške u zavarenim spojevima koje mogu nastati u izradi
- greške u zavarenim spojevima koje mogu nastati u eksploataciji.

U ovom radu će se naglasak dati na greške koje mogu nastati u izradi, odnosno metode kontrole kvalitete koje se koriste za otkrivanje grešaka koje mogu nastati u izradi zavarenih konstrukcija i proizvoda.

Postoji više mogućih podjela grešaka u zavaru, pa se tako greške dijele s obzirom na:

- Uzrok nastajanja greške (konstrukcijske greške, metalurške greške i tehnološke greške),
- Položaj greške (unutrašnje greške, površinske i podpovršinske greške, te greške po cijelom presjeku),
- Po obliku greške (kompaktne greške, izdužene greške, oštre greške, zaobljene greške, ravninske greške i prostorne greške),
- Po veličini greške (male greške, greške srednje veličine I velike greške),
- Po brojnosti grešaka (pojedinačne greške, učestale greške i gnijezdo grešaka), te
- Po vrsti greške (plinski uključci, uključci u čvrstom stanju, naljepljivanje, nedostatak provara, pukotine i greške oblika i dimenzija).

Kada se govori o greškama u zavarenim spojevima, važno je naglasiti da za svaku vrstu greške postoje kriteriji prihvatljivosti ovisno o zahtijevanoj kvaliteti i pouzdanosti zavarenog spoja, odnosno zavarene konstrukcije. Sve greške nemaju isti utjecaj na pouzdanost i sigurnost zavarene konstrukcije, pa je tako pukotine imaju najveći negativni utjecaj na pouzdanost i sigurnost s obzirom na činjenicu da se teže otkrivaju (napr. podpovršinske pojedinačne pukotine manjih dimenzija), te da tijekom eksploatacije zavarene konstrukcije dolazi do „rasta i razvoja" pukotine koja nakon nekog vremena eksploatacije, ukoliko se ne otkrije, može poprimiti kritičnu dimenziju i dovesti do otkaza zavarene konstrukcije ili proizvoda).

Na slici 1 daje se primjer hladne (a) i tople kristalizacijske pukotine(b) u zavarenom spoju nekoliko primjera grešaka u zavarenom spoju, a na slici 2 se daju primjeri drugih karakterističnih pukotina u

zavarenom spoju /zajeda, poroznost, uključci troske, nedostatak provara – naljepljivanje, nedostatak provara i preveliko nadvišenje sa strane lica zavara)

a) Hladna pukotina nastala kod ispitivanja zavarljivosti Tekken metodom

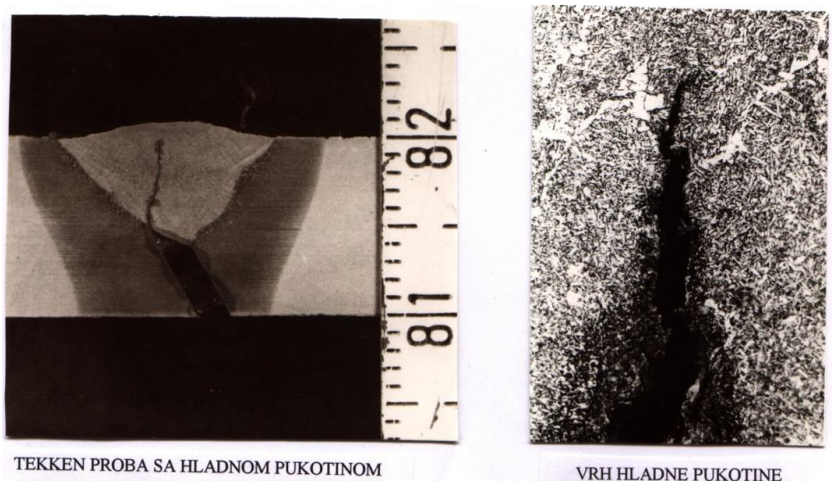

b) Tople pukotine na austenitnom visokolegiranom čeliku

Slika 1. Primjer hladne (a) i tople kristalizacijske pukotine (b) u zavarenom spoju

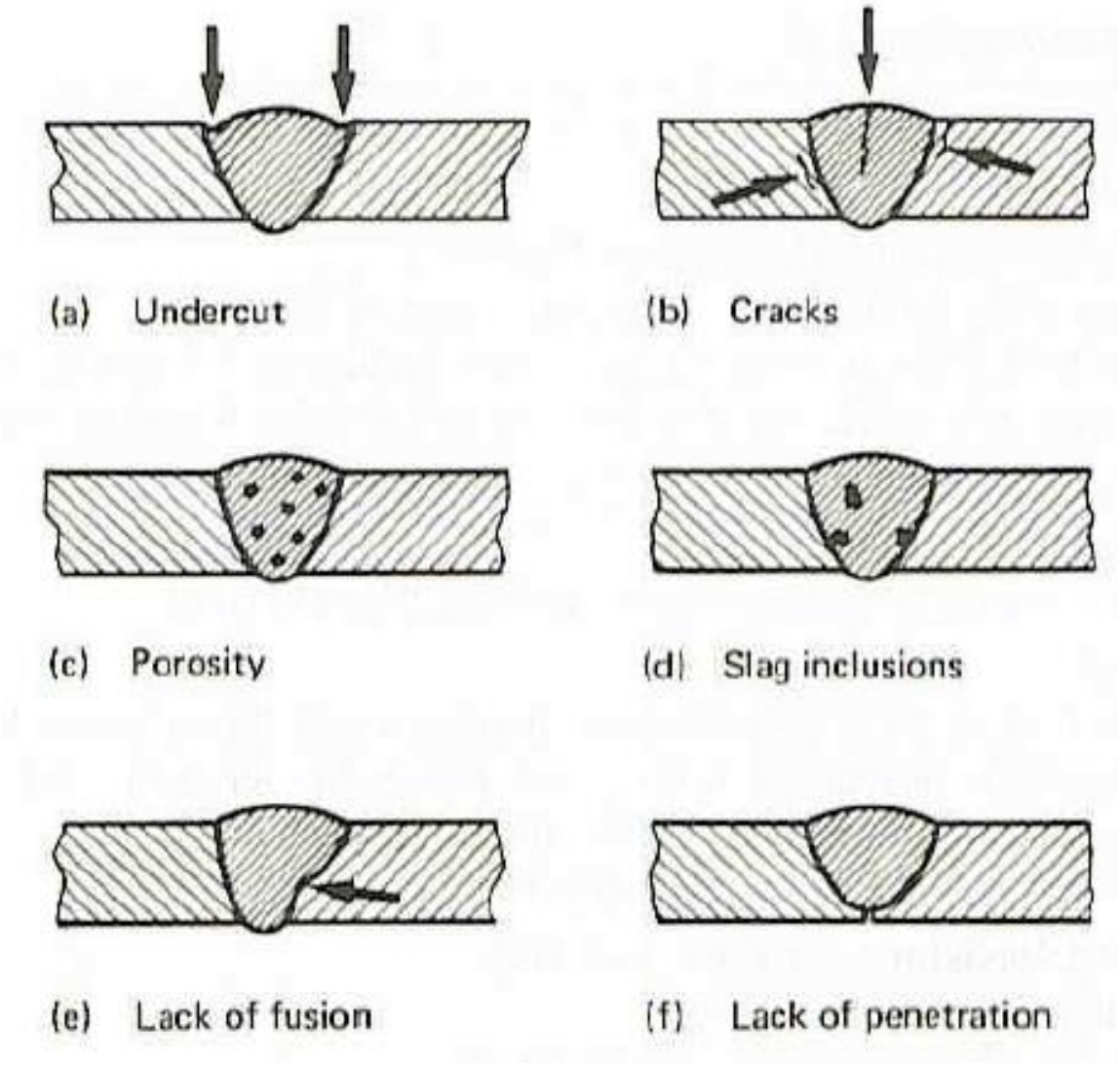
(a) Undercut
(b) Cracks
(c) Porosity
(d) Slag inclusions
(e) Lack of fusion
(f) Lack of penetration

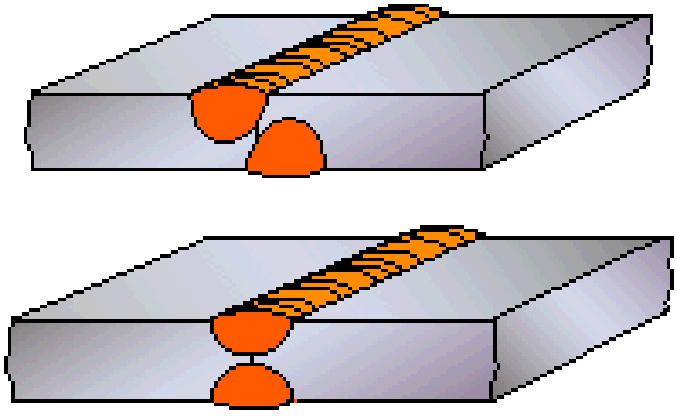

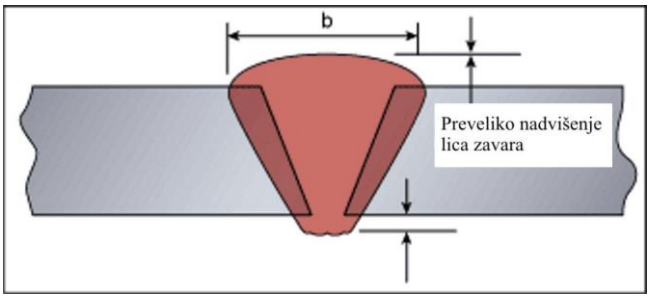

3. Kontrola kvalitete kod izrade zavarene konstrukcije/proizvoda provodi se:

a) prije zavarivanja,
b) tijekom zavarivanja i
c) nakon zavarivanja.

Kontrola kvalitete prije zavarivanja najčešće obuhvaća sljedeće provjere:
- atesta postupaka zavarivanja, te atesta pogona za izvođenje zavarivačkih radova (ukoliko se radi o vanjskoj provjeri),
- atesta zavarivača koji će izvoditi zavarivanje ,
- atesta peći za sušenje i držanje dodatnog materijala (tobolci za prijenos i držanje elektroda)
- atesta za osnovne i dodatne materijale,
- uvjeta skladištenja osnovnog i dodatnog materijala, te vizualnu kontrolu stanja kvalitete osnovnog materijala,
- atesta za uređaje i opremu za zavarivanje i žljebljenje, tr vizualnu kontrolu stanja iste
- atesta peći i opreme za naknadnu toplinsku obradu, ukoliko je ista predviđena tehnološkim postupkom,
- atesta uređaja i opreme za kontrolu parametara zavarivanja i temperature (amper-volt-ohm metri, digitalni termometri, …), te
- oblika i kvalitete pripreme žljebova za zavarivanje i rugih elemenata, specifičnih sa stajališta pojedinih postupaka zavarivanja.

Navedene aktivnosti kontrole provode se u cijelosti prije zavarivanja, a po mogućnosti i po potrebi i tijekom zavarivanja (npr. nije dopušteno je da zavarivanje izvode zavarivači kojima je istekao atest ili koji su bez odgovarajućeg atesta za zavarivanje). O efikasnosti provođenja kontrole prije zavarivanja uvelike će ovisiti kako kvaliteta provođenja tehnološkog postupka, tako i kvaliteta izvedenih zavara.

Kontrola kvalitete tijekom zavarivanja najčešće obuhvaća provjeru:
- temperature predgrijavanja,
- glavnih parametara zavarivanja (napon, jakost struje, brzina zavarivanja),
- temperature međuprolaza, temperature dogrijavanja, …)

Kontrola kvalitete nakon zavarivanja može se podjeliti na kontrolu metodama bez razaranja (KBR/ DT Destructive Testing) i kontrolu metodama s razaranjem (KSR/NDT Non Destructive Testing).

Metode kontrole s razaranjem obično se provode na zavarima pri certifikaciji postupaka zavarivanja, ali se ponekad provode i nakon izvođenja zavara na proizvodima i konstrukcijama iz pogona (npr. "nastavne pločice" kod kružnih zavara na plaštu vagonske cisterne, tlačna proba sa razaranjem u proizvodnji propan/butan boca za domaćinstvo i dr.).

Uobičajene metode kontrole s razaranjem su:
- vlačno kidanje epruvete (najčešće se traže naprezanje tečenja, vlačna čvrstoća, prekidna čvrstoća, kontrakcija i izduženje),
- mjerenja tvrdoće (najčešće jedna od sljedećih metoda: HV30, HV10, HV5, HV1),
- ispitivanje udarne žilavosti / radnje loma (napr. Charpy - V),
* ispitivanje savijanjem lica i korijena zavara,
- ispitivanja iz područja mehanike loma (COD, CTOD, J_{IC} , K_{IC} , ...),
- različita korozijska ispitivanja,
- različita dinamička ispitivanja,
- tlačne probe s razaranjem,
- različite radioničke probe i probe zavarljivosti,
- ispitivanja sadržaja kemijskih elemenata i ostale metode.

Na slici 3 je shematski prikazana oprema koja se koristi za osnovna ispitivanja zavarenih spojeva metodama s razaranjem (vlačni pokus, tvrdoća, udarna radnja loma / žilavost, savijanje).

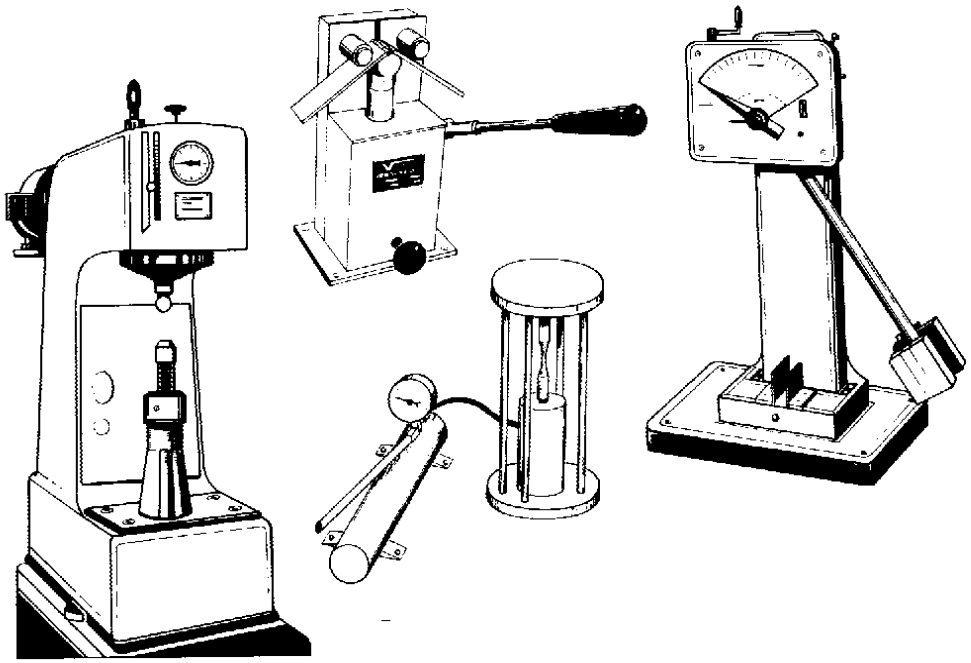

Slika 3. Shematski prikaz opreme za ispitivanje zavarenih spojeva s razaranjem

Metode kontrole kvalitete bez razaranja koje se češće koriste:
- Vizualna kontrola bez ili uz pomoć pomagala (povećala, endoskop)
- Penetrantska kontrola Radiografska kontrola - Ultrazvučna kontrola
- Magnetska kontrola
- Kontrola vrtložnim strujama
- Kontrola nepropusnosti: detektori, sapunica, vakuum, tlačna proba, …

U ovom radu će se ukratko osvrnuti na dvije temeljne metode koje se mogu koristiti u svakom pogonu i za korištenje kojih nisu potrebna značajna sredstva i ulaganja u kadrove.
Kako bi se ove kontrole kvalitete (ali i sve ostale metode) uspješno primjenile u praksi, osobe koje provode ove aktivnosti kontrole kvalitete trebaju završiti stručnu izobrazbu kod za to ovlaštenih institucija, temeljem čega dobivaju odgovarajuće certifikate kojim potvrđuju da su kvalificirane za primjenu ovih metoda, što je zakonska obveza poduzeća koja se bave zavarivanjem. Rok valjanosti certifikata je 5 godina, nakon čega je kod iste ili druge ovlaštene institucije potrebno obnoviti certifikat.

Sve ostale metode mogu biti nadgradnja na ove dvije metode ukoliko se radi o proizvodima s povećanim rizikom od otkaza, što se odražava na povećane zajtjeve za kvalitetu, pa tako i na opseg i vrste metoda kontrole kvalitete koje će se prmjeniti na zavarenoj konstrukciji / proizvodu.

Prije primjene bilo koje druge metode kontrole zavara (KBR ili KSR), primjenjuje se vizualna kontrola koja može uštediti vrijeme i novac, jer je ovom metodom moguće detektirati neke površinske greške. Za pomoć kod vizualne kontrole u skučenim i nepristupačnim dijelovima konstrukcije koriste se različita povećala – lupe, uz osvjetljenje, endoskopi i kamere.

Sljedeća metoda koja je relativno jednostavna za primjenu je penetrantska metoda. I ova se metoda koristi za otkrivanje površinskih grešaka, a na slici 4 a do d su prikazane faze primjene ove metode kontrole kvalitete zavarenih spojeva.

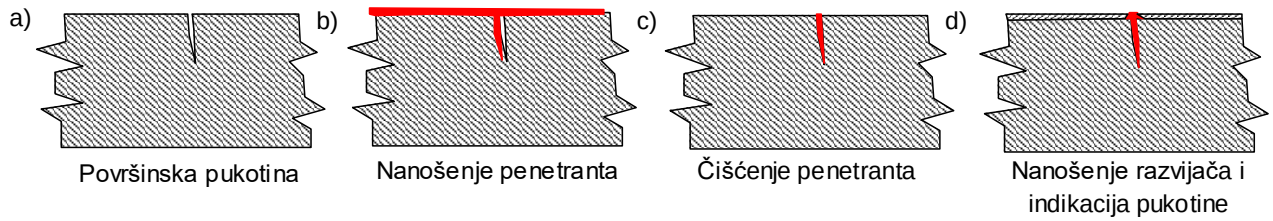

Slika 4. Faze primjene penetrantske kontrole zavarenih spojeva

Na prethodno očišćenu i odmašćenu površinu nanosi se penetrant. Nakon penetriranja u eventualnu pukotinu (ovisi o vrsti penetranta i o dimenzijama pukotine potrebno je približno uzima 10 do 15 minuta), odstranjuje se penetrant na odgovarajući način (vodom ili suhom krpom).

Nakon sušenja površine lima (suha krpa) nanosi se razvijač (obično je crvene boje), koji izvlači penetrant iz pukotine, pa je na bijeloj površini lima lako uočljiva bijela linija od penetranta iz pukotine.

Kod tanjih limova na jednu se stranu nanosi penetrant, a na drugu razvijač. Ukoliko postoji pukotina kroz cijelu debljinu lima, tada će razvijač izvući penetrant na svoju stranu, što će se detektirati kao lako uočljiva crvena linija od penetranta iz pukotine na bijeloj (od razvijača) površini lima.

Kontrola tekućim penetrantima ne primjenjuje se kod zavarenih spojeva zavarenih proizvoda za prehrambenu industriju, kao ni kod zavarenih spojeva gdje postoji sklonost prema koroziji (posebno koroziji uz naprezanje).

a) Koncentracija crvenih točaka - poroznost i piting b) naglo crvenjenje, kontinuirano ravno - velike pukotine i otvaranja c) slomljene linije od točaka koje se pojavljuju nakon nekoliko minuta - sitne pukotine d) niz crvenih točaka formiran u nepravilnu liniju - pukotine od umaranja	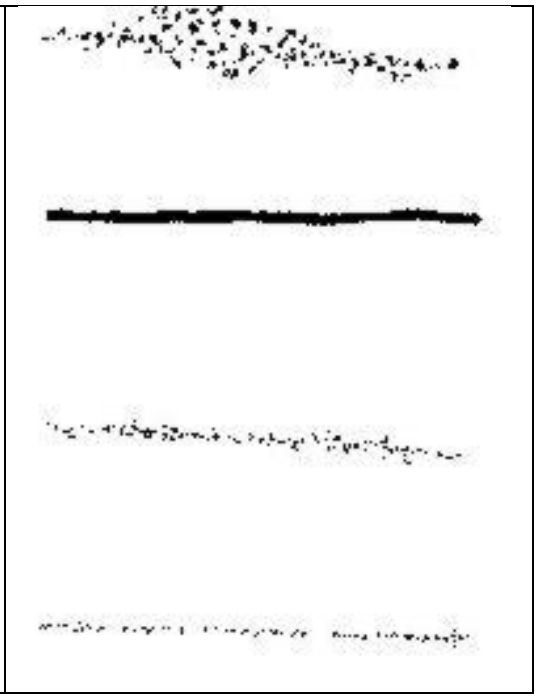

Slika 5. Nekoliko shematskih primjera indikacija kod kontrole penetrantima

4. Kriteriji osjetljivosti metoda kontrole kvalitete metodama bez razaranja

Prije primjene bilo koje druge metode kontrole zavara (KBR ili KSR), primjenjuje se vizualna i dimenzionalna kontrola. Te metode nisu skupe, ne oduzimaju jako puno vremena, a mogu dati vrlo korisne informacije i uštedjeti vrijeme i novac ukoliko se ovim metodama otkriju nedozvoljene greške. Za pomoć kod vizualne kontrole u skučenim i zamračenim dijelovima konstrukcije koriste se različita pomagala: lupe uz osvjetljenje i povećala, dok se za dimenzionalnu kontrolu koriste različita pomagala za mjerenje debljine zavara, visine nadvišenja zavara i sl. Greške u izradi mogu se otkriti različitim metodama kontrole kvalitete bez razaranja, a svaka od metoda kontrole bez razaranja ima „prag osjetljivosti", tj. minimalne dimenzije greške koju je moguće otkriti uz primjenu pojedine metode kontrole.

U tablici 1 navedene su orijentacijske vrijednosti minimalnih dimenzija greške koju je moguće detektirati pojedinim metodama KBR.

Tablica 1. Orijentacijska osjetljivost otkrivanja pukotina kod pojedinih metoda KBR.

Metoda KBR	Širina pukotine, mm	Duljina pukotine, mm	Dubina pukotine, mm	Primjedba
Penetranti	0,1	2	-	Ovisno o stanju površine i optičkim pomagalima
Magnetske čestice	0,01	1	0,2	Ovisno o stanju površine
Ultrazvuk	0,01	1	0,2	Samo za feromagnetske materijale
Radiografija	0,3	5	0,3	-
Akustička emisija	0,001	0,001	0,001	-

Kod primjene pojedinih metoda kontrole kvalitete bez razaranja važno je znati kriterije prihvatljivosti grešaka, odnosno kritične dimenzije pojedinih grešaka. Slijedom toga se propisuje jedna ili više metoda kontrole bez razaranja primjenom kojih je moguće detektirati tu grešku i sastaviti odgovarajuće izvješće koje će biti podloga za daljnje postupanje.

5. Zaključak

U radu se daje pregled aktivnosti na kontroli kvalitete zavarenih spojeva u praksi. Kontrola kvalitete nerazdvojno je povezana s tehnologijom zavarivanja jer potvrđuje kvalitetu zavarenih spojeva na zavarenoj konstrukciji / proizvodu koji nije gotov dok aktivnosti kontrole kvalitete i kompletna tehničko-tehnološka dokumentacija nije finalizirana i predana krajnjem kupcu. Danas smo svjedoci da se aktivnostima kontrole i osiguranja kvalitete (ali i osiguranju pouzdanosti i integralnoj logističkoj podršci) pridaje sve veći značaj zbog potencijalno mogućih rizika od otkaza i posljedica za ljude, čovjekov okoliš i materijalna dobra.

6. Literatura

[1] Vjera Krstelj, Ana Lypolt (Penetrantska kontrola). HDKBR Hrvatsko društvo za kotrolu bez razaranja, Zagreb, 2005.
[2] Sveučilište u Zagrebu fakultet strojarstva i brodogradnje, Vjera Krstelj (Ultrazvučna kontrola) odabrana poglavlja, Zagreb,2003.
[3] K. Siva kishore babu, B. Koteswararao, Y. Suresh, D. Ravi. Analysis Of Quality In Solid State Welding (Copper-Copper) By Using NDT And DT By Altering Physical Properties At Constant Time, Materials Today: Proceedings, Volume 4, Issue 8, 2017, 7351-7356.
[4] T. Warren Liao, Jiawei Ni. An automated radiographic NDT system for weld inspection: Part I - Weld extraction, NDT & E International, Volume 29, Issue 3, 1996, 157-162.
[5] Li Yan. Optimizing radiographic NDT techniques for welds, NDT & E International, Volume 27, Issue 1, 1994, 15-20.

Društvo za tehniku zavarivanja Slavonski Brod

13. Međunarodno znanstveno-stručno savjetovanje SBZ 2025

„STROJARSKE TEHNOLOGIJE U IZRADI ZAVARENIH KONSTRUKCIJA I PROIZVODA, SBZ 2025."
Slavonski Brod, 08. i 09. 05. 2025.

Application of FDM 3D printing technology for V-bending tool used in the small batch production of thin sheet metal handles

J. Cumin[1,*], K. Cahun[1], D. Novoselović[1], M. Duspara[1]

[1]Mechanical Engineering Faculty in Slavonski Brod, University of Slavonski Brod, Croatia

[*] Corresponding Author. E-mail: jcumin@unisb.hr

Abstract

This paper presents possibility of practical application of FDM 3D printing technology for production of V-bending tool made from ABS polymer material. Both FDM technology and various ABS filaments are easily available in markets nowadays. For the design of simple, thin sheet metal handle, a V-tool was design and printed, taking into account handle material, handle mounting and pre-stressing due to design, DIN EN 10130/10209 (DC04) deep drawing steel mechanical properties and elastic springback. Results are presented through the scope of gradual tool wear visible as bending angle errors, and tool wear as a function of number of bent handles.

Keywords: bending, FDM, V-tool, accuracy

1. Introduction

Nowadays rapid protyping and 3D printing technologies are widespread in mainstream population. It has brought many benefits for testing purposes, visualization, representation of assemblies, pre-production of functional prototypes tests etc., [1].

The most spread consumer 3D printers nowadays, are printers which work on Fused Deposition Modelling (FDM) system. Sometimes these technologies are referred as Fused Filament Fabrication (FFF) technologies [2,3]. There is also a wide spread selection of filaments used for various purposes. From simple prototype visualization and smaller part structural strength, a Polylactic Acid (PLA) filament is mostly used, and for more robust functional prototypes the Acrylonitrile Butadiene Styrene (ABS), Polyoxymethylene (POM) [4].

Recent research in this field is based on high end filament materials such as carbon fiber-reinforced polymers (CFRP) [5,6], and materials infused with silicon carbide or aluminum oxide. Besides good

printing material, the printing strategy and percentage of layer infill have a definitive impact on printed tool life, strength, rigidity and wear [7].

2. Materials and methods

Fig. 1 shows base outline of the drawer handle. Since it is planned to be made of very thin sheet metal (s = 0,75 mm), a design feature is to let 5° allowance at the leg of the handle. Thus when mounted on drawer and tensioned up, the hump of the handle will slightly protrude outwards with large diameter, thus constantly providing arch with slight tension in order to prevent buckling of the sheet metal (compared to regular design if this should not be taken into account).

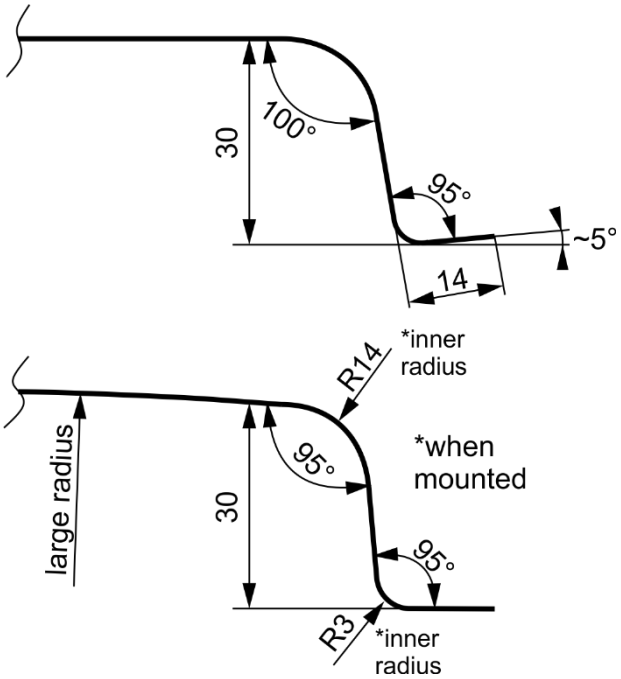

Figure 1. Desired angles and slightly tensioned outer arch when handle is in mounted position.

Material of the handle is chosen to be DC04 (EN10130; 1.0338) deep drawing steel. It is widespread material in the sheet metal industry, and easily available. Tab. 1 shows chemical composition, and Tab. 2 gives mechanical properties overview.

Table 1. Chemical composition of DC04 (EN 1.0338) steel [8,9].

Element	C	Mn	P	S	Si	N	Cu	Al
Content / %	≤ 0,08	≤ 0,4	≤ 0,03	≤ 0,03	≤ 0,03	≤ 0,008	≤ 0,02	≤0,02

Table 2. Mechanical properties of DC04 (EN 1.0338) [8,9].

Yield strength, R_y / MPa	Tensile strength, R_m / MPa	Elongation, A / %	Anisotropy / R_{value}	Strain hardening exponent n
140-180	270-370	28-38	1,6	0,18

In order to define tool design, geometry and dimensions the calculation of bending parameters is required.
Based on the literature [10], the following bending factors were calculated.

a) tensile extension of the outer fiber in the bent piece [10]:

$$\varepsilon_{i1} = \frac{1}{\frac{2R_i}{t}+1} = \frac{1}{\frac{2\cdot 14}{0,75}+1} = 0,0261 \text{ for the radius } R_i = 14 \text{ mm} \quad (1)$$

$$\varepsilon_{i2} = \frac{1}{\frac{2R_i}{t}+1} = \frac{1}{\frac{2\cdot 3}{0,75}+1} = 0,11 \text{ for the radius } R_i = 3 \text{ mm} \quad (2)$$

b) position on the neutral axis, (which is practically in the same spot as half of the sheet thickness which is characteristic for thin sheet metal plates) [10]:

$$R_{n(14)} = \sqrt{R_i \cdot R_o} = \sqrt{14 \cdot 14,75} = 14,37 \text{ mm; for } R_i = 14 \text{ mm} \quad (3)$$

$$R_{n(3)} = \sqrt{R_i \cdot R_o} = \sqrt{3 \cdot 3,75} = 3,354 \text{ mm; for } R_i = 3 \text{ mm} \quad (4)$$

c) reduction radius of neutral surface [10]:

$$R_{r(14)} = \frac{R_n}{s} = \frac{14,37}{0,75} = 19,16; \text{ for } R_i = 14 \text{ mm} \quad (5)$$

$$R_{r(3)} = \frac{R_n}{s} = \frac{3,354}{0,75} = 4,472; \text{ for } R_i = 3 \text{ mm} \quad (6)$$

Radius of neutral surface $R_{r(14)}$ lies between intervals $5 \leq R_{r(14)} \leq 200$ indicating elastic-plastic bending (Fig. 2a) where position z_0 can be determined based on the Hook's law and elongation (or compression) of this fiber that can be calculated from eq. (1). A larger elastic springback is usually expected after unloading [10].

Radius of neutral surface $R_{r(3)} < 5$ indicating theoretical pure plastic deformation (Fig. 2b) through the whole sheet thickness. In this cases, the elastical part of deformation (and subsequently elastic springback) is smaller than in previous case (a).

Maximum sheet bending diameter where plastic deformation can occur (if this radius is any larger, only elastic deformation is observed in the bent segment) can be calculated as follows [10]:

$$R_{i(max)} = \frac{s \cdot E}{2 \cdot R_m} = \frac{0{,}75 \cdot 210000}{2 \cdot 320} \approx 246\,\text{mm} \tag{7}$$

where E / MPa – Young's modulus, R_m / MPa – average value of ultimate tensile stress obtained from Tab. 2.

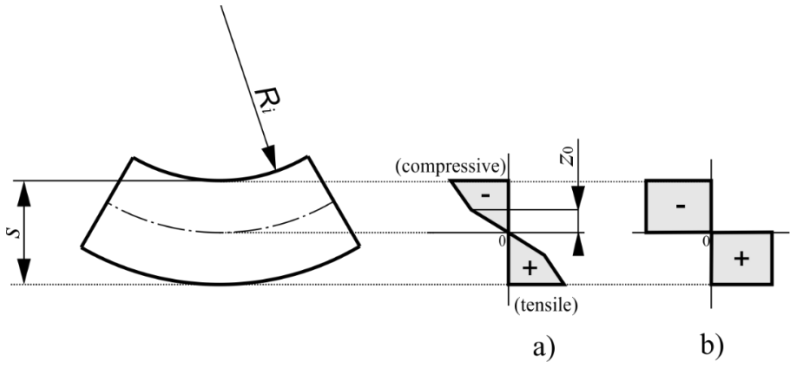

Figure 2. Type of bending based on the reduction radius of neutral surface.

With respect to the shown parameters, an estimation of elastic springback after unloading can be calculated by [10]:

$$\frac{R_i}{R_f} \approx 4\left[\frac{R_i \cdot R_m}{E \cdot s}\right]^3 - 3\left[\frac{R_i \cdot R_m}{E \cdot s}\right] + 1 \tag{8}$$

$$K_s = \frac{R_i + \frac{s}{2}}{R_f + \frac{s}{2}} = \frac{180° - \alpha_2}{180° - \alpha_1} \tag{9}$$

Where K_s – springback factor; R_f / mm – radius of the unloaded sheet metal; α_1 / ° – sheet bend angle before unloading; α_2 / ° – sheet bend angle after unloading (see Fig. 3.).

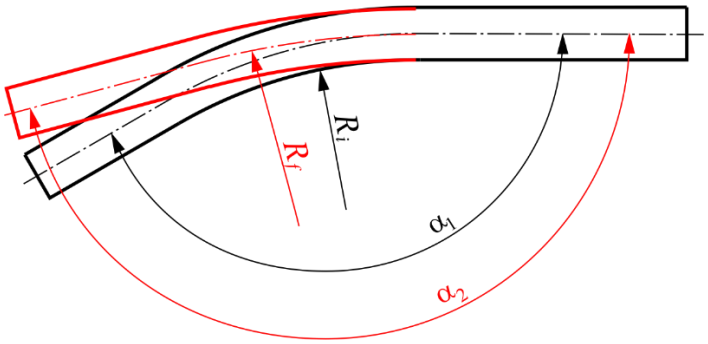

Figure 3. Elastic springback with bending factors from (8,9) [10].

Based on the iterative procedure, the values of bending diameter, and desired bend angles have been obtained – see Tab. 3.

Table 3. Bending angles and springback.

R_i	R_i/R_f	α_1 / °	α_2 / °
14	0,91476	92,6	100,05
3	0,98172	93,4	94,98

Fig. 4. shows general dimensions and respective bend angles for the 3D printed tool.

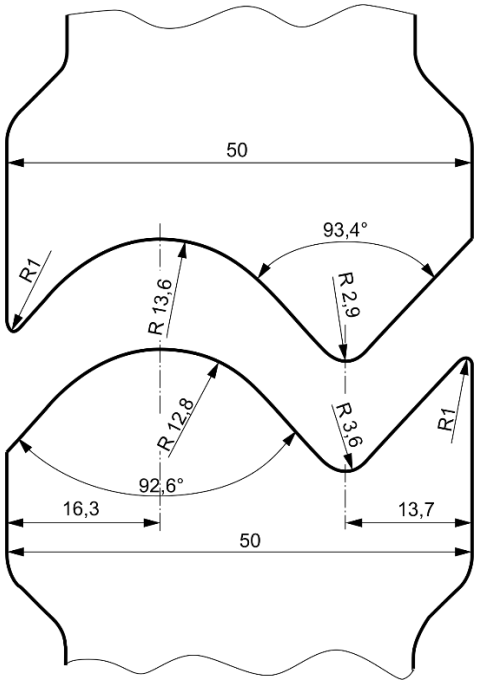

Figure 4. Geometry for the 3D print bending tool.

Fig. 5. shows printed bending tools (ABS filament, 100% infill on UP mini 3D printer; 0,3 mm layer thickness, 41 grams). Since properties of 3D printed layers are anisotropic and depend on layout and filament deposit thickness, temperature, deposit cooling rate etc. [11], only thing that could be checked is approximation of strain in the loaded state with maximal axial tool force of 5000 N, which was done in Autodesk Fusion 360, v2.0.16490 (Fig. 5.) and it shows acceptable tool deformation.

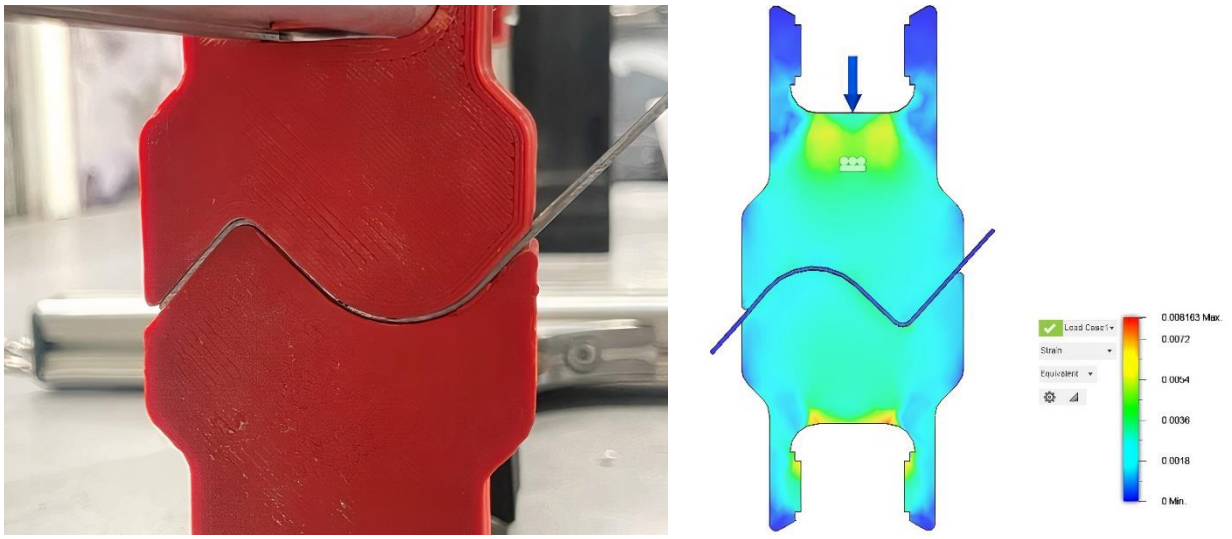

Figure 5. Geometry of the tool with associated approximation of strains in Autodesk Fusion 360, and on the right printed tool.

For the bending part, a total of 40 pieces was produced in series of 10, after which the last part was measured for bend angles and accuracy. Fig. 6. shows a fragment of produced parts (left), and on the right tested parts – the first one followed by each 10th produced part.

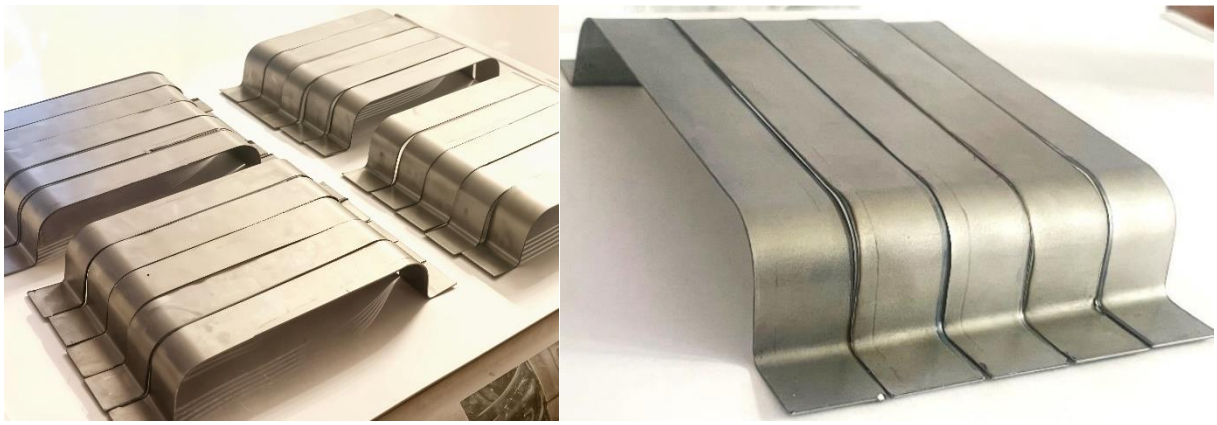

Figure 6. Series of produced parts (left), and on the right first produced piece, with follow up of each 10th produced part.

Fig. 7. shows surface deformations of the bending tool after all parts have been produced (left), and on the right is the reference surface for the deformation measurement.

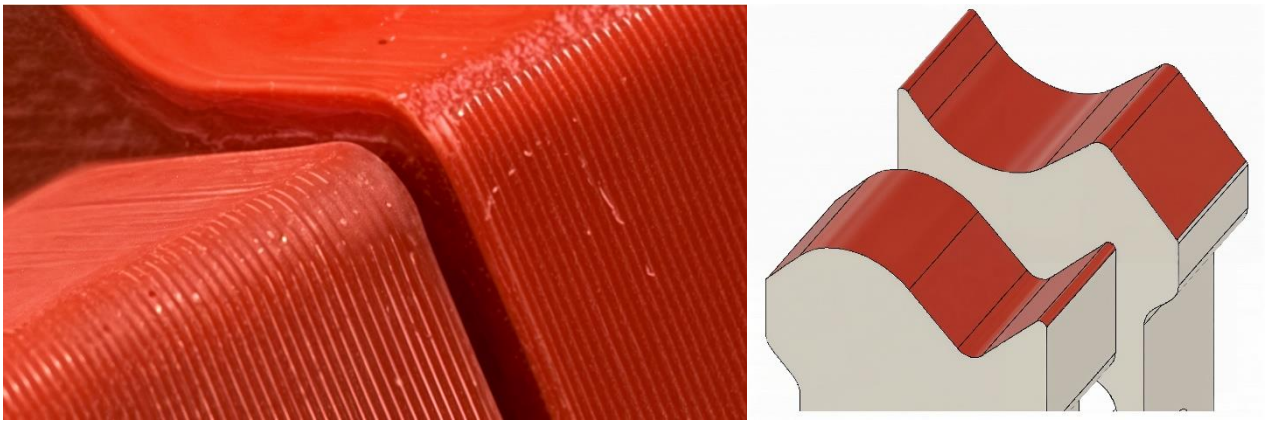

Figure 7. Deformed surface of the 3D printed tool, and reference surface for deformation measurement.

Fig. 8. shows deformation of upper tool surface after bending, with respect to the and original reference surface from Fig. 8. Measurements were done with non-contact 3D optical measuring scanner ATOS Core 300 (GOM), and results were processed with dedicated ATOS Professional suite (2021).

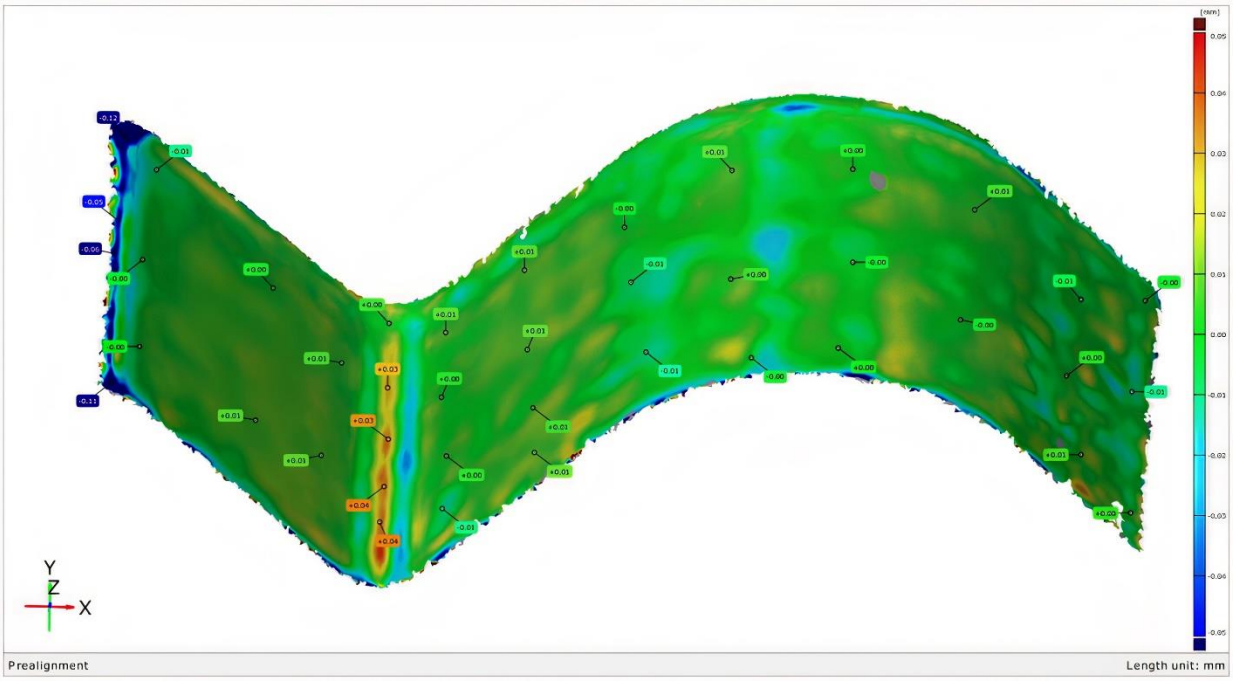

Figure 8. Deformation of upper bending tool in comparison to the reference area from Fig. 8.

Fig. 9. shows lower tool surface deformation after bending, and original reference surface from Fig. 8.

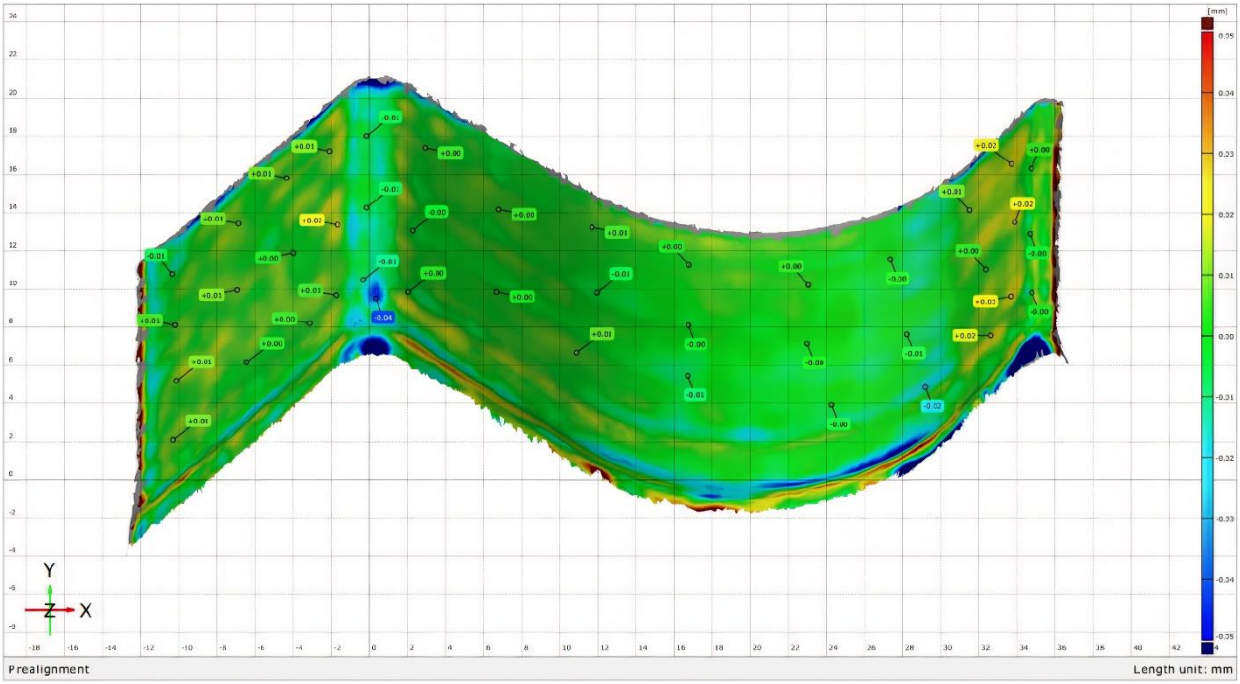

Figure 9. Comparison of deformed lower bending tool in comparison to the reference area from Fig. 8.

Fig. 10. shows measured angles and radii of the a) first piece; b) 10th piece; c) 40th piece. Tab. 4 places all the measured values in one place.

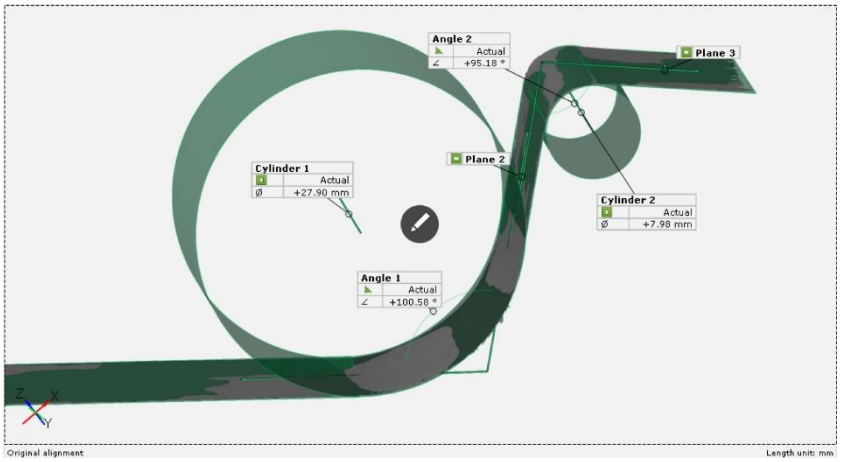

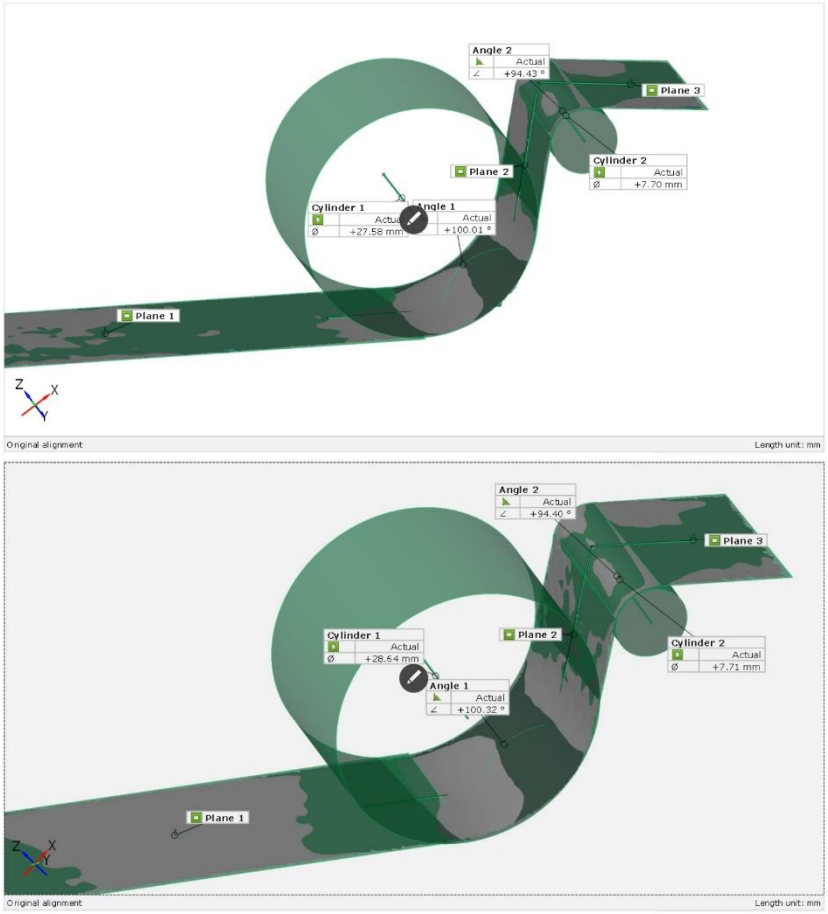

Figure 9. Measured angles and radii, a) first image and first piece; b) middle image and 20th piece; c) last image and 40th piece

Table 3. Measured values related to bent workpiece segments.

	1st piece	10th piece	20th piece	30th piece	40th piece
R_1 / mm	13,95	13,86	13,79	13,52	14,32
R_2 / mm	3,99	3,79	3,85	3,84	3,86
α_1 / °	100,58	99,22	100,01	97,77	100,32
α_2 / °	95,18	94,10	94,43	93,9	94,40

Tab. 4. gives comparison of minimal and maximal measured values. It can be shown that they are in the vicinity value of 5%, which is acceptable for engineering and prototype testing purpose.

Table 4. Comparison of minimal and maximal obtained values

	MAX.	MIN.	$\Delta_{APSOL.}$	Δ / %
R_1 / mm	14,32	13,52	0,8	5,59

R_2 / mm	3,99	3,79	0,2	5,01
α_1 / °	100,58	97,77	2,81	2,79
α_2 / °	95,18	93,9	1,28	1,34

5. Conclusions

This paper gives overview of application of FDM printing technology for printing of bending tools made form ABS polymer, and testing of tool life during bending of 40 samples. FDM technology has become mainstream in recent years, which has led to the availability of different filament materials, and respectively different mechanical properties of the printed parts. Although ABS is little tougher than PLA filament, it has its disadvantages in use.

For the design of drawer handle, the bending tool was produced, and this tool has been used for bending of 40 (+1) sheet metal pieces, after which tool deformation was measured with non-contact measuring system ATOS Core 300 (GOM). This preliminary results show promising application for quick production of small batch sheet metal products used for the purpose of prototype testing. This results can be improved by utilizing tool design with inserted metal rods for higher tool rigidity. Also some of the future research goals is usage of carbon fiber-reinforced polymers (CFRP) in conjunction with metal bar reinforcements to test the very limits of FDM technology for utilization in sheet metal forming technologies.

6. References

[1] Bandinelli, Francesco; Peroni, Lorenzo; Morena, Alberto. (2023). Elasto-Plastic Mechanical Modeling of Fused Deposition 3D Printing Materials. *Polymers*, 15(1). https://doi.org/10.3390/polym15010234.

[2] Kuznetsov, Vladimir; Solonin, Alexey; Tavitov, Azamat.; Urzhumtsev, Oleg; Vakulik, Anna. (2020). Increasing Of Strength Of FDM (FFF) 3D 495 Printed Parts By Influencing On Temperature-Related Parameters Of The Process, *Rapid Prototyping Journal*, 26(1), 107–496 121. DOI: 10.20944/preprints201803.0102.v1.

[3] Tang, Chi-Long; Seeger, Stefan; Mathias, Mathias. (2023). Improving the comparability of FFF-3D printing emission data by adjustment of the set extruder temperature. *Atmospheric Environment: X Journal*, 18. No. March. DOI: 10.1016/j.aeaoa.2023.100217.

[4] Ray, Sudip; Cooney, Ralph. (2018). Handbook of Environmental Degradation of Materials - Chapter 9 - Thermal Degradation of Polymer and Polymer Composites. William Andrew applied science publishers. DOI: https://doi.org/10.1016/B978-0-323-52472-8.00009-5.

[5] Patel, Kautilya; Shah, Dhaval; Joshi, Shashikant; Patel, Kaushik. (2023). Developments in 3D printing of carbon fiber reinforced polymer containing recycled plastic waste: A review. *Cleaner Materials* 9. DOI: https://doi.org/10.1016/j.clema.2023.100207.

[6] Markforged: Onyx® Micro carbon fiber filled nylon that forms the foundation of Markforged composite parts. URL: https://markforged.com/materials/plastics/onyx (31.3.2025).

[7] Zaragoza, Veronica Geraldine; Rane, Kedarnath; Strano, Matteo; Monno, Michele. (2021). Manufacturing and performance of 3D printed plastic tools for air bending applications. Journal of Manufacturing Processes 66, 460-469 . DOI: https://doi.org/10.1016/j.jmapro.2021.04.045.

[8] Steel pro Group. DC04 Steel | 1.0338. URL: https://steelprogroup.com/galvanized-steel/grades-galvanized-steel/dco4-steel-guide/ (2.4.2025).

[9] ThyssenKrupp. DC04 | 1.0338. URL: https://www.thyssenkrupp-materials-processing-europe.com/en/c-steel/cold-rolled-sheet/dco1-dc07/dc04. (2.4.2025).

[10] Boljanović, Vukota (2004). Sheet metal forming processes and die design. New York: Industrial Press. ISBN 0-83 1 1-3 182-9.

[11] N. da Conceição, Marceli; M. da Fonseca, Henrique; M. S. M. Thiré, Rossana. (2025). Temperature Profile from Parts Produced by Fused Filament Fabrication (FFF) Measured by In Situ Infrared Thermography. *Processes 13(1)*, 60. https://doi.org/10.3390/pr13010060.

Društvo za tehniku
zavarivanja Slavonski Brod

13. Međunarodno znanstveno-stručno savjetovanje SBZ 2025

„STROJARSKE TEHNOLOGIJE U IZRADI ZAVARENIH KONSTRUKCIJA I PROIZVODA, SBZ 2025."
Slavonski Brod, 08. i 09. 05. 2025.

Challenges in determining fracture toughness of pipe material

D. Damjanović[1,*], N. Gubeljak[2], I. Samardžić[1], D. Kozak[1], J. Stojšić[1], A. Milinović[1]

[1]Mechanical Engineering Faculty in Slavonski Brod, University of Slavonski Brod, Croatia
[2]Mechanical Engineering Faculty, University of Maribor, Slovenia

[*] Corresponding Author. E-mail: ddamjanovic@unisb.hr

Abstract

In the last few tens of years, several methods have been proposed for measuring the fracture toughness of pipe material, but all of them have some drawbacks. Starting from 1995 when one of first methods was proposed until nowadays, few procedures are proposed regarding CT specimen (curved or modified CT specimen). The only available study that analyses an alternative to the SENB specimen is a study in which authors analyses the curved SENB specimen. Meanwhile, in 1996, another alternative method called SSM method (Stress-Strain Microprobe) has been proposed. Despite a large number of studies on this topic, no simple and economically viable procedure for measuring the fracture toughness of pipe material has been designed and standardized up to nowadays.
Ring-type test specimen (PRNB – Pipe Ring Notched Bend specimen) which is alternative to SENB test specimen is proposed in 2015. Making a PRNB specimen is simpler and cheaper than making standard SENB or CT specimens because PRNB is simply cut from a pipe. A notch is made on the PRNB specimen most often by wire electro erosion, and then the specimen is ready for the three-point bending test. A lot of research has been conducted on PRNB test specimen and it was generally concluded that PRNB specimen cut from pipe can be an adequate substitute for measuring the fracture toughness of pipe material.

Keywords: fracture toughness, pipe, tube, crack, fatigue pre-cracking

1. Introduction

Pipelines represent the most common and most reliable way of transporting energy media and are a key part of energy, industrial, and utility infrastructure. Maintaining their integrity is key to maintaining the stability of these systems. If a pipeline bursts or leaks due to material weaknesses or fatigue, the consequences can be catastrophic, including explosions, fires, and environmental disasters. This can also lead to significant economic losses due to the loss of resources, the need for remediation and repairs, as well as potential penalties or lawsuits. Knowledge of elasto - plastic and

fracture - mechanical behavior of materials is the basis for assessing the deformation capacity of pipelines, which is a key feature for production, installation and operation of pipelines. In the case of pipelines made of thin-walled pipes, it is difficult to measure the fracture toughness of the material, because it is necessary to use standardized test specimens like SENB or CT, which are impossible to produce from thin wall of pipe. To nowadays, slightly less than ten alternative test specimens and/or methods of measuring the fracture properties of pipe material have been proposed, but no specimens and/or methods are standardized. Scientists intensively researched this issue and Evans introduced one of the first method in 1995 by proposing a curved CT test specimen cut from a piece of pipe and a specialized testing device. Evans proved that it was possible to use known expressions to calculate the fracture toughness of a standard CT specimen on the proposed curved CT specimen as well [1]. Furthermore, in 2008, a similar procedure for a specimen cut from a pipe was proposed by Dlouhy and Gubeljak who used a modified CT specimen and also a specially developed testing device [2]. However, there was a problem that when generating a fatigue pre-crack in such a specimen, uneven crack growth occurred through the wall thickness of the specimen, which was not in line with the standard for measuring fracture toughness. In 2012, Gajdos and Sperl also presented a similar method and specially developed testing device [3], [4]. In the following years, the authors continued to deal with curved CT specimens [5], but this type of test specimen was never standardized because special test device was required for each new pipe geometry. Meanwhile, in 2009, a group of authors presented and patented an alternative to a CT specimen called the CP Specimen (Compact Pipe specimen) [5]. To nowadays, there are several studies performed on such a specimen [6], [7]. Yet, such studies are scarce due to the fact that the great disadvantage of this kind of specimen is that it simulates a transverse crack in the pipe, which is very rare in pipes. The only available study that analyses an alternative to the SENB specimen is a study in which authors analyses the curved SENB specimen [8]. However, when compared to the standard CT specimen used in the same study, such curved SENB specimen described crack propagation differently. Meanwhile, in 1996, another alternative method called SSM method (Stress-Strain Microprobe) [9], [10], with a completely different approach to integrity assessment was introduced by Haggag. In the following years, that method has been applied also by other authors together with the inventor [11], [12]. This method is patented [13] and it refers to a non-destructive test method in terms of measuring the footprint in a material derived from the injection of a tungsten carbide ball. However, the wider scientific community has not accepted this method, so it is very rarely used. Furthermore, in [14], [15], [16], and in book [17], Capelle presented another alternative method for measuring the fracture properties of test specimens cut from pipes. This is a non-standard test specimen called Roman tile, which allows the measurement of fracture properties in the transverse direction. However, this measurement method and the proposed test specimen are not efficient in description of the stress state in real pipes. Some of the described non-standard test specimens are shown in Figure 1, while Table 1 shows chronological overview of the proposed alternative non-standard test specimens for measuring the fracture toughness of pipe material.

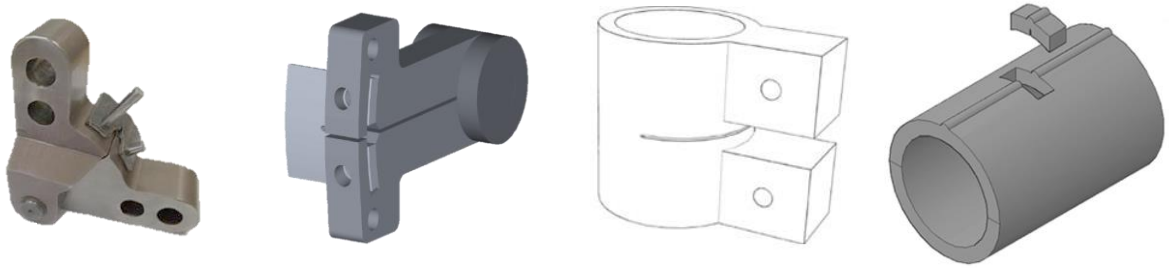

a) modified CT test specimen [2] b) curved CT test specimen [3] c) CP test specimen [7] d) curved SENB test specimen [9]

Figure 1. Alternative specimens for measuring fracture toughness of pipe material

Table 1. Chronological overview of the proposed alternative non-standard test specimens for measuring the fracture toughness of pipe material

Authors	Year	Type of specimen	Crack direction	Remark
Evans, J. T.; Kotiskos, G.; Robey, R. F. [1]	1995	curved CT	longitudinal	The need to make a special device that is not universal
Capelle, J.; Gilgert, J.; Matvienko, Y.; Pluvinage, G. [16], [17], [18]	2007	roman tile	transversal	This type of specimen is not efficient in describing the stress state and the mode of crack opening
Dlouhy, Ivo; Gubeljak, Nenad [2]	2008	modified CT	longitudinal	The need to make a special device that is not universal
Gajdoš, Ľubomír; Šperl, Martin [3]	2012	curved CT	longitudinal	The need to make a special device that is not universal
Park, Soo; Yoo, Sang-Soo; Min, Jun-Ki; Koo, Jae-Mean; Seok, Chang-Sung [5]	2012	curved CT	longitudinal	The paper does not mention the problem of uneven crack propagation, but it is certainly present
Koo, J. M.; Park, S.; Seok, C.S. [7]	2013	compact pipe	transversal	Compact pipe specimen simulates a transverse crack in a pipe, while a longitudinal crack is the most common in pipes

Gajdoš, Ľ.; Šperl, M.; Crha, P. [4]	2014	CT cut from pipe and flattened	longitudinal	By flattening the CT specimen cut from the pipe, large plastic deformations are introduced into the specimen itself
Angeles-Herrera, D.; Albiter-Hernandez, A.; Cuamatzi-Melendez, R.; Gonzalez-Velazquez, J. L. [9]	2014	curved SENB	longitudinal transversal	Compared to the standard CT examined in the paper, curved SENB describes different crack propagation then the examined CT
Mahajan, G.; Saxena, S.; Mohanty, A. [8]	2016	compact pipe	transversal	Compact pipe specimen simulates a transverse crack in a pipe, while a longitudinal crack is the most common in pipes

2. Pipe – Ring Notched Bend specimen

Traditional ways of measuring fracture properties, such as SENB and CT specimens, are often not applicable to pipelines, especially those with thin walls or small diameters. No simple and economically viable procedure for measuring the fracture properties of pipe material has been designed and standardized up to present. In that sense, Matvienko and Gubeljak proposed a ring-type test specimen known as Pipe Ring Notched Bend specimen – PRNB. Figure 2 shows the basic geometry of the newly proposed PRNB test specimen.

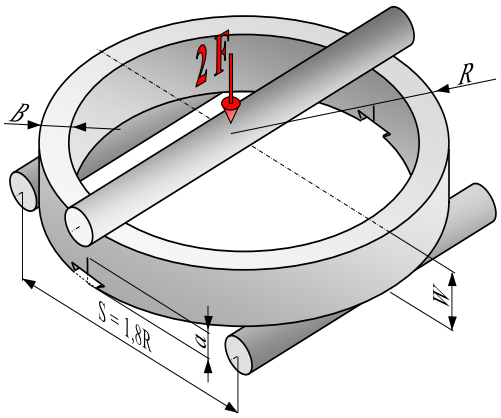

Figure 2. Pipe Ring Notched Bend specimen (PRNB)

2.1. Previous research on Pipe Ring Notched Bend specimen

As an introduction to the study of fracture mechanics parameters of PRNB specimens loaded in bending, the authors Likeb, Gubeljak and Matvienko in [18] conducted research on the ring-shaped specimen without notches and cracks in order to prove the applicability of expressions from strength of materials for determination of stresses and strains in critical ring cross-sections. In order to predict pipeline loading capacity, as well as its resistance to crack initiation and propagation, the pipeline integrity assessment requires solutions for Stress Intensity Factor and Limit Load [19]. The Limit Load is the main input parameter for assessing the possibility of plastic collapse [20], [21]. By research conducted in [19] authors proved that the PRNB specimen showed similar fracture behavior as the standard SENB specimen, and that the solution for Stress Intensity Factor and Limit Load of the PRNB specimen were well correlated with the SENB specimen. The same authors showed in [22] that the variation of the outer radius of the PRNB specimen had a negligible effect on the Limit Load value in case of constant values referring to the specimen ratio of the outer radius R and the height W ($R/W = 4$), and the ratio of the height W and the wall thickness B ($W/B = 2$), and in case of crack depth ratios ranging $0{,}45 \leq a/W \leq 0{,}55$. Furthermore, an experimental study was conducted to compare the fracture behavior of the PRNB specimen and the standard SENB specimen made of the same material [23]. The study showed that the results were in good correlation with the results obtained by both specimens. In [24], the authors compared several types of specimens: standard SENB and CT, as well as PRNB specimen with a notch and PRNB specimen with a notch and fatigue pre-crack (non-uniform propagation). Comparison of CTOD - R resistance curves for all the above test specimens showed very similar fracture behavior in the area of stable crack propagation. Although in the mentioned studies the PRNB test specimen with only a notch or with a non-uniform fatigue pre-crack was taken into consideration, it was generally concluded that PRNB specimen cut from pipe can be an adequate substitute for measuring the fracture toughness of pipe material [25]. All above described researches related to PRNB specimens were conducted on specimens cut from a sheet metal plate with the intention to eliminate the impact of residual stresses caused by pipe production. So, all researches focused strictly on studying the PRNB specimen fracture behavior without imperfections.

In [26], different geometries of the PRNB test specimen with and without residual stresses were investigated on specimens made from real pipes for the first time. The paper presents the dependence of the force and Crack Mouth Opening Displacement in means of F - CMOD curves in order to evaluate the influence of residual stresses on the deformation behavior of the PRNB test specimen. In paper [27], investigation of residual stresses on PRNB test specimens before and after the annealing for residual stress reduction procedure were presented. In paper [28], the correlation between the measured fracture toughness was studied using the newly proposed PRNB test specimen and the standardized SENB test specimen made from the same pipe as the PRNB test specimen. The research showed a very good correlation in the obtained values using both type of test specimens, but with a significant difference. Namely, fatigue pre-crack was performed in the SENB test specimen in order to generate real crack in specimen, while the PRNB test specimen was tested only with a notch, without fatigue crack, which was not a valid test according to available standards for measuring fracture toughness [29], [30].

2.2. Problem of uneven crack propagation of Pipe Ring Notched Bend specimen

Currently, the biggest disadvantage of the PRNB test specimen is that it is very difficult to perform the correct fatigue pre-cracking of the specimen because of uneven crack propagation through the wall thickness. In [31], the influence of residual stresses on fracture behavior of PRNB test specimens is analyzed. The analysis of PRNB test specimens and measured values of residual stresses on them proved that residual stresses have effects on fracture behavior only at the beginning of three-point bending test. With a further increase in force, bending stresses completely prevail in the test specimen and the influence of residual stresses becomes negligible.
Standards prescribe that the deviation in the depth of fatigue crack propagation through the wall thickness of the test specimen must not exceed 10% [29]. Due to torsion that is most pronounced in the crack propagation plane the roller through which the loading is transmitted to PRNB test specimen loads more greatly the test specimen on the inner wall and therefore the fatigue crack propagates faster from the inside of the test specimen, Figure 3.

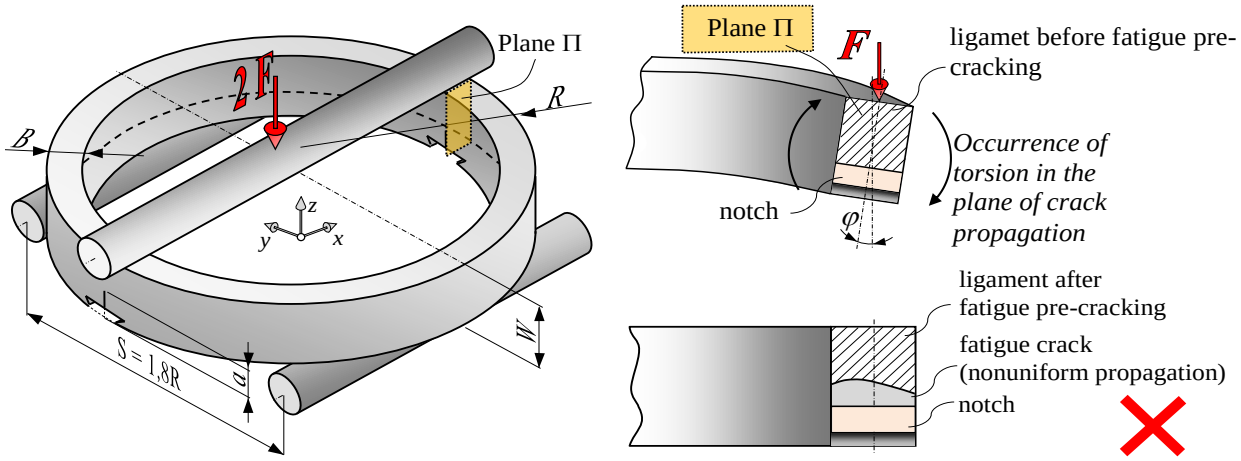

Figure 3. Occurrence of torsion in the plan of crack propagation of Pipe Ring Notched Bend specimen (PRNB)

In previous studies, authors are numerically analyzed the occurrence of the torsion [32]. Those studies showed that the torsion effect had a significant influence on the fracture behavior of the PRNB test specimen at lower *a*/*W* ratios (0,2 to 0,45). When increasing this ratio (0,45 to 0,7), torsion had no significant effect on the fracture behavior of PRNB test specimen. Ratio's *a*/*W*=0,45 to 0,7 were in the range of those covered by the ASTM E1820 standard, so it was concluded that the torsion effect did not affect the fracture behavior of the PRNB test specimen for *a*/*W* ratios defined by the standard as marginal.

Figure 4 shows real example of uneven fatigue crack propagation on PRNB specimen made from pipe with dimensions ϕ 114,3 x 12,5. In this case, Chevron notch is applied.

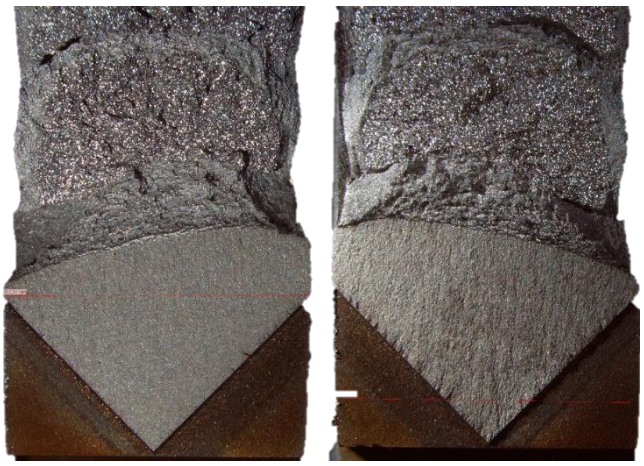

Figure 4. Real example of uneven fatigue crack propagation on PRNB specimen made from pipe with dimensions ϕ 114,3 x 12,5

To conclude, torsion effect can be neglected, however, torsion is the main reason for uneven propagation of fatigue crack through the wall thickness of the PRNB test specimen, so it is certainly a major problem that has not been solved up to now, and therefore such a test specimen cannot be used in practice on a global scale.

EU project *Collaborative research to increase the level of development of a new innovative method of testing fracture toughness using a ring-type test specimen (KIRIMI) NPOO.C3.2.R3-I1.04.0117* aims to solve the problem of uneven fatigue crack propagation on PRNB specimen, which will be certainly a big step to the final goal of standardizing the PRNB test specimen on a global level.

5. Conclusions

Until nowadays, numerous methods have been proposed for measuring the fracture toughness of pipe material, but all of them have drawbacks. Most method are dealing with CT specimens (curved or modified CT specimen), the only available study that analyses an alternative to the SENB specimen is a study in which authors analyses the curved SENB specimen. Despite a large number of studies on this topic, no simple and economically viable procedure for measuring the fracture toughness of pipe material has been designed and standardized up to nowadays.

As an alternative to the SENB test specimen, the PRNB test specimen is presented for measuring the fracture toughness of pipe materials from pipes from which standardized SENB and CT test specimens cannot be made. Currently, the biggest disadvantage of the PRNB test specimen is that it is very difficult to perform the correct fatigue pre-cracking of the specimen because of uneven crack

propagation through the wall thickness. Within the EU project NPOO.C3.2.R3-I1.04.0117, researchers will aim to prove the applicability of proposed patent solution in order to achieve uniform crack propagation during the fatigue pre-cracking of the PRNB test specimen using an exhaustive numerical and experimental approach. This will be a big step towards the final goal of standardizing the PRNB test specimen on a global level.

Acknowledgments and Funding: The authors would like to acknowledge the EU Research Project (NPOO.C3.2.R3-I1.04.0117) financed from The Recovery and Resilience Facility (NextGenerationEU).

6. References

[1] J. T. Evans, G. Kotiskos i R. F. Robey, »A method for fracture toughness testing cylinder material,« u *Engineering Fracture Mechanics*, svez. 50, Elsevier Science Ltd, 1995., pp. 295-300

[2] I. Dlouhy i N. Gubeljak, »Personal discussion about testing the thin pipeline wall by using modified CT specimen and especial developed testing device,« Alger, 2008.

[3] Ľ. Gajdoš i M. Šperl, »Evaluating the Integrity of Pressure Pipelines by Fracture Mechanics,« u *Fracture Toughness of Metal Castings, Science and Technology of Casting Processes*, InTech, 2012., pp. 283-310

[4] Ľ. Gajdoš, M. Šperl i P. Crha, Comparison of fracture toughness of curved and flat CT specimens for the gas pipeline ingerity management, IGRC - International Gas Union Research Conference, Copenhagen: International Gas Union, 2014, Copenhagen.

[5] S. Park, S.-S. Yoo, J.-K. Min, J.-M. Koo i C.-S. Seok, »Evaluation of fracture toughness characteristics for nuclear piping using various types of specimens,« *International Journal of Pressure Vessels and Piping*, Sves. %1 od %290-91, pp. 9-16, 2012.

[6] C. S. Seok, S. K. Cho, K. S. Seon, K. H. Lee i S. Park, »Compact pipe specimen«. Patent WO2009075475, 18. 06. 2009.

[7] J. M. Koo, S. Park i C. Seok, »Evaluation of fracture toughness of nuclear piping using real pipe and tensile compact pipe specimens,« *Nuclear Engineering and Design*, svez. 259, pp. 198-204, 2013.

[8] G. Mahajan, S. Saxena i A. Mohanty, »Numerical characterization of compact pipe specimen for stretch zone width assessment,« *Fatigue & Fracture of Engineering Materials & Structures*, svez. 39, br. 7, pp. 859-865, 2016.

[9] D. Angeles-Herrera, A. Albiter-Hernandez, R. Cuamatzi-Melendez i J. L. Gonzalez-Velazquez, »Fracture toughness in the circumferential–longitudinal and circumferential–radial directions

of longitudinal weld API 5L X52 pipeline using standard C(T) and nonstandard curved SE(B) specimens,« *International Journal of Fracture,* svez. 188, pp. 251-256, 2014.

[10] F. M. Haggag, A. J. Wang i T. J. Theiss, »Using Portable/In-Situ Stress-Strain Microprobe System to Measure Mechanical Properties of Steel Bridges During Service,« u *SPIE. Digital Library*, Nondestructive Evaluation of Steel Bridges ur., 1996., pp. 65-75

[11] F. M. Haggag, J. A. Wang, M. A. Sokolov i K. L. Murty, »Use of Portable/In Situ Stress-Strain Microprobe System to Measure Stress-Strain Behavior and Damage in Metallic Materials and Structures,« *Nontraditional Methods of Sensing Stress, Strain and Damage in Materials and Structures ASTM STO 1318,* pp. 85-98, 1997.

[12] K. L. Murty, M. D. Mathew, P. Q. Miraglia, V. N. Shah i F. M. Haggag, »Non-destructive evaluation of deformation and fracture properties of materials using stress-strain microprobe,« u *Non-destructive Characterisation of Materials in Aging Systems*, Pennsylvania, Materials Research Society, 1998., pp. 327-337

[13] K. L. Murty i M. D. Mathew, »Nondestructive monitoring of structural materials using automated ball indentation (ABI) technique,« u *Nuclear Engineering and Design*, 228 ur., Elsevier, 2004., pp. 81-96

[14] F. M. Haggag, »Field indentation microprobe for structural integrity evaluation«. USA Patent 4852397, 1989.

[15] J. Capelle, J. Gilgert, Y. Matvienko i G. Pluvinage, »Comparison of methods to measure the resistance to fracture emanating from scratches in gas pipes,« u *Proceeding of the ICF Interquadrennial Conference "Fracture Mechanics in design of Fracture Resistant Materials and Structures"*, 2007.

[16] J. Capelle, J. Gilgert, I. Dmytrakh i G. Pluvinage, »Hydrogen effect on fatigue and fracture resistance of a pipe steel,« u *Structural integrity and life*, 2009., pp. 9-14

[17] J. Capelle, J. Gilgert, Y. Matvienko i G. Pluvinage, »Measurement of the resistance to fracture emanating from scratches in gas pipes using non-standard curved specimens,« u *Security and Reliability of Damaged Structures and Defective Materials*, 2009., pp. 157-174

[18] G. Pluvinage i M. H. Elwany, Safety, Realiability and Risks Associated with Water, Oil and Gas Pipelines, Netherlands: Springer, 2008, pp. 205-217

[19] A. Likeb, N. Gubeljak i Y. G. Matvienko, »Analiza napetostno deformacijskega stanja upogibno obremenjenega obroča,« *Zbornik del / Kuhljevi dnevi 2013,* pp. 105-112, rujan 2013.

[20] A. Likeb, N. Gubeljak i Y. Matvienko, »Stress Intensity Factor and Limit Load Solutions for New Pipe–Ring Specimen with Axial Cracks,« u *Procedia Materials Science,* svez. 3, 2014., pp. 1941-1946.

[21] F. I. Sattari, »Finite element analysis of limit loads for surface cracks in plates,« u *International Journal of Pressure Vessels and Piping*, svez. 57, 1994., pp. 237-243

[22] Y. Lei, »Use of local and global limit load solutions for plates with surface cracks under tension,« u *International Journal of Pressure Vessels and Piping*, svez. 84, 2007., pp. 545-559

[23] N. Gubeljak, A. Likeb i Y. G. Matvienko, »Determination of Limit Loads for New Pipe – Ring Specimens,« u *High Strength Steels for Hydropower Plants, Design Concepts - Pressure Conduits: Proceedings of the 3rd International Conference*, Graz, Graz University of Technology, 2013., pp. 283-290

[24] N. Gubeljak, A. Likeb, J. Predan i Y. Matvienko, »Comparison between Fracture Behaviour of Pipe - Ring Specimens and Standard Specimens,« u *Key Engineering Materials*, 2013., pp. 637-640

[25] N. Gubeljak, A. Likeb i Y. Matvienko, »Fracture Toughness Measurement by Using Pipe - Ring Specimens,« u *Procedia Materials Science*, svez. 3, 2014, pp. 1934-1940

[26] D. Damjanović, D. Kozak, N. Gubeljak i V. Tropša, »Proposal of new Pipe-Ring specimen for fracture mechanics,« Procedia Engineering, svez. 149, pp. 33-39, 2016.

[27] D. Damjanović, D. Kozak, S. Marsoner i N. Gubeljak, »Residual stress state in pipe cut ring specimens for fracture toughness testing,« Materialpruefung/Materials Testing, svez. 59, br. 6, pp. 530-535, 2017.

[28] D. Damjanović, D. Kozak, Y. Matvienko i N. Gubeljak, »Correlation of Pipe Ring Notched Bend (PRNB) specimen and Single Edge Notch Bend (SENB) specimen in determination of fracture toughness of pipe material,« Fatigue & Fracture of Engineering Materials and Structures, svez. 40, br. 8, pp. 1251-1259, 2017.

[29] K. H. Schwalbe, J. Heerens, U. Zerbst, H. Pisarski i M. Kocak, »EFAM GTP 02 - The GKSS test procedure for determining the fracture behaviour of materials,« GKSS Forschungszentrum Geesthacht GmbH, Geesthacht, 2002.

[30] ASTM E 1820 - 13, »Standard Test Method for Measurement of Fracture Toughness,« ASTM International, West Conshohocken, 2013.

[31] D. Damjanovic, D. Kozak i N. Gubeljak, »The influence of residual stresses on fracture behavior of Pipe Ring Notched Bend specimen (PRNB),« Engineering fracture mechanics, svez. 205, pp. 347-358, 2019.

[32] D. Damjanovic, D. Kozak, I. Gelo i N. Gubeljak, »The influence of torsion effect on fracture behavior of Pipe Ring Notched Bend specimen (PRNB),« Theoretical and Applied Fracture Mechanics, svez. 103, 2019.

Društvo za tehniku
zavarivanja Slavonski Brod

13. Međunarodno znanstveno-stručno savjetovanje SBZ 2025

„STROJARSKE TEHNOLOGIJE U IZRADI ZAVARENIH KONSTRUKCIJA I PROIZVODA, SBZ 2025."
Slavonski Brod, 08. i 09. 05. 2025.

Vibracije zbog prepusta alata kod glodanja

M. Stoić[1,*], K. Marićak[1], A. Stoić[2], M. Duspara[2], M. Čuletić Čondrić[1]

[1]Technical Department, University of Slavonski Brod, Croatia
[2] Mechanical Engineering Faculty in Slavonski Brod, University of Slavonski Brod, Croatia

[*] Corresponding Author. E-mail: mstoic@unisb.hr

Abstract

Vibracije na strojevima tijekom obrade postupcima odvajanja čestica su različite. U sustavu alatni stroj - radni predmet mogu se uočiti tri vrste vibracija: slobodne, prisilne i samopobudne vibracije. Razlozi za pojavu pojedinih vibracija su različiti. U radu se promatraju samopobudne vibracije, općenito, koje mogu biti posljedica uvjeta obrade, a ovise o materijalu koji se obrađuje, dubini i širini reza, geometriji alata itd. Tijekom procesa glodanja jedan od razloga za pojavu samopobudnih vibracija je prepust alata, odnosno glodala.
Ponekad je potreban veliki prepust alata zbog geometrije izratka, izrade raznih utora i sl. Povećanjem prepusta alata povećavaju se i vibracije koje izravno utječu na kvalitetu obrade u vidu hrapavosti obrađene površine, geometrijskih i dimenzijskih odstupanja, ali i istrošenosti oštrice alata.
U radu je analiziran utjecaj pojedinih parametara obrade na veličinu vibracija.
Smanjenje prepusta rezultira nižim vibracijama, a time i boljom kvalitetom obrade u vidu hrapavosti površine i dimenzijskih odstupanja.

Keywords: glodanje, vibracije alata, prepust alata, kvaliteta površine

1. Uvod

Obrada odvajanjem čestica obuhvaća različite tehnološke postupke u kojima dolazi do pojave vibracija u sustavu alatni stroj – alat - obradak. Vibracije koje nastaju tijekom procesa obrade mogu imati značajan utjecaj na kvalitetu obrade s smislu dimenzijskih i geometrijskih odstupanja i hrapavosti obrađene površine, ali i na vijek trajanja alata te ukupnu učinkovitost proizvodnog procesa.
U praksi se najčešće susreću tri osnovne vrste vibracija: slobodne, prisilne i samopobudne vibracije.
Slobodne vibracije nastaju kao posljedica kratkotrajnog poremećaja sustava, kada je sustav jednom pobuđen te nakon toga oscilira vlastitom frekvencijom bez daljnjeg vanjskog utjecaja. Ovakve vibracije najčešće su prolaznog karaktera i javljaju se, na primjer, nakon dodira alata s obratkom (pri ulazu i izlazu alata na početku i na kraju obrade) ili promjene uvjeta rezanja.

Prisilne vibracije uzrokovane su vanjskim periodičkim silama, na primjer neuravnoteženost stroja ili ekscentričnosti stezne naprave, neravnomjernog toka odvojene čestice, nesimetrične geometrije alata ili nepravilnosti na obratku. Također mogu biti uzrokovane i neravnotežom između ležajeva, vretena i drugih dijelova alatnog stroja. Kada se utvrde uzroci, relativno ih je jednostavno izbjeći, smanjiti ili ukloniti. Frekvencija ovih vibracija odgovara frekvenciji vanjskog uzroka, a njihov intenzitet ovisi o amplitudi pobude i rezonanciji sustava.
Samopobudne vibracije predstavljaju poseban izazov jer nastaju kao rezultat međudjelovanja reznih sila i promjenjive krutosti sustava tijekom obrade. Upravo te samopobudne vibracije, poznate i kao regenerativne vibracije, mogu dovesti do pojave tzv. „chattera" – nestabilnog i neželjenog stanja u obradi. [1] Do vibriranja dolazi kada alat, držač alata i vreteno vibriraju na rezonantnoj frekvenciji sklopa. Chatter se obično prevodi kao brbljanje ili klepetanje jer u pozadini stvar zvuk klepetanja.
U ovom radu naglasak je stavljen na analizu samopobudnih vibracija koje nastaju tijekom procesa glodanja, s posebnim fokusom na utjecaj prepusta alata. Povećanjem prepusta alata, osobito kod obrade dubljih ili teško dostupnih površina, dolazi do smanjenja ukupne krutosti sustava, što pogoduje razvoju vibracija. Posljedice takvih vibracija uključuju smanjenje kvalitete obrađene površine, povećana dimenzijska odstupanja te ubrzano trošenje rezne oštrice.
Cilj ovog rada je istražiti povezanost između odabranih parametara obrade i intenziteta vibracija, s ciljem optimizacije procesa i postizanja veće stabilnosti tijekom glodanja.

2. Samopobudne vibracije – chatter

Samopobudne vibracije, poznate i kao regenerativne vibracije ili „chatter", najozbiljniji su oblik vibracija jer nastaju kao posljedica povratne sprege između procesa rezanja i elastičnosti sustava stroj – alat - obradak. Ove vibracije se ne javljaju zbog vanjske sile, već su rezultat međudjelovanja reznih sila i dinamike sustava. Prvi pokušaji razumijevanja chatter fenomena zabilježeni još 1907. godine od strane F. W. Taylora, ali i dalje predstavljaju izazov u automatizaciji strojne obrade. Prisutnost chattera negativno utječe na kvalitetu površine, točnost obrade, uzrokuje neugodan zvuk te ubrzava trošenje alata, što ga čini jednim od ključnih problema u suvremenoj proizvodnji. [2]
Tipičan primjer pojave chattera vidljiv je kod glodanja: kako se alat rotira i reže, čak i male promjene u dubini reza (zbog savijanja alata) mogu uzrokovati nestabilnost. Na primjer, do chattera dolazi kada valovita površina nastala prethodnim prolazom alata utječe na promjenu debljine odvojene čestice u sljedećem rezu, što zatim mijenja reznu silu i uzrokuje nove oscilacije. Također, ako je sustav slabije krutosti, na primjer stezanje obradka s velikim prepustom izvan stezne naprave ili kod većeg prepusta alata, dolazi do razvoja samopobudnih vibracija. Vizualno, ovo se očituje kao nepravilna, valovita i grubo obrađena površina. (Slika 1.)

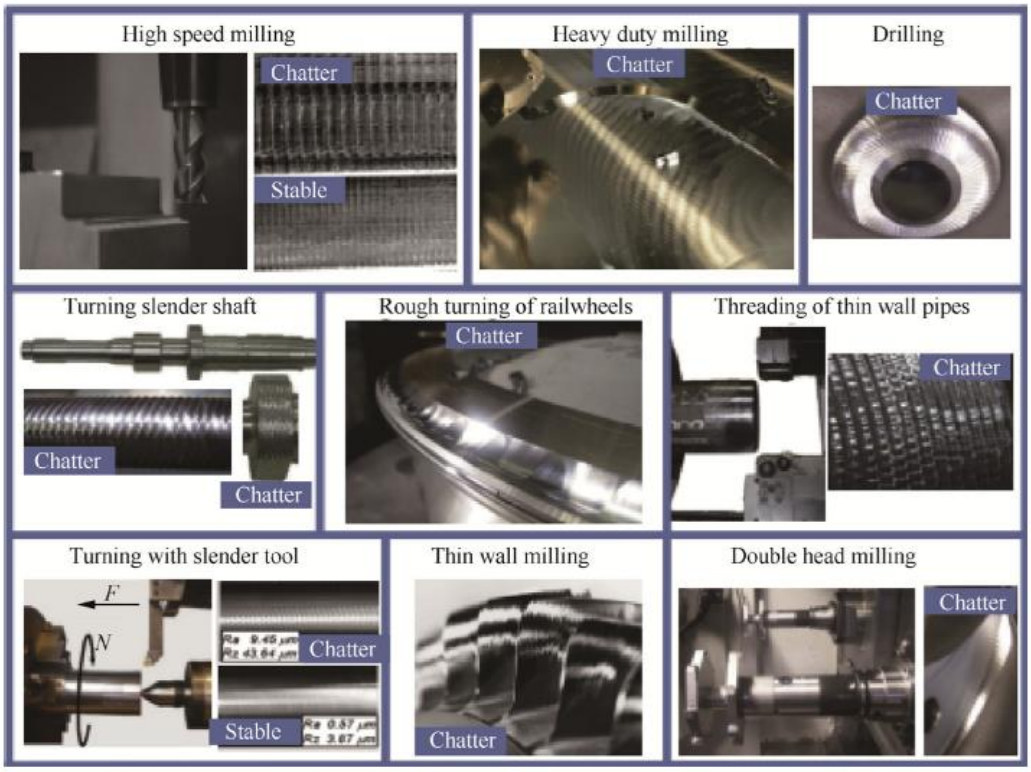

Slika 1. Primjeri utjecaja chattera kod različitih postupaka obrade [2]

Frekvencija samopobudnih vibracija obično ne odgovara frekvenciji vrtnje alata, već ovisi o rezonantnim svojstvima sustava i dinamici rezanja. Kritični parametri koji utječu na pojavu chattera su:

- krutost sustava (alat – stroj - obradak),
- geometrija alata (broj oštrica, kutovi rezanja),
- parametri obrade (brzina rezanja, posmak, dubina rezanja),
- prepust alata.

Chatter vibracije mogu se podijeliti u tri glavne skupine: uzrokovane trenjem, uzrokovane spojem te regenerativne vibracije. [2] Vibracije uzrokovane trenjem nastaju zbog međusobnog trenja između alata i obratka. Pojava sile trenja javlja se na dijelu trošenja alata na stražnjoj površini alata. Zatupljenjem noža dolazi do povećanja pojasa trošenja što dovodi do povećanja natražne sile, a time i sile trenja. Ove nestabilnosti se često manifestiraju pri većim brzinama rezanja i neadekvatnoj geometriji alata. Vibracije uzrokovane spojem rezultat su razlike u krutosti konstrukcijskih elemenata te mogu dovesti do rezonancije i uzrokovati nestabilnost sustava. Stabilno stanje moguće je postići analizom sustava i eksperimentalnim modeliranjem. Nepravilnosti mogu biti, na primjer, netočno izvedena ozubljenja, hidraulički udar u hidrauličkom prijenosnom sustavu, sile trenja između vratila i drugih dijelova alatnog stroja, zračnost i trenje u ležajevima i slično. Regenerativne vibracije, koje se smatraju najčešćim oblikom chattera u praksi, rezultat su promjena u debljini odvojene čestice koje

nastaju zbog razlike između valovite površine prethodnog reza i trenutačnog prolaza alata. (Slika 2.) Ovaj tip vibracija je posebno izražen kod glodanja, gdje više reznih oštrica ulaze u kontakt s materijalom. [2]

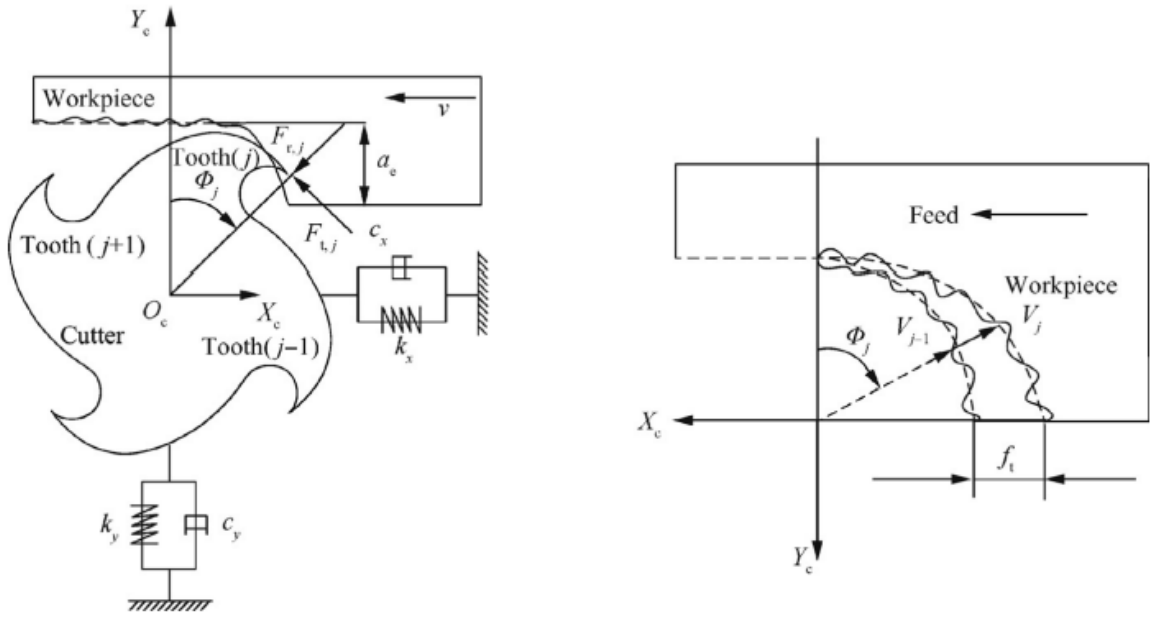

Slika 2. Dinamički model postupka glodanja [2]

Osim promjene debljine odvojene čestice dolazi i do promjene kutova alata, ali i kutova obrade, a rezultat je promjena sile rezanja u odgovarajućem pravcu i može se izraziti formulom:

$$dF = \sum_{i=1}^{4} dF_{(1)}$$

gdje su dF promjena sile nastala zbog četiri komponente:

- pri promjeni trenja između prednje površine alata i odvojene čestice
- pri promjeni prednjeg i stražnjeg kuta zbog vibracija
- pri relativnom pomaku alata i obratka što dovodi do promjene poprečnog presjeka odvojene čestice
- zbog grešaka u prijenosnicima i drugim elementima stroja [1]

3. Vibracije kod čeonog glodanja

Glodanje je postupak obrade alatima s više reznih oštrica, a koristi se pri obradi ravnih površina, različitih profila, površina specijalnog i složenog oblika. Za obradu različitih površina koriste se i različite vrste glodala koja djelimo:

a) Prema kinematici postupka: istosmjerno i protusmjerno
b) Prema položaju reznih oštrica na glodalu:obodno i čeono

Osim ove podjele može se razmatrati i podjela ovisno o kvaliteti obrađene površine i obliku obrađene površine.

Obzirom na veliki broj različitih vrsta glodala, bitno je poznavanje parametara obrade i njihovog utjecaja na proces obrade. Parametri obrade određuju karakteristike procesa obrade, pri čemu treba voditi računa i o formiranju odvojene čestice. Tijekom rotacije glodala, obradni materijal se pomiče prema alatu određenom brzinom, brzinom posmaka, a svaki zub glodala odstranjuje male količine materijala. Veličina i oblik odvojene čestice su bitni radi lakšeg odvođenja iz zone rezanja, a ovise o nizu čimbenika, među kojima su najvažniji: dubina rezanja, brzina posmaka, brzina rezanja, broj zuba, geometrija umetka ili zuba, te vrsta materijala koji se obrađuje.

Parametri obrade kod glodanja su:

a_p - aksijalna dubina (mm)
a_e - radijalna dubna (mm)
f_z - posmak po zubu (mm/zub)
f - posmak po okretaju (mm)
v_f - posmična brzina (mm/min)
D_c - promjer glodala (mm)
z_n - broj reznih oštrica
z_c - efektivni broj oštrica
v_c - brzina rezanja (m/min)
n - frekvencija vrtnje (min^{-1}),
a prikazani su na slici 3.

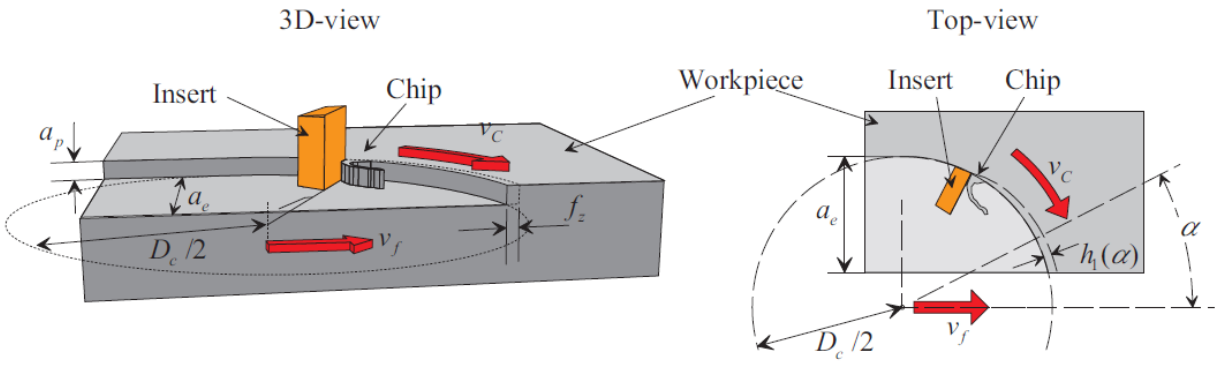

Slika 3. Parametri obrade kod glodanja [3]

Osim parametara obrade, važan faktor je i smjer posmaka obradka u odnosu na smjer vrtnje alata, pa tako kod čeonog glodanja razlikujemo:

- protusmjerno čeono glodanje → posmak ide suprotno od smjera vrtnje alata u točki kontakta.
- istosmjerno čeono glodanje → posmak ide u istom smjeru kao i rotacija alata u točki kontakta.

U praksi, istosmjerno glodanje kod čeonog glodanja daje bolju površinsku obradu i manji otpor rezanju, ali zahtjeva veću stabilnost i veću krutost sustava (alat + stroj + obradak).

Kod glodanja utora, za slučaj kad radimo puni utor, glodalo reže s obje strane jednakomjerno pa je i opterećenje ravnomjerno, ali je otpor rezanju veći. Ovo ne predstavlja veliki problem kod malog prepusta alata jer je i krutost obratka velika. Ponekad je zbog geometrije obratka potrebno imati veći prepust alata, a koji će onda utjecati i na pojavu većih vibracija. Kod velikog prepusta alata obrada postaje teža jer dolazi do savijanja alata u smjeru brzine rezanje, a što uzrokuje vibracije na vrhu alata poznate kao chatter (klepetanje). Sve to dovodi do lošije kvalitete obrađene površine.

Za smanjenje vibracija zbog velikog prepusta provedena su različita ispitivanja, a neke od preporuka prema DMG MORI [5] su:

- vibracije se mogu smanjiti smanjenjem natražne sile i glavne sile rezanja pri čemu je i otpor materijala obrade manji,
- povećanje prednjeg kuta rezne oštrice γ do 30 ˚ čime se glavna sila rezanja smanjuje i do 33 %, a smanjuju se i natražna i posmična sila (slika 4.)

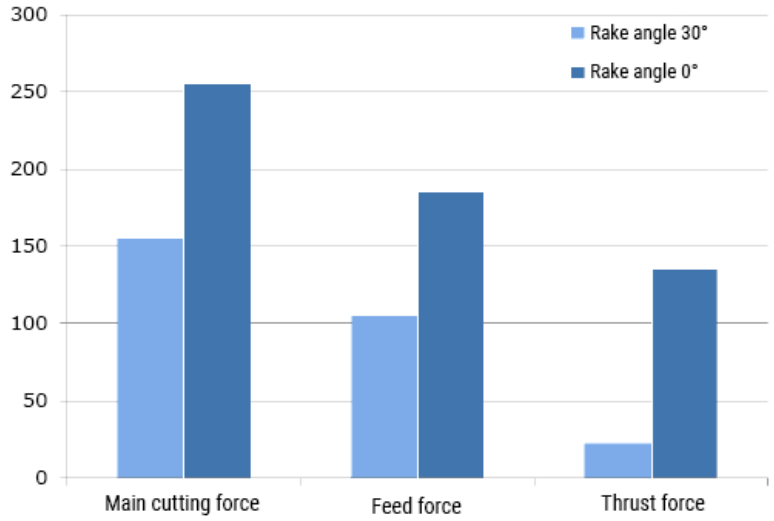

Slika 4. Usporedba otpora rezanja za različite prednje kutove γ (materijal: S50C) [5]

- smanjiti kut vrha rezne oštrice alata ε_r, a rezultati ispitivanja su prikazani na slici 6. Na glavnoj sili rezanja nije uočena velika promjena, ali natražna sila se povećavala, a sila posmaka smanjivala kako se povećavao kut vrha rezne oštrice. Smanjenjem kuta vrha rezne oštrice može se smanjiti i chatter.

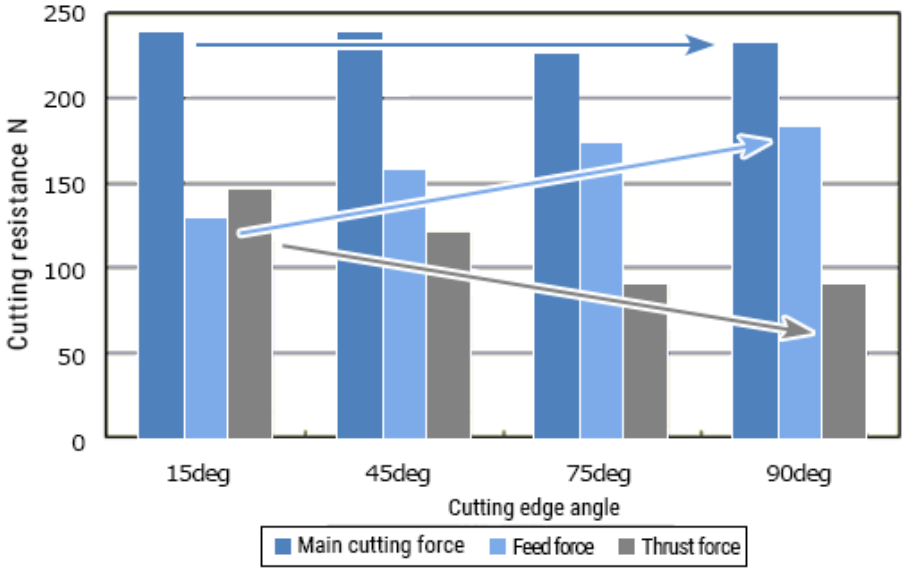

Slika 6. Utjecaj promjene kuta vrha rezne oštrice na sile u procesu rezanja [5]

- održavati konstantan broj oštrica u zahvatu – veći broj oštrica koje ulaze i izlaze iz zahvata s materijalom obrade uzrokuje i veća dinamička opterećenja što dovodi do pojave chatter-a. Veći broj oštrica u zahvatu smiruje vibracije, ali zahtjeva i veće sile rezanja (slika 7.). Stoga je bitno voditi računa i o veličini alata i o smjeru otpora rezanja.

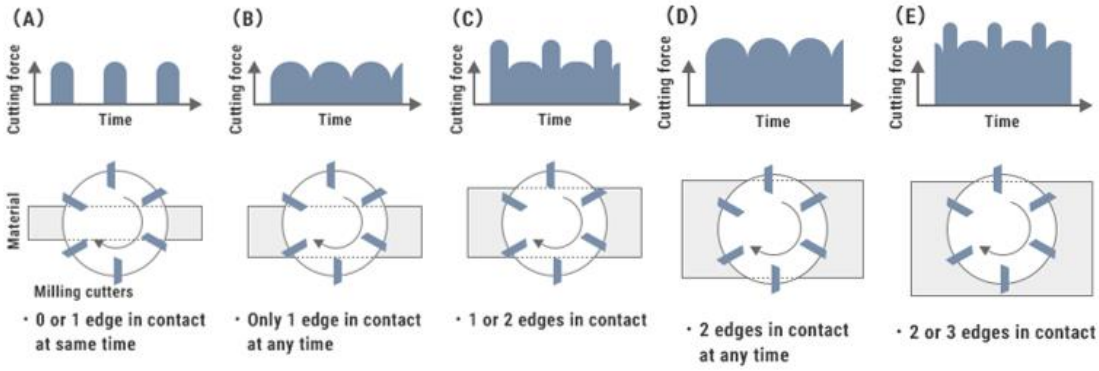

Slika 7. Odnos sile rezanja i broja reznih oštrica u zahvatu [5]

Različite tehnike suzbijanja chatter vibracija [6] su:

- izrada dijagrama procesa stabilnosti (SLD dijagram) – odabir odgovarajućih parametara procesa
- promjene brzine vrtnje glavnog vretena – s manjom brzinom rezanja dobije se bolje obrađena površina [7]
- povećati krutost sustava

4. Eksperimentalni dio

Na temu vibracija kod čeonog glodanja postoje različita istraživanja i preporuke različitih načina smanjivanja tih vibracija. Veliki dio tih istraživanja bavi se chatter vibracijama kod čeonog glodanja različitih materijala, ali i površina većih od promjera glodala. Za smanjenje chatter vibracija često se ističe krutost sustava koja podrazumijeva i odgovoarajući način stezanja obradka i alata sa što manjim prepustom alata. Međutim, ponekad je zbog geometrije samog obradka i izrade utora potreban veći prepust alata. Eksperimentalni dio ovog rada istražuje utjecaj promjene parametara obrade na kvalitetu obrađene površine s promjenom duljine prepusta alata kod glodanja utora širine promjera glodala.

Eksperiment je rađen na ručno upravljanoj glodalici Prvomajska GUK-1 koja nema mogućnost promjene brzine vrtnje tijekom obrade, već je brzina rezanja određena zadanim brojem okretaja na početku obrade i promjerom glodala. Korišteno glodalo je Wattson HSS promjera 26 mm s 5 reznih oštrica. Materijal obrade je konstrukcijski čelik za strojne dijelove S235JR.

Cilj eksperimenta je analizirati utjecaj prepusta alata, dubine obrade i posmaka na vibracije (RMS, PEAK) i na hrapavost površine (Ra, Rz) kod glodanja pri konstantnom broju okretaja.

Kratki opis eksperimenta: radi se obrada glodanjem s dvije vrijednosti prepusta alata: jedan od 80 mm i jedan od 210 mm. Za svaki prepust alat mijenjaju se vrijednosti dubine obrade od 0,5 mm, 1 mm, 1,5 mm i 2 mm. Za sve dubine rezanja posmak je bio 0,4 mm po okretaju, a za dubinu obrade od 2 mm napravljena je dodatno obrada i sa posmakom od 0,1 mm po okretaju. Za svaki prepust alata i za sve obrade (sve dubine i posmak) izmjerene su vrijednosti vibracija (RMS i PEAK) u određenim rasponima. Isto tako izmjerene su i hrapavosti obrade Ra i Rz. Izmjerene vrijednosti prikazane su u tablici 1.

Uzorci na kojima su mjerene vibracije i hrapavost prikazani su na slici 8.

Mjerenje vibracija tijekom obrade je pomoću vibrometra (bilježe se RMS i PEAK vrijednosti u određenim frekvencijskim rasponima) Adash A4900 Vibro M Ex.

Mjerenje hrapavosti površine nakon obrade uređajem za hrapavost (Ra, Rz) Mitutoyo SJ-301.

Tablica 1. Izmjerene vrijednosti vibracija i hrapavosti površina

prepust alata, mm	n [okr/min]	f [mm]	a [mm]	µm [PEAK]	mm/s [RMS]	Ra, µm	Rz, µm
80	808	0,4	0,5	11 - 13	0,59	4,512	23,15
80	808	0,4	1	212 - 216	0,78	3,51	18,072
80	808	0,4	1,5	221 - 281	0,82	3,907	20,027
80	808	0,4	2	38 - 45	1,18	2,15	13,273
80	808	0,1	2	10 - 28	1,25	2,958	16,87
210	808	0,4	0,5	20 - 23	0,60	2,832	17,12
210	808	0,4	1	254 - 265	0,86	5,263	25,343
210	808	0,4	1,5	241 - 270	1,03	4,568	23,258
210	808	0,4	2	43 - 53	1,52	2,822	15,422
210	808	0,1	2	18 - 30	0,79	3,642	17,353

Slika 8. Primjeri uzoraka na kojima su rađena mjerenja

Analiza dobivenih rezultata prikazana je u grafovima odnosa dubina obrade i vibracija (slika 9. i slika 10.) te odnosa dubine obrade i hrapavosti površine (slika 12. i slika 13.).

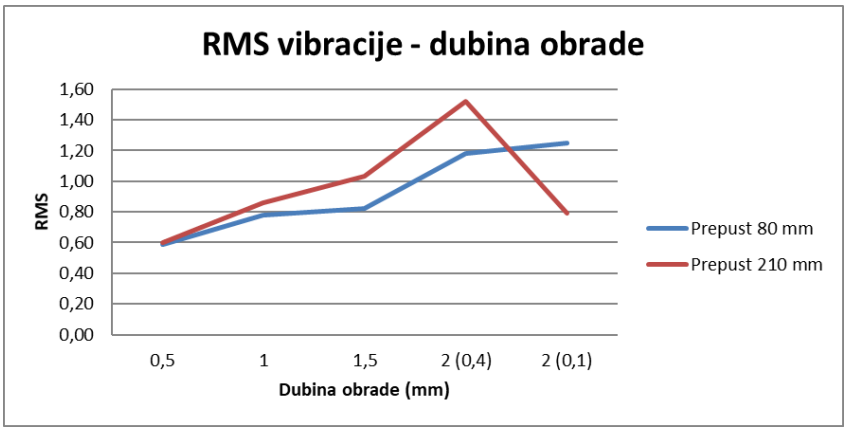

Slika 9. Odnos RMS i dubine obrade

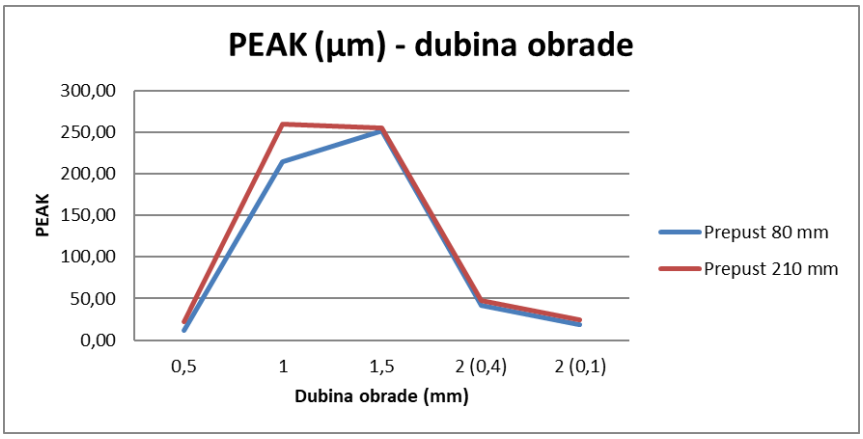

Slika 10. Odnos PEAK i dubine obrade

RMS pokazuje prosječnu razinu vibracija odnosno daje dojam koliko je sustav "nemiran", dok PEAK pokazuje najgori trenutni udar, a što je važan podatak kod mogućnosti oštećenja ili rezonancije.
Na slici 10. na grafu se može vidjeti nagli skok vibracija – trenutni udar pri dubini obrade od 1 mm, za prepust od 210 mm, a zatim i nastavak tog skoka do dubine 1,5 mm. Također i kod prepusta od 80 mm na dubini od 1,5 mm došlo je do naglog skoka vibracija. Veća dubina obrade zahtjeva i veće sile rezanja, a što je dovelo do naglog trošenja alata s povećanjem dubine rezanja sa 1 mm na 1,5 mm što se posebno manifestiralo kod prepusta od 210 mm taljenjem dijela obradka i pojavom velike količine naljepka na obradku. (slika 11.)

Slika 11. Naglo trošenje alata i stvaranje naljepka na obrađenoj površini

Na dubini rezanja od 2 mm može se primjetiti pad i za posmak od 0,4 mm i za posmak od 0,1 mm. Ako bi se povukla trend linija kroz grafove RMS i PEAK u odnosu na dubinu obrade primjećuje se da grafovi padaju s dubinom od 2 mm. Jedan od zaključaka bi mogao biti da će veća dubina obrade dodatno smiriti vibracije.

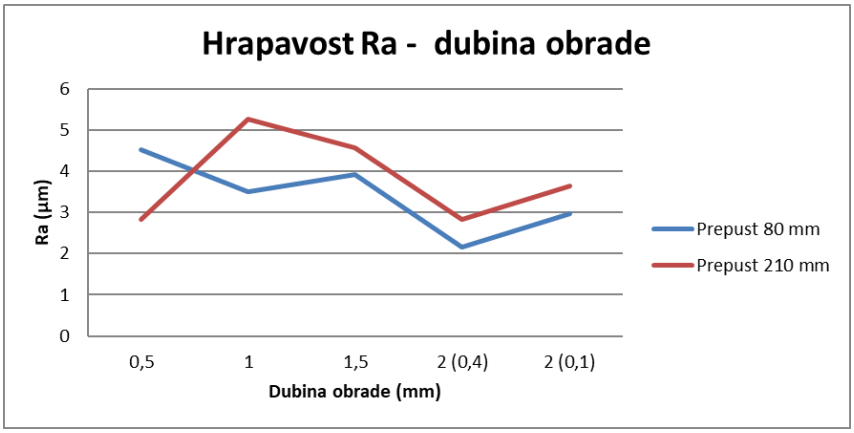

Slika 12. Odnos hrapavosti Ra i dubine obrade

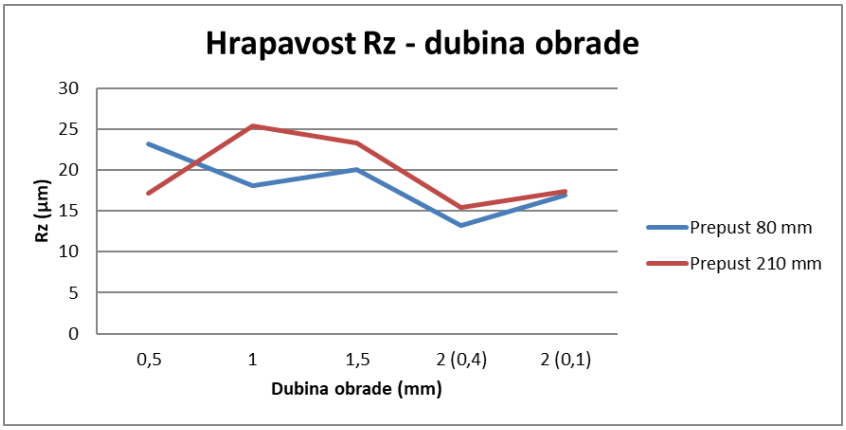

Slika 13. Odnos hrapavosti Rz i dubine obrade

Iz grafova se može primjetiti da Ra I Rz pokazuju blago poboljšanje hrapavosti pri prepustu od 80 mm s povećanjem dubine obrade i posmakom od 0,4 mm dok s promjenom posmaka hrapavost raste. Slično se može primjetiti i kod prepusta od 210 mm gdje na početku s povećanjem dubine obrade do 1 mm imamo rast hrapavosti, a nakon toga pad i za Ra i za Rz, dok će smanjenjem posmaka za istu dubinu obrade od 2 mm doći do ponovnog rasta hrapavosti.
Utjecaj vibracija zbog prepusta alata na hrapavost obrađene površine može se vidjeti iz grafova na slikama 14. i 15.

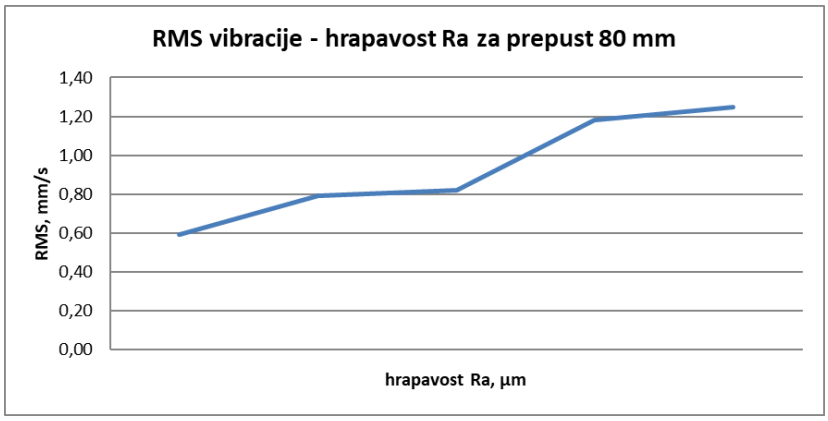

Slika 14. Utjecaj vibracija na hrapavost pri prepustu od 80 mm

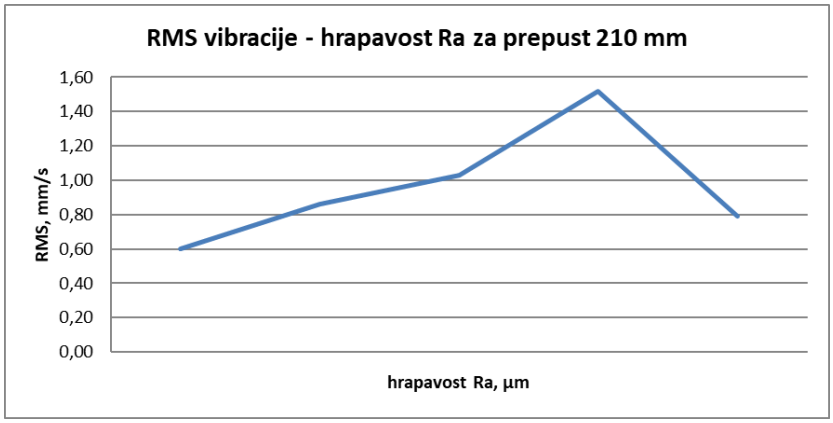

Slika 15. Utjecaj vibracija na hrapavost pri prepustu od 210 mm

Povećanjem vibracija povećava se i hrapavost površine, što je vidljivo iz grafa na slici 14.
Treba napomenuti da se zbog grube obrade površine hrapavost mjerila u više točaka za svaku promjenu dubine obrade i za svaki prepust te je na kraju uzeta srednja vrijednost hrapavosti i za Ra i za Rz.

5. Zaključak

Kod većeg prepusta (210 mm) primijećene su veće vrijednosti vibracija (i RMS i PEAK) u usporedbi s manjim prepustom (80 mm). Osim toga veći prepust rezultirao je povećanjem hrapavosti površine (Ra i Rz su u prosjeku veće vrijednosti).
Nagli trenutni udar vibracija dogodio se pri dubini obrade od 1 mm i 1,5 mm, a nakon čega je, povećanjem dubine rezanja došlo do smirivanja vibracija.
Odnos vibracija i hrapavosti površine pokazuje da se povećanjem vibracija pogoršala I kvaliteta obrađene površine, odnosno došlo je do povećanja hrapavosti.

6. Reference

[1] K. Khalili; M. Danesh. (2013.) Investigation of overhang effect on cutting tool vibration for tool condition monitoring. The University of Birjand, Birjand, Iran (ISSN ONLINE 2424-4635)

[2] Caixu YUE; Haining GAO; Xianli LIU; Steven Y. LIANG; Lihui WANG. (2019.) A review of chatter vibration research in milling. Chinese Society of Aeronautics and Astronautics. Production and hosting by Elsevier Ltd. This is an open access article under the CC BY-NC-ND license (http://creativecommons.org/licenses/by-nc-nd/4.0/).

[3] Henrik Ĺkesson; Tatiana Smirnova; Lars HÍkansson; Thomas Lagö; Ingvar Claesson. (2009.) Investigation of the Dynamic Properties of a Milling Tool Holder. Blekinge Institute of Technology. (ISSN: 1103-1581 Research report No. 2009:07)

[4] DMG MORI. (2019.) Tips on Machining Vol. 28How to prevent chatter in long-overhang face milling. Machining know-how/knowledge

[5] J. Munoa; X. Beudaert; Z. Dombovari; Y. Altintas; E. Budak; C. Brecher; G. Stepan. (2016.) Chatter suppression techniques in metal cutting. CIRP Annals - Manufacturing Technology 65 (2016) 785–808

[6] Amel Karić; Arnel Jašarević. (2023.) Analiza uticaja parametara obrade i vibracija na kvalitet obrađene površine pri čeonom glodanju tanke ploče od aluminijuma. 13. Naučno-stručni skup sa međunarodnim učešćem, "QUALITY 2023", Neum, B&H, 19. – 21. juni 2023.

Društvo za tehniku zavarivanja Slavonski Brod

13. Međunarodno znanstveno-stručno savjetovanje SBZ 2025

„STROJARSKE TEHNOLOGIJE U IZRADI ZAVARENIH KONSTRUKCIJA I PROIZVODA, SBZ 2025."
Slavonski Brod, 08. i 09. 05. 2025.

Artificial Intelligence in the Optimization of Parameters and Cutting Layouts in Thermal Cutting Processes

Katić[1,*], T. Šarić[1], G. Šimunović[1]

[1]Mechanical Engineering Faculty in Slavonski Brod, University of Slavonski Brod, Croatia

[*] Corresponding Author. E-mail: kkatic@unisb.hr

Abstract

In modern industry, the optimization of thermal cutting processes plays an important role in increasing production efficiency, reducing costs, and ensuring effective material utilization. Since the development of artificial intelligence has a significant impact on manufacturing, this paper presents an overview of thirty available AI-based tools used for the optimization of nesting and cutting parameters in plasma, oxy-fuel, and laser cutting processes. The focus is placed on tools that automate complex nesting processes, adapting cutting paths to the geometry of parts and minimizing waste. Additionally, tools that enable the optimization of key technological cutting parameters — such as speed, power, gas pressure, and nozzle height — are analyzed with the aim of achieving greater precision and reducing unwanted thermal deformations. A dedicated chapter explains how artificial intelligence functions in this application, from machine learning and evolutionary algorithms to models that analyze large datasets in order to optimize processes and provide automatic recommendations. The comparative analysis of the presented tools highlights their significant potential to improve production processes, while also recognizing challenges related to system integration and the need for additional user training, and opens up opportunities for further development and application of these technologies in industrial practice.

Keywords: artificial intelligence, cutting optimization, nesting, thermal cutting processes

1. Introduction

In recent years, the manufacturing industry has experienced a significant transformation driven by the rapid advancement and integration of artificial intelligence (AI) technologies. Among the various sectors influenced by this evolution, thermal cutting—comprising plasma, oxy-fuel, and laser cutting—stands out as one of the most promising areas for AI-driven optimization. As global competition intensifies, manufacturers are under increasing pressure to reduce costs, minimize material waste, increase product quality, and improve overall process efficiency. Thermal cutting

plays a central role in the production of metal components, and its performance is directly tied to the precise configuration of numerous parameters, such as cutting speed, power, gas pressure, and nozzle height. Traditional approaches to managing these parameters often rely on manual tuning or basic automation, which can lead to suboptimal performance, variability in quality, and higher operational costs. AI introduces new paradigms for process control and decision-making in thermal cutting. By harnessing the power of machine learning, deep learning, computer vision, and evolutionary algorithms, AI enables real-time data analysis, predictive modeling, and adaptive regulation of process variables. Furthermore, AI systems can automate the complex task of nesting — the optimal arrangement of parts on raw material — which is essential for maximizing material utilization and minimizing waste. This is particularly relevant in industries such as aerospace, automotive, shipbuilding, and heavy machinery, where high material efficiency and tight tolerances are crucial. This paper investigates the role of AI in the dual optimization of nesting layouts and cutting parameters, offering a comprehensive review of thirty state-of-the-art software tools currently available on the market. These tools employ a variety of AI techniques, including support vector machines (SVM), long short-term memory (LSTM) networks, convolutional neural networks (CNN), reinforcement learning, genetic algorithms (GA), and hybrid models, each contributing to process improvements in unique ways. The study aims to provide a comparative analysis of these tools, focusing on their technical capabilities, adaptability to different production environments, and overall impact on key performance indicators such as cutting accuracy, material efficiency, and production time. The significance of this research lies in its potential to inform practitioners, researchers, and decision-makers about the current state and future direction of AI-driven thermal cutting solutions. By understanding the capabilities and limitations of available tools, industries can make informed investments, accelerate their digital transformation, and move closer to achieving smart manufacturing systems. Moreover, the study addresses the practical challenges associated with AI implementation, such as data requirements, system integration, infrastructure needs, and workforce training - all of which are critical factors for successful deployment. Ultimately, this paper contributes to the ongoing discourse on intelligent manufacturing by highlighting how AI technologies can enhance process control, reduce resource consumption, and support the transition to more sustainable and autonomous production systems.

2. Fundamentals of the Cutting Process

Thermal cutting technologies represent fundamental processes in modern material processing, enabling the separation of materials through precise directing of a heat source. This chapter presents the three most commonly used technologies – plasma, gas (oxygen), and laser cutting – which differ in their physical principles, energy requirements, and fields of application. Each of these methods has specific advantages and challenges, depending on the type of material, thickness, required precision, and industrial conditions. Their analysis provides a foundation for understanding the potential for optimization through artificial intelligence in the following chapters of the paper. Plasma cutting uses

ionized gas to melt and remove material. It enables precise cutting of thicker metals at lower costs [1, 2]. The methods differ as follows: standard (nitrogen, oxygen, argon-hydrogen), water-injected, underwater, and precision (0.5–25 mm) [3, 4]. Air is inexpensive but causes oxidation, while inert gas mixtures offer better stability and cut cleanliness [3]. Secondary gases increase energy density and reduce slag formation [2]. Gas (oxy-fuel) cutting is used for carbon and low-alloy steels. The material is heated with a flame (acetylene, propane, hydrogen), after which oxygen is injected to induce oxidation [5]. Advantages include low cost and the ability to cut thicker plates, while drawbacks involve a larger heat-affected zone and slower cut initiation. The use of hydrogen allows for faster heating and reduced heat input, while high-purity oxygen improves cutting speed and quality [6]. Laser cutting uses a focused beam to melt or vaporize the material. With the aid of gases such as oxygen or nitrogen, clean and precise cuts are achieved [7]. It is used in industries requiring micron-level accuracy [8, 9]. Fiber lasers (12–40 kW) enable fast and energy-efficient cutting of various materials [10, 11]. Ultrafast lasers reduce the heat-affected zone and allow processing of sensitive materials [12]. The integration of AI enables automatic adjustment of parameters and optimization of cutting layouts [13]. This technology supports sustainable manufacturing by reducing energy consumption and waste.

3. The Role of Artificial Intelligence in Cutting Processes

Artificial intelligence (AI) is increasingly taking on a key role in cutting technologies. Through machine learning and deep learning, AI analyzes data on temperature, speed, tool (e.g. electrodes and nozzles) wear, and cut quality, automatically adjusting parameters such as power, speed, and gas pressure [11]. Predictive models prevent thermal deformations, computer vision with CNN detects defects, and predictive maintenance boosts productivity [11]. Hybrid AI systems, digital twins, and generative design further expand capabilities [9]. Machine learning algorithms such as Random Forest and SVM detect tool wear with up to 99.9% accuracy, while CNN identifies microcracks with 95.1% precision [14, 15]. Genetic algorithms reduce energy consumption by 25%, and reinforcement learning enables autonomous control at frequencies up to 200 Hz [16, 17]. Unsupervised algorithms classify materials and detect anomalies. GAN models simulate optimal paths, while LSTM and transformers enable real-time analysis. Hybrid models (e.g., LSTM + SVM) reduce downtime by 40%, and material utilization increases up to 98% [17]. Although AI delivers high performance, challenges include the need for large datasets, GPU capacity (e.g., 16 GB), and high integration costs (Nature, 2024). The future points toward Edge AI (response time <5 ms) and quantum approaches for faster optimization. Evolutionary algorithms, especially GA (Genetic Algorithms), optimize parameters such as speed and feed rate [18]. In one-dimensional cutting problems and production planning, GA shortens time by up to 40% [19]. Differential Evolution (DE) yields better results in tool condition prediction [20], while combining GA with neural networks or the Taguchi method further improves accuracy [21]. Advanced methods include Pareto optimization, digital twins, and

quantum algorithms. Industrial applications are broad, and the future includes integration with IoT and generative design to reduce costs by up to 40% [18, 19, 20].

4. Artificial Intelligence Tools for Automated Nesting and Optimization of Cutting Parameters

In the context of modern industry, where high precision, shortened production cycles, and cost reduction are dominant priorities, artificial intelligence is becoming a key technology for enhancing thermal cutting processes [22]. The application of AI systems in this field enables significant technological and economic benefits, particularly in the areas of nesting process automation and optimization of cutting parameters, including tool movement speed, energy source power, working gas pressure, and nozzle height above the material [23]. The analysis presented in this chapter covers thirty available software solutions based on AI systems, focusing on tools with demonstrated capabilities for optimizing thermal cutting processes—specifically plasma, laser, and gas cutting [24]. The tools were selected based on clearly defined criteria, which include:

- The level of automation in the nesting process,
- The ability to automatically regulate key cutting parameters in real time,
- The application of predictive models for managing thermal deformations, and
- The adaptability of tools to various part geometries and material types.

The methodology used involved a review of the most widely available and utilized AI systems. The tools were classified and analyzed in tabular format, with a focus on their functional capabilities, advantages in industrial application, level of flexibility and accuracy, as well as the complexity of integration into existing production systems. This approach enables an objective evaluation of each solution and a comparison based on relevant technical and operational parameters. The goal of this analysis is to provide a systematic overview of currently available AI tools that support advanced control of cutting processes, and to assist users and decision-makers in industry in selecting the technology that best meets their technical and organizational needs.

The comparative analysis of AI tools is conducted with the goal of identifying solutions that best meet the needs of modern manufacturing in the field of thermal cutting. The analysis includes criteria that directly affect cut quality, process efficiency, and material usage economy. The first criterion relates to nesting functionalities, as an optimized layout of parts on the material reduces waste and enables more efficient use of raw materials [25]. The second criterion, automatic regulation of cutting parameters (speed, power, gas pressure, and nozzle height), is essential for process stability and result repeatability, especially in serial production [26]. The third aspect involves models for predicting and controlling thermal deformations, which ensure greater precision and reduce the need for additional finishing [23]. The fourth criterion – tool accuracy and flexibility – is important as it reflects the system's ability to adapt to various geometries and materials without compromising cut quality. By comparing these criteria, it becomes possible to select the tool that best fits the specific characteristics of a given technological process, production capacity, and market demands [27] (Table 1).

Table 1. Comparative Analysis of AI Tools

The name of the AI tool	Functionality of the tool	Automatic regulation of cutting parameters	Models for prediction and control of thermal deformations	Comparison of tool accuracy and flexibility
SigmaNEST [28]	Advanced nesting and regulation of all parameters	Yes	Yes	High accuracy, medium flexibility
NestFab [29]	Basic nesting without full parameter control	Partially	Partially	Medium accuracy, high flexibility
Cut Rite [30]	Advanced nesting and regulation of all parameters	Not	Yes	Medium accuracy and flexibility
ProNest [31]	Basic nesting without full parameter control	Yes	Partially	High accuracy, medium flexibility
Lantek Expert [32]	Advanced nesting and regulation of all parameters	Partially	Yes	Medium accuracy, high flexibility
AlmaCAM Nest [33]	Basic nesting without full parameter control	Not	Partially	Medium accuracy and flexibility
Optimation Nesting [34]	Advanced nesting and regulation of all parameters	Yes	Yes	High accuracy, medium flexibility
Deepnest [35]	Basic nesting without full parameter control	Partially	Partially	Medium accuracy, high flexibility
MyNesting [36]	Advanced nesting and regulation of all parameters	Not	Yes	Medium accuracy and flexibility
JetCAM Expert [37]	Basic nesting without full parameter control	Yes	Partially	High accuracy, medium flexibility
NestingWorks [38]	Advanced nesting and regulation of all parameters	Partially	Yes	Medium accuracy, high flexibility
TPA CAD/CAM Nesting [39]	Basic nesting without full parameter control	Not	Partially	Medium accuracy and flexibility
Metamation MetaCAM [40]	Advanced nesting and regulation of all parameters	Yes	Yes	High accuracy, medium flexibility
ESAB Columbus [41]	Basic nesting without full parameter control	Partially	Partially	Medium accuracy, high flexibility
FlexiNest [42]	Advanced nesting and regulation of all parameters	Not	Yes	Medium accuracy and flexibility

RadANest [43]	Basic nesting without full parameter control	Yes	Partially	High accuracy, medium flexibility
Thermoptimize [44]	Advanced nesting and regulation of all parameters	Partially	Yes	Medium accuracy, high flexibility
Hypertherm SureCut [45]	Basic nesting without full parameter control	Not	Partially	Medium accuracy and flexibility
CNCsoft Nest [46]	Advanced nesting and regulation of all parameters	Yes	Yes	High accuracy, medium flexibility
Smart2DCutting [47]	Basic nesting without full parameter control	Partially	Partially	Medium accuracy, high flexibility
Xteg Nest AI [48]	Advanced nesting and regulation of all parameters	Not	Yes	Medium accuracy and flexibility
Hexagon RADAN [49]	Basic nesting without full parameter control	Yes	Partially	High accuracy, medium flexibility
PlasmaSensAI [50]	Advanced nesting and regulation of all parameters	Partially	Yes	Medium accuracy, high flexibility
TopNest [51]	Basic nesting without full parameter control	Not	Partially	Medium accuracy and flexibility
AI NestPro [52]	Advanced nesting and regulation of all parameters	Yes	Yes	High accuracy, medium flexibility
OptiCut AI [53]	Basic nesting without full parameter control	Partially	Partially	Medium accuracy, high flexibility
TrueShape Nesting [54]	Advanced nesting and regulation of all parameters	Not	Yes	Medium accuracy and flexibility
AI-Cut Optimizer [55]	Basic nesting without full parameter control	Yes	Partially	High accuracy, medium flexibility
NestMaster AI [56]	Advanced nesting and regulation of all parameters	Partially	Yes	Medium accuracy, high flexibility
LaserCut AI Studio [57]	Basic nesting without full parameter control	Not	Partially	Medium accuracy and flexibility

The implementation of AI tools in industrial practice brings a range of challenges, but also significant potential for improving manufacturing processes. A study by Zavodna et al. [58] shows that companies successfully implementing AI tools achieve a reduction in operational costs by 15–30% and a productivity increase of 22% thanks to predictive maintenance and optimization of production parameters. Additionally, AI systems enable rapid adaptation of production lines to different materials, increasing process flexibility by 73% without the need for manual intervention. One of the key challenges is the integration of AI tools into existing systems, which often requires additional

adjustments to both software and hardware infrastructure. According to the U.S. Department of Education Report [59], beyond technical compatibility, there is also a need for user training and education, as effective use of AI systems requires an understanding of their algorithms and capabilities. Security aspects must not be overlooked either – data protection, system resilience to errors, and clearly defined organizational responsibilities are crucial factors when introducing new technologies. Despite the challenges, development prospects remain highly positive [60]. It can be concluded that ongoing research and the increasing availability of computing power contribute to AI tools becoming more accurate, faster, and more accessible, opening the door to further optimization of cutting and manufacturing processes as a whole.

4. Conclusion

This paper presents a concise overview of contemporary AI tools applicable to the optimization of nesting processes and technological parameters in thermal cutting. The focus is placed on analyzing functionality, efficiency, and integration potential within an industrial environment. Special attention is given to the tools' ability to automatically manage parameters such as cutting speed, power, nozzle height, and gas pressure, as well as to predict and reduce thermal deformations in materials. Significant differences were observed among the tools in terms of accuracy, adaptability to various production conditions, and the level of integration into existing systems. While most available solutions are based on traditional optimization algorithms, the application of machine and deep learning is still in development, yet it shows great potential for future improvements in cutting processes. The limitations of this paper stem from its reliance on available technical data and promotional materials from manufacturers, as well as the absence of experimental validation under controlled conditions. Despite this, the paper contributes by providing a systematic overview that can serve as a foundation for professionals and researchers in the selection, evaluation, and further development of AI tools in this technological field. Furthermore, the paper opens up space for future research aimed at experimental performance validation, return on investment (ROI) analysis, development of standardized tool selection criteria, and deeper integration of machine learning methods within the context of adaptive control of thermal cutting processes.

5. Literatura / Izvori

[1] Nemchinsky, Valerian. (2017). *Heat Transfer in Plasma Arc Cutting*. https://doi.org/10.1007/978-3-319-32003-8_28-1 **(book chapter)**

[2] Adhikari, Babu Ram & Khanal, Raju. (2013). *Introduction to the Plasma State of Matter*. *Himalayan Physics, 4* (60). 10.3126/hj.v4i0.9430. **(book)**

[3] Kudrna, Lukáš; Fries, Jiri; Merta, Marek. (2019). Influences on plasma cutting quality on CNC machine. *Multidisciplinary Aspects of Production Engineering, 2*, 108–117. https://doi.org/10.2478/mape-2019-0011 **(journal article)**

[4] Karthick, M.; Anand, P.; Meikandan, M.; Sekar, S.; Natrayan, L.; Bobe, K. (2022). Optimization of plasma arc cutting parameters on machining of Inconel 718 superalloy. *Journal of Nanomaterials, 2022*(1), 7181075. **(journal article)**

[5] Eckert Cutting. (2024a). *Oxygen cutting technology*. Retrieved April 14, 2025, from https://eckert-cutting.com/technologies/oxygen-cutting.html **(web source, accessed: 14. April 2025.)**

[6] Eckert Cutting. (2024b). *Hydrogen – A new potential for oxy-fuel cutting technology*. Retrieved April 14, 2025, from https://eckert-cutting.com/knowledge-base/hydrogen-a-new-potential-for-oxy-fuel-cutting-technology.html **(web source, accessed: 2. April 2025.)**

[7] ETASR. (2023). *Laser cutting: Principle and applications*. Retrieved April 14, 2025, from https://etasr.com/index.php/ETASR/article/view/6733 **(web source, accessed: 2. April 2025.)**

[8] Hymson Laser. (2025). *Top trends in laser metal cutting machines for 2025*. Retrieved April 14, 2025, from https://www.hymsonlaser.net/article/top-trends-in-laser-metal-cutting-machines-for-2025.html **(web source, accessed: 2. April 2025.)**

[9] AIMSPress. (2025). *Laser cutting in high-precision industries*. Retrieved April 14, 2025, from https://www.aimspress.com/article/doi/10.3934/matersci.2025002?viewType=HTML **(web source, accessed: 2. April 2025.)**

[10] Scoop Market. (2025). *Laser cutting machine statistics*. Retrieved April 14, 2025, from https://scoop.market.us/laser-cutting-machine-statistics/ **(web source, accessed: 2. April 2025.)**

[11] ScienceDirect. (2024). *AI-based optimisation of total machining performance: A review*. Retrieved April 14, 2025, from https://www.sciencedirect.com/science/article/pii/S1755581724000105 **(web source, accessed: 2. April 2025.)**

[12] Fero Lézervágás. (2025). *The future of laser cutting: Innovations, trends, and transformations*. Retrieved April 14, 2025, from https://fero-lezervagas.hu/en/the-future-of-laser-cutting-innovations-trends-and-transformations/ **(web source, accessed: 2. April 2025.)**

[13] The Fabricator. (2025). *The rapid evolution of modern laser cutting technology*. Retrieved April 14, 2025, from https://www.thefabricator.com/thefabricator/article/lasercutting/the-rapid-evolution-of-modern-laser-cutting-technology **(web source, accessed: 2. April 2025.)**

[14] University of Huddersfield. (2024). *Prediction of cutting force via machine learning: State of the art*. Retrieved April 14, 2025, from https://pure.hud.ac.uk/en/publications/prediction-of-cutting-force-via-machine-learning-stat-of-the-art **(web source, accessed: 2. April 2025.)**

[15] ASTRJ. (2024). *Application of machine learning algorithms for recognizing the wear of the cutting tool*. Retrieved April 14, 2025, from https://www.astrj.com/Application-of-machine-learning-algorithms-for-recognizing-the-wear-of-the-cutting,196706,0,2.html **(web source, accessed: 2. April 2025.)**

[16] AIML Programming. (2024). *AI-enabled metal cutting optimization*. Retrieved April 14, 2025, from https://aimlprogramming.com/services/ai-enabled-metal-cutting-optimization/ **(web source, accessed: 2. April 2025.)**

[17] Plataine. (2024). *FabricOptimizer: Cutting & kitting optimization*. Retrieved April 14, 2025, from https://www.plataine.com/application/fabricoptimizer-cutting-kitting-optimization/ **(web source, accessed: 2. April 2025.)**

[18] Pustejovsky, Zbynek; Pekaric, Miroslav. (2011). Application of genetic algorithms for optimization of cutting parameters in turning process. *Journal of Production Engineering, 14*(3), 11–14. https://scindeks.ceon.rs/article.aspx?artid=0354-68291103011P **(journal article)**

[19] Cubonova, Nikola; Dodok, Tomáš; Sagova, Zuzana. (2019). Application of genetic algorithm for scheduling optimization. *Scientific Journal of Silesian University of Technology. Series Transport, 104*, 153–161. https://doi.org/10.20858/sjsutst.2019.104.15 **(journal article)**

[20] Ali, M. Y.; Sharma, V.; Zitoune, R. (2021). Multi-objective optimization of machining parameters using differential evolution algorithm. *Measurement, 177*, 109280. https://doi.org/10.1016/j.measurement.2021.109280 **(journal article)**

[21] Mansour, Ahmed; Gabriel, Khaled. (2013). Optimization techniques for machining operations. *International Journal of Modern Manufacturing Technologies, 5*(1), 56–62. http://ijmmt.ro/vol5no12013/Mansour_Gabriel_1.pdf **(journal article)**

[22] Altuğ, Mehmet; Söyler, Hüseyin. (2023). Optimization with artificial intelligence of the machinability of Hardox steel, which is exposed to different processes. *Sci Rep, 13*, 14100. https://doi.org/10.1038/s41598-023-40710-8 **(journal article)**

[23] Zhang, Lei; Wang, Hong. (2024). Application of artificial intelligence in energy management systems. *E3S Web of Conferences, 2024*(70), 06015. https://doi.org/10.1051/e3sconf/20247006015 **(conference paper)**

[24] Kumar, Rakesh; Singh, Ankit. (2024). Artificial intelligence approaches for predictive power consumption modeling in machining – Short review. *E3S Web of Conferences, 540*, 06015. https://doi.org/10.1051/e3sconf/202454006015 **(conference paper)**

[25] Van der Veen, Bart. (2024). *Developing a plate nesting algorithm for a steel processing company*. University of Twente Student Theses, University of Twente. https://essay.utwente.nl/102916/1/Final%20version.pdf **(master's thesis)**

[26] Outemsaa, Omar; El Farissi, Omar; Hamouti, Lahcen. (2024). Cutting parameters optimization to minimize surface roughness and carbon emission in turning process using AI tools and intelligent algorithms. *International Journal on Technical and Physical Problems of Engineering (IJTPE), 16*(2), 7–16. https://www.iotpe.com/IJTPE/IJTPE-2024/IJTPE-Issue59-Vol16-No2-Jun2024/2-IJTPE-Issue59-Vol16-No2-Jun2024-pp7-16.pdf **(journal article)**

[27] Grigoriev, Sergey N.; Fedorov, Sergey V.; Hamdy, Khaled. (2019). Materials, properties, manufacturing methods and cutting performance of innovative ceramic cutting tools – a review. *Manufacturing Review, 6*, 19. https://doi.org/10.1051/mfreview/2019016 **(journal article)**

[28] SigmaTEK Systems. (n.d.). *SigmaNEST*. https://www.sigmanest.com/en **(web source, accessed: 2. April 2025.)**

[29] Efficient Software Ltd. (n.d.). *NestFab*. https://www.nestfab.com/ **(web source, accessed: 2. April 2025.)**

[30] HOMAG Group. (n.d.). *Cut Rite cutting optimization software*. https://www.homag.com/en/product-detail/software/work-preparation/cut-rite-cutting-optimization-software **(web source, accessed: 2. April 2025.)**
[31] Hypertherm, Inc. (n.d.). *ProNest CNC part nesting software*. https://www.hypertherm.com/hypertherm/pronest/pronest-cadcam-nesting-software/ **(web source, accessed: 2. April 2025.)**
[32] Lantek. (n.d.). *Lantek Expert*. https://www.lantek.com/us/nesting-cad-cam-2d-software **(web source, accessed: 2. April 2025.)**
[33] Alma. (n.d.). *AlmaCAM Nest*. https://almacam.com/alma-an-expert-in-nesting-software-for-cutting/ **(web source, accessed: 2. April 2025.)**
[34] Optimation. (n.d.). *Optimation Nesting Software*. https://optimation.com/ **(web source, accessed: 2. April 2025.)**
[35] Deepnest. (n.d.). *Deepnest*. https://deepnest.io/ **(web source, accessed: 2. April 2025.)**
[36] Efficient Software Ltd. (n.d.). *MyNesting*. https://www.mynesting.com/ **(web source, accessed: 2. April 2025.)**
[37] JETCAM International. (n.d.). *JETCAM Expert*. https://www.jetcam.net/ **(web source, accessed: 2. April 2025.)**
[38] Geometric Americas, Inc. (n.d.). *NestingWorks*. https://www.solidworks.com/partner-product/nestingworks **(web source, accessed: 2. April 2025.)**
[39] TPA S.p.A. (n.d.). *CADnesting*. https://www.tpaspa.com/cadnesting **(web source, accessed: 2. April 2025.)**
[40] Metamation. (n.d.). *MetaCAM CAD CAM*. https://metamation.com/metamation-metacam-cad-cam/ **(web source, accessed: 2. April 2025.)**
[41] ESAB. (n.d.). *Columbus CAD/CAM Nesting Software*. https://esab.com/us/nam_en/products-solutions/product/cutting-automation/software/columbus/ **(web source, accessed: 2. April 2025.)**
[42] ThinkSAi. (n.d.). *Flexi*. https://www.thinksai.com/ **(web source, accessed: 2. April 2025.)**
[43] Hexagon. (n.d.). *RADAN*. https://www.radan.com/ **(web source, accessed: 2. April 2025.)**
[44] Thermoptimize. (n.d.). *Thermoptimize*. https://thermoptimize.com/ **(web source, accessed: 2. April 2025.)**
[45] Hypertherm, Inc. (n.d.). *SureCut*. https://www.hypertherm.com/ **(web source, accessed: 2. April 2025.)**
[46] CNCsoft. (n.d.). *CNCsoft Nest*. https://www.cncsoft.com/ **(web source, accessed: 2. April 2025.)**
[47] Smart2DCutting. (n.d.). *Smart2DCutting*. https://www.smart2dcutting.com/ **(web source, accessed: 2. April 2025.)**
[48] Xteg. (n.d.). *Nest AI*. https://www.xteg.com.au/ **(web source, accessed: 2. April 2025.)**
[49] Hexagon. (n.d.). *RADAN*. https://www.radan.com/ **(web source, accessed: 2. April 2025.)**
[50] PlasmaSensAI. (n.d.). *PlasmaSensAI*. https://plasmasensai.com/ **(web source, accessed: 2. April 2025.)**

[51] TopNest. (n.d.). *TopNest*. https://www.topnest.com/ **(web source, accessed: 2. April 2025.)**
[52] AI NestPro. (n.d.). *AI NestPro*. https://www.ainestpro.com/ **(web source, accessed: 2. April 2025.)**
[53] OptiCut. (n.d.). *OptiCut AI*. https://www.opticut.com/ **(web source, accessed: 2. April 2025.)**
[54] TrueShape. (n.d.). *TrueShape Nesting*. https://www.trueshape.com/ **(web source, accessed: 2. April 2025.)**
[55] AI-Cut. (n.d.). *AI-Cut Optimizer*. https://www.aicutoptimizer.com/ **(web source, accessed: 2. April 2025.)**
[56] NestMaster AI. (n.d.). *NestMaster AI*. https://www.nestmaster.ai/ **(web source, accessed: 2. April 2025.)**
[57] LaserCut AI Studio. (n.d.). *LaserCut AI Studio*. https://www.lasercut.ai/ **(web source, accessed: 2. April 2025.)**
[58] Zavodna, Lucie; Ueberwimmer, Margarethe; Frankus, Elisabeth. (2024). Barriers to the implementation of artificial intelligence in small and medium sized enterprises: Pilot study. *Journal of Economics and Management, 46*, 331–352. https://doi.org/10.22367/jem.2024.46.13 **(journal article)**
[59] U.S. Department of Education. (2023). *Artificial intelligence and the future of teaching and learning: Insights and recommendations*. Washington, DC: Office of Educational Technology. https://www.ed.gov/sites/ed/files/documents/ai-report/ai-report.pdf **(government report)**
[60] Cloud Security Alliance. (2024). *AI organizational responsibilities: Core security responsibilities*. https://cloudsecurityalliance.org/artifacts/ai-organizational-responsibilities-core-security-responsibilities **(web source, accessed: 2. April 2025.)**

Društvo za tehniku zavarivanja Slavonski Brod

13. Međunarodno znanstveno-stručno savjetovanje SBZ 2025

„STROJARSKE TEHNOLOGIJE U IZRADI ZAVARENIH KONSTRUKCIJA I PROIZVODA, SBZ 2025."
Slavonski Brod, 08. i 09. 05. 2025.

Automatic Classification of Welding Defects Using Neural Network

I. Petrović[1,*], M. Stojkov[2], I. Samardžić[2], M. Mišić[3], M. Lovrić[4]

[1]Faculty of Electrical Engineering, Computer Science and Information Technology Osijek, Josip Juraj Strossmayer University of Osijek, Croatia
[2]Mechanical Engineering Faculty in Slavonski Brod, University of Slavonski Brod, Croatia
[3]High School Dugo Selo
[4]Industrial High School Slavonski Brod

[*] Corresponding Author. E-mail: ipetrovic81@gmail.com

Abstract

Technological development accompanied the need to get a high-quality welding. In this research, an automatic technique is introduced to detect, recognize and classify welding defects in radiographic (x-ray) images, using texture features. Image processing techniques, including converting color images to grayscale, filtering and resizing images were applied to help in the image array of weld images and welding defect detection. Therefore, a proposed program was built in-house to automatically classify and recognize the most common types of welding defects met in practice. The introduced technique has been tested on eleven welding defects which are: center line crack, cap undercut, elongated slag lines, lack of interpass fusion, lack of root penetration, lack of side wall fusion, misalignment, root crack, root pass aligned, root undercut, and transverse crack. The introduced technique can find promising application of digital image processing technique to the field of welding defect inspection compared with traditional methods.

Keywords: Radiographic image, Welding defects, Neural network, Image processing

1. Introduction

Quality control of manufactured products has become one of the main objectives of production processes. Inspection of welded structures is essential to ensure that the quality of welds meets the requirements of the design and operation, thus, to assure safety and reliability. Although it is one of the oldest techniques of non-destructive inspection, radiography is still accepted as essential for the control of welded joints in many industries such as petroleum, nuclear, naval, chemical, and aeronautical. It is particularly important for critical applications, where weld failure can be catastrophic, such as in pressure vessels, load-bearing structural members, and power plants [1].

The reliable detection of defects is one of the most important tasks in nondestructive tests, mainly in the radiographic test, since the human factor still has a decisive influence on the evaluation of defects in the film. Radiographic inspection is a well-established testing and quality control method to detect weld defects [2].
Flaws resulted from welding operations are detrimental to the integrity of the fabricated artifacts/structures. Commonly seen weld flaws include lack of fusion, lack of penetration, gas holes, porosities, cracks, inclusions, etc. Of course, some flaw types might appear more often than others for a particular welding process. To maintain the desirable level of structural integrity, welds must be inspected according to the established standard. The results of weld inspection also provide useful information for identifying the potential problems in the fabrication process, which are necessary for improving the welding operations. In the current industrial practice, weld inspection is often carried out by certified inspectors; Previous studies show that the capability of improving inspection systems depending on computer-aids through radiographic images to improve the objectivity and productivity of weld inspection operations [3].

2. Classification of welding defects

The method of welding defect classification could include feature extraction [1-8], thermal image analysis and ultrasonic inspection [9-11], and image histogram [12-16].

2.1. Feature extraction

An automatic detection system to recognize welding defects in radiographic images was described by Vilar et al. [4]. They aimed to analyze ANN modifying the performance function for different neurons in the input and hidden layer in order to obtain a better performance on the classification stage. Zapata was described as an automatic system et al. [1, 2], to detect, recognize, and classify welding defects in radiographic images and to evaluate the performance for two neuro-classifiers based on an artificial neural network (ANN) and an adaptive-network-based fuzzy inference system (ANFIS). An expert vision system for automatic inspection is introduced by Shafeek et al. [5-6], to detect and to assess the welding defects of gas pipelines from the radiographic images. This system has many advantages such as enhancing the captured images and eliminating the loss of images details, so this system is considered very effective where it helps to make the defects more clearly.
An automatic control and inspection of welding defects is introduced by Yahia et al. [7], using edge detection method of radiographic images, based essentially on the use of a multilayer perceptron, aiming to classify and to increase the successful recognition default percentage. A new approach for feature extraction from radiography images acquired with gamma rays was proposed by Kasban et al. [8], in order to detect weld defects. Neural networks are used for matching features in the proposed approach. The experimental results show that the proposed approach can be used in a reliable way for automatic detection from radiography images in the presence of noise and blurring.

2.2 Image Histogram

A feature selection methodology is proposed by Garcia-Allende et al. [12], to solve the uncertainty regarding the selection of the optimum spectral band, which allows the employment of the line-to-continuum method for on-line welding diagnostics. Field test results have been conducted to demonstrate the feasibility of the solution. Daillant et al. [13], proposed a complete acquisition and processing line of weld radiographies, from which must be highlighted cavity shaped defects. They presented a study of three trend removal methods allowing improving the signal/noise ratio of the edge's pictures. The segmentation is derived from the edges picture by the mean of a constrained watershed algorithm. A new approach that allows automatic weld defect detection and classification based in the combined use of principal component analysis and an artificial neural network is proposed by Mirapeix et al. [14]. Arc-weld tests on stainless steel were reported, showing a good correlation between the ANN outputs and the classical interpretation of the electronic temperature profile. Therefore, and due to the problems associated with manual detection, this work aims to classify automatically welding defects using image histogram method via neural network.

3.Theoretical background

This work depends on theoretical background to enhance the practical part of it, which consists of welding and its defects, computer vision and its related process, preprocessing for image, and artificial neural network.

3.1 Welding and welding defects

Industries, such as power plants, oil refineries, chemical plants, and food processing plants depends on the networks of pipe-lines. Today, most pipes are joined by welding, but this was not always true, for until about 35 years ago pipe was joined by screw threads or by bolted flanged joints. Welding now considered the best method for connecting pipes, is used even in the most demanding high-pressure and high temperature service. Only high-quality pipe welds are acceptable in modern industry; for the failure of a pipe weld not only can disrupt the operation of a plant, but it can also be the cause of a serious accident with the possible loss of life and property [15]. Arc welding is a welding process in which the heat is generated by an electric arc between an electrode and the work. In DC welding, the work is generally the positive pole with the electrode the negative pole, but reverse polarity may be used in which the work is the negative pole, and the electrode is the positive pole. Welding pipelines is an important process to join pipelines and its accessories, defects due to welding could occur and the need for methods to test welding process is a must to achieve quality control and quality assurance. The advantages of this process are:

a) the most efficient way to join metals.
b) lowest cost joining method.
c) affords lighter weight through better utilization of materials.

d) joins all commercial metals.
e) Provides design flexibility.
Welding discontinuities may be divided into three board classifications: Design related, welding process related and metallurgical related. Include problems with design or structural details, choice of the wrong type of weld joint for a given application, or undesirable changes in cross section.
Defects due to process itself are undercut, slag inclusions, overlap, and porosity, tungsten inclusions, backing peace left on shrinkage voids, oxide inclusions, lack of penetration, craters, melt-through, spatter, arc strikes, under fill, and lack of fusion [16].

3.2 Computer vision and image process

Developments in image processing, computer vision, artificial intelligence and other related fields have significantly improved the capability of visual inspection techniques. It was reported that about 60–90% of all existing machine vision applications were classified as automated visual inspection [6].
Images are stored in computers as a 2-dimensional array of numbers. The numbers can correspond to different information such as color or gray scale intensity, luminance, chrominance, and so on. Before we can process an image on the computer, we need the image in digital form.
Image processing is the first stage in most computer vision applications, namely the use of image processing to preprocess the image and convert it into a form suitable for further analysis.

3.3 Image pre-processing

3.3.1 Noise reduction

Digital image processing techniques are employed to lessen the noise effects and to improve the contrast, so that the principal objects in the image can be more apparent than the background. The gray level values of the noise pixels are much higher than those of their immediate neighbors. As noise is characterized as high frequency values, low pass filtering methods, like a median filter, can be used to effectively remove the noise pixels. Median filter is a spatial filtering operator; it uses a 2D mask applied to each pixel in the input image. The median filtering allows mainly the attenuation/elimination of noise. Indeed, the acquired images should pass through a stage of image filtering in order to remove distracting and useless information [8]. The application of a low-pass filter is used to remove noise in radiographic images.

3.3.2 Contrast enhancement

Radiographic images usually have poor contrasts and a lack of detail. The target of contrast enhancement is to improve the radiographic images quality by highlighting the useful information while leaving the unimportant information intact. In the original radiographic image, the distribution

of gray levels is highly skewed towards the darker side. Defects in these areas can hardly be recognized; therefore, it is desirable to stretch the histogram distribution to an evenly distributed one, like a rectangular shape instead of a skewed shape. The histogram equalization algorithm proportionally modifies the original gray level values to the range of 0 and 255.

3.3.3 Image histogram

Histogram is a graph showing the number of pixels in an image at each different intensity value found in that image, as shown in Fig.1. For an 8-bit gray scale image, there are 256 intensity values are possible. The intensity histogram features are first order statistics. The histogram is plotted from the image and from the histogram four features are extracted that can discriminate between different classes of x-ray images. Four features such smoothness, uniformity, third moment and entropy is calculated using intensity histogram graph. The histogram graph is constructed by counting the number of pixels at each intensity value [19].

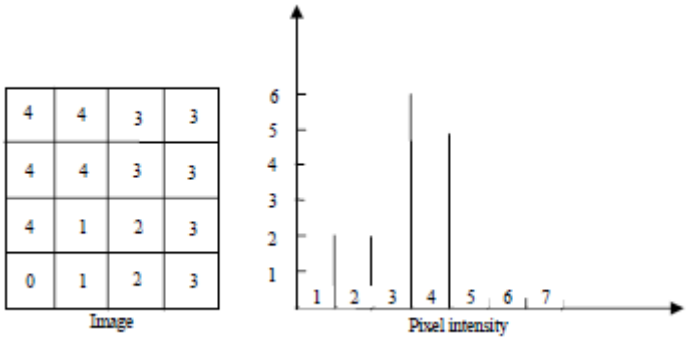

Fig.1. Simple image with histogram

3.4 Artificial Neural Network (ANN)

A neural network is an interconnected assembly of simple processing elements, units or nodes, whose functionality is loosely based on the animal neuron. The processing ability of the network is stored in the inter-unit connection strengths, or weights, obtained by a process of adaptation to, or learning from, a set of training patterns. Recently, there has been an increased interest on neural research; in the next some of those researches as an example for detecting welding defect by using neural network. ANNs are machine learning programs based on neuron like building blocks similar to the neurons in the human brain. Most of the research and applications of neural networks involve feed-forward networks trained by the back-propagation algorithm. These ANNs usually undergo a training phase by feeding it a set of inputs with known outcome, and then back propagating the known results to adjust the weights among the neural elements. After many iterations of training, called epochs, the NN is able to detect subtle patterns in large data sets and make predictions based on what it has

learned through past observations [18]. Feed forward neural network architecture was selected based on the flexibility and applicability of the approach in a variety of problems [20].

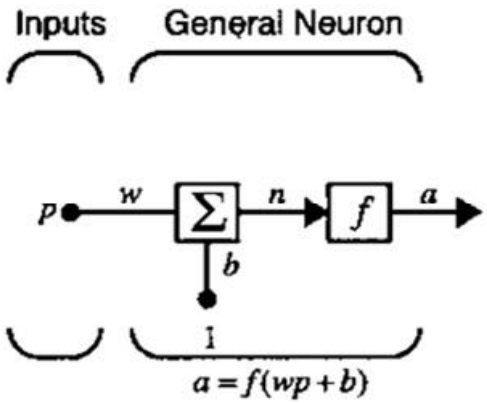

Fig.2 Network procedure

Where: *p* is an input, weight (*w* = *wp*) and *b* are the bias (*offset*). It's like a weight except that it has a constant input of 1. A neuron may have or may not have a bias. Summer output (*n*) (net input), transfer function (activation function) (*f*) is chosen by the designer, neuron output (*a*), and w and b are adjustable scalar parameters of the neuron (by a learning rule).
The network shown in Fig.2 can be described as follows:
Back-propagation: The back-propagation (gradient descent) algorithm and the more sophisticated variants described, are used for training.
Multilayer: The neurons are arranged in layers, with input, hidden and output layers.
Perceptions: The neurons each have a transfer function, either hard limit, linear, sigmoid or tanh.
Supervised: The networks are trained with an example set of galaxies classified by humans.
Feed forward: The training has no effect on the input parameters, just the weights and biases.
Static: There is no time dependence in the network.

4. Experimental methodology

The quality of radiographic images is related to the technique employed, as well as the inspected material, as well as the choice of a standard filter for noise elimination. Film digitizing is a critical part of the weld recognition system. Hence, selecting optimized resolution of scanning and acceptable quality of digitizing plays an important role in whole system performance.
The radiographic films can be digitized by several systems according to ASME V [10]. The more common way of digitization is through scanners, which works with light transmission – usually called transparency adapters. Another method also used is image acquisition by camera CCD (Charge Couple Device).

In this case, the film is placed in a light box and the camera captures the digital image and transmits it for a computer. The system which described in this research is an inspection system for welding defects. The main elements of machine vision system are as follows:
a) image acquisition system,
b) lighting system, and
c) Data processing system, as shown in

Fig.3 Welding defects capturing system

4.1 Preprocessing of the image

After digitization of the films, it is very common to use a preprocessing stage, seeking mainly the attenuation/elimination of noise and contrast improvement.
The application of low pass filters is the more frequently used tool to remove noise in a radiographic image [21, 22].

4.2 Histogram Features

Observing the magnitude of the pixel values, it is found that the range of intensity varies from class to class. A better graph to show the range of variation is the histogram plot. The information derived from a histogram plot can be used as features for visual inspection. A representative sample (images for each case) was taken, and the corresponding histogram was plotted. Table 1 shows the output of the produced program for 7 samples of welding defects and their images with their histograms.

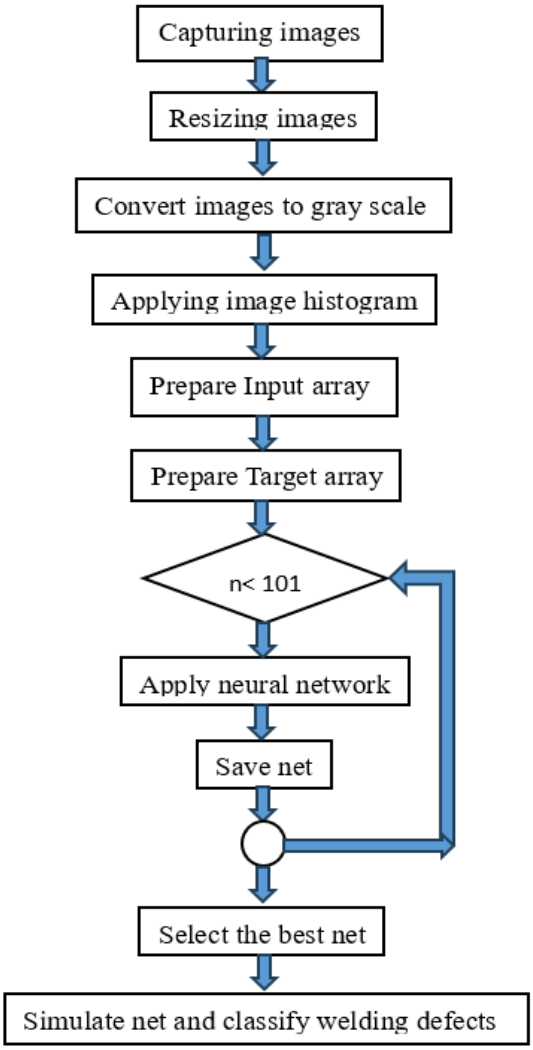

Fig.4 Block diagram of the procedure

Table 1. X ray images of welding defects and no defects

No.	Defect type	Image number	Image	Histogram
1	No defect	T0037	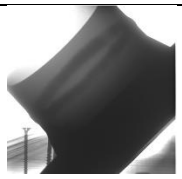	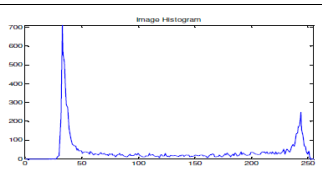

2	Lack of fusion	T0067	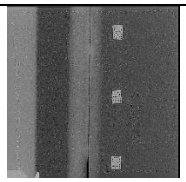	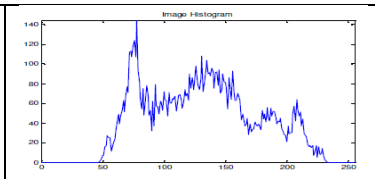
3	Porosity	T0129	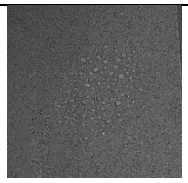	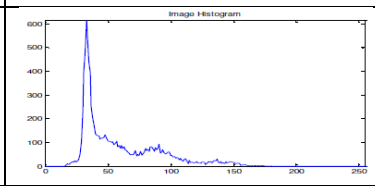
4	Undercut	T0215	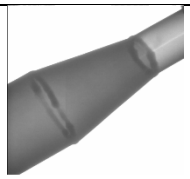	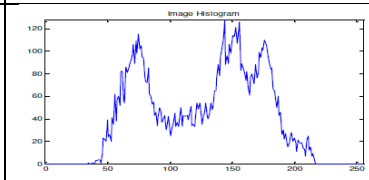
5	Cavity	T0242		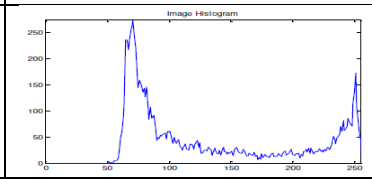
6	Slag	T0195	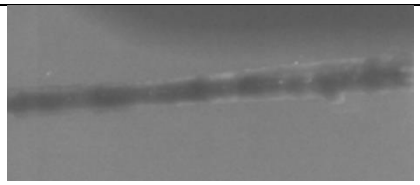	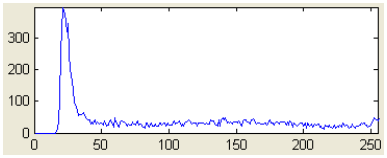
7	Crack	T0010	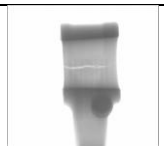	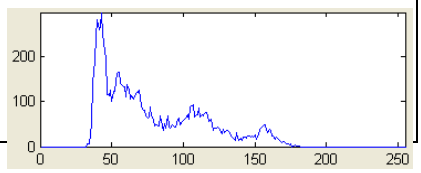

Thirty-eight radiographic films represent seven cases of welding defects that were collected in order to apply the proposed method of welding defect classification.

Radiographic films were holding on a backlighting then an image was acquired by a digital camera and saved to a file.

All radiographic images were cropped and resized using a commercial program from the captured image to form a total of 222 images. These images were classified to seven cases as mentioned before. In order to evaluate the effect of image resolution, these images were resized to be 100×100 pixels, 70×70 pixels, and the 50×50 pixels.

These images were loaded by software written specially for that work using Matlab package, to convert the colored images to gray scale image, and then filtered by a suitable method (Median filter). Image histogram was performed for each image using Matlab image processing toolbox and stored in an array called *input* array.

Target array was created so as each case was represented in one row. For example, case one 'Crack' is defined as: [1 0 0 0 0 0] and in case of two defects as case one and case four the array is defined as: [1 0 0 1 0 0 0 0 0]. The output dataset is an array of 222 × 7 (222 image × 7 cases) as follows:

$$T=\begin{bmatrix} 1 & 0 & 0 & 0 & 0 & 0 & 0 \\ 1 & 0 & 0 & 0 & 0 & 0 & 0 \\ :: & :: & :: & :: & :: & :: & :: \\ 0 & 1 & 0 & 0 & 0 & 0 & 0 \\ 0 & 1 & 0 & 0 & 0 & 0 & 0 \\ : & : & : & : & : & : & : \\ 0 & 0 & 0 & 0 & 0 & 0 & 1 \\ 0 & 0 & 0 & 0 & 0 & 0 & 1 \end{bmatrix}$$

A feed forward neural network with error back propagation algorithm was adopted for the neural network system as in Fig.5. Here it is used to classify welding defects through captured images.

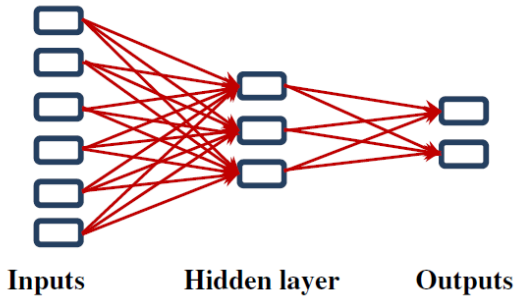

Fig 5. Neutral Network Architecture

Input/output datasets were used to train the network. A procedure was employed to optimize the hidden layer neurons and select the transfer function for which a program was generated in Matlab package.

About 100 training processes were performed and the best net was extracted and saved for later use. The best net elected as the results of its output have the heist percentage value of successful prediction. A program was built especially for the classification of welding defects named Welding Defects Inspection using Neural Network Program "*WDINProg*". This program was built using Matlab Software Packages. Fig. 6 shows the main interface of the program.

The Matlab Neural Network Toolbox is one example of such a toolset, and it is available in a standard form to all. High performance computers would enable more runs and shorter training times. Feed-forward artificial neural networks allow signals to travel one way only – from input to output.

There is no feedback (looping), i.e. the output of any layer does not affect the same or earlier layers. Feed-forward artificial neural networks tend to be straightforward networks that associate inputs with outputs.

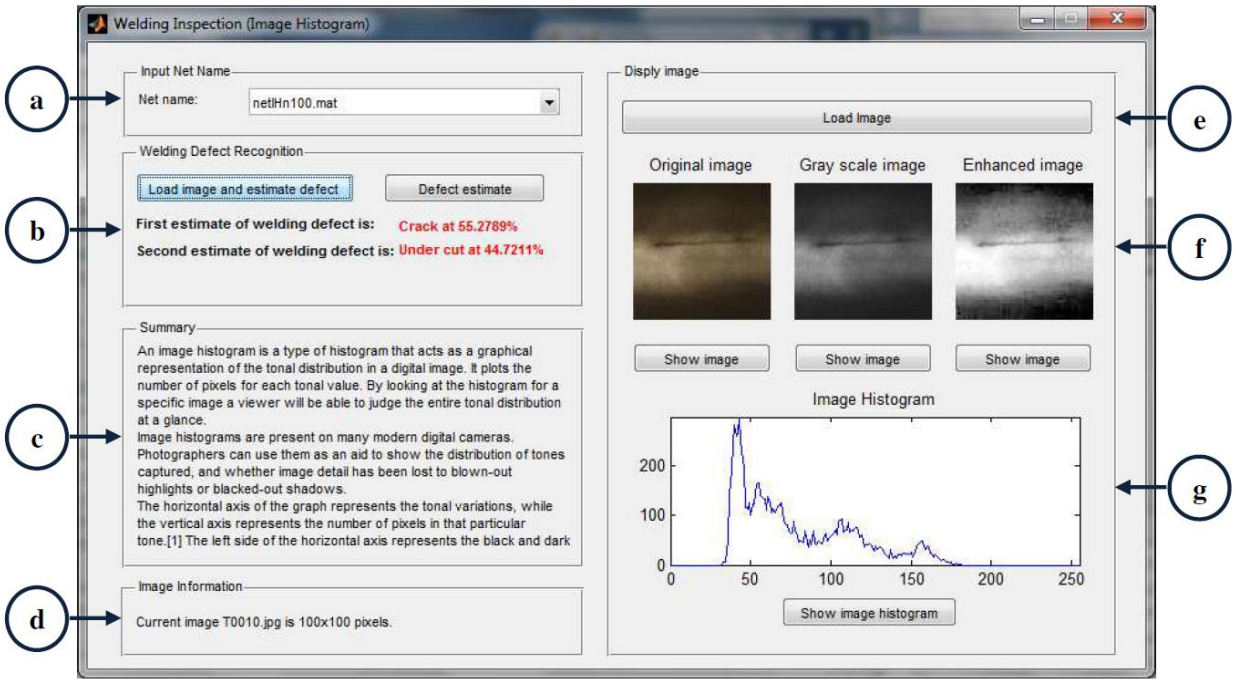

Fig.6 Detection of weld defects by WDINProg.

Figure 6 shows the graphical user interface of the *WDINProg* that is used for detecting welding defects using image histogram method. The *Input Net Name* section (a) represents a drop-down selection of all available pre-created nets. In section (b), the user can load an x-ray image to estimate the defects (if exists), then showing the results as illustrated. Section (c) shows a brief information about image histogram, whereas section (d) shows the current image information (Name and size). The user can only load any image (e) to display the selected image as original, grayscale and enhanced forms (f). Therefore, image histogram was calculated and plotted in section (g).

5. Conclusion

Design and build a program to detect and to classify the welding defects based on X-ray images and relying on artificial neural networks and image analysis processes, and depends on the design and program of two ways: (a) depends on the discovery of a defect, and only one in the image, (b) the discovery of more than flawing in the image, and have found the following:

1. The effect of varying the size of the image on the degree of success of defects for all cases and has turned out that the detection of defects does not depend on the size of the image.
2. It has turned out that the average college success percentages when detected on only one defect was 75,4 % ± 1,1.
3. As it turns out, the average college success percentages detected at more than one defect was 94,3% ± 0,3.

4. Led the development of the program for detects of more than one defect to a significant increase in the percentages of detection of different cases

6. References

[1] Zapata J; Vilar R; Ruiz R; (2011). Performance evaluation of an automatic inspection system of weld defects in radiographic images based on neuro-classifiers, Expert Systems with Applications, Vol. 38, pp. 8812 – 8824 **(conference paper)**

[2] Zapata J: Vilar R; and Ruiz R; (2011). Automatic Inspection System of Welding Radiographic Images Base on ANN Under a Regularization Process, J. Nondestruct. Eval; doi: 10.1007/s10921-011-0118-4 **(journal article)**

[3] Liao, T.W; (2009). Improving the accuracy of computer-aided radiographic weld inspection by feature selection, NDT&E International, Vol. 42, pp. 229–239 **(journal article)**

[4] Vilar, R; Zapata, J; and Ruiz, R; (2009). An automatic system of classification of weld defects in radiographic images, NDT & E International, Vol. 42, pp.467–476 **(journal article)**

[5] Shafeek H.I; Gadelmawla E.S; AbdelShafy A. A. and Elewa I.M; (2004). Assessment of welding defects for gas pipeline radiographs using computer vision, NDT&E International, Vol.37, pp. 291–299 **(journal article)**

[6] Shafeek H.I; Gadelmawla E.S; AbdelShafy A.A; Elewa I.M; (2004). Automatic inspection of gas pipeline welding defects using an expert vision system, NDT & E International, Vol. 37, pp. 301–307 **(book/ chapter in book)**

[7] Yahia N.B; Belhadj T; Brag S. and Zghal A; (2011). Automatic detection of welding defects using radiography with a neural approach, Procedia Engineering, Vol. 10, pp. 671–679 **(book/ chapter in book)**

[8] Kasban H; Zahran O; Arafa H; El-Kordy M; Elaraby S. M. S. AbdEl-Samie F. E; (2011). Welding defect detection from radiography images with a cepstral approach, NDT&E International, Vol. 44, pp. 226–231 **(book/ chapter in book)**

[9] Sreedhar U; Krishnamurthy C. V; Balasubramaniam K; Raghupathy V. D; Ravisankar S; (2012). Automatic defect identification using thermal image analysis for online weld quality monitoring, Journal of Materials Processing Technology, Vol. 212, pp.1557– 1566 **(journal article)**

[10] Kafieh R; Lotfi T; Fattahi R.A; (2011). Automatic detection of defects on polyethylene pipe welding using thermal infrared imaging, Infrared Physics & Technology, Vol. 54, pp. 317–325 **(journal article)**

[11] Garcia-Allende P.B; Mirapeix J; Conde O.M; Cobo A; and Lopez-Higuera J.M; (2009). Defect Detection in Arc-Welding Processes by Means of the Line – to-Continuum Method and Feature Selection, Sensors 2009 Vol. 9, 7753-7770; doi:10.3390/s91007753, pp. 7753-7770 **(journal article)**

[12] Mirapeix J; García-Allende P.B; Cobo A; Conde O.M. and López-Higuera J.M; (2007). Real-time arc-welding defect detection and classification with principal component analysis and artificial neural networks, NDT&E International, Vol. 40, pp. 315–323 **(journal article)**

[13] Abdelhay A.M; (2002). Application of Artificial Neural Networks to Predict the Carbon Content and the Grain Size for Carbon Steels, Egypt. J. Sol., Vol. 25, No. 2, pp. 229 **(journal article)**

[14] Wang, G; Liao, T.W; (2002). Automatic identification of different types of welding defects in radiographic images, NDT&E International, Vol. 35, pp. 519–528 **(journal article)**

[15] Lashkia, V., (2001). Defect detection in X-ray images using fuzzy reasoning, Image and Vision Computing, Vol. 19, pp. 261-269 **(journal article)**

[16] Petrović, Ivan; Kolić Matko (2024). Quality Control of Aluminum die castings in the Automotive Industry, Croatian Association for Castings, Ferrous and non-ferruos metallurgy in the 21st Century, Sceintific- Expert Seminar, Trakošćan **(journal article)**

[17] Petrović Ivan; Stojkov Marinko; Markešić Zoran; (2024). Control Quality of welded joints using Automatic Defect Recognition System for Digital Radiography, 22nd Natural Gas, Heat and Water Conference, 15th International Natural Gas, Heat and Water Conference, Osijek **(journal Article)**

Društvo za tehniku zavarivanja Slavonski Brod

13. Međunarodno znanstveno-stručno savjetovanje SBZ 2025

„STROJARSKE TEHNOLOGIJE U IZRADI ZAVARENIH KONSTRUKCIJA I PROIZVODA, SBZ 2025."
Slavonski Brod, 08. i 09. 05. 2025.

Implementacija ultrazvučne tehnike totalnog fokusiranja u proces ispitivanja zavarenih spojeva

Z. Nikolić[1,*], V. Nikolić[2]

[1]Siemens Mobility d.o.o. Cerovac, Sobovica BB, 34321 Kragujevac, Srbija
[2]Departman za fiziku, Prirodno-matematički fakultet, Univerzitet u Novom Sadu, Trg Dositeja Obradovića 4, Novi Sad, Srbija

[*] Corresponding Author. E-mail: ferrumcarbon@gmail.com

Sažetak

Usled ubrzanog razvoja industrije zavarivanja usavršene su različite metode i tehnike ispitivanja bez razaranja zavarenih spojeva. Inženjerska dostignuća u smislu informatičkih softvera, unapredila su mogućnosti ultrazvučnih uređaja i opreme dajući im na taj način znatnu računarsku snagu, veliki propusni opseg podataka, zavidan memorijski kapacitet, jednostavnost u rukovanju i dr. Sve to je dovelo do nastanka različitih novih tehnika ultrazvučnog ispitivanja među kojima je zasigurno u samom vrhu tehnika totalnog fokusiranja, poznatija kao TFM. Ma koliko bile savršene i napredne, njihove primene često zahtevaju različita dokazivanja i potvrde u praksi. Sve što je novo i savremeno pretpostavlja se i da je bolje, ali je to potrebno verifikovati i uskladiti sa pravilima iz standarda, zahtevima naručioca ispitivanja, zahtevima kupca itd. To je uglavnom zahtevan posao koji podrazumeva značajno operativno vreme, angažovanje većeg broja ljudi iz struke i po nepisanom pravilu niz problema. U ovom radu će biti opisano iskustvo u postupku uvođenja ultrazvučne tehnike totalnog fokusiranja (TFM) za ispitivanje zavarenih spojeva u našoj fabrici.

Ključne reči: Tehnika totalnog fokusiranja (TFM), implementacija ultrazvučne tehnike, proces ispitivanja zavarenih spojeva.

1. Uvod

Prilikom ispitivanja zavarenih spojeva metodama bez razaranja uglavnom je dovoljno pridržavati se uputstava i preporuka iz relevantnih standarda. U njima stoje do detalja opisani postupci, redosled, kriterijumi za ocenjivanje kao i eventualna ograničenja metode ili tehnike, odnosno sve ono što je potrebno kako bi izabrana NDT metoda dokazala opravdanost primene i na taj način potvrdila ili opovrgla kvalitet predmetnog zavarenog spoja. U tom smislu, poznavanje standarda je od ključnog

značaja za uspeh primene određene NDT metode kako za operatere, tako i za sve ostale učesnike u procesu ispitivanja.
Operateri stiču znanja o poznavanju i primeni pravila iz standarda prolazeći kroz proces obuke i kvalifikacije, odnosno sertifikacije za određenu metodu NDT [1]. Svi ostali učesnici u procesu ispitivanja i ne moraju da budu sertifikovani za tu metodu, ali moraju biti upoznati sa procesom kroz radna uputstva i pisane procedure koje opet, mora sastaviti i overiti lice koje je kvalifikovano i sertifikovano za oblast ispitivanja bez razaranja. Tako postavljen sistem deklarativno garantuje da će sva zahtevana pravila iz standarda biti ispoštovana i na taj način biti osiguran zahtevani kvalitet određenog proizvoda.
Iz takve perspektive i svega gore navedenog proizilazi da je prilično jednostavno sprovesti ispitivanje neke komponente kada postoje utvrđena pravila i kada je metoda, odnosno tehnika već verifikovana u primeni [2]. Međutim, problem nastaje kada to nije slučaj i kada imamo zahteve kupaca koji nisu obuhvaćeni standardima ili se kose sa pravilima iz njih i kada se zahtevaju metode ili tehnike za ispitivanje koje mi nismo primenjivali u praksi i nemamo potvrdu o njihovoj pouzdanosti za naš proizvod. To je onaj slučaj koji se navodi u standardima kao specifičan zahtev kupca i gde je opisano u kojim situacijama zahtevi kupca imaju prioritet u odnosu na neka pravila iz standarda.
U ovom radu će biti opisana iskustva iz prakse u slučaju kada smo za ispitivanje određenog zavarenog spoja imali uputstvo od strane kupca i u slučaju kada za ispitivanje drugog zavarenog spoja nismo imali nikakva određena uputstva i procedure od kupca. Dakle u drugom slučaju smo sami morali dokazati i potvrditi kupcu pouzdanost tehnike TFM u primeni na ovom spoju.

2. Sprovođenje i tok procesa

U oba slučaja se radi o ispitivanju zavarenih spojeva od legura aluminijuma iz grupe 5xxx i 6xxx [3]. Zahtev je bio da se ispitivanje obavi ultrazvučnom metodom, tehnikom FMC/TFM (Full Matrix Capture/Total Focusing Method) [4].

2.1. Primer za prvi slučaj

Kod ovog slučaja se radilo o zavarenom spoju bez potpunog uvarivanja sa pripremom "HY" zavarenim postupkom MIG(131). Debljina materijala je 8mm sa zatupljenjem od 2mm i uglom pripreme od 55º. Standardi za ultrazvučna ispitivanja navode određena ograničenja kod ispitivanja ove vrste spojeva bez obzira na primenjenu tehniku. Međutim, mi smo dobili od eksperata našeg kupca uputstvo prema kome ćemo izvršiti ispitivanje spoja bez obzira na ta ograničenja. Uputstvo je sadržalo tehniku podešavanja uređaja i opreme i ilustraciju predmetnog spoja. Naime, zahtev se ogledao u tome da se spoj ne ispituje do potpune dimenzije debljine od 8mm već je bilo dovoljno ispitati zapreminu deponovanog materijala u spoju, tj. samo 6mm i konstatovati da li u tom delu postoje ili ne postoje nehomogenosti u metalu šava i ZUT. Tehnika TFM to omogućava bez pojave tzv. fantomskih ehoa, nejasnih šumova i sl.

U uputstvu na ilustraciji jasno su bile ograničene dve zone za ocenjivanje do dubine 6mm. Prva zona od 0-5mm i druga od 5-6mm sa različitim kriterijumima za ocenjivanje mogućih reflektora. Za prvu zonu su kriterijumi bili blaži dok su za drugu, od 5-6mm bili dosta rigorozniji i kompleksniji za ocenjivanje, ali su nam bili predstavljeni i pojašnjeni. Ovde jasno dolazi do izražaja ona smernica iz standarda koja govori o prioritetu zahteva kupca u odnosu na preporučena pravila.
Uz takvu podršku eksperata od strane kupca, mi smo lako i brzo osvojili ispitivanje tog spoja tehnikom FMC/TFM i postigli zadovoljavajuće rezultate koje i danas sa uspehom održavamo. Uz učešće našeg rukovodstva kontrole kvaliteta, inženjera zavarivanja, stručnjaka i operatera za NDT iz sektora kontrole zavarenih spojeva i svih ostalih relevantnih osoba, postignuta je saglasnost sa predstavnicima kupca za primenu uputstva u našoj fabrici.
Na taj način je relativno jednostavno završen proces implementacije nove tehnike i ona je verifikovana i uvedena u redovan plan kontrole zavarenih spojeva koji i danas primenjujemo. Time je okončan proces za primer prvog slučaja u ovom radu.

2.2. Primer za drugi slučaj

U jednom momentu smo od kupca dobili zahtev za ispitivanje zavarenog spoja sa oznakom 5V. Predmet ispitivanja je takođe zavreni spoj od legura aluminijuma debljine 5mm sa punom penetracijom i tipom pripreme spoja "V". Zavareni spoj je izveden polumehanizovanom tehnikom "traktorom" u položaju "PC", postupkom MIG. Ovoga puta u zahtevu je bilo navedeno samo šta je potrebno ispitati i kojom metodom i tehnikom, ali ne i kako to izvesti. Nikakvog uputstva i pomoći nije bilo. Uz rezultate je bilo potrebno kreirati i izveštaj o sprovedenom ispitivanju metodom ultrazvuka, tehnikom FMC/TFM što je tražilo dodatnu ozbiljnost i pristup poslu [5].

3. Planovi, podela aktivnosti i ciljevi

Budući da za ovaj slučaj nismo imali detaljne informacije morali smo da organizujemo sastanak na nivou relevantnih osoba kako bi zauzeli stav i delegirali aktivnosti. Ovako postavljen zadatak pred našu službu zahtevao je pažljivo razmatranje svih detalja i veliku odgovornost pojedinaca. Učešće su uzeli rukovodioci kontrole kvaliteta, operateri kontrole zavarivanja i stručnjaci za NDT, odgovorni inženjeri zavarivanja i odabrani zavarivači i operateri zavarivanja sa instruktorom zavarivanja na čelu. Plan je bio da se zavari uzorak, koji je po svojim karakteristikama identičan originalnom uzorku koji će se ispitivati u serijskoj proizvodnji. Ta aktivnost je dodeljena iskusnom operateru zavarivanja i njegovom instruktoru. U takav spoj je bilo potrebno uneti veštačke reflektore koji će biti markirani i koji se mogu očekivati u tom spoju shodno postupku i tehnici zavarivanja, grupi materijala i sl. (slika 1) i u jednom delu spoja uneti u uređaj takve parametre zavarivanja koji će zasigurno izazvati pojavu neprovara u korenu i nalepljivanja na stranici žleba [6] (slika 2). Ovaj zadatak je poveren iskusnom NDT operteru trećeg nivoa, sa dokazanim sveobuhvatnim znanjem iz oblasti metalurgije i tehnologije zavarivanja koje je verifikovano međunarodnim sertifikatima, kao i instruktoru zavarivanja.

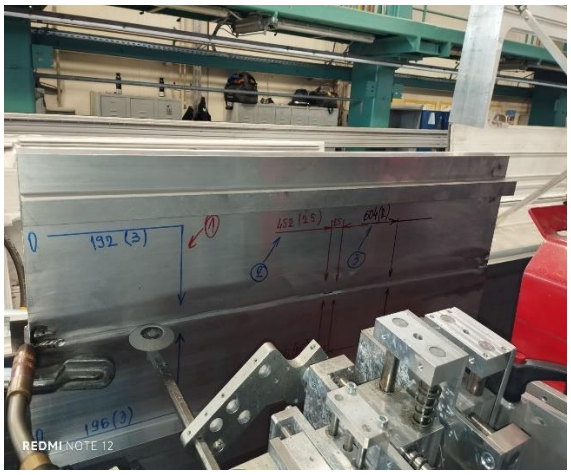

Slika 1. Veštački uneti reflektori i njihovo markiranje na uzorku

Slika 2. Unošenje neadekvatnih parametara za postizanje neprovara i nalepljivanja

Pisanje i overa procedure i uputstva za ispitivanje predmetnog spoja takođe je poverena NDT operateru sa kvalifikacijama i sertifikatom za metodu ispitivanja ultrazvukom trećeg nivoa. Priprema tehničke dokumentacije, crteža i skica pala je na teret odgovornom inženjeru zavarivanja.
Eventualnu uspešnost i potvrdu primenjene tehnike ispitivanja za ovu vrstu spoja verifikovaće rukovodstvo kontrole kvaliteta uz usaglašavanje sa kupcem, rukovodilac proizvodne tehnologije zavarivanja i operater kontrole zavarenih spojeva trećeg nivoa koji će sprovoditi ispitivanje.

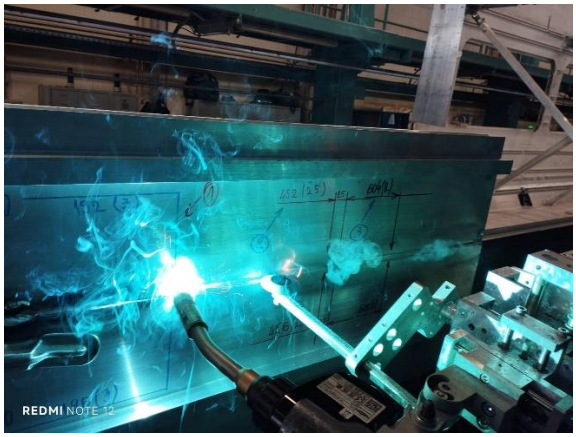

Slika 3. Zavarivanje preko veštački unetih reflektora

Slika 4. Izgled lica šava u toku zavarivanja preko veštački unetih reflektora

Kalibracija uređaja i opreme za ispitivanje, konfiguracija sistema, podešavanje ispitne osetljivosti, tumačenje i evaluacija dobijenih rezultata i izrada završnog izveštaja o ispitivanju takođe su deo aktivnosti koje pripadaju NDT ispitivaču trećeg nivoa.

Jedan od primarnih ciljeva ovog tima bio je da se dobijeni rezultati ispitivanja na probno zavarenom uzorku uporede sa stvarnim pozicijama, karakteristikama i orijentacijama veštački unetih reflektora na njemu. Ukoliko bi dobili tačne rezultate, na taj način bi mogli dokazati pouzdanost primene TFM tehnike za ispitivanje ove vrste spoja čime bi bio dostignut krajnji cilj.

3.1. Aktivnosti posle zavarivanja uzorka

Nakon zavarivanja uzorka sa veštački unetim reflektorima pristupilo se vizuelnoj kontroli zavarenog spoja gde je već tom metodom bilo moguće utvrditi da se baš na mestima na kojima su veštački uneti reflektori nalaze i nesavršenosti u zapremini metala šava [7]. Bilo je jednostavno utvrditi pojavu nadvišenja ili utonuća lica šava, poroznost, razbrizgavanje, prelivanje, nepravilnosti oblika i mera i dr. (slika 4). To je dalo nadu da smo blizu uspeha. Međutim, uzimajući u obzir da je pri ispitivanju takvih spojeva tehnikom FMC/TFM potrebno obrusiti lice šava na nivo osnovnog materijala, dolazimo do zaključka da nam VT inspekcija ne može dati ništa više od nepouzdanih rezultata. Nama je bila potrebna potvrda kvaliteta u zapremini metala šava i ZUT. Zavar je obrušen na nivo osnovnog materijala i ponovo smo vraćeni na početak.

4. Rezultati ispitivanja i analiza

Prvi veštački unet reflektor predstavljao je metalni uključak. Za tu svrhu smo uzeli vrh igle za obeležavanje od tvrdog metala. On je postavljen u korenu šava. Za drugi reflektor smo odabrali komadić čelične žice za zavarivanje postupkom MAG, prečnika 1mm i dužine 25mm. Kao treći reflektor zabušili smo rupu u stranicu pripreme osnovnog materijala prečnika 1,5mm u dubini do 8mm. Za četvrtu nepravilnost smo odabrali nepotpuno uvarivanje u korenu i nalepljivanje na stranici žleba. Na aparatu za zavarivanje smo smanjili struju i napon za približno 30-40% u odnosu na parametre u WPS listi za taj spoj i tako bili prilično sigurni da ćemo postići ono što želimo.
Nadvišenje lica šava je prerbrušeno na nivo osnovnog materijala i time je moglo da počne ispitivanje uzorka. U ultrazvučni uređaj su uneti svi potrebni dostupni parametri. Ovaj zavareni uzorak je zapravo služio kao uporedno telo za kalibraciju. Imali smo poznate parametre koji nisu promenljivi u odnosu na spojeve koji se trebaju ispitivati u serijskoj proizvodnji. Akustičke karakteristike materijala su identične. I uzorak i materijal koji se koristi u serijskoj proizvodnji imaju iste izotropne karakteristike. Metalurška svojstva oba materijala su jednaka. Te poznate vrednosti su nam u velikoj meri olakšale podešavanje ispitne osetljivosti budući da nismo imali standardizovani kalibracioni blok za tu grupu materijala. Ispitno pojačanje i još neke bitne vrednosti za podešavanje osetljivosti smo proračunali matematičkim putem na osnovu obrazaca iz literature. Podatke o ispitnoj sondi sa kojom smo ispitivali pronašli smo u specifikaciji koju je dostavio proizvođač. Njih je takođe trebalo uneti u uređaj. Put skeniranja koji je bilo potrebno da nam zabeleži enkoder odredili smo na osnovu dužine zavarenog spoja na ispitnom uzorku. Sve ostalo odradio je moćni softver ultrazvučnog uređaja koji smo koristili.

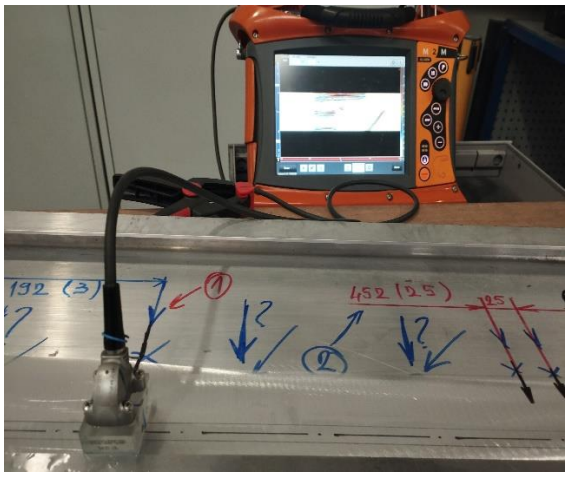

Slika 5. Lokacija prvog reflektora

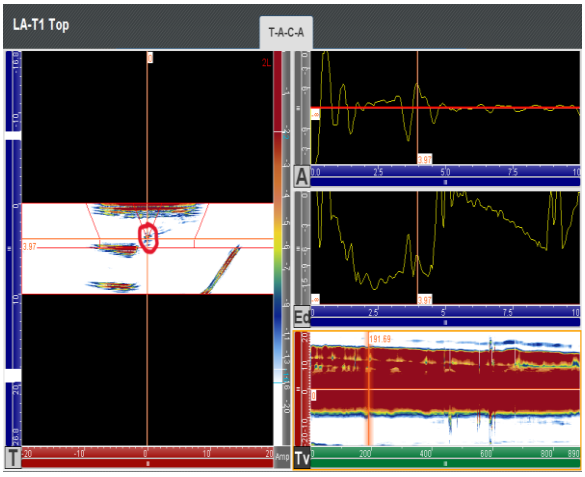

Slika 6. Prikaz reflektora na ekranu uređaja

Detektovanje prvog veštački unetog reflektora, određivanje njegove lokacije, mogućnost njegovog dimenzionisanja i veran prikaz na monitoru uređaja već su garantovali uspeh. Zahvaljujući naprednim mogućnostima ultrazvučnog uređaja sa kojim smo ispitivali i na osnovu značajnih ranijih iskustava u radu sa ovim uređajem bili smo sigurni da smo na pravom putu.
Sve ostale reflektore u nizu nepogrešivo smo detektovali i uz pomoć 3D prikaza na uređaju potvrdili da se radi upravo o onima koje smo veštački izazvali. Rezultati su bili nedvosmisleni. Sa aspekta operativnih aktivnosti i tehničkih detalja, za nas je ovaj izazov bio završen na najbolji mogući način.

5. Zaključak

Nakon prezentovanja celokupnog procesa i dobijenih rezultata kupcu našeg proizvoda dobili smo njihovu saglasnost za primenu tehnike. Pristupili smo izradi procedure i uputstva za ispitivanje predmetnog zavarenog spoja. U uputstvo smo uneli sve neophodne detalje za ispitivanje kao što su: obim ispitivanja, kriterijumi prihvatanja, nivoi testiranja i dr. Kreirali smo i specifični šablon završnog izveštaja o ispitivanju tih spojeva. Sledeći korak je bio overa dokumentacije i verifikacija primenljivosti tehnike FMC/TFM za ispitivanje spoja sa oznakom 5V i uvođenje u redovni plan kontrole zavarenih spojeva u fabrici.
Zajedničkim zalaganjem svih stručnjaka iz tima, primenom pravila iz standarda i operativnim iskustvom iz prakse postigli smo zacrtani cilj. Drugačije i ne bi bilo izvodljivo. Dobijanjem saglasnosti od strane kupca završen je kompletan proces implementacije i verifikacije jedne tehnike ispitivanja ultrazvukom uz pomoć koje i danas isporučujemo zavarene spojeve vrhunskog kvaliteta za globalno poznatog kupca.

6. Literatura

[1] SRPS EN ISO 9712:2013 - Ispitivanje bez razaranja – Kvalifikacija i sertifikacija osoblja za IBR, ISS, Institut za Standardizaciju Srbije, Beograd
[2] ISO 17640:2018 - Non-destructive testing of welds – Ultrasonic testing – Technique, testing levels, and assessment, ISO, Vernier, Geneva, Switzerland.
[3] Prokić Cvetković, R., Popović, O., : Metalurgija zavarivanja, Mašinski fakultet Univerziteta u Beogradu, Beograd, 2019, str., 307-312.
[4] ISO 23865:2021 – Non-destructive testing – Ultrasonic testing – General use of full matrix capture / total focusing technique (FMC / TFM) and related technologies, ISO, iiw, Vernier, Geneva, Switzerland.
[5] ISO 23864:2021 – Non-destructive testing of welds – Ultrasonic testing – Use of automated total focusing technique (TFM) and related technologies, ISO, iiw, Vernier, Geneva, Switzerland.
[6] SRPS EN ISO 6520-1:2013 – Zavarivanje i srodni procesi – Klasifikacija geometrijskih nesavršenosti u metalnim materijalima – Deo 1: Zavarivanje topljenjem i pritiskom, ISS, Institut za Standardizaciju Srbije, Beograd
[7] EN ISO 17637:2016 - Non-destructive testing of welds – Visual testing of fusion – welded joints, CEN, European Committee for Standardization, Brussels.

Društvo za tehniku
zavarivanja Slavonski Brod

13. Međunarodno znanstveno-stručno savjetovanje SBZ 2025

„STROJARSKE TEHNOLOGIJE U IZRADI ZAVARENIH KONSTRUKCIJA I PROIZVODA, SBZ 2025."
Slavonski Brod, 08. i 09. 05. 2025.

High quality with high speed - TWIN welding

M. Jagnjić[1], T. Marijanović[2] , Ž. Čubrilo[3], K. Didić[4,*]

[1]Director of QM in in Đuro Đaković Special
[2]Deputy of welding engineer in Đuro Đaković Special vehicles
[3]Head of welding school and labos in Đuro Đaković Special vehicles
[4] Responsible welding engineer in Đuro Đaković Special vehicles

[*] Corresponding Author. E-mail: Kresimir.Didic@duro-dakovic.com

Abstract

Twin welding is a lastes tested and proven innovation of welding technologies which improve quality, efficiencies and cost in the process. The main advantages of using twin welding are that it is highly efficient, requires minimum heat input, provides superior quality results to name but a few.

Keywords: twin, high quality, high speed, efficiencies, deposition rate

1. Introduction

Twin welding is a process that involves using two welding arcs simultaneously to join metal together. It is often employed in industrial settings where high productivity and efficiency are required. One of those companies are Đuro Đaković Special vehicles wich produce over 1000 wagons per year. In twin welding, two welding torches (or welding machines) are used, with each torch creating its own arc. The arcs are positioned side by side or slightly offset, and the metal being welded is melted by both arcs, allowing for a wider and deeper penetration than single-arc welding.

2. Key features of twin welding

Twin welding is a specialized technique designed to improve welding efficiency, quality, and speed, particularly in high-volume and high-performance applications. Adjust only the most essential aspects becuase there is a possibillity achieve better results automatically. During the welding process, twin system regulates the welding parameters and welding variables independently in the background to keep both arcs perfectly regulated at all times.
TeachMode, TouchSense, SeamTracking, WireSense and short circuit detection within the gas nozzle. Twin assistance systems simplify handling of the welding system and thereby increase welding efficiency, which saves a lot of time.

Processing large, heavy components has never been easier. This is possible thanks to the power of 2 welding power sources in one system, leading to particularly high deposition rates and excellent gap-bridging ability, deposition rate, up to 25 kg/h.
Fast welding speeds up to 4 m/min without loss of quality: This is par for the course owing to the high deposition rate—just like the reliable penetration and notch-free welds.
While the total energy input is higher, the heat input to each individual weld is lower compared to conventional single-arc processes. This can reduce the risk of distortion and warping in the material. The dual arcs allow for deeper penetration into the base material, which can be beneficial for thicker materials or when a high-quality joint is required.

3. Research result

For manually welding, the weld joint had a K preparation, a bevel angle of 60°, a gap between positions of 0 mm and a root face of 1 mm (Figure 1).

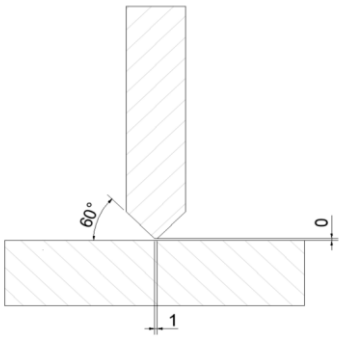

Figure 1. Preparation of joint for manually welding

After the decision to automate welding on the bogie line, numerous tests were performed to obtain the required welding speed.
The test data can be found in the table below. All samples were prepared according to the sketch in Figure 2.

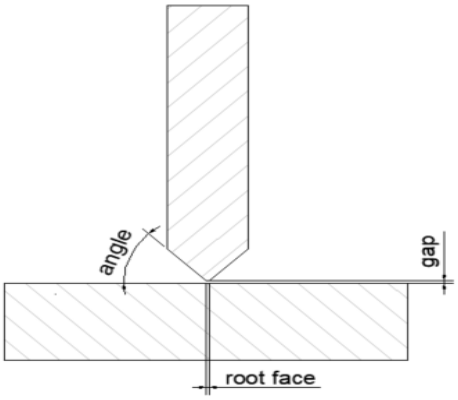

Figure 2. Preparation of joint for robotic welding

Table 1. Comparison of test welds

Test No.	Preparation	Results
1.	- angle 30 ° - root face 1.5 mm - weld. gap 0mm	- is more efficient for welding speed than an angle of 60 ° - there is no place for the MAG tacking - the stitch fills the whole bevel - (TIG alternative better but inefficient) - Non-penetration in the root of the weld
2.	- angle 45 ° - root face 1.5 mm - weld. gap 0mm	- is more efficient for welding speed than an angle of 60 ° - there is more space for the MAG tacking - the stitch partially fills the bevel (no need to tack TIG) - penetration in spices is guaranteed
3.	- angle 45 ° - root face 1.5 mm - weld. gap 1.25mm	- is more efficient for welding speed than an angle of 60 ° - there is more space for the MAG tacking - the stitch partially fills the bevel (no need to tack TIG) - penetration in spices is guaranteed - there is a visible penetration in the root along the entire length and at the site of the tack
4.	- angle 45 ° - root face 1.5 mm - weld. gap 2 mm	- failed due to excessive clearance, the material burns and it is not possible to weld with such a gap.

After testing, testing no. 2 is applied in production, but during exploitation we changed the angle of the gun, which ensures complete penetration, and in this way we ensured that the materials are joined. Bevel preparation of the positions must be done strictly on the milling machine, and position cutting strictly on the laser.

4. Evidence of quality

The welding sequence is shown in Figure 3. Twin welding enables for a sufficient amount of deposit to be produced from a single pass without leaving insufficient penetration or insufficient weld overhang.

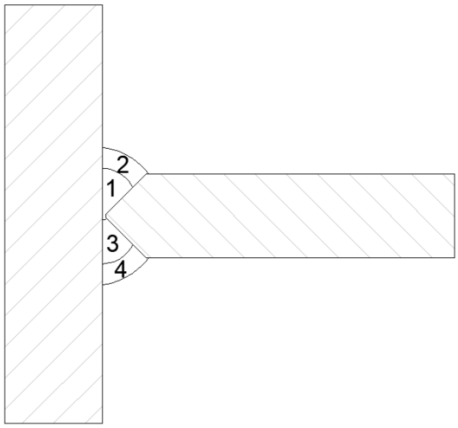

Figure 3. Welding sequence

The macrostructure of the welded joint can be seen in Figure 4. Surface of the cross-section of the welded joint was polished with diamond grinding plate with a grain size of 15μm. Acid for surface etching are nital 3%.

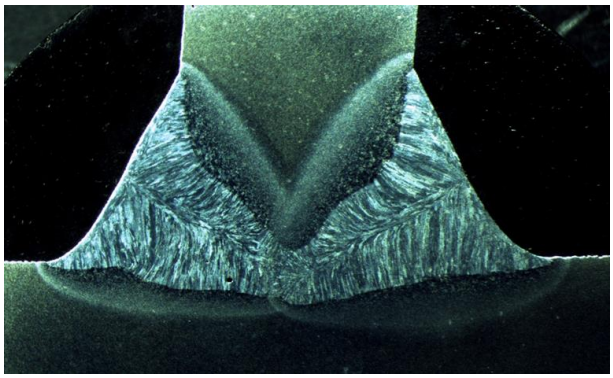

Figure 4. Macrostucture with enlargement 3x

The Vickers hardness test method consists of indenting the test material with a diamond indenter, in the form of a right pyramid with a square base and an angle of 136 degrees between opposite faces subjected to a load of 98 N. The load is normally applied for 10 to 15 seconds.

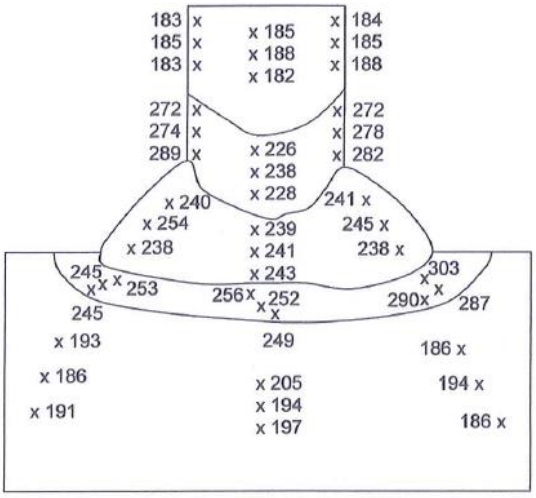

Figure 5. Hardness testing

The final product are weld with high quality and same dimension of weld in every point of cross section. The visual appearance of the weld are welded in accordance with EN 5817 klasification B or EN 15085-3 CPC2 (Figure 6).

Figure 6. Final appearance of weld

5. Quality and quantity

Twin brings a high quality welded joint with a high welding speed. The welding speed of 50 cm/min in the normal position made it possible to achieve annual production plans.
Twin requires maximum precision preparation to avoid problems and errors that may occur due to incorrect preparation.

The production increased by 400%, which brought a great saving of time, ensuring the necessary production capacity, saving the costs of filler material. The product warranty has been extended because each product is welded in the same way where the human factor has no influence.

6. References

[1] Robot welding system; Fronius FRW COMPACT Twin Sidebar
[2] J. P. Lee, M. H. Park , D. H. Kim , B. J. Jin, J. Y. Shim, B. Y. Kang, I.S. Kim: An experimental study on optimizing for tandem gas metal arc welding process, Journal of Achievements in Materials and Manufacturing Engineering, Vol.68, Issues 2, February 2015, p.72-79;
[3] H. Mori, T.Asada: Flexible tandem welding system, KOMATSU Technical Report, Vol.50, No 154, 2004, p.1-5;

Društvo za tehniku zavarivanja Slavonski Brod

13. Međunarodno znanstveno-stručno savjetovanje SBZ 2025

„STROJARSKE TEHNOLOGIJE U IZRADI ZAVARENIH KONSTRUKCIJA I PROIZVODA, SBZ 2025."
Slavonski Brod, 08. i 09. 05. 2025.

Bitne varijable EPP zavarivanja membranskih zidova na vodocijevnim kotlovima

SAW essential variables of membrane walls on water-tube boiler

M. Činkl[1,*], T. Marsenić[1], B. Despotović[2], D. Marić[3]

[1]ANDRITZ TEP d.o.o, Slavonski Brod, Hrvatska
[2]Društvo za tehniku zavarivanja Slavonski Brod, Slavonski Brod, Croatia
[3]Strojarski fakultet u Slavonskom Brodu, Sveučilište u Slavonskom Brodu, Hrvatska

[*] Corresponding Author. E-mail: monika.cinkl@andritz.com

Sažetak

U radu je opisano zavarivanje membranskih panela izrađenih od 13CrMo4-5 cijevi u tvornici ANDRITZ TEP d.o.o. Zavarivanje je izvedeno EPP postupkom. Također, u radu su navedeni zahtjevi za te zavarene spojeve specificirani prema normi EN 12952-5.

Ključne riječi: Elektrolučno zavarivanje pod praškom (EPP), EN 12952-5

Abstract

The paper describes the welding of membrane panels made from 13CrMo4-5 of the well-known name; in the ANDRITZ TEP d.o.o. factory. The welding was performed using the SAW process. The paper states the requirements for these welded joints according to EN 12952-5.

Keywords: Submerge arc welding (SAW), EN 12952-5

1. Uvod

Membranski zidovi predstavljaju vanjske granice kotla, odnosno gabarite kotla uključujući i pregradne zidove unutar kojih se odvija proces izgaranja različitih tipova goriva; fosilnih goriva, otpada ili biomase i strujanja produkata izgaranja koji prenose toplinu. Primjenjuju se za izradu

vodocijevnih kotlova čije je volumen veći od 2 litre za proizvodnju pare ili tople vode, tlaka većeg od 0,5 bar i temperature koja prelazi 110˚C [1]. Kroz cijevi membranskih zidova protječe voda ili para, a osnovna funkcija ovih zidova je apsorpcija topline koja nastaje izgaranjem goriva unutar ložišta. Sastoje se od zavarenih cijevi i traka pogodnih za primjenu u eksploataciji, slika 1. Ponekad, se paneli membranskih zidova savijaju spiralno, čime se formira tzv. spiralni membranski zid, kakav je primijenjen u Termoelektrani Nikola Tesla B2. Spiralnim rasporedom omogućena je ravnomjernija raspodjela toplinskog opterećenja po cijeloj površini ložišta, čime se smanjuju lokalna pregrijavanja i produžuje vijek trajanja kotla. Istovremeno, spiralna konstrukcija pridonosi kompaktnijem dizajnu, boljim hidrodinamičkim svojstvima kotla i primjenjuje se kod kotlova s prinudnom cirkulacijom. Membranski zavari na kotlovskim postrojenjima su po svom opsegu najveći i stoga se zavarivanje ovih spojeva najčešće mehanizira.

Slika 1. Membranski zid vodocijevni kotao

2. Osnovni podaci o zavarenom uzorku; osnovni i dodatni materijal

2.1 Osnovni Materijal

Materijal koji se primjenjuje za izradu kotlovskih cijevi membranskih zidova treba biti izrađen i kontroliran u skladu s normama, specifikacijama za tlačnu opremu koje su usvojene kao harmonizirane europske norme za materijale ili imaju Europsko odobrenje za materijale ili se na temelju postupka ocjene odobrava njegova primjena. Odabir materijala, čelika za izradu membranskih zidova treba biti u skladu s EN 12952-2, Annex A. Cijevi koje se primjenjuju za izradu membranskih zidova se proizvode u skladu sa harmoniziranom europskom normom EN 10216-2 [2]. U normi se navode osnovni zahtjevi za naručivanje cijevi i ispitivanje, odnosno ispitna kategorija. Temeljem ispitne kategorije određuje se zahtjevani opseg ispitivanja;

- kemijski sastav, (cast analysis),
- vlačna čvrstoća pri sobnoj temperaturi,
- test spljoštavanja,

- test ekspanzije, širenja,
- radnja loma,
- test ispitivanja nepropusnosti,
- dimenzionalna kontrola cijevi,
- vizualna kontrola cijevi,
- ispitivanje bez razaranja površine cijevi s ciljem otkrivanja uzdužnih nepravilnosti.

Osnovni materijal i dimenzije zidova se definiraju na temelju namjene kotla, tipa goriva, radnih uvjeta, na primjer temperature u ložištu, radnog tlaka i temperature pare, te ostalih uvjeta u eksploataciji uključujući koroziju. Zavarivanje i ispitivanje proizvodnog ispitnog uzorka je provedeno na cijevi sljedećih dimenzija; promjera 38 mm i debljine stijenke 5 mm, a dimenzije trake su 6x24 mm. Kvalitet cijevi i trake je 13CrMo4-5. Materijal pripada klasičnoj grupi čelika otpornih na puzanje. Čelik se isporučuje u normaliziranom i popuštenom stanju. U Tablici 1. se vidi zahtjevani kemijski sastav čelika prema normi i sastav čelika isporučene cijevi (uzorak oznaka 42616).

Tablica 1. Kemijski sastav cijevi

Cast no.	-	C [%]	Mn [%]	Si [%]	P [%]	S [%]	Cu [%]	Cr [%]	Ni [%]	Al [%]	Mo [%]
		Requirements - zahtjevi									
	min. max.	0,10 0,17	0,40 0,70	0,35	0,025	0,010	0,30	0,70 1,15	0,30	0,040	0,40 0,60
42616		0,13	0,52	0,23	0,008	0,006	0,16	0,92	0,06	0,015	0,46

U Tablici 2. je prikazan toplinski tretman cijev. Isporučena cijev je normalizirana na 945˚C i popuštena na 710˚C u zraku što je u skladu s normom.
U Tablici 3. su prikazana zahtjevana mehanička svojstva i svojstva isporučene cijevi. Granica tečenja ReH i vlačna čvrstoća Rm su u skladu sa zahtjevima norme.

Tablica 2. Toplinski tretman cijevi

Steel grade-Čelik		Heat Treatment Toplinski tretman	Austenitizing Normalizacija		Tempering Popuštanje	
Steel name Naziv	Steel number Oznaka		Temperature Temperatura °C	Cooling medium Rashladni medij	Temperature °C Temperatura	Cooling medium Rashladni medij
13CrMo4-5	1.7335	+NT	900 to 960	air	660 to 730	air
Chg 42616	1.7335	+NT	945	air	710	air

Tablica 3. Mehanička svojstva cijevi

Steel grade-Čelik		Tensile properties at room temperature Čvrstoća pri sobnoj temperaturi							Impact properties Radnja loma				
Steel name Čelik	Steel number Oznaka	Upper yield strength or proof strength ReH or Rp0,2 for wall thickness T min./ Granica tečenja ReH ili Rp0,2 ovisno o debljini stijenke Tmin.				Tensile strength Vlačna čvrstoća Rm	Elongation Izduženje A min. %		Minimum average absorbed energy KV2 J at a temperature of °C Minimalna prosječna absorbirana energija KV2 kod sobne temperature				
		T≤16	16<T≤40	40<T≤60	60<T≤100		l	t	l			t	
		MPa	Mpa	MPa	Mpa	MPa			20	0	-10	20	0
13CrMo4-5	1.7335	290	290	280	-	440to590	22	20	40	-	-	27	-
Chg 42616	1.7335	327	-	-	-	484	31,1	-	-	-	-	-	-

Traka je izrađena u skladu s normom EN 10028-2, u Tablici 4. je naveden kemijski sastav trake.

Tablica 4. Kemijski sastav trake

Chemical composition- Kemijski sastav													
Item	Cast.-No.	-	C	Mn	Si	P	S	Cr	Al	Cu	Mo	Ni	N
0001	190156	min.	0,080	0,400	-	-	-	0,700	-	-	0,400	-	-
		Isporučeno	0,125	0,605	0,250	0,0120	0,0032	0,917	0,018	0,025	0,469	0,029	0,0079
		max.	0,180	1,000	0,350	0,025	0,010	1,150	-	0,300	0,600	-	0,0120

2.2 Dodatni materijal za zavarivanje

Za zavarivanje membranskih zavara koristi se postupak elektrolučnog zavarivanje pod praškom (EPP). Dodatni materijali koji su korišteni za zavarivanje proizvodnog ispitnog uzorka;

- žica za zavarivanje klasifikacijske oznake EN ISO 24598-A: S S CrMo1,
- prašak za zavarivanje EN ISO 14174: S A AR/AB 1 78 AC H5.

Žica za zavarivanje je odabarana na osnovu kvalitete cijevi i trake, odnosno približno je jednakog kemijskog sastava. U Tablici 5. je kemijski sastav žice koji je u skladu s normom EN ISO 24598.

Tablica 5. Kemijski sastav žice za zavarivanje naveden u certifikatu

	Chemical composition – Kemijski sastav %											
Cast No.	**C**	**Si**	**Mn**	**P**	**S**	**Cu**	**Al**	**Cr**	**Mo**	**Ni**	**V**	**Ti**
758410	0,11	0,12	0,84	0,006	0,008	0,009	0,002	1,22	0,48	0,02	0,003	0,001
758410	**Nb**	**Co**	**Pb**	**Sn**	**B**	**As**	**Zr**	**Ta**	**Sb**	**Ca**	**N**	**O**
	-	-	-	0,001	-	-	0,003	-	0,0020	-	-	-

Prašak za zavarivanje sastoji se od minerala. U Tablici 6. je naveden kemijski sastav praška. Najveći udio ima aluminijev oksid pa se taj tip praška povezuje s alumino rutilnim praškom.

Tablica 6. Kemijski sastav praška iz certifikata

Flux composition – Sastav praška (%)										
Al2O3	SiO2	TiO2	ZrO2	K2O	Na2O	MnO	CaO	MgO	CaF2	FeO
37.6	14.3	9.7	0.2	0.40	2.10	16.5	1.4	1.8	10.3	5.50
Al203+TiO2		Al2O3+CaO+MgO								
47.30		40.80								

Na temelju povećanog udjela silicija koji djeluje kao dezoksidator i mangana koji povećava čvrstoću metala zavara može se zaključiti da se radi o aktivnom prašku koji zbog svog kemijskog sastava povećava otpornost na poroznosti i poboljšava izgled gusjenice, lica zavara. Aktivni prašci se primarno primjenjuju za jednoprolazno zavarivanje.

Tablica 7. pokazuje veličinu zrna praška i udjele pojedinih veličina zrna praška. Ovaj praška spada u sitno zrnati prašak („fine grain"). Odlike ovog praška su mogućnost zavarivanja velikim brzinama, glatka površina zavara bez zajeda i geometrijskih nepravilnosti. Alumino-rutilni prašak omogućuje zavarivanje velikim brzinama zavarivanja oko 100 cm/min. i jednostavno uklanjanje troske s površine zavara, dok sitno zrno praška poboljšava operativnu zavarljivost, stabilnost procesa zavarivanja i metaruluških procesa tijekom zavarivanja.

Tablica 7. Veličina zrna praška % (Sleve analysis %)

> 1.7 mm	> 0.85 mm	> 0.425 mm	> 0.25 mm	< 0.25 mm
0.00	12.30	45.90	33.80	8.00

3. Zahtjevi norme za membranski zavar

Na slici 2. je pokazan tipičan detalj spoja membranska cijev – traka. Prije zavarivanja cijev i traka trebaju biti očišćeni. Između simetrala dviju cijevi je definiran razmak „korak - t", koji je bitan pri zavarivanju trake i cijevi kako bi se održale dimenzije zidova u zadanim tolerancijama.

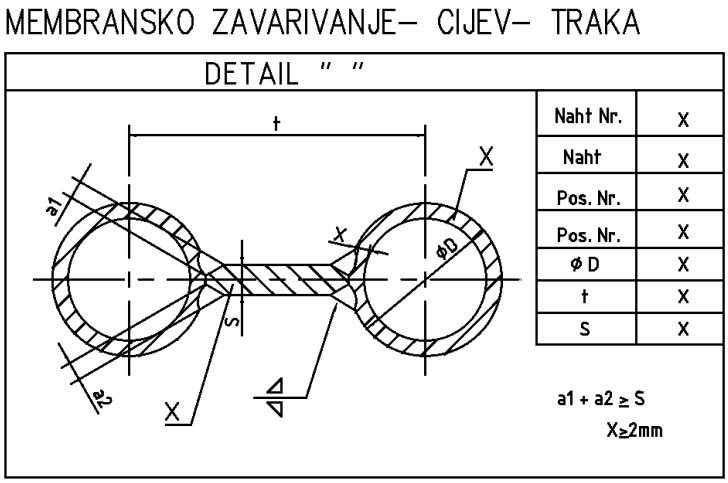

Slika 2. Detalj zavarivanja sa crteža koji definira korak, veličinu zavara i dubinu penetracije

Prije početka proizvodnog zavarivanja potrebno je zavariti i ispitati proizvodni ispitni uzorak. Ispitni uzorak se ponavlja za svaku promjenu;

- dimenzije cijevi ili trake,
- materijala cijevi ili trake,
- stroja na kojem se izvodi mehanizirano ili automatsko zavarivanje,
- parametara zavarivanja.

Prema normi EN 12952-5 definirani su zahtjevi za membranske zavare:

- zavar treba biti dimenzioniran tako da ukupna debljina zavara ($a_1 + a_2$) bude jednaka debljini stijenke trake (s), slika 3.,
- nepenetrirani dio stijenke cijevi (er) treba minimalno iznositi 2 mm,

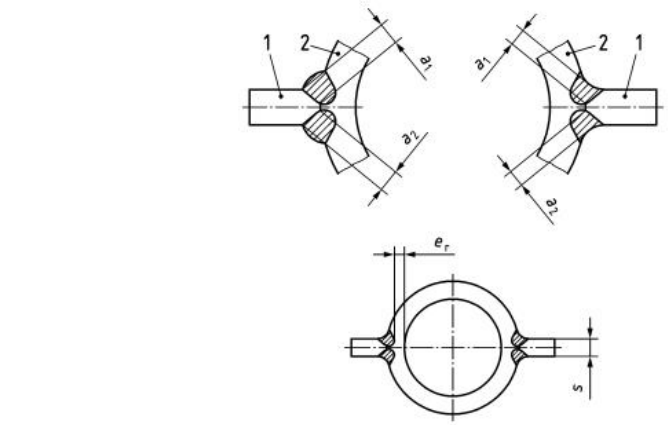

Key

$e_r \leq 2$ mm; see C.4.2.2 a)

$a_1 + a_2 \geq s$

1 fin

2 tube

Slika 3. Veličina kutnog zavara i preostalog dijela cijevi

- linearno odstupanje trake u odnosu na simetralu cijevi može iznositi $\Delta \leq 2$ mm, slika 4. Ovo odstupanje se definira kako bi se dobio kvalitetan zavaran spoj i zahtjevana veličina zavara koja omogućuje traženi prijenos topline s trake na cijevi i medij unutar cijevi, odnosno kako bi se postiglo zadovoljavajuće hlađenje trake,

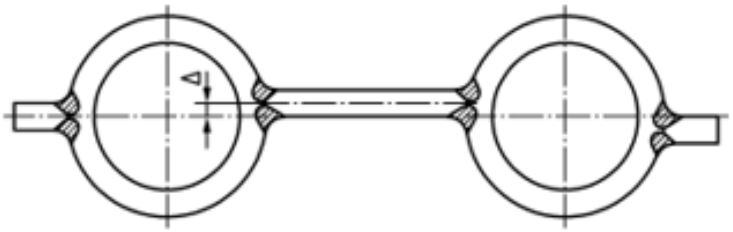

a) Linear misalignment

Slika 4. Linearno odstupanje trake u odnosu na simetralu cijevi

- kutno odstupanje položaja trake, slika 5. je razlika položaja trake s lijeve i desne strane trake i ne smije biti veća od 3 mm; $b_1 - b_2 \leq 3$ mm,

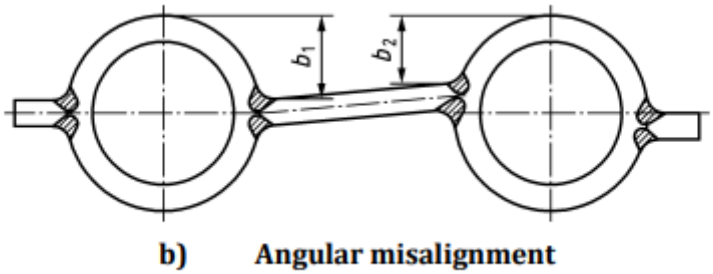

Slika 5. Kutno odstupanje položaja trake

- maksimalna ispupčenost zavara je specificirana pomoću kuta, slika 6. Zavar treba imati blagi prijelaz na cijev i traku, kako bi se smanjila koncentracija naprezanja, odnosno α<30°. Izbjegava se ispupčeni – konveksan zavar, slika 6.

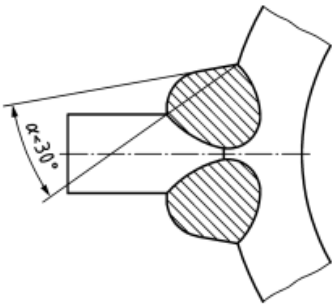

Figure C.4 — Allowable excessive convexity for fin to tube welds

Slika 6. Maksimalno dopuštena ispupčenost zavara definirana kutem

Također norma propisuje prihvatljivost ostalih nepravilnosti i grešaka na membranskim zavarima koji se vizualno ispituju;

- pukotine nisu dopuštene,
- poroznosti na površini membranskih zavara mogu iznositi max. 2 mm ako nisu na kraju ili ponovnom početku zavarivanja,
- uključci nisu dopušteni na površini membranskog zavara,
- greške vezivanja nisu dopuštene,
- zajed, maksimalna veličina iznosi ≤ 0,5 mm,
- propaljivanje i popravak cijevi nije dopušten,
- loš nastavak nije dopušten,
- greške oštećenja od brušenja ili oštrog alata na površini cijevi nisu dopuštene,

- oštećenja od električnog luka nisu dopuštena, moraju se obrusiti i ispitati magnetskim česticima
- prskotine od procesa zavarivanja normalno se trebaju ukloniti.

Posebno treba izdvojiti greške oštećenja, onečišćenja cijevi kontaktnom provodnicom kao posljedicu kolizije tijekom zavarivanja kada kontaktna provodnica dotakne površinu cijevi. Ovaj tip greške je zapravo uključak bakra na cijevi i nije posebno naveden u normi, ali predstavlja najopasniju grešku koja može uzrokovati propuštanje cijevi. To su najteže greške za otkrivanje tijekom kontrole, stoga je potrebna posebna edukacija zavarivačkog osoblja kako bi se izbjegao ovaj tip grešaka.

4. Bitne varijable kod elektrolučnog zavarivanja pod praškom (EPP)

Zavarivanje membranskih panela izvodi se na stroju prikladnim za takvu vrstu zavarivanja. Uglavnom postoje dva tipa ovakvih strojeva; stroj gdje se panel giba tijekom zavarivanja i stroj gdje je panel učvršćen, a glave za zavarivanje se kreću. Prije početka zavarivanja podešava se sljedeće;

- postavljaju se rolne određenog profila za vođenje ovisno o promjeru cijevi koja se zavaruju,
- podešava se držač trake koji centrira traku u odnosu na simetralu cijevi,
- podešava se kut, visina gorionika, i razmak između gorionika ovisno o koraku panela koji se zavaruje,
- postavlja se dodatni materijal za zavarivanje; žica za zavarivanje koja može biti na kolutima mase 350 kg i prašak za zavarivanje,
- postavlja se traka na napravu koja omogućuje njeno odmatanje tijekom zavarivanja,
- podešava se stroj za kalibriranje širine trake.

Bitne varijable zavarivanja su:

- prije zavarivanja cijevi i traka se čiste, uglavnom sačmarenjem kako bi se spriječile nečistoće koje uzrokuju poroznosti u zavaru i zajede,
- postupak zavarivanja, za zavarivanje membranskih zavara najadekvatnije se pokazao EPP postupak zavarivanja,
- stupanj mehanizacije postupka zavarivanja, najčešće se primjenjuje potpuno mehanizirani ili automatski postupak zavarivanja koji utječe na konstrukciju stroja, brzinu zavarivanja, kvalitetu zavarenih membranskih zidova,
- struja zavarivanja ovisi o promjeru i debljini stijenke cijevi, debljini trake, kvaliteti materijala i promjeru žice za zavarivanje,
- vrsta struje, istosmjerna ili izmjenična utječe na broj EPP glava koji se primjenjuje tijekom zavarivanja, zbog pojave puhanja električnog luka,
- broj EPP glava koje istodobno izvode zavarivanje utječe na brzinu zavarivanja i kapacitet stanice
- napon zavarivanja ovisi o struji zavarivanja, kvaliteti osnovnog materijala i zahtjeva za geometriju zavara,

- brzina zavarivanja ovisi o postupku zavarivanja, stupnju mehanizacije, tipu praška i veličini zrna koji se primjenjuje. Primjena aluminu rutilnog praška omogućuje velike brzine zavarivanja pri čemu se postiže zahtjevana kvaliteta zavarenog spoja,
- unos topline koji je definiran parametrima specificiranim iznad,
- temperatura predgrijavanja ovisi o mikrostrukturi čelika koji se zavaruje
- promjer žice zavarivanja ovisi o postupku zavarivanja i debljini osnovnog materijala, cijevi i trake,
- položaj trake u odnosu na simetralu cijevi treba biti u skladu s EN 12952-5,
- slobodan kraj žice, kut gorionika i međusobni uzdužni razmak između gorionika.

5. Rezultati ispitivanja

Prije početka proizvodnje ispitan je proizvodni ispitni uzorak od strane kontrole Andritz TEP-a [3]. U prvoj fazi, provedena je vizualna kontrola zavarenog spoja prema zahtjevima iz poglavlja 3. Prilikom vizualne kontrole nisu zabilježene nepravilnosti. U drugoj fazi pripremljeni su makro uzorci iz četverocijeva, slika 7. u ispitnom labaratoriju prema zahtjevima kupca.

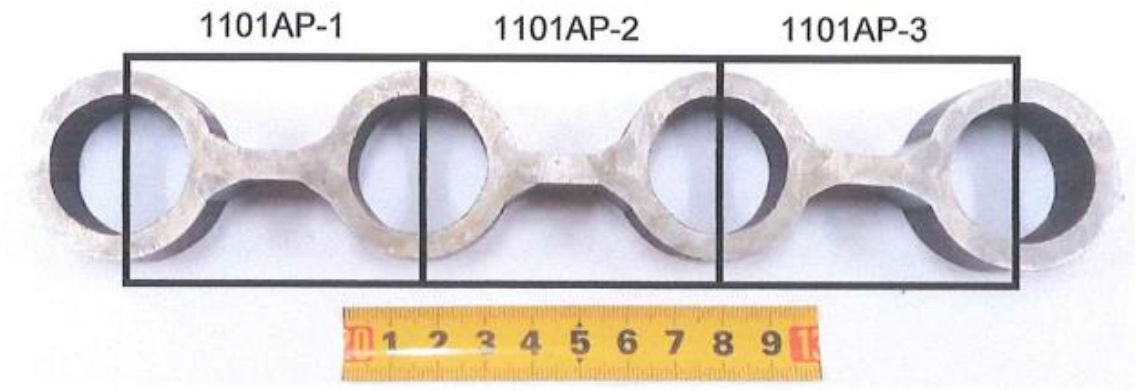

Slika 7. Uzorak za makro ispitivanje membranskih zavara na zavarenom četverocijevu

Izmjerene veličine zahtjevane normom na makro uzorcima su navedne u Tablici 8.;

- minimalna veličina kutnog zavara, odnosno suma kutnih zavara a1+a2 iznosi 8,43 mm što je veće od debljine trake s=6 mm,
- minimalno izmjerena preostala debljina stijenke nakon zavarivanja iznosi er=2,59 mm što je veće od 2 mm,
- maksimalno linearno odstupanje trake u odnosu na simetralu cijevi iznosi Δ=1,9 mm, a dopušteno je 2 mm,
- maksimalno kutno odstupanje trake b1-b2 ili b4-b3 iznosi 0,5 mm, a dopuštena razlika je 3 mm,

- zavar ima blagi prijelaz na osnovni materijal tako da je kut α<30˚, potpuno prihvatljiv.

Tablica 8. Izmjerene veličine ne makro uzorcima prema zahtjevu norme EN 12952-5 sa skicom veličina

DIMENZIJA DIMENSION	UZORAK SPECIMEN			ZAHTJEVI REQUIREMENTS
	1101AP-1	1101AP-2	1101AP-3	
a_1	4,75	4,77	4,96	$a_1 + a_2 \geq s$ $a_3 + a_4 \geq s$
a_2	4,62	4,71	4,36	
a_1+a_2	9,37	9,48	9,32	
a_3	4,69	5,07	4,70	
a_4	4,42	3,36	4,74	
a_3+a_4	9,11	8,43	9,44	
er_1	2,78	2,59	3,61	er ≥ 2 mm
er_2	3,03	2,76	2,81	
er_3	2,81	2,65	3,13	
er_4	3,25	3,21	3,12	
Δ1	0,50	1,10	0,00	Δ ≤ 2 mm
Δ2	0,50	1,00	0,30	
Δ3	1,00	0,90	0,13	
Δ4	1,20	1,90	0,95	
b_1	15,40	17,40	16,10	$b_1 - b_2 = \Delta \leq 3$ mm $b_4 - b_3 = \Delta \leq 3$ mm
b_2	14,90	17,20	15,90	
b_2-b_1	0,50	0,20	0,20	
b_3	16,10	14,20	15,70	
b_4	16,20	14,20	15,90	
b_4-b_3	0,10	0,00	0,20	
α1, α2, α3, α4	< 30°	< 30°	< 30°	α < 30°

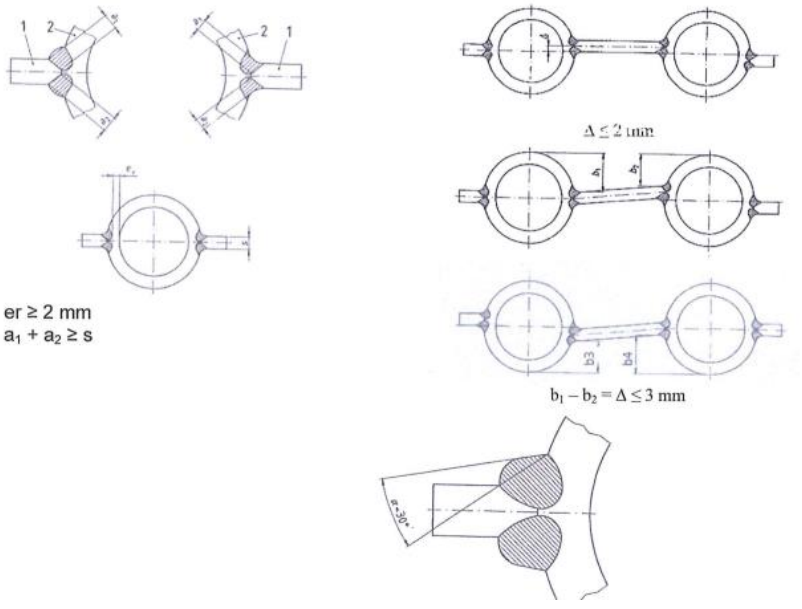

Na makro uzorcima, slika 8., može se zabilježiti da su spojevi bez anomalija, pukotina, grešaka vezivanja, s pravilnom geometrijom zavarenog spoja.

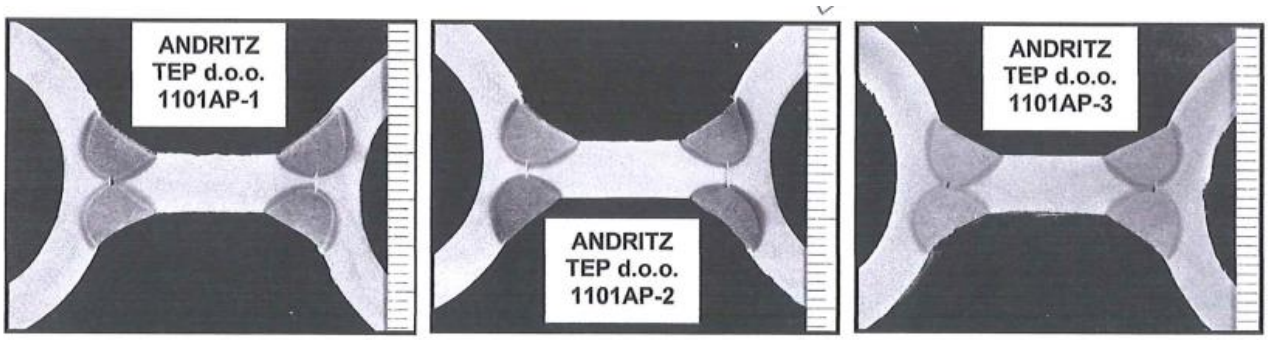

Slika 8. Makro ispitivanje membranskih zavara

Osim zahtjevanih ispitivanja provedeno je ispitivanje tvrdoće jer se radi o nisko legiranom čeliku bainitne mikrostrukture, slika 9. Mjerenje tvrdoće se zahtjeva kod kvalifikacije postupka zavarivanja, i bitna je informacija koja može odrediti primjenu predgrijavanja ili toplinske obrade nakon zavarivanje. Izmjerene tvrdoće HV10 za ovaj čelik su u zahtjevanom području;

- osnovni materijal se kreće od 167 do 183 HV10,
- zona utjecaja topline od 269 do 290 HV
- zona metala zavara od 270 do 279 HV.

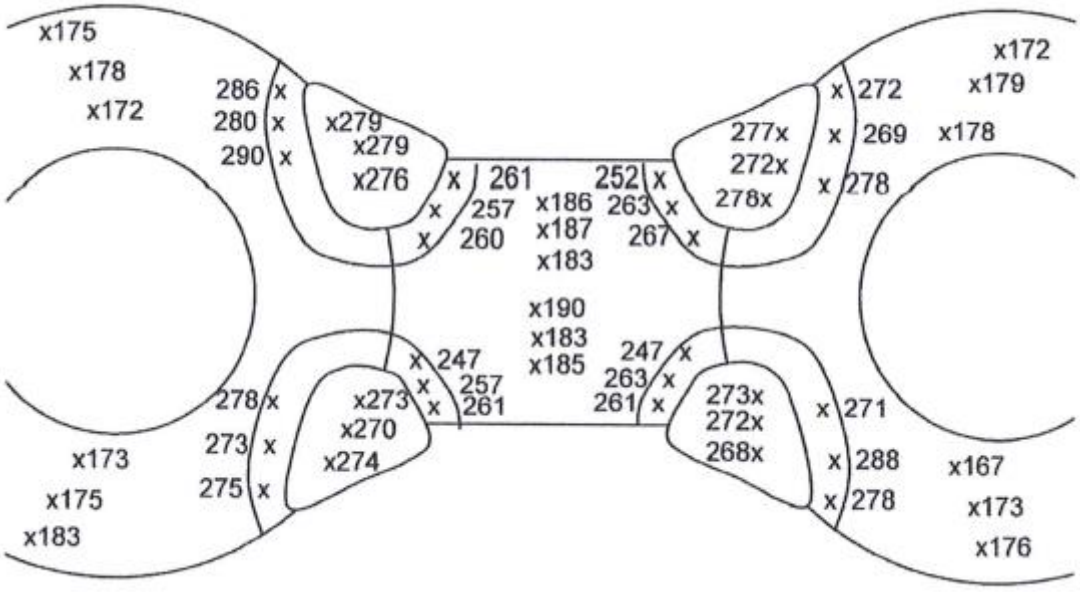

Slika 9. Raspored tvrdoća membranski zavari

Što se tiče rezultata ispitivanje može se zaključiti da su na temelju ispitivanja i izmjerenih vrijednosti u području zahtjevanih normama EN 12952-5 i EN ISO 15613 (EN ISO 15614-1)

6. Zaključak

Membranski zavari po svom opsegu, odnosno dužini i masi su najzastupljeniji na vodocijevnim kotlovima. Na pojedinim kotlovima dužina membranskih zavara može iznositi 500 km i više. Ovisno o broju EPP glava od 2 do 10 ovisi kapacitet stroja. Zbog svoje opsežnosti, zavarivanje membranskih zavara se izvodi na visokoučinskim strojevima posebno konstruiranim za tu namjenu kako bi se postigla zahtjevana kvaliteta zavarenih spojeva i ostale bitne veličine koje definiraju kvalitetu membranskog zida; dimenzije i ravnost panela membranskih zidova. Ovi tipovi strojeva spadaju u kapitalne strojeve tvrtki koje proizvode vodocijevne kotlove i sastavni su dio stanice gdje se zavaruju i proizvode paneli membranskih zidova. Na brzinu zavarivanja značajno utječe prašak za zavarivanje i njegova veličina zrna. Alumino rutilni prašci omogućuju zavarivanje brzinama većim od 1m/min. Priprema i čistoća spoja, parametri zavarivanja, podešavanje kuta EPP glava, položaj trake u odnosu na simetralu cijevi utječu na kvalitetu zavara. Operateri zavarivanja, upravljaju i nadziru sam proces membranskog zavarivanja i po potrebi korigiraju bilo kakva odstupanja, tako da kvaliteta zavarenih spojeva prvenstveno ovisi o njima. Osim stečenih vještina, iskustva i znanja, operateri zavarivanja trebaju biti upoznati o fatalnim posljedicima koje greške tipa propaljivanja cijevi i onečišćenja cijevi bakrenim uključcima mogu uzrokovati tijekom eksploatacije, stoga se od njih traži maksimalna odgovornost i suradnja po ovom pitanju.

7. Literatura

[1] EN 12952-1 izdanje 2015; Vodocijevni kotlovi i pomoćne instalacije – 1. dio: Općenito
[2] EN 10216-2 izdanje 2020; Bešavne čelične cijevi za tlačne namjene - Cijevi od nelegiranih i legiranih čelika s utvrđenim svojstvima pri povišenim temperaturama
[3] Marija Balažić, Tihomir Marsenić, QWI08-04 rev.5, Opća uputa za zavarivanje i popravke (ANDRITZ TEP d.o.o.)

Društvo za tehniku zavarivanja Slavonski Brod

13. Međunarodno znanstveno-stručno savjetovanje SBZ 2025

„STROJARSKE TEHNOLOGIJE U IZRADI ZAVARENIH KONSTRUKCIJA I PROIZVODA, SBZ 2025."
Slavonski Brod, 08. i 09. 05. 2025.

Application and Possibilities of Robotic Welding in the Freight Wagons Production

D. Novak[1,*], L. Burušić[1], D. Tomerlin[1,2], D. Kozak[2], I. Samardžić[2]

[1]TŽV Gredelj Rolling Stock Factory, Croatia
[2]Mechanical Engineering Faculty in Slavonski Brod, University of Slavonski Brod, Croatia

[*] Corresponding Author. E-mail: david.novak@tzv-gredelj.hr

Abstract

The rolling stock industry in general refers to various railway vehicles, including both powered and unpowered vehicles, such as locomotives, freight wagons, passenger cars (i.e. coaches) and non-revenue cars. The freight wagons are unpowered railway vehicles that are used for the transportation of various cargo. In scope of this paper, the application and possibilities of implementing robotic welding processes in the freight wagons production at the TŽV Gredelj company is presented. The main components of a freight wagon are bogies and the wagon frame. Due to the complexity and specifics of the design of these components, their breakdown into subassemblies suitable for the robotization production process are being done. The paper investigates manufacturing processes of such subassemblies, using several robotic welding systems. The general dimensions and weight of the subassemblies and their accessibility during welding are considered. The functionalities and modes of robotic welding are considered, to achieve optimal production and ensure welded joints with required mechanical and exploitation properties. Inspection of welded joints and manufactured welded assemblies in scope of quality control during production is described. Finally, the economic aspects of shifting production from manual to robotic welding is presented through a comparison of the two production approaches.

Keywords: Freight wagon, robotic welding, welded joint, bogie, wagon frame

1. Introduction

Today, in the modern world, railway transport represents one of the most important ways of transporting people and goods around the world. Its importance is constantly growing, which creates a constant need for technological improvements. In the railway industry, the unpowered rail vehicles are generally referred to "wagons". Wagons are designed and used for several purposes, such as transport of cargo (freight wagons), transport of passengers (passenger coaches) or other purposes.

Such cars, when coupled together and hauled by one or more locomotives, form a train. Wagons substantially vary in design and features, depending on the requirements for types of cargo to be transported, as well as the rail route and conditions the need to operate on. Wagon, depending on the design, can include a number of main components [1]:

- Wagon body
- Wagon frame (underframe)
- Bogies
- Wheelsets
- Suspension components, couplings and brakes

Freight wagons can be designed as heavy haul wagons that carry bulk material, and 'mixed' freight wagons that can carry a variety of freight from construction materials to liquids to retail goods and general freight. TŽV Gredelj rolling stock factory, with more than 130 years long tradition, is one of the leading rolling stock factories in this part of Europe. The company is engaged in new vehicles design and manufacturing and also in modernization, rehabilitation and maintenance of various rolling stock vehicles and products (e.g. passenger coaches, low floor trams, diesel and electric locomotives, freight wagons, container wagons, car transportation wagons, etc.) [2].
In scope of this paper, the universal freight wagon from TŽV Gredelj production line, that can transport different goods using different upper structures mounted and connected to the base frame, will be elaborated in more detail. Since the paper is covering the application and possibilities of robotic welding manufacturing processes, the welded structures of freight wagons, and their production, will be put in focus [1], [2].
On the global level, welding technology and manufacturing processes play a key role in the development of railway infrastructure and vehicles, significantly affecting their reliability and safety. Advances in welding technologies enable the optimization of production, increase the durability of structures and reduce maintenance costs, which contribute to more efficient and sustainable railway transport. With constant need for improvements in welding processes, the robotic welding, has established itself as an indispensable production technology. Robotic welding is one of the most advanced technologies in modern industry, enabling high precision, speed and repeatability, especially required during the serial production of railway wagons and products. It is nowadays commonly used in the railway industry where the demands for quality and productivity are very high.

2. Freight wagon structural design

As already mentioned in the introductory part of this paper, the typical freight wagon is built around the several major structural components. Since the paper is discussing the welding processes, it is only relevant to present and describe in more detail the main welded structural assemblies: the welded wagon frame and bogies welded assembly.

2.1. Bogie

Bogies are the structural arrangements that contains the wheelsets and are directly connected to the wagon body/frame. Freight wagons generally use a three-piece bogie design, consisting of two wheelsets, two sideframes (i.e. longitudinal beams) and a crossmember. The bogie is connected to the wagon body by "centre bowl", which allows the bogie to rotate relative to the wagon body. The passenger coaches typically use solid "H" frame-type bogies with primary and secondary air suspension to provide a better ride dampening and dynamics [1].

The freight wagons bogies design which will be reviewed in this paper is the Y25 bogie. Such bogies have a proven design, have been used in freight wagons for over 50 years, with a positive opinion in many European countries. Y25 is the 2-axle bogie for freight wagons with axle load 22.5 t. Maximum wagon speed at an axle load 20/22.5 t can be 120/100 km/h [3].

The 3D model of the Y25 bogie, manufactured by TŽV Gredelj is shown in Figure 1. The main components of this railway bogie are: 1) 2x longitudinal beams, 2) crossmember, 3) 2x wheelsets, 4) 4x axle boxes and suspension elements, 5) brake system, and other components [2].

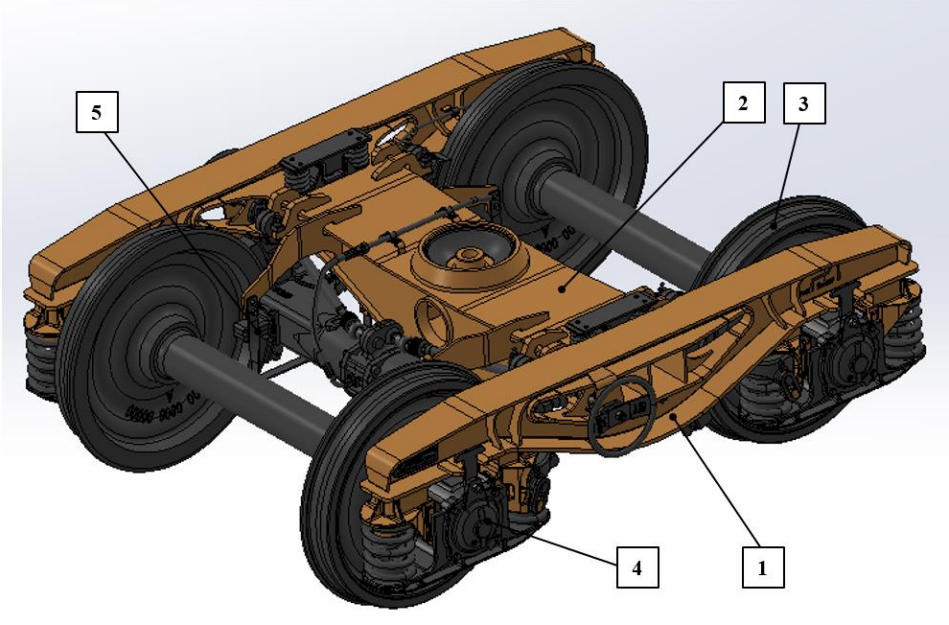

Figure 1. Y25 bogie (TŽV Gredelj) [2]

The Y25 bogie structural components, that are applicable and are currently being produced in TŽV Gredelj using a robotic welding processes are shown in Table 1.

Table 1. The Y25 bogie components applicable for robotic welding

Component	Model

Longitudinal beam	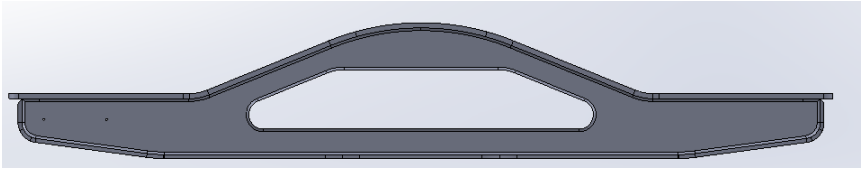
Crossmember	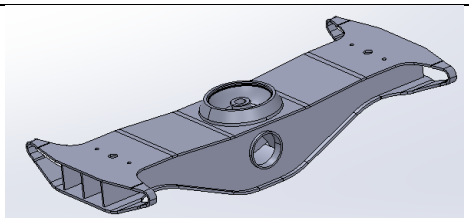

The longitudinal beam and the crossmember are subassemblies of the bogie that are applicable for robotic welding manufacturing processes. The longitudinal beam is welded with the HV8 + z10/5K compound weld (half V weld with fillet weld a5 reinforcement), while the crossmember is welded with a5 and a6 fillet welds. The material of these components is S355J2+N which belongs to material group 1.2 according to ISO/TR 15608.

2.2. Wagon frame

The wagon frame (underframe) has two primary functions. First function is related to supporting the external load the wagon is carrying, and the other function is to transmit longitudinal forces from one wagon to the adjacent wagons in the train composition. Mixed freight wagons and passenger coaches both rely on a low wagon frame on which different body types are further attached. The freigh wagon frame for container transport, is generally designed with continuous longitudinal beams in the centre of the wagon that run the length of the wagon. These longitudinal beams support the external cargon load of the wagon, and also transmit the longitudinal train force to adjacent wagons. Heavy haul wagons (e.g. coal wagon) have the structural design incorporating the frame with the wagon body to allow larger volumetric payloads [1].

Wagon frame welded structures are typically manufactured from structural steel grades. Such structural steel grades reduce the material and manufacturing costs of wagons, provide the ease of manufacture, and also ensure good mechanical properties combined with high fatigue resistance of the welded frame structures. The wagon frame design process generally relies on CAD + FEM software combined approach to achieve optimal design and structural life. The wagon frame design is required to ensure the welded frame structure capable of enduring the maximum longitudinal, vertical, and lateral forces experienced during both regular haulage and shunting operations [1].

The 80ft freight wagon frame from the TŽV Gredelj production line is shown in Figure 2. It is the 24.4 m long freight wagon, and depending on the containers and pallets attached, capable of transporting woodchips or wood in a bulk form, steel slabs, plates or pipes, palletized goods etc.

Figure 2. Freight wagon frame 80ft (TŽV Gredelj) [2]

The 80ft freight wagon frame 3D model is shown in Figure 3.

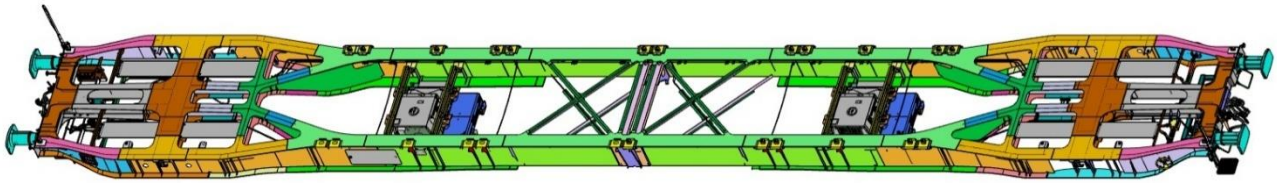

Figure 3. Freight wagon frame 3D model (TŽV Gredelj) [2]

The welded wagon frame itself consists of various subassemblies and parts. The frame is built around the longitudinal support beams with transverse stiffeners, and two headstock assemblies being the end members of the frame assembly. Subassemblies applicable to robotic welding processes are: the longitudinal beam, headstock beam, "S" beam, cross, coupler carrier, transverse beams, shown in Table 2.

Table 2. The wagon frame components applicable for robotic welding

Component	Model

Longitudinal beam	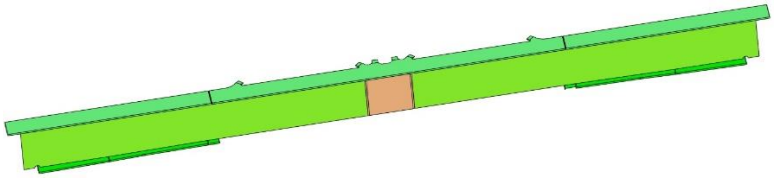
Headstock beam	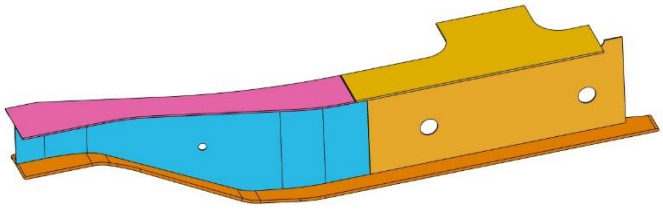
"S" beam	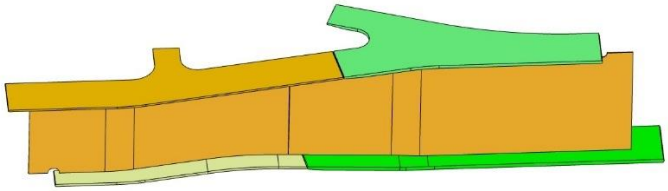
Cross	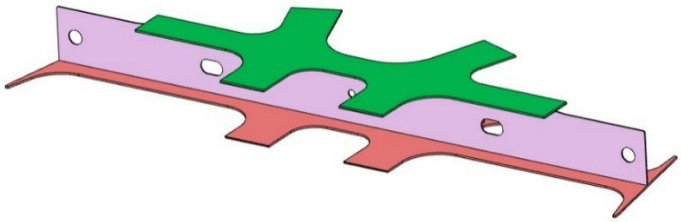
Coupler carrier	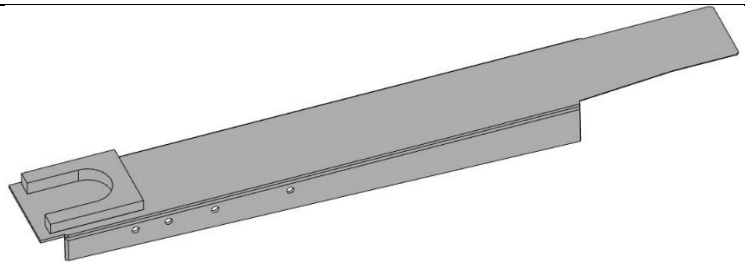
Transverse beam	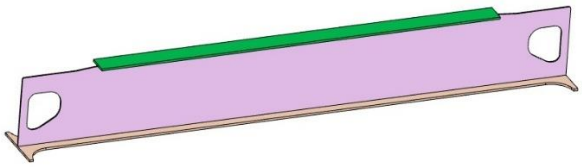

The material from which these components are made is S355J2+N/S355J2C+N which belongs to material group 1.2 according to ISO/TR 15608. The welds performed on these components are fillets a2.5, a3, a4, a5, and Y or V butt welds 7HY, 10HV.

3. Robotic welding

The welding robot station is an automated system in which industrial robots perform welding operations on components. These stations use robots equipped with specialized welding tools, sensors, and computer systems to control the welding process, ensuring high precision, repeatability, and efficiency in production. The requirements in railway vehicle construction are constantly increasing. Higher safety standards, increased efficiency and growing cost pressure are presenting challenges of switching from manual to robotic production. The automated welding systems increase the production quality, reduce production times and cut operating costs.
TŽV Gredelj company currently uses four robotic stations:

- Daihen Varstroj using OTC robots (1 unit),
- Cloos robotic station (2 units),
- Yaskawa (1 unit)

3.1. Robotic station Daihen Varstroj

The welding robotic station VRC 2x FD-B6L 1GM/2d is intended for welding the longitudinal beams of the Y25 bogie. The welding process used is MIG/MAG, and the robotic station is shown in Figure 4. [4].

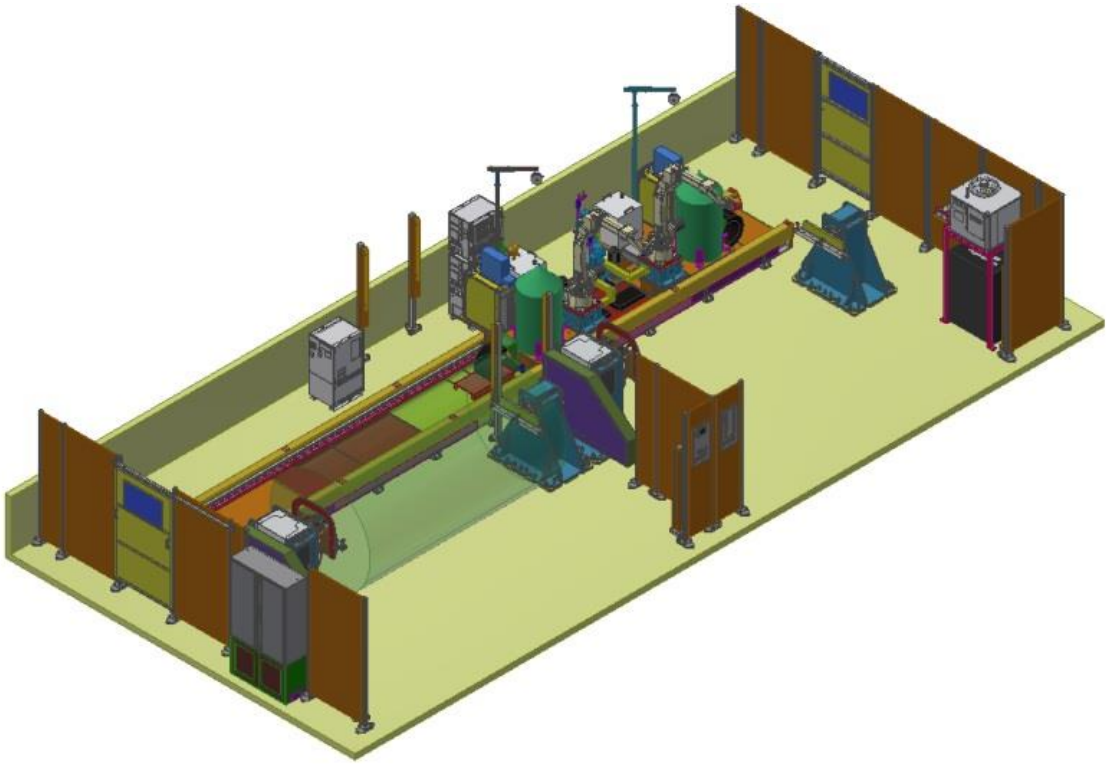

Figure 4. Robotic welding station 2x FD-B6L 1GM/2d [4]

The welding robot station consists of the following components [4], [5]:

- robot; OTC FD-B6L (2x)

- welding source; WB-P502L (2x)
- welding torch; Binzel ABIROB W500 (2x)
- positioner P-1500K ROBO (2x)
- robot trolley (2x)
- slider for the robot trolley

Hydraulic clamping devices for the longitudinal beam are mounted on the single-axis positioners P-1500K ROBO. Since there are two types of longitudinal beams, A and B, the robotic station includes two workstations: one for welding the type A longitudinal beam, and the other for welding the type B longitudinal beam.
The FD-B6L robot (Figure 5) is a 6-axis robot with a weight of 278 kg. The positional repeatability of the tool center point (TCP) is 0.08 mm. The payload capacity of the robot arm is 6 kg for all welding tasks, and it can be equipped with various torches and sensors. This robot is equipped with an integrated iCAT shock sensor and a Abicor Binzel ABIROB W500 welding torch. A touch sensor is used for part scanning [5].

Figure 5. OTC FD-B6L [5]

Figure 6. WB-P502L [6]

The listed welding power source, Welbee Inverter P502L, supports DC, DC pulse, DC TIG, and DC STICK/MMA welding processes. For welding the longitudinal beam, DC is used for the root pass (spray transfer of filler material), while DC Pulse is used for the fill passes. The welding power source provides 400 A at 100% duty cycle (DC process) and is shown in Figure 6 [6].

3.2. Robotic station Cloos

The Cloos QRC350 welding robot station is intended for welding the subassemblies of the wagon frame presented in chapter 2.2. Wagon frame. The welding process is MIG/MAG, and the robotic station itself consists of the following components (Figure 7):

- robot; QRC350
- welding source; Cloos GLC 603 Quinto II (2x)
- welding torches:
  - single; MRW350
  - tandem
- positioners:
  - single – axis WPV – 5000N
  - two – axis WPEK 25000N
- robot trolley
- slider for the robot trolley

Figure 7. Robotic welding station Cloos QRC350

The fixtures used for holding the wagon frame subassemblies are mechanical fixtures. Three fixtures are used for welding the mentioned subassemblies of the wagon frame, two of which are interchangeable on the two-axis positioner, while one is mounted on the single-axis positioner.
The QIROX QRC 350 (Figure 8) is a 6-axis articulated arm robot with a weight of 235 kg. The robot is mostly used in upright or overhead position (this setup is implemented at TŽV Gredelj) and is mounted on a base or directly at a robot positioner (robot trolley). QIROX QRC-350 robot has a classic wrist, capable of mounting welding torches, flame cutters, and other tools with a weight of up to 15 kg. The integration of a tool changer on the wrist allows the robot to perform multiple processes. An anti – collision sensor is integrated in the robot flange [7].

Figure 8. Cloos QRC350 [7]

Figure 9. GLC 603 Quinto II [8]

The listed welding power source, Cloos GLC 603 Quinto II (Figure 9), supports DC, DC pulse, TIG DC, MIG brazing and tandem welding processes. The current range of this welding power source is from 40 to 600 A [8].

3.3. Subassembly production

This section of the paper will describe three examples of robotic production, of bogie and wagon frame subassemblies, presented in chapters 2.1 and 2.2. The production of the longitudinal beam of the Y25 bogie will be described first. Before robotic welding, the longitudinal beam, which consists of three parts, must be assembled and tack welded inside the fixture shown in figure 10.

Figure 10. Longitudinal beam fixture

Figure 11. Hydraulic fixture (Daihen Varstroj)

After the assembly, the longitudinal beam is placed into a hydraulic fixture (Figure 11) on the Daihen Varstroj robotic station. The beam is first clamped using hydraulic components, then the robot is set to automatic mode and the welding process is commenced. The welding sequence is as follows: first, root passes are welded on both sides of the longitudinal beam, followed by the second pass (i.e. the fill pass) on both sides. Two welding robots perform welding simultaneously. After welding, the part remains in the hydraulic fixture for 25 minutes to cool down. The welding sequence is shown in Figure 12, and all welds are performed in the PB position according to standard EN ISO 6947.

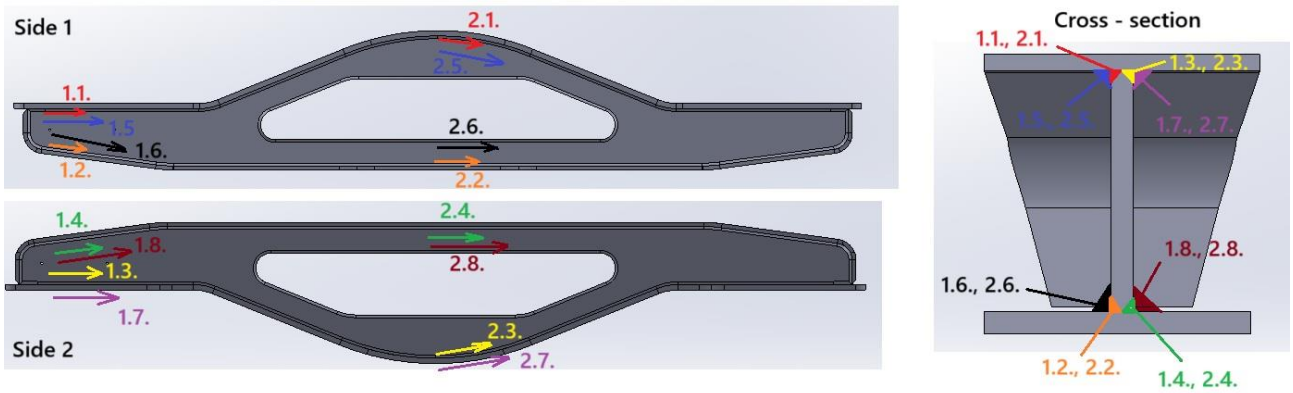

Figure 12. Welding sequence of the Y25 longitudinal beam

The welding parameters are given in Table 3.

Table 3. Welding parameters for Y25 longitudinal beam

Parameters	Welding process	Pass	
		Robot 1	Robot 2
Welding current, I = 360 [A] Voltage, U = 33 [V] Welding speed, v = 60 [cm/min]	DC	1.1., 1.2.	2.1., 2.2.
Welding current, I = 362 [A] Voltage, U = 33 [V] Welding speed, v = 54 [cm/min]	DC	1.3., 1.4.	2.3., 2.4.
Welding current, I = 310 [A] Voltage, U = 35 [V] Welding speed, v = 32 [cm/min]	PDC	1.5., 1.6.	2.5., 2.6.
Welding current, I = 310 [A] Voltage, U = 35 [V] Welding speed, v = 33 [cm/min]	PDC	1.7., 1.8.	2.7., 2.8.

The HV8 + z10/5K compound weld (half V weld with fillet weld a5 reinforcement) on the longitudinal beam is shown in Figure 13.

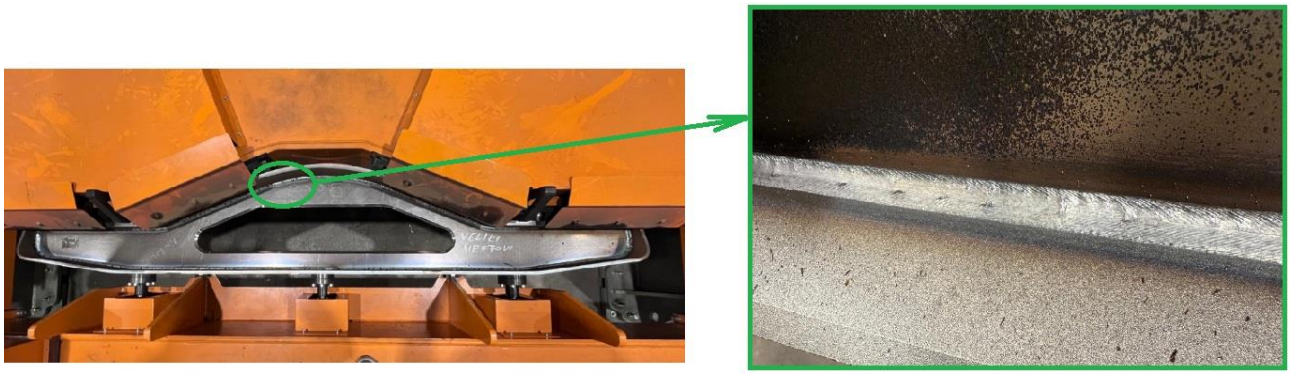

Figure 13. Weld HV8 + z10/5K on the longitudinal beam

On the Cloos robotic station, described in Chapter 3.2 of this paper, subassemblies of the wagon frame are welded. As an example, the "S" beam and the transverse beam will be considered. The fixture for holding the "S" beam is mounted on the two-axis positioner, while the fixture for the transverse beam is located on the single-axis positioner. First, the "S" beam is assembled using tack welds in the fixture, as shown in Figure 14.

Figure 14. "S" beam fixture

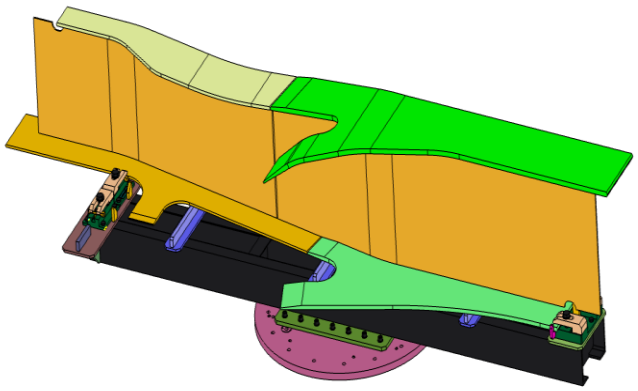

Figure 15. "S" beam fixture (Cloos)

After the assembly, the "S" beam is placed on the positioner, the robot is set to automatic mode, and the welding process begins. Since the fixture is not hydraulic, rather mechanical (Figure 15), and the subassembly is clamped only at three points, which leads to inevitable deformations during welding, an arc sensor is integrated into the welding process to compensate for these deformations. Before welding, the starting point of welding is located using a touch sensor. The welding sequence (Figure 16) is defined, and all welds are performed in the PA position according to standard EN ISO 6947.

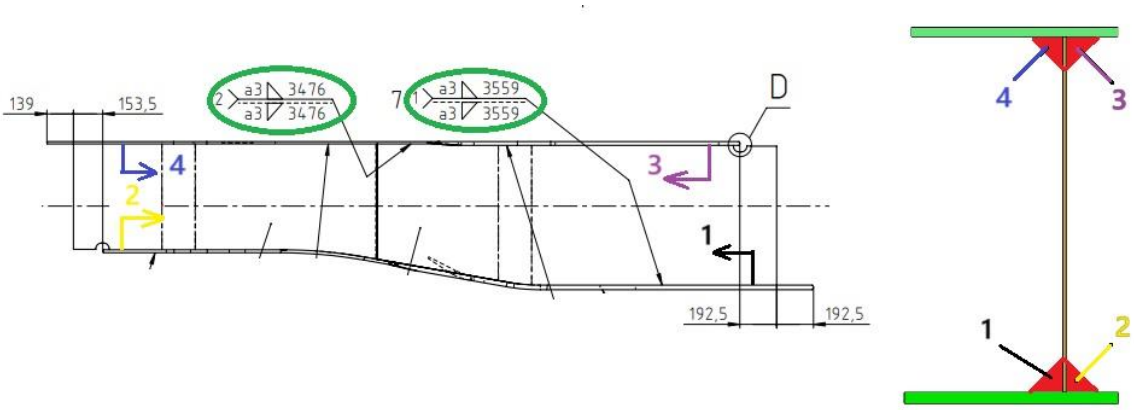

Figure 16. Welding sequence of "S" beam

The welding parameters are given in Table 4.

Table 4. Welding parameters for "S" beam

Parameters	Welding process	Pass
Welding current, I = 340 [A]	PDC	1, 2, 3, 4
Voltage, U = 34.8[V]		
Welding speed, v = 55 [cm/min]		

The a3 double sided fillet weld on the "S" beam is shown in Figure 17.

Figure 17. Weld a3 on the "S" beam

The same applies to the transverse beam. It is assembled and tack welded in the fixture, after which it is transferred to the robotic station and placed in the fixture on the single-axis positioner. Before

welding begins, a touch sensor is used to locate the starting point of the weld, while during welding, an arc sensor is used to compensate for deformations caused by the welding process. The welding sequence (Figure 18) is defined, and all welds are performed in the PA position according to standard EN ISO 6947.

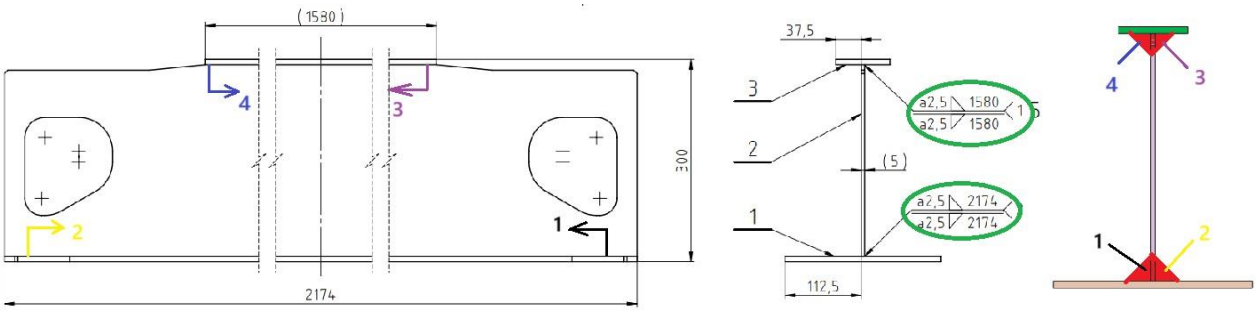

Figure 18. Welding sequence of transverse beam

The welding parameters are given in Table 5.

Table 5. Welding parameters for transverse beam

Parameters	Welding process	Pass
Welding current, I = 295 [A]	PDC	1, 2, 3, 4
Voltage, U = 33 [V]		
Welding speed, v = 56 [cm/min]		

3.4. Quality of robotic welding process

The evolution from manual to robotic welding has significantly transformed modern manufacturing, particularly in industries where precision, consistency, and efficiency are critical. The robotic welding processes offers noticeable improvements over manual methods, such as improved repeatability and round-the-clock productivity. One of the most prominent benefits of robotic welding is its ability to consistently repeat identical welds with high precision. This level of repeatability minimizes variability and deviations in weld quality (e.g. geometry of welds), which is particularly important in applications that demand structural reliability and visual uniformity. However, robotic welding systems are not inherently applicable to nonconformities and unique cases. Unlike skilled human welders, robots cannot intuitively respond to slight changes in joint configuration or unexpected circumstances. To mitigate this limitation, additional technologies such as arc sensors and vision systems must be integrated to allow real-time adjustments. Without these tools, even minor inconsistencies in joint alignment can lead to weld defects. The success of robotic welding relies heavily on precise preparation of the workpieces. Subassemblies must be manufactured within narrow tolerance fields, as even small deviations can disrupt the robot's programmed path. Joint geometry

should be simple and uniform, avoiding abrupt changes in shape that could confuse the robotic arm or reduce the weld quality. Cleanliness is equally critical, surfaces must be free from contaminants such as rust, oil or grease, as robots lack the capacity to detect or clean such imperfections prior to welding. In addition to surface preparation, misalignments, gaps, or irregularities can easily go unnoticed by the robot and result in weak or incomplete welds. Quality assurance remains a vital component of robotic welding. Non-destructive testing methods like visual inspection (VT), magnetic particle inspection (MT) and ultrasonic inspection (UT) are often employed to verify weld integrity. Destructive testing of welds, in form of macro sections (Figure 19 and Figure 20) is also included to verify the weld geometric features and possible surface and volumetric defects. The high initial investment in robotic welding is justified by the long-term quality gains. Reduced rework, fewer defects, and improved product performance lower overall production costs.

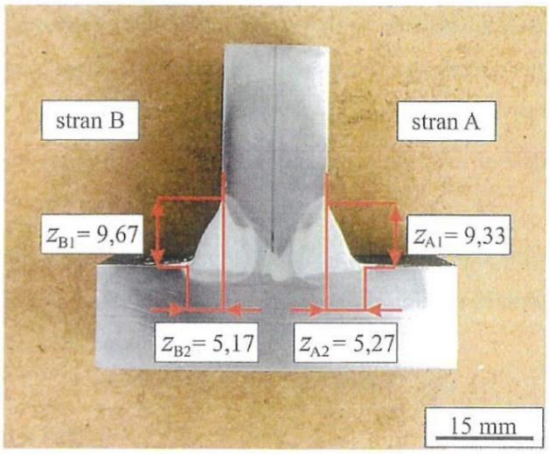

Figure 19. Weld HV8 + z10/5K macro section dimensions

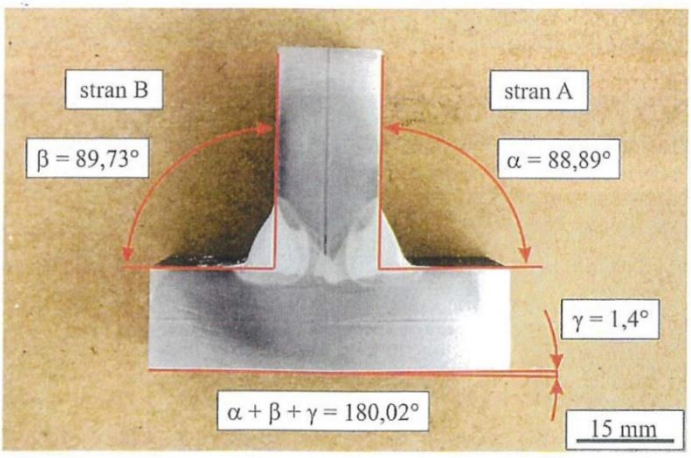

Figure 20. Weld HV8 + z10/5K macro section angularity

3.5. Economic aspects

Considering the economic and technological parameters, automated welding offers several advantages over conventional manual technology that justify its higher initial investment. The most obvious benefit is the significant increase in the productivity. Robots can work continuously without breaks, which leads to higher throughput and shorter cycle times. This consistent operation translates into a faster return on investment in high-volume production settings.

Another key economic benefit is improved weld quality and consistency. Robots eliminate human error and fatigue, which results in fewer defects and less rework. Less rework means less wasted material and time, both of which are cost drivers in a manufacturing environment. Robotic systems also optimize material usage, reducing over-welding and minimizing filler material consumption. In terms of operational costs, robotic welding minimizes safety incidents, thus lowering insurance premiums and downtime from workplace injuries.

Energy consumption is another factor. Automated systems can be programmed to use energy more efficiently than humans. Over time, these savings contribute significantly to lowering the cost per unit. While the upfront cost of installing robotic systems is high, their operational lifespan and low maintenance requirements balance the investment.

4. Conclusion

Robotic welding has proven to be a transformative technology in the production of freight wagons, particularly in achieving consistently high-quality welds. At TŽV Gredelj, the implementation of robotic welding on several critical structural components, demonstrated how automation can enhance structural integrity and production reliability.

The precision and repeatability offered by robotic welding systems significantly reduce human error and inconsistencies, ensuring each weld meets strict mechanical and exploitation criteria. Unlike manual processes, robots maintain consistent parameters throughout every cycle, which leads to uniform heat input and less weld defects such as porosity, undercuts, and incomplete penetration. This is especially vital in railway applications where weld quality directly correlates with the safety and longevity of the rolling stock.

The key factor in ensuring weld quality is the preparation of the components to be welded. Robotic welding requires clean surfaces and simplified joint geometry to fully capitalize on the system's capabilities. At TŽV Gredelj, dedicated attention is given to tack welding, surface treatment and adherence to validated Welding Procedure Specifications (WPS). The result is not only visually and structurally conforming weld, but one that consistently meets inspection standards, including non-destructive testing methods like ultrasonic testing.

The data-driven nature of robotic welding further enhances quality assurance. Real-time monitoring of parameters such as voltage, current, and wire feed speed enables operators to maintain full process control, detect anomalies immediately and document every weld for traceability. This traceability is essential in meeting the utmost quality standards required in the rail industry.

5. References

[1] Spiryagin, Maksym et al. (2014). Design and Simulation of Rail Vehicles. 1st Edition, CRC Press (ISBN ISBN 978-1-4665-7566-0)

[2] TŽV Gredelj (Rolling Stock Gredelj) documentation

[3] Dusza, Mirosław (2023). Freight car model with Y25 bogies stability analysis. *Rail Vehicles/Pojazdy Szynowe,* 3-4, 13-24. https://doi.org/10.53502/RAIL-175725

[4] TŽV Gredelj (2023). Tehnično navodilo za varno uporabo, preizkušanje in vzdrževanje: Robotska varilna celica tip: *VRC 2x FD-B6L 1GM/2d*

[5] Daihen (2020). Arc Welding Robot FD-B6L. https://daihen.mx/wp-content/uploads/2020/04/FD-B6L-brochure.pdf

[6] OTC Daihen (2021). Pulzni MAG/MIG Varilni izvor, navodilo za uporabu
[7] Carl Cloos Schweisstechnik GmbH *Welding robot:* Systematic automated welding and cutting. https://www.cloos.de/
[8] Cloos (2012). Product catalogue. https://www.alterct.com/images/Katalog_2012_EN_cloos.pdf

Društvo za tehniku zavarivanja Slavonski Brod

13. Međunarodno znanstveno-stručno savjetovanje SBZ 2025

„STROJARSKE TEHNOLOGIJE U IZRADI ZAVARENIH KONSTRUKCIJA I PROIZVODA, SBZ 2025."
Slavonski Brod, 08. i 09. 05. 2025.

ZAVARIVANJE Cu-Al-Ni LEGURE S PRISJETLJIVOSTI OBLIKA TIG POSTUPKOM

M. Gojić[1,2,*], S. Kožuh[1], I. Ivanić[1], D. Dumenčić[1], F. Kozina[1], I. Garašić[3], I. Juraga[3], B. Kosec[4], A. Nagode[4]

[1]Sveučilište u Zagrebu Metalurški fakultet, Aleja narodnih heroja, 3, 44000, Sisak
[2]Sveučilište Sjever, Trg Dr. Žarka Dolinara, 1, 48000, Koprivnica
[3]Fakultet strojarstva i brodogradnje Sveučilišta u Zagrebu, Ivana Lučića 5, 10000 Zagreb
[4]Prirodoslovnotehnički fakultet Sveučilišta u Ljubljani, Aškerčeva 12, 1000 Ljubljana

Autor za korespodenciju: gojic@simet.unizg.hr

Sažetak

U ovom radu prikazan je dio znanstvenih istraživanja pri zavarivanju legura s prisjetljivosti oblika na bazi bakra. Kao osnovni materijal korištena je šipka promjera 8 mm iz Cu-12,8Al-4,1Ni (mas. %) legure s prisjetljivosti oblika koja je dobivena postupkom kontinuiranog lijevanja u indukcijskoj peći. Nakon lijevanja provedena je toplinska obrada, zavarivanje te karakterizacija legure prije i nakon zavarivanja (mikrostrukturna analiza i mjerenje mikrotvrdoće). Toplinska obrada se sastojala od austenitizacije na 850 ^{o}C u trajanju 30 minuta uz naknadno hlađenje u vodi. Sučeljeno zavarivanje je provedeneo TIG postupkom uz 100 % argon (brzina protoka 10 l/min.) kao zaštitni plin kod sljedećih parametara: jakost struje 80 A, napon 13 V, brzina zavarivanja 14,4 cm/min. s unosom topline od 1,63 kJ/cm. Dodatni materijal je pripremljen strojnom obradom (tokarenje) na promjer 3 mm iz osnovnog materijala. Za karakterizaciju su korištene optička mikroskopija, pretražna elektronska mikroskopija i energijsko disperzijska spektroskopija, te mjerenje mikrotvrdoće (HV_{10}) na osnovnom materijalu, zoni utjecaja topline i u zoni taljenja. Kao sredstvo za nagrizanje korištena je otopina 2,5 mg $FeCl_3$, 48 ml metanola i 10 ml HCl. Utvrđena je martenzitna mikrostruktura u lijevanom stanju, nakon toplinske obrade kao i nakon zavarivanja. Martenzitna mikrostruktura je osnovni preduvjet za efekt prisjetljivosti oblika. Prosječna vrijednost mikrotvrdoće osnovnog materijala je 396,5 HV_{10}, zone utjecaja topline je 456,1 HV_{10}, a zone taljenja je 411,9 HV_{10}.

Ključne riječi: legure s prisjetljivosti oblika, lijevanje, TIG zavarivanje, martenzit, mikrotvrdoća

Abstract

In this work the part of scientific research during welding of shape memory alloys based on copper is shown. As base material used of the bar with diameter of 8 mm from Cu-12.8Al-4.1Ni (% by weight) shape memory alloy which obtained by means of continuous casting in the induction furnace. After casting, the heat treatment, welding as well as characterization of alloy before and after welding (microstructural analysis and testing of microhardness). Heat treatment consisted from austenitatization at 850 ^{o}C for 30 minutes followed by quenching in water. Butt welding is carried out using TIG procedure by 100 % Ar (flow rate of 10 l/min.) as the protective gas at following parameters: current intensity of 80 A, voltage of 13 V, speed welding of 14.4 cm/min with input heat of 1.63 kJ/cm. The filler material was prepared by machine treatment (turning) on diameter 3 mm from the base material. For characterisation the optical microscopy, scanning electron microscopy and energy dispersive spectroscopy as well as testing of microhardness (HV_{10}) on the base material, heat affected zone and weld metal are used. As reagent for etching the solution 2,5 mg $FeCl_3$, 48 ml metanola and 10 ml HCl was used. It is found the martenzite microstructure in casting condition, after heat treatment as well as after welding. Martenzite microstrucute is the basic precondition for shape memory effect. Avarage value of microhardness of the base material is 396,5 HV_{10}, heat affected zone is 456,1 HV_{10} and the weld metal is 411,9 HV_{10}.

Keywords: Shape memory alloys, casting, TIG welding, martenzite, microhardness

1. Uvod

Efekt prisjetljivosti oblika legura u suštini je prisjećanje prethodno deformacijom unesenog oblika materijala, a u fizikalnom smislu je posljedica martenzitne fazne transformacije u strukturi homogene tvari [1]. Ta se fazna transformacija može potaknuti mehaničkim i/ili toplinskim putom. Ove legure karakteriziraju jednosmjerni i dvosmjerni efekt prisjetljivosti oblika, te svojstva pseudoelastičnosti i superplastičnosti [2]. Legure s prisjetljivosti oblika imaju primjenu u brojnim područjima (strojarstvo, elektroindustrija, medicina itd.). Efekt prisjetljivosti oblika prvi je primijetio švedski istraživač Ölander 1932. godine na Au-47,5 at. % Cd leguri [2-5] kada je uočeno da martenzitna faza može poprimiti oblik koji se mijenja s promjenom temperature. Ozbiljniji interesi za ove legure počinju tek kad je isti efekt uočen na leguri Ni-Ti, poznatoj kao nitinol. Ova legura sadrži oko 50 mas. % Ni i 50 mas. % Ti i prvi put je dobivena početkom 1960.-ih. godina u američkom laboratoriju Naval Ordinance Laboratory (NOL). Stoga i naziv nitinol potječe od inicijala kemijskih elemenata (Ni, Ti) i navedenog američkog laboratorija.
Međutim zbog previsoke cijene nitinola provode se istraživanja s ciljem dobivanja i drugih legura s prisjetljivosti oblika koje imaju prihvatljiviju cijenu izrade. Među njima su najpoznatije legure na bazi bakra (Cu-Al-Ni, Cu-Al-Zn, Cu-Al-Mn itd.), na bazi željeza (Fe-Mn, FePt, FeMnSi, FeCoNiTi itd.), na bazi plemenitih metala (Au-Cd, Au-Ag, Pt-Al, Pt-Ti itd.) [6-8]. Legure s prisjetljivosti

oblika na bazi bakra zbog svojih dobrih električnih i toplinskih svojstava i niže cijene te lakšeg dobivanja su dobra alternativna skupljim Ni-Ti legurama. Postoji niz prednosti Cu-Al-Ni legura, u odnosu na NiTi leguru: lakše taljenje, lijevanje i kontrola kemijskog sastava, veći Youngov modul elastičnosti, viša radna temperatura (do 200°C) i što je najvažnije bolja stabilnost dvosmjernog efekta prisjetljivosti oblika. No primarni njihov nedostaci su slabija deformabilnost i sklonost prema krhkom lomu zbog visoke elastične anizotropije, velikih zrna te izlučivanja sekundarnih faza (precipitati) i nečistoća po granicama zrna.
Općenito je zavarljivost legura s prisjetljivosti oblika otežana i kompleksna, zbog niže čvrstoće zavarenog spoja, mogućnosti nastajanja intermetalnih spojeva, potrebe za što užom zonom utjecaja topline itd. Prisutni problemi su u prvom redu povezani s procesom rafinacije u zoni taljenja zavarenog spoja i u potrebnom razvoju dodatnih materijala. Primarno, iz područja zavarivanja, se provode na Ni-Ti legurama [9-13], posebno laserski, plazmom, elektronskim snopom, trenjem, TIG postupkom itd. Vrlo je malo istraživanja na području zavarivanja legura s prisjetljivosti oblika na bazi bakra [14, 15]. Stoga su u ovom radu prikazana dijelom istraživanja Cu-12,8Al-4,1Ni (mas. %) legure s prisjetljivosti oblika zavarene TIG postupkom kao prva u Republici Hrvatskoj.

2. Eksperimentalni dio

Za izradu Cu-Al-Ni predlegure s prisjetljivosti oblika provedeno je taljenje tehnički čistih komponenti (Cu, Al i Ni) u vakuum indukcijskoj peći u zaštitnoj atmosferi argona. Peć za taljenje spojena je na uređaj za vertikalno kontinuirano lijevanje te se cijeli postupak (taljenje predlegure mase 15 kg i lijevanje šipki promjera 8 mm) provodio u zaštitnoj atmosferi argona (slika 1). Temperatura taline iznosila je 1230°C, a brzina lijevanja iznosila je 295 mm/min. Za lijevanje korištena je grafitna kokila promjera 8 mm koja je postavljena u Cu-vodom hlađeni kristalizator. Duljina oscilacije kokile je iznosila 2-5 mm, a vrijeme mirovanja između oscilacije kokile je bilo 0,3-0,1 s.

a) b) c)

Slika 1. Dobivanje legure Cu-Al-Ni postupkom kontinuiranog lijevanja

Nakon lijevanja provedena je toplinska obrada šipki koja se sastojala od austenitizacije na 850 °C u trajanju 30 minuta uz naknadno hlađenje u vodi. Sučeljeno zavarivanje je provedeno TIG postupkom (uređaj Fronius 230i AC/DC) uz 100 % argon (brzina protoka od 10 l/min.) kao zaštitni plin kod sljedećih parametara: jakost struje 80 A, napon 13 V, brzina zavarivanja 14,4 cm/minuta, s unosom topline od 1,63 kJ/cm (slika 2). Dodatni materijal (elektroda) je pripremljen strojnom obradom (tokarenje) na promjer 3 mm iz kontinuirano lijevanih šipki.

Metalografska priprema obuhvaćala je abrazivno rezanje uzoraka, ulaganje u vodljivu masu, brušenje te grubo i fino poliranje. Uzorci su rezani pomoću uređaja Struers Secotom-60 uz stalno hlađenje emulzijom kako bi se spriječilo njihovo pregrijavanje. Nakon rezanja, uzorci su toplo prešani u bakelitnu masu pomoću uređaja Struers CitoPress. Proces se odvijao pri temperaturi od 180 °C i tlaku od 250 bara, u trajanju od 2 minute. Po završetku prešanja uzorci su automatski hlađeni vodom i zadržani u cilindru još 5 minuta. Brušenje i poliranje provedeni su na automatskom uređaju Struers Tegramin-30 standardnim postupkom za pripremu Cu-legura: brušenje na SiC brusnom papiru gradacije 320 uz hlađenje vodom, grubo poliranje na podlozi MD-Largo uz dodatak suspenzije DiaPro 9,0 µm, fino poliranje na podlozi MD-Mol uz dodatak suspenzije DiaPro 3,0 µm i završno poliranje na podlozi MD-Chem uz dodatak suspenzije DiaDuo 1,0 µm. Korištena otopina za nagrizanje uzoraka je 2,5 g $FeCl_3$, 48 ml metanola i 10 ml HCl.

Metalografska analiza izvedena je pomoću optičkog mikroskopa DSX1000 te pretražnih elektronskih mikroskopa (TESCAN VEGA TS 5136 MM i SEM ThermoScientic Quattro S). Kemijski sastav osnovnog materijala, zone utjecaja topline i zone taljenja određen je pomoću energetsko disperzijskog spektrometra (EDS Ultim, Oxford Instruments). Mjerenje mikrotvrdoće osnovnih elemenata zavarenog spoja provedeno je pomoću Vickers metode (HV_{10}) mikrotvrdomjerom Leica VMHT s vremenom utiskivanja od 15 s.

a) b) c)

Slika 2. Pripremljeni V-spoj (a), operativni postupak TIG zavarivanja (b) i zavareni spoj (c)

3. Rezultati i diskusija

Na slikama 3-7 prikazane su mikrografije dobivene optičkim mikroskopom (OM) i pretražnim elektronskim mikroskopom (SEM) u struji sekundarnih i raspršenih elektrona s odgovarajućim spektrima snimljenih energetsko disperzijskom spektrometrijom (EDS). Na dobivenim

metalografskim snimkama Cu-Al-Ni legure vidljiva je tipična martenzitna mikrostruktura u lijevanom stanju (slika 3) kao i u svakom dijelu zavarenog spoja (osnovni materijal, zona utjecaja topline i zona taljenja) nakon zavarivanja (slike 4a i b - 6a, i b). Očito da je brzina hlađenja prilikom skrućivanja i nakon lijevanja i nakon zavarivanja bila dovoljno velika da nije postojala mogućnost nastajanja niskotemperaturnih faza te je eutektoidni raspad zaustavljen i odvijala se samo martenzitna fazna transformacija. Na OM i SEM mikrografijama jasno su vidljive granice zrna, a martenzitne iglice imaju različitu orijentaciju u pojedinim zrnima.

Može se ustvrditi da se mikrostruktura sastoji od spontano nastalog martenzita igličastog oblika. Također je i orijentacija kristala različita. Martenzitne iglice imaju različitu orijentaciju unutar pojedinog zrna, što se može objasniti nukleacijom grupa martenzitnih pločica na brojnim mjestima unutar zrna i stvaranjem lokalnog naprezanja unutar zrna koje omogućuje nastajanje više grupa različito orijentiranih pločica. Na rubu kristali nastaju pod određenim kutem te prema literaturi [16] taj kut iznosi oko 60 °. Prema istraživanju kojeg su proveli Lojen i suradnici [17], maksimalna postignuta brzina fronte skrućivanja je oko 2,1 mm/s, stoga je moguće da fronta kristalizacije, započinjući od vanjskog ruba uzorka prema sredini, uzrokuje nastajanje preferirane orijentacije rastućih zrna. Mikrostrukturna analiza u ovom istraživanju potvrdila je potpunu transformaciju β faze u martenzitnu fazu u lijevanom stanju te nakon toplinske obrade (kaljenjem) i nakon zavarivanja u svim elementima zavarenog spoja. Nastala mikrostruktura je rezutirala transformacijom β faze u martenzit ispod M_s temperature. Martenzit je nastao primarno kao igličasti martenzit tzv. V-oblika. Morfologija nastale martenzitne mikrostrukture je tipična samoprilagođavajuća zig-zag morfologija [18]. Cu-Al-Ni legure sa sadržajem aluminija iznad 11 mas. % transformiraju iz austenitne β faze u β_1 sređenu fazu s DO_3 tipom kristalne strukture, prije nego započne martenzitna transformacija. Legure sa sadržajem aluminija od 11-13 mas. % u mikrostrukturi imaju 18R (β_1') martenzit. Viši sadržaj aluminija (>13 mas. %) prati formiranje 2H (γ_1') martenzita. Ako se kemijski sastav nalazi na granici između nastanka oba martenzita, tada oba mogu postojati u mikrostrukturi. Koji od njih će se pojaviti u mikrostrukturi ovisi o kemijskom sastavu, temperaturnim uvjetima i uvjetima naprezanja [19, 20]. Uz nastanak martenzitne faze iz početne austenitne (β) faze, došlo je za vrijeme zavarivanja i do promjene veličine zrna u zoni utjecaja topline. Veličina zrna je iznimno bitna karakteristika mikrostrukture jer o njoj ovise i druga mehanička i funkcionalna svojstva legure.. Nedostatak legura s prisjetljivošću oblika je krupnozrnata mikrostruktura koja negativno utječe na ponašanje legure.

Zapažena je velika homogenost kemijskog sastava od osnovnog materijala (slike 4c i d), preko zone utjecaja topline (slike 5 c i d) do zone taljenja (slike 6c i d) što je potvrđeno kemijskim sastavom iz prikazanih EDS spektara (tablica 1). Prosječni kemijski sastav osnovnog materijala je: 82,26Cu-13,21Al-4,53Ni (mas. %), zone utjecaja topline je 82,30Cu-13,30Al-4,40Ni (mas. %), a zone taljenja 82,34Cu-13,16Al-4,50Ni (mas.%). Može se primijetiti da je dobivena krupnozrnata martenzitna mikrostruktura u zoni utjecaja topline (slika 5). Navedene promjene krupnozrnate mikrostrukture je praćena i promjenom vrijednosti mikrotvrdoće (tablica 2), posebno u zoni utjecaja

topline (slika 5) čija prosječna vrijednost je iznosila 456,1 HV_{10}. Širina martenzitnih iglica u zoni utjecaja topline je iznosila oko 7,4 µm, dok je širina metalne osnove oko 8 µm (slika 7).

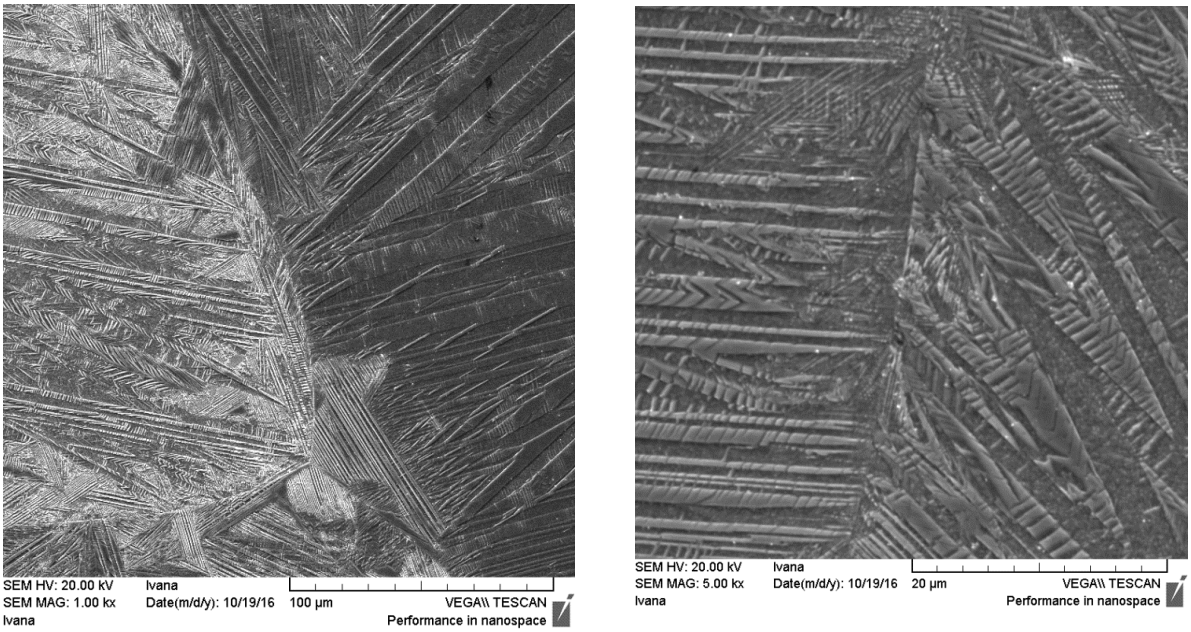

a) b)

Slika 3. SEM mikrografije Cu-Al-Ni legure nakon lijevanja pri različitim povećanjima; a – 1000x, b – 5000x

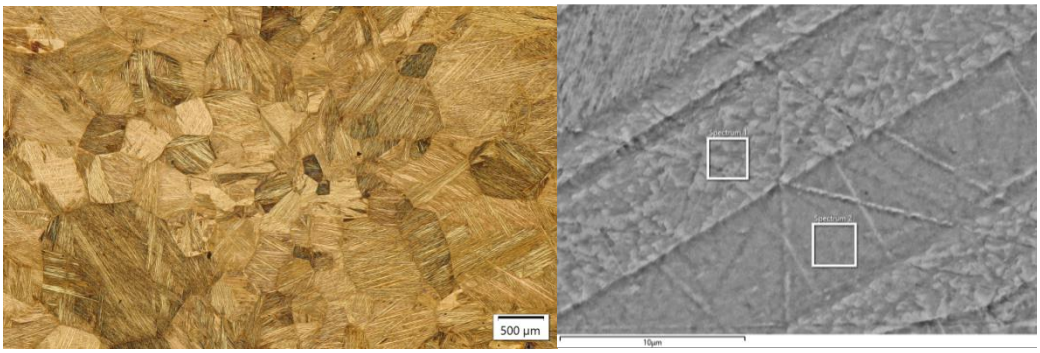

a) b)

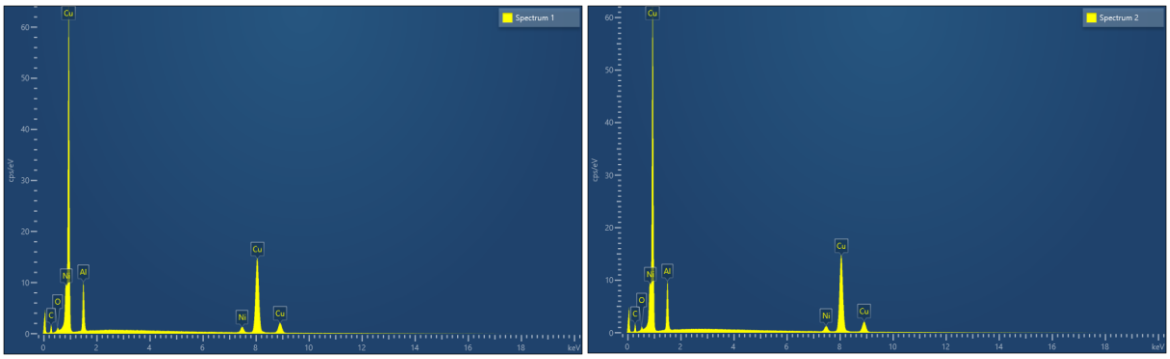

c) d)

Slika 4. OM (a) i SEM mikrografije (b) i EDS spektri (c i d) osnovnog materijala nakon toplinske obrade

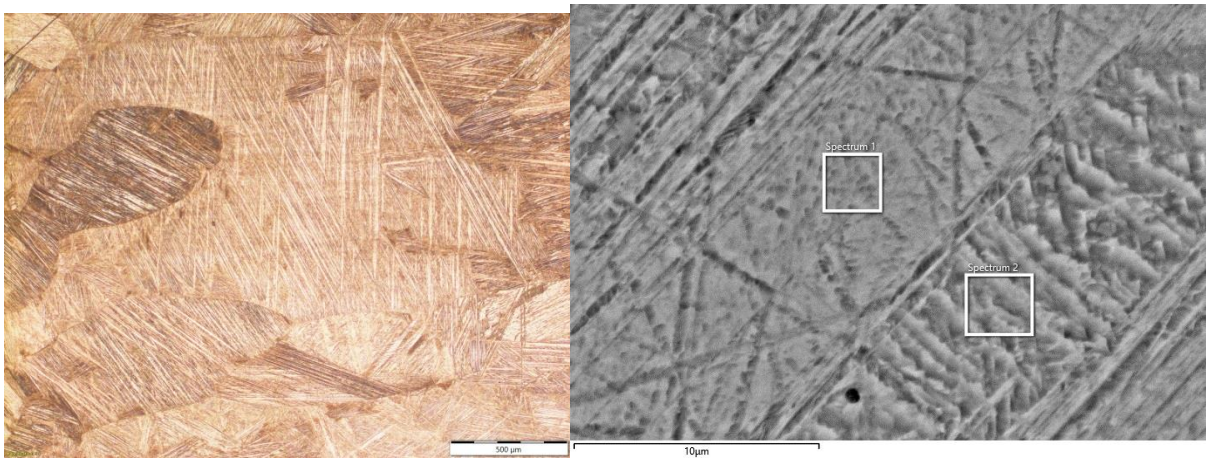

a) b)

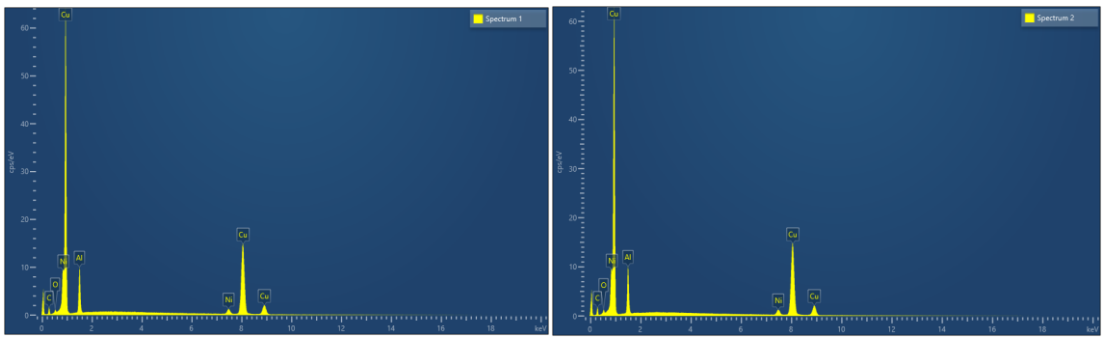

c) d)

Slika 5. OM (a) i SEM mikrografije (b) i EDS spektri (c i d) zone utjecaja topline

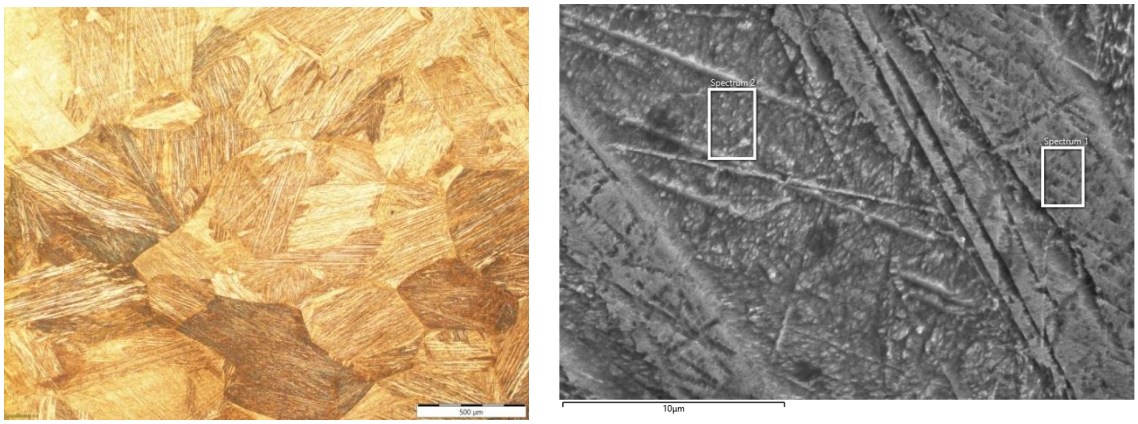

a) b)

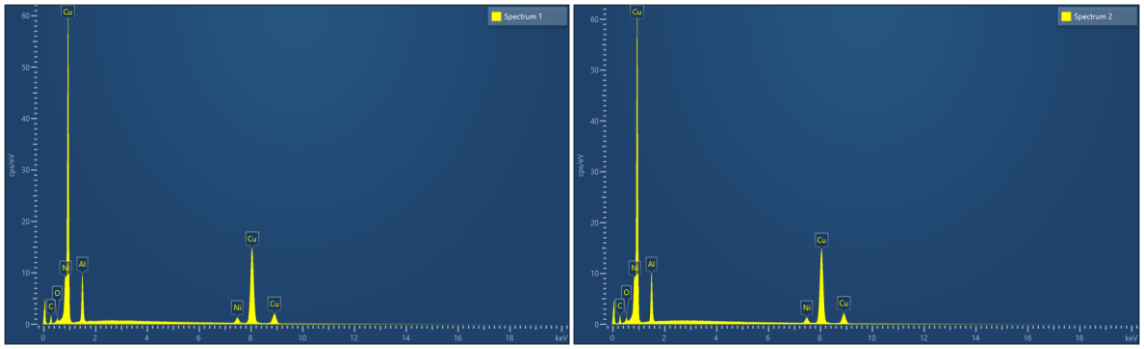

c) d)

Slika 6. OM (a) i SEM mikrografije (b) i EDS spektri (c i d) zone taljenja

Tablica 1. Kemijski sastav iz EDS spektara osnovnih elemenata zavarenog spoja, mas. %

Element zavarenog spoja	Broj EDS spektra sa slika 4c i d – 6 c i d	Cu	Al	Ni
Osnovni materijal	1 2	82,12 82,40	13,27 13,16	4,61 4,44
Zona utjecaja topline	1 2	82,45 82,14	13,21 13,38	4,34 4,47
Zona taljenja	1 2	82,56 82,13	13,01 13,31	4,43 4,57

Tablica 2. Vrijednosti mikrotvrdoće osnovnih elemenata zavarenog spoja, HV_{10}

Osnovni materijal	Zona utjecaja topline	Zona taljenja
394,5	456,4	408,7
398,1	454,7	414,2

396,9	457,1	412,7

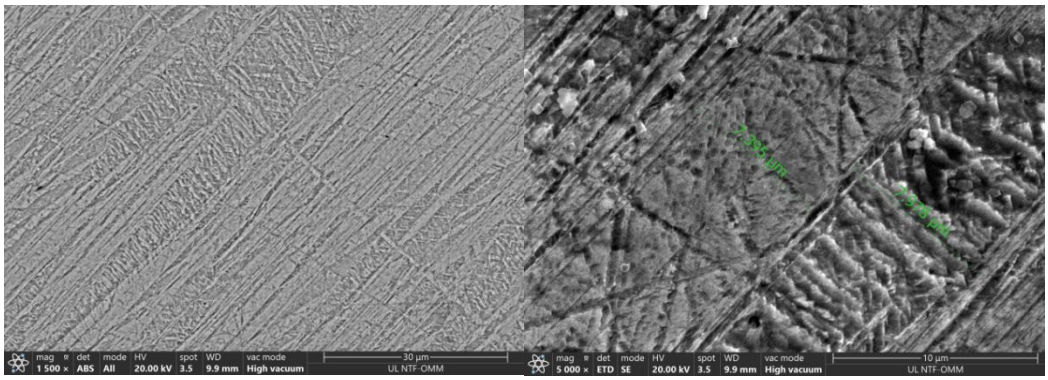

a) b)

Slika 7. SEM mikrografije u struji raspršenih elektrona zone utjecaja topline kod različitih povećanja (a – 1500 X i b – 5000 X

4. Zaključak

Na osnovi provedenih istraživanja može se zaključiti da istraživana Cu-12,8Al-4,1Ni (mas. %) legura s prisjetljivosti oblika dobivena kontinuiranim lijevanjem u lijevanom i toplinski obrađeno stanju ima martenzitnu mikrostrukturu što je osnova za efekt prisjetljivosti oblika. Nakon provedenog zavarivanja TIG postupkom svi elementi zavarenog spoja također imaju martenzitnu igličastu strukturu s homogenim kemijskim sastavom. Prosječni kemijski sastav osnovnog materijala je: 82,26Cu-13,21Al-4,53Ni (mas. %), zone utjecaja topline je 82,30Cu-13,30Al-4,40Ni (mas. %), a zone taljenja 82,34Cu-13,16Al-4,50Ni (mas.%). Zapažen je porast veličine zrna u zoni utjecaja topline sa širinom martenzitnih iglica oko 7,4 µm. Prosječna vrijednost mikrotvrdoće osnovnog materijala je 396,5 HV_{10}, zone utjecaja topline je 456,1 HV_{10}, a zone taljenja je 411,9 HV_{10}.

5. Literatura

[1] M. Gojić, Legure s efektom memorije oblika, Metalurgija, 31 (1992) 2/3, 77-82.
[2] K. Otsuda, C. M. Wayman, Shape Memory Materials, Cambridge University Press, Cambridge, 1998. 97-377.
[3] C. Lexcellent, Shape-memory Alloys Handbook, John Wiley&Sons Inc., Hobogen, 2013, 11-47.
[4] D. Ćorić, M. Franz, Svojstva i primjena slitina s efektom prisjetljivosti oblika, Zavarivanje, 50 (2007) 5/6, 179-187.
[5] I. Ivanić, M. Gojić, S. Kožuh, Slitine s prisjetljivosti oblika (I. dio): najznačajnija svojstva, Kemija u industriji, 63 (2014), 9-10, 323-329.

[6] M. Gojić, S. Kožuh, I. Ivanić, L. Vrsalović, T. Holevac Grgurić, Razvoj legura s prisjetljivosti oblika na bazi bakra u okviru znanstveno-istraživačkih projekata na Metalurškom fakultetu Sveučilišta u Zagrebu, Kemija u industriji, 72 (2023) 7-8, 478-503.
[7] M. Gojić, L. Vrsalović, S. Kožuh, A. Kneissl, I. Anžel, S. Gudić, B. Kosec, M. Kliškić, Electrochemical and microstructural study of Cu-Al-Ni shape memory alloy, Journal of Alloys and Compounds, 509 (2011) 9782-9790.
[8] G. Lojen, M. Gojić, I. Anžel, Continuously cast Cu-Al-Ni shape memory alloy - Properties in as-cast condition, Journal of alloys and compounds, 580 (2013), 497-505.
[9] W. Wang, H. Li, The welability of Shape Memory Alloys, Journal of Physics: Conf. Series 1168 (2019) 022076, 1-6. https://doi:10.1088/1742-6596/168/2/022076.
[10] M. H. Sadati, Y. Javadi: Investigation of mechanical properties in welding of shape memory alloys, Procedia Engineering, 149 (2016) 438-447.
[11] N. Sari, H. Doğan, Microstructural Charcterisation of Welded Shape Memory Alloys, Celal Bayer University Journal of Science 15 (2019) 4, 415-421. https://doi: 10.18466/cbayarfbe.497388
[12] T. Kramár, J. Taurer, P. Vondrouš, Welding of Nitinol by Selected Technologies, Acta Polytecnica, 59 (2019) 1, 42-50. https://doi:14311/AP.2019.590042
[13] J. P. Oliviera, R. M. Miranda, F. M. Braz Fernandes, Welding and Joining of NiTi Shape Memory Alloys: A Review, Progress in Materials Science, 88 (2017) 412-466.
[14] J. P. Oliviera, Z. Zeng, S. Bervieiller, D. Bouscaud, F. M. Braz Fernandes, R.M. Miranda, N. Zhou, Laser welding of Cu-Al-Be shape memory alloys: Microstructure and mechanical Properties, Materials&Design, 148 (2018) 145-152.
[15] A. A. De Albuquerque, H. Lache, D. F. De Oliviera, J. C. A., Brito, Rotary friction welded applied to Cu11.8Al0.45Be shape memory alloy, Journal of Advanced Procesess, 10 (2024) 100233, 1-10. https://doi.org/10.10167/jajp2024 100233
[16] M. Gojić, S. Kožuh, I. Anžel, G. Lojen, I. Ivanić, B. Kosec, Microstructural and phase analysis of CuAlNi shape-memory alloy after continuous casting, Materials and Technology, 47 (2013) 2, 149-152.
[17] G. Lojen, A. C. Kneissl, M. Gojić, R. Rebeka, M. Čolić, I. Anžel, Continuous casting of Cu-Al-Ni shape memory alloys, Livarski vestnik, 57 (2010) 4, 172-193.
[18] U. Sari, I. Aksoy, Micro-structural analysis of self-accommodating martensites in Cu–11.92 wt%Al–3.78 wt%Ni shape memory alloy, Journal of Materials Processing Technology, 195 (2008), 72-76.
[19] G. Lojen, I. Anžel, A. Kneissl, A. Križman, E. Unterweger, B. Kosec, M. Bizjak, Microstructure of rapidly solified Cu-Al-Ni shape memory alloy ribbons, Journal of Materials Processing Tehnology, 162-163 (2005) 220-229.
[20] S. H. Chang, Influence of chemical composition on the damping characteristics of Cu-Al-Ni shape memory alloys, Materials Chemistry and Physics, 125 (2011) 358-363.

Društvo za tehniku
zavarivanja Slavonski Brod

13. Međunarodno znanstveno-stručno savjetovanje SBZ 2025

„STROJARSKE TEHNOLOGIJE U IZRADI ZAVARENIH KONSTRUKCIJA I PROIZVODA, SBZ 2025."
Slavonski Brod, 08. i 09. 05. 2025.

Sučeono zavarivanje blokova od Cogidura (1.8715 grupa 3.2.) za tramvajske skretnice MAG postupkom

D. Mitić[1,*], M. Mitić[1], N. Jović[2], Đ. Hadži Đokić[3], D. Gruber[4], M. Mijajlović[3]

[1]Nivar d.o.o. Niš, Srbija
[2]Vossloh MIN Skretnice Niš, Srbija
[3] Mašinski fakultet u Nišu, Univerzitet u Nišu, Srbija
[4] DGNDT DOO Niš, Srbija

[*] Corresponding Author. E-mail: mitanivar@gmail.com

Rezime

U radu je predstavljena tehnologija zavarivanja tramvajske skretnice MAG postupkom sučeonog spoja blokova od Cogidura (1.8715,grupa 3.2) sa podloškom od bakra. Takodje u radu je dat pregled ispitivanja zavarenih spojeva (VT, PT i UT), makro ispitivanje, ispitivanje tvrdoće, kao i dinamičko ispitivanje zavarenog uzorka na lom.

Ključne reči: zavarivanje, skretnice, ispitivanje, Cogidur, tvrdoća

1. Uvod

Postupci kojim se spajaju tramvajske skretnice prema standardu EN 14811 su:
Aluminotermijsko zavarivanje AT
Elektrootporno zavarivanje ET
Zavarivanje samozaštitnom punjenom žicom FCAW
Elektrootporno zavarivanja šina ET se najčešće upotrebljava u radioničkim uslovima,mada danas postoje mobilni uređaji za zavarivanje na terenu, dok se najčešće upotrebljava aluminotermijsko zavarivanje šina AT, kako u radionici, tako i na terenu.
Od 1996. god. spajanje šina počinje da se primenjuje zavarivanjem samozaštitnom punjenom žicom FCAW, američka firma Lincoln Electric uz odobrenje Deutsche Bahn AG, za zavarivanje šinskih skretnica, čvrstoće materijala od Rm 685N/mm² do Rm 885N/mm², za pruge sa osovinskim opterećenjem od 10t i brzinom manjom od 80km/h. Ovaj postupak se odlikuje time što je unos energije znatno veći, nego kod zavarivanja MAG postupkom. Kod zavarivanja samozaštitnom žicom, prečnik elektrodne žice je Ø2,0mm, a kod MAG postupka je 1.2mm.

Pošto je zavarivanje samozaštitnom žicom američka tehnologija zavarivanja, dodatni materijal i oprema za zavarivanje ovim postupkom se proizvodi u USA, dok se u Evropi, a naročito u Francuskoj javila težnja, da se tramvajske skretnice zavaruju evropskom tehnologijom, dodatnim materijalom i opremom koja se proizvodi u Evropi. Jedno je želja, a sasvim drugo je ostvarenje te želje, pogotovo kada se zavaruju blokovi debljine preko 150mm, pri čemu se zavaruje prečnikom žice Ø1,2mm, a zavareni uzorci podvrgavaju dinamičkom ispitivanju na lom.

2. Osnovni materijal

Prilikom izrade tramvajskih skretnica na ukrštajima, izvršena je zamena šina blokovima od Cogidura (Hardox 400), zbog veće tvrdoće blokova. Na njima se nakon zavarivanja mašinskom obradom pravi žleb, kao kod šine. Materijal blokova je Cogidur (1.8715 grupa 3.2) tvrdoće veće od 400HB.

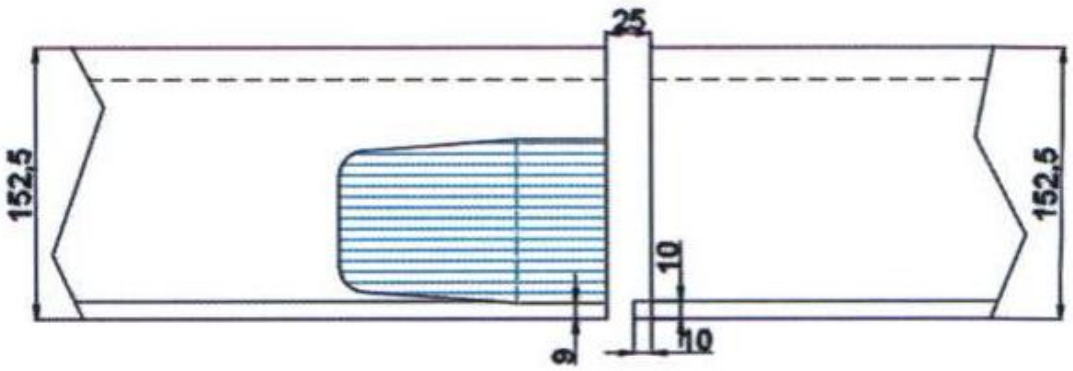

Slika 1. Crtež pripreme spoja blokova

Tabela 1. Hemijske karakteristike osnovnog materijala

Osnovni materijal	C %	Mn %	Si %	Ni %	Cr %	Mo %	Ti %	V %	Cu %
Cogidur	0,168	1,305	0,417	0,469	1,859	0,180	0,005	0,003	0,359

Tabela 2. Mehaničke karakteristike osnovnog materijala

Osnovni materijal	Rm N/mm²	Rv N/mm²	L %	Pv J	Tvrdoća HB
Cogidur	1355	1005	13	-40°C 53	414-427

Pre zavarivanja, blokovi se postavljaju na rastojanju od 25mm. Ivice blokova su obrušene do metalnog sjaja, a nakon provere centričnosti blokova, postavljaju se stege, koje ih drže na tačnom

rastojanju. Nakon toga se postavljaju bakarni podmetači sa strane blokova, dok je pre toga postavljen bakarni podmetač sa žlebom ispod blokova.
Pre samog zavarivanja, predgrevaju se blokovi propan-butanom u dužini od 500mm levo i desno od spoja, kako bi se materijal predgrejao po dubini bloka.Temperatura predgrevanja iznosi 150°C, a maksimalna je 200°C. Nakon predgrevanja, zavaruju se blokovi u dva prolaza, a nakon toga se skidaju bakarni podmetači i zavaruje još jedan prolaz.

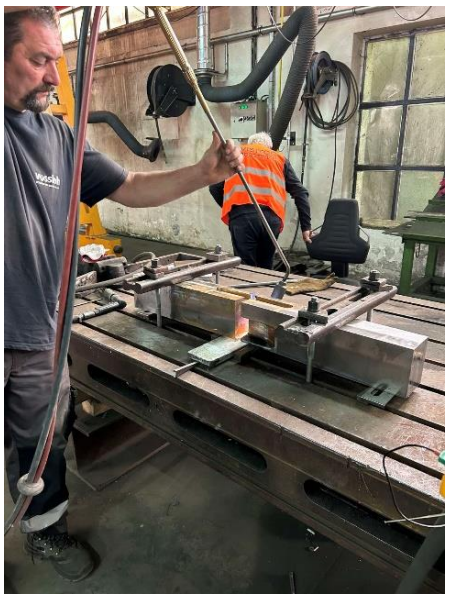

Slika 2. Predgrevanje spoja

Slika 3. Merenje temperature predgrevanja

Pošto su postavljeni bakarni podmetači ,ponovo se vrši predgrevanje, zato što dolazi do gubitka toplote i podhlađivanja materijala, jer postavljanje bakarnih podmetača na predhodno zagrejani spoj nije lako izvesti i zahteva veštinu zavarivača. Merenjem temperature materijala blokova i ako ona ne odstupa više od 10% od preporučene vrednosti, nastavlja se zavarivanjem i to neprekidno sve dok se ne dođe do nekih 30mm do kraja visine spoja. Tada se sklanjaju bakarni podmetači, zavar se očisti od šljake pneumatskim uređajem sa vibrirajućim žicama. Sledećih 30mm visine spoja se zavaruje nerdjajućom elektrodnom žicom. Sve vreme zavarivanja prate se vrednosti jačine struje, koje minimalno odstupaju od vrednosti koje su date u WPS listi.

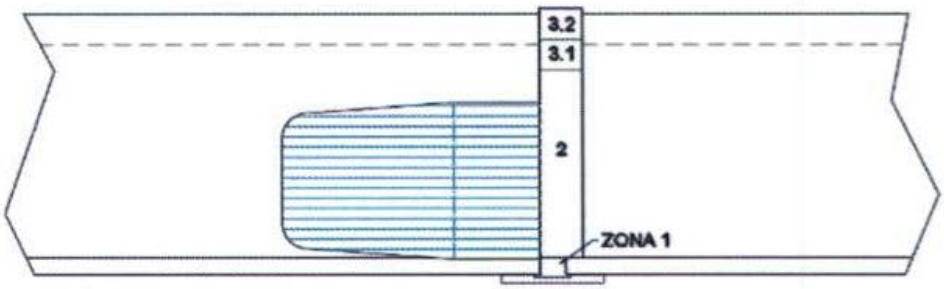

Slika 4. Zavareni spoj presek po visini

2.1 Dodatni materijal za zavarivanje spoja

Za zavarivanje blokova od Cogidura MAG postupkom, koristili smo elektrodnu žicu EN 14341-A G42 5 M/CG3Si1, komercijalne oznake OK AristoRod 12.50, prečnika Ø1,2mm, dok zadnjih 30mm zavaruje se nerđajućom elektrodnom žicom EN 14343-A G 18 8 Mn,komercijalne oznake OK Autrod 16.95,p rečnika žice Ø1,2mm.

Tabela 3. Hemijske karakteristike dodatnog materijala

Dodatni materijal	C %	Si %	Mn %	P %	S %	Cr %	Ni %	Mo %	Ti %	Cu %
OK AristoRod 12.50	0,07	0,87	1,46	0,009	0,013	0,02	0,01	0,01		0,02
OK AutRod 16.95	0,08	0,9	6,9	0,03	0,01	19,0	8,1	0,02		

Tabela 4. Mehaničke karakteristike dodatnog materijala

Dodatni materijal	Rm N/mm²	Rv N/mm²	Izduženje %	Pv jJ
OK AristoRod 12.50	560	480	26	-40°C 60
OK AutRod 16.95	640	450	41	20²C 130

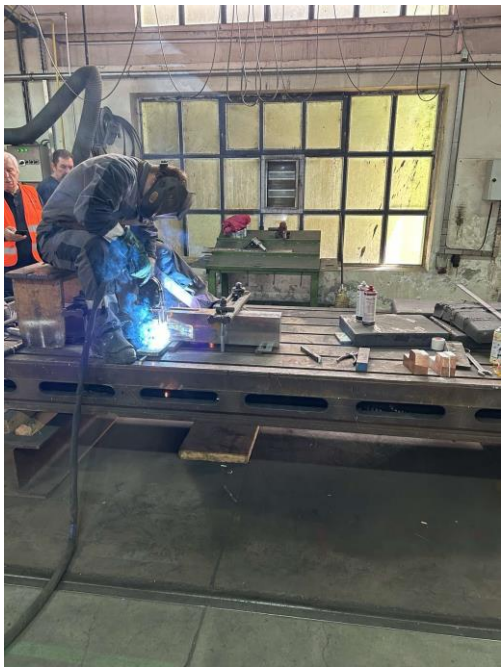

Slika 5. Zavarivanje bloka

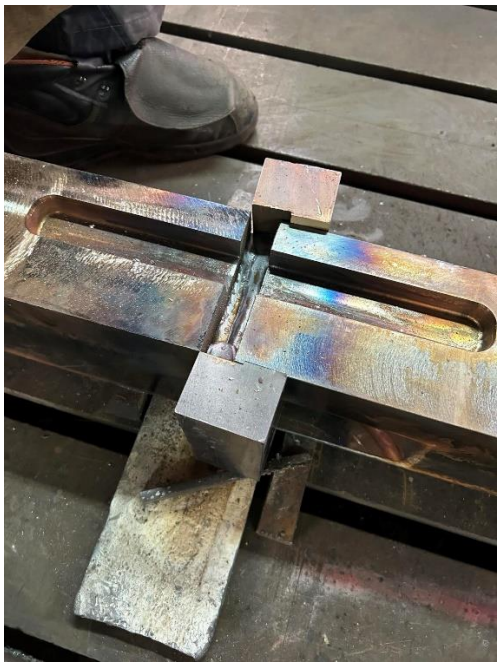

Slika 6. Izgled spoja pre završnog zavarivanja

3. Zavarivanje

Postoje dve tehnike zavarivanja MAG postupkom, u prvoj električni luk se vodi po sredini spoja, ali se zavaruje sa većim vrednostima jačine struje. Druga tehnika podrazumeva niže vrednosti jačine struje, ali se električni luk usmerava u jednom prolazu na levu stranu spoja ,a u drugom prolazu na desnu stranu. Ova tehnika omogućava veće uvarivanja u bokove.

Nakon zavarivanja uzorak se dogreva na temperaturu od 200°C u trajanju od 1h, a nakon toga se pokriva vatrostalnim platnom i ostavlja da se polagano hladi.

Parametri zavarivanja dati su wps listi, a vrednost jačine struje se kreće od 250A do 270A, napon je oko 29V, brzina zavarivanja od 25cm/min do 27cm/min, zavisno da li se zavaruje podnožje spoja ili se zavaruju završni prolazi. Unos toplote se kreće između 1,22KJ/mm do 1,39KJ/mm.

Slika 7. Zavareni uzorak

Slika 8. Ispitivanje ultrazvukom

4. Ispitivanje bez razaranja

Nakon 24h izvršena je vizuelno dimenzionalna kontrola, kako samog zavarenog spoja, tako i paralelnost blokova, kao i moguća deformacija-skupljanje. Posle su urađena ispitivanja penetrantskom tečnošću i ultazvukom zavarenih uzoraka. Kritično mesto je ,kada se skidaju bakarni kalupi i nakon čišćenja i predgrevanja, nastavlja sa zavarivanjem. Tada se mogu javiti greške-nalepljivanje i nemetalni uključci.

5. Ispitivanje sa razaranjem

Pošto su rezultati ispitivanja bez razaranja uzoraka bili zadovoljavajući, jedan uzorak se podvrgava ispitivanju sa razaranjem (makro i ispitivanje tvrdoće), a drugi uzorak se dinamički ispituje na lom sa promenjivim opterećenjem. Ispitivanje sa razaranjem je obavila laboratorija RD Dijagnostika d.o.o. Beograd, koja ima ovlašćenje od TUV SUD Industrie Service GMBH.

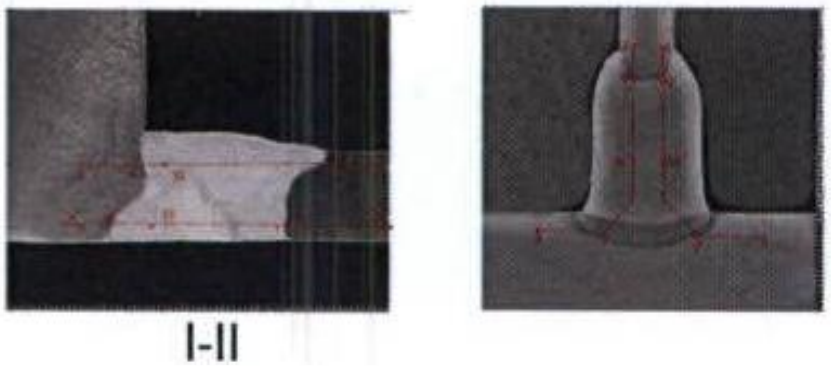

Slika 9. Presek spoja - makro

Slika 10. Presek spoja – makro

6. Ispitivanje tvrdoće

Tabela 5. Merenje tvrdoće

Art /Last: - *Type / Load:* - *Type / Charge:* HV 10 – nur informationen / *only information*

Nr. *No.* *N°*	Meßreihe *Measuring Line* *Ligne de mesure*	Grundwerkstoff *Base Material* *Métal de base*			WEZ *HAZ* *ZAT*			Schweißgut *Weld Metal* *Métaldéposé*			WEZ *HAZ* *ZAT*			Grundwerkstoff *Base Material* *Métal de base*		
366/24	1-5-11-7-3	423	425	420	212	214	216	161	164	158	225	224	221	430	428	427
366/24	2-6-13-8-4	426	419	422	215	218	219	163	161	157	218	216	220	431	426	424
366/24	1-5-11-7-3	421	420	425	214	212	215	159	157	155	224	220	218	432	430	427
366/24	2-6-13-8-4	420	421	427	218	220	221	161	162	158	219	223	225	428	427	424
366/24	1-5-11-7-3	414	424	426	208	210	212	158	156	154	224	221	218	420	424	425
366/24	2-6-13-8-4	422	425	427	211	213	215	159	161	163	216	214	217	415	417	419
366/24	1-5-11-7-3	417	419	421	210	212	215	157	159	161	215	217	218	421	419	417
366/24	2-6-13-8-4	415	414	418	213	216	218	155	157	159	210	212	214	414	415	418

7. Ispitivanje na lom

Test opterećenja je urađen na uzorku CQB429 AWBW Cogidur an Cogidur-VMS, prema proceduri T15002P01, ukupne dužine uzorka 1200mm, koji je zavaren MAG postupkom u preduzeću VOSSLOH MIN SKRETNICE d.o.o. Niš.
Test savijanja u četiri tačke je obavljen u Tehnološkom centru Vossloh Cofiger u Reichshoffen-Francuska. Rastojanje između osloncaje 1100mm, a dva laserska senzora se koriste za merenje amplitude. Pre ispitivanja izvršena je sertifikacija hidrauličkog cilindra i etaloniranje laserskih senzora. Maksimalno opterećenje je 130Mpa sa amplitudom od 13 do 130Mpa, broj ciklusa 3.000.000, a frekvencija 5HZ. Ispitivanje je urađeno u periodu od 24.06. do 01.07.2024.

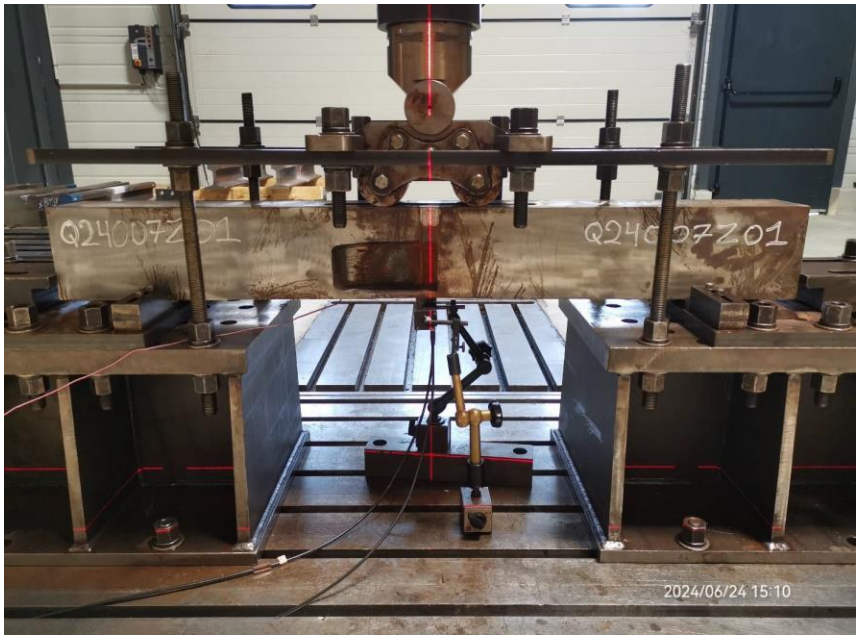

Slika 11. Uređaj za ispitivanje uzoraka na lom

Type	Nb cycles	Frequency	L5 Amplitude (mm)	L6 Amplitude (mm)
Qualification	1 000	5 Hz	0.73	0.78
Qualification	3 Mo	5 Hz	0.75	0.81

Slika 12. Izgled zavarenog uzorka nakon ispitivanja na lom i ispitivanja penetrantima

Nakon ispitivanja na lom nakon 3.000.000 ciklusa promenljivim opterećenjem, nije došlo do pojave prslina u zavarenom spoju.

8. Zaključak

Zavarivanje MAG postupkom je je mnogo zahtevnije za zavarivanje nego što je zavarivanje samozaštitnom žicom, zbog toga što je mnogo manji unos toplote MAG postupkom,te je mogućnost pojave nalepa na bokovima blokova, mnogo izvesniji. Takođe produktivnost MAG postupkom je značajno manja nego zavarivanje innershield postupkom.

9. Literatura

[1] Atlas of Fatique Curves ASM International Materials Park,Ohio 44073-0002
[2] Kralj S,Dunđer M,Ispitivanje sklonosti zavarenih spojeva čelika 25 CrMo4 i Ck45 prema nastajanju hladnih pukotina.Zavarivanje (0044-1902)43 (2000) 1/2 ,5-16 43
[3] Kou S,Welding Metallurgy Handbook,2nd ed.New York,USA,John Wiley and Sons,2002

Društvo za tehniku zavarivanja Slavonski Brod

13. Međunarodno znanstveno-stručno savjetovanje SBZ 2025

„STROJARSKE TEHNOLOGIJE U IZRADI ZAVARENIH KONSTRUKCIJA I PROIZVODA, SBZ 2025."
Slavonski Brod, 08. i 09. 05. 2025.

Ecological Aspects and Occupational Safety in Welding Processes: Contemporary Approaches and Challenges

Z. Trišović[1,4,*], T. Mankovits[2], M. Čavić[3], A. S. Petrović[4], D. Kozak[5], N. Trišović[4]

[1]Academy of Applied Studies Polytechnic, Belgrade, Serbia
[2]University of Debrecen, Department of Mechanical Engineering, Hungary
[3]Faculty of Technical Science, University of Novi Sad, Serbia
[4]Mechanical Engineering Faculty in Belgrade, University of Belgrade, Serbia
[5]Mechanical Engineering Faculty in Slavonski Brod, University of Slavonski Brod, Croatia

[*] Corresponding Author. E-mail: zaga.app@gmail.com

Abstract

The welding process is one of the most important technological procedures in modern industry, with applications in the automotive, aerospace, shipbuilding and other sectors. However, alongside its advantages, welding also presents a range of ecological and health-related challenges. The emission of harmful gases and particles, energy consumption and waste generation have a significant impact on the environment and workers' health. This paper provides an overview of the ecological aspects of welding, as well as modern technologies and practices aimed at improving energy efficiency and occupational safety.

1. Introduction

Welding is an indispensable process in modern manufacturing and construction industries, yet it presents considerable environmental and occupational health challenges. A substantial body of literature has addressed the environmental impacts of welding processes, as well as the health and safety concerns associated with workers' exposure to welding fumes, radiation and noise. O'Brien (1991) provides a foundational understanding of welding processes in the "Welding Handbook", outlining the environmental effects associated with different welding techniques. The author emphasizes the types of hazardous gases released during welding operations - such as ozone, carbon monoxide and nitrogen oxides - and discusses mitigation techniques, including the use of protective shielding gases and enclosed systems that aim to minimize emissions. These early insights set the stage for further exploration into sustainable welding practices. Building upon the technical foundations, Messler (2008) delves deeper into the physics, chemistry and metallurgy of welding in "Principles of Welding", emphasizing the chemical composition of welding fumes and their potential health impacts. He underlines the importance of applying emission-reducing strategies, not only to

protect workers but also to limit broader ecological harm. Similarly, Kou (2003) in "Welding Metallurgy" links metallurgical properties of materials to process efficiency and environmental sustainability, highlighting the need for cleaner technologies and improved energy management in welding operations. Research on environmental and safety issues in welding has been extensively explored in the scientific literature. Schneider and Meyers (1999) offer a thorough overview of the environmental and occupational consequences of welding in their study published in the "Journal of Environmental Science and Technology". They underscore the dual challenge of protecting worker health while also minimizing atmospheric pollution, advocating for stricter regulatory frameworks and improved process control. Recent works have placed increasing focus on the health implications of welding fumes. Silva and Gomes (2018), in a comprehensive review in the "International Journal of Occupational Safety and Ergonomics", assess long-term occupational exposure to toxic gases. Their study reinforces the critical role of ventilation systems and personal protective equipment (PPE) in mitigating these risks, aligning with global occupational health guidelines. Environmental sustainability in welding has gained attention in recent years. De Moraes and Lima (2017) explore the environmental burden of welding-related waste and propose sustainable practices such as recycling of metal waste and the adoption of energy-efficient equipment. Their article in the "Journal of Manufacturing Processes" presents welding as an integral part of the circular economy, particularly when cleaner technologies and material recovery systems are implemented. Technological advancements have also enabled better control of occupational hazards. Dufresne and Desjardins (2015) investigate various engineering controls, including localized fume extraction and filtration systems. Their research, published in the "Journal of Occupational and Environmental Hygiene", shows how integrated safety solutions can drastically improve air quality in welding environments. The health risks related to inhalation of welding fumes, including respiratory and systemic effects, are further detailed by Lindqvist and Holmberg (2004). They highlight the need for comprehensive safety protocols that combine monitoring, regulation and worker education. Their findings, published in the "International Journal of Occupational Safety and Ergonomics", support a growing consensus that both engineering and administrative controls are necessary. Environmental engineering perspectives are offered by Baucom and McNeely (1997), who assess the atmospheric impacts of welding and propose waste management and emission control strategies. Their article in the "Journal of Environmental Engineering" outlines actionable recommendations for reducing the carbon and pollution footprint of welding operations through process innovation and policy enforcement. Finally, Höhler and Sobolev (2010) provide an integrated view of sustainable welding technologies in their article in the "Welding Journal". They highlight current innovations in fume extraction, energy-saving techniques and AI-based process optimization. These advancements are increasingly vital in aligning welding practices with international environmental and occupational safety standards, such as ISO 14001 and OSHA guidelines. Collectively, these sources present a comprehensive understanding of the ecological and health-related challenges in the welding industry. The literature emphasizes a shift toward cleaner, more energy efficient technologies, improved fume control and stronger regulatory compliance. It also points to the importance of integrating sustainability into core

welding operations through automation, recycling and real-time process optimization - making the welding industry more aligned with global sustainability goals.

2. Ecological Aspects of Welding

2.1 Emissions of Harmful Gases and Particles

During the welding process, gases such as ozone (O_3), carbon monoxide (CO), nitrogen oxides (NO_x) and fumes from heavy metals are released. These gases can negatively affect air quality, cause respiratory issues among workers and contribute to atmospheric pollution. One example of emission reduction involves the use of enclosed systems with controlled atmospheres, which utilize shielding gases such as argon and helium to minimize the formation of harmful oxides. These techniques not only improve the quality of welded joints but also significantly reduce the environmental impact.

2.2 Energy Consumption and Carbon Footprint

Welding is an energy-intensive process and its carbon footprint varies depending on the technique used. For instance, laser and ultrasonic welding are more energy - efficient compared to traditional arc welding. The use of renewable energy sources in production facilities can further reduce the environmental impact. Moreover, the growing adoption of hybrid welding methods, which combine conventional techniques with modern digital control systems, enables more precise process control and reduces unnecessary energy consumption. Such approaches are already being implemented in leading industries, particularly in the automotive and aerospace sectors.

2.3 Waste Management and Recycling

Industrial waste generated by welding includes metal scraps, flux particles and chemical substances from shielding gases. The application of recycling strategies and proper disposal can significantly mitigate negative environmental consequences. In some manufacturing systems, waste metal material is reused through melting and reprocessing into new components, reducing the need for primary raw materials and contributing to the circular economy.

3. Occupational Safety in the Welding Industry

3.1 Risks in the Welding Process

In addition to environmental aspects, welding also poses significant health risks for workers, including exposure to heat and UV radiation, metal fumes and high noise levels. Prolonged exposure can lead to occupational diseases such as pneumoconiosis and hearing loss. Some companies are introducing advanced workplace monitoring systems, which include sensors for detecting harmful gases and automatic alarms that alert workers when pollutant levels exceed permitted limits.

3.2 Ventilation and Filtration Systems

One of the key factors in protecting workers is an adequate ventilation and air filtration system. Modern technologies allow for the efficient removal of harmful gases and particles directly at the source, significantly reducing health risks. A successful example of implementation is the use of mobile extraction systems combined with HEPA filters, which capture even the finest metal particles before they reach workers' respiratory tracts.

3.3 Personal Protective Equipment (PPE)

Proper use of PPE, such as respirators with filters, protective gloves, specialized helmets with automatic darkening and heat-resistant clothing, is essential to reducing the risk of welding-related injuries and illnesses. The development of new materials for protective equipment - such as lightweight yet highly durable fabrics with excellent thermal insulation - further contributes to worker comfort and safety.

4. Comparative Analysis of Environmentally Friendly Welding Technologies

The environmental impact of welding processes is a critical factor in determining the sustainability of modern industrial practices. Different welding techniques offer varying levels of energy efficiency, emissions and suitability for recycling, all of which contribute to their environmental footprint. A comparative analysis of some commonly used welding techniques - MIG/MAG, TIG, laser and ultrasonic - provides insight into their environmental implications.

1. MIG/MAG Welding

MIG/MAG (Metal Inert Gas / Metal Active Gas) welding offers medium energy efficiency. While it is widely used due to its versatility and speed, this technique generates high emissions compared to others, primarily due to the release of gases and particulates into the air. In terms of recycling suitability, MIG/MAG welding is considered medium, as the process can be adjusted to minimize waste, but it still produces considerable amounts of scrap metal that need to be managed.

2. TIG Welding

TIG (Tungsten Inert Gas) welding is known for its low energy efficiency as it tends to be slower and requires more precise control, often resulting in higher power consumption. However, TIG welding produces low emissions, making it an environmentally friendlier option in terms of air quality. The technique is highly suitable for recycling, as it generates minimal waste and the materials used are often recyclable, resulting in a high recycling suitability.

3. Laser Welding

Laser welding stands out with its high energy efficiency. This process uses a focused laser beam to join materials, which minimizes energy consumption. It generates minimal emissions,

making it one of the cleaner welding techniques in terms of air pollution. Like TIG, laser welding also scores high for recycling suitability, as it produces less waste and is highly precise, reducing the need for rework and scrap materials.

4. Ultrasonic Welding

Ultrasonic welding offers the highest energy efficiency among the techniques analyzed, as it uses high-frequency ultrasonic vibrations to create heat and join materials without the need for external heat sources. This results in a significant reduction in energy usage. The emissions from ultrasonic welding are minimal, making it an environmentally friendly process in terms of air quality. Additionally, it has very high suitability for recycling because it generates virtually no waste and the materials used are easily recyclable.

While MIG/MAG welding is widely used in many industries, it produces higher emissions and has moderate energy efficiency and recycling potential. TIG and laser welding offer improved environmental performance, with laser welding standing out due to its precision and minimal waste generation. However, ultrasonic welding leads the pack in terms of energy efficiency, low emissions and recycling suitability, making it the most environmentally friendly option. This analysis suggests that the shift toward more sustainable welding technologies will likely involve adopting methods like laser and ultrasonic welding, which offer both superior environmental performance and high recycling potential (Table 1)

Table 1. Comparative Analysis of Environmentally Friendly Welding Technologies

Welding Technique	Energy Efficiency	Emissions	Recycling Suitability
MIG/MAG	Medium	High	Medium
TIG	Low	Low	High
Laser	High	Minimal	High
Ultrasonic	Very High	Minimal	Very High

5. Current Trends and Regulations

International environmental and occupational safety frameworks are playing an increasingly important role in guiding technological development in modern industry. The ISO 14001 standard, established by the International Organization for Standardization (ISO), provides a systematic approach for organizations to manage their environmental responsibilities in a manner that contributes to sustainability. Similarly, regulations concerning workplace safety, such as those developed by the Occupational Safety and Health Administration (OSHA) in the United States, aim to ensure safe and healthy working conditions. Although OSHA standards are specific to the U.S., they are widely recognized and often influence international best practices. In alignment with these regulations, industries are progressively turning to environmentally conscious technologies. One area

that has seen significant advancement is welding technology, where the integration of automation and artificial intelligence (AI) has enabled more accurate and consistent welding processes. These innovations help to minimize material waste and reduce emissions of harmful substances generated during conventional welding operations. AI-powered systems are capable of real-time monitoring and adjustment of welding parameters, such as current, voltage, speed, and torch position, based on data from sensors and vision systems. This real-time optimization not only improves the quality of welds but also reduces the frequency of defects and rework, thereby lowering operational costs and decreasing the overall environmental impact of the manufacturing process.

6. Conclusion

The environmental aspects and occupational safety in the welding industry represent key challenges for modern manufacturing. Process optimization, the implementation of innovative technologies and strict adherence to regulatory standards can significantly reduce the negative impact on the environment and improve working conditions. Future developments in this field should focus on increasing energy efficiency and expanding automation, which will contribute to a more sustainable welding industry. With continued research and the application of emerging technologies, significant progress can be made in protecting workers' health and preserving the environment.

7. Acknowledgment

This research is supported by the Ministry of Science, Technological Development and Innovation of the Republic of Serbia, under the 2024 Agreement on Financing Scientific Research, No. 451-03-137/2025-03/200105, dated February 4, 2025, Serbian-Hungarian Bilateral Cooperation for the Years 2025-2026: Structural optimization of additively manufactured cellular titanium implant using artificial intelligence. Additional support provided by COST (European Cooperation in Science and Technology) CA21155, CA21112 and CA21106.

8. References

[1] O'Brien, R. L. (1991). *Welding Handbook: Welding Processes, Part 1*. American Welding Society.
[2] Messler, R. W. (2008). *Principles of Welding: Processes, Physics, Chemistry and Metallurgy*. Wiley.
[3] Kou, S. (2003). *Welding Metallurgy*. Wiley-Interscience.
[4] Schneider, D. E., Meyers, M. A. (1999). "Environmental and Safety Issues in Welding Processes." *Journal of Environmental Science and Technology*, 33(2), 131–138.

[5] Silva, P. A., Gomes, L. M. (2018). "Welding Fume and Health: A Review on the Impact of Occupational Exposure." *International Journal of Occupational Safety and Ergonomics*, 24(4), 495–502.
[6] De Moraes, M. A., Lima, E. (2017). "Environmental Impact and Sustainable Practices in Welding." *Journal of Manufacturing Processes*, 29, 101–110.
[7] Dufresne, A., Desjardins, D. (2015). "Welding Fume Control and Safety in the Workplace." *Journal of Occupational and Environmental Hygiene*, 12(5), 302–312.
[8] Lindqvist, M., Holmberg, H. (2004). "Health Risks and Environmental Impact of Welding." *International Journal of Occupational Safety and Ergonomics*, 10(4), 381–391.
[9] Baucom, R. D., McNeely, J. D. (1997). "Environmental Considerations in Welding Operations." *Journal of Environmental Engineering*, 23(2), 211–223.
[10] Höhler, J., Sobolev, K. (2010). "Sustainable Welding Technology: Environmental and Safety Considerations." *Welding Journal*, 89(7), 32–42.

Društvo za tehniku
zavarivanja Slavonski Brod

13. Međunarodno znanstveno-stručno savjetovanje SBZ 2025

„STROJARSKE TEHNOLOGIJE U IZRADI ZAVARENIH KONSTRUKCIJA I PROIZVODA, SBZ 2025."
Slavonski Brod, 08. i 09. 05. 2025.

A review paper: Influence of welding defects to structural integrity of welded joints

M. Aranđelović[1], A. Petrović[2,*], B. Đorđević[1], D. Kozak[3], T. Mankovits[4]

[1]Innovation Centre of Faculty of Mechanical Engineering, Kraljice Marije 16, Belgrade, Serbia
[2]University of Belgrade, Faculty of Mechanical Engineering, Kraljice Marije 16, Belgrade, Serbia
[3]University of Slavonski Brod, Faculty of Mechanical Engineering, Trg Ivane Brlić Mažuranić 2, Slavonski Brod, Croatia
[4]University of Debrecen, Faculty of Engineering, Department of Mechanical Engineering, Ótemető utca 2, Debrecen, Hungary

[*] Corresponding Author. E-mail: aspetrovic@mas.bg.ac.rs

Abstract

This paper presents a review of the most notable cases involving welded joint defects and their influence on structural performance. It examines examples where imperfections such as undercuts, incomplete penetration, lack of fusion, and so on, have compromised the integrity of welded structures. By analyzing these cases, the paper highlights how such defects contribute to stress concentration, reduced load-bearing capacity, and, in severe instances, failure. The review underscores the critical importance of identifying and mitigating these flaws to ensure the safety and reliability of constructions like bridges, buildings, and industrial frameworks.

Keywords: welded joints, structural integrity, welding defects, numerical-experimental approach

1. Introduction

Welded joints are an unavoidable element in the processes of remediation, repair, and, more broadly, the most common method of connecting structural components. However, they simultaneously represent the locations on a structure that have the greatest impact on its integrity and service life [1,2]. Experience has shown that it is impossible to create ideal welded joints, and thus, the subject of this paper is a brief overview of the issue of imperfections and irregularities in welded joints. These imperfections can arise due to various factors, including flaws in welding techniques, inadequate

material preparation, or the influence of external conditions during the process. Irregularities such as cracks, porosity, or incomplete weld penetration can significantly weaken a structure, often leading to a reduction in its load-bearing capacity or even catastrophic failures. Therefore, understanding the nature of these defects is crucial for improving the quality of welded joints and extending the lifespan of structures. In this paper, we will address the most common types of defects, and their consequences.

2. Short Studies about Welded Joints Single Defect

Kozak and his team [3] explored the impact of incomplete root penetration in welds, adhering to the EN ISO 6520-1 standard. They examined defects such as lack of fusion and incomplete penetration in a butt joint between a pipe and an elbow, finding that the weld root was not fully fused. This was illustrated in Figure 1. The base material, 10 CrMo 9-10, was analyzed for stress distribution near the defect tip using the finite element method (FEM). Simulations revealed that the incomplete root penetration, a site of high stress concentration, was the most critical area. Various defect depths were tested, and all load curve points fell within the safe zone of the Failure Assessment Diagram (FAD), though identifying the critical intersection with the material's resistance curve remains necessary. The study concluded that failure pressures matched limit pressures, negating the need for further calculations, and focused solely on the effect of one defect on structural integrity.

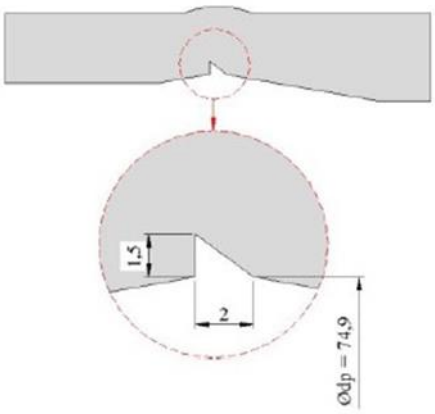

Figure 1. Dimensions and geometry of weld defect [3]

In a separate study, Dimić and colleagues [4] assessed how weld imperfections shown in Figure 2 affect the integrity of a pipe elbow under constant internal pressure. They identified incomplete root penetration on the pipe's inner surface via ultrasonic testing and analyzed its impact using FEM in ABAQUS software. The research also evaluated the weld's plastic reserve through FEM to determine the structure's load capacity when a surface defect leads to cracking. Results showed that load capacity decreases only when a crack stems from a surface defect like incomplete penetration. External factors that might influence these findings were not considered in this study.

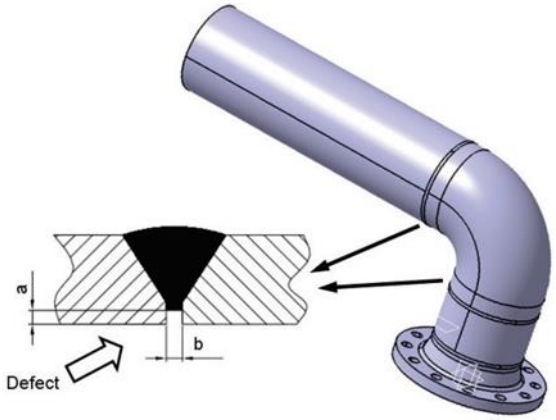

Figure 2. Welded joint with incompletely filled groove [4]

Lack of fusion, another prevalent weld defect, was examined by Tušek and his team [5]. They identified it as the most frequent welding flaw, attributing it to insufficient heat input. Although modern welding processes are reliable, Otersbok [6] noted that the actual weld geometry deviates from the intended design due to thermal and dynamic effects during welding. These local geometric variations significantly alter stress concentration in the welded joint. An undercut, shown in Figure 3, was scanned with a 3D scanner for detailed statistical analysis. The study introduced a method to assess the transition radius between the base material and weld metal, using the resulting data to compute stress concentrations at different joint locations via notch-effect approximation equations. Numerical models reflecting real weld geometry were validated against FEM, showing strong agreement. However, in areas with significant undercuts, stress concentrations were notably underestimated. An enhanced approach was proposed to refine existing notch factor equations. This method for evaluating local weld geometry parameters can enhance production quality control, while the derived stress concentration factor approximation supports localized fatigue assessments of critical joint areas.

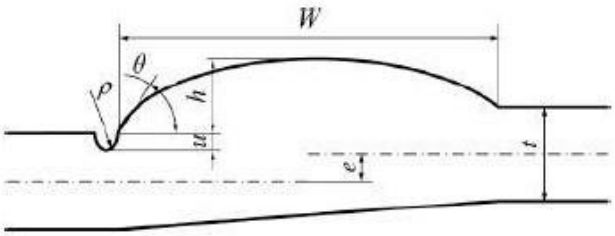

Figure 3. Welded joint with undercut [6]

Shen [7] pointed out that conventional welding of thin sheets often introduces initial defects like bending and deformation due to heat input, with misalignment being a common issue. He suggested that advanced techniques, such as laser or hybrid laser welding, which reduce heat input, could

mitigate these problems. Similarly, Tomerlin and his team [8] analyzed welding challenges with 6 mm thick S690QL steel sheets using MIG/MAG techniques, identifying lack of fusion and incomplete root penetration as frequent defects. Odanović [9] emphasized that these issues can be avoided by optimizing welding parameters and selecting suitable filler materials.

Cerit [10] studied stress concentration distribution in a butt-welded joint with defects, as shown in Figure 4. The analysis focused on an undercut, varying its depth and radius, and excess weld metal, adjusting its height and angle relative to the base material. The joint's response to uniaxial tension was modeled using FEM across multiple simulations. The findings underscored excess weld metal as a key driver of stress distribution, especially when paired with an undercut. Stress concentration in the undercut increased with greater depth and diameter, and it intensified as the angle between the undercut and excess weld metal decreased. Both defects amplify stress in the joint, with the study concluding that a pronounced excess weld metal combined with an undercut creates a critical hotspot where stress concentration exceeds that of either defect alone. This makes the site prone to crack formation, risking structural failure.

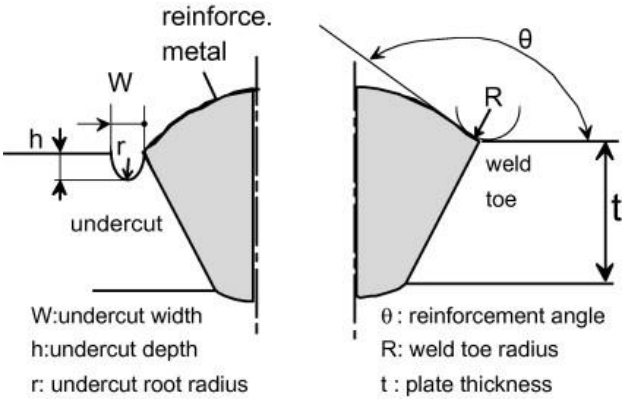

Figure 4. Welded joint with undercut and excess metal [10]

3. Welded joints with multiple imperfections

Following studies investigated the effects of two weld imperfections-excess weld metal and cracks-on the integrity of welded joints. The research demonstrated a clear interaction between these defects, with excess weld metal serving as a stress concentrator that initiates and propagates cracks. Beyond this observed relationship, the work posed new questions, notably: how does the interplay of these defects affect the structure's service life, and what additional factors, beyond weld geometry, influence defect behavior?

The failure analysis of a welded joint with multiple imperfections was conducted by considering the collective impact of all defects, rather than isolating the most prominent one. Four scenarios involving multiple defects in a welded joint under uniaxial tensile loading were examined using the extended Finite Element Method (XFEM) as shown by Aranđelovic and his collegues [11-13]. Two-

dimensional Finite Element Models were constructed based on tensile test specimens, each with an initial crack positioned in a critical zone of the welded joint, identified as a vulnerable area. For each of the four defect scenarios (Excess weld metal, weld face undercut and incomplete root penetration, which represent plates for Group 1 specimens; Incomplete root penetration and weld face sagging, which represent plates for Group 2 specimens; Excess weld metal, weld face undercut and misalignment, which represent plates for Group 3 specimens; Incomplete root penetration, misalignment and weld face undercut, which represent plates for Group 4 specimens) shown in Figure 5, numerical simulations were run with three varying initial crack depths to thoroughly evaluate their effects.

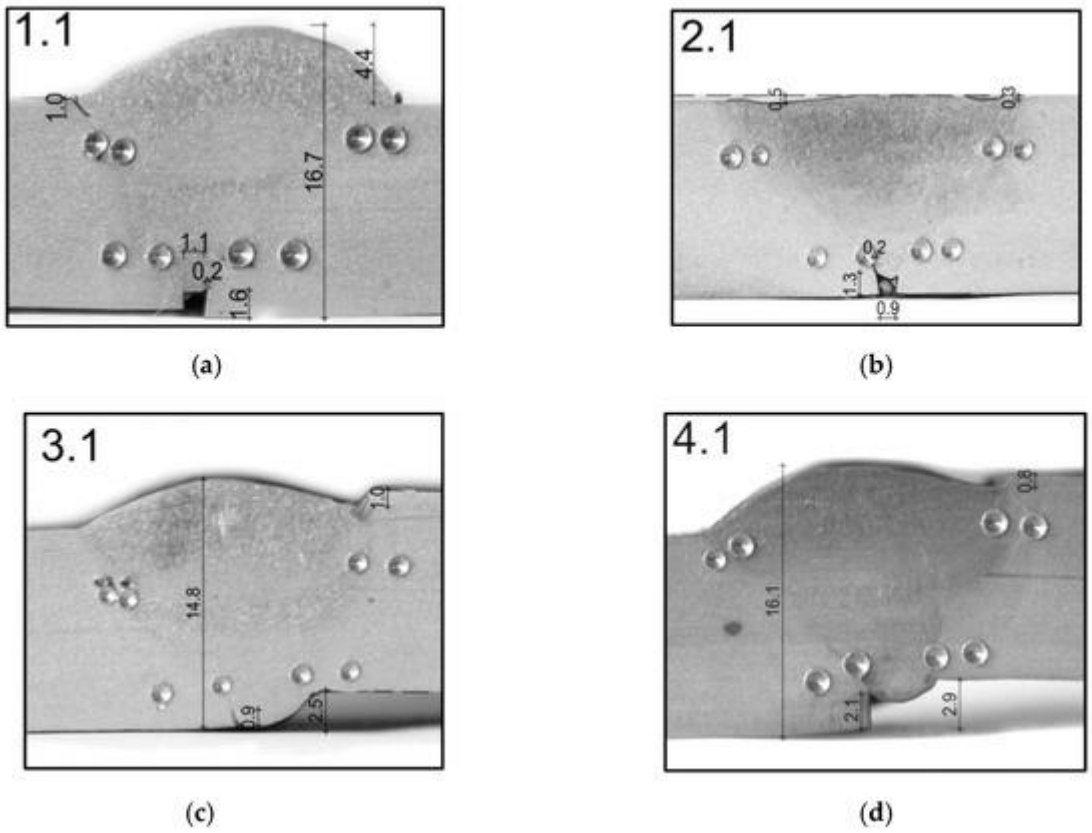

Figure 5. Weld metal and defects geometry for (a) Group 1; (b) Group 2; (c) Group 3; (d) Group 4 [13]

An Engineering Critical Assessment was performed using Failure Assessment Diagrams (FAD) for each defect deemed critical in its respective welded joint case. The simulations indicated that the geometry of the defects significantly influenced the structural integrity, with one defect emerging as the most critical in terms of potential failure risk. The analysis concluded that a combination of vertical misalignment paired with a secondary defect had the most severe impact, greatly increasing the risk of structural failure in the welded joint. It should be highlighted that misalignment in a welded

joint, as a form of defect, represents the most severe case due to its impact on multiple aspects. The altered geometry caused by misalignment, combined with a reduced load-carrying capacity, increased stress concentration, and a more complex state of strain, significantly compromises the joint's performance. The asymmetry introduced by this defect causes the specimen to deform not only axially but also in other directions, leading to unpredictable and amplified deformations. This multi-directional strain intensifies local stresses, making misalignment a critical factor that severely undermines the structural integrity and durability of the welded joint.

4. Conclusions

The analysis of welded joints presented in this paper underscores their critical role in structural integrity while highlighting the persistent challenge of imperfections that threaten their performance. The case studies demonstrate that defects such as excess weld metal, cracks, incomplete root penetration, lack of fusion, undercuts, and misalignment—often arising from welding techniques, material preparation, or thermal effects—can individually and collectively compromise a structure's load-bearing capacity and longevity. Notably, the interaction between defects, such as excess weld metal amplifying crack propagation or misalignment inducing complex strain states, emerges as a key factor in elevating stress concentrations and increasing failure risk. This study reinforces the need for a holistic approach to weld imperfection analysis, ensuring safer and more durable structural design.

5. Acknowledgement

This work is contribution to the Ministry of Science and Technological Development of Serbia funded contracts no. 451-03-137/2025-03/ 200105 and 451-03-137/2025-03/ 200213 from 04.02.2025. and Serbian-Hungarian joint research project no. 9 (period 2024-2026) – Structural optimization of additively manufactured cellular titanium implant using artificial intelligence.

6. References

[1] Miladinov, Milan; Đorđević, Branislav; Sedmak, Simon; Vučetić, Filip; Jeremić, Lazar; Sedmak, Aleksandar; Popović, Olivera. (2025). Cracking of HSLA Steel Nioval 47 Caused by Exploitation Condition and Repair Welding. *Tehnički vjesnik, 32 (2),* 683-691. https://doi.org/10.17559/TV-20240613001772

[2] Miladinov, Milan; Đorđević, Branislav; Sedmak, Simon; Bratu, Ciprian; Radu, Dorin; Sedmak, Aleksandar; Aleksić, Nikola. (2024). Damage analysis and restoring of structural integrity of pelton runner after repair welding: case study. *Structural integrity and life, 24,* 217-221.

[3] Kozak, Dražan; Damjanović, Darko; Katinić, Marko. (2016). Integrity assessment of the butt weld joint with defect according to EN ISO 6520-1, series 400. *Structural integrity and life, 16(2),* 120-124.

[4] Dimić, Ivana; Arsić, Miodrag; Međo, Bojan; Stefanović, Ana; Grabulov, Vencislav. (2013). Effect of welded joint imperfection on the integrity of pipe elbows subjected to internal pressure. *Tehnički vjesnik, 20(2),* 285-290.

[5] Tušek, J.; Bajcer, B.; Taljat, B.; Hrženjak, M. (2007). Analysis of lack of fusion in welds at water heaters. *Metalurgija, 46(2),* 111-116.

[6] Ottersbock, M.J.; Leitner, M.; Stoschka, M. (2021). Characterisation of actual weld geometry and stress concentration of butt welds exhibiting local undercuts. *Engineering Structures, 240,* 112266

[7] Shen, W.; Qui, Y.; Xu, L.; Song, L. (2019). Stress concentration effect of thin plate joints considering welding defects. *Ocean Engineering, 184,* 273-288.

[8] Tomerlin, Damir; Kozak, Dražan; Gubeljak, Nenad; Damjanović, Darko. (2020) Numerička analiza distorzija i zaostalih naprezanja pri zavarivanju kutnih spojeva S690QL limova. *10. susret Hrvatskog društva za mehaniku, Slavonski Brod.*

[9] Odanović, Zoran; Grabulov, Vencislav; Arsić, Miodrag; Đurđević, Mile; Katavić, Boris. (2011). Selection of the optimal filler material for on-site repair welding of the turbine shaft at the hydropower plant. *Zavarivanje i zavarene konstrukcije, 56(4),* 149-166.

[10] Cerit, M.; Kokumer, O.; Gelner, K. (2010). Stress concentration effects of undercut defect and reinforcement metal in butt welded joint. *Engineering Failure Analysis, 17,* 571-578.

[11] Aranđelović, Mihajlo; Đorđević, Branislav; Sedmak, Simon; Radu, Dorin; Petrović, Ana; Dikić, Stefan; Sedmak, Aleksandar. (2024). Failure analysis of welded joint with multiple defects by extended Finite Element Method and Engineering Critical Analysis. *Engineering Failure Analysis, 160,* 108176. https://doi.org/10.1016/j.engfailanal.2024.108176

[12] Aranđelović, Mihajlo; Sedmak, Simon; Jovičić, Radomir; Perković, Srđa; Burzić, Zijah; Radu, Dorin; Radaković, Zoran. (2021). Numerical and Experimental Investigations of Fracture Behaviour of Welded Joints with Multiple Defects. *Materials, 14(17),* 4832. https://doi.org/10.3390/ma14174832

[13] Aranđelović, Mihajlo; Petrović, Ana; Đorđević, Branislav; Sedmak, Simon; Sedmak, Aleksandar; Dikić, Stefan; Radu, Dorin. (2023). Effects of Multiple Defects on Welded Joint Behaviour under the Uniaxial Tensile Loading: Fem and Experimental Approach. *Sustainability 15(1),* 761. https://doi.org/10.3390/su1501076

Društvo za tehniku zavarivanja Slavonski Brod

13. Međunarodno znanstveno-stručno savjetovanje SBZ 2025

„STROJARSKE TEHNOLOGIJE U IZRADI ZAVARENIH KONSTRUKCIJA I PROIZVODA, SBZ 2025."
Slavonski Brod, 08. i 09. 05. 2025.

PRODUCTION AND USE OF HYDROGEN FOR INDUSTRIAL PURPOSES

E. Bjelajac[1,*], B. Hildebrandt[2], L. Sohler[3], A. Skumavc[4], D. Klobčar[5], T. Vuherer[6]

[1] Messer Slovenija d.o.o., Jugova 20, 2342 Ruše
[2] Messer SE & CO. KGaA, Krefeld
[3] Messer Cutting Systems GmbH, Otto-Hahn-Straße 2-4, 64823 GroßUmstadt, Germany
[4] SIJ Acroni d.o.o., Cesta Borisa Kidriča 44, 4270 Jesenice
[5] Faculty of Mechanical Engineering, University of Ljubljana, Aškerčeva ulica 6, 1000 Slovenia
[6] Faculty of Mechanical Engineering, University of Maribor, Smetanova ulica 17, 2000 Maribor Slovenia

*Corresponding Author: E mail: edvard.bjelajac@messergroup.com

Abstract

Metals are an essential material for the construction of buildings, transportation structures, process equipment and other products for industrial and individual use, including the manufacture of renewable energy equipment. A significant amount of energy is required to convert them. Reducing carbon dioxide emissions in the smelting and metals forming industry is important for the overall reduction of greenhouse gas emissions. To decarbonize the metals industry, it makes sense to replace the combustible gases acetylene and propane with carbon-neutral hydrogen. It is estimated that in the near future, as hydrogen from renewable sources increases, it will also be affordable to use it as a replacement for the current combustible gases in industrial machining. At the same time, by using hydrogen, the user avoids paying CO2 emision coupons.

Keywords: Oxyfuel-hydrogen cutting, environmentally friendly.

1. Introduction

Fossil fuels dominate the global energy system and are responsible for over 80% of the world's energy supply and three quarters of all greenhouse gas emissions. In order to reduce greenhouse gas emissions and limit global warming in line with the goals of the Paris Agreement, fossil fuels should be reduced or partially replaced by fuels with lower greenhouse gas emissions. Experts believe that the production of green hydrogen is the key to reducing greenhouse gas emissions in the future [1] The EU's energy strategy aims to reduce greenhouse gas emissions through the increased use of

renewable and low greenhouse gas sources and has allocated significant resources to this through projects.

Around 120 million tons of hydrogen are produced every year, of which around two thirds is pure and one third is produced in combination with other gases. Depending on how the hydrogen is produced, there is grey, brown, blue, green and possibly pink hydrogen, Figure 1. Currently, around 95% of hydrogen is grey or brown, which is produced from coal or natural gas and whose greenhouse gas emissions are released into the atmosphere [2]. The production of grey hydrogen, which is obtained from natural gas, produces fewer emissions than the production of brown hydrogen from coal. Hydrogen is also released when aluminium is cut in the presence of water [3]. The name blue hydrogen is used when greenhouse gases have been captured in the production process. Pink hydrogen is produced by electrolysis, which is powered by nuclear energy, while green hydrogen, which is produced from renewable energy sources, is usually produced by electrolysis.

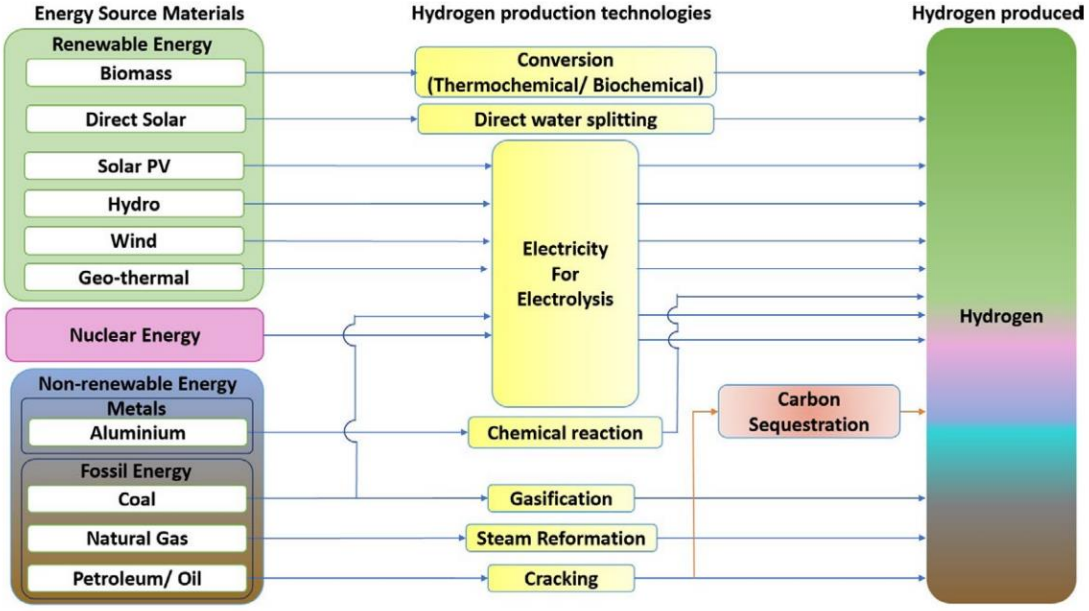

Figure 1. Energy sources for hydrogen production [1]

The primary use of hydrogen is primarily in the industrial sector, followed by transportation, with significantly fewer applications in the energy, power generation and construction sectors.

In the coming years, we expect to see an increase in hydrogen fuel cell electric vehicles (FCEVs), both for private and commercial use. In the energy sector, hydrogen can be used as a fuel in gas turbines or "fuel cells", which reverse the reaction in the electrolysis of water so that hydrogen reacts electrochemically with oxygen (air) to release energy.

In industry, hydrogen is expected to replace some fossil fuels in metallurgy in the future, and in the chemical industry it will be used to synthesize ammonia, methanol, crude oil and coal chemicals. In welding, hydrogen is already used as a component of shielding gases for TIG welding due to its

excellent thermal conductivity Figure 2, for welding high-alloy stainless steels with an austenitic structure. A few percent hydrogen is added to the argon; 2-7.5 % is used in the Messer Group's commercially developed mixtures, the higher the addition of hydrogen for thicker base materials. The addition of hydrogen significantly reduces the welding current, increase welding speed, decrease deformations of base material, and oxidation on the weld surface.

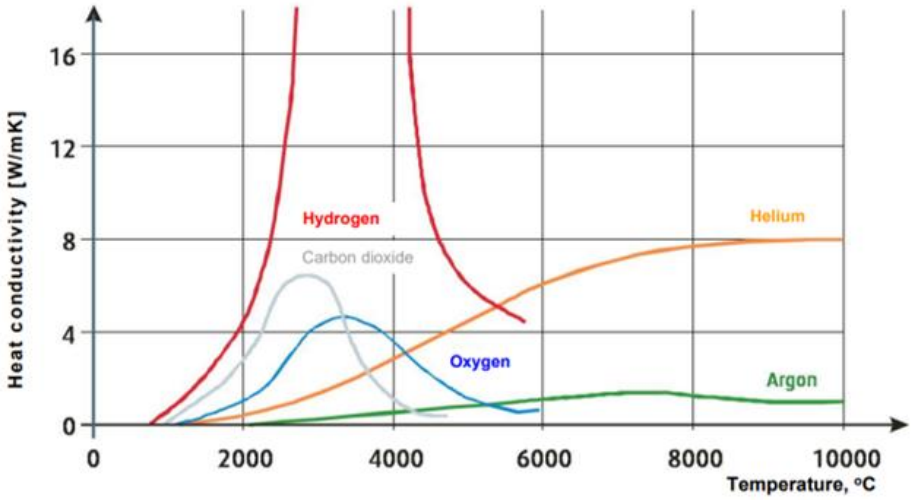

Figure 2. Thermal conductivity of gases [4]

The most used flammable gases for oxy-fuel cutting are acetylene and propane mixtures. The use of hydrogen for industrial cutting purposes has gained momentum in the EU in recent years. The main driving force behind this is the implementation of the ESG Regulation. The price of hydrogen appears very high in terms of kg-bass, but due to the low density, the cost share is relative in the overall view in relation to a cutting meter.

It is expected that the cost of producing hydrogen from renewable sources will be competitive with other combustible gases in the coming years and that green hydrogen will become cheaper. The use of hydrogen in industry will be further strengthened by the fact that its use will avoid the payment of CO2 coupons.

The main properties of hydrogen are: It is the lightest gas, its specific gravity is 14 times less than that of air, it is a very diffusible gas, it requires minimal energy to ignite (five times less than gasoline), it has a high combustion rate, and it has a high thermal conductivity [5].

The advantages of hydrogen over acetylene and propane/butane are: high quality of the cut surface, environmentally friendly gas, no carbon dioxide or carbon monoxide is produced during combustion, significantly less dust is produced compared to acetylene and propane, less work for processing the parts after cutting, high cutting speed and lower cutting costs [6]. In oxy-fuel cutting with an oxy-acetylene flame, the heat-affected area is significantly larger compared to an oxy-hydrogen flame [5].

The hardening of cut surfaces cut with hydrogen behaves similarly to those cut with propane or acetylene.
As a manufacturer of autogenous systems with a 100-year tradition and its own production in the EU, Messer Cutting invests considerable resources in the development of autogenous systems in which hydrogen is used as a combustible gas for heating, straightening, and cutting.

2. The advantages of using hydrogen for cutting

The combustion of hydrogen with air reaches a temperature of 1700 °C and with oxygen is flame temperature much higher. The ignition temperature is 585 °C and the upper and lower explosion limits are 4 and 75 % [7], **Table *1***. Properties of cutting gasesTable 1. When hydrogen burns, 2 kg of hydrogen combines with 16 kg of oxygen to form 18 kg of water, according to the following equation [1].

$$H_2 + 0.5O_2 = H_2O \quad [1]$$

Table 1. Properties of cutting gases

Gas	Formula	Ignition temperature, [°C]	Lower explosion limit (air), [vol %]
Vodik	H2	585	4~
Acetylene	C2H2	335	2,5 ~
Propane	C3H8	467	2,2 ~

The hydrogen and acetylenic flames are shown, Figure 3.
The properties of a hydrogen flame are:
- bright, non-dazzling, transparent flame,
- concentrated energy source enables little shorter piercing times and faster cutting,
- no carbon dioxide and carbon emissions, monoxide,
- reduced dust lower noise levels emission,
- low oxygen consumption,
- safer gas, higher ignition temperature and lower explosion limit compared to acetylene and propane, Table 1.

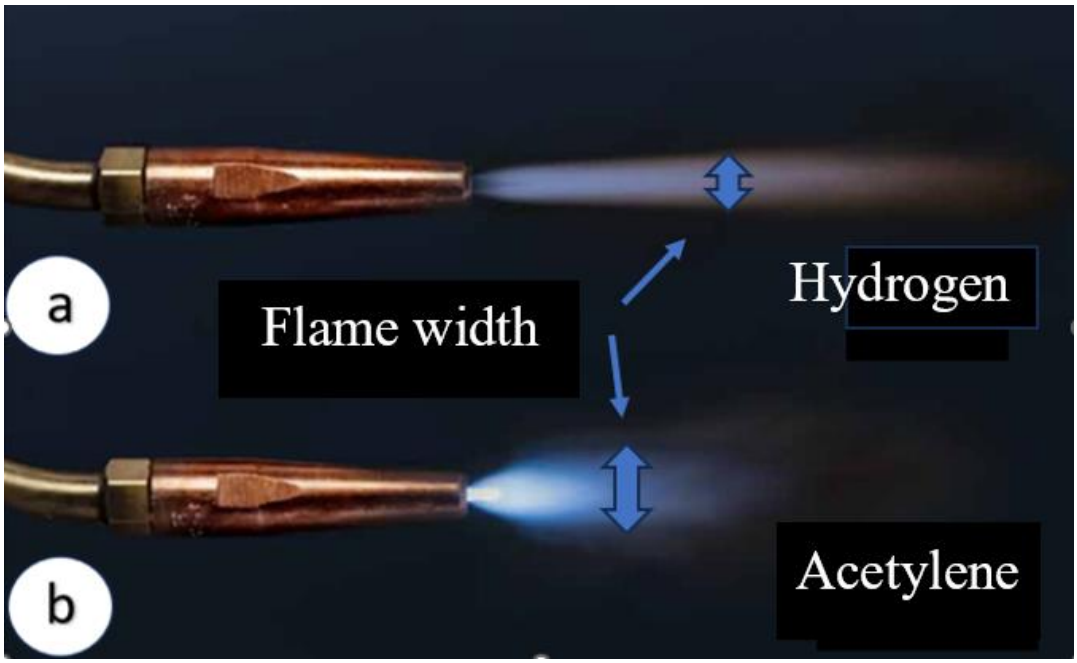

Figure 3. Oxyfuel cutting, a) hydrogen flame, b) acetylene flame [8]

2.1. Clean, environmentally friendly and safe cutting process

The cutting of hydrogen is environmentally friendly; compared to acetylene and propane, the combustion of hydrogen does not produce carbon dioxide. A comparative analysis of the measurement of flue gases from the combustion of acetylene, propane and hydrogen with oxygen, carried out at Leibniz University in Hannover, showed that the amount of CO2 measured when using the combustible gas hydrogen was 400 ppm, Figure 4a, which is significantly lower than for acetylene and propane, where the values are over 3000 ppm in both cases. Combustion of hydrogen with oxygen alone does not produce CO2 emissions, Equation 1, the value shown in Figure 3 also considers the CO2 content of the surrounding atmosphere. When cutting with other combustible gases, a CO2 concentration value of 1400 ppm is considered as an influence of the surrounding atmosphere, as the deterioration of air quality due to emissions is much faster than when cutting with hydrogen. The amount of NOx produced with hydrogen is around 15 ppm, with the highest amount being over 60 ppm when burning acetylene, Figure 4b. Hydrogen cutting also produces significantly less fumes, and small-scale cutting of unalloyed steels can be carried out indoors with virtually no fume extraction. From this point of view, hydrogen cutting represents the future of oxyfuel cutting. Testing equipment is shown on Figure 5.

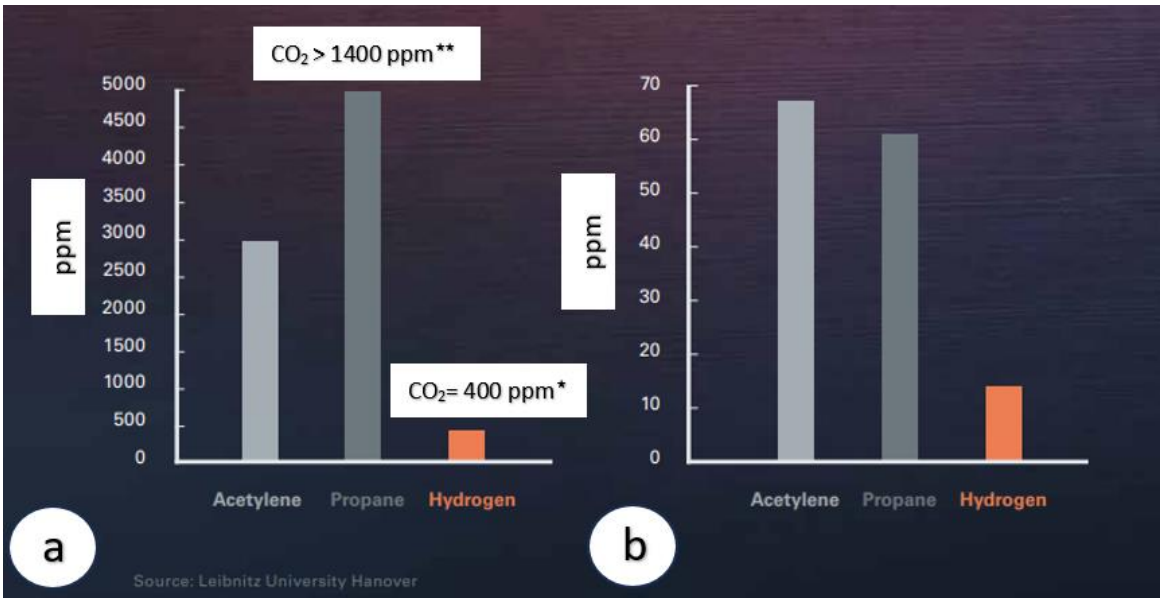

Figure 4. The amount of exhaust gases from oxyfuel cutting, a) CO2 emissions, b) NOx emissions [8]

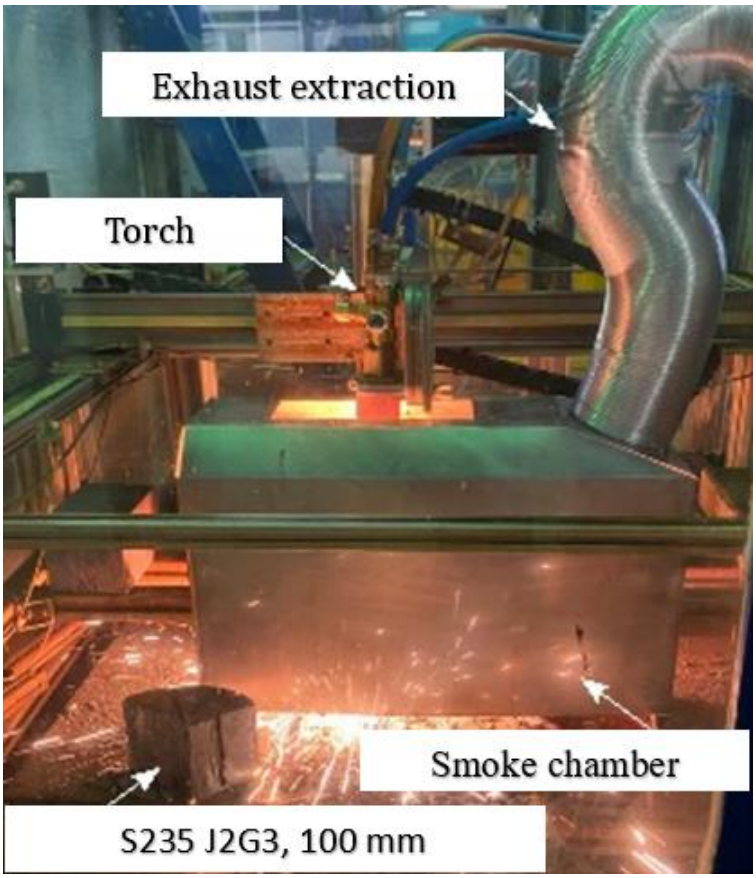

Figure 5. Test device for fume gas separation

3. Conclusions

The comparison of the results of the acetylene-oxygen, propane-oxygen and hydrogen-oxygen tests showed that:

- the amount of greenhouse gases produced directly when using hydrogen is 0, compared to acetylene and propane, where the values vary between 3000 and 5000 ppm, the captured fume gases consider the concentration of carbon dioxide in the surrounding atmosphere,
- the amount of NOx produced when using hydrogen is sometimes lower than when using acetylene and propane,
- flame is more concentrated than in propane and acetylene and consequently cutting speed is higher than with other mentioned gases,
- amount of fume gases are much lover with hydrogen, than with other standard flame gases like acetylene and propane,
- with combination of CO2 emission coupons is expected, that hydrogen will play important role like advance burning gas for industry in future.

4. Reference

[1] C. L. M. Eh, A. N. T. Tiong, J. Kansedo, C. H. Lim, B. S. How, and W. P. Q. Ng, "Circular Hydrogen Economy and Its Challenges," *Chem Eng Trans*, vol. 94, pp. 1273–1278, 2022, doi: 10.3303/CET2294212.

[2] *Hydrogen : a renewable energy perspective*. International Renewable Energy Agency, 2019.

[3] K. Uehara, H. Takeshita, and H. Kotaka, "Hydrogen gas generation in the wet cutting of aluminum and its alloys."

[4] "Complex Properties of Shielding Gases," 2016.

[5] J. Tušek and M. Šraj, "OXY-HYDROGEN FLAME FOR CUTTING OF STEELS," *METALURGIJA*, vol. 46, pp. 211–215, 2007.

[6] "Hydrogen Gas Cutting System".

[7] "X.2 PROPERTIES OF HYDROGEN X.2.1 GASEOUS HYDROGEN."

[8] "HYCUT Hydrogen makes oxyfuel technology more cost-effective and better for the environment and human health."

Društvo za tehniku zavarivanja Slavonski Brod

13. Međunarodno znanstveno-stručno savjetovanje SBZ 2025

„STROJARSKE TEHNOLOGIJE U IZRADI ZAVARENIH KONSTRUKCIJA I PROIZVODA, SBZ 2025."
Slavonski Brod, 08. i 09. 05. 2025.

Fatigue behaviour of welded joints with multiple defect combinations

S. Sedmak[1,*], M. Aranđelović[1], A. Petrović[2], D. Kozak[3], B. Đorđević[1]

[1]Innovation Center of Faculty of Mechanical Engineering, Belgrade, Serbia
[2]University of Belgrade, Faculty of Mechanical Engineering, Belgrade, Serbia
[3]University of Slavonski Brod, Mechanical Engineering Faculty, Slavonski Brod, Croatia,

[*] Corresponding Author. E-mail: simon.sedmak@yahoo.com

Abstract

This research represents a continuation of extensive investigation of the effects of multiple defects in welded joint on their integrity [1-4]. Up to this point, all of the research was focused on static loads and determining which defect combination is the least favourable one. Based on the previous results, it was determined that vertical plate misalignment was the most critical defect, as its presence would also result in a number of other stress concentrators in the welded joints. The next steps in analysing the exact ways in which defect combinations which include vertical misalignment affect the integrity of welds included, among others, analysing of the microstructure in welded joint regions, mainy focusing on the heat affected zone, where most critical locations in terms of stress were observed. Additionally, fatigue was included as one of the important factors which needs to be considered. The goal here was to determine how the presence of different defects affects the fatigue life of welded structures by developing representative numerical models using finite element method. It needs to be pointed out that this is the initial stage, which aims to develop prototypical models which can then be used for other materials and weld geometries.

Keywords: Welding defects, Fatigue, Finite Element Method

1. Introduction

While the effect of single defects on welded joints is well researched and documented, the issue of multiple defects being present at the same time is still a relatively new subject, which is not covered by relevant standards, such as EN-ISO-5817 series [5]. Extensive research into this matter, [1-4], was conducted by the authors of this work, involving four different groups of multiple defects, as well as test specimens without any defects. Comparing of obtained results confirmed that the specien groups with vertical plate misalignment as the dominant defect were the most critical, and it was decided to

continue the analyses with these two groups. The most recent efforts in this direction include the development of numerical models which would simulate fatigue crack growth [6-8] in specimens with multiple defects. This research will also include the experimental tests in the future, which will be used to verify the newly developed models. Hence, the goal here was to obtain functional finite element models, which can be compared to each other in order to gain insight into the extent to which different defect combinations affect the fatigue life of welded joints. Once proper experimental data is obtained, these models can be effectively used for realistic applications, as changing of input data for numerical models is a simple process. An additional goal of this research was to create a base which can later be applied to different geometries, and more importantly, different materials.

2. Base for the FE models

All numerical models which will be shown here were made based on the geometries of actual tensile test specimens, including the exact dimensions of each defect [3,4]. Some examples of these geometries, for defect combinations which include vertical misalignments, can be seen in Figure 1. As indicated in the figure, one of the welded plates is slightly sloped, whereas the other remained horizontal during the welding. This was also taken into account when designing the numerical models. All specimens were taken from welded plates made of low-carbon low-alloyed structural steel S275JR, which is known for its solid mechanical properties, but has low resistance to fatigue compared to some of the other groups of steel.

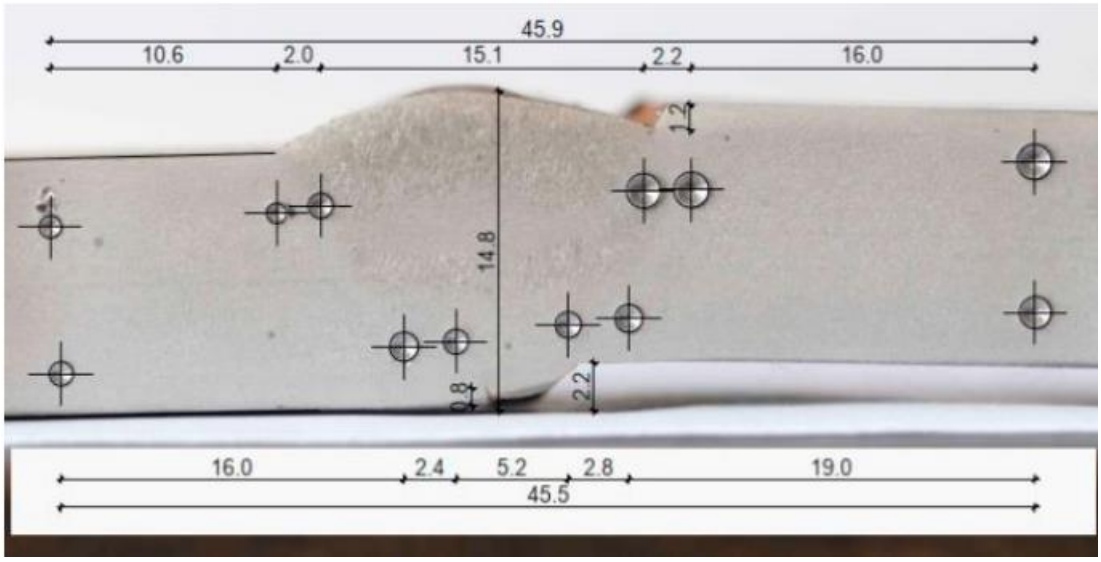

Figure 1. Welded joint specimen with vertical misalignment, incomplete root penetration and a weld face undercut [4].

Originally, finite element models were made in ABAQUS, as two-dimensional, and included all three welded joint regions (parent material, weld metal and heat affected zone), as individual zones with

specific tensile properties - yield stress, tensile strength and deformation at failure - which were determined by combining experimental and iterative numerical approaches [9].
Numerical models for the analysis of fatigue crak growth were made using ANSYS R2022 version, and in this case, three-dimensional geometry was adopted, in order to represent crack growth as realistically as possible. However, due to certain limitations of the used method (SMART crack growth, [10,11]), some approximations of the models had to be adopted. Defning several different materials within the model, which would correspond to each individual weld region, was not an option, as it would cause the model to stop working due to issues with contacts between these regions. Hence, a more simplified approach was adopted, and the whole specimen was modeled as if it was made of the heat affected zone, since this was the region where cracks would initiate during actual tensile tests. For this reason, initial fatigue cracks were assumed in the same critical locations where highest stresses were observed in real specimens. It should also be noted that the cracks in the tensile tests would propagate only through the HAZ, which is why the whole finite element model was appxorimated with its tensile properties.
Another important approximation was related directly to fatigue crack growth - the defining of Paris law coefficient C and exponent m [12]. Since there is currently no experimentally obtained values for the research presented here (as these experiments will be a part of the future research), values of C and m were adopted based on data available in literature for steels such as the one used here. Final values that were selected were 1.5×10^{-12} for C and 2.8 for m. Since the main goal here was to create prototype numerical models made from the same material, with different geometries, this was sufficiently accurate. As it was previously pointed out, once real Paris law parameters are obtained experimentally, they can be easily updated in the existing finite element models.

3. Development of numerical models

This stage of research involved the importing of model geometry, defining and positioning of the initial fatigue crack, along with boundary conditions and loads, both of which were made in a way that corresponds to the experiments. As previously mentioned, all finite element models and analyses presented ih this paper were made using ANSYS software, and fatigue crack growth was simulated via SMART crack feature. For this reason, it was necessary to mesh the models using tetrahedral elements, as can be seen in Figure 2, for all three models - two with defects and a "clean" one. Initial fatigue cracks can also be seen in the most critical location for all three models, which was located in the root side of the weld, close to the region which would correspond to weld metal in the real specimens. These locations were previously determined, both numerically and experimentally, during various static analyses [1-4].

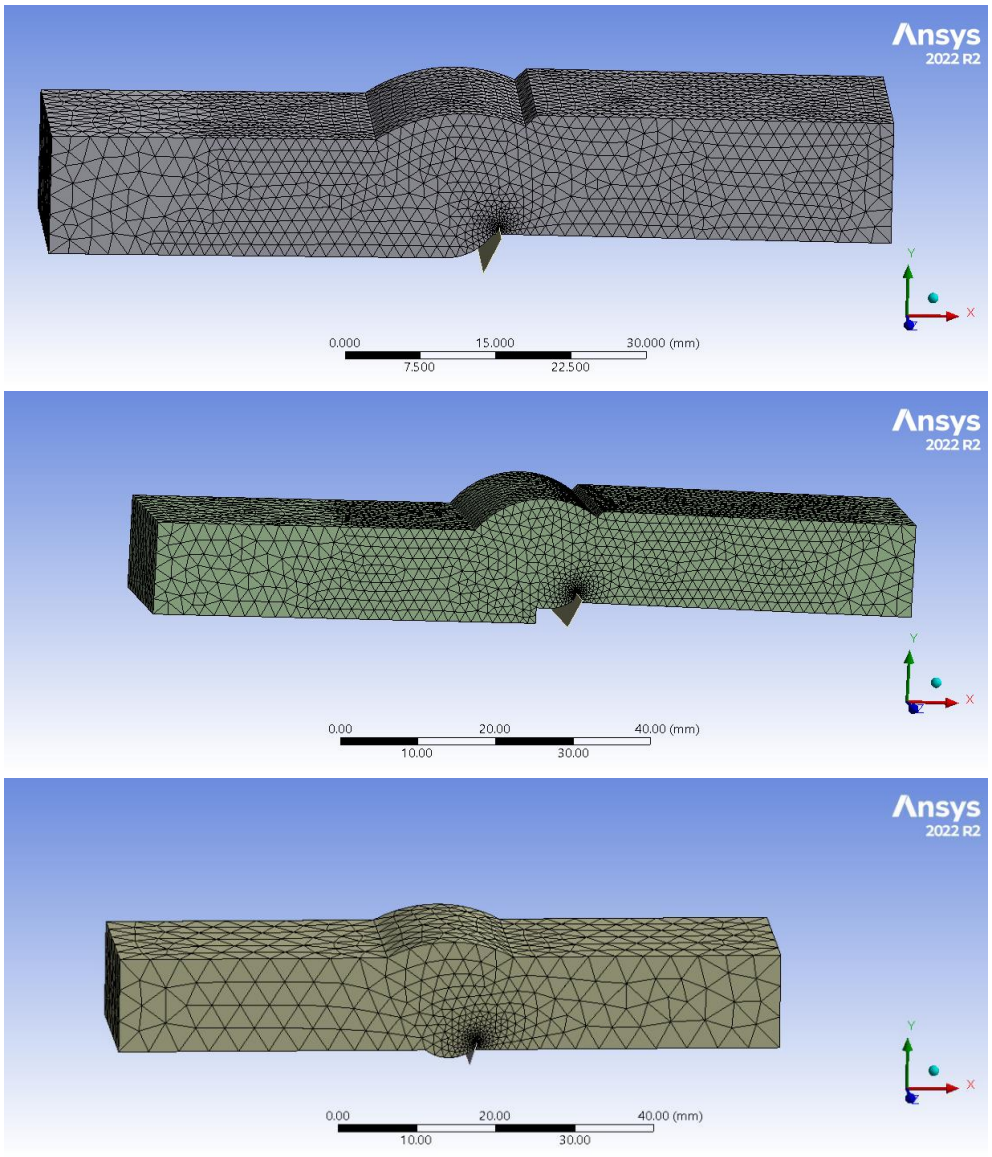

a)

b)

c)

Figure 2. Finite element meshes for models with: a) misalignment, excess weld metal and undercut; b) misalingment, incomplete root penetration, undercut; c) no defects

Boundary condition and load were defined in the same way for all three models, and an example can be seen in Figure 3. One end of the specimen was fixed, whereas the opposite was subjected to pressure load with a magnitude of 100 MPa. This value was selected based on one of the static models, which entered plasticity for load magnitude of 170 MPa (which in turn corresponded to the force of around 41kN, which was obtained in the experiment. Since fatigue loads cause failure at stress levels lower than the yield stress of a given material, a value of around two-thirds of the plasticity load (170 MPa) was selected, which would correspond to dividing the original load with a typical safety factor of 1.5. Of course, once actual experiments are completed, this load magnitude will be adequately

updated. Mechanical properties used as input included yield stress of 405 MPa and tensile strength of 505 MPa, in accordance with previous results [9]. Initial crack length was adopted as 1 mm, in accordance with common practice in these cases.

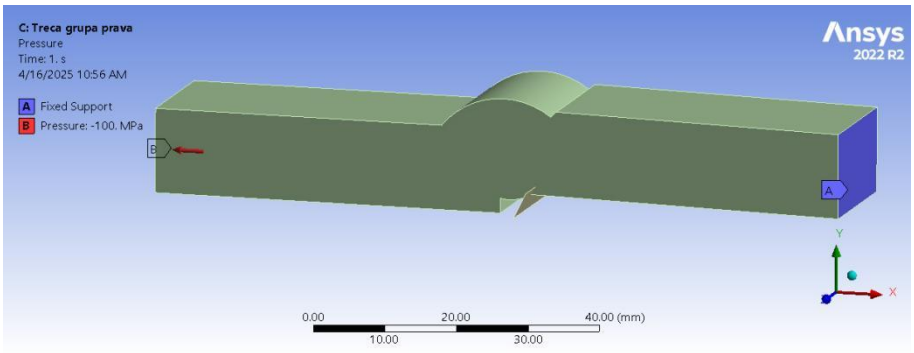

Figure 3. Boundary condition (fixed end) and the load (100 MPa pressure)

4. Results of FEM simulations and discussion

This chapter will include the results of all three fatigue crack growth simulations, in terms of stress intensity factors around the crack tip and number of load cycles until failure, which will be presented in the form of a-N (crack extension vs. Number of cycles) diagrams. It should be noted that these results do not refer to critical crack length (hence the term "extension"), and that critical crack length is actually a combination of initial crack length and total extension obtained during the simulations. Stress intensity factors for all three cases are given in figure 4.

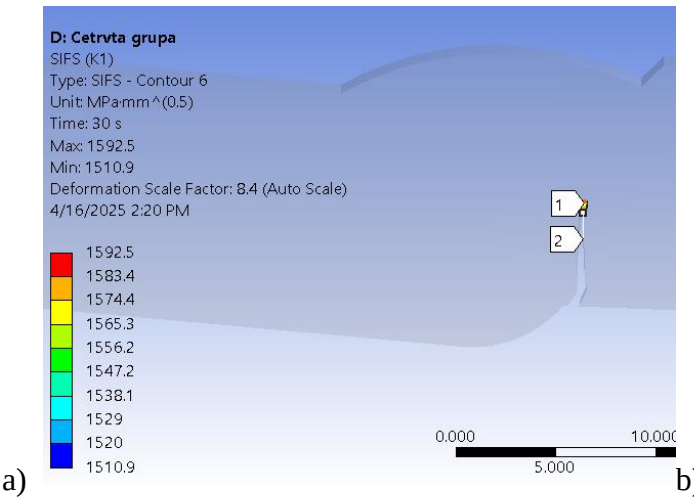

a)

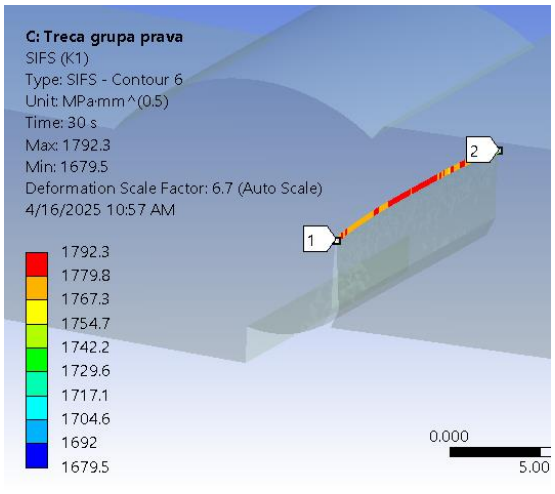

b)

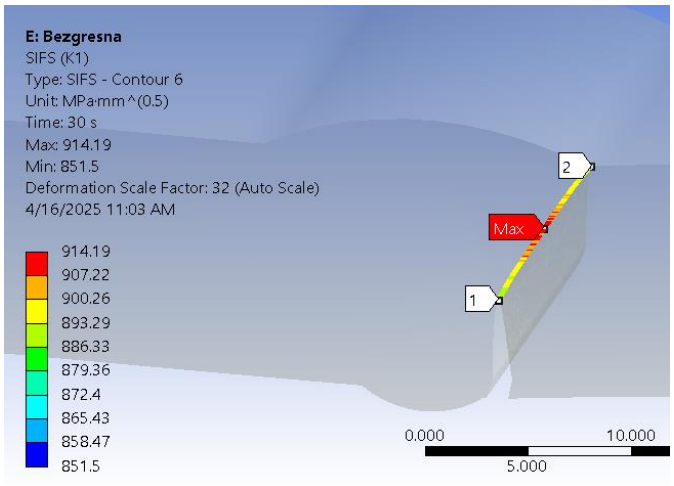

c)

Figure 4. SIF values for models with : a) misalignment, excess weld metal and undercut; b) misalingment, incomplete root penetration, undercut; c) no defects

Diagrams showing the relationship between the number of cycles and crack extension are given in figure 5.

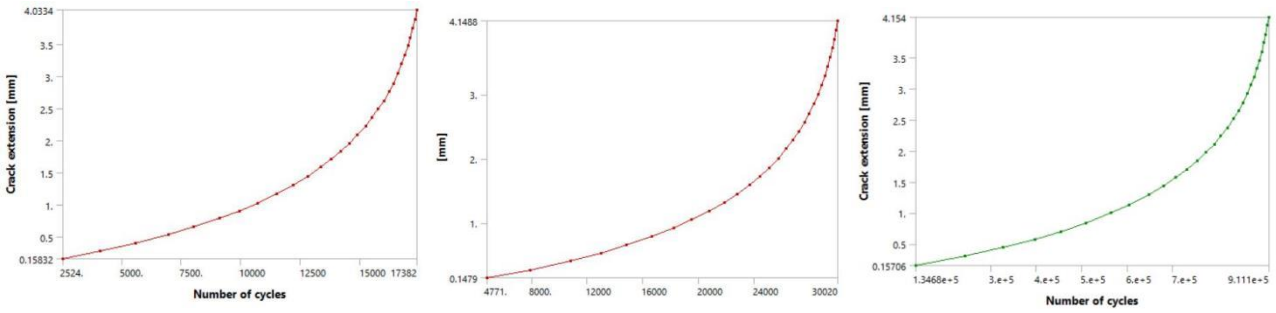

Figure 5. a-N diagrams for models with: a) misalignment, excess weld metal and undercut; b) misalingment, incomplete root penetration, undercut; c) no defects

All of the presented results were obtaind during calculations which consisted of 30 steps. This number was determined iteratively, by slightly increasing the total number of steps - which controls the total crack growth - up to a point where the a-N curve would go into the unstable fatigue crack growth region, as can be clearly seen in all three diagrams from Figure 5. Total crack extension was very similar between all of the models, a bit longer than 4 mm, which suggests that critical crack lengths for all three cases were around 5 mm, including the initial crack length.

For each model, fatigue cracks would change their paths from their initial position, propagating in a more vertical direction. Similar behaviour was observed in experiments with static loads/cracks, wherein these cracks would propagate through the HAZ towards the weld metal. While it was assumed that such behaviour was related to microstructures in each regions, new models (with only

one material) have confirmed that geometry of the specimen also plays a very important role. Although this was expected from the beginning, it was not taken into consideration up until these results were obtained. This also suggests that the crack propagation path could change considerably in the case the boundary conditions and loads are "reversed", i.e., if the load and fixed BC are applied on the opposite side of the model. This behaviour is specific to the models presented here, due to noticeable asymmetry resulting from several welded joint defects which were present.

While crack lengths for all three models were the same, noticeable differences were observed in terms of SIFs, and especially, total number of cycles. In this case, stress intensity factor values for models with defects were 70-95% greater compared to the model without defects (which was 914 $MPa \cdot mm^{1/2}$), which can be easily explained with significant stress concentration in certain parts of the first two models, which was absent in the defectless specimen.

Fatigue behaviour exhibited the most prominent differences - even the two models with defects differed by over 40%, with the incomplete root penetration group taking around 17,300 cycles to reach critical crack extension/length, and the excess weld metal model requiring around 30,000 cycles. This gives clear insight into which group of defects is the most critical, and it should be noted that the same conclusion was reached during previous research, with static loads - this particular defect combination was the least favourable in terms of structural integrity of the weld. Both of these results for number of cycles are negligible when compared to the specimen model without defects, as it needed over 900,000 cycles to reach the same critical length. This implies that multiple defects in welded joints can decrease fatigue life more than 30 times.

5. Acknowledgements

This work is contribution to the Ministry of Science and Technological Development of Serbia funded contracts no. 451-03-137/2025-03/ 200105 and 451-03-137/2025-03/ 200213 from 04.02.2025. and Serbian-Hungarian joint research project no. 9 (period 2024-2026) – Structural optimization of additively manufactured cellular titanium implant using artificial intelligence.

6. Conclusions

Research presented in this paper involved the initial stages of developing finite element models which would simulate fatigue crack growth in welded joints with multiple defects, based on previously obtained results for static loads. Since there is still no actual experimental basis for fatigue results, a number of approximations and assumptions had to be made, so that models which can be at least compared to each other, could be obtained. Hence, the goal was to determine how much the presence of different defects affects the fatigue life of such specimens. This goal was ultimately achieved, providing realistic initial models, which will be further improved as future research progresses. It should be noted that significant differences in number of cycles for defectless model and the other two were an expected result, only confirming what was already known in practice - that none of the

defects presented here are acceptable in structures subjected to fatigue. Due to this, results obtained as this point can only be used as a reference for future work, and should be considered purely from a theoretical point of view. Comparison to real cases represents the goal of the next step, which will involve analysing the behaviour of welded joints made of different types of steels, with different combinations of defects.

6. References

[1] Aranđelović, Mihajlo; Petrović, Ana; Đorđević, Branislav; Sedmak, Simon; Sedmak, Aleksandar; Dikić, StefanČ Jovičić, Radomir. (2022). Effects of Multiple Defects on Welded Joint Behaviour Under the Uniaxial Tensile Loadring: Numerical and Experimental Approach, CIBv 2022 International Scientific Conference on Civil Engineering and Building Services, Brašov, Romania

[2] Aranđelović, Mihajlo; Sedmak, Simon; Jovičić, Radomir; Kozak, Dražan; Đorđević, Branislav. (2021). Numerical simulation of crack growth in welded joints with defects, *Procedia Structural Integrity, 33(C)*, pp. 850-857, DOI:10.1016/j.prostr.2021.10.095

[3] Aranđelović, Mihajlo; Sedmak, Simon; Jovičić, Radomir; Perković, Srđa; Burzić, Zijah; Đorđević, Branislav; Radaković, Zoran. (2021). Numerical simulation of welded joints with multiple various defects, *Structural Integrity and Life, 21(1)*, pp. 103-107

[4] Aranđelović, Mihajlo; Sedmak, Simon; Jovičić, Radomir; Petrović, Ana; Dikić, Stefan. (2022), Optimisation of numerical models of welded joints with multiple defect combinations, *Procedia Structural Integrity 42*, pp. 985-991

[5] Sedmak, Simon; Jovičić, Radomir; Sedmak, Aleksandar; Aranđelović, Mihajlo; Đorđević, Branislav, (2018). Influence of multiple defects in welded joints subjected to fatigue loading according to sist en iso 5817: 2014, *Structural Integrity and Life, 18(1)*, pp. 77-81

[6] Singh, I.V.; Mishra, B.K.; Bhattacharya, S.; Patil, R.U.. (2012), The numerical simulation of fatigue crack growth using extended finite element method, *International Journal of Fatigue, 36(1)*, pp. 109-119, https://doi.org/10.1016/j.ijfatigue.2011.08.010.

[7] Sarzosa, F.B. Diego; Godefroid, B. Leonardo; Ruggieri, Claudio. (2013). Fatigue crack growth assessments in welded components including crack closure effects: Experiments and 3-D numerical modeling, *International Journal of Fatigue, 47*, pp. 279-291, https://doi.org/10.1016/j.ijfatigue.2012.09.009.

[8] Sedmak, Aleksandar. (2024). Fatigue crack growth simulation by extended finite element method: A review of case studies, *FFEMS, 47(6)*, pp. 1819-1855, https://doi.org/10.1111/ffe.14277

[9] Aranđelović, Mihajlo; Petrović, Ana; Đorđević, Branislav; Sedmak, Simon; Sedmak, Aleksandar; Dikić, Stefan; Radu, Dorin. (2023). Effects of Multiple Defects on Welded Joint Behaviour under the Uniaxial Tensile Loading: Fem and Experimental Approach. *Sustainability 15(1):761*. https://doi.org/10.3390/su15010761

[10] Alshoaibi, M. Abdulnaser. (2021). Numerical Modeling of Crack Growth under Mixed-Mode Loading. *Applied Sciences. 11(7):2975*. https://doi.org/10.3390/app11072975

[11] Alshoaibi M., Abdulnaser; Fageehi A., Yahya. (2022). Finite Element Simulation of a Crack Growth in the Presence of a Hole in the Vicinity of the Crack Trajectory. *Materials, 15(1):363.* https://doi.org/10.3390/ma15010363

[12] Ancona, F.; Palumbo, D.; De Finis, R.; Demelio, G.P.; Galietti, U. (2016). Automatic procedure for evaluating the Paris Law of martensitic and austenitic stainless steels by means of thermal methods, *Engineering Fracture Mechanics, 163*, pp. 206-219, https://doi.org/10.1016/j.engfracmech.2016.06.016.

Welding Society in Slavonski Brod

Univerza v Mariboru Fakulteta za strojništvo

University in Slavonski Brod

The Faculty of Materials Science and Technology in Trnava

Đuro Đaković Group Slavonski Brod

GLAVNI SPONZORI

SPONZORI

PARTNERI